



Space engineering

**Structural materials handbook -
Part 6: Fracture and material
modelling, case studies and design
and integrity control and inspection**

NOTE:

This pdf-file does not contain automatic cross-references. To make use of the cross-references please use the MS Word version of this document.

Foreword

This Handbook is one document of the series of ECSS Documents intended to be used as supporting material for ECSS Standards in space projects and applications. ECSS is a cooperative effort of the European Space Agency, national space agencies and European industry associations for the purpose of developing and maintaining common standards.

This handbook has been prepared by the ECSS-E-HB-32-30 Working Group, reviewed by the ECSS Executive Secretariat and approved by the ECSS Technical Authority.

Disclaimer

ECSS does not provide any warranty whatsoever, whether expressed, implied, or statutory, including, but not limited to, any warranty of merchantability or fitness for a particular purpose or any warranty that the contents of the item are error-free. In no respect shall ECSS incur any liability for any damages, including, but not limited to, direct, indirect, special, or consequential damages arising out of, resulting from, or in any way connected to the use of this document, whether or not based upon warranty, business agreement, tort, or otherwise; whether or not injury was sustained by persons or property or otherwise; and whether or not loss was sustained from, or arose out of, the results of, the item, or any services that may be provided by ECSS.

Published by: ESA Requirements and Standards Division
 ESTEC, P.O. Box 299,
 2200 AG Noordwijk
 The Netherlands

Copyright: 2011© by the European Space Agency for the members of ECSS

Change log

ECSS-E-HB-32-20 Part 6A	First issue
20 March 2011	

Table of contents

Change log	3
Introduction.....	27
64 Behaviour of advanced composites	28
64.1 Introduction.....	28
64.2 Summary of material behaviour	29
64.2.1 Metal matrix composites.....	29
64.2.2 Inorganic ceramic matrix composites	30
64.3 Significant behavioural characteristics	30
64.3.1 General.....	30
64.3.2 Modulus mismatch.....	30
64.3.3 Matrix-to-reinforcement interface.....	31
64.3.4 In-situ fibre strength.....	32
64.3.5 CTE mismatch	32
64.3.6 Thermal history and residual stresses.....	33
64.3.7 Multiple cracking.....	33
64.3.8 Thermo-mechanical fatigue (TMF)	33
64.4 Basic fracture characteristics	33
64.4.1 General.....	33
64.4.2 Particulate reinforced MMC	34
64.4.3 Fibre reinforced MMC.....	35
64.4.4 Fibre reinforced CMC	36
64.4.5 Defining design values	37
64.5 Failure criteria for CMC	37
64.5.1 Introduction.....	37
64.5.2 Design aspects	37
64.6 References	40
64.6.1 General.....	40
65 Particulate reinforced metals	41
65.1 Introduction.....	41

65.1.1	Materials	41
65.1.2	Composites.....	41
65.1.3	Particulate reinforcement.....	42
65.2	Damage mechanisms.....	43
65.2.1	Unnotched specimen.....	43
65.2.2	Notched specimen.....	44
65.2.3	Influence of particles.....	44
65.2.4	Composite performance	45
65.3	Failure modes and fracture behaviour.....	45
65.3.1	Matrix effects	45
65.3.2	Failure mode studies	46
65.3.3	Particulate shape and aspect ratio	46
65.3.4	Particulate fracture	48
65.3.5	Void nucleation and growth	48
65.3.6	Fracture toughness.....	49
65.4	Thermo-mechanical fatigue (TMF) and creep	50
65.4.1	Residual stresses	50
65.4.2	Temperature	50
65.4.3	Superplasticity	50
65.4.4	Applications	50
65.5	References	50
65.5.1	General.....	50
66	Fibre reinforced metals	53
66.1	Introduction.....	53
66.1.1	Materials	53
66.2	Damage mechanisms.....	54
66.2.1	General.....	54
66.2.2	Effect of lay-up.....	54
66.3	Failure modes.....	55
66.3.1	General.....	55
66.3.2	Matrix dominated failure	55
66.3.3	Fibre-dominated damage	55
66.3.4	Self-similar damage growth	55
66.3.5	Fibre-matrix interfacial failures	56
66.4	Thermo-mechanical and creep response	56
66.4.1	General.....	56
66.4.2	Application.....	57

66.5 References	57
66.5.1 General.....	57
67 Inorganic ceramic matrix composites	59
67.1 Introduction.....	59
67.1.1 General.....	59
67.1.2 Matrix.....	60
67.1.3 Interface.....	60
67.1.4 Fibres.....	60
67.2 Damage mechanisms.....	60
67.2.1 Material effects	60
67.2.2 Microcracking	61
67.2.3 Porosity.....	62
67.2.4 Manufacturing and in-service effects.....	63
67.2.5 Crack propagation	63
67.3 Fracture behaviour	64
67.3.1 Toughness parameters.....	64
67.3.2 Test specimens	69
67.3.3 ' <i>R</i> curves	69
67.4 References	71
68 Modelling advanced materials.....	72
68.1 Introduction.....	72
68.1.1 Polymer composites	72
68.1.2 Metal matrix composites.....	72
68.1.3 Inorganic ceramic matrix materials.....	72
68.1.4 Summary of models.....	73
68.2 Particulate reinforced metals	74
68.2.1 Use of models.....	74
68.3 Fibre reinforced metals.....	74
68.3.1 Use of models.....	74
68.4 Inorganic ceramic matrix composites	75
68.4.1 Use of models.....	75
68.5 References	78
68.5.1 General.....	78
69 High-temperature structures	80
69.1 Introduction.....	80
69.1.1 Applications	80

69.1.2 Performance	80
69.1.3 High-temperature materials	80
69.1.4 Development approach	81
69.2 Functions	81
69.2.1 General	81
69.2.2 Aerodynamic heating	82
69.2.3 Propulsive power generation	83
69.3 Operating environments	84
69.4 Integration	84
69.5 Heat management	85
69.6 Life expectancy	85
69.6.1 General	85
69.6.2 Launcher	85
69.6.3 Spaceplane	85
69.6.4 Satellite	86
69.7 Materials selection	86
69.8 Manufacturing	86
69.9 Applications	87
69.9.1 Future reusable launch vehicles	87
69.9.2 Flight-vehicle dependent	88
69.9.3 Non-vehicle dependent	92
69.9.4 Summary of European capabilities	95
69.10 References	96
69.10.1 General	96
70 Thermo-structural designs	98
70.1 Introduction	98
70.1.1 General	98
70.1.2 Single mission	98
70.1.3 Reusable vehicles	99
70.2 Spaceplanes	99
70.2.1 Hermes	99
70.2.2 HOPE	99
70.2.3 Single- and two-stage-to-orbit	100
70.3 Hermes	100
70.4 HOPE	101
70.5 HOTOL	105
70.6 SÄNGER	107

70.7	National aerospace plane (NASP)	108
70.8	Demonstrator panels	110
70.8.1	General.....	110
70.8.2	NASP	110
70.9	Nose cones	110
70.9.1	General.....	110
70.9.2	Shuttle orbiter	110
70.9.3	Hermes	112
70.9.4	HOPE	114
70.9.5	NASP	114
70.9.6	HOTOL	114
70.9.7	SÄNGER	115
70.9.8	X-38	115
70.10	Wing leading edges (WLE).....	116
70.10.1	General.....	116
70.10.2	Shuttle orbiter	116
70.10.3	Buran	116
70.10.4	Hermes	118
70.10.5	HOPE	119
70.10.6	Others.....	119
70.11	Box sections	120
70.11.1	NASP	120
70.11.2	Hermes	120
70.12	Cryogenic tanks.....	121
70.13	Heat shield designs	121
70.14	Air inlet-intakes	124
70.15	Earth re-entry capsules	125
70.16	Manned re-entry vehicles	127
70.17	Deep space missions	128
70.17.1	CNSR ROSETTA: Earth return capsule	128
70.18	Mars landers.....	129
70.18.1	General.....	129
70.18.2	NASA Pathfinder/MESUR network landers	129
70.18.3	MARSNET	130
70.19	Cassini-Huygens	130
70.19.1	General.....	130
70.19.2	C-C aerobrake (heat shield)	130

70.19.3 Nose cap front shield with AQ60	131
70.20 Planetary probes	131
70.21 Aerobrake designs	131
70.21.1 General.....	131
70.21.2 NASA/ESA Cassini-Huygens mission	131
70.22 PRORA: USV – unmanned space vehicle	133
70.22.1 Background	133
70.22.2 USV programme.....	135
70.22.3 USV systems and flight test beds.....	136
70.22.4 External configuration of FTB_1 and FTB_2	137
70.22.5 External configuration of FTB_3	138
70.23 X-38 Body flap	140
70.23.1 Background	140
70.23.2 Body flaps.....	142
70.23.3 Mechanical fasteners.....	143
70.23.4 CMC to metal attachment.....	144
70.23.5 Ceramic bearings	145
70.23.6 Ceramic seals.....	146
70.24 X-38 Nose cap.....	147
70.24.1 Background	147
70.24.2 Concept	148
70.24.3 Thermal profiles.....	148
70.24.4 Flexible insulation design	149
70.24.5 Integration and qualification testing	150
70.24.6 Summary	152
70.25 Aerobrake: Deployable CMC decelerator.....	153
70.25.1 Background	153
70.25.2 Mars ISRU mission ‘in-situ resource unit’	154
70.25.3 Mars ISRU mission – Concept	154
70.25.4 Mars ISRU mission – Environmental aspects	157
70.26 References	158
70.26.1 General.....	158
71 Thermal protection systems.....	163
71.1 Introduction.....	163
71.1.1 Application.....	163
71.1.2 European development programmes	164
71.1.3 Concepts	165

71.1.4	Non load-carrying TPS	167
71.1.5	Load-carrying TPS.....	168
71.1.6	Reusable structures.....	168
71.2	Cooling modes	169
71.2.1	General.....	169
71.2.2	Passive TPS.....	170
71.2.3	Active cooling concepts.....	170
71.3	Early re-entry capsules.....	171
71.4	Ablative designs	173
71.4.1	General.....	173
71.4.2	Programmes	174
71.4.3	Materials	174
71.5	Space Shuttle orbiter.....	177
71.5.1	General.....	177
71.5.2	Materials and configurations.....	178
71.5.3	In-Service TPS Performance.....	182
71.6	Buran.....	182
71.6.1	General.....	182
71.6.2	Materials and configurations.....	184
71.7	Advanced carbon reinforced composites	184
71.7.1	Carbon-carbon composites	184
71.7.2	ACC - Advanced carbon-carbon.....	184
71.7.3	Aerospatiale - Aerotiss® 2.5D	185
71.7.4	Carbon-silicon carbide composites.....	186
71.8	Durable metallic TPS.....	188
71.8.1	General.....	188
71.8.2	Multiwall TPS.....	189
71.8.3	Developments.....	190
71.9	Titanium-based composites	192
71.9.1	NASP	192
71.10	Internal multiscreen insulation (IMI)	192
71.10.1	Concept	192
71.10.2	Development and characterisation.....	195
71.10.3	Potential applications.....	198
71.11	Flexible external insulation (FEI)	198
71.11.1	General.....	198
71.11.2	Design concept.....	198

71.11.3 Key features	199
71.11.4 Product range	200
71.11.5 Hermes	200
71.11.6 MSTP programme	201
71.11.7 ARD programme.....	204
71.11.8 Future reusable vehicles	205
71.11.9 Verified performance	205
71.11.10 IFI - Internal flexible insulation development	206
71.12CMC shingles	208
71.12.1 Hermes design concept.....	208
71.12.2 TETRA/X-38 programme panels	210
71.12.3 SPFI - Surface protected flexible insulation.....	212
71.13Heat pipes	223
71.13.1 General.....	223
71.13.2 Shuttle-type heat pipe cooled wing leading edge	225
71.13.3 Sodium-Hastelloy-X heat pipe for advanced space transportation system	225
71.13.4 Refractory metal-CMC heat pipe for NASP	226
71.14Cooled panels	227
71.14.1 General.....	227
71.14.2 Demonstrator units	228
71.14.3 Active cooling on NASP.....	229
71.15Beryllium TPS.....	231
71.15.1 General.....	231
71.15.2 Cassini-Huygens heat shield: Phase A configuration.....	231
71.16Aerobrakes	233
71.17Heat shields.....	233
71.17.1 General.....	233
71.17.2 SEPCORE® TPS concept.....	233
71.17.3 Ceramic heatshield assembly (CHA).....	234
71.17.4 MIRKA - Micro re-entry capsule	242
71.17.5 ALSCAP - Alternative low-cost, short-manufacturing-cycle ceramic assessment programme	244
71.18Aeroshell	247
71.18.1 General.....	247
71.18.2 Semi-integrated aeroshell TPS (S.I.A.T)	247
71.18.3 Demonstrator aeroshell design.....	247
71.19Cryogenic tanks.....	254

71.19.1 General.....	254
71.19.2 European programmes.....	254
71.19.3 Concepts: TPS panel array	255
71.19.4 Concepts: LH tank cryogenic insulation	256
71.20 TPS mass budgets	258
71.20.1 Allocation.....	258
71.20.2 Examples.....	258
71.21 TPS verification	259
71.22 Polymer foam cryogenic insulation.....	259
71.22.1 General.....	259
71.22.2 Polymer foam characteristics	259
71.22.3 Properties	260
71.22.4 Materials.....	261
71.22.5 Ranking of polymer foam cryogenic insulation	263
71.22.6 Further work	265
71.23 High temperature insulation (HTI)	265
71.23.1 Background	265
71.23.2 Development factors.....	266
71.23.3 Development approach	267
71.23.4 Materials.....	270
71.23.5 Testing.....	270
71.23.6 Summary	274
71.24 References	274
72 SPF/DB titanium designs	284
72.1 Introduction.....	284
72.1.1 General.....	284
72.1.2 Aircraft components.....	284
72.1.3 Space applications	284
72.2 Basic SPF/DB process	285
72.2.1 Superplastic forming.....	285
72.2.2 Diffusion bonding.....	285
72.3 Process attributes.....	287
72.4 Titanium alloys	288
72.5 Aluminium alloys	289
72.6 Access doors and ducting	290
72.6.1 General.....	290
72.6.2 Slat track/jack cans.....	290

72.6.3	Underwing access doors	291
72.6.4	Other SPF/DB components	292
72.7	Spars and stiffened panels	293
72.8	Struts and cylinders	293
72.9	Leading edges and lateral fins	293
72.10	Firewalls	294
72.11	Pressure vessels	294
72.12	Cost aspects	295
72.13	European facilities	295
72.14	References	295
72.14.1	General	295
73	Propulsion technologies	297
73.1	Introduction	297
73.2	Propulsion unit requirements	297
73.2.1	Launcher engines	297
73.2.2	Shuttle engines	297
73.2.3	Spaceplane engines	298
73.2.4	Thrusters	298
73.2.5	Nozzles	298
73.3	Fuels	298
73.3.1	General	298
73.3.2	Solid propellants	298
73.3.3	LH/LOX	299
73.3.4	Monopropellants	299
73.3.5	Bipropellants	299
73.4	Ariane 5	299
73.4.1	General	299
73.4.2	MPS solid rocket motor	299
73.5	Vulcain engine	300
73.5.1	General	300
73.5.2	Specification	301
73.5.3	Materials	301
73.6	HM 7 engine	302
73.6.1	General	302
73.6.2	Nozzle geometry	303
73.7	Mage 2 motor	303
73.8	Nozzles	303

73.9 Space Shuttle Main Engine (SSME)	304
73.10 Air breathing engines	304
73.10.1 General.....	304
73.10.2 NASP nozzle development.....	305
73.10.3 European ramjet technology.....	305
73.11 CMC rocket stator	305
73.12 Metal thrusters.....	307
73.13 CMC thrusters	307
73.14 References	307
73.14.1 General.....	307
74 Protective coatings	310
74.1 Introduction.....	310
74.2 Coating functions.....	311
74.2.1 General.....	311
74.2.2 Application requirements	312
74.3 Passivation	312
74.3.1 General.....	312
74.3.2 Materials	313
74.3.3 Coating adhesion.....	313
74.4 Basic coating types	314
74.4.1 General.....	314
74.4.2 Diffusion coatings	314
74.4.3 Overlay coatings.....	314
74.5 Coating processes.....	315
74.5.1 General.....	315
74.5.2 Slurry coating.....	315
74.5.3 Physical vapour deposition (PVD)	315
74.5.4 Enhanced physical vapour deposition (PVD)	316
74.5.5 Thermal spraying.....	316
74.5.6 Chemical vapour deposition (CVD)	317
74.5.7 Enhanced chemical vapour deposition (CVD).....	317
74.5.8 Other processes	317
74.6 Coatings: Titanium components.....	318
74.6.1 NASP	318
74.7 Coatings: Superalloy components.....	318
74.7.1 General.....	318
74.7.2 Aluminide diffusion coatings	319

74.7.3	MCrAlY overlay coatings	319
74.8	Thermal barrier coatings (TBC)	320
74.8.1	Ni-based superalloy components	320
74.8.2	Shuttle Main Engine HPFTP blades	320
74.8.3	Fibre-reinforced TBC's	321
74.8.4	Coating technology	321
74.8.5	Seals.....	321
74.9	Carbon-Carbon: Oxidation protection.....	321
74.9.1	General.....	321
74.9.2	Applications	321
74.9.3	Coating systems	321
74.9.4	Basic problem.....	322
74.10	Multiplex coatings.....	322
74.10.1	General.....	322
74.10.2	Constituents.....	323
74.10.3	Application examples.....	324
74.11	Coatings: C-SiC and SiC-SiC	325
74.11.1	General.....	325
74.11.2	C-SiC	325
74.11.3	SiC-SiC.....	325
74.12	Carbon-Carbon: Surface coatings	326
74.12.1	Dimensionally stable structures.....	326
74.13	References	330
74.13.1	General.....	330
75 Seal technology	334	
75.1	Introduction.....	334
75.1.1	Uses	334
75.1.2	Structural assemblies	334
75.1.3	Dynamic seals	335
75.1.4	Materials	335
75.2	Structural seals.....	335
75.3	Seal materials.....	336
75.3.1	General.....	336
75.3.2	Elastomers.....	336
75.3.3	Types of elastomers	339
75.3.4	Viscoelasticity.....	343
75.3.5	Physical properties	344

75.3.6	Chemical properties.....	351
75.3.7	Rubber-to-metal bonding.....	354
75.3.8	Engineering design with elastomers.....	355
75.3.9	Finite element analysis.....	358
75.3.10	Applications	360
75.3.11	Thermoplastic elastomers	361
75.4	Energised metal seals	361
75.4.1	General.....	361
75.4.2	Materials.....	362
75.5	NASP engine developments	363
75.5.1	General.....	363
75.5.2	Developments.....	363
75.6	Fibrous seals	364
75.7	Elastomeric seals	365
75.7.1	Materials	365
75.7.2	Design aspects.....	365
75.7.3	Causes of leakage.....	366
75.7.4	Aerospace applications	367
75.8	References	368
75.8.1	General.....	368
75.8.2	ECSS standards	369
75.8.3	ASTM standards.....	370
75.8.4	ISO standards.....	370
76	Integrity control of high temperature structures	371
76.1	Introduction.....	371
76.2	Materials.....	371
76.2.1	Integrity control.....	371
76.2.2	Fracture control	372
76.3	Failure characteristics	372
76.3.1	Advanced alloy systems	372
76.3.2	Composite materials.....	372
76.4	High temperature.....	373
76.5	Coatings	373
76.5.1	General.....	373
76.5.2	Manufacturing.....	373
76.5.3	Inspection	373
76.6	Considerations	374

76.6.1	Mass optimisation.....	374
76.6.2	Approach	374
76.7	Case study: Developments in integrity control	375
76.8	Case study: Phase 1 - Material characterisation.....	377
76.8.1	General.....	377
76.8.2	Materials, manufacturing and NDT.....	377
76.8.3	Defect detection by selected NDI methods	378
76.8.4	Maximum applied stresses	379
76.8.5	High-temperature tests	380
76.8.6	Residual strengths.....	381
76.8.7	Analysis	381
76.8.8	Conclusions.....	381
76.9	Case study: Phase 2 - Structural sub-component behaviour	382
76.10	References	382
76.10.1	General.....	382
77	Defect types	383
77.1	Introduction.....	383
77.2	Advanced metal alloys	384
77.2.1	General.....	384
77.2.2	ODS alloys.....	384
77.2.3	SPF alloys	384
77.3	Metal matrix composites.....	384
77.3.1	General.....	384
77.3.2	Standard product forms	384
77.3.3	Near-net shape manufacture	385
77.4	Ceramic matrix composites	386
77.5	Coatings	386
77.6	Joints	387
77.6.1	General.....	387
77.6.2	Uses	387
77.6.3	Mechanical fastened joints	388
77.6.4	Fusion joints	388
77.7	Structural parts	389
77.7.1	General.....	389
77.7.2	Composite materials.....	389
77.8	In service	389
77.9	References	391

77.9.1	General.....	391
78 Damage tolerance.....		392
78.1	Introduction.....	392
78.1.1	Materials.....	392
78.1.2	Structure.....	392
78.1.3	Fracture mechanics.....	392
78.1.4	Initial material quality (IMQ).....	392
78.2	MMC: Particulate and whisker reinforced.....	393
78.2.1	Fatigue behaviour.....	393
78.2.2	Fracture mechanics.....	394
78.3	CMC: Whisker reinforced	395
78.4	MMC: Continuous fibre reinforced.....	395
78.4.1	Fatigue.....	395
78.5	CMC: Continuous fibre reinforced	397
78.5.1	Failure characteristics.....	397
78.6	Coatings	398
78.6.1	Coating performance	398
78.6.2	Process and material selection.....	399
78.6.3	Failure characteristics.....	399
78.7	References	400
78.7.1	General.....	400
78.7.2	ECSS standards	400
79 Fracture control		401
79.1	Introduction.....	401
79.1.1	Application.....	401
79.2	References	401
79.2.1	General.....	401
79.2.2	ECSS standards	401
80 NDT techniques		402
80.1	Introduction.....	402
80.2	Advanced metal alloys	403
80.2.1	General.....	403
80.2.2	Brittle materials.....	403
80.2.3	Multi-phase microstructures	403
80.3	Metal matrix composites.....	403
80.4	Carbon-Carbon and ceramic matrix composites	404

80.5 Coatings	407
80.6 Joints	407
80.6.1 General.....	407
80.6.2 Fused joints	407
80.6.3 Mechanically fastened and interlock joints	408
80.7 Fusion joints	408
80.7.1 General.....	408
80.7.2 Thin-walled seam welded tubes	409
80.7.3 Diffusion bonded joints	409
80.8 References	409
80.8.1 General.....	409
81 High-temperature testing	412
81.1 Introduction.....	412
81.2 Purpose of testing	412
81.3 Material behaviour.....	413
81.3.1 Basic fracture modes.....	413
81.3.2 Metal matrix composites.....	413
81.3.3 Inorganic and ceramic matrix composites	413
81.4 Degradation mechanisms.....	414
81.4.1 Materials	414
81.4.2 Degradation rate.....	414
81.5 Coupon testing	415
81.5.1 General.....	415
81.5.2 Single-fibre tests.....	415
81.5.3 Fibre push through	415
81.5.4 Net-shape components	415
81.5.5 Flexural and ILSS testing	415
81.5.6 Small coupon tests	416
81.5.7 Machining	416
81.5.8 Extensometry.....	416
81.5.9 End tabs	417
81.5.10 Coatings	417
81.5.11 Material gradation.....	417
81.5.12 Specimen alignment.....	418
81.5.13 Linear elasticity.....	418
81.6 Mechanical properties	418
81.6.1 General.....	418

81.6.2 Tensile	419
81.6.3 Compression	420
81.6.4 Shear	420
81.6.5 Open-hole tension	421
81.6.6 Fatigue.....	421
81.7 Fracture toughness	421
81.8 Physical properties	422
81.8.1 General.....	422
81.8.2 Standards	422
81.9 Status of test standards.....	422
81.9.1 General.....	422
81.9.2 Metal matrix composites	423
81.9.3 Ceramic matrix composites	423
81.10 Demonstrator testing	427
81.11 References	428
81.11.1 General.....	428

Figures

Figure 64.4-1 - Representative stress-strain curve: Particulate reinforced MMC.....	34
Figure 64.4-2 - Representative stress-strain curves: Monofilament reinforced MMC	35
Figure 64.4-3 - Representative stress-strain curves: Bidirectional SiC-SiC composite.....	36
Figure 64.5-1 – Failure criteria: Comparison between predicted failure curves for	38
Figure 64.5-2 – Failure criteria: ‘Hour-glass’ test specimen for C-C/SiC composites	39
Figure 65.2-1 - Relative stress-strain behaviours of optimised (good) and non- optimised (poor) MMCp composites	44
Figure 65.3-1 - Features of particles in MMCp materials	47
Figure 65.3-2 - Possible crack propagation paths in MMCp materials.....	48
Figure 67.2-1 - Glass matrix composite material: Microcracking sequence	62
Figure 67.2-2 - Bidirectional glass-ceramic matrix composite: Schematic of tunnelling cracks in 90° layers.....	63
Figure 67.3-1 - Schematic representations of load-displacement (P/u) curves: (a) Linear elastic behaviour	65
Figure 67.3-2 - Schematic representations of load-displacement (P/u) curves: (b) Linear non-elastic behaviour.....	65
Figure 67.3-3 - Schematic representations of load-displacement (P/u) curves: (c) Non-linear elastic behaviour	66
Figure 67.3-4 - Schematic representations of load-displacement (P/u) curves: (d) Non-linear non-elastic behaviour	66
Figure 67.3-5 - CMC materials: Possible fracture mechanisms	67

Figure 67.3-6 - SENB and delamination test specimens.....	69
Figure 67.3-7 - Fracture energy (J , Rice) as a function of crack increment: Short random fibre materials	70
Figure 67.3-8 - Fracture energy (J , Rice) as a function of crack increment: Multidirectional materials	70
Figure 70.4-1 - HOPE: Distribution of surface temperatures.....	101
Figure 70.4-2 - HOPE: Distribution of TPS.....	102
Figure 70.4-3 - HOPE structural materials to be applied.....	103
Figure 70.4-4 - OREX structure and TPS.....	104
Figure 70.4-5 - HYFLEX: Structural Configuration	104
Figure 70.5-1 - HOTOL: Configuration 'g'.....	105
Figure 70.5-2 - HOTOL: Rear Fuselage and Aft LOX Tank	107
Figure 70.6-1 - SÄNGER: Surface temperatures at Mach 6.8	108
Figure 70.7-1 - NASP: Basic configuration.....	109
Figure 70.9-1 - Shuttle: Nose cap system components	111
Figure 70.9-2 - Shuttle: RCC chin panel system components	112
Figure 70.9-3 - Hermes: C-C INOX® nose cone (0.6 scale)	113
Figure 70.9-4 - HOPE: Heat resistant structural configuration	114
Figure 70.9-5 - HOTOL: Nose cone and nose shell	115
Figure 70.10-1 - Shuttle orbiter: Wing leading edge system components.....	116
Figure 70.10-2 - Buran: Wing leading edge construction	117
Figure 70.10-3 - Buran: Temperature of wing leading edge with time	118
Figure 70.10-4 - Hermes: Hot structure leading edge	119
Figure 70.11-1 - Hermes: C-SiC box for thermal structure.....	120
Figure 70.13-1 - Double wall heat shield.....	122
Figure 70.13-2 - Heat shield and stringer stiffened panels.....	123
Figure 70.13-3 - MARSNET: Heat shield for planetary entry probe	124
Figure 70.14-1 - Air intake ramp in C-SiC	125
Figure 70.15-1 - COMET recovery system.....	126
Figure 70.15-2 - MIRKA capsule: Exploded view of spherical heat shield	127
Figure 70.16-1 - ACRV flight vehicle: General layout.....	128
Figure 70.17-1 - CNRS ROSETTA: Aerocapsule configuration	129
Figure 70.19-1 - Huygens: C-C decelerator design.....	130
Figure 70.19-2 - Huygens: Nose cap front shield.....	131
Figure 70.21-1 - Cassini-Huygens: Stretched carbon skin decelerator.....	132
Figure 70.21-2 - Cassini-Huygens: Separation sequence.....	133
Figure 70.22-1 - PRORA – USV: FTB_2 external configuration	138
Figure 70.22-2 – VEGA launcher: Large fairing	139

Figure 70.22-3 - PRORA – USV: FTB_3 external configuration	140
Figure 70.23-1 – X-38: Test vehicle	141
Figure 70.23-2 – X-38 body flap: Construction.....	142
Figure 70.23-3 – X-38 body flap: Mechanical fasteners.....	143
Figure 70.23-4 – X-38 body flap: CMC to metal attachment.....	145
Figure 70.23-5 – X-38 body flap: Ceramic bearing	146
Figure 70.23-6 – X-38 body flap: Ceramic dynamic seal	147
Figure 70.24-1 – X-38 Nose assembly	148
Figure 70.24-2 - X-38 Nose assembly: Thermal profiles.....	149
Figure 70.24-3 – X-38 Nose assembly: Flexible insulation distribution.....	150
Figure 70.24-4 – X-38 Nose assembly: Flexible insulation assembly	151
Figure 70.24-5 – X-38 Nose cap with insulation mounted on vehicle nose structure.....	153
Figure 70.25-1 – Deployable CMC hot structures - Mars ISRU mission	156
Figure 71.2-1 - TPS concepts	169
Figure 71.2-2 - Principal passive thermal control architectures	170
Figure 71.3-1 - Galileo entry probe	172
Figure 71.4-1 - Ablatives: Basic decomposition mechanisms	173
Figure 71.4-2 - CARINA: General layout.....	175
Figure 71.5-1 - Orbiter: Design surface temperatures (°C) in ascent and re-entry trajectories	177
Figure 71.5-2 - Orbiter: TPS - Thermal protection systems	178
Figure 71.5-3 - Orbiter: RSI system configuration.....	181
Figure 71.6-1 - BURAN: External thermal protection	183
Figure 71.7-1 - TPS: ACC multi-post stand-off concept	185
Figure 71.8-1 - TPS: Multiwall panel scheme.....	189
Figure 71.10-1 - TPS: IMI design concept.....	194
Figure 71.11-1 - TPS: Schematic of FEI blanket.....	198
Figure 71.11-2 - TPS: IFI internal flexible insulation blanket.....	207
Figure 71.11-3 - TPS: IFI blanket configuration in X-38 nose cap	208
Figure 71.12-1 - TPS: Hermes CMC shingle support cross-section	209
Figure 71.12-2 – SPFI surface protected flexible insulation panel	213
Figure 71.12-3 – SPFI Surface protected flexible insulation: Design	214
Figure 71.12-4 – SPFI: Summary of thermal performance	216
Figure 71.12-5 – SPFI: Thermal performance during vehicle re-entry and landing	217
Figure 71.12-6 – SPFI: Structural performance - Shaker test	219
Figure 71.12-7 – SPFI: Structural performance – spectral distribution and OASPL	220
Figure 71.12-8 – SPFI: SHEFEX TPS demonstrator	223

Figure 71.13-1 - Heat pipe: Operation principle for leading edge cooling	224
Figure 71.13-2 - Heat pipe: Wing leading edge design for advanced space transportation system	226
Figure 71.13-3 - Heat pipe: NASP wing leading edge.....	227
Figure 71.14-1 - Convective cooling systems	228
Figure 71.14-2 - Cooled structure: Design concepts.....	229
Figure 71.14-3 - NASP: SiC-Ti-Titanium aluminide D-groove panel	230
Figure 71.15-1 - Cassini-Huygens: Exploded view	232
Figure 71.15-2 - Cassini-Huygens: Beryllium TPS design solution.....	232
Figure 71.17-1 - CHA - Ceramic heatshield assembly	236
Figure 71.17-2 – CHA: Insulation and bolt assembly	237
Figure 71.17-3 – CHA-element: Temperature profiles during full mission testing.....	241
Figure 71.17-4 – MIRKA/FOTON: Configuration.....	243
Figure 71.18-1 – Aeroshell: Design concept	247
Figure 71.18-2 – Aeroshell: SIAT test model assembled cross-section.....	248
Figure 71.18-3 – Aeroshell: Down-scaled demonstrator design features	249
Figure 71.19-1 – TPS panel array concept: Cryogenic tanks.....	256
Figure 71.19-2 – Cryogenic insulation: LH tank concepts	257
Figure 71.23-1 - TPS: Flow diagram of HTI development testing for X-38 nose cap assembly.....	269
Figure 71.23-2 - TPS: HTI temperature gradient test set-up, parameters and sample configuration	273
Figure 72.2-1 - SPF/DB: Two sheet configuration.....	285
Figure 72.2-2 - SPF/DB: Three sheet configuration	286
Figure 72.2-3 - SPF/DB: Four sheet configuration	287
Figure 72.4-1 - Superplastic forming: Strain rate sensitivity in formability trials on Ti alloy IMI 834	289
Figure 72.6-1 - SPF/DB titanium alloy: Slat track and jack for Airbus A310.....	291
Figure 72.6-2 - SPF/DB Ti: A310 underwing access door locations	292
Figure 72.9-1 - SPF/DB: Principle of four-sheet technique for leading edge	294
Figure 73.5-1 - Vulcain engine: Schematic diagram	300
Figure 73.6-1 - Ariane 4 HM 7 engine: Thrust chamber	302
Figure 73.10-1 - NASP: Modified government baseline engine configuration.....	305
Figure 73.11-1 - Rocket stator CMC components	306
Figure 74.3-1 - Coatings: Properties of coating, substrate and interface	313
Figure 74.10-1 - Multiplex coatings: Basic configuration.....	323
Figure 74.10-2 - C-C multiplex coatings: Crack and sealing mechanisms	324
Figure 74.12-1 – Coatings: Dimensionally stable carbon-carbon – concept	327

Figure 74.12-2 – Coatings: Dimensionally stable carbon-carbon – Potential materials	328
Figure 74.12-3 – Coatings: Dimensionally stable carbon-carbon – Manufacturing method.....	330
Figure 75.3-1 – Elastomers: Schematic of crosslinked rubber molecular network.....	337
Figure 75.3-2 – Elastomers: Typical tensile strength at 23°	340
Figure 75.3-3 – Elastomers: Typical tensile strength at 100°C	341
Figure 75.3-4 – Elastomers: Viscoelasticity – hysteresis effect	344
Figure 75.3-5 – Elastomers: Creep of a weighted rubber strip.....	350
Figure 75.3-6 – Elastomers: Creep of a weighted rubber strip (logarithmic time)	350
Figure 75.3-7 – Elastomers: Effect of sample thickness on oxidation rate at 110°C.....	351
Figure 75.3-8 – Elastomers: Arrhenius plot example	354
Figure 75.3-9 – Elastomers: Simple rubber block in shear	355
Figure 75.3-10 – Elastomers: Increasing compression stiffness by lamination.....	357
Figure 75.3-11 – Elastomers: Elastomeric torsion disc	358
Figure 75.4-1 - Metal seals: 'C' profile and serpentine	362
Figure 75.5-1 - NASP: Ceramic wafer seal	363
Figure 75.5-2 - NASP: Braided rope seal.....	364
Figure 76.7-1 - Integrity control for high-temperature applications: Study logic	376
Figure 76.7-2 - Integrity control for high temperature applications: Approach	376
Figure 78.2-1 - Whisker and particle reinforced MMC: Fatigue response	394
Figure 78.4-1 - MMC potential failure mechanisms under cyclic loading	395
Figure 78.4-2 - Failure modes of MMC	396
Figure 78.4-3 - MMC: Fatigue response showing matrix failure.....	397
Figure 81.5-1 - Coupon testing: Scanning laser extensometry system.....	417
Figure 81.6-1 - CMC high temperature tensile testing: CEN recommended sample types	420

Tables

Table 64.3-1 - Modulus mismatch in composites: Examples	31
Table 64.3-2 - CTE mismatch in composites: Examples.....	32
Table 65.1-1 - Particulate reinforced MMCs.....	41
Table 66.1-1 - Fibre reinforced MMC	53
Table 66.3-1 - Ti/SiC MMC: Calculated stresses	56
Table 67.1-1 - Inorganic/ceramic matrix composites.....	59
Table 69.9-1 – Summary of high temperature materials technologies: Flight-vehicle dependent.....	90
Table 69.9-2 – Summary of high temperature materials technologies: Non-flight vehicle dependent.....	93

Table 69.9-3 – Summary of high temperature materials technologies: European expertise	95
Table 70.23-1 – X-38 body flap: Mechanical fasteners – properties	144
Table 71.1-1 - TPS: Summary of candidate characteristics	166
Table 71.1-2 - TPS and Thermo-structural designs: Material classes	167
Table 71.3-1 – Early re-entry capsules: TPS mass fractions	171
Table 71.4-1 – Ablative TPS: ALS051 properties.....	176
Table 71.5-1 - Orbiter: TPS material temperature limits.....	179
Table 71.5-2 - TPS: RSI Typical Properties	180
Table 71.7-1 – Aerotiss® 2.5D coated carbon-carbon: Properties.....	186
Table 71.7-2 – CMC carbon-silicon carbide: Various TPS programmes and applications.....	187
Table 71.7-3 – CMC TPS: MAN carbon-silicon carbide - Properties	188
Table 71.10-1 - TPS: IMI material candidates for different applications.....	194
Table 71.10-2 – TPS: Summary - IMI characterisation test results	197
Table 71.11-1 - TPS: Mechanical loads and sources on FEI components	199
Table 71.11-2 – FEI-TPS product range	200
Table 71.11-3 – TPS: FEI nominal flutter test envelopes.....	204
Table 71.11-4 – FEI-TPS: Summary of verified performances	206
Table 71.12-1 – Hermes TPS REI-shingle mass breakdown.....	210
Table 71.12-2 – TETRA/X-38 TPS: C-SiC panel qualification test matrix.....	211
Table 71.12-3 - TETRA/X-38 TPS: Shingle qualification test matrix	212
Table 71.12-4 - SPF1: Thermal property evaluation	221
Table 71.17-1 – CHA: Subcomponents mass breakdown	238
Table 71.17-2 - SEPCARB-INOX 272-01: Properties	239
Table 71.17-3 – CHA: Functional test matrix	240
Table 71.17-4 – ALSCAP: Thermo-physical data for C/SiC.....	246
Table 71.18-1 - Aeroshell demonstrator: Predicted and actual temperatures	250
Table 71.19-1 – Cryogenic insulation: Technical considerations for LH tank concepts	257
Table 71.22-1 - Cryogenic insulation: Polymer foam candidate materials	261
Table 71.22-2 - Cryogenic insulation: Polymer foam mechanical properties	263
Table 71.22-3 – Cryogenic insulation: Ranking criteria and values	264
Table 71.23-1 - TPS: HTI development tests for X-38 nose cap assembly	268
Table 71.23-2 - TPS: HTI candidate materials	270
Table 71.23-3 - TPS: HTI thermal stability test results.....	271
Table 72.4-1 - Titanium alloys: Superplastic characteristics	288
Table 75.3-1 – Elastomers: Typical glass transition temperatures.....	338
Table 75.3-2 – Elastomers: Summary of common materials and characteristics	340

Table 76.6-1 - Integrity control parameters for new materials	375
Table 77.3-1 - MMC: Typical material defects.....	385
Table 77.4-1 - CMC: Typical material defects	386
Table 77.5-1 - Coating materials: Typical defects	387
Table 77.6-1 - Fusion joints: Example of techniques and use.....	388
Table 77.6-2 - Fused joints: Defects	388
Table 77.7-1 - Defects in composite materials after further processing	389
Table 77.8-1 - Typical in-service defects.....	390
Table 78.2-1 - MMC: Effect of particle size on fatigue and fracture toughness.....	394
Table 78.6-1 - Coatings: Damage tolerance aspects	398
Table 80.3-1 - NDI techniques for MMCs.....	404
Table 80.4-1 - NDI techniques for defect detection and measurement of C-C and CMC materials	405
Table 80.4-2 - Technical and economical aspects of NDI techniques	406
Table 80.5-1 - Coatings: Inspection techniques	407
Table 80.7-1 - Fused joints: Inspection techniques.....	408
Table 80.7-2 - Standards for inspection of welded tubes	409
Table 81.9-1 - Test methods: CEN standards for advanced technical ceramic composites.....	425
Table 81.9-2 - Test methods: CEN standards for advanced technical ceramics - monolithic.....	426
Table 81.9-3 - Test methods: CEN standards for advanced technical ceramics - coatings	427
Table 81.9-4 - Test methods: CEN standards for advanced technical ceramics – others	427

Introduction

The Structural materials handbook, ECSS-E-HB-32-20, is published in 8 Parts.

A glossary of terms, definitions and abbreviated terms for these handbooks is contained in Part 8.

The parts are as follows:

Part 1	Overview and material properties and applications	Clauses 1 - 9
Part 2	Design calculation methods and general design aspects	Clauses 10 - 22
Part 3	Load transfer and design of joints and design of structures	Clauses 23 - 32
Part 4	Integrity control, verification guidelines and manufacturing	Clauses 33 - 45
Part 5	New advanced materials, advanced metallic materials, general design aspects and load transfer and design of joints	Clauses 46 - 63
Part 6	Fracture and material modelling, case studies and design and integrity control and inspection	Clauses 64 - 81
Part 7	Thermal and environmental integrity, manufacturing aspects, in-orbit and health monitoring, soft materials, hybrid materials and nanotechnologies	Clauses 82 - 107
Part 8	Glossary	

64

Behaviour of advanced composites

64.1 Introduction

The fracture behaviour of metallic and ceramic matrix composites is more complex than that of unreinforced alloys or monolithic ceramics. The fracture characteristics of the more isotropic variants are now well understood and predictive models are widely accepted, e.g. Linear Elastic Fracture Mechanics (LEFM), [See also: ECSS-E-32-01 – Fracture control].

For newer composite materials, attempts have been made to describe and predict their behaviour by extending the models for their more isotropic counterparts. Success has been limited by the anisotropy of the composites, especially for those with continuous fibres. In reality, anisotropic metallic and ceramic composites need to be considered as new classes of materials. Some CMC materials, destined for use in TPS on reusable vehicles, have been investigated for appropriate selection and use of failure criteria, [See: 64.5].

Metal matrix composites are particularly difficult as they show elastic-plastic deformation characteristics, where the degree of plastic deformation is influenced by many factors.

Ceramic composites are elastic in behaviour, although accumulated matrix microcracking gives non-linear deformation characteristics. These composites are desirable because of their high temperature operating capabilities.

This chapter covers three discrete groups of composites:

- Particulate reinforced metals (MMC_p).
- Fibre reinforced metals (MMC_f).
- Inorganic ceramic matrix composites (ICMC_f).

Whisker reinforced metals or ceramics are not explicitly covered because they are primarily of non-European origin and in some European countries whiskers are thought to present health hazards.

The different fracture behaviours of each are described. In particular, the interrelation between residual stresses and thermo-mechanical fatigue effects is highlighted. As materials are pushed towards their physical and chemical limits, the shorter the period that they can sustain the combined effects of thermal cycling, mechanical and thermal stresses and oxidation.

64.2 Summary of material behaviour

64.2.1 Metal matrix composites

64.2.1.1 Particulate reinforced (MMCp)

This group consists mainly of aluminium matrix composites. The levels of particulate addition are normally in the range of 10 vol.% to 20 vol.% in order to retain the ‘metallic characteristics’ of ductility, fracture toughness and formability.

Features include:

- 10 vol.% to 20 vol.% particulate reinforcement
- Basically isotropic in macro composition and can be compared with conventional alloys, e.g. LEFM
- Initially elastic materials at low strains, then elastic-plastic to plastic, with limited ductility (4% to 8% maximum).
- Failure determined by particulate-to-matrix adhesion and matrix microstructure plus heat treatment.
- High particulate contents (>20%) show very poor fracture toughness

64.2.1.2 Fibre reinforced (MMCf)

Composites are mainly based on aluminium and titanium, although copper, nickel (superalloy) and magnesium variants have some space applications.

The fracture behaviour of continuous fibre MMCf materials is very different to those of MMCp and conventional alloys. They are highly anisotropic, with very low failure strains. In this respect they are more closely aligned to CFRP materials, but the matrix does display elastic-plastic characteristics as opposed to elastic. High processing temperatures result in high residual stresses within the composite.

Features include:

- 35 vol.% to 50 vol.% fibre reinforcement.
- No direct comparison with the fracture behaviour of conventional alloys can be made.
- Highly anisotropic, low strain to failure materials.
- Fully elastic to very low strains, then complex elastic-plastic behaviour.
- Failure characteristics closer to CFRP than alloys.
- Properties determined by in-situ fibre strength and modest transverse strengths between fibre and matrix.
- Both matrix microstructure and heat treatment are important.
- The presence of reinforcement can change the microstructure of the matrix and alter the matrix yield strength.
- Fibre to matrix adhesion is very important.

64.2.2 Inorganic ceramic matrix composites

64.2.2.1 Fibre reinforced (ICMCf)

The group of materials includes:

- GMC,
- GCMC,
- CMC and
- C-C.

These materials do not display the classic brittle, low strain-to-failure and catastrophic fracture behaviour of monolithic ceramics. Instead they rely on multiple crack stoppers at the fibre-matrix interfaces to avoid catastrophic failure. Such materials can function with high levels of microcracking in thermo-structural roles, i.e. where thermal shock resistance and modest strengths are required.

Features include:

- 30 vol.% to 50 vol.% fibre reinforcement.
- No direct comparison with monolithic ceramics can be made.
- Highly anisotropic with modest strength characteristics.
- Possess high temperature, insulative, thermal shock and thermo-cyclic capabilities.
- Benign fracture characteristics exhibited despite low overall strain to failure.
- Fibre to matrix interface is very important as poor bonding is essential and provides a de-coupling mechanism.

[See also: [64.4](#); [64.5](#)]

64.3 Significant behavioural characteristics

64.3.1 General

In order to understand the behaviour of metal and ceramic composites, the significance of some of their basic characteristics has to be considered.

64.3.2 Modulus mismatch

In most composites, the matrix and reinforcement (particulate or fibre) have different moduli (E). [Table 64.3.1](#) shows some representative examples.

When external load is applied, the stresses sustained by the matrix and reinforcement respectively are determined by the ratio of their moduli and their respective volume fractions.

The stress-strain response of composites is dependent on the combined contributions of the matrix and reinforcement. The ‘Law of Mixtures’ applies to the initial modulus of the composite provided that all the constituents behave elastically.

With MMC and CMC materials, true linear elasticity exists only at very low strain levels. As the strain increases, one or more effects can occur:

- Plastic deformation of the matrix (MMC).
- Matrix failure, i.e. microcracking (CMC).
- Accumulation of microcracks with or without matrix-to-reinforcement interface failure (MMC and CMC).
- Particulate fracture and plastic flow of matrix (MMCP).
- Ultimate fibre failure (MMCf and CMC).

With CMC materials, accumulated matrix microcracking can give apparent non-linear and non-elastic behaviour, even though the constituent materials are themselves behaving elastically.

Table 64.3-1 - Modulus mismatch in composites: Examples

Composite						Mismatch ratio † ($E_m - V_m / E_f - V_f$)
Matrix type	E_m (GPa)	V_m (%)	Reinforcement type	E_f (GPa)	V_f (%)	
Al	72	80	SiC_p	400	20	0.72
Al	72	60	C_f	240	40	0.45
Ti	110	60	SiC_f	390	40	0.42
SiC	400	60	SiC_f	193	40	3.1
Glass	75	60	SiC_f	193	40	0.58

Key † The lower the value, the greater the contribution by the reinforcement in sustaining stresses under elastic conditions.
Also, the lower the value, the greater the compressive stresses retained in the reinforcement on cooling. This, in turn, increases the residual stresses in the matrix when there is a CTE mismatch between reinforcement and matrix.
The SiC-SiC composite is unlike the others in having a matrix with a modulus significantly greater than the reinforcement.

64.3.3 Matrix-to-reinforcement interface

The effective strength of the interface bond between matrix and reinforcement is a critical factor in determining the overall composite fracture behaviour, Ref. [64-1].

Conflicting requirements exist between the need for 'good, strong' and 'poor, weak' bonding.

- Good bonding in theory enables the maximum strength of the reinforcement to be utilised. However, in MMC and CMC materials, good bonding is also synonymous with fibre surface degradation through chemical diffusion mechanisms with the matrix. This causes a loss in fibre strength.
- Poor bonding is essential in CMC materials to promote de-coupling between the fibre and matrix in order to achieve benign fracture behaviour, i.e. acceptable fracture toughness.

A compromise should be sought to meet the specific features of each composite.

64.3.4 In-situ fibre strength

All reinforcing fibres have attractive tensile strengths before being incorporated into composites (2000MPa to 7000MPa). In reality, it is extremely difficult to fully utilise this potential in MMC and CMC composites. The actual in-situ strength contribution made by the fibres is influenced by:

- Fibre to matrix adhesion (interface).
- Fibre degradation caused by:
 - composite manufacturing,
 - chemical diffusion, or
 - attack by aggressive environmental exposure, e.g. oxidation.

The fibre's in-situ tensile strength can be reduced to 20% to 70% of theoretical strength. This level can be even lower in poorly constituted composites (poor materials selection) or composites with severe environmental degradation, e.g. thermo-oxidative.

64.3.5 CTE mismatch

The coefficient of thermal expansion (CTE) for matrix and reinforcement are different. For a metallic matrix with a ceramic reinforcement the difference is considerable. The matrix usually has the higher expansion, as shown in Table 64.3.2.

Reinforcement fibres possess higher CTEs in the transverse than in the longitudinal direction.

The significance of the CTE mismatch centres on the residual stresses induced on cooling because the matrix is contracting more than the reinforcement. The matrix experiences retained tensile stresses whilst the reinforcement is under compression. Composites with significant mismatches between their constituents CTE and moduli are particularly susceptible to high residual tensile stresses in the matrix phase.

Table 64.3-2 - CTE mismatch in composites: Examples

Matrix type	Composite			CTE mismatch † ($CTEm - CTe_r$)	Process temperature (°C)
	$CTEm$ (10^{-6}°C^{-1})	Reinforcement type	$CTEr$ (10^{-6}°C^{-1})		
Al	23	SiC _p	5	18	650
Al	23	C _f	-1	24	650
Ti	9	SiC _f	3.5	5.5	900
C (PG)	2	C _f	-1	3	1100 - 2000
SiC	5	SiC _f	3.1	2.9	1200
Glass	8	SiC _f	3.1	4.9	800

Key † Ideally the CTE mismatch should be as small as possible.
 Aluminium alloys have very high CTE values and combining them with carbon fibres creates a significant CTE mismatch. The residual tensile stresses in the aluminium on cooling are compounded by this and the low $E_m V_m / E_f V_f$ value, [See: Table 64.3.1].
 Where CTE mismatch is smaller, e.g. SiC/SiC and C/C, this compensates for the large temperature range between processing to ambient.

64.3.6 Thermal history and residual stresses

The thermal history of a composite is important in determining fracture behaviour, Ref. [64-1]. The processing or forming temperature establishes the level of residual stresses when cooled to ambient. Sub-ambient temperatures induce greater residual stresses. Exceeding the processing temperature of ceramic composites reverses the stressing to compression in the matrix and tension in the reinforcement.

With metals, the use of heat treatments can alter the matrix microstructure and alleviate residual stressing. Residual stresses can influence the creep behaviour of MMC materials. Excessive thermal shock, persistent thermal cycling and uneven heating are further mechanisms of relieving internal stresses through the formation of microcracking, matrix yielding and delaminations.

64.3.7 Multiple cracking

64.3.7.1 Fibre reinforced materials

The majority of MMC and CMC materials experience multiple cracking phenomena during progressive fracture in the unnotched condition. Matrix microcracks, ply cracking, voidage and delamination can reach high population densities with the composite still sustaining useful applied loads.

64.3.7.2 Particulate reinforced materials

Only particulate MMC materials show fracture behaviours close to the single crack mechanism of alloys conforming to the LEFM philosophy. Where notched specimens are used to characterise toughness, cracking becomes more localised at the point of maximum stress.

64.3.8 Thermo-mechanical fatigue (TMF)

For MMC and CMC materials, potential uses are applications experiencing both mechanical loading and thermal cycling.

As temperature excursions affect residual stresses within the composite, they can have a compounding effect when coupled with external mechanical loads, Ref. [64-2], [64-3], [64-4]. Material behaviour can be strongly influenced depending on whether thermal stresses and applied stresses are in-phase or out-of-phase with each other, [See: 47.9 for an example of TMF of titanium-matrix composites].

64.4 Basic fracture characteristics

64.4.1 General

An example from each group of composites demonstrates their basic fracture characteristics because they affect tensile stress-strain behaviour. The stress-strain curves are idealised representations and cannot be used for design data.

64.4.2 Particulate reinforced MMC

Figure 64.4.1 represents the stress-strain behaviour of a particulate reinforced aluminium alloy, with 17 vol. % silicon carbide particles.

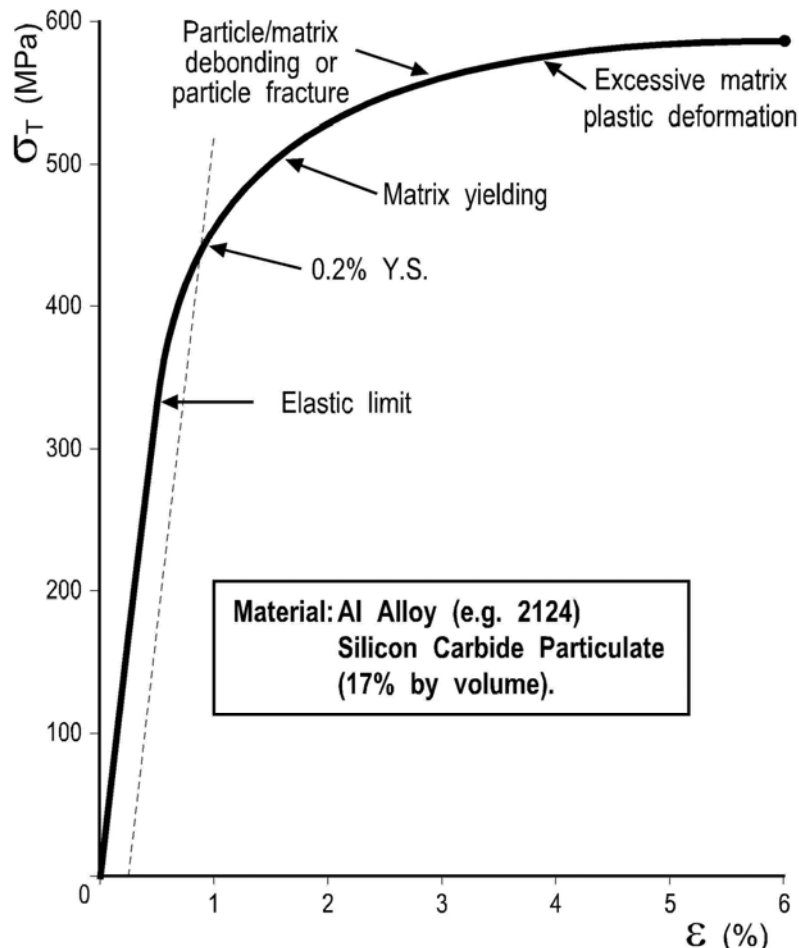


Figure 64.4-1 - Representative stress-strain curve: Particulate reinforced MMC

The material is elastic at very low strain levels with both matrix and particles elastically deforming in unison. Overall linear elasticity is only exhibited to strain levels as low as 0.2% to 0.4%, whereas an unreinforced alloy can be expected to be elastic to approximately 0.5%. Above the elastic limit, permanent deformation and plastic behaviour of some form is shown. The initial deformation process can be difficult to establish. As strain levels exceed 0.5%, a massive accumulation of deformation features makes the picture very confusing. However, important features are:

- The particles themselves have an individual strain to failure less than approximately 0.2%. It is therefore impossible for them to continue straining elastically beyond this level. Consequently they either fracture or debond from the matrix enabling the matrix to continue deforming.
- The matrix retains residual stresses due to CTE mismatch before any external load is applied. The matrix can therefore be expected to start yielding (plastically deforming) at lower overall applied strain, i.e. less than the 0.5% of unreinforced alloys. Matrix behaviour is dominant in MMC_p materials.

This behaviour is important when stating mechanical properties:

- Tensile modulus: quoted as the initial, secant or tangential value.
- Yield strength. For conventional alloys, the 0.2% offset yield value is used against the initial linear elastic portion of the stress-strain curve.

[See: Chapter 65 for further details of MMCp materials]

64.4.3 Fibre reinforced MMC

Figure 64.4.2 uses continuous silicon carbide monofilament reinforced titanium as the example to represent the MMCf group.

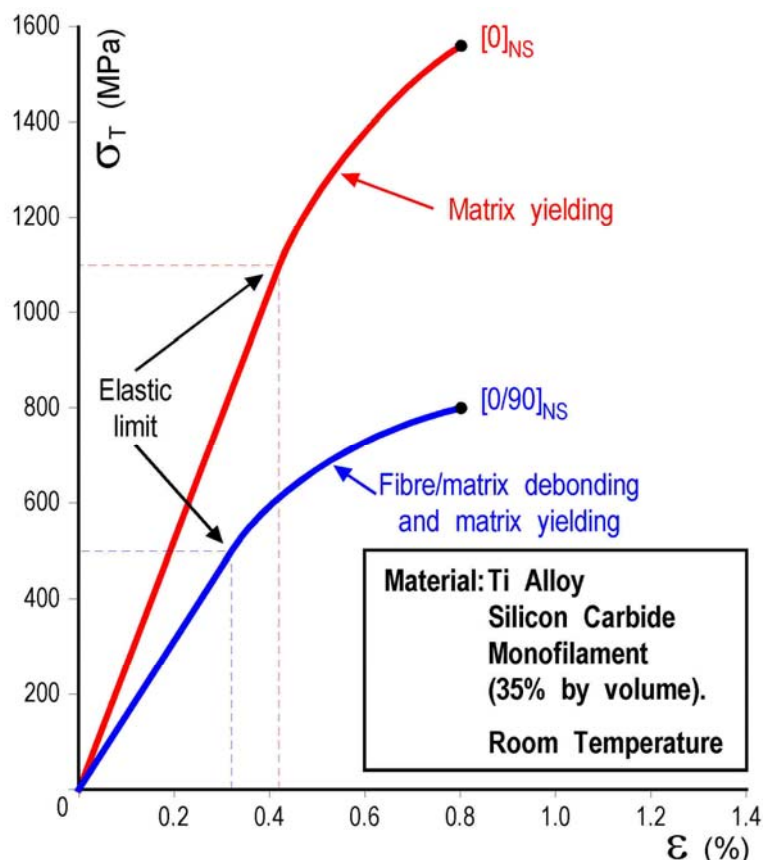


Figure 64.4-2 - Representative stress-strain curves: Monofilament reinforced MMC

The overall composite failure strains are low because they are fibre dominated. Both unidirectional and bi-directional materials exhibit initial linear elastic behaviour. The UD composite shows a gradual reduction in modulus as the overall failure point is approached. This modulus reduction can be explained by the onset of matrix yielding and low level individual fibre failure. The 0°/90° composite shows a reduction in modulus at a much lower strain level. It corresponds to transverse ply failure through debonding of the fibre-matrix interface. This equates to the first-ply failure (FPF) phenomenon seen in CFRP materials where the 90° plies fail first.

For Ti/SiC materials, the FPF weakness is particularly sensitive to the residual matrix stresses and brittle nature of the fibre-matrix interface.

64.4.4 Fibre reinforced CMC

With ICMCf materials, the generic grouping covers brittle elastic matrices combined with brittle elastic fibres. The stress-strain curve in Figure 64.4.3 depicts a multidirectional SiC-SiC material. The composite modulus is therefore very high. If a glass or carbon matrix were used, an appreciably lower composite moduli results.

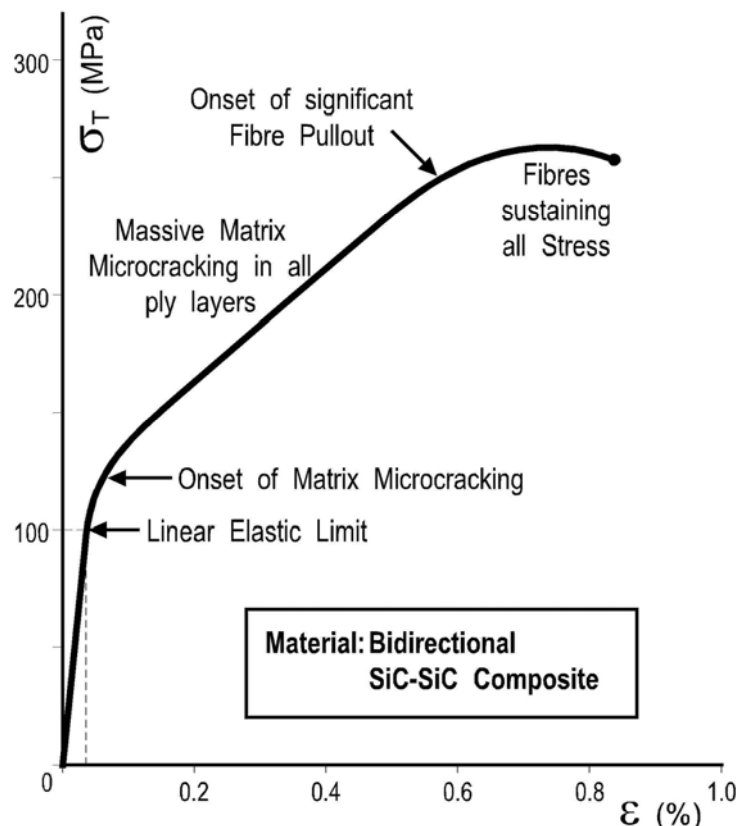


Figure 64.4-3 - Representative stress-strain curves: Bidirectional SiC-SiC composite

This group of composites are always used in with multidirectional (3D or nD) reinforcements because transverse tensile strengths are very low.

The composite tensile strength is very much dependent on the in-situ fibre strength and the ability to de-couple fibre and matrix. The truly linear elastic region of these composites is very small. The majority of the stress-strain curve depicts the accumulation of a massive microcracking population with the modulus contribution by the matrix diminishing as ultimate failure is approached.

64.4.5 Defining design values

64.4.5.1 General

With all the metal and ceramic matrix composites, the issue of defining design values for modulus, strength and permissible strain needs close examination.

A compromise is applied between attainable modulus and strength demands. Stiffness realisation against strength retention is an important issue as significant overall stiffness loss can be experienced at higher stress levels. The loss of stiffness results from some form of permanent deformation or damage in the matrix phase.

64.4.5.2 Failure criteria

Compared with polymer-based composites, confidence in establishing and the use of failure criteria for metal- and ceramic-based composites is lower.

The problem arises because the MMCs and CMCs are not as widely-used in space structures as fibre-reinforced polymer composites. Consequently, the knowledge-base is much reduced and tends to be limited to a small number of organisations. The material applications usually have more hostile conditions than for fibre-reinforced plastics, e.g. hot structures made of CMCs. The materials themselves are complex and their overall characteristics are highly processing-dependent, Ref. [64-5].

Design guidelines have been established for the appropriate use of failure criteria during space structure design as part of an ESTEC-funded study on failure criteria for non-metallic materials, conducted in Germany by HPS and DLR, Ref. [64-7].

The ESTEC study covered FRP, [See: 11.8] and CMC, [See: 64.5].

64.5 Failure criteria for CMC

64.5.1 Introduction

As part of an ESTEC-funded study on failure criteria for non-metallic materials, conducted in Germany by HPS and DLR, design guidelines have been established for the appropriate use of failure criteria during the design phases of space structures, Ref. [64-5], [64-6], [64-7].

64.5.2 Design aspects

64.5.2.1 General

Design guidelines have been established based on structural configuration examples from the TETRA/X-38 nose cap design-development. This used C-C/SiC grades of CMC material developed by DLR, Ref. [64-7].

[See also: 70.24]

64.5.2.2 Materials

The C-C/SiC composite materials investigated are produced by DLR using the LSI (liquid silicon infiltration) process. Grades of material, with different characteristics, are produced by varying the fibre preconditioning and processing parameters. For TPS-type applications, the main grades are designated as XB or XT. A further grade of XT is used for mechanical fasteners (bolts), Ref. [64-7].

64.5.2.3 Failure loads

Although some specifically-derived failure criteria for CMCs exist, the criteria applied to polymer composites are also used. Of these, either maximum stress or maximum strain tends to be the first choice. Classical criteria based on continuum mechanics are not always appropriate for CMCs, Ref. [64-6].

Various failure criteria used for polymer composites were applied to CMC materials. Of these, some performed better than others, e.g. ZTL-hypothesis provides more realistic values than Tsai-Wu. Puck appears inappropriate for CMCs because of the difference in failure modes exhibited by CMCs compared with FRPs, Ref. [64-6]. An example of a comparative failure curve, with high-temperature experimental data is shown in Figure 64.5.1, Ref. [64-6].

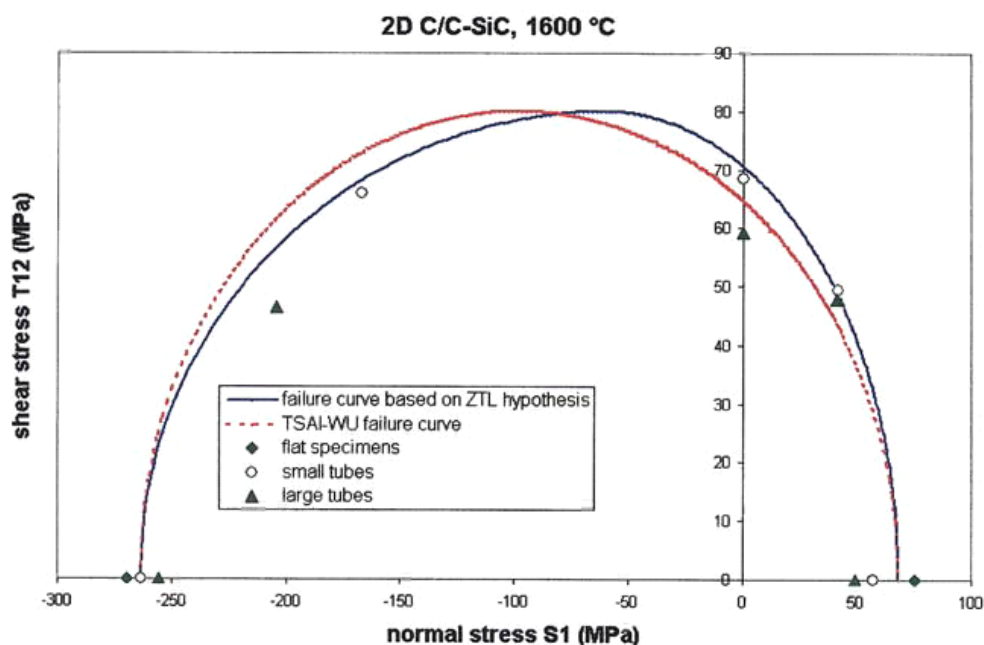


Figure 64.5.1 – Failure criteria: Comparison between predicted failure curves for C-C/SiC composites with experimental data

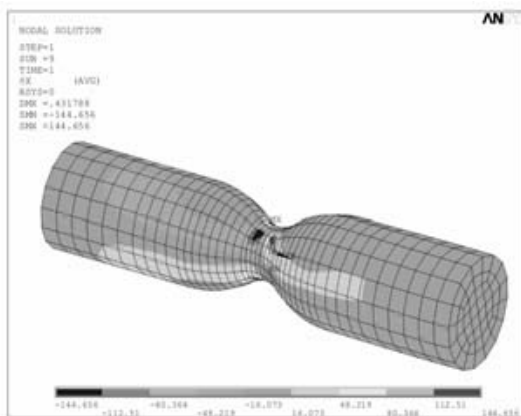
Since CMC material properties tend to improve with temperature, the use of RT-generated data can provide a conservative estimate of the performance of hot structures, Ref. [64-6].

Based on the evaluation of DLR's materials, a practical approach to estimate the failure loads appears to be the maximum stress criterion, which is similar to that used for monolithic ceramics. The significant difference is that the Weibull modulus is completely different. This means that designers need reliable strength values rather than the statistically-derived probability values used for monolithic ceramics, Ref. [64-6], [64-7].

64.5.2.4 Test and analysis

A new test approach was developed and evaluated to confirm the assumption about failure load data, Ref. [64-6], [64-7].

The outcome of this phase of the work was an ‘hour-glass’ shaped test specimen, as shown in Figure 64.5.2, Ref. [64-6]. The results using this showed reasonable consistency with the maximum stress criterion and enabled combinations of tension and shear load interaction, such as the conditions found at load introduction points. Hence, it enables a full set of test data to be generated within the range ($+\sigma_1/\tau_{12}$), Ref. [64-6], [64-7].



FEM model of ‘hour-glass’ test specimen



Fractured ‘hour-glass’ test specimen in high-temperature test rig

Figure 64.5-2 – Failure criteria: ‘Hour-glass’ test specimen for C-C/SiC composites

64.5.2.5 Load introduction points

To meet the NASA stipulation of avoiding damage to the X-38 CMC shell, joint-related designs were studied in detail. This enabled a series of design guidelines to be established, Ref. [64-7]:

- Permanent joints:
 - castable, which is a combination of an adhesively bonded and potted connection, using a high-temperature ceramic-based compound; an approach used in the CETEX programme.
 - bolted joints, where the component parts of the mechanical fasteners were made of CMC.
- Non-permanent joints, i.e. ceramic rivet-type, which enable inspection, maintenance and repair of the TPS on RLVs.
- Elastic joints, e.g. CMC stand-off concept developed under the FESTIP programme. These connections retain some flexibility in order to cope with thermal mismatch between the CMC TPS and the proposed CFRP or Al-Li alloy cryotank structures.
- Kinematic joints, e.g. X-38 nose cap attachment, which needed to cope with thermal mismatch between the TPS and the aluminium alloy substructure, but which was not feasible using the FESTIP elastic joint (stand-off) configuration.

In the design of elastic and kinematic joints, the aim is to obtain a suitable compromise between the thermal expansion properties of the CMCs and the support structure, usually made from light alloy (flexibility), whilst retaining sufficient mechanical performance (stiffness) under mechanical loading.

64.6 References

64.6.1 General

- [64-1] M. Taya & R.J. Arsenault
'Metal Matrix Composites: Thermomechanical Behaviour'
Pergamon Press, 1989, ISBN 0-08-036983-9
- [64-2] T. Fujita et al
'Temperature-Dependent Tensile and Shear Response of P100/6061 Graphite-Aluminium'
ASTM STP 1080, 1990, p165-182
- [64-3] J.J. Schubbe & Shankar Mall
'Damage Mechanisms in a Cross-Ply Metal Matrix Composite under Thermal-Mechanical Cycling'; ICCM 8, p20/B/1-9, 1991
- [64-4] H. Sehitoglu & M. Karayaka
'Thermo-Mechanical Fatigue of Al-SiCp Composites'
Proceedings of the 4th International Conference on Fatigue and Fatigue Thresholds, July 1990, Vol.3, p1693-1698
- [64-5] C. Kaiser et al: HPS/DLR/Kayser Threde/ESTEC
'Failure criteria for FRP and CMC: Theory, Experiments and Guidelines'
Proceedings of the European Conference on Spacecraft Structures, Materials and Mechanical Testing, ESTEC, Noordwijk, NL 10-12 May 2005, ESA SP-581 CDROM
- [64-6] C. Kaiser et al: HPS/DLR/Invent GmbH/ESTEC
'Failure criteria for Non-metallic materials: Part II Ceramic Matrix Composites'
Proceedings of ECCM III, Rhodes, Greece, May-June 2004
- [64-7] C. Kaiser & H. Weihs: HPS/DLR (D)
'Failure Criteria for Non-metallic Materials: CMC Failure Criteria Guidelines'
Contractor Report No. FAIL-DLR-TN-001 (Issue 1), March 2005
ESTEC Contract No. 16162/02/NL/CP

65

Particulate reinforced metals

65.1 Introduction

65.1.1 Materials

65.1.1.1 General

The most common materials are shown in [Table 65.1.1](#).

Table 65.1-1 - Particulate reinforced MMCs

Matrix	Particulate	Sources
Al	SiC	A217 and A817 (BP Composites)
		Duralcan (Alcan)

[See: [46.13](#) for material properties]

65.1.1.2 Microstructure

The accepted microstructural features which can influence fracture behaviour are:

- In-situ matrix yield strength (for solution heat-treatable alloys with precipitation hardening mechanisms)
- Dispersion strengthening, e.g. ODS with particles sub-micron in size, $0.01\mu\text{m}$ to $0.1\mu\text{m}$.
- Small particulates in the $2\mu\text{m}$ to $3\mu\text{m}$ range.
- Large particulates in the range $10\mu\text{m}$ to $20\mu\text{m}$ range.

65.1.2 Composites

65.1.2.1 Matrix

Matrix selection can affect the composite behaviour. Composites can be prepared that out-perform the base alloy, providing that some basic guidelines are followed.

The composite modulus, yield strength and UTS reflect that at least 80% by volume of the composite is matrix.

An aluminium matrix is likely to be a 2XXX, 7XXX series, aluminium-lithium, ODS, wrought or cast alloy, [See: Chapter [46](#)]. Heat treatments and mechanical working are also influential.

The matrix options are equally considerable for copper or magnesium.

[See: Chapter 45 for copper, Chapter 44 for magnesium].

The matrix metal or its alloying elements can react chemically with the particulate, e.g. aluminium reacts with SiC but not with Al₂O₃.

The microstructure and hence properties of an alloy in a selected heat-treated and mechanically worked condition can be disrupted by the presence of particulates acting as nucleating agents, Ref. [65-1].

65.1.3 Particulate reinforcement

65.1.3.1 Types

Types of particulate materials investigated include:

- Alumina (Al₂O₃), Ref.[65-2], [65-3],
- Silicon carbide (SiC), Ref.[65-4] to [65-10],
- Titanium diboride (TiB₂), and
- Boron carbide (B₄C).

SiC is the most widely used particulate reinforcement with aluminium, not least because good bonding can be achieved between matrix and particle by chemical interaction.

65.1.3.2 Size

The size of particulate reinforcement is important, Ref. [65-11]. Very small particles are the most efficient for achieving high strengths. This is reflected in oxide dispersion strengthened alloys, where oxide phases are 0.01µm to 0.1µm but their volumetric percentage is small. The deliberate addition of significant volumetric quantities of discrete particles has the effect of raising both modulus and strength. Again, smaller sizes are preferable given cost and other practical constraints. An evenly distributed dispersion is desirable for reproducible behaviour. Particulate sizes in the range 2µm to 3µm are preferable for high strengths, but expensive powder-metallurgy routes are used. Larger, 15µm+, particles are less efficient, giving lower strength, but are cheaper to incorporate using casting processes.

Some of the factors influencing particle-reinforced composite fracture behaviour are, Ref. [65-5], [65-6], [65-9], [65-10]:

- Aspect ratio,
- Size distribution, and
- Particle shape. Particles can be slightly:
 - elongated,
 - rounded,
 - angular,
 - faceted, and
 - pre-cracked.

All particles are ceramic, which have high moduli but with low strain to failures of approximately 0.2%.

Particulate MMC materials always have an initial, low-strain tensile modulus which is higher than the base alloy. The strength characteristics, i.e. 0.2% YS, UTS, fracture toughness and ultimate elongation are not always as good because particles have been added.

It is possible to prepare ‘good’, ‘indifferent’ or even ‘poor’ composites from similar constituents. Only composites which are better in performance than their unreinforced counterparts are used where strength requirements prevail, because of the additional cost. If stiffness is the prime requirement, then MMC_p materials can be attractive.

65.2 Damage mechanisms

65.2.1 Unnotched specimen

For particulate MMC the overall fracture behaviour can be closely related to that of the unreinforced base alloy with some additional features. The base alloy undergoes elastic deformation to the elastic limit, after which irreversible plastic deformation accumulates. The plastic deformation is a result of dislocation growth and grain boundary slippage. Ultimately, the combined elastic and plastic deformation gives rise to excessive yielding, necking and failure. This broadly describes the behaviour of an unnotched alloy and is translated to the stress-strain curve in Figure 65.2.1.

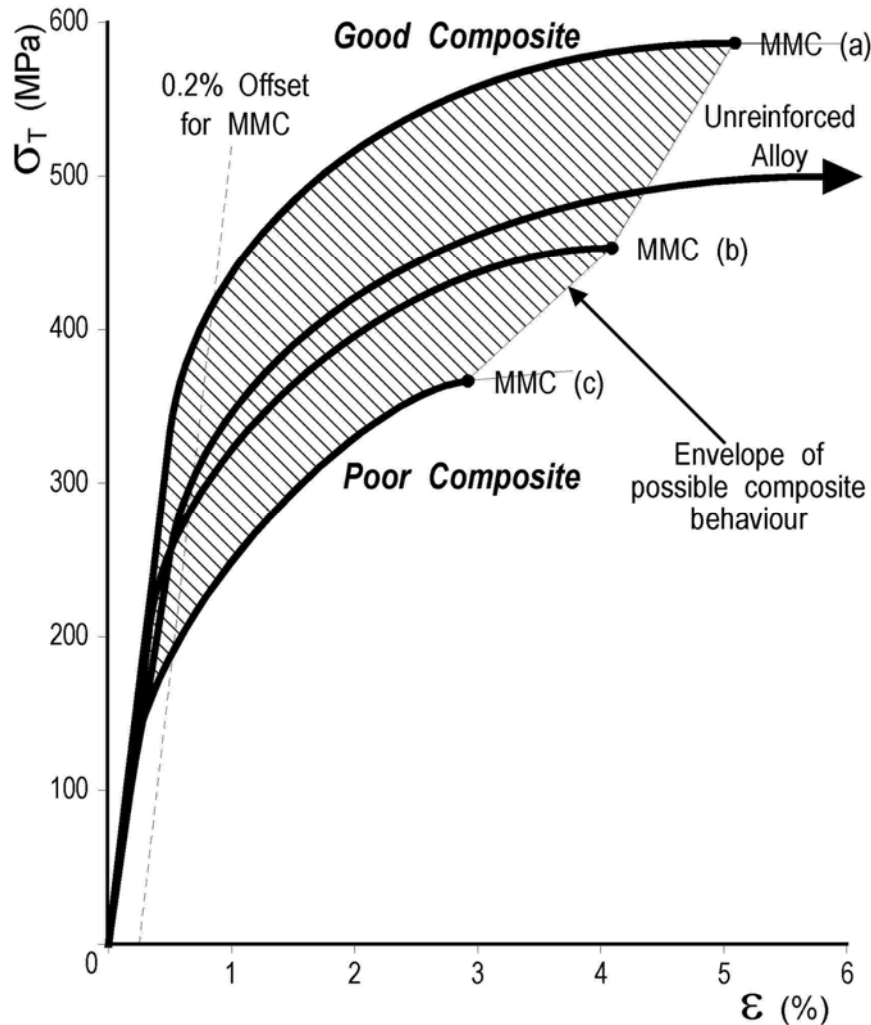


Figure 65.2-1 - Relative stress-strain behaviours of optimised (good) and non-optimised (poor) MMCp composites

65.2.2 Notched specimen

A single crack forms with the plastic deformation occurring ahead of the crack as it propagates until the critical size is reached. Whereupon the energy stored in the loaded specimen is sufficient to cause rapid crack growth and catastrophic failure.

65.2.3 Influence of particles

The inclusion of a large population of particles, whilst of small size, each influences the local 'matrix' volume. Their presence does not affect the gross mode of failure for loaded unnotched or notched material. This is ultimately a single propagating crack. However, the accumulated local events around each particle fashions the overall composite behaviour both before and after the elastic limit, Ref. [65-12].

The particles are there to provide reinforcement, i.e. sustain load that would otherwise be carried by the matrix. However, the strain capacity of the particles is much lower than that of the surrounding matrix. The matrix can deform to 5%, 10% or 20% extension, whilst the particle can only manage approximately 0.2%. A point is therefore reached at a very low strain when the two can no longer

strain elastically together and relative movement between the two occurs. The ideal behaviour is for the adjacent matrix to remain adhering to the particle, whilst the remainder plastically deforms and ultimately begins to flow until the overall strains are in the 4% to 8% region. Whilst this is occurring, the particle is still performing a function because it is elastically deformed but its ultimate strength and strain to failure have not been reached. Something close to this can be achieved in optimised composites.

Other behaviour can also occur in varying degrees, which lowers the overall composite strength and strain to failure:

- Particles are over-stressed and fracture, Ref. [65-1]. The two parts no longer act in unison and have a gap between them which can grow as a crack in response to plastic deformation around it.
- The particle separates from the matrix through lack of adhesion. Again, an interface forms which can grow into a crack. The particle loses some of its ability to sustain elastic deformation and becomes less efficient as a reinforcing medium. In the worst case, the particle acts as a solid inclusion which is a hindrance rather than a benefit.

65.2.4 Composite performance

A 'performance envelope' exists [See: [Figure 65.2.1](#)], which describes that exhibited by a composite in comparison with the unreinforced alloy.

The top portion, designated 'Good', represents an optimised composite whilst the lower portion, occupied by MMC (b) and MMC (c), represent a composite that does not achieve the baseline performance of the unreinforced alloy.

The 'Good' position, MMC (a), is achieved by having:

- Good particle dispersion
- Good particle to matrix adhesion
- Optimum particle shape and size distribution
- Matrix microstructure and heat treatment optimised for the presence of particles in the composite.

The composite matrix microstructure or heat-treatment processes used can vary from those of an unreinforced alloy.

65.3 Failure modes and fracture behaviour

65.3.1 Matrix effects

65.3.1.1 General

MMCP composites cannot be viewed simply as an accepted alloy containing solid phases whose addition is aimed at achieving some form of reinforcement.

The presence of the particles alters the accepted microstructure of the isotropic alloy before any external load is applied. In effect, the accumulation of dislocations in the matrix is modified. The basic strengthening mechanisms prevailing in the composite are an accumulation of, Ref. [65-13]:

- High dislocation densities in the matrix, due to dislocation generation as a result of differences in coefficient of thermal expansion.
- Small subgrain size, as a result of the generation of high dislocation density.
- Residual elastic stresses.
- Differences in texture.
- Dispersion strengthening in the matrix, by the formation of intermetallic particles that otherwise do not form in the unreinforced alloy.
- Classical composite strengthening, through load transfer to the particles.

As such the matrix cannot be viewed as truly isotropic. The macro-yielding of the composite is controlled by the inhomogeneous matrix which is a mixture of high and low dislocation regions. This accounts for the difficulties experienced in modelling MMCp materials beyond their initial, very low strain elasticity.

65.3.1.2 Duplex microstructures

Understanding MMCp behaviour is further complicated by deliberately produced duplex microstructures as a means of improving fracture toughness by:

- Larger particles which, provided they do not exceed an upper critical size, give resistance to unstable crack propagation.
- Finer particles, equivalent to dispersions of less than a lower critical size (no longer classified as particle additions), which provide matrix strengthening and crack initiation toughness.

65.3.2 Failure mode studies

For MMCp materials, differences are recognised between:

- straightforward macro-behaviour of simple tensile tests on unnotched specimens, and
- localised micro-behaviour more prevalent in single crack (notched) propagation studies which are defining fracture toughness.

Most studies attempt to explain composite behaviour by following the slow progression of a single crack and identifying deformation of fracture features in and around the crack tip.

65.3.3 Particulate shape and aspect ratio

No introduced particles are truly spheroid in shape nor elliptical as hypothesised by models, e.g. Eshelby. In reality they are of variable size distribution, usually angular and possess some aspect ratio exceeding unity.

- Aspect ratio >3: Alignment through mechanical working influences the directional properties.
- Aspect ratio >10: Implies that the reinforcement is a whisker or very short discontinuous fibre.

Figure 65.3.1 shows a schematic representation of the features found in MMCp materials.

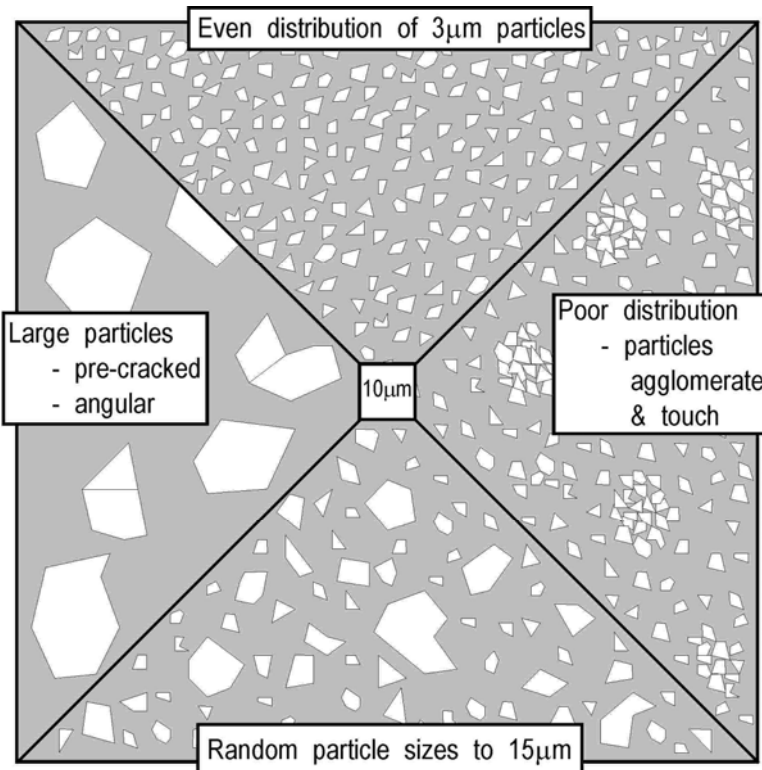


Figure 65.3-1 - Features of particles in MMCp materials

As a single crack propagates, the crack tip can follow a path which is influenced by the features around it, e.g.

- An even particulate distribution is essential for reproducible material behaviour and is an assumption for all models.
- Larger particles ($>15\mu\text{m}$) do not hinder crack progress in the same way as a population of smaller particles of the same volumetric contribution.
- The angularity of particles influences the presence of stress concentrations in the adjacent matrix. End-effects of sharp tips and whisker or fibre ends influence crack propagation depending on their orientation.

Figure 65.3.2 shows the effect of weak interfaces and cracked particles on crack propagation. The random fracture path is indicative of a good MMCp material where no apparent points of weakness have influenced the propagation of the crack.

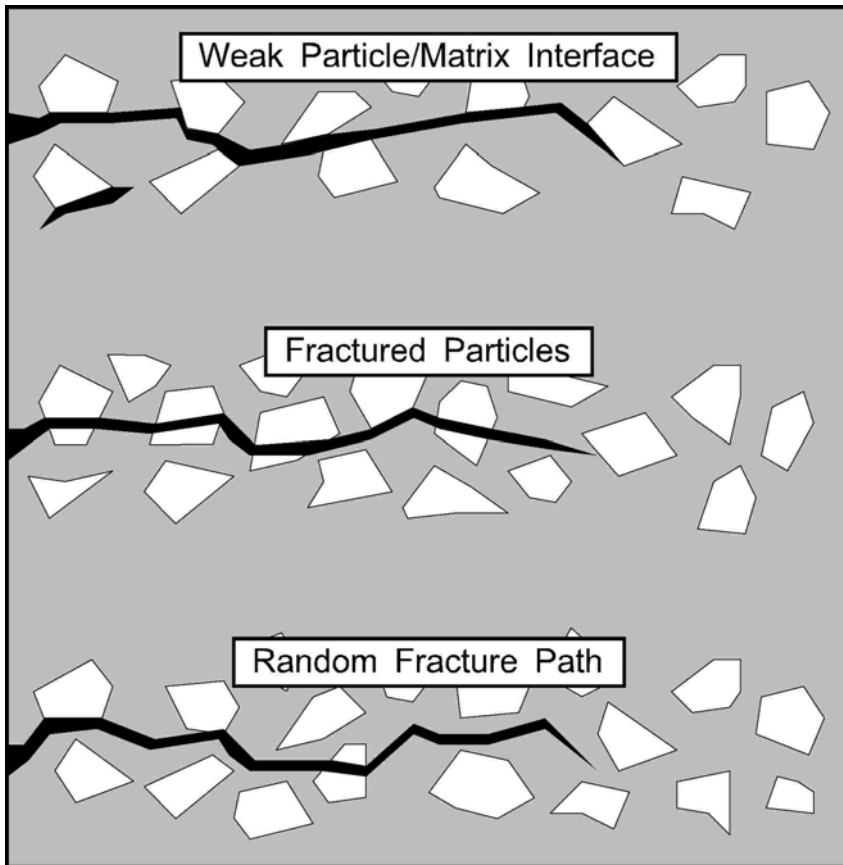


Figure 65.3-2 - Possible crack propagation paths in MMCp materials

65.3.4 Particulate fracture

A particle's fracture behaviour is influenced by:

- Shape, particularly if its surface is recessed.
- The inherent fracture toughness of the particle itself, where the particle can be weakened or cracked during mechanical working of the composite.

[See: [Figure 65.3.2](#) for crack propagation through fractured particles]

65.3.5 Void nucleation and growth

When a single crack propagates, evidence suggests that the crack path is attracted towards particles adjacent to the fracture plane. The ductile fracture of the matrix is characterised by void nucleation and growth (VNG). The spacing between the void nucleating particles is generally considered to be a critical microstructural parameter that, taken together with the tensile properties, controls the toughness of a given composite.

The toughness of Al/SiC composites can be improved when the size of the SiC particles is increased, provided that at least one of the assumptions is met:

- Voids are nucleated by SiC particles.

- The response of the Al/SiC system to the change in centre-to centre particle spacing remains the same regardless of whether this change is caused by varying the volume fraction or size of particles.

65.3.6 Fracture toughness

65.3.6.1 General

Toughness tests are governed by the principles of LEFM or elastic-plastic fracture mechanics (EPFM).

- LEFM: The plastic zone associated with the developing crack is restricted to a small region at the crack tip.
- EPFM: Gross yielding can occur across the whole of the uncracked portion of the specimen.

The implication being that initial crack growth comes under LEFM whereas EPFM is applicable when the crack has grown appreciably, Ref. [65-14].

65.3.6.2 Common terms

The testing of MMCp materials is complicated by the difficulties in obtaining stable crack growth. It is generally accepted that these composites have lower fracture toughness values than their unreinforced counterparts.

K_{IC}	Plane strain <u>fracture toughness</u> , a measure of a material's resistance to unstable crack extension when the stress state at the crack tip is plane strain and the opening mode (I) load is applied. The opening mode corresponds to a load applied perpendicular to the crack plane.
K_Q	A provisional value of K_{IC} , not confirmed until checks made on P_{max}/P_Q , thickness B , and ligament width $W-a$, are compared with validity criteria in standards.
K_R	Measure of resistance to stable crack growth.
R -curve	Continuous record of toughness, K_R , plotted against stable crack extension.
K_c	Plane stress fracture toughness. The value of K_c , is an instability condition determined by the tangent between the R -curve and the applied K -curve of the specimen.
G_c	Critical strain energy release rate : for plane stress $G_c = K_c^2/E$.

EPFM

In EPFM there are terms analogous to those used in LEFM, such as J or J_R for EPFM energy release rate and R -curves are also measured (known as J/R -curves). However other terms such as T , tearing modulus, are also given.

65.4 Thermo-mechanical fatigue (TMF) and creep

65.4.1 Residual stresses

Residual tensile stresses are retained in the matrix and can be as high as 100MPa to 150MPa at room temperature. Such levels represent a considerable portion of the yield strength of aluminium alloys, for example.

65.4.2 Temperature

The presence of residual stresses provides a motivating force for relaxation if the right conditions prevail. An increase in temperature is such an impetus. For aluminium MMC_p material, a modest temperature of 200°C and a modest external load provide an incentive for creep.

The creep characteristics of any particular composite are dependent on the heat treated condition.

65.4.3 Superplasticity

If a very ductile matrix is used, e.g. pure aluminium, the composite can exhibit superplastic tendencies giving rise to phenomena such as, Ref. [65-15]:

- Enhanced deformation: a superplasticity effect at low stress.
- Internal stress superplasticity (ISS), Ref. [65-15].
- Mismatch induced superplasticity (MISP), Ref. [65-15].

65.4.4 Applications

The use of particulate reinforcement is useful for increasing room temperature modulus and yield strength. However, dimensional changes can occur at elevated temperatures or with repeated thermal cycling.

65.5 References

65.5.1 General

- [65-1] N. Bourgeois et al
'Modelization of Microstructure Influence on the Macroscopic Properties of Discontinuously Reinforced MMCs'

Proceedings of the Microstructure and Properties of Metal Matrix Composites Conference, Roskilde, Denmark
2-6 Sep 1991, p235-240

- [65-2] S.V. Kamat et al
'Mechanical Properties of Particulate-Reinforced Aluminium-Matrix Composites'
Acta metall. Vol.37, No9, p2395-2402, 1989
- [65-3] A.F. Whitehouse & T.W. Clyne
'Effects of Reinforcement Content and Shape on Cavitation and Failure in Metal-matrix Composites'
Composites 24 No.3 (1993) p256-261 Part 2
- [65-4] K. Schmidt et al
'Mechanical and Thermal Properties of Silicon-Carbide Particle-Reinforced Aluminium'
ASTM STP 1080, 1990, p155-164
- [65-5] C.P. You et al
'Proposed Failure Mechanism in a Discontinuously Reinforced Aluminium Alloy'
Scripta METALLURGICA, Vol.21, p181-185, 1987
- [65-6] J.K. Shang & R.O. Ritchie
'On the Particle-Size Dependence of Fatigue-Crack Propagation Thresholds in SiC-Particulate-Reinforced Aluminium-Alloy Composites: Role of Crack Closure and Crack Trapping'
Acta metall. Vol.37, No8, p2267-2278, 1989
- [65-7] M. Manoharan & J.J. Lewandowski
'Microstructural Effects on the Toughness of Aluminium Alloy Based Metal-Matrix Composites'
Fundamental Relationships Between Microstructure & Mechanical Properties of Metal-Matrix Composites. Edited by P.K.Liau and M.N.Gungor. The Minerals, Metals & Materials, 1990
- [65-8] D.M. Knowles & J.E. King
'Role of Reinforcement/Matrix Interfacial Strength in Fatigue Crack Propagation in Particulate SiC Reinforced Aluminium Alloy 8090'
Materials Science and Technology, June 1992, Vol.8, p500-509
- [65-9] T.J.A. Doel et al
'Mechanical Properties of Aluminium-based Particulate Metal-matrix Composites'
Composites 24 No.3 (1993) p270-275 Part 2
- [65-10] T.J. Downes & J.E. King
'The Effect of Microstructure on the Fracture Toughness of a Metal-matrix Composite'
Composites 24 No.3 (1993) p276-281 Part 2
- [65-11] Y. Flom & R.J. Arsenault
'Effect of Particle Size on Fracture Toughness of SiC/Al Composite Material'
Acta metall. Vol.37, No9, p2413-2423, 1989

- [65-12] D.L. Davidson
'Fatigue and Fracture Toughness of Aluminium Alloys Reinforced with SiC and Alumina Particles'
Composites 24 No.3 (1993) p248-255 Part 2
- [65-13] M. Taya & R.J. Arsenault
'Metal Matrix Composites: Thermomechanical Behaviour'
Book. Pergamon Press, 1989, ISBN 0-08-036983-9
- [65-14] B. Roebuck & J.D. Lord
'Fracture Toughness Testing for Metal Matrix Composites'
IOP Short Meetings Series No28, 1990
ISBN 0-85498-530-1, p110 - 128
- [65-15] S.M. Pickard & B. Derby
'The Deformation of Particle Reinforced Metal Matrix Composites During Temperature Cycling'
Acta Metall. mater. Vol.38, No.12, p2537-2552
- [65-16] Yong-Ching Chen & G.S.Daehn
'The Thermal Cycling Deformation of a Particle Reinforced Metal Matrix Composite: Comparison between a Model and Experimental Observations'
Scripta Metallurgica et Materialia, Vol.25, p1543-1548, 1991

66

Fibre reinforced metals

66.1 Introduction

66.1.1 Materials

66.1.1.1 General

The most common materials are shown in Table 66.1.1.

Table 66.1-1 - Fibre reinforced MMC

Matrix	Fibre	Comments
Al	SiC	Nicalon fibre
	C	Any carbon fibre
	B	Filament
Ti	SiC	Sigma or AVCO monofilaments.

[See: [46.14](#) and [46.15](#) for details of materials and properties]

Microstructural features which can influence fracture behaviour are:

- In-situ matrix yield strength
- Fibre to matrix interface adhesion
- Transverse fibre-matrix strength
- In-situ fibre tensile strength

Composite fracture behaviour and strength are fibre dominated because the full yielding characteristics of the matrix cannot be used.

66.1.1.2 Matrix

- Matrix selection determines the stress and strain levels at the elastic limit.
- To minimise residual stresses within the composite, the composite process temperature are kept as low as possible.
- Contact between molten alloy and fibres is avoided if possible, to restrict chemical interactions.

66.1.1.3 Fibre reinforcement

- Between 35 vol.% and 40 vol.% of reinforcement usually enables an even dispersion of fibres that are not touching.
- Fibre surface treatments and coatings are beneficial to control the interface characteristics and maximise the fibre in-situ strength.

66.2 Damage mechanisms

66.2.1 General

The use of continuous fibres excludes a single crack failure mode for the composite. The fibre behaviour dominates, with the matrix not experiencing strains much beyond 1%, but with yielding.

66.2.2 Effect of lay-up

66.2.2.1 General

In a simple tensile test, some loss of modulus is experienced as the matrix yields. If 90° plies are present, their contribution diminishes quickly due to fibre-matrix interface failure. Most studies on damage mechanisms have concentrated on the response to notched conditions and the application of mechanical load and thermal cycling. There are differences in response between aluminium, Ref. [66-1], [66-2] and titanium matrix composites, Ref. [66-3] to [66-13].

Damage in the form of localised fracture or cracking is predominantly initiated in off-axis, i.e. 90° and ±45°, plies. With sufficient strain, the cracks propagate to give transverse ply cracking. The accumulation of multiple transverse cracks results in complete separation of transverse plies from axial, 0° plies causing delaminating. Where good fibre-matrix bonding exists, as with Ti/SiC, the transverse cracks begin (under fatigue conditions) to penetrate the axial plies. This can lead to a single crack propagation through the 0° fibres and a catastrophic failure.

Crack initiation is likely where fibres are very close or touching; hence excluding the matrix. This is more common with boron and SiC monofilament reinforced metals. An even fibre spacing is essential. During fatigue cycling, voids are generated in the fibre-matrix interface that eventually develop to full debonding of the interface.

66.2.2.2 Boron reinforced aluminium

In notched boron fibre reinforced aluminium, flaws initiate at locations of highest shear stress in the matrix. Initially, the flaws grow out to the first unflawed fibre, then parallel to the fibre until failure occurs across the net section.

66.2.2.3 Titanium matrix composites

In titanium-based materials, the flaws initiate at the maximum strain location. They grow irregularly across and along the fibres until the energy is great enough to crack through the fibres out to the specimen edge in a manner similar to that in unreinforced metals.

66.3 Failure modes

66.3.1 General

Based on the relative strain to fatigue failure of the fibre and matrix, as well as the interface properties, the possible failure mechanisms can be grouped into four categories:

- Matrix dominated,
- Fibre-dominated,
- Self-similar damage growth, and
- Fibre-matrix interface failure, Ref. [66-14].

66.3.2 Matrix dominated failure

In Al/B composites, the boron fibres are not very sensitive to fatigue. The matrix begins yielding at 0.1% to 0.2% strain which is far below the failure strain of the fibre at 0.85%. Therefore, fatigue damages the matrix but does not affect the fibres.

Local plastic straining can be permitted in the composite during the first few load cycles, provided the composite ‘shakes down’ during these few cycles, Ref. [66-2], [66-14]. The shakedown stress is reached if the matrix cyclically hardens to a cyclic yield stress such that only elastic deformation occurs under subsequent load cycles. The stress relates to the onset of fatigue damage but not to laminate failure, i.e. failure of the load carrying 0° fibres.

For Al/B, 70% of UTS can be considered as a safe design load for a life without a significant loss of stiffness.

If all of the initial stiffness needs to be retained for a 2×10^6 cycle lifetime, then the cyclic stress range cannot exceed 35% of UTS. Here the maximum permissible applied strain is about 0.3% without the effect of notches, Ref. [66-14].

66.3.3 Fibre-dominated damage

To predict composite fatigue life, the stress level in the 0° fibres is the governing factor. Initial modulus is lost, particularly through fibre-matrix interface failures in the case of Ti/SiC. Once the stiffness has stabilised, the laminate does not fail until the 0° fibres fail. The in-situ fibre strength determines the maximum permissible fatigue stresses.

66.3.4 Self-similar damage growth

In some composites, e.g. Ti-15-3/SCS6, the fibre and matrix can have similar fatigue endurance strain ranges, i.e. 0.33% to 0.36% at $R=0.1$ for these particular constituents. Damage can initiate and grow as a self-similar crack. Although these composites have rather weak fibre-matrix interfaces, a combination of the residual radial compressive matrix stresses around the fibre and the Poisson effect (when pulling a UD laminate in tension), results in interface strengths sufficient to enable self-similar crack growth in the composite.

66.3.5 Fibre-matrix interfacial failures

The strength expectations are greater for titanium materials (690MPa to 1350MPa) than for aluminium materials (350MPa to 700MPa). This suggests that titanium matrix composites demand much more strength from the fibre-matrix interface than do aluminium matrix composites.

Where fatigue endurance limits are being established, in many instances titanium composites are limited by the interface, whereas aluminium composites are restricted by fatigue of the matrix.

For the simple case of a SiC fibre embedded in a titanium alloy, the calculated stresses in the matrix near the fibre-matrix interface are given in Table 66.3.1, Ref. [66-7].

Table 66.3-1 - Ti/SiC MMC: Calculated stresses

Stress	Value
Radial stress	-138 MPa (compressive)
Tangential hoop stress	+276 MPa (tensile)
Axial stress (fibre direction)	+207 MPa (tensile)

The high reactivity of hot titanium with silicon carbide and hot aluminium with carbon produces composites where fibre degradation can be acute unless a fibre coating is applied which is also optimised for the desired interface characteristics.

The maximum permissible strain under fatigue conditions ultimately determines the viability of MMC_f materials over their unreinforced alloy counterparts. If full stiffness retention is essential, then the in-situ elastic limit of the matrix or fibre-matrix interface is the limiting factor. For multidirectional MMC_f materials, the 'margin of superiority' is proven by test rather than assumed.

66.4 Thermo-mechanical and creep response

66.4.1 General

In continuous fibre MMC materials, the fibres are assumed to be elastic under all conditions. The matrix has elastic-plastic characteristics where plastic deformation becomes more probable as:

- temperature increases, and
- applied strain increases above 0.2%.

The composites are assumed to be power-law creep materials at elevated temperatures, Ref. [66-15].

Creep occurs when the applied load at a given temperature causes a permanent dimensional change over a selected time. Creep rupture characteristics are studied for isotropic metal alloys to assess the maximum permissible application temperature under a predetermined loading condition.

Particulate MMC materials exhibit significant matrix dominated creep.

Continuous fibre MMC materials are less susceptible to creep, due to the dominance of the fibre elasticity. The anisotropy of MMC_f is also greater so that for:

- UD plies: The amount of permanent yielding possible is extremely small. The matrix can yield slightly under an applied strain but the elasticity of the fibres largely restores the composite

once the load is removed. This mechanism can contribute to a ratcheting phenomenon where thermal cycling can compound small dimensional changes on each cycle, Ref. [66-2].

- Transverse plies: Their matrix domination enables considerable capacity for yielding and creep.
- Bi-directional composites: Whilst fibre-dominated, they exhibit creep even at modest strain levels. The residual stresses in the matrix are significant to the onset of permanent deformation.

66.4.2 Application

For long-life structures undergoing thermo-mechanical loading the onset of significant creep limits the maximum permissible strain levels.

66.5 References

66.5.1 General

- [66-1] T. Fujita et al
'Temperature-Dependent Tensile and Shear Response of P100/6061 Graphite-Aluminium'
ASTM STP 1080, 1990, p165-182
- [66-2] A.C.F. Cocks et al
'Effect of Cyclic Thermal Loading on the Properties of Metal Matrix Composites'
Journal of Thermal Stresses, 15: p175-184, 1992
- [66-3] W.S. Johnson et al
'Mechanical Characterisation of Unnotched SCS6/Ti-15-3 Metal Matrix Composites at Room Temperature'
ASTM STP 1080, 1990, p193-218
- [66-4] G.M. Nemez et al
'Thermal Cycling Response of Quasi-Isotropic Metal Matrix Composites'
Journal of Engineering Materials and Technology, Vol. 114, p156-191, 1992
- [66-5] J.J. Schubbe & Shankar Mall
'Damage Mechanisms in a Cross-Ply Metal Matrix Composite under Thermal-Mechanical Cycling'
ICCM 8, p20/B/1 - 9, 1991
- [66-6] P.G. Ermer & S. Mall
'Damage Mechanisms in a Unidirectional Metal Matrix Composite during Thermal Cycling'
Proceedings of the 5th Technical Conference on Composite Materials in Transition, p528-536, 1990
- [66-7] W.S. Johnson
'Damage Development in Titanium Metal-matrix Composites'

Composites 24 No. 3 (1993) p187-196 Part 2

- [66-8] P.J. Cotterill & P. Bowen
'Fatigue Crack Growth in a Fibre-reinforced Titanium MMC at Ambient and Elevated Temperatures'
Composites 24 No. 3 (1993) p214-221 Part 2
- [66-9] C. Barney et al
'Fatigue Crack Propagation in SiC Continuous Fibre-reinforced Ti-6Al-4V alloy Metal-matrix Composites'
Composites 24 No. 3 (1993) p229-234 Part 2
- [66-10] I. Greaves et al
'The Bending Fatigue Behaviour of Unidirectional Reinforced SCS6/Ti-15-3'
Composites 24 No. 3 (1993) p235-240 Part 2
- [66-11] A.R. Ibbotson et al
'Damage Assessment and Lifting of Continuous Fibre-reinforced Metal-matrix Composites'
Composites 24 No. 3 (1993) p241-247 Part 2
- [66-12] D.M. Harmon & C.R. Saff
'Damage Initiation and Growth in Fiber Reinforced Metal Matrix Composites'
ASTM STP 1032, 1989, p237-250
- [66-13] L. Molliex et al
'Temperature Dependence Prediction of SiC/Titanium Composites Tensile Properties from a Micromechanical Approach'
Proceedings of the Interfacial Phenomena in Composite Materials Sept. 1991, p183-186
- [66-14] C.R. Saff et al
'Damage Initiation and Growth in Fiber-Reinforced MMCs'
Journal of Metals, November 1988, p58-63
- [66-15] G.S. Daehn
'Effects of Environmental and Microstructural Variables on the Plastic Deformation of Metal Matrix Composites under changing temperature conditions'
ASTM STP 1080, 1990, p70-86

67

Inorganic ceramic matrix composites

67.1 Introduction

67.1.1 General

The most common materials are shown in [Table 67.1.1](#).

Table 67.1-1 - Inorganic/ceramic matrix composites

Matrix	Fibre
Glass matrix (GMC)	
Borosilicate	C SiC
Glass-ceramic matrix (GCMC)	
LAS	Silicon fibres
MAS	
CAS	
Ceramic matrix (CMC)	
SiC	C SiC
Carbon-Carbon (C-C)	
Carbon	C †
Graphite	

Key: † 2D, 3D or nD fibre orientation

[See: Chapters [52](#), [53](#) and [54](#) for details of materials]

Microstructural features influencing composite fracture behaviour are:

- Matrix modulus and failure strain determined by grain size.
- Matrix porosity and distribution.
- Interface thickness and consistency.
- In-situ fibre condition (tensile strength).

Composite fracture behaviour is influenced significantly by:

- Matrix.
- Interface.
- Fibres.

The ultimate strength comes solely from the in-situ fibre performance, Ref. [67-1], [67-2].

67.1.2 Matrix

The modulus and strain to failure of the matrix determine the linear elastic limit of the composite. Residual stresses in the matrix are influenced by the processing temperature.

Most matrices contain residual porosity of uneven size distribution caused by the pyrolysis process. Up to 10 vol.% porosity is acceptable.

The differences in moduli for the respective matrices are significant, e.g. <100GPa for glass and carbon and >400GPa for silicon carbide.

67.1.3 Interface

To decouple brittle matrix and fibre, an interface material is usually introduced as a fibre coating. This is usually a 'soft' material such as carbon or pyrolytic boron nitride at around 0.1µm to 0.5µm thick. Not only does the interface act as a decouplant, but it also provides surface protection to the fibre from chemical degradation.

67.1.4 Fibres

Silicon carbide (Nicalon and Tyranno) and carbon fibres are predominantly used because of their high strength retention to 1200°C (minimum). Alumina fibres and aluminosilicate fibres are less strong. Multidirectional fibre reinforcement is essential for composite integrity.

67.2 Damage mechanisms

67.2.1 Material effects

The main difference between CMC and MMC materials is that the constituents of CMCs are all elastic in nature and no plastic deformation is possible. A non-linear elastic behaviour occurs with gradual fibre pull-out and incomplete crack closure.

Owing to the brittle nature of constituents in CMC materials, there is an incentive to use three-dimensional reinforcement (3D, nD) to avoid interlaminar planes of weakness. The fracture behaviour of such composites is more complex, Ref. [67-3], [67-4], [67-5].

67.2.2 Microcracking

In MMCs, stress relief occurs by plastic deformation of the matrix; in CMC materials it is by matrix microcracking. As strain increases the population of microcracks grows enormously and the damage area is very large.

Figure 67.2.1 shows the crack accumulation in a glass-ceramic composite, but is representative of CMC materials as a whole.

Transverse plies begin to crack at very low stress levels. At later stages the cracks penetrate the 0° layers. The cracks propagate around the fibres and the fibre-matrix interface decouples. The fibres remain intact bridging the crack.

The material appears to be simultaneously elastic, 'plastic' (irreversible dimensional changes) and damageable, whilst retaining integrity. Such composites are used with the knowledge that they contain some level of damage. The maximum permissible microcrack population density has to be determined. This is complicated by aggressive, corrosive species entering cracks and degrading the fibres.

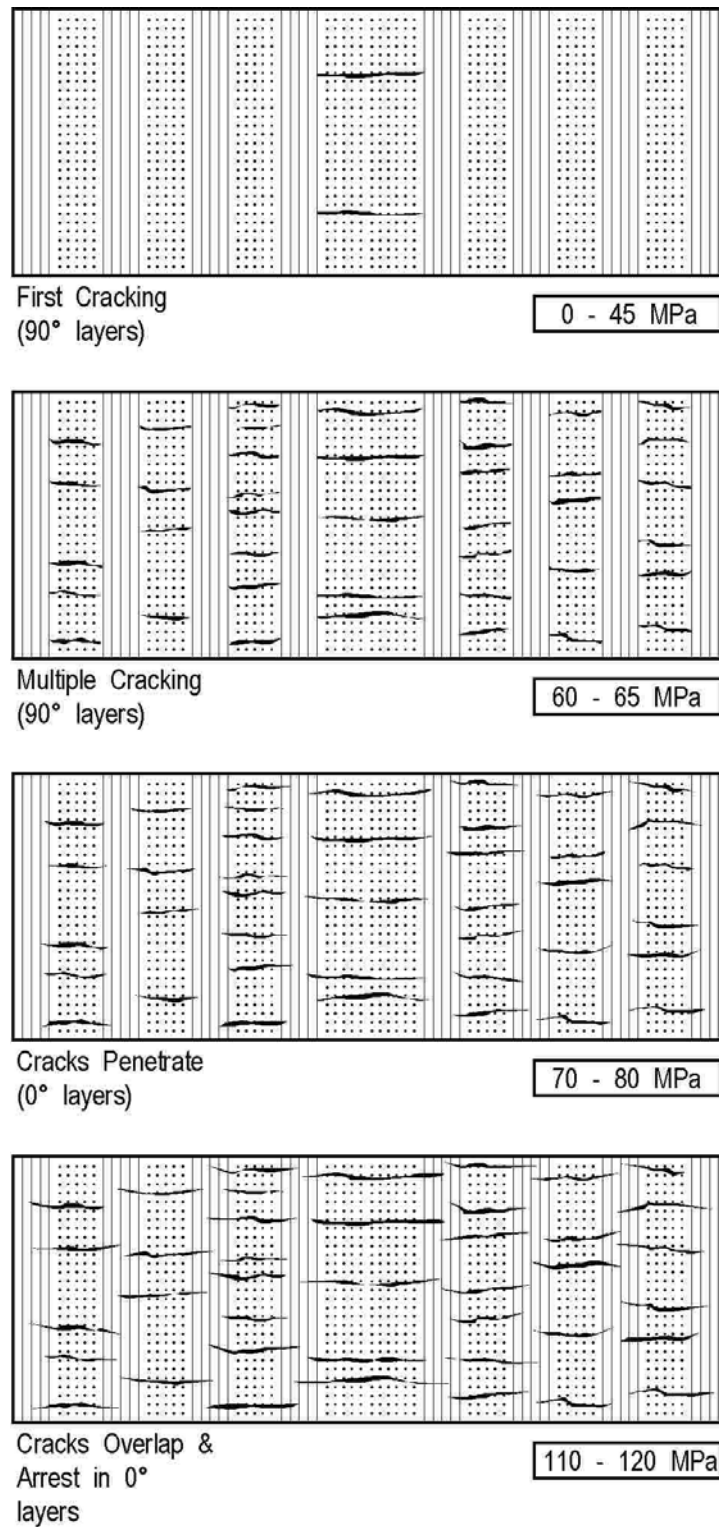


Figure 67.2-1 - Glass matrix composite material: Microcracking sequence

67.2.3 Porosity

Most ceramic matrix composites have retained porosity resulting from the manufacturing route, usually precursor pyrolysis. Retained porosity levels of 5% to 10% by volume are unavoidable. Evenly distributed fine porosity is preferable to larger discrete pores.

For GMC and GCMC materials porosity can be minimised during hot-pressing, with the matrix in a near molten state. Matrix cracking can occur where a defect, e.g. porosity, is present in combination with local residual stresses.

67.2.4 Manufacturing and in-service effects

As with all high-temperature composites, lowering the process (manufacturing) temperature assists in reducing residual tensile stresses in the matrix.

ICMC materials tend to experience acute thermal shock and cycling coupled with applied mechanical loads, hence local conditions conducive to crack formation exist much of the time.

67.2.5 Crack propagation

To demonstrate the three-dimensional aspects of crack orientation, [Figure 67.2.2](#) describes the tunnelling growth that can be expected from a crack spanning the 90° layer. Such cracks have the capacity to run the entire length of the ply and provide a crack tip front to penetrate the unidirectional plies. This type of behaviour is likely to occur in well-consolidated, low-porosity GMC and GCMC materials based on unidirectional plies.

With more irregular microstructures, as in multiple-deposition CVI composites, crack propagation is less planar and more readily terminated or deflected. The use of 2D fabrics and 3D constructions severely inhibits planar crack growth.

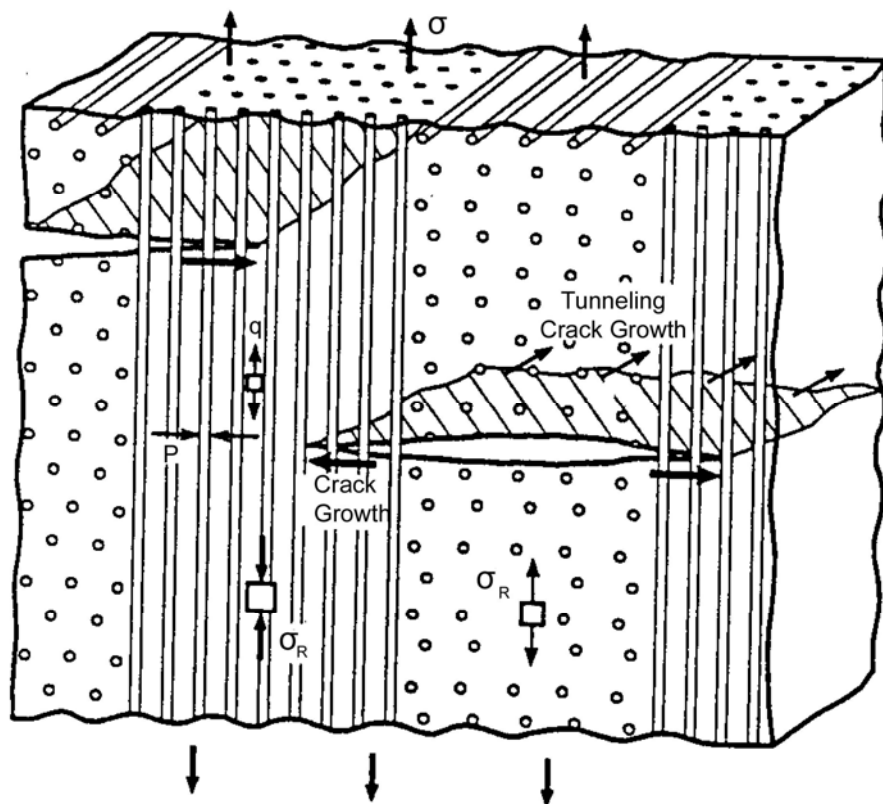


Figure 67.2-2 - Bidirectional glass-ceramic matrix composite: Schematic of tunnelling cracks in 90° layers

Cracks form locally to relieve stress. Once a crack has occurred it is more likely that, with increasing load, further cracks form rather than propagation of the original one.

Propagation is a result of gross over-stressing or elastic energy input under fatigue loading. Fibre pull-out becomes critical as the applied strain and stress reach the ultimate capacity of the material, which is determined by the interface and in-situ fibre strength.

For ICMC materials, the presence of porosity (<10%) and matrix microcracking is unavoidable but is not considered as an unacceptable defect level. These composites are likely be applied to structures in a linear nonelastic state, but possibly as nonlinear, nonelastic materials, depending on the intended life of the structure.

67.3 Fracture behaviour

67.3.1 Toughness parameters

67.3.1.1 General

The use of unique toughness parameters, such as K_{IC} , G_{IC} , J_{IC} are not appropriate for ICMC materials as they do not behave as perfectly elastic or brittle materials. Instead a crack growth resistance (R -curve) can be used which describes the energy needed for crack extension as a function of crack increment. Theorists prefer to work with the assumption that stable crack growth prevails, but this is rare in practice.

67.3.1.2 Testing

Fracture behaviour has been studied with notched and unnotched specimens, which fail in different modes. The single edge notched beam (SEN_B) is popular for studying crack growth, [See: [Test specimens](#)].

With commercial materials, the crack growth mechanisms differ between [GMC](#), [GCMC](#), [CMC](#) and [C-C](#). Significant characteristics are:

- interface properties,
- fibre pull-out,
- reinforcement geometries, orientation and bundle size, and
- crack debris.

Once cracking occurs, the original low-strain, linear elastic modulus of the composite is lost. To quantify the toughness of the material, the crack propagation from length a to $a+\delta a$ is described. Four modes that can describe a load-displacement response are, Ref. [67-8]:

- Linear elastic: where the process is reversible, i.e. the specimen returns to zero strain on removal of the load, [See: [Figure 67.3.1](#)].
- Linear non-elastic: incremental permanent strains result after each increasing load application, [See: [Figure 67.3.2](#)].
- Non-linear elastic: change in residual modulus with displacement but no residual strain, [See: [Figure 67.3.3](#)].

- Non-linear non-elastic: permanent strain and nonlinear elasticity, [See: [Figure 67.3.4](#)].

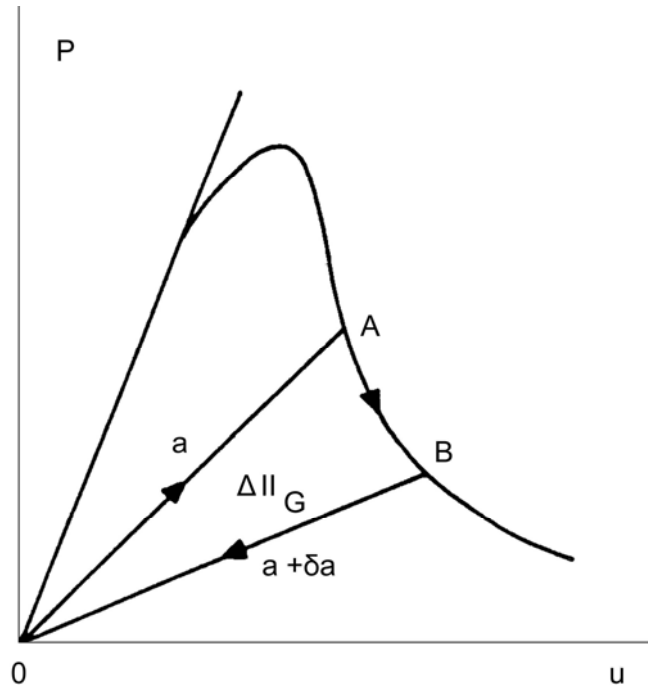


Figure 67.3-1 - Schematic representations of load-displacement (P/u) curves: (a)
Linear elastic behaviour

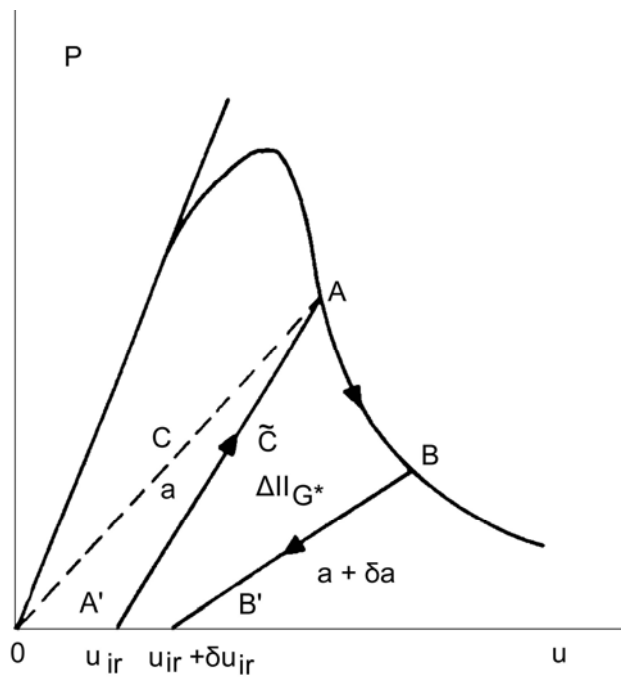
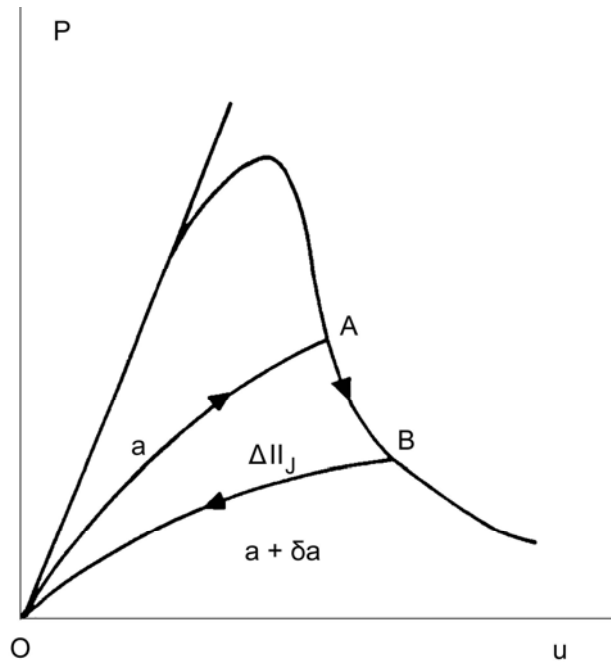
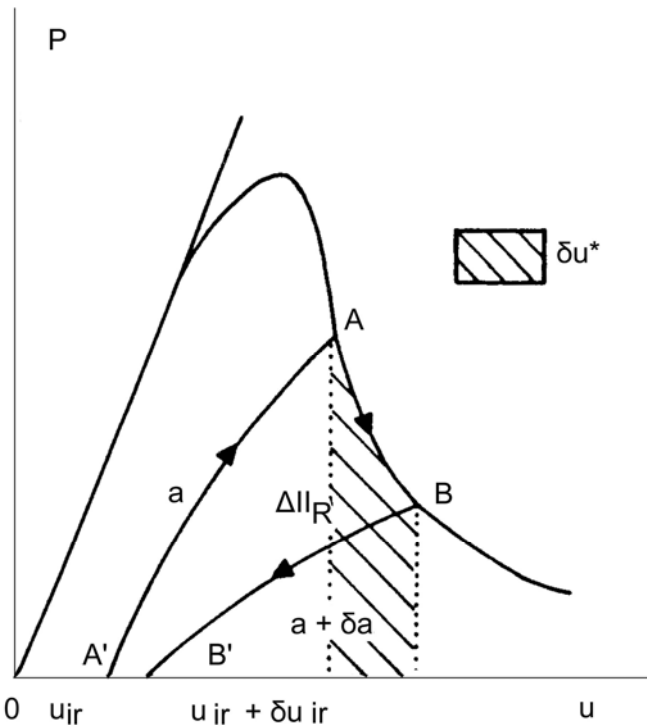


Figure 67.3-2 - Schematic representations of load-displacement (P/u) curves: (b)
Linear non-elastic behaviour



**Figure 67.3-3 - Schematic representations of load-displacement (P/u) curves: (c)
Non-linear elastic behaviour**



**Figure 67.3-4 - Schematic representations of load-displacement (P/u) curves: (d)
Non-linear non-elastic behaviour**

The reasons for a nonelastic response centre on the strained material being unable to return to its original volume, i.e. cracks do not fully close up. This can be explained by debris jamming the cracks or fibre pull-through. The nonlinearity suggests the fibre contribution to modulus is being reduced by applied load, presumably through fibres pulling through the matrix. Nonelasticity becomes

increasingly obvious as the composite strain nears its limit and more fibre pull-through and pull-out occurs.

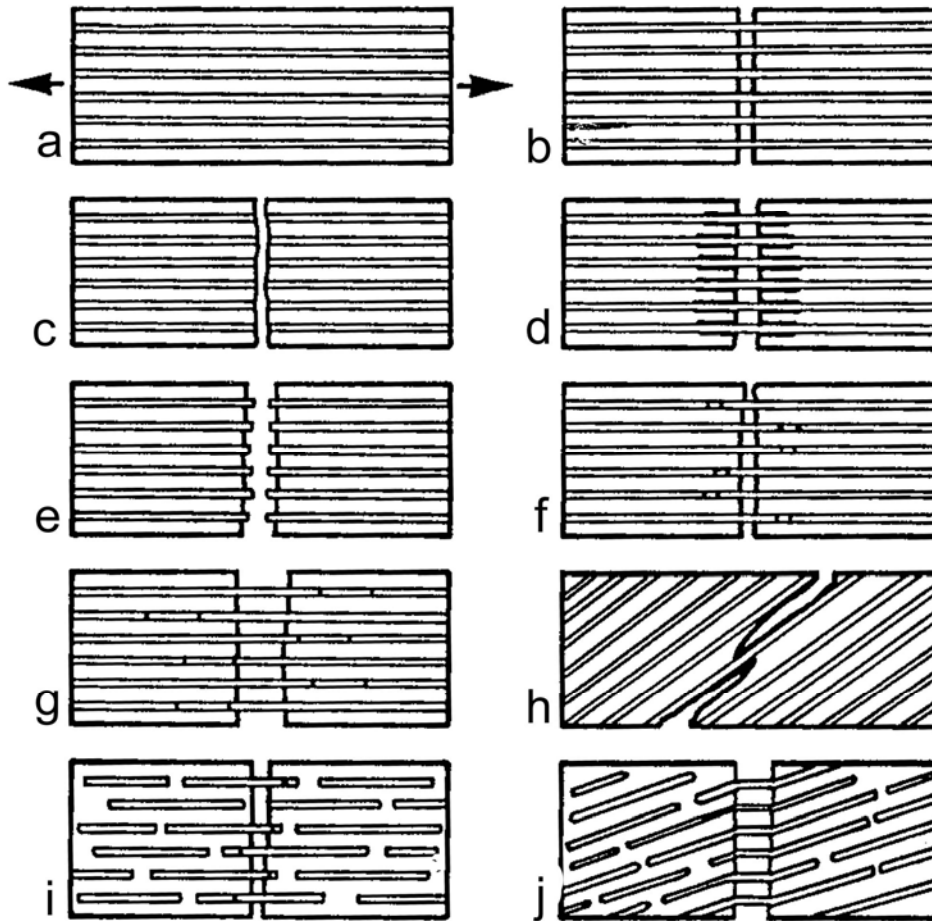


Figure 67.3-5 - CMC materials: Possible fracture mechanisms

Details of localised failure are shown in [Figure 67.3.5](#) and the sequence of events is described.

Under applied load, composite (a) experiences a matrix crack, as in (b). The critical stress in the interface is given by, Ref. [67-7]:

$$\sigma_f^D = \left(\frac{4E_f G_{IIC}}{r} \right)^{\frac{1}{2}} \quad [67.3-1]$$

Where:

E_f = Young's modulus of fibres

G_{IIC} = Mode II toughness of the fibre-matrix interface

r = radius of the fibres

Where the critical stress is greater than the fibre strength, a mode (c) failure occurs, which is undesirable in ICMC materials.

If $\sigma_f^D < \sigma_f^R$ (fibre stress), then fibre-matrix debonding occurs before fibre fracture. As loading continues the debonding extends and the fibres elongate while dissipating energy by friction on the matrix (d). If the fibre strength is not distributed (Weibull's modulus, m , high) the fibres break at the line of the matrix crack, as in mode (e).

The fracture energy, R is then:

$$R_2 = R_1 + \frac{V_f r (\sigma_f^R)^3}{3E_f \tau^*} \quad [67.3-2]$$

and:

$$R_1 = 2(V_f \gamma_f + V_m \gamma_f) \quad [67.3-3]$$

Where:

γ = surface energy

V = volume fraction

τ^* = shear friction stress at the interface

If the Weibull modulus of the fibres is small, the fibres have a non-negligible probability of breaking on one side or the other of the matrix crack, as in mode (f). Separation then requires the pull-out of the fibres, which leads to another important dissipation of supplementary energy, mode (g). Here:

$$R_3 = R_2 + \left(\frac{V_f \tau^* L_p^2}{3r} \right) \quad [67.3-4]$$

Where:

L_p = is pull-out length.

The pull-out length increases with σ_f^R and r , and with decreasing m and G_{IIC} or τ^*

Modes (h), (i) and (j) are further special cases.

67.3.2 Test specimens

67.3.2.1 Single edge notched beam (SENB) specimens

The SENB specimen is a popular means of obtaining data for '*R*' curves, Ref. [67-7]. The simplicity of a bend test does conceal that true tensile stresses do not occur in the notched face. There are shear stresses present which influence the details of crack propagation mechanisms.

A typical SENB specimen is shown in Figure 67.3.6. These are a useful qualitative way of comparing materials. Any quantitative results are considered with care.

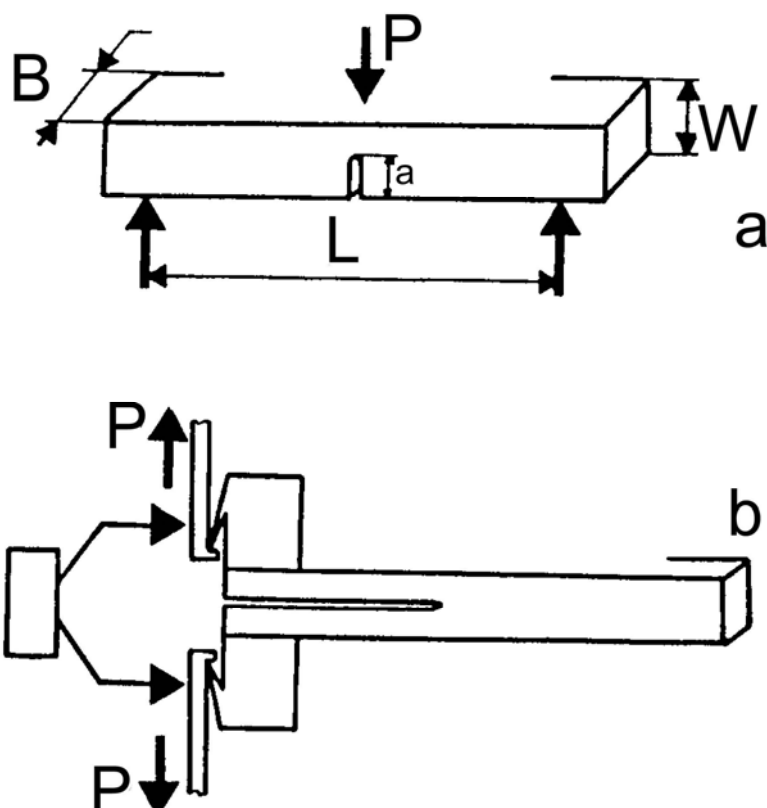


Figure 67.3-6 - SENB and delamination test specimens

67.3.3 '*R*' curves

An '*R*' curve presents a calculated fracture energy for the material against the change in crack length, Ref. [67-8], [67-9]. A plateau is usually reached once the crack length has reached a certain value, usually 1mm.

This is true for 2D and 3D continuous fibre composites. Short fibre, random composites show a different behaviour.

The *R* value for the plateau is usually in the range 2000 J/m² to 6000J/m². Examples of *R* curves are given in Figure 67.3.7 for short random fibre materials and Figure 67.3.8 for multidirectional materials.

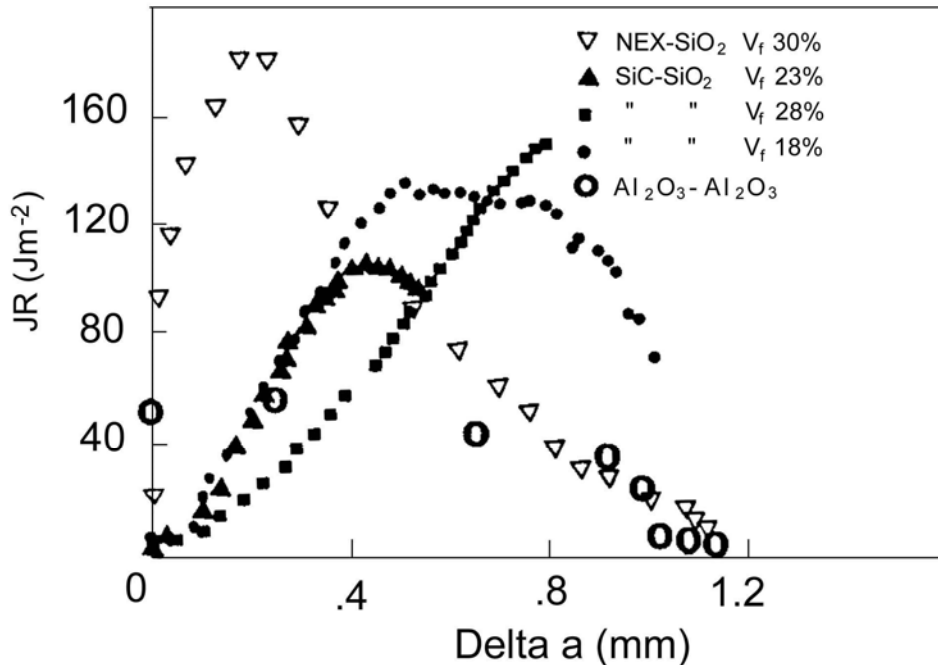


Figure 67.3-7 - Fracture energy (J , Rice) as a function of crack increment: Short random fibre materials

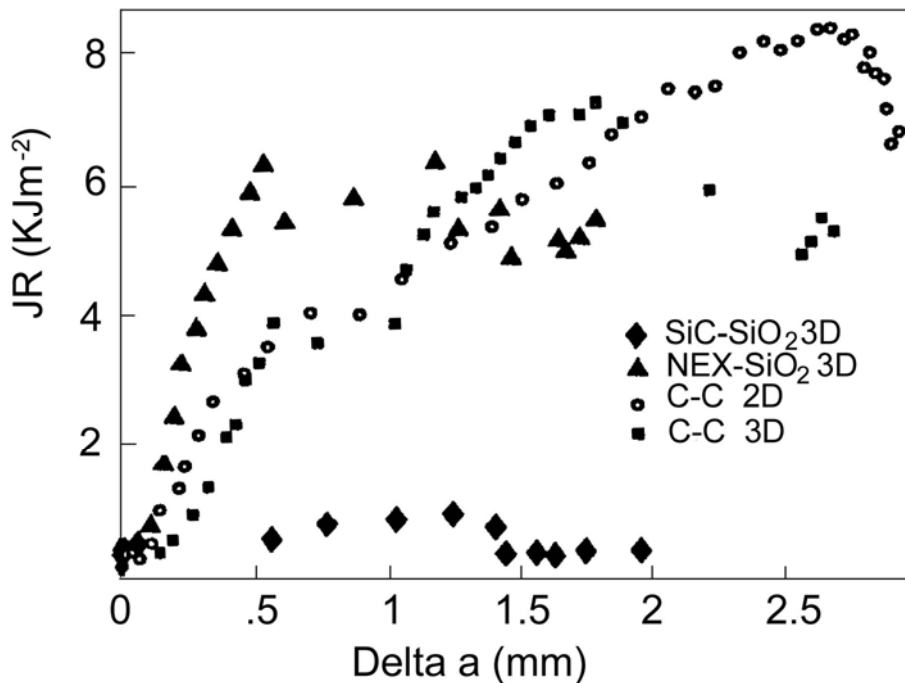


Figure 67.3-8 - Fracture energy (J , Rice) as a function of crack increment: Multidirectional materials

A rigorous comparison of different SiC-SiC and C-SiC composites, using the same specimen geometry, has yet to be conducted.

Various means of determining ' R' and ' J ' values are available. Work undertaken in France is the most detailed to date, Ref. [67-7], [67-10], [67-11].

67.4 References

- [67-1] I.M. Daniel et al
'Failure Mechanisms in Ceramic Matrix Composites'
Conference on Experimental Mechanics, 1989, p832-838
- [67-2] S. Mall & R.Y. Kim
'Failure Mechanisms in Laminates of Silicon Carbide/Calcium-Aluminosilicate Ceramic Composite'
Composites. Vol. 23. No 4. July 1992. p215-222
- [67-3] A. Chulya et al
'Damage Mechanisms in Three-Dimensional Woven Reinforced Ceramic Matrix Composites under Tensile and Flexural Loading at Room and Elevated Temperatures'
AIAA-92-2492-CP
- [67-4] A. Chulya et al
'Failure Mechanisms of 3-D Woven SiC/SiC Composites under Tensile and Flexural Loading at Room and Elevated Temperatures'
Ceram. Eng. Sci. Proc. 13[7-8], p420-432, 1992
- [67-5] E.P. Butler et al
'Interactions of Matrix Cracks with Inclined Fibers'
Ceram. Eng. Sci. Proc. 13[7-8], p475-482, 1992
- [67-6] D.S. Beyerle et al
'Damage Mechanisms and the Mechanical Properties of a Laminated 0/90 Ceramic/Matrix Composite'
J. Am. Ceram. Soc., 75 [12] p3321-3330 (1992)
- [67-7] H. Osmani et al
'Toughness, Microstructure and Interface Characteristics for Ceramic-Matrix Composites'
Composites Science and Technology 37 (1990) p191-206
- [67-8] J. Llorca & M. Elices
'Fracture Resistance of Fiber-Reinforced Ceramic Matrix Composites'
Acta. metall. mater, Vol.38, No. 12, p2485-2492, 1990
- [67-9] K.R. Stull & A. Parvizi-Majidi
'Fracture Toughness of Fiber-Reinforced Glass Ceramic Matrix Composites'
Ceram. Eng. Sci. Proc. 12[7-8], p1452-1461, 1991
- [67-10] M. R'Mili et al
'Energy Toughness Parameters for a 2D Carbon Fibre Reinforced Carbon Composite'
Composites Science and Technology 37 (1990) p207-221
- [67-11] M. Bouquot et al
'Toughness Assessment of Ceramic Matrix Composites'
Composites Science and Technology 37 (1990) p223-248
- [67-12] 'Fatigue and Fracture of Inorganic Composites'
Composites 24 No 2 (1993) p65-184 Part 1

68**Modelling advanced materials**

68.1 Introduction**68.1.1 Polymer composites**

The modelling of polymer composite fracture behaviour is not a precise science despite many years of research. The elastic behaviour can be described, i.e. prediction of modulus (stiffness), but strength values vary depending on the failure criteria applied, of which there are many, [See: Chapter 11].

68.1.2 Metal matrix composites**68.1.2.1 General**

The behaviour of MMC materials is even more difficult to predict than that of CFRP. MMC materials show true elasticity only to very low strain levels before plasticity in the matrix shows in the composite behaviour, Ref. [68-1]. The contribution of the metal matrix is significant because its modulus is similar to that of the reinforcement. Models therefore cannot ignore or minimise the matrix contribution, as is the case for polymer matrix composites.

68.1.2.2 Fibre reinforced MMC

The fibre reinforced MMC materials are close to CFRP in overall failure strain and models can be modified accordingly.

68.1.2.3 Particulate MMC

The MMCP materials conform to elastic models as far as initial stiffness predictions are concerned but accurate strength predictions can prove elusive. This primarily stems from the composite properties being matrix dependent. The microstructure and properties of the matrix are influenced by many parameters.

68.1.3 Inorganic ceramic matrix materials

ICMC materials contain only elastic phases, suggesting that good prediction of elastic constants is feasible. However, calculating ultimate strength is difficult because non-linear and non-elastic behaviour is apparent once significant microcracking and fibre pull-out occurs.

68.1.4 Summary of models

68.1.4.1 General

Some generic models are highlighted, Ref. [68-1].

68.1.4.2 Law of mixtures

The basic assumption of the law of mixtures is that the externally applied strain (in tension, compression or shear) is equal to the strains in all the phases present, i.e. reinforcement and matrix. The contribution of each phase is therefore directly dependent on its volume fraction within the composite. This simple method of modelling relies on all phases being elastic. It is therefore realistic to use this model to predict stiffness values of MMC and CMC materials but only to very low strain levels. The model can also provide reasonably accurate tensile strength values for unidirectional composites provided that fibre degradation has not occurred. For multidirectional MMC and CMC materials, the law of mixtures is inappropriate and gives high, inaccurate strength values.

68.1.4.3 Shear lag model

This is best suited to aligned short fibre reinforced composites; preferably with an even fibre distribution and with fibre alignment in the loading direction, Ref. [68-1]. It can be used in conjunction with the law of mixtures, but it is based on some simpler assumptions and gives a poorer approximation than more rigorous models. It has been applied to MMC materials to predict the flow stress during the plastic deformation seen in the stress-strain curve.

68.1.4.4 Laminated plate model

For laminate composites, i.e. most CFRP constructions, the basic element is a lamina of unidirectional composite with continuous fibres aligned in one direction. The overall behaviour of a laminate depends strongly on the stacking sequence of laminae which have different fibre orientations.

The laminate plate model provides an analytical tool with which to predict the overall mechanical or physical properties of the laminate. The most popular laminated plate model is based on a special lamina, an orthotropic plate under plane stress conditions. Such models are widely applied to polymer matrix composites and can predict strength reasonably accurately by summing the contributions of each lamina. Such models have been applied to MMC_f materials, but principally for the physical properties, thermal conductivity and thermal expansion.

68.1.4.5 Eshelby's models

Eshelby's models provide a more rigorous mathematical treatment of composites from a three-dimensional perspective, Ref. [68-1]. They are applicable to short fibre reinforced composites and can be modified to address particulate and continuous fibre MMCs. These models contain 'Eshelby's tensor' which is a function of the reinforcement geometry and the matrix Poisson's ratio when the matrix is isotropic. Eigenstrains can be incorporated for CTE mismatch strains and plastic strain in the matrix.

68.1.4.6 Other models

Several other rigorous models have been proposed. Among these, self-consistent models and those based on variational principles are the most popular. These are grouped by their applicability to various material types and described further.

[See: [68.2](#) for particulate-reinforced MMCs; [68.3](#) for fibre-reinforced MMCs; [68.4](#) for ICMCs]

68.2 Particulate reinforced metals

68.2.1 Use of models

The law of mixtures and shear lag approaches to material modelling have limited uses for describing particulate metal matrix composites, Ref. [68-1].

There is no consensus on which models are appropriate and various approaches are being put forward involving:

- Eshelby's models and equivalent inclusion method, Ref. [68-1], [68-2].
- Levy-Von Mises rules and equations, Ref. [68-3].
- Self-consistent philosophies, Ref. [68-1].
- Mori and Tanaka's average strain approach, Ref. [68-2].

The lack of consensus stems from a confusion created by the:

- Many different materials assessed, i.e. matrix and particulate combinations.
- Variations in fracture characteristics between composites.
- High proportion of plastic deformation in the yielding and fracture process.

68.3 Fibre reinforced metals

68.3.1 Use of models

The models applied include:

- Law of mixtures, Ref. [68-1], [68-4].
- Laminated plate, e.g. micromechanics with METCAN (Metal Matrix Composite Analyser), Ref. [68-1], [68-5], [68-6], [68-7].
- Gokhfeld shakedown theory of continua, Ref. [68-8].
- Power-law creep models, Ref. [68-9], [68-10].
- Vanishing fibre diameter (VFD) model, Ref. [68-11], [68-12], [68-13].
- Thermo-viscosity theory based on overstress (TVBO), Ref. [68-12].

The plastic element of MMC_f behaviour is the problematical feature. The models are largely theoretical and have yet to be rigorously proven. Most are in the form of 'in-house' software programs.

68.4 Inorganic ceramic matrix composites

68.4.1 Use of models

68.4.1.1 General

The 'Law of Mixtures' approach is appropriate for predicting the very low strain elastic constants before the onset of microcracking.

Any models for predicting strength require measurement of some fundamental material parameters, most notably:

- In-situ fibre strength
- Shear friction stress at the interface (τ)
- Mode II toughness of the fibre-matrix interface
- Surface energies

Modelling of ICMC behaviour is at the tentative level. Both elasticity and energy theories are being used to describe the progressive failure modes that produce non-linear effects, Ref. [68-4] to [68-9].

68.4.1.2 On-set of matrix cracking

$$\varepsilon_m = \left[\frac{12\gamma_m \tau}{d} \frac{V_f}{V_m} \frac{(1-\nu^2)^2 E_f}{E_m^2 E_c} \right]^{1/3} \quad [68.4-1]$$

where:

ε_m = matrix strain

γ_m = fracture energy of matrix

τ = shear stress

d = fibre diameter

V = volume fraction

ν = Poisson's ratio

suffixes:

m = matrix

f = fibre

c = composite

This relationship is the basis of the ACK analysis (Aveston-Cooper-Kelly). The crack initiation strain is increased by raising fibre volume fraction and reducing fibre diameter, Ref. [68-18].

68.4.1.3 Distance between cracks

Up to the saturation density:

$$\Delta = \frac{d\epsilon_m E_f}{2\tau} \frac{E_m}{E_f} \left(\frac{1-V_f}{V_f} \right)^{\frac{1-V_f}{V_f}} \quad [68.4-2]$$

Where:

$$\Delta = \text{matrix crack distance}$$

The corresponding stress is the 'Saturation Stress', (σ_s).

68.4.1.4 Crack 'closure' effect

Separation of the surfaces of a crack is restrained by fibre reinforcement. This 'closure' effect inhibits further crack growth. If fibres are broken or pulled through the matrix, the 'closure' effect is relevant within the immediate vicinity of the crack tip. Accordingly, crack initiation is controlled by a critical fracture toughness parameter of the matrix and friction forces at the interface between the fibre and matrix τ , Ref. [68-18].

$$\sigma_m = \left[\frac{12(1-\nu^2)K_c^2 \tau E_f V_f^2 (1-\nu^2)(1+\eta)^2}{E_m d} \right]^{1/3} \quad [68.4-3]$$

where:

$$\eta = \frac{E_f V_f}{E_m (1-V_f)}$$

Small fibre diameters and high volume fractions both inhibit matrix cracking. However, high τ values are inappropriate and fibre breakage is promoted by strong matrix-to-fibre bonding.

68.4.1.5 Crack growth parameters

The crack growth parameters described are, Ref. [68-20]:

\tilde{G} Potential energy release rate (crack extension force) for elastic behaviour.

G^* Potential energy release in non-elastic behaviour.

R Crack propagation resistance. When $G = R$, there is stable crack growth.

ϕ_{ir}	Irreversible deformation.
J	General relation of energy release rate used instead of G particularly for non-linear elastic behaviour.
J_s	Energy released in crack extension from a to δa
J_R	Parameter based on methods proposed by Rice et al for non-linear behaviour.
J_G	Relationship for non-elastic non-linear behaviour developed by Garwood.

This gives three types of distinguishable parameters:

- Elastic contribution: G , J_R and J_s
- Non-elastic contribution: ϕ_{ir}
- Total resistance: $J_{G^*}, R = J_s + \phi_{ir}$

Where J is usually of the same magnitude as R .

It is claimed that the fracture parameters J_R, ϕ_{ir} and R do not depend on either:

- specimen shape and size, or
- initial notch length.

Therefore, they can be considered as intrinsic fracture parameters with which to describe composite behaviour.

68.5 References

68.5.1 General

- [68-1] M. Taya & R.J. Arsenault
'Metal Matrix Composites: Thermomechanical Behaviour'
Book. Pergamon Press, 1989, ISBN 0-08-036983-9
- [68-2] N. Bourgeois et al
'Modelization of Microstructure Influence on the Macroscopic Properties of Discontinuously Reinforced MMCs'
Proceedings of the Microstructure and Properties of Metal Matrix Composites Conference, Roskilde, Denmark, 2-6 Sept. 1991 p235-240
- [68-3] S.M. Pickard & B. Derby
'The Deformation of Particle Reinforced Metal Matrix Composites During Temperature Cycling'
Acta Metall. mater. Vol.38, No.12, p2537-2552
- [68-4] D.M. Harmon et al
'Strength Predictions for Metal Matrix Composites'
ASTM STP 1032, 1989, p222-236
- [68-5] G.M. Nemez et al
'Thermal Cycling Response of Quasi-Isotropic Metal Matrix Composites'
Journal of Engineering Materials and Technology, Vol. 114 p156-191, 1992
- [68-6] C.C. Chamis & C.A. Ginty
'Fundamental Aspects and Failure Modes in High-temperature Composites'
SAMPE Quarterly, July 1990, p20-26. Also 35th SAMPE Symposium, 1990, p 492-503
- [68-7] C.C. Chamis et al
'Computational Simulation of High-Temperature Metal Matrix Composites Cyclic Behaviour'
ASTM STP 1080, 1990, p56-69
- [68-8] A.C.F. Cocks et al
'Effect of Cyclic Thermal Loading on the Properties of Metal Matrix Composites'
Journal of Thermal Stresses, 15: p 175-184, 1992
- [68-9] G.S. Daehn
'Effects of Environmental and Microstructural Variables on the Plastic Deformation of Metal Matrix Composites under changing Temperature Conditions'
ASTM STP 1080, 1990, p70-86

- [68-10] Y.S. Lee et al
'Modelling of Transverse Mechanical Behaviour of Continuous Fiber Reinforced Metal-Matrix Composites'
Journal of Composite Materials, Vol.25, May 1991, p536-555
- [68-11] W.S. Johnson et al
'Mechanical Characterisation of Unnotched SCS6/Ti-15-3 Metal Matrix Composites at Room Temperature'
ASTM STP 1080, 1990, p193-218
- [68-12] Nan-Ming Yeh & E. Krempl
'A Numerical Simulation of the Effects of Volume Fraction, Creep and Thermal Cycling on the Behaviour of Fibrous Metal-Matrix Composites'
Journal of Composite Materials, Vol.26, No.6, 1992, p900-915
- [68-13] W.S. Johnson
'Damage development in Titanium Metal-matrix Composites'
Composites 24 No3 (1993) p187-196 Part 2
- [68-14] J. Llorca & M. Elices
'Fracture Resistance of Fiber-Reinforced Ceramic Matrix Composites'
Acta. metall. mater, Vol.38, No. 12, p2485-2492, 1990
- [68-15] D.S. Beyerle et al
'Damage Mechanisms and the Mechanical Properties of a Laminated 0/90 Ceramic/Matrix Composite'
J. Am. Ceram. Soc., 75 [12] p3321-3330 (1992)
- [68-16] Wen-Shyong Kuo & Tsu-Wei Chou
'Modelling of the Thermomechanical Behaviour of Glass Matrix Composites'
Metal & Ceramic Matrix Composites: Processing, Modelling & Mechanical Behaviour. Edited by R.B. Bhagat et al, 1990
p311-318
- [68-17] L.R. Dharani
'Analysis of a Ceramic Matrix Composite Flexure Specimen'
ASTM STP 1080, 1990, p87-97
- [68-18] D. Sygulla et al
'Integrated Approach in Modelling, Testing and Design of Gradient-CVI Derived CMC Components'
AGARD Workshop 'Introduction of Ceramics into Aerospace Structural Components', 21/22 April 1993, Antalya, Turkey
- [68-19] 'Fatigue and Fracture of Inorganic Composites'
Composites 24 No2 (1993) p65-184 Part 1
- [68-20] M. R'Mili et al
'Energy Toughness Parameters for a 2D Carbon Fibre Reinforced Carbon Composite'
Composites Science and Technology 37 (1990) p207-221

69

High-temperature structures

69.1 Introduction

69.1.1 Applications

Space applications for high-temperature materials are normally associated with:

- Launcher propulsion systems,
- Re-entry vehicles,
- Hyper-velocity transport (spaceplanes),
- Planetary exploration spacecraft.

[See also: [69.9](#)]

69.1.2 Performance

Each application has a range of different performance criteria. All have combined thermal and mechanical requirements that can push materials close to their limits of physical stability. The key issues to be resolved include:

- Structural functions [See: [69.2](#)],
- Operating environments [See: [69.3](#)],
- Structural integration [See: [69.4](#)],
- Heat management [See: [69.5](#)],
- Life expectancy [See: [69.6](#)],
- Mass budgets,
- Materials selection [See: [69.7](#)],
- Manufacturing [See: [69.8](#)].

69.1.3 High-temperature materials

The external temperatures experienced on re-entry can range from 400°C to almost 2000°C for some regions of RLV concepts.

Most applications far exceed the thermal capabilities of fibre-reinforced polymer composites ([FRP](#)) or conventional [aluminium](#) based materials (250°C to 350°C), so metal-, carbon- and ceramic-based materials are used, often as combinations of alloys, composites and fibrous insulation.

[See also: Chapter [42](#)]

69.1.4 Development approach

As space programmes evolve there is a continuing pressure to improve the mass efficiency of structures, Ref. [\[69-1\]](#), [\[69-2\]](#), [\[69-3\]](#), [\[69-4\]](#). This is generally achieved by use of improved materials and design concepts. Often more than one solution can satisfy a structural requirement.

Within Europe, high-temperature material development programmes have tended to be flight-vehicle biased, e.g. materials technology developed for thermo structures or thermal protection systems within a particular vehicle concept. The technology can then be applied, if appropriate, to future programmes.

A NASA review (2007) of European hot-material capabilities for thermo structures and TPS concluded, Ref. [\[69-7\]](#):

- A lot of good development work is being done in Europe.
- Strong emphasis is placed on CMC and metallic TPS, with CMC tile TPS having a higher technology readiness level than metallic (whereas the situation is reversed in the USA).
- Companies tend to have niche technologies with little competition in that area,
- Companies collaborate a great deal.
- Many of the companies have both the fabrication and design expertise within the same organisation.
- Europe appears focused on developing technology for flight experiments, but understands that flight experiments sometimes fail and moves on.

[See: [69.9](#)]

69.2 Functions

69.2.1 General

Heat energy and high temperatures are generated by:

- aerodynamic effects at high speed.
- combustion of fuels for propulsion.

Both give a wide spectrum of temperatures, originating at localised regions of extremely high heat flux. Surrounding areas experience a diminishing temperature gradient away from the focal point. The duration of heating defines the overall heat management problem.

69.2.2 Aerodynamic heating

69.2.2.1 Heat flux

The external surfaces of spaceplanes, re-entry vehicles and capsules experience heating when passing through gaseous environments at extremely high velocities. The heat flux experienced is structure dependent but typically varies between 0.5MW/m^2 and 15MW/m^2 . Higher localised fluxes can be experienced for some SSTO vehicles or planetary capsules. In spaceplane designs, this can result in surface temperatures up to 1700°C .

To withstand the peak temperatures, ceramics should be in the form of:

- Rigid composites (C-SiC, SiC-SiC),
- Fibre felts and cloths, or
- Rigid foams.

Lower temperatures can be tolerated by metallic systems based on nickel superalloys or titanium.

The external surface of spaceplanes can therefore be made from a range of materials depending on the temperature distribution. The aerodynamic surfaces perform a thermal-barrier function in conjunction with a load-carrying role.

They can be classified as either, Ref. [69-5], [69-6]:

- thermo-structural designs, [See: Chapter 70], or
- thermal protection systems (TPS), [See: Chapter 71].

69.2.2.2 Other factors

The design and material selection is influenced by:

- Surface catalicity,
- Oxidising species,
- Material thermal conductivity,
- Life requirements (single or multiple mission),
- Acoustic response,
- Proven experience.

Ablative materials are an option for missions with only a single re-entry [See: 71.4 - Ablative designs].

69.2.3 Propulsive power generation

69.2.3.1 Fuels

A range of fuels can be burnt, including:

- Solid fuels for boosters,
- Liquid H₂/O₂,
- Monopropellants for thrusters,
- Bipropellants for thrusters, e.g. MMH/NTO.

69.2.3.2 Temperature

All propellants produce extremely high gas temperatures (>2500°C) from which the containment materials are protected by controlled gas flows and the use of cooling. This ensures that these containment materials remain at temperatures within their capabilities.

For the range of possible service temperatures these include:

- Carbon-carbon to 2000°C (possibly 2500°C),
- SiC-SiC to 1600°C,
- Niobium alloys to 1400°C,
- Titanium alloys to 600°C,
- Copper alloys to 540°C.

69.2.3.3 Spaceplanes

With the advent of spaceplanes (SSTO or TSTO), the range of propulsion-system designs has broadened to include:

- Air-breathing engines,
- Scram-Jets,
- Ram Jets.

All propulsion systems experience a spread of temperatures away from the region of fuel combustion, enabling a range of different materials to be used in the reduced temperature zones.

For spaceplane concepts, the main propulsion unit and the necessary air intakes are usually integrated into the airframe and external aerodynamic profile.

69.2.3.4 Other design factors

Additional parameters affecting designs include:

- Oxidative and corrosive exhaust gases,
- Thermal shock,
- Material compatibility with fuels,
- Optimum life requirement,

- Specific impulse,
- Active cooling,
- Material limitations.

69.3 Operating environments

When materials are used at high temperatures, there is a narrow margin between stability and unacceptable material degradation. In general, the shorter the life requirement, the higher the operating temperature.

For reusable structures, a sufficient margin is established in order to guarantee material and structural integrity for multiple missions.

The operating environment for hot structures imposes a range of conditions, which, compounded, can give mechanisms for material failure, including:

- Thermal cycling,
- Thermal shock,
- Thermo-mechanical fatigue (TMF),
- Oxidising and corrosive gases,
- Embrittlement (effects of hydrogen or cryogenic conditions),
- Aggressive fuels,
- Impact,
- High temperature creep.

[See: Chapter [83](#) for thermo-mechanical fatigue; Chapter [85](#) for high-temperature environmental stability]

69.4 Integration

Hot structures are integrated with the cooler parts of the vehicle:

- The loaded, hot external aerodynamic surfaces of the spaceplane are connected to the cooler, primary airframe structures.
- Thrust from a hot propulsion unit is transmitted to the vehicle via a suitable load path.

Integration takes into account:

- Differences in thermal expansion between components,
- Joining techniques, [See: Chapter [60](#) and Chapter [61](#)].
- Assembly methods.
- Inspection, [See: Chapter [80](#)].
- Seal technologies, [See: Chapter [75](#)].

69.5 Heat management

The generation of high thermal fluxes and energy densities at the surface of a component or structure creates problems in heat management. The amount of heat absorbed is determined by:

- Surface emissivity,
- Material thermal conductivities,
- Specific heat capacities,
- Gas flow velocities and heat capacities,
- Overall thermal inertia,
- Location of thermal insulation,
- Opportunities for active cooling.

Heat management is a controlling factor in the design of thermal protection systems ([TPS](#)), [See: Chapter [71](#)].

69.6 Life expectancy

69.6.1 General

The greater the life expectancy placed on a component or structure, the greater the opportunity for a degradation mechanism to occur that can compromise material integrity.

Life expectancy is determined by:

- Maximum temperature,
- Thermal shock,
- Time at temperature,
- Number of thermal cycles,
- Presence of corrosive species.

In propulsion systems, material erosion is permissible provided that it is constrained to acceptable levels within the defined operating life.

69.6.2 Launcher

Total life expectancy for a launcher main engine is a matter of minutes for a single launch cycle.

69.6.3 Spaceplane

The engine can be operational for a few tens of hours with possibly one hundred cycles. A similar life requirement is applicable for the vehicle [TPS](#).

69.6.4 Satellite

A satellite attitude control thruster has a few hours total use, but this can be spread over 5000 firings (thermal cycles) under acute oxidising conditions at 1400°C.

69.7 Materials selection

The selection of an appropriate structural material is largely influenced by:

- Maximum operating temperature,
- Life expectancy,
- Operating environment,
- Availability of technology,
- History of proven performance.

Given that surface behaviour is all important in high-temperature environments, coatings have an important role in protection and compatibility. Coatings provide:

- Oxidation and hot corrosion protection,
- Controlled catalytic response,
- Desired emissivity.

[See: Chapter 74]

69.8 Manufacturing

High-temperature materials require specialised process techniques which are capital intensive. Net-shape or near net-shape forming processes are common as the finished materials are difficult to process. The overall designs are therefore strongly influenced by the availability of manufacturing facilities and expertise. Sound reasons can be put forward for using materials with lower cost manufacturing routes in preference to more costly, though perhaps technically more desirable, options.

- Superplastic forming and diffusion bonding (SPF/DB) enables production of complex designs in titanium sheet.

[See: Chapters 47 and 72 for Ti-alloys; Chapter 88 for manufacturing techniques]

- CMCs can be produced by resin pyrolysis or sol-gel routes at a lower cost than that of chemical vapour deposition (CVD/CVI).

[See: Chapter 52 for CMCs; Chapter 88 for manufacturing techniques]

- Load transfer can be achieved by a range of methods each of which has various attractions and limitations.

[See: Chapters 58, 59, 60, and 61]

69.9 Applications

69.9.1 Future reusable launch vehicles

69.9.1.1 European perspectives and objectives

Research and development on TPS and hot structures is crucial for future space vehicles. In general, the high-temperature material technologies can be grouped as:

- Flight-vehicle dependent.
- Non-vehicle dependent.

According to a NASA review in 2007, the next generation of TPS and hot-structure technologies are under development within Europe for numerous experimental launch vehicles concepts (whereas the USA is seen to have concentrated on Space Shuttle-derived technology). Other comments can be summarised as, Ref. [69-7]:

- European TPS and hot structure emphasis:
 - Development of ceramic matrix composite and metallic TPS with fibrous insulation.
 - Larger unit item size (reduced part count).
 - More durable (reduced inspection and repair).
 - Development of ceramic matrix composites and metallic hot structures.
 - No ceramic tile development.
 - Only limited developments using blanket insulation.
 - Waterproofing generally not necessary.
- Technology development has a broad base, including:
 - Fabrication.
 - Testing facilities, developed for TPS and hot structures, e.g. thermal/structural test chamber; arc-jet tunnels.
 - Large components.
 - Fasteners.
 - Bearings.
 - Oxidation protection.
 - Damage repair.
 - Life cycle.
- Long-term funding is based on technology needs. Europe-wide industry support and financial commitment to X-38 program, with significant resources available for future space vehicle TPS and hot structures:
 - C/SiC body flaps (estimated US\$ 20 million); Technology developments (estimated US\$ 50 million by Germany).
 - Many companies committing resources in developing C/SiC hot structures.

- Large thermal/structural test chamber developed specifically for verification of hot structures.

69.9.2 Flight-vehicle dependent

69.9.2.1 Summary of concept vehicles

Many concepts for RLVs of various complexities have been proposed. All of these vehicles have thermo-structures or TPS and hence contribute to the technological advances made with high-temperature materials. The expertise and experience gained during these earlier programmes has contributed to recent vehicle concepts:

- Space Shuttle Orbiter (USA), [See also: [71.5](#)]
- BURAN (ex-USSR) , [See also: [71.6](#)]
- Hermes (Europe), [See also: [70.3](#)]
- HOPE (Japan), [See also: [70.4](#)]
- HOTOL (UK), [See also: [70.5](#)]
- Sänger (D), [See also: [70.6](#)]
- X-program vehicles, e.g.
 - X-33.
 - X-38, [See also: [70.23](#) – body flap; [70.24](#) – nose cap].
 - X-43, part of NASA's Hyper-X program to develop a hypersonic air vehicle powered by an air-breathing engine.
 - X-51 'WaveRider', NASA's scramjet engine demonstrator (SED-WR), to undergo test flights end-2009 into 2010.
- NASP or X-30 (USA), [See also: [70.7](#)], an air-breathing SSTO single stage to orbit concept vehicle.
- Hopper (D), an unmanned commercial launcher system that forms part of the Phoenix programme. Intended to test technologies. A joint initiative by Daimler-Chrysler Aerospace with a consortium of industrial and scientific partners (started in 1999).
- Foton (Russia), a flight experiment test-bed (15 days in orbit) for DLR's LSI - liquid silicon infiltration C/C-SiC, [See: [52.3](#)] and protective coatings (yttrium silicate), [See also: [71.17](#)].
- PRORA-USV unmanned space vehicle (I), funded by Italian Space Agency / CIRA, an orbital FTB (flying test bed) for technology development of sharp hot structures (wing leading edge and nose cap), [See: [70.22](#)].
- IXV - Intermediate Experimental Vehicle (ESA), part of ESA FLPP, run by NGL Prime, joint venture of Astrium (F, D) and Finmeccanica (I), PDR end of 2007, first flight end of 2010.
- EXPERT - European eXPERimental Re-entry Testbed (ESA): Flight Experiment TPS, comprising a blunt cone configuration with a pyramidal shape (called KHEOPS) having four flat surfaces, each with a fixed flap (two fixed flap settings).
- SHEFEX - Sharp Edge Flight Experiment (D), which is DLR-funded to evaluate performance of multi-facetted leading edges. Flew October 2006 (Mach 7 between 90-20 km, 300km apogee)

- SHyFE - Sustained Hypersonic Flight Experiment (UK), which is funded by UK Ministry of Defence, to design and fly a prototype ramjet capable of sustained hypersonic flight. 1st flight August 2009, 2nd flight in 2010.
- LEA (F), by MBDA and ONERA, destined Mach 4 to 8 test flights between 2010 and 2013. Key technology fuel-cooled composite structures for combustion chambers.

[See also: [71.1](#) for description of other European programmes which have contributed to TPS technologies]

69.9.2.2 Summary of high-temperature structural materials

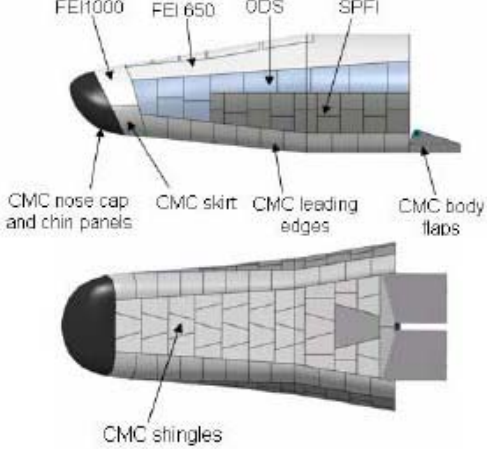
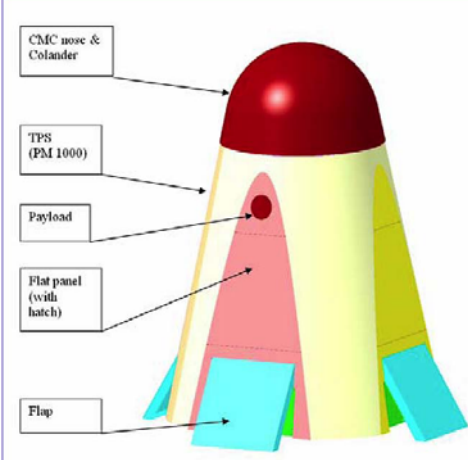
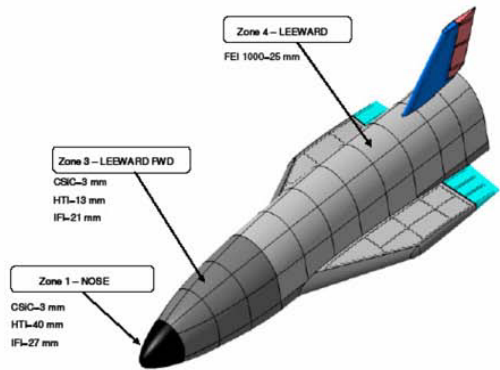
[Table 69.9.1](#) summarises the various high-temperature material technologies developed for the thermo structures and TPS of particular vehicle concepts, Ref. [\[69-7\]](#).

69.9.2.3 Summary of hypersonic engine materials technologies

The propulsion systems of several of the hypersonic concept vehicles rely on air-breathing scramjets. Development engines use hydrogen or hydrocarbon fuels, Ref. [\[69-10\]](#), [\[69-8\]](#). Other materials, such as silanes, are also suggested. Materials for scramjets need to demonstrate extreme combined thermal and chemical resistance, [See also: Chapter [73](#)]. Engine concepts tend to use:

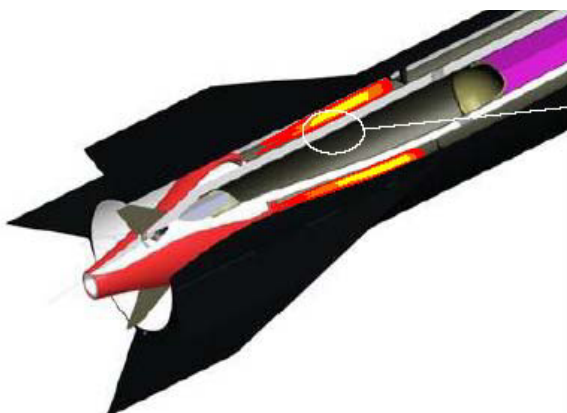
- High-temperature alloys, often cooled by the fuel, [See also: [48](#) – superalloys; [49](#) – intermetallics].
- Ceramics or CMCs, [See: [52](#)], either uncooled or cooled, e.g. Cooled C/SiC CMC concepts destined for the hydrogen fuelled French LEA scramjet, Ref. [\[69-9\]](#); DLR's CMC combustion chamber in Germany, Ref. [\[69-7\]](#).

Table 69.9-1 – Summary of high temperature materials technologies: Flight-vehicle dependent

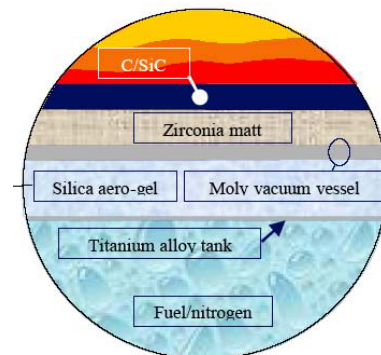
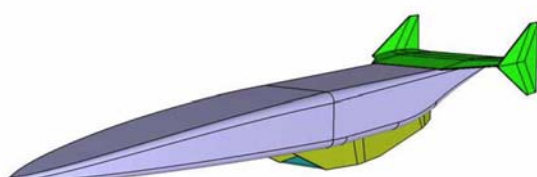
IXV - Intermediate Experimental Vehicle (ESA)	
	Leeward and base side : FEI flexible external insulation (FEI 1000, 650, 450), [See: 71.11] ODS metallic TPS: Metallic sandwich TPS stainless steel hollow sphere core; HollowMet ODS hollow sphere core (Alcatel Alenia Space (I) & and Plansee (A)); Metallic honeycomb TPS TIMETAL 1000; ODS superalloys based on IN 617 (Dutch Space)
EXPERT - European experimental re-entry test bed (ESA) - KHEOPS	
	C/SiC nose cap (DLR) EXPERT metallic TPS (Plansee PM 1000) CMC open flaps (MT Aerospace)
USV - unmanned Space Vehicle (I)	
	UHTC ultra high temperature ceramics: <ul style="list-style-type: none"> - Nose: bulk graphite core; truncated conical C/SiC frame (Fabbricazioni Nucleari), with ZrB₂-SiC coating on C/SiC frame by plasma spray (Centro Sviluppo Materiali); UHTC conical tip from hot pressing (National Research Council Institute for Ceramic Materials) - Wing leading edge: Actively cooled: Inconel; UHTC. Hybrid sandwich panel (to 2000°C on windward surface) with C/C face sheets, carbon foam core. - Leeward surface: MMC of Ni sheets and SiC/Al₂O₃ fibres
	.../continued

SHEFEX - Sharp Edge Flight Experiment (D)

CMC's with some metallic TPS (C/C-SiC leading edge; CMC LSI panels liquid silicon infiltration process (DLR); Fibrous matt insulation, [See: [71.12](#)]; CMC fasteners)

SHyFE - Sustained Hypersonic Flight Experiment (UK),

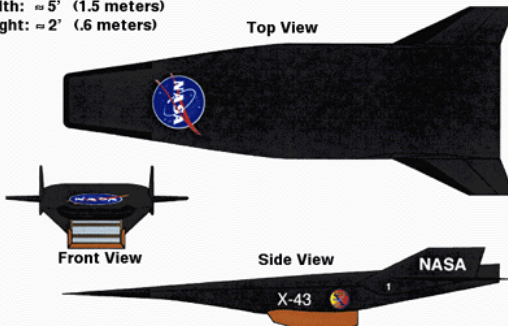
C/SiC used for vehicle construction:
almost entire flight experiment is CVI
C/SiC (MT Aerospace)
Titanium alloy tank

**LEA (F)**

Actively-cooled composite combustion chamber:

- A3CP - C/SiC Novoltex CVI, with machined cooling channels. Brazing of another sheet of C/SiC Novoltex.
- Sepcarbinox® CMC C/SiC
- PTAH-SOCAR monoblock structure obtained by weaving with stitching yarns through removable mandrel (burn-out), liquid densification

.../continued

X-program vehicles (USA)	
X-43A - Hyper-X	 <p>Length: ≈ 12' (3.7 meters) Width: ≈ 5' (1.5 meters) Height: ≈ 2' (.6 meters)</p>  <p>The X-43A was a hypersonic aircraft developed by NASA. It had a black, aerodynamic body with a distinctive pointed nose and a flat underside. The aircraft was primarily used for testing air-breathing scramjet engines. It completed its flight trials in 2004, reaching a maximum speed of Mach 9.6.</p> <p>X-43A known as Hyper-X completed flight trials in 2004 and flew at Mach 9.6 for a few seconds, X-43A has a tile-based C-C TPS (Boeing) and high-temperature resistant metals that also resist shock waves forces on the airframe generated in hypersonic flight. The air-breathing scramjet (developed by ATK) uses gaseous hydrogen fuel. The copper-based engine was not designed to survive the test flight. Ref.[69-13]</p>
X-51 - WaveRider	 <p>Test flights (end-2009 – 2010) to fly hypersonic (> Mach 6) for 5 minutes using air-breathing hypersonic scramjet. The vehicle obtains some lift from its shock waves in-flight. The Pratt & Whitney X-51 'Falcon' engine is made from standard Ni-alloy and cooled during flight by its fuel. Ref. [69-13]</p>

69.9.3 Non-vehicle dependent

69.9.3.1 General

Some broad categories created to classify applications for high-temperature materials include:

- Thermo-structural designs, [See: Chapter 70],
- Thermal protection systems (TPS), [See: Chapter 71],
- Propulsion technologies, [See: Chapter 73],
- Protective coatings, [See: Chapter 74],
- Seal technologies, [See: Chapter 75].

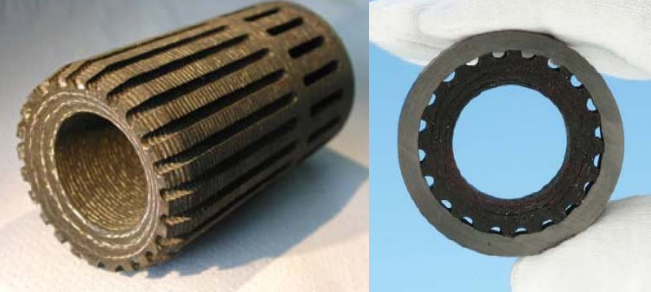
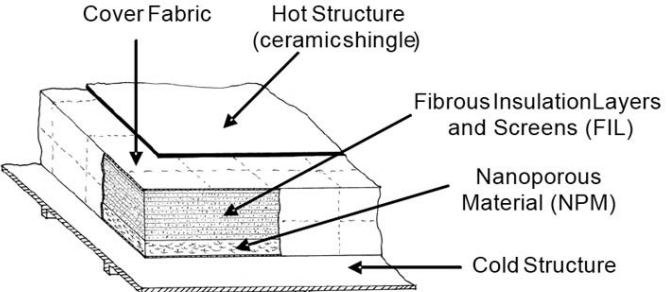
These Chapters contain a series of case studies describing aspects of design and materials selection. Many of the concepts have not necessarily been applied or flown.

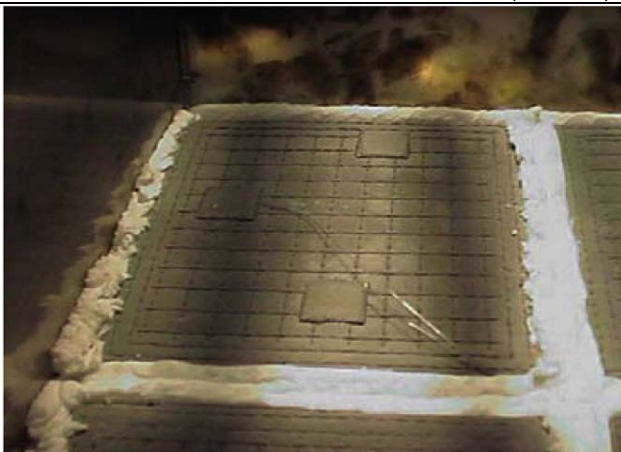
69.9.3.2 Technologies

High temperature material developments for non-vehicle specific RLVs tend to be associated either with TPS or scramjet propulsion systems. Some TPS developments evolved from previous work, e.g. layered insulation materials, panels.

Within Europe, ESA funds work within the framework of future launcher programmes, e.g. FLPP-1 Materials and Structures Program. Some examples of technologies developed that are not vehicle-specific are summarised in [Table 69.9.2](#), Ref. [69-7], [69-12].

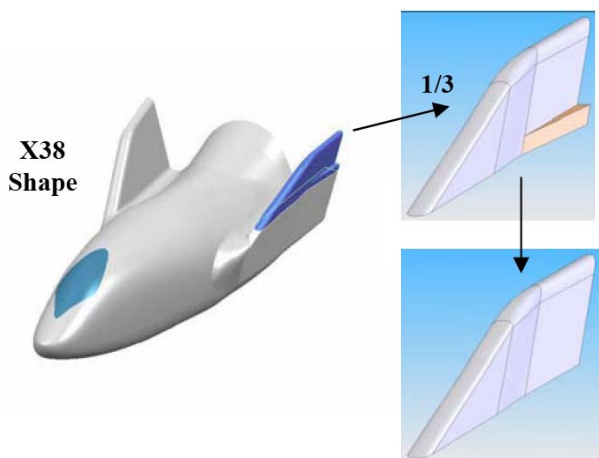
Table 69.9-2 – Summary of high temperature materials technologies: Non-flight vehicle dependent

Actively cooled CMC thrust chamber (DLR)	 <p>C/C used for inner material (porosity 13% to 22%; 0°/90° lay-up; 10 mm thick) Temperature gradients (1000°C/mm due to low k of 1 W/mK to 1.2 W/mK; 30 mm chamber diameter) CFRP jacket (internal pressure loads; longitudinal compression loads due to attachments and thrust; 5 mm thick.; needs H₂ barrier)</p>
MLI - multi-layer insulation (MT Aerospace)	 <p>Medium Temperature (~1000°C): Weight limit* 4 kg/m² and 40 mm thick; Nextel 312 fabric containment; Pryogel superior to Microtherm (density, vibration, humidity, handling); Consists of IMI and Pyrogel (6 mm). High Temperature (~1600°C): Limits* 8.5 kg/m², 80 mm; Nextel 440 fabric containment; IMI [See also: 71.10] with Zircar APA-2 for highest temperature regions and Pyrogel for lower temperature regions. Seals (DLR): Saffil filled Nextel 312 bag impregnated by MTMS (up to 1300K); Saffil filled Nextel 440 bag impregnated by MTMS (up to 1900K); Kept in place by C/SiC guard.</p> <p>* ESA imposed limit .../continued</p>

FEI - flexible external insulation (EADS)

FEI blankets new developments:
High emittance coating developed
with better stability; Less toxic
waterproofing for initial and re-
waterproofing (now methyl
triethoxy silane); Refurbishment
and repair procedures defined;
Applied to FEI-1000 blankets and
subjected to 10-flight
environmental testing; Water-
proofing and coating refurbished
after 4 cycles.

[See also: 71.11]

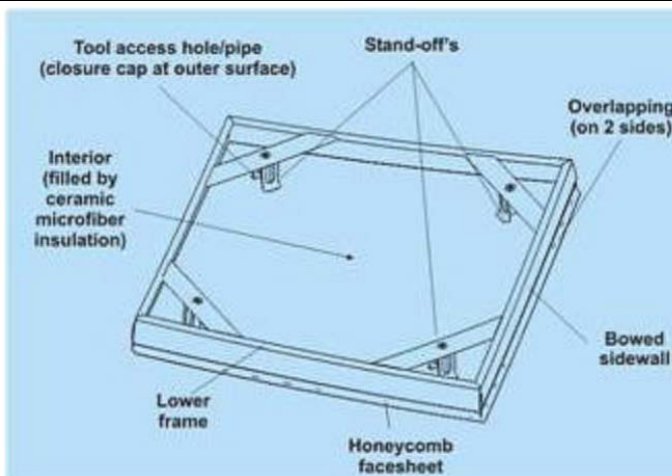
Hybrid Metal/CMC Winglet Hot Structure (Alenia)

General configuration: 1/3 size
of X-38, removed hinge step.
Design and analysis complete,
with fabrication and PWT test
planned.

Outboard panel and wing leading
edge: MT Aerospace C/SiC, 3
mm thick

Inboard (3 panels): Plansee PM
2000, 1 mm thick with 2 mm
thick ribs

Seals: Nextel wrapped Saffil

ULTIMATE Metallic TPS (EADS)

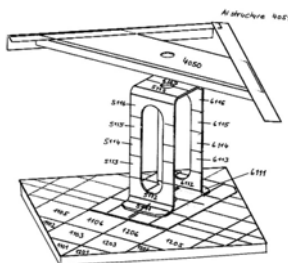
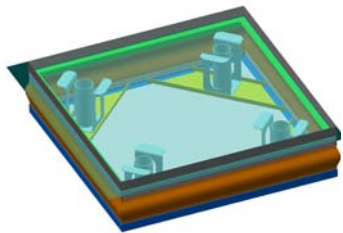
General configuration: Load-
carrying metallic box with
standoffs and internal
insulation; Outer surface
honeycomb sandwich (10 mm
thick, hexagonal cells); γ -TiAl;
 Ω -standoffs. SHEFEX flight
similar to ULTIMATE design.

Panel size: Development 200mm \times
200mm; Final design 500mm \times
500mm;

Panel test (Vibration*, Acoustic,
Thermal to $\sim 850^{\circ}\text{C}$); Assembly
tests (Vibration*, Thermal IR,
PWT)

* HOPPER loads

.../continued

MERIT Metallic TPS (EADS)

Further development of ULTIMATE using a β -Ti alloy instead of the γ -TiAl in ULTIMATE. Reason for change: Aluminide brittle at RT.

ESA-funded study within the framework of FLPP-1 Materials & Structures Program.

Passive-to-Active Oxidation (Germany)**Research into a reproducible phenomenon seen during PWT tests.**

Under some steady state conditions, a small increment in energy (1 mm closer) caused a small hot spot that within 30 seconds covered the entire sample with a temperature of 2050°C.

Cause of temperature rise at passive to active transition attributed to half energy released during active oxidation from oxidative reactions, half from nitrogen recombination (tested with N₂ plasma, low oxygen).

Effect seen at: 1720°C/800 Pa, 1700°C/500 Pa, 1720°C/800 Pa, 11800°C/2000 Pa, 1840°C/3500 Pa, 1940°C/7000 Pa

69.9.4 Summary of European capabilities

European capabilities for high-temperature materials destined for hot-structures and TPS are summarised in Table 69.9.3, Ref. [69-7]. It is not an exhaustive list.

Table 69.9-3 – Summary of high temperature materials technologies: European expertise

Organisation (Country)	Activities
ESA (F) ESTEC (NL)	Future launchers programs.
MT Aerospace (D) (formerly MAN Technologie)	CVI C/SiC hot structures fabrication and design.
DLR (D)	LSI C/C-SiC hot structures and general hot structures design.
Plansee (A)	High temperature metal (Ti, Superalloy, intermetallics and refractory metals) fabrication.
IABG (A)	Hot structures testing.
SNECMA (F)	CVI C/SiC acreage TPS fabrication and design.
Dutch Space (NL)	Metallic TPS and hot structures fabrication and design.
EADS-Astrium Group (Europe-wide, D and F)	Complete portfolio of TPS and hot structures design.
CIRA (I)	Aerospace R&D Centre, world's largest PWT.

69.10 References

69.10.1 General

- [69-1] ESTEC Workshop - Advanced Structural Materials : Design for Space Applications
23-25 March 1988
ESA WPP-004 (October 1988)
- [69-2] ESA Symposium on Space Applications of Advanced Structural Materials
March 1990
ESA SP-303, p227-232
- [69-3] Proceedings of the International Conference: Spacecraft Structures and Mechanical Testing
ESTEC, 24-26 April 1991
ESA SP-321, p299-308
- [69-4] ESA Symposium on Advanced Materials for Lightweight Structures
March 1992; ESA SP-336
- [69-5] Proceedings of a NASA Workshop: Current Technology for Thermal Protection Systems
11-12 February 1992, Langley Research Centre, Virginia
NASA Conference Publication 3157
- [69-6] First ESA/ESTEC Workshop on Thermal Protection Systems
ESTEC, Noordwijk, 5-7 May 1993
ESA-WPP-053 (August 1993)
- [69-7] D.E. Glass: NASA Langley Research Center (USA)
'European Directions for Hypersonic Thermal Protection Systems and Hot Structures'
31st Annual Conference on Composites Materials and Structures, Daytona Beach, Florida, USA, January 2007
- [69-8] G. J. Dadd et al: QinetiQ - Farnborough (UK)
'Sustained Hypersonic Flight Experiment (SHyFE)'
Paper: AIAA 2006-7926, 14th AIAA/AHI Space Planes and Hypersonic Systems and Technologies Conference, Canberra, 6-10 November, 2006
- [69-9] L. Serre & F. Falempin: ONERA/MBDA (F)
'French R&T Activities on High-Speed Airbreathing Propulsion'
14th AIAA/AHI Spaceplanes & Hypersonic Systems & Technologies Conference, Canberra, 6-10 November, 2006
- [69-10] M.R. Tetlow et al: University of Adelaide (Australia)
'Orbital Payload Delivery using Hydrogen and Hydrocarbon-fuelled Scramjet Engines'
Presented at IEEE Aerospace Conference 2006.
- [69-11] W P.P. Fischer & Jörg Bolz et al: DaimlerChrysler Aerospace Bremen, (D)
'SPFI - A New TPS for Re-entry Vehicles'
SAE Paper 1999-01-2165 (1999)

- [69-12] W P.P. Fischer: EADS Astrium Space Transportation GmbH, Bremen,
(D)
'Beta-Titanium Alloy Thermal Protection System for Re-entry Vehicles'
SAE Paper 08ICES-0013 (2008)
- [69-13] Extracts from NASA Press website (June 2009)

70

Thermo-structural designs

70.1 Introduction

70.1.1 General

This chapter aims to demonstrate how space structure designs have developed to function in high-temperature environments. Material selection has been driven by the need to combine load-bearing functions with heat management. There have been a number of contributory factors to the evolution of designs:

- A move from single to multiple-mission, reusable structures,
- Higher payload requirements,
- More efficient liquid fuel propulsion systems,
- More efficient structural materials,
- Advances in high-temperature materials technology.

A historical view shows the initial investment on which subsequent space projects have been built. Space programmes consume small quantities of materials which are costly to evaluate and approve for space use. Proven materials and construction methods are always attractive in comparison with unproven technologies.

In many cases a thermo-structural design also forms the external thermal protection system of a space vehicle.

[See also: Chapter [71](#) for thermal protection systems]

70.1.2 Single mission

Initial man-rated space vehicles were small capsules, such as the Gemini, Mercury and Apollo series launched on Saturn rockets. These non-reusable capsules were designed for single missions and had to withstand the heat generated on re-entry into the earth's atmosphere. The heat shields ([TPS](#)) were of an ablative design attached to the metal capsule (cold structure), [See: [71.3](#)]. They performed their role efficiently and [ablative](#) designs are appropriate for some future space missions such as planetary exploration.

70.1.3 Reusable vehicles

With the advent of the Space Shuttle Orbiter and Buran, the requirements were extended to multiple-mission capabilities and greater payloads. The external structure of these vehicles therefore had to withstand multiple re-entries with minimal maintenance, so ablative technologies were excluded. These early spaceplanes were essentially aircraft designs of predominantly aluminium airframe construction. Insulative tiles were added to the external surfaces to provide the insulation for keeping the airframe cool, [See: 71.5 and 71.6].

Critical aerodynamic surfaces such as the nose-cone were made of carbon-carbon composites and were essentially thermo-structural designs. The success with carbon-carbon composites (RCC on the Shuttle), promoted the move to designs on newer spaceplane concepts which require the extensive use of thermo-structural materials such as SiC-SiC, C-SiC and CMCs. Whilst functional, the ceramic tiles on the Shuttle are now thought of as mass inefficient and troublesome in maintenance requirements. Low maintenance and inspection costs are now deemed essential for future reusable spaceplanes with short turn-round times.

Spaceplanes form the focal point for thermo-structural design concepts, Ref. [70-1]. However, with the costs envisaged for their construction the technology can also be applied elsewhere, such as deep-space planetary exploration.

70.2 Spaceplanes

70.2.1 Hermes

The Hermes programme was a continuation of the Shuttle concept, but used more advanced technologies. In 1993 the Hermes programme was terminated and the vehicle was never built.

Hermes was intended to be launched by Ariane 5 and placed in Low Earth Orbit (LEO). The Hermes engines were small but sufficient for orbital manoeuvring. Each spaceplane was intended to perform 30 missions with the vehicle designed to sustain 100 flights. The structure and thermal protection system therefore had to be capable of sustaining this number of re-entries.

Most of the external aerodynamic surfaces were intended to be rigid CMC tiles or shingles [See: 71.12]. The external surfaces were thermo-structural in sustaining aerodynamic loads and thermal fluxes on re-entry. As with the Shuttle, the nose-cone was of a C-C construction with an oxidation protection coating system. As part of the Hermes demonstrator programme various assemblies were manufactured, including:

- Nose cone, [See: 70.9],
- Wing leading edges, [See: 70.10],
- Box section [See: 70.11], and
- Shingles, [See: 71.12].

70.2.2 HOPE

HOPE is the Japanese equivalent of the ‘shuttle’ concept, i.e. a spaceplane with a disposable launcher having some recoverable components, Ref. [70-33]. The level of technology is similar to that of Hermes as a demonstrator for more advanced materials with thermo-structural design concepts.

70.2.3 Single- and two-stage-to-orbit

The next generation of spaceplanes are intended to be truly reusable in eliminating the disposable launcher. This requires the spaceplanes to have their own launch capability with an efficient power plant and appropriate fuel capacity. The payload then represents a small proportion of the total (gross) mass.

Only very efficient designs enable sufficient payload to be economically viable. These spaceplanes are intended to be operated in a similar fashion to aircraft and to offer significant economies in placing payloads into orbit. They are subjected to the thermal excursions both on launch and re-entry. High profile programmes included:

- NASP and HOTOL single-stage-to-orbit (SSTO) vehicles, and
- Sänger a two-stage-to-orbit (TSTO) system.

Subsequent RLV concepts include those arising from the European FESTIP and FLTP programmes; resulting in the EXTV (European Experimental Test Vehicle). The PHOENIX collaborative programme in Germany includes the 'Hopper' vehicle concept. This builds on the technology base investigated for Sänger.

Within the US X-programme, the X-33 Venture Star, X-34 and DC-XA Delta Clipper are all technology demonstrator vehicles for RLVs. The X-38 CTV is a re-entry demonstrator and the forerunner to the Crew Rescue Vehicle (CRV) for the International Space Station (ISS). The X-38/TETRA demonstrator vehicle contains a significant amount of European-based technology and expertise, Ref. [70-33].

[See: Chapter 52 for CMC]

[See also: Chapter 90 to Chapter 94 for smart technologies]

The information presented reflects the development of suitable technologies. No endorsement of any one technology in preference to another is intended or implied.

70.3 Hermes

Beneath the outer surface is a load-bearing airframe made principally of aluminium alloy with titanium in localised areas. The maximum temperature that aluminium alloys can withstand is around 175°C, so thermal soak to the airframe has to be efficiently controlled.

For thermo-structural designs, the outer rigid skin possesses certain surface emissivity and catalytic characteristics determined by the surface coating. The thermal conductivity or diffusivity then determines the amount of heat that can enter the structure. The diffusivity and density of underlying ceramic insulation determines the spacing needed between skin and airframe and the remainder of the mass budget.

Hermes was restricted to 24 tonnes gross mass, that being the maximum lift capacity of Ariane 5. Maximum payload was around 3 tonnes. The US Space Shuttle in comparison has a 22.8 tonne payload. Hermes was very vulnerable to erosion of the 3 tonne payload capacity, necessitating a very efficient structural and thermal design package.

A resumé of the thermo-structural configurations developed is given in Ref. [70-2]. Prior to cancellation of the European Hermes programme, the areas of materials technology to the fore were:

- C-SiC and SiC-SiC thermo-structural designs manufactured by SEP using CVI processing routes.
- C-C thermo-structural designs manufactured by Aerospatiale.
- Dassault Aviation assembled parts in CMC.
- FEI (flexible external insulation) concepts by MBB-ERNO (DASA), [See: 71.11].
- Rapid C-SiC processing for CMC shingles by Dornier/DASA and MAN Technologie, [See: 71.12].

Work on these technologies has largely continued under more recent European and joint US RLV programmes, [See: 70.2].

70.4 HOPE

Whereas Hermes dispensed with a composite airframe and reverted back to an aluminium construction, HOPE retains a polyimide CFRP structure, Ref. [70-3].

The external surfaces rely heavily on C-C designs and ceramic tiles for the hotter regions. The surface temperature profile, shown in Figure 70.4.1, has similarities with that of Hermes.

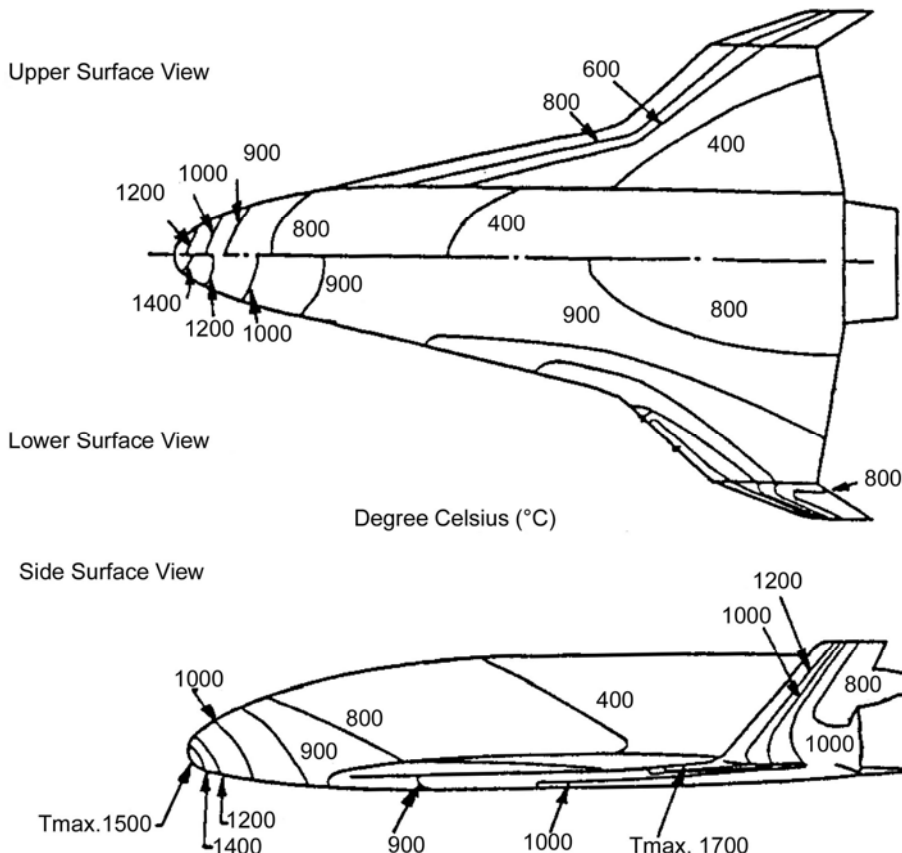


Figure 70.4-1 - HOPE: Distribution of surface temperatures

HOPE is a small vehicle designed with the H-II launcher lift capabilities as the major constraint. The gross mass is 20 tonnes with a 3 tonne payload on launch (5 tonne on return). Diagrammatic representations of the structural configuration and material allocations are shown in [Figure 70.4.2](#) and [Figure 70.4.3](#), Ref. [70-4].

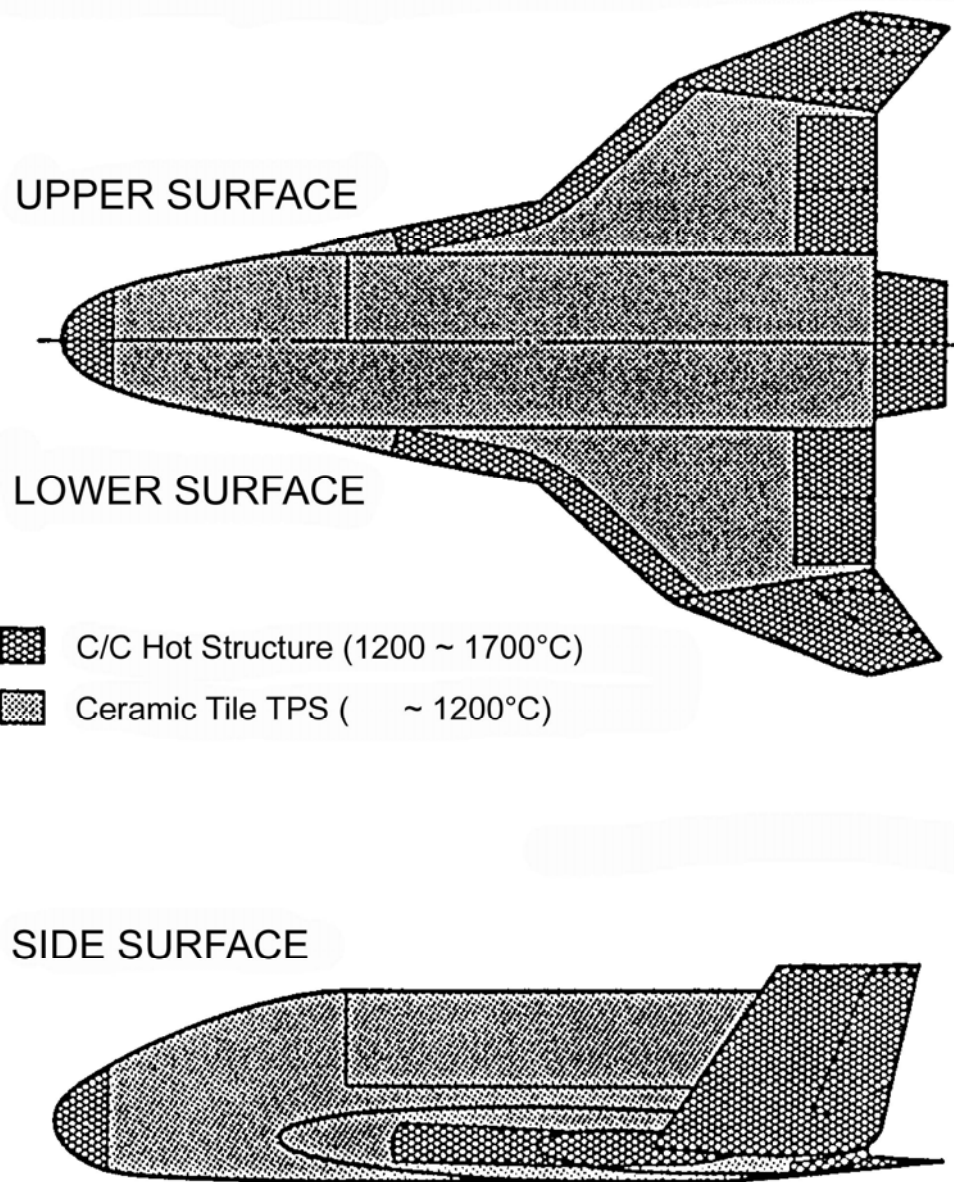


Figure 70.4-2 - HOPE: Distribution of TPS

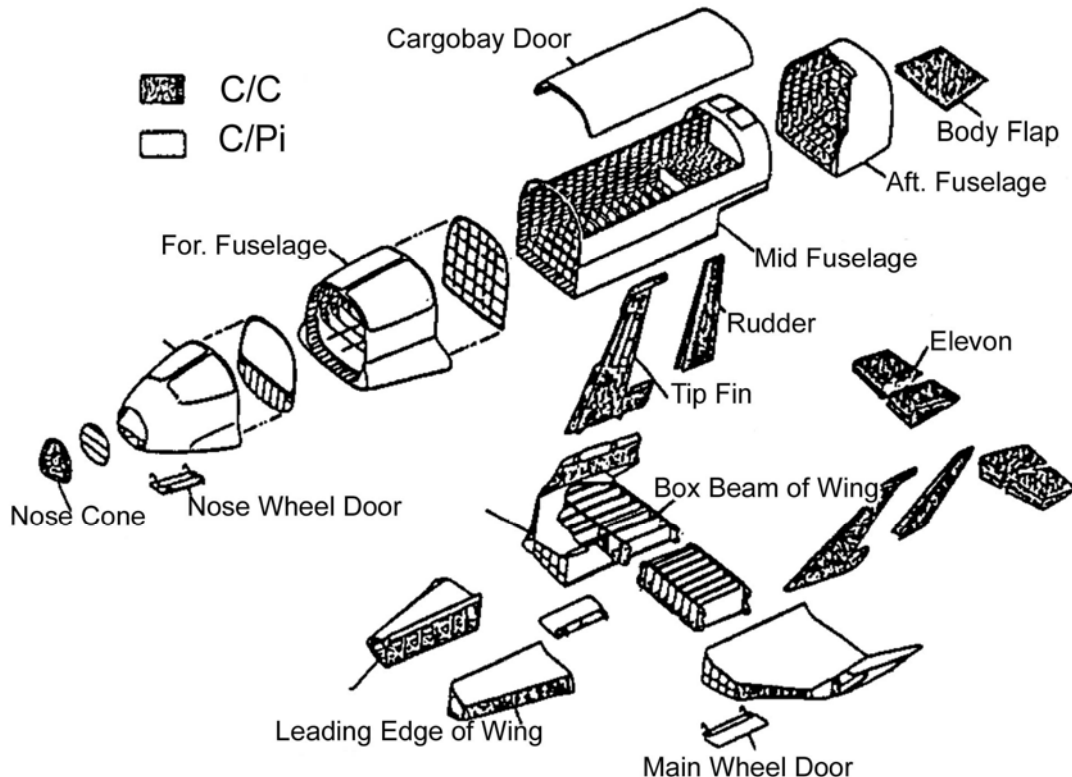


Figure 70.4-3 - HOPE structural materials to be applied

The National Space Development Agency of Japan (NASDA) is applying selected technologies to experimental test vehicles, Ref. [70-4]:

- OREX (Orbital Re-entry EXperiment) intended launch in 1994.
- HYFLEX (HYpersonic FLight EXperiment) in 1996.

These aim to evaluate the effect of re-entry on materials and structures.

Representative diagrams of the two test vehicles are shown in Figure 70.4.4 and Figure 70.4.5, Ref. [70-4].

The HYFLEX configuration has an aluminium airframe as opposed to the PI CFRP intended for HOPE.

Attached C-C Panels & Ceramic Tiles to Aluminium Honeycomb Panel

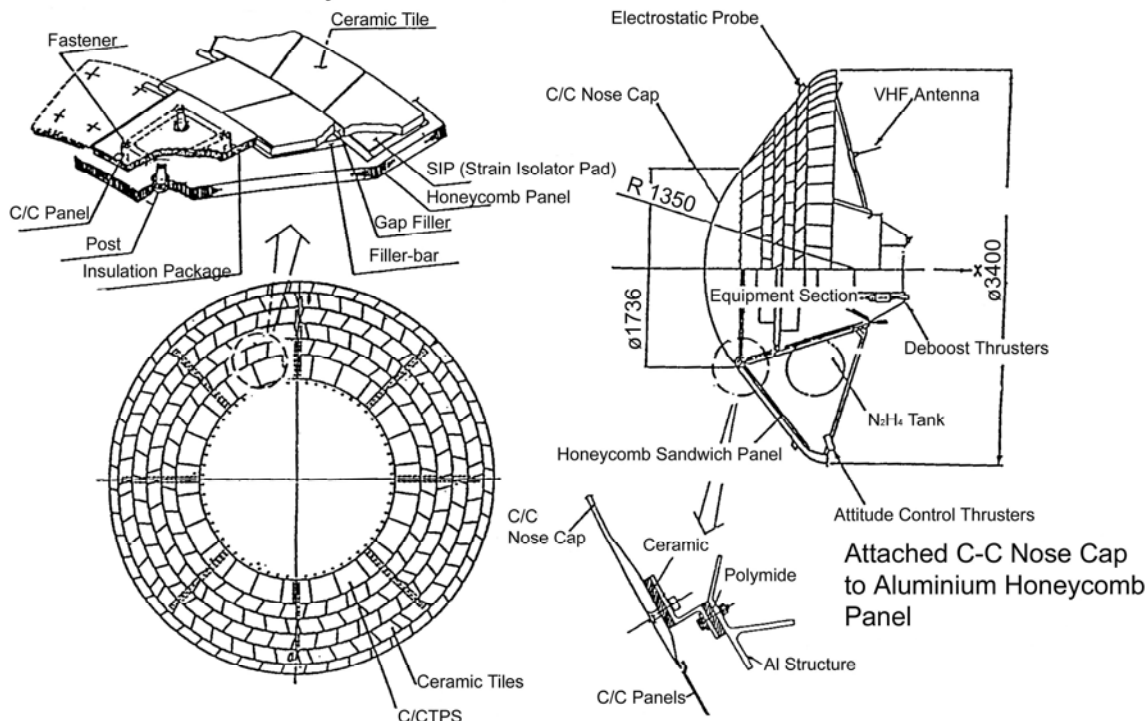


Figure 70.4-4 - OREX structure and TPS

Length	4.4m
Width	1.36m
Height	1.04m
Weight	850kg

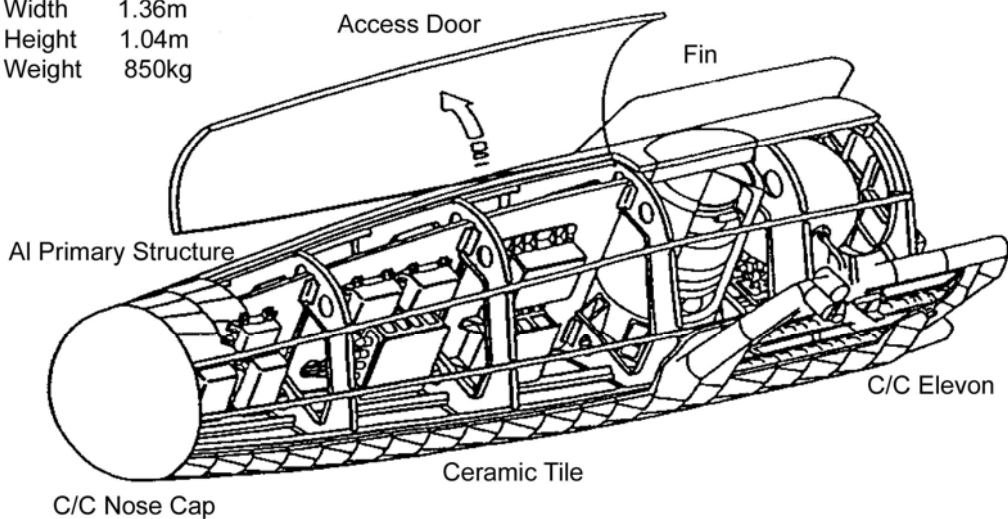


Figure 70.4-5 - HYFLEX: Structural Configuration

The primary material technologies under investigation include:

- titanium constructions, including multiwall TPS (up to 550°C),
- carbon-carbon composites thermo-structures and TPS,
- soft ceramic tile TPS, and
- polyimide CFRP airframe technology.

70.5 HOTOL

HOTOL (HOrizontal Take Off and Land) is a fully reusable SSTO unmanned launch vehicle. For take-off, the original design proposed using a powered sledge to propel the vehicle down the runway. This reduced fuel demands and lowered undercarriage weight.

Subsequent concepts have proposed launching HOTOL from the top of a modified Antonov AN-225 heavy-lift aircraft flying at high altitude.

All HOTOL concepts require the vehicle to have a large LH/LOX capacity and efficient propulsion system. A unique engine has been proposed which is capable of switching from air-breathing ramjet to rocket propulsion and back again for landing manoeuvres. The vehicle would have four to six engines.

The basic conceptual shape of HOTOL is shown in [Figure 70.5.1](#), Ref. [70-5]. In simple terms, it is a flying fuel tank with a payload bay, air intake and engine cluster. The forward portion of the fuselage contains the LH-tank. The fuselage cross-section is more or less cylindrical and shielded against re-entry heating by the carry-through wings and the engine nacelles.

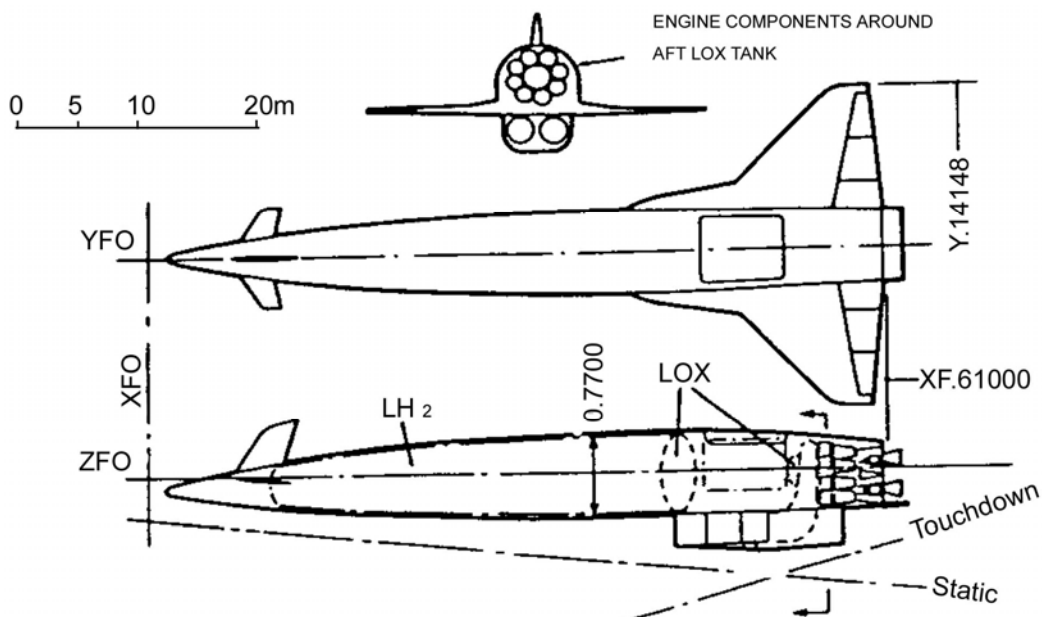


Figure 70.5-1 - HOTOL: Configuration 'g'

A wide range of materials have been proposed for various parts of the structure with differing thermal regimes, Ref. [70-5]:

- Nose cone (1480°C): C-SiC sandwich structure supported by C-SiC frames.
- Nose shell: Sandwich structure of Ti/SiCf with additional TPS. This sustains fin loads via a bearing in the nose shell frame.
- Fin (630°C): Reinforced titanium alloy torsion box and spigot. The torsion box is a multi-spar design with honeycomb sandwich skins. The leading edge, trailing edge and tip are C-SiC sandwich constructions experiencing 1430°C.
- Liquid hydrogen tank (LH): Forms the front fuselage structure, carrying shear, torque, end load and bending moment due to gusts, manoeuvres, take-off, landing, lift, drag and fuel sloshing. The tank is tapered with domed ends and end skirts to transfer the fuselage-tank

loads to the adjacent structures. Tank construction is based on filament wound PEEK thermoplastic CFRP.

- Thermal protection system (TPS): Cryogenic insulation is used for the LH tank coupled with protection from the re-entry temperatures of 930°C on the lower surface and 430°C on the upper surface by ceramic fibre insulation incorporating foil radiation screens. The insulation is protected from the airflow by C-SiC sandwich aeroshell panels 1m x 0.3m. The aeroshell panels are designed to withstand acoustic, thermal and pressure loading and sized to prevent the occurrence of panel flutter.
- Payload bay: Aft of the liquid hydrogen tank is the payload bay, 7.5m in length and 4.6m width. The doors, which open sideways, are designed to carry fuselage bending moments, end loads, shear loads and aerodynamic pressures when closed. Corrugated titanium alloy sandwich constructions are envisaged to sustain temperatures approaching 430°C.
- Thrust structure: The main rocket chambers are supported by a mounting ring connected to an array of struts. Some of the struts are directly attached to the aft LOX tank (PEEK CFRP) and the remainder are connected to the fuselage longerons. The maximum bay temperature is 150°C. The longeron maximum temperature is 430°C. The LOX tank experiences thermal cycles between -183°C and +150°C. Titanium is the intended construction material, but polyimide CFRP can also be justified in places.
- Wing: Consisting of five main components:
 - Torsion box of reinforced titanium honeycomb sandwich with external protection from the 930°C re-entry temperature.
 - Centre section providing wing support from the fuselage by four main frames. The frames are located at the front and rear spars with the two other frames between them. Another frame supports the strake and trolley. The frames experience 430°C, so require reinforced titanium.
 - The leading edge is C-SiC in 1m sections with each joint providing thermal expansion.
 - Trailing edge controls consist of two flaperons each side of rib stiffened C-SiC sandwich construction for 1430°C application.
 - The strake is attached to both the fuselage (by swinging links) and the wing (by a hinge) in order to enable differential thermal expansion. Again a C-SiC construction is essential.
- Rear fuselage: This consists of an arrangement of longerons in reinforced titanium with insulation adjacent to the air intake, as shown in Figure 70.5.2, Ref. [70-5]. Skinning consists of titanium sandwich panels, with a large number of access points. Noise levels up to 165dB are anticipated. The body flap is C-SiC to resist temperatures of 930°C.
- Air intake: The air intake is open during the air breathing ascent to Mach 5 and 25km altitude, and is closed thereafter. It is subjected to a maximum temperature of 1430°C and a C-SiC construction is intended.

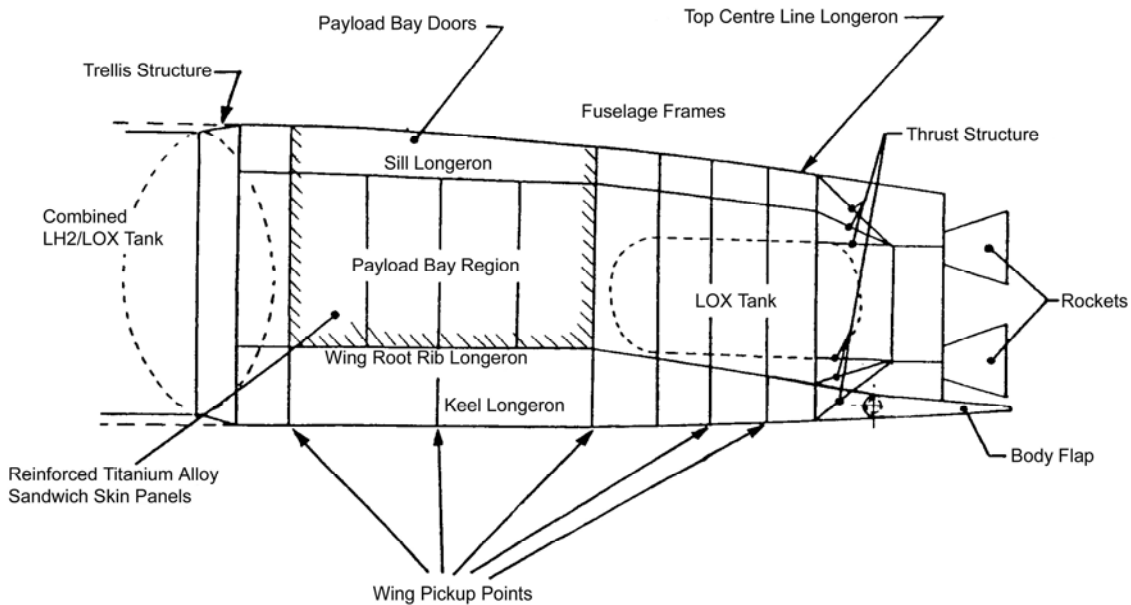


Figure 70.5-2 - HOTOL: Rear Fuselage and Aft LOX Tank

HOTOL is a concept under further development. The design revolves around an investment in C-SiC, TMC, fibrous insulation and PEEK CFRP technologies. The payload is small (circa 3%) in relation to the gross mass of the vehicle with fuel.

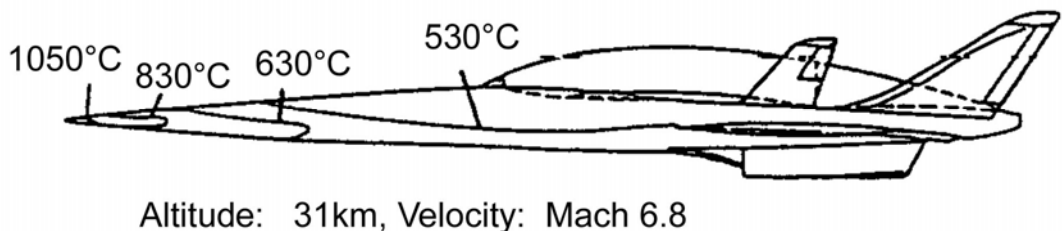
Recent studies have indicated the need to optimise total vehicle design and construction, including parameters such as, Ref. [70-6]:

- trajectory optimisation,
- cross range performance,
- heat pulse shaping,
- TPS thermal diffusivity,
- TPS thermal conductivity, which affects on-ground and in-orbit fuel boil off,
- TPS density,
- Total TPS mass.

This shows that the materials used in the construction can be characterised very well.

70.6 SÄNGER

The German Sänger project is a two-stage-to-orbit system and is a very large transportation concept, in length and gross mass. The winged first stage of Sänger uses a cluster of turbo-ramjets to propel it and its payload to Mach 6.8. The maximum temperature over major areas of the airframe are in the 600°C range with local hot spots up to 1100°C, as shown in Figure 70.6.1, Ref. [70-7].



Altitude: 31km, Velocity: Mach 6.8

Figure 70.6-1 - SÄNGER: Surface temperatures at Mach 6.8

Most of the structure could be made of titanium. The aerodynamic loads are comparable to those of supersonic transports up to the stage separation phase. The manned lower stage takes off and lands on a conventional runway. The upper stage (HORUS) is the actual spaceplane capable of a 7 tonne payload. It requires rocket propulsion to achieve final orbit. The similarities between HORUS and Hermes or HOPE in term of structural configurations then become more obvious.

HORUS is designed with similar constraints to achieve reusable status for multiple re-entries. Similar material technologies are appropriate. Two proposed advantages for the Sänger project are that the:

- two stages operate independently in reasonably well-known environments.
- lower stage could be readily converted to a hypersonic craft, for a potential commercial market.

Whilst high-temperature materials technology can find uses in any spaceplane concepts, within Sänger and German hypersonic programmes emphasis has been placed on:

- multiwall titanium and nickel alloy TPS concepts, [See: Chapter 71].
- low cost CMC (C-SiC and SiC-SiC) production techniques, [See: Chapter 52].

70.7 National aerospace plane (NASP)

NASP is a USA SSTO vehicle on which various technologies have been demonstrated, Ref. [70-8]. It has an ambitious scram-jet propulsion system to attain Mach 25 velocities, Ref. [70-1].

Figure 70.7.1 gives the basic X-30 NASP configuration, Ref. [70-9].

MATERIALS APPLICATIONS

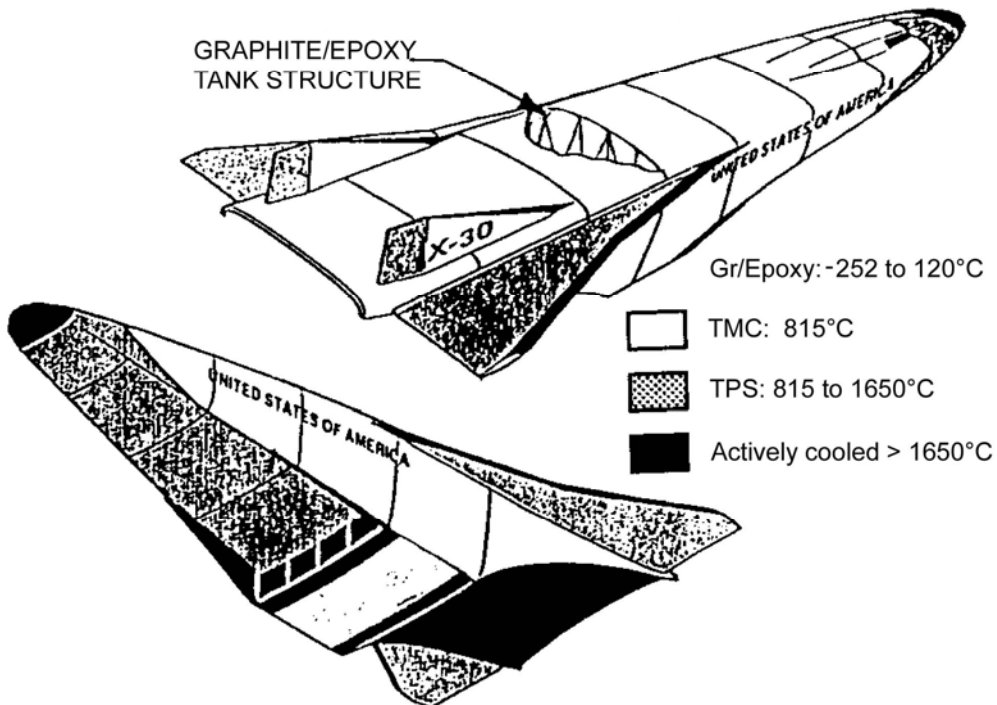


Figure 70.7-1 - NASP: Basic configuration

Producing an efficient airframe construction for NASP poses considerable challenges. This is due largely to kinetic heating which, being more critical in the ascent phase, leads to temperatures at stagnation points well above 2500°C. Materials selection then becomes a greater uncertainty as this maximum temperature range is some 800°C higher than anticipated on European and Japanese spaceplane concepts. Active cooling of structures around the engine controls material temperatures within acceptable limits.

To predict the flow characteristics through and around prospective aerodynamic concepts considerable investment has been made in Computational Fluid Dynamics (CFD).

Within the NASP programme, heavy investment has been made in materials technologies, with large demonstrator panels being prepared, Ref. [70-8]:

- Titanium aluminides and titanium aluminide composites, [See: Chapter 49].
- TMC materials of continuous silicon carbide monofilament reinforced beta-titanium alloys (Timet Beta 21S), [See: Chapter 47].
- High conductivity copper, beryllium and carbon compositions, [See: Chapter 45 for Cu; Chapter 51 for Be].
- Advanced carbon-carbon composites (ACC) with multiplex oxidation protection schemes, [See: Chapter 54].
- High-temperature coating technology, e.g. hafnium compounds, [See: Chapter 74].

[See also: Chapter 71 for TPS]

70.8 Demonstrator panels

70.8.1 General

The various spaceplane programmes have resulted in a range of demonstrators produced by different materials technologies. The information highlights the achievements given that no full-scale vehicles have been constructed and flown.

70.8.2 NASP

TMC constructions based on formed, plasma-sprayed, filament preforms include, Ref. [70-8]:

- tubes up to 3m long,
- I-beam sections,
- top-hat stiffened sections and panels,
- NASP skin panels ~2.4m x ~1.2m (8ft x 4ft),
- box beam channels,
- assembled torque box,
- fuselage assembly.

Titanium aluminide panels (760mm x 2030mm) have been constructed from SPF/DB Ti3Al material, Ref. [70-8].

Detailed technical publications on the NASP programme are awaited, Ref. [70-9].

Aerospatiale have prepared a NORSIAL® C sandwich structure consisting of two skins with a corrugated core, 80mm x 80mm x 25mm, Ref. [70-10], [70-11]. This used MAS/Nicalon SiC material for applications up to 1000°C. A demonstrator leading edge was also made in this material.

70.9 Nose cones

70.9.1 General

As the leading aerodynamic surface, the nose cones of spaceplanes experience high thermal loadings coupled with pressure loadings. Carbon-carbon constructions are used on the Shuttle Orbiter and Buran. C-C has proved reliable and is the first choice for many thermo-structural applications. Improved C-C materials and constructions were specified for Hermes, HOPE and NASP nose cones. C/SiC, developed in Germany, was specified for the X-38 vehicles.

70.9.2 Shuttle orbiter

The nose cap and chin panel are structural fairings which transmit aerodynamic loads to the airframe structure through discrete mechanical attachments, Ref. [70-12], as shown in Figure 70.9.1 and Figure 70.9.2.

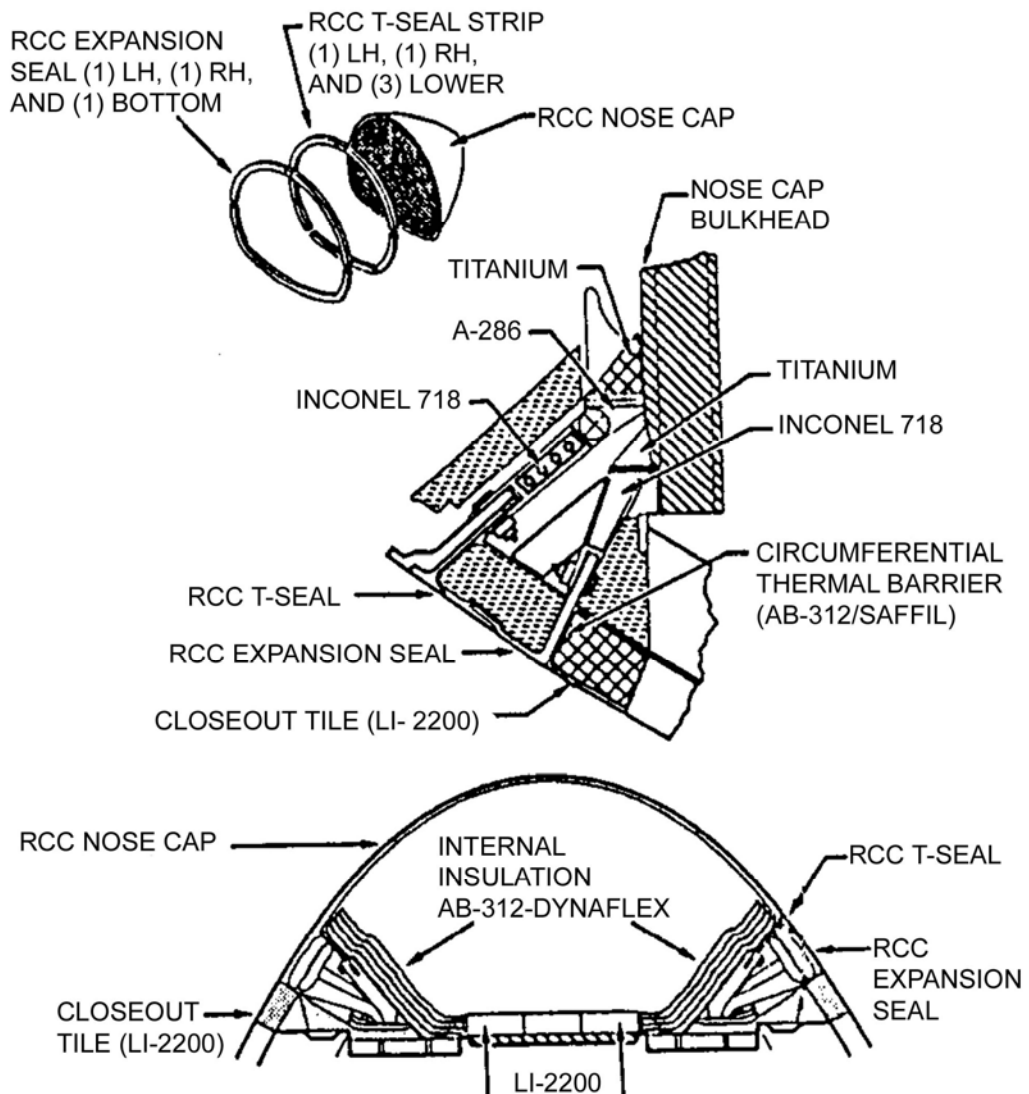


Figure 70.9-1 - Shuttle: Nose cap system components

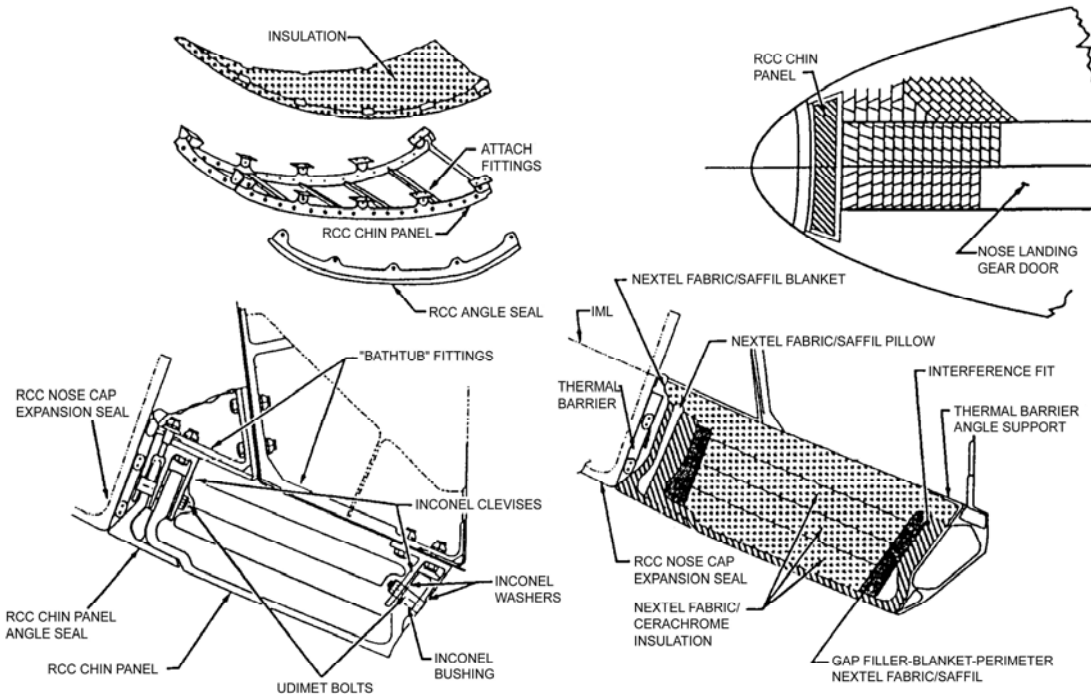


Figure 70.9-2 - Shuttle: RCC chin panel system components

The older generation carbon-carbon composite (RCC) is used for the main parts. Inconel 718 and A-286 stainless steel fittings are bolted to flanges formed on the RCC components. These in turn are fixed to the titanium nose cap bulkhead.

Since RCC is not an insulator, the metallic attachments are protected from internal radiation and conduction by insulation blankets. These consist of:

- cerachrome insulation, contained in formed and welded Inconel foil,
- blankets fabricated from AB-312 ceramic cloth, Saffil and cerachrome insulation,
- ceramic tiles (RSI LI-2200).

70.9.3 Hermes

Part-scale demonstrator nose cones were fabricated, Ref. [70-11], [70-13]. The basic carbon fibre preform was woven by Aerospatiale or SEP. During the early stages of the programme both C-C (0.6 scale) and C-SiC (0.5 scale) nose shells were manufactured. SEP produced a Skinex® C-SiC version in 2D woven form. Aerospatiale used their AEROTISS® automated winding and weaving process to achieve a 3D construction for densification with carbon by phenolic resin pyrolysis (C-C INOX®).

- C-C INOX® version: A thin-walled structure locally reinforced with 5 stiffeners and a thick flange to transfer loads to a titanium ring which links the nose cap to the airframe, as shown in Figure 70.9.3. The AEROTISS technique enables the skin thickness to be varied between 3mm and 15mm. It is also applicable to wing leading edges.
- C-SiC Skinex® version: Less well developed than the C-C version and used chemical vapour infiltration (CVI) for densifying the fibre preform with SiC.

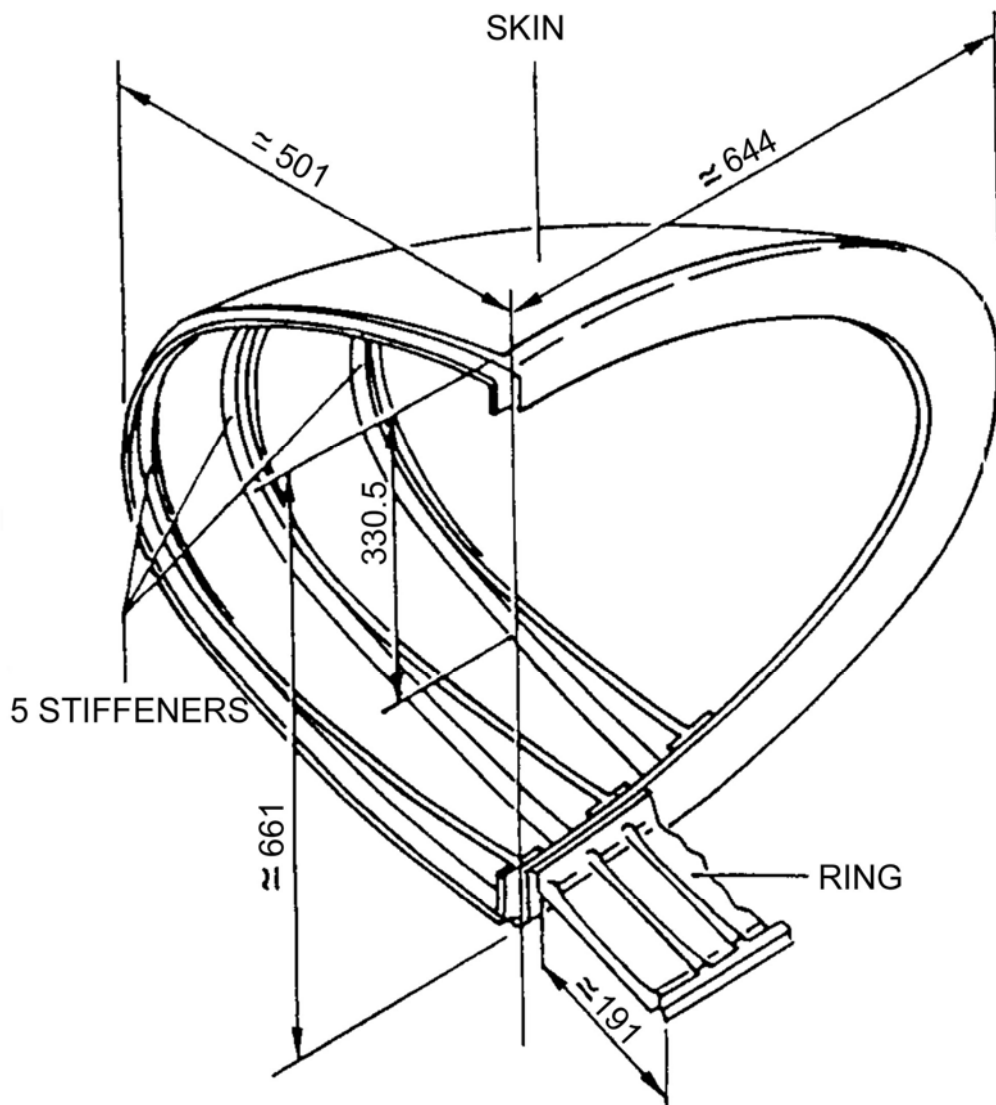


Figure 70.9-3 - Hermes: C-C INOX® nose cone (0.6 scale)

70.9.4 HOPE

Figure 70.9.4 shows that the outline resembles that of the Shuttle orbiter, Ref. [70-4].

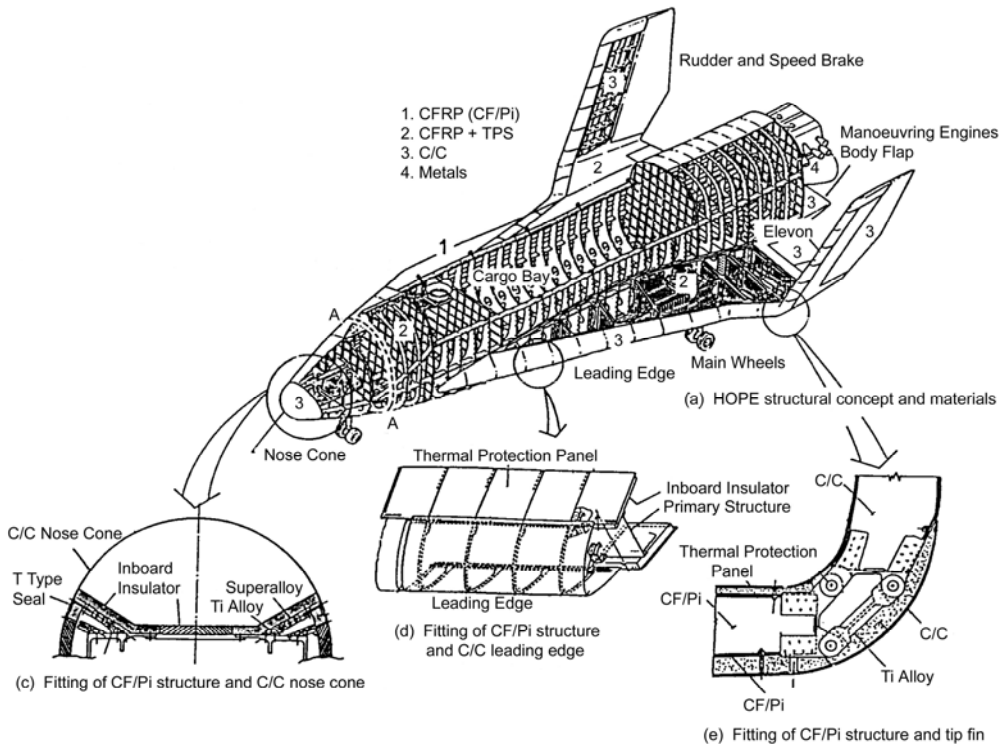


Figure 70.9-4 - HOPE: Heat resistant structural configuration

[See: Figure 70.4.4 for details of the transition between the C-C nose cone and the cold structure for the OREX demonstrator vehicle]

The cone has a diameter of 1.736m with a radius of curvature of 1.35m. The cellular through-thickness of the construction is 4mm.

Attachment to the aluminium structure is by a progressive change of materials in the spacers and fasteners, from ceramic, steel, titanium through to polyimide adjacent to the aluminium. All fasteners are located on the outer circumference of the shell. The SiC conversion coated C-C cone experiences temperatures up to 1700°C.

70.9.5 NASP

The NASP nose cone experiences very high heat fluxes depending on its mode of operation. Advanced carbon-carbon (ACC) constructions are envisaged with advanced protection systems. The cone could require active cooling, [See: 71.14].

70.9.6 HOTOL

C-SiC nose cone constructions proposed for HOTOL are shown in Figure 70.9.5, Ref. [70-5].

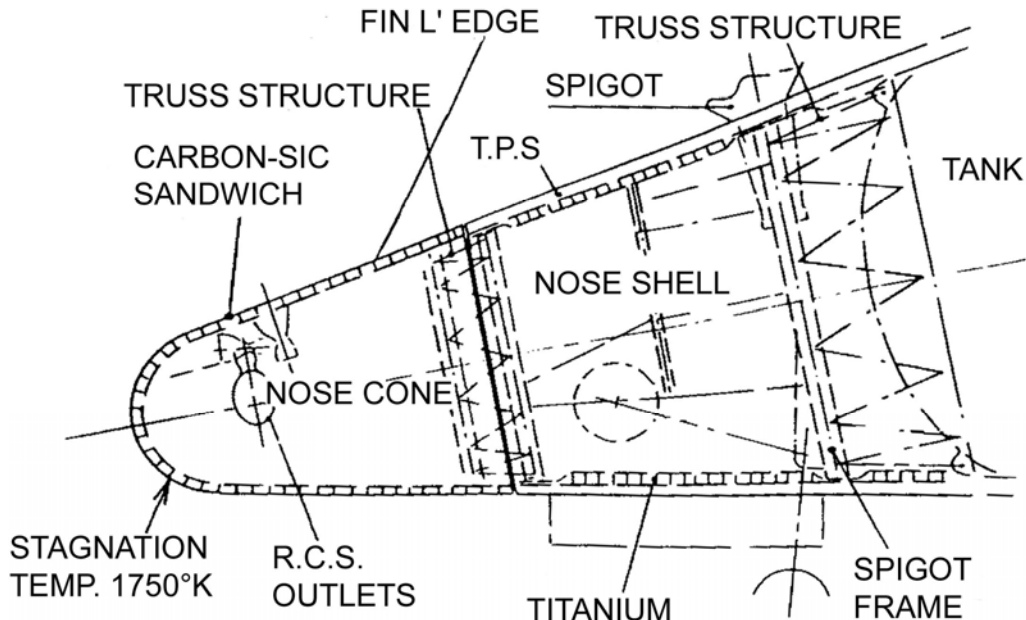


Figure 70.9-5 - HOTOL: Nose cone and nose shell

70.9.7 SÄNGER

The HORUS upper stage resembles Hermes in general construction.

The Sänger first stage experiences lower temperatures, therefore the material options for the nose cone are not as limited.

70.9.8 X-38

The X-38 nose cap overall TPS system comprised, Ref. [70-40], [70-41]:

- C/SiC panels (external surface) developed by DLR.
- Flexible insulation blankets, which were used to fill the remaining volume between the substructure and the C/SiC nose shell. Different types of insulation, developed by Astrium SI, were used:
 - IFI internal flexible insulation on the cold substructure; an existing side-development of FEI blankets, [See: 71.11].
 - HTI high temperature insulation on the outermost region; a new development to provide higher thermal performance than existing FEI and IFI types of products, [See: 71.23].

The overall TPS system for the nose assembly was a collaborative exercise conducted by Astrium SI, DLR-Stuttgart and MAN Technologie in Germany. NASA cancelled the project when the integration of the X-38 demonstrator vehicle V201 was 90% complete.

[See: 70.24 – X-38 Nose cap; See also: 70.23 – X-38 Body flap].

70.10 Wing leading edges (WLE)

70.10.1 General

The choice of materials for wing leading edges are basically the same as those for the nose cone, [See: [70.9](#)].

On any spaceplane the same material and manufacturing technologies apply to both nose cones and WLEs. The materials gaining preference are C-C or C-SiC.

70.10.2 Shuttle orbiter

The C-C WLE for the Orbiter is shown in [Figure 70.10.1](#), Ref. [[70-12](#)].

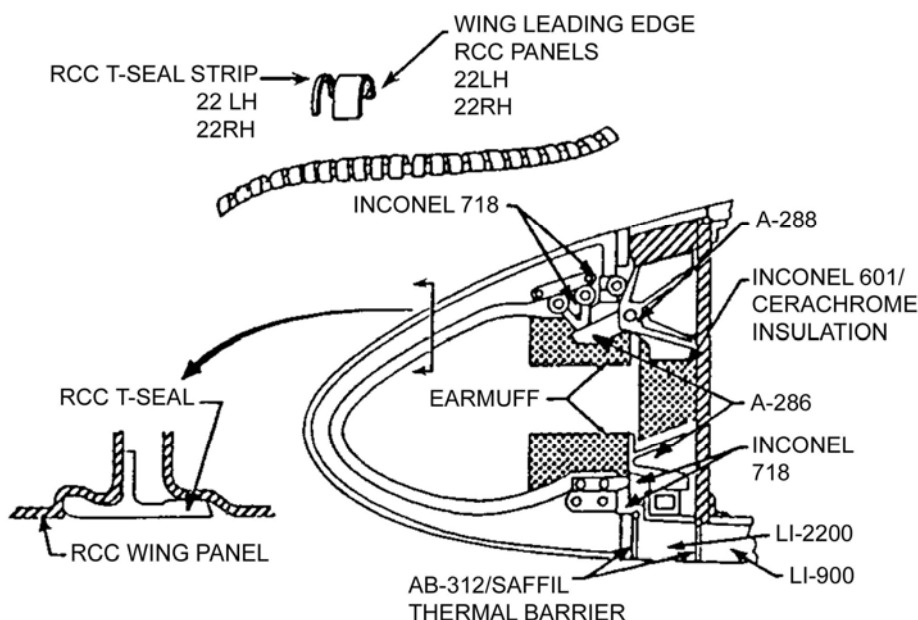


Figure 70.10-1 - Shuttle orbiter: Wing leading edge system components

Each WLE consists of 22 panels joined by 22 T-Seals. This segmentation is used not only to enable its manufacture, but also to accommodate the thermal expansion during re-entry and to prevent large gaps or interference between parts.

In addition, the T-Seals prevent ingestion of the boundary-layer gases into the WLE cavity. The range of materials is similar to that for the nose-cone, [See: [70.9](#)].

70.10.3 Buran

The construction is similar to that of the Orbiter, as shown in [Figure 70.10.2](#), Ref. [[70-14](#)].

A time-temperature profile for the WLE is shown in [Figure 70.10.3](#), Ref. [[70-16](#)]. This demonstrates how heat management through the use of radiation heat exchange was successful in lowering peak temperatures between 100°C and 150°C, so extending the working life of the C-C.

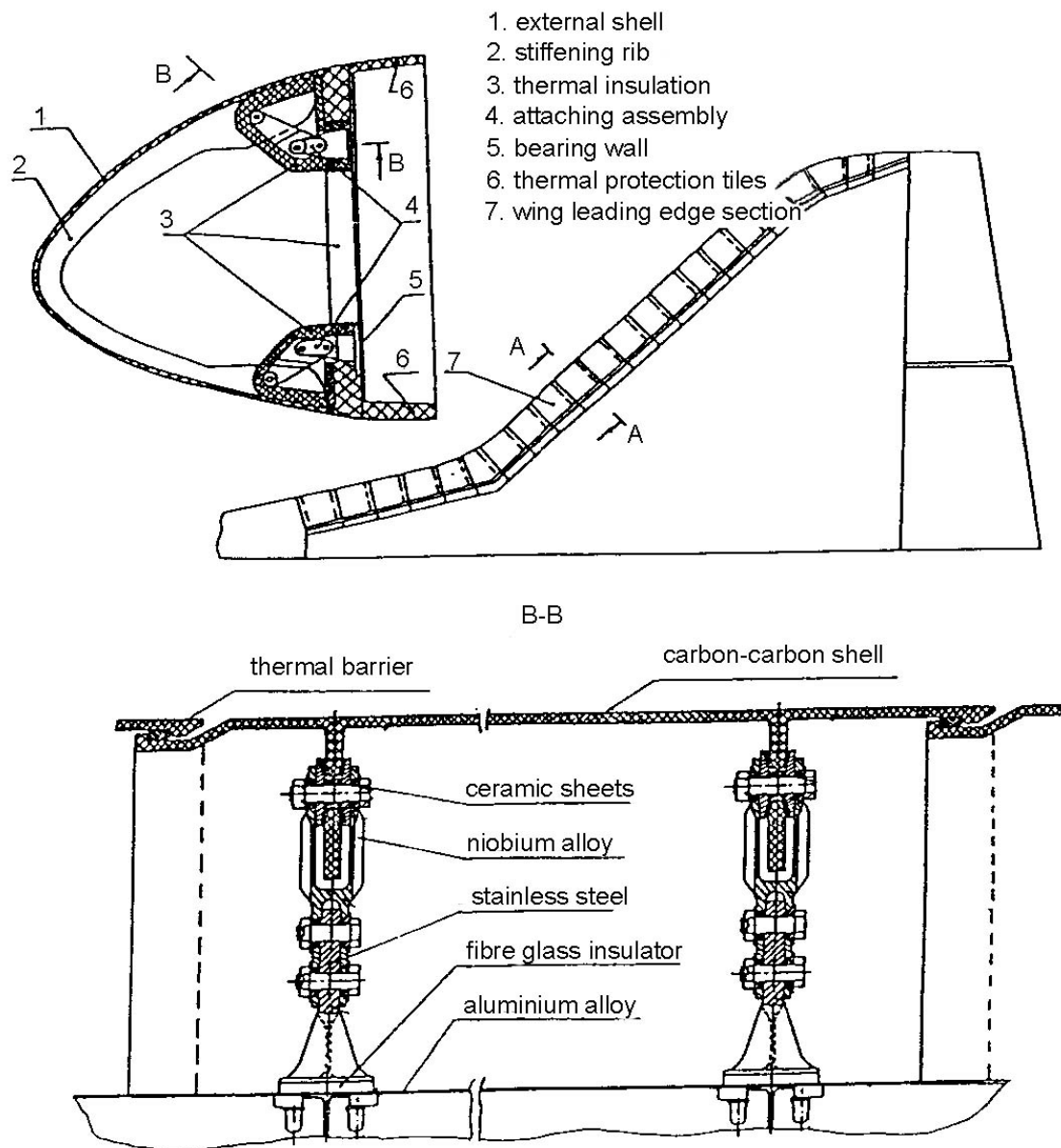


Figure 70.10-2 - Buran: Wing leading edge construction

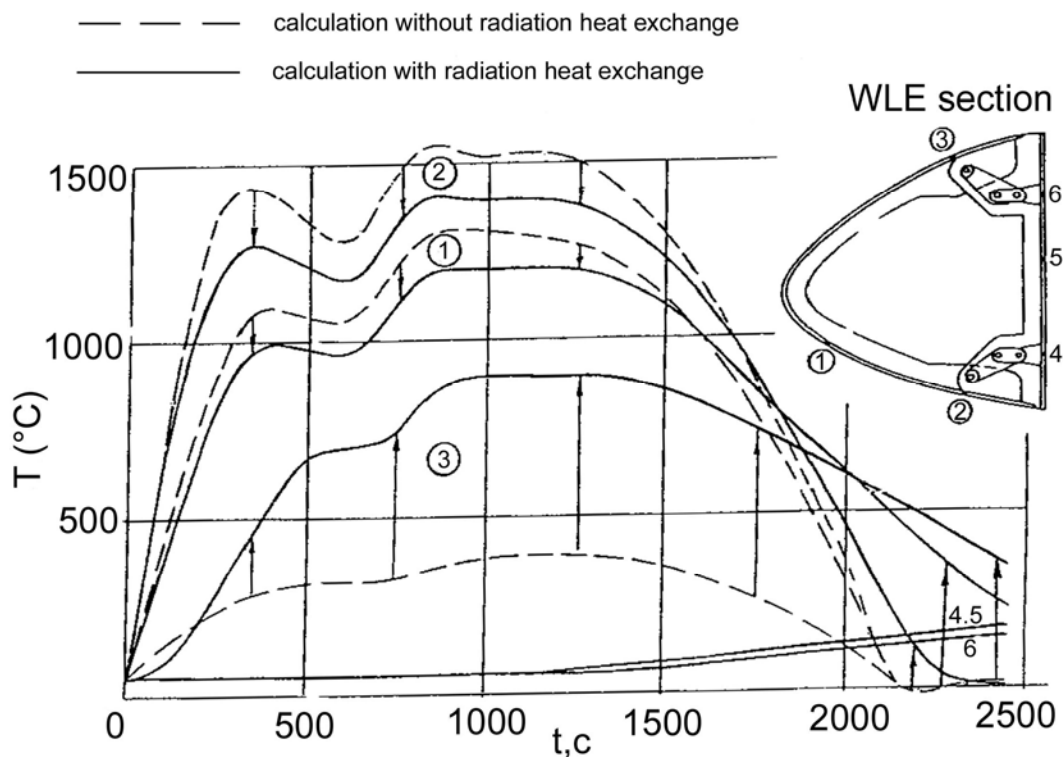


Figure 70.10-3 - Buran: Temperature of wing leading edge with time

70.10.4 Hermes

Various WLE configurations have been made by Aerospatiale, Ref. [70-10], [70-11], SEP and Dassault Aviation based on their respective expertise in CMC materials and manufacturing technologies.

SEP prepared a C-SiC WLE section of dimensions 400mm (height) \times 310mm (width) \times 210mm (depth). This integrally stiffened section was manufactured by the CVI route. It successfully sustained 16 cycles to 1550°C in air and 2 cycles to 1700°C whilst under mechanical load, Ref. [70-15].

A schematic representation of a Hermes WLE is shown in Figure 70.10.4, Ref. [70-1], [70-10].

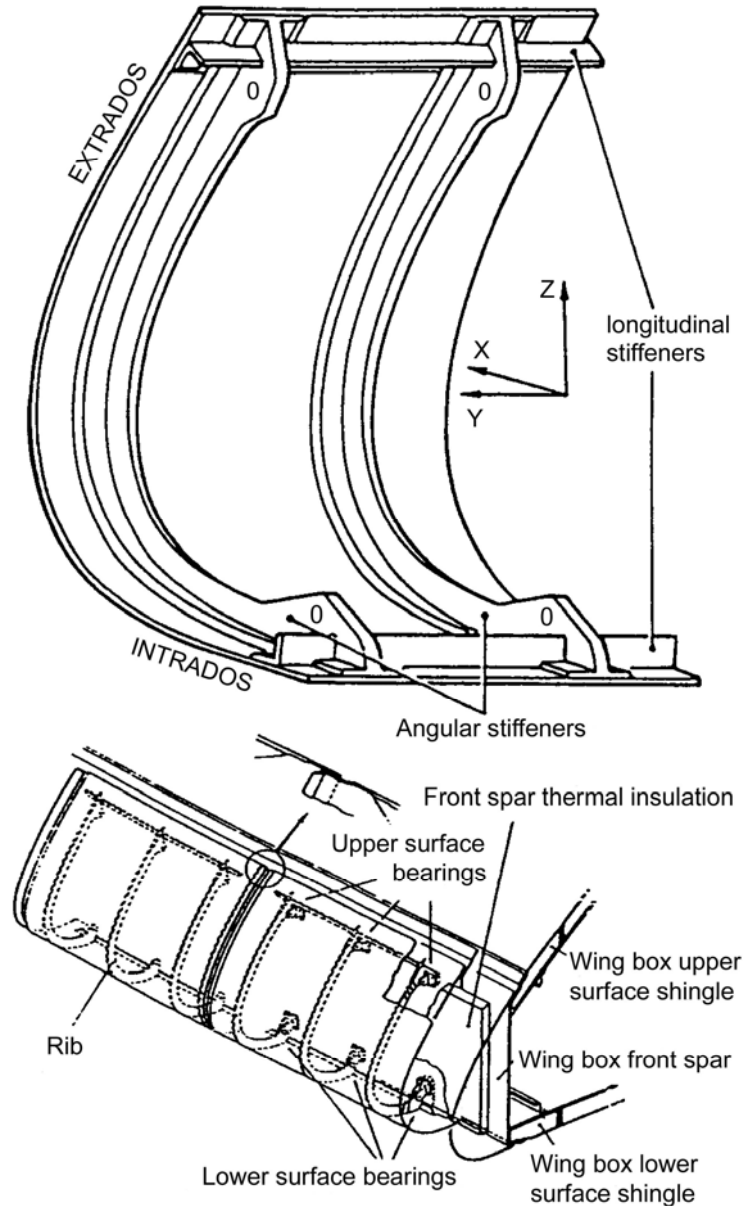


Figure 70.10-4 - Hermes: Hot structure leading edge

70.10.5 HOPE

The main wing and the wing tip fins (elavons) both have leading edge sections. C-C is the intended material for the construction, [See: [Figure 70.4.3](#)].

HYFLEX has a C-C elevon to enable an assessment of the technology, Ref. [\[70-17\]](#).

70.10.6 Others

Dornier produced a wing leading edge by a low-cost manufacturing route for C-SiC. The unit avoids fasteners through the use of integral flange stiffeners, Ref. [\[70-16\]](#).

Aerospatiale have made a WLE section in a GCMC material.

70.11 Box sections

70.11.1 NASP

An assembled TMC NASP 'Torque box' assembly measures some 2.4m x 1.2m (8ft x 4ft). It consists of a mechanically fastened construction of skin panels, channel sections and I-beams.

70.11.2 Hermes

The box-section is shown in Figure 70.11.1 and had an overall length of 1.77m, Ref. [70-13].

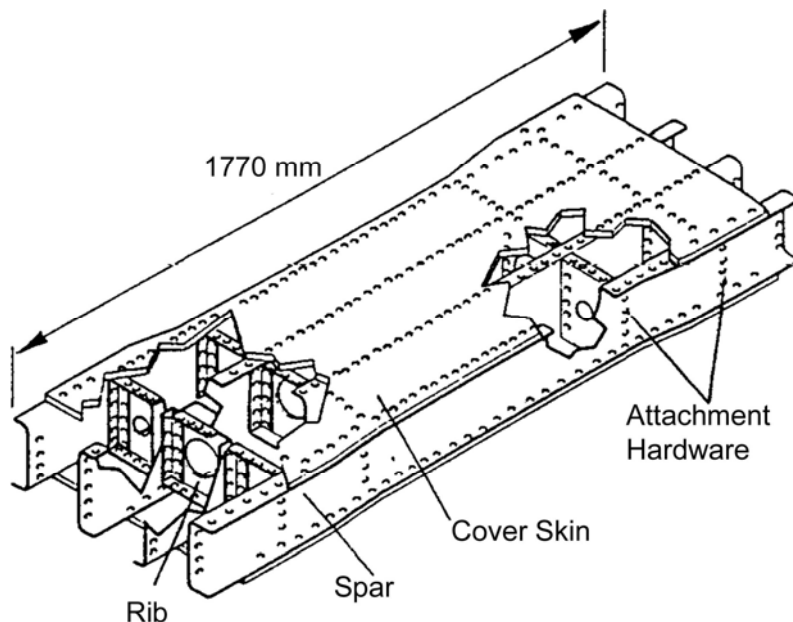


Figure 70.11-1 - Hermes: C-SiC box for thermal structure

SEP used their SEPCARBINOX® C/SiC material in its developed form SKINEX® to manufacture a Hermes wing box section, which included, Ref. [70-13], [70-15], [70-32]:

- textile processing to prepare 3-D preforms,
- SiC infiltration by CVI,
- application of anti-oxidation protection,
- assembly by fastening, with TZM metallic fasteners, and
- design optimisation.

The outer skin was 1.6m long and 0.6m wide, with thicknesses varying from 1.9mm to 9.9mm in spar assembly zones. The spars were 1.8m in length and 0.2m wide with a constant thickness of 3.5mm. The total assembled mass was 41.5kg.

Mechanical loading trials were undertaken at IABG, as a prelude to high-temperature testing, Ref. [70-32].

70.12 Cryogenic tanks

Cryogenic fuel tanks (cryotanks) are a special case in their construction and mode of operation. They form a significant part of SSTO and TSTO vehicle designs. For concepts like HOTOL, they effectively form the load-bearing fuselage.

The actual tank is usually considered as a cold structure (as in HOTOL) and protected by efficient TPS to ensure that elevated temperatures are not experienced. For the HOTOL tank, PEEK CFRP is envisaged as the main construction material.

For more ambitious designs, such as NASP, the tank and its contents can be specifically designed to absorb heat. Therefore higher temperature materials are used for the construction, e.g. advanced titanium-based materials.

70.13 Heat shield designs

Dornier designed and manufactured a demonstrator heat shield panel based on C-C and C-SiC materials, Ref. [70-16], [70-17], [70-18].

Various manufacturing routes were studied in conjunction with different two-stiffener concepts:

- Double-wall version: The inner C-SiC panel was reinforced by stiffening corrugations and acted as the load-carrying part of the double wall. The outer thin C-C panel acted as a heat emitting layer. Both panels were joined by oxidation-protected niobium bolts. The configuration and fastening are shown in Figure 70.13.1, Ref. [70-17].
- Stringer reinforced single panel: A carbon fibre fabric preform was prepared with stitched-on stiffeners. The preform was resin infiltrated by RTM and then pyrolysed to C-C. The basic configurations are shown in Figure 70.13.2, Ref. [70-17]. The overall shield diameter was 4m. Protective coatings were applied to the C-C.

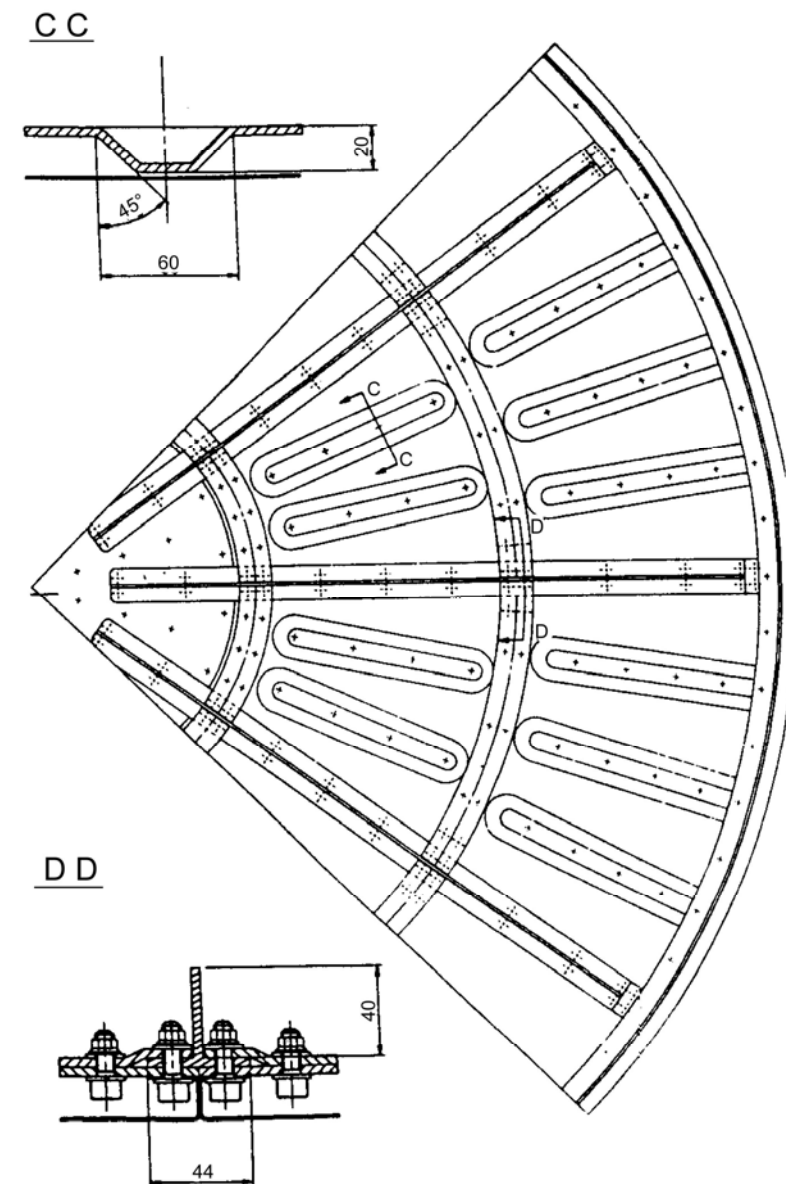


Figure 70.13-1 - Double wall heat shield

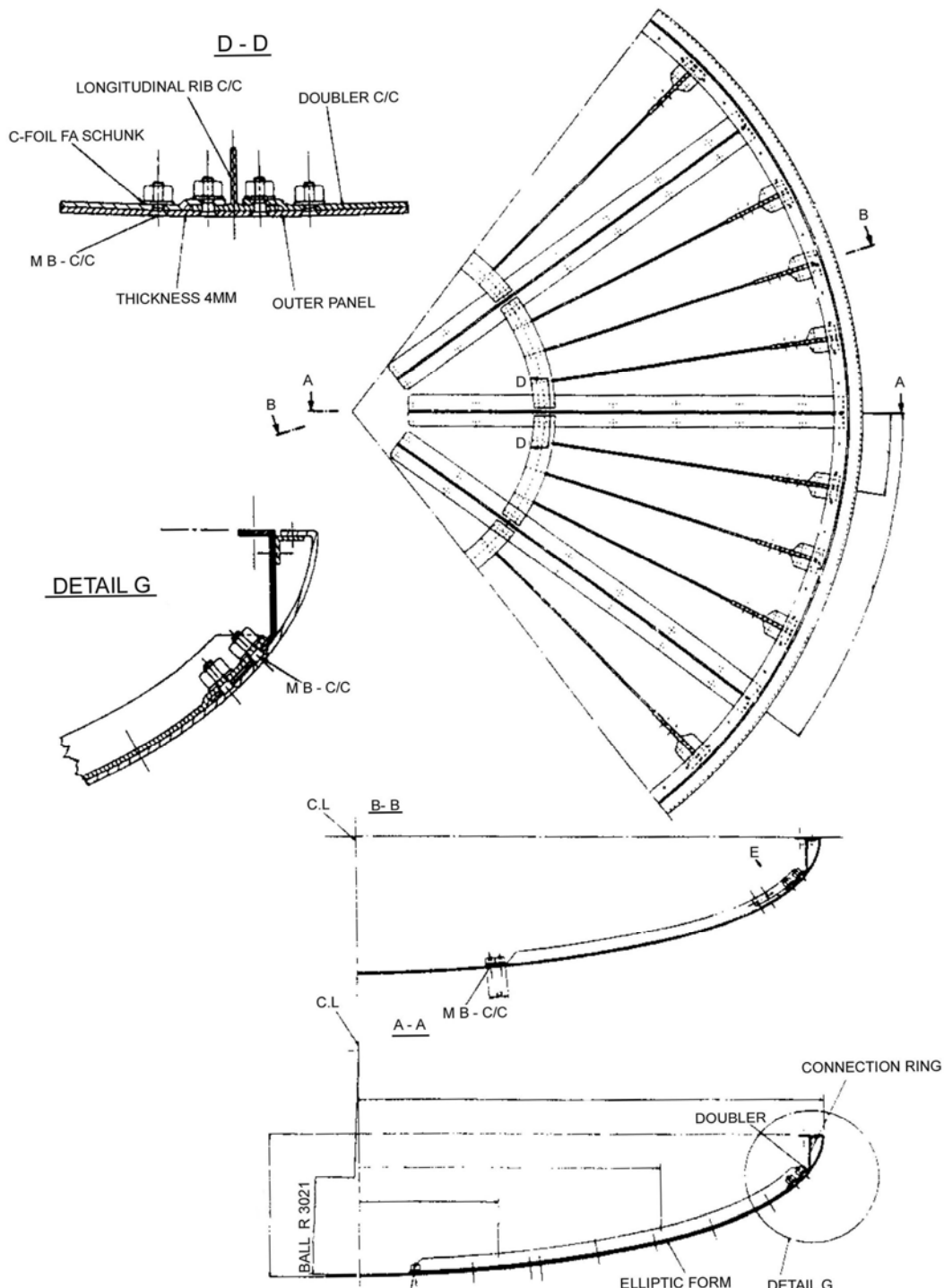
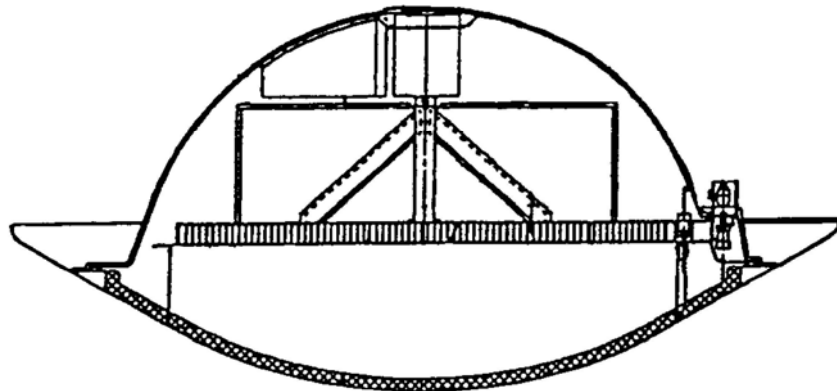


Figure 70.13-2 - Heat shield and stringer stiffened panels

These designs could be used on a Mars Lander, e.g. MARSNET, as shown in Figure 70.13.3, Ref. [70-18].



C/SiC decelerator and TPS

Figure 70.13-3 - MARSNET: Heat shield for planetary entry probe

SEP produced a C-C heatshield for Huygens, Ref. [70-19].

[See: 70.19]

70.14 Air inlet-intakes

As part of the German Hypersonic Technology programme, MAN Technologie and Dornier (DASA) produced an air intake ramp in C-SiC, Ref. [70-20], [See also: 52.7 for the X-38 Body Flap].

MAN used liquid infiltration and pyrolysis of silicon-based polymers in conjunction with gradient CVI manufacturing techniques. The component is shown in Figure 70.14.1, Ref. [70-20]. The manufacturing also incorporated an open face sheet with holes produced by laser.

The assembled component has been tested under thermal and mechanical loads at IABG and has demonstrated its integrity.

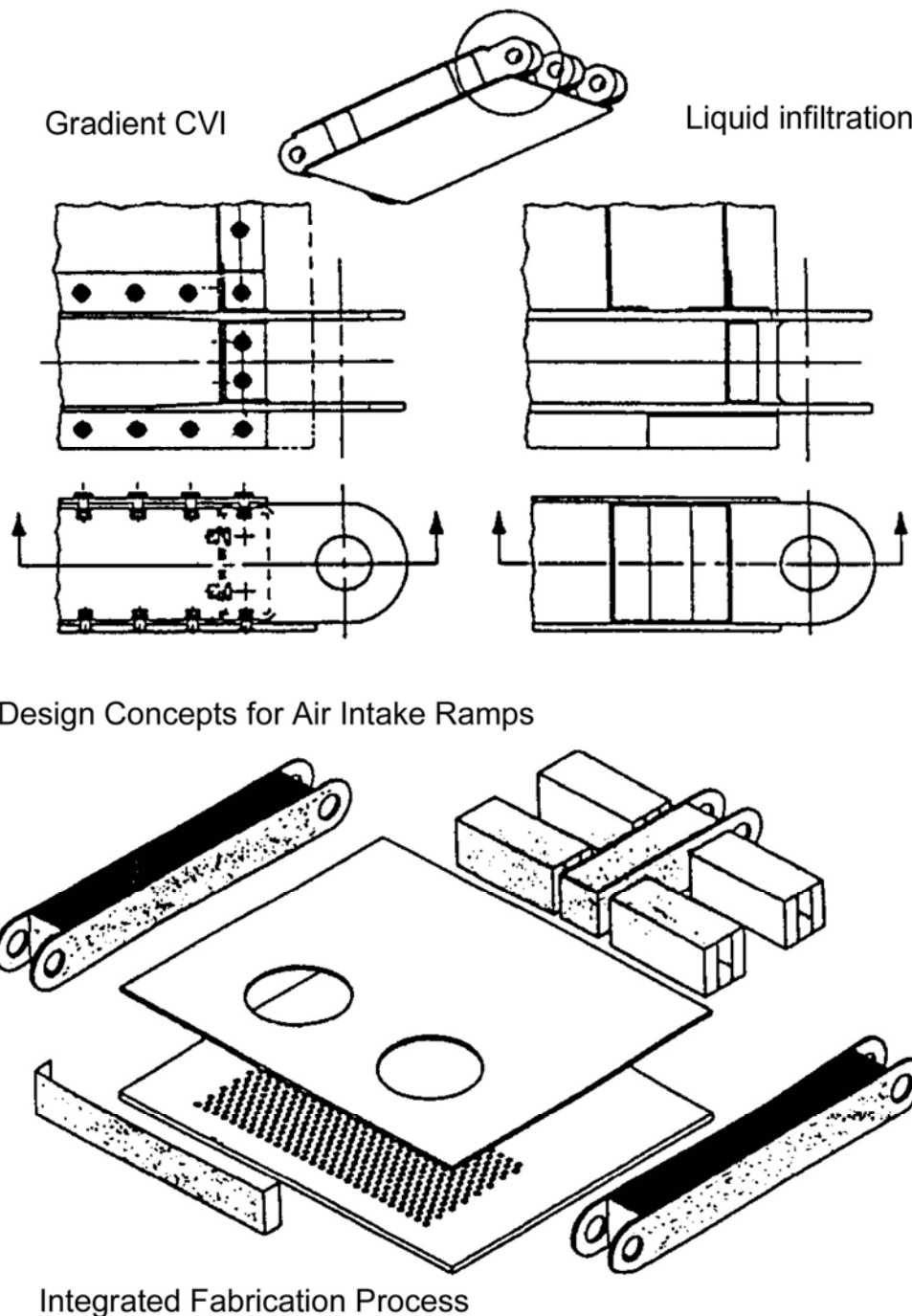


Figure 70.14-1 - Air intake ramp in C-SiC

70.15 Earth re-entry capsules

This group of vehicles includes non-man rated capsules used to retrieve experiments from space for return to earth. The success of the Apollo missions provides the starting point for improved designs and means of construction.

Projects which can be highlighted in this field are:

- CARINA LEO microgravity experiment recovery vehicle, Ref. [70-21].

- [See: [71.4](#) for ablative TPS concept and structural configuration].
- CNSR Rosetta capsule (ERC) for returning comet nucleus samples, Ref. [[70-22](#)]. [See: [70.17](#)].
- COMET microgravity experiment recovery capsule, Ref. [[70-23](#)]. The structural configuration is shown in [Figure 70.15.1](#). Away from the TPS, the capsule consists of a stainless steel forebody structure which acts as a radiator. The capsule structure for the nose cap, aft structure and end cap are in epoxy CFRP.
- [See: [71.4](#) for ablative TPS concept]
- EXPRESS and MIRKA re-entry capsules, Ref. [[70-24](#)]: As part of the German Hypersonic Technology Programme, these two re-entry capsules are flight experiments to assess hot structure technologies. They follow the 1992 flight of TPS materials on the Russian mission FOTON-8.
 - EXPRESS (EXPeriment Re-entry Space System) is a joint German-Russian-Japanese project, intended to fly in 1994. A 300mm diameter C-SiC tile (5mm thick) with a mass of 1kg is attached and expected to reach 2700°C on re-entry (CETEX: CEramic Tile EXperiment).
 - MIRKA is a ballistic re-entry capsule intended to have an Apollo-type ablative shield with an outer layer of C-SiC to provide erosion resistance, known as 'Surface Protected Ablator' (SPA) from DASA-Dornier. The experiment is intended to fly 1995. The structure is shown in [Figure 70.15.2](#), showing the spherical heatshield with a diameter of 1m and total mass of 60kg, Ref. [[70-24](#)].

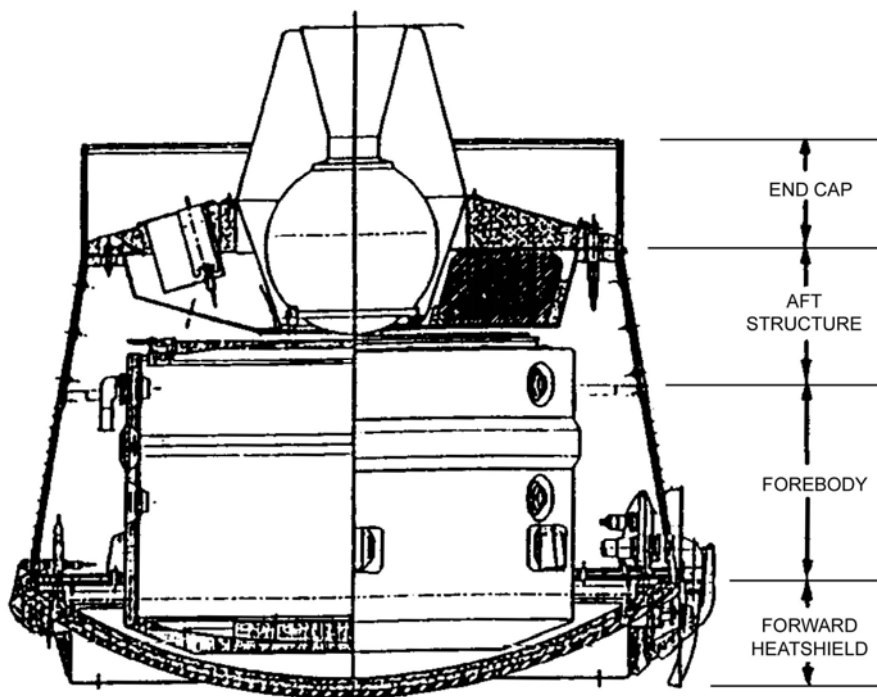


Figure 70.15-1 - COMET recovery system

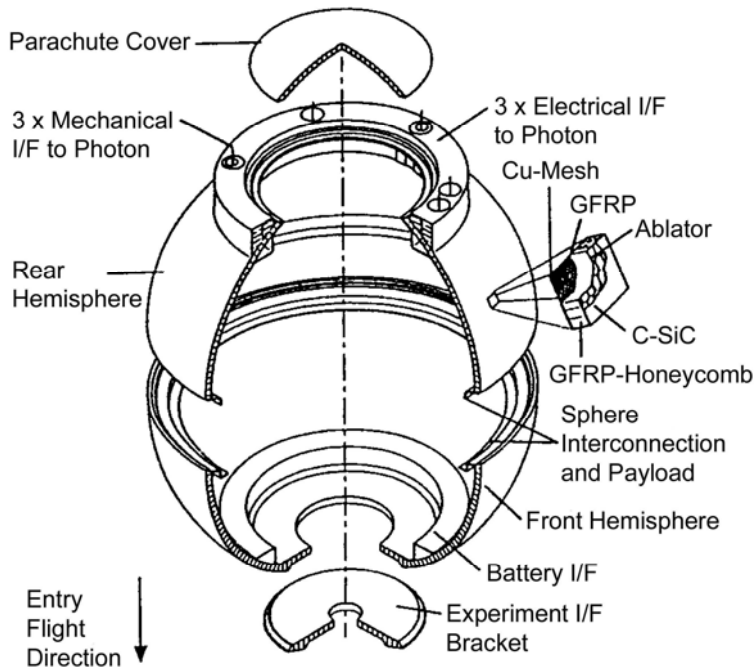


Figure 70.15-2 - MIRKA capsule: Exploded view of spherical heat shield

70.16 Manned re-entry vehicles

Apollo capsules were successful in bringing astronauts back from space through the earth's atmosphere.

With the advent of manned space stations, concepts for an escape module for emergencies or ACRVs (Assured Crew Return Vehicles) have been proposed. They have been studied both in the USA, Ref. [70-25] and Europe, Ref. [70-26]. The studies take account of all the experience gained with re-entry capsules to earth and other planets.

Figure 70.16.1 shows the general layout of an ACRV, where an ablative TPS is proposed, Ref. [70-26]. To this can be added the experience gained with thermo-structures within the Hermes programme.

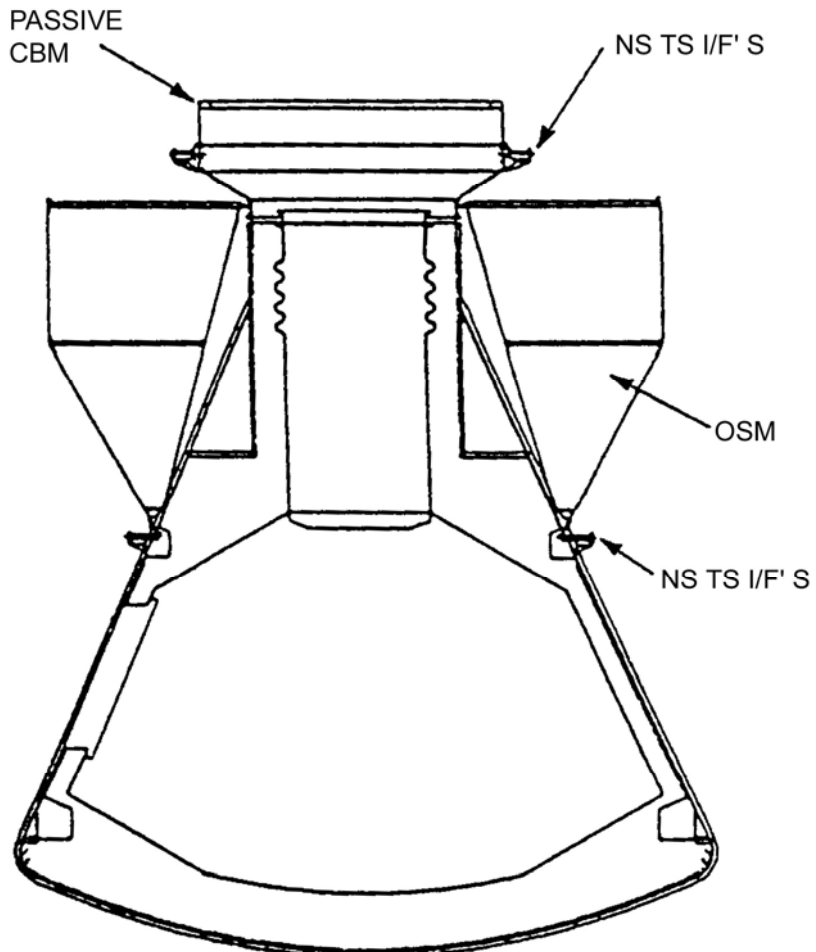


Figure 70.16-1 - ACRV flight vehicle: General layout

70.17 Deep space missions

70.17.1 CNSR ROSETTA: Earth return capsule

The capsule concept is shown in [Figure 70.17.1](#), Ref. [70-22].

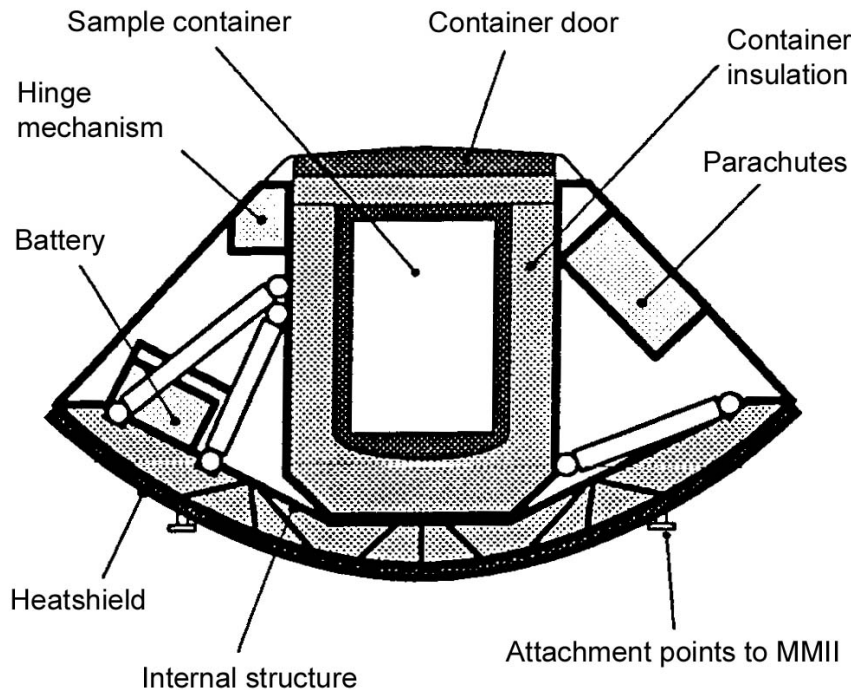


Figure 70.17-1 - CNRS ROSETTA: Aerocapsule configuration

It has a SEPCORE® layered protection system, where the load-bearing heat shield is SEPCARBINOX® C-SiC with an external ablative layer and internal thermal insulation.

The capsule total mass was 320kg, an external diameter of 1.63m and a 60° cone forward shape, Ref. [70-22].

Severe conditions were anticipated for a peak deceleration of 55 g and heat fluxes to 10MW/m² at the stagnation points. The mass budget of 140kg for the SEPCORE® heatsheet, i.e. 44% of total, reflects the heat management problem.

70.18 Mars landers

70.18.1 General

Viking Mars lander was the first successful visit to the planet. Further exploration programmes are planned.

70.18.2 NASA Pathfinder/MESUR network landers

The MESUR (Mars Environment SURvey) vehicle is based on the Viking vehicle's forebody aerobrake shape, Ref. [70-27]. A parachute-assisted descent aids separation of the payload package from the aeroshell. The aerobrake's diameter is 2m. A peak stagnation heat flux of 0.8MW/m² is envisaged which is not particularly high, enabling a range of TPS options to be considered, including improved silica tiles (ex-Shuttle), silicone ablatives (SLA-561, ex-Viking) or AVCOAT 5026 material (ex-Apollo).

70.18.3 MARSNET

The application of C-SiC thermo-structures is envisaged for the decelerator and heat shield, Ref. [70-28].

[See: 71.18 for aeroshell concepts for Mars landers]

70.19 Cassini-Huygens

70.19.1 General

For entry into the Titan atmosphere, NASA and ESA have sponsored programmes to study different thermo-structural configurations. These being the Cassini orbiter (NASA) and the Huygens probe (ESA). Cassini-Huygens is due for launch in 1997 and will reach Titan in the year 2004.

The Huygens heat shield construction falls into two possible categories:

- beryllium-based technology, Ref. [70-29], [70-30], [See: 71.15], or
- C-C constructions.

Titan has a non-oxidising atmosphere which enables the use of unprotected C-C.

70.19.2 C-C aerobrake (heat shield)

The Huygens concept is shown in Figure 70.19.1. It has an outer diameter of 3.1m with an inner diameter of 1.65m, Ref. [70-13], [70-15], [70-19].

The development deployable system is based on six SEP manufactured C-C panels linked together by a fish-plate and fastener system. The C-C skin is 0.5mm thick, reinforced by stringers and stiffeners. Each 3D multilayer woven conical panel is 600mm x 600mm, [See: Figure 70.19.1]. The total mass of the system is 21.3kg. This design was successfully both mechanically and acoustically tested, Ref. [70-19].

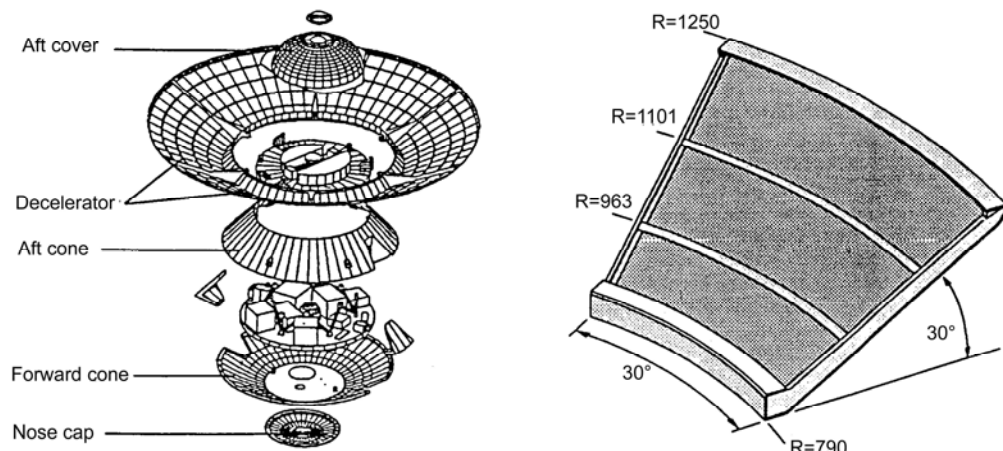


Figure 70.19-1 - Huygens: C-C decelerator design

70.19.3 Nose cap front shield with AQ60

This Huygens concept is manufactured by Aerospatiale, Ref. [70-31], to withstand the high heat fluxes (1.35MW/m^2).

The shield is a CFRP/aluminium honeycomb sandwich structure with AQ60 TPS applied, as shown in Figure 70.19.2, Ref. [70-31]. The TPS is an Aerospatiale development consisting of silica-fibre felt impregnated with phenolic resin.

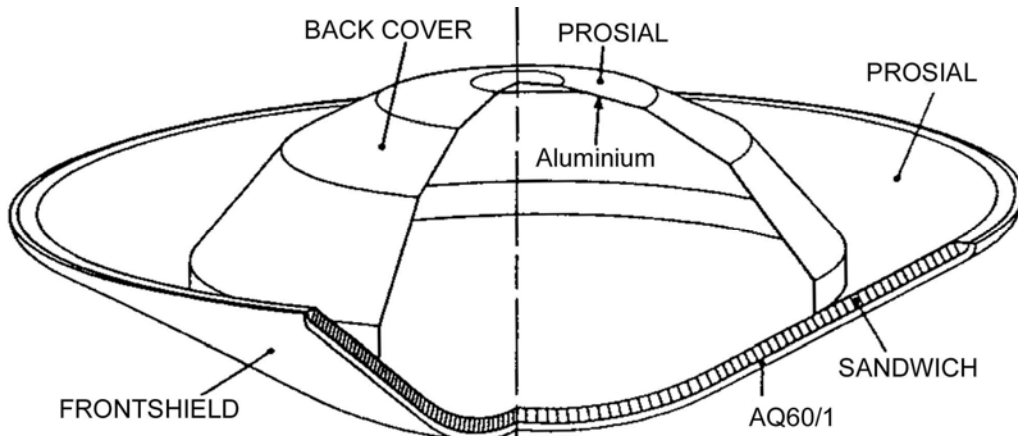


Figure 70.19-2 - Huygens: Nose cap front shield

70.20 Planetary probes

Planets reached by exploratory probes include:

- Venus, [See also: 71.3], Pioneer,
- Mars, [See: 70.18, 71.18], NASA Pathfinder, MESUR and MARSNET,
- Saturn, [See: 70.19], Cassini-Huygens,
- Jupiter, [See also: 71.3], The Galileo orbiter and probe reached Jupiter in December 1995, Ref. [70-27].

70.21 Aerobrake designs

70.21.1 General

The forward shield or face of an entry vehicle reacts against the atmosphere to provide a braking action. Aerobrake, heatshield and aeroshell are terms used variously to describe this part of a vehicle, [See also: 70.25].

70.21.2 NASA/ESA Cassini-Huygens mission

A deployable high-drag decelerator has been investigated, Ref. [70-29]. The vehicle decelerator is a means of increasing the overall braking area, in conjunction with the forward cone. The decelerator, connected to an aft cover, and forward cone are jettisoned once their role has been fulfilled.

Originally a thin skin C-C construction was proposed. This, however, proved inadequate because the skins buckled. The elimination of the matrix was suggested, with the basic carbon fibre fabric retained and stretched between a structure. The fabric forms an axisymmetric concave shape, as indicated in [Figure 70.21.1](#), for assembly with the overall vehicle shown in [Figure 70.21.2](#), Ref. [70-29]. Beryllium was proposed for the struts of the deployment armature. The total mass of the deployable decelerator was estimated at 25kg and experiences temperatures up to 600°C.

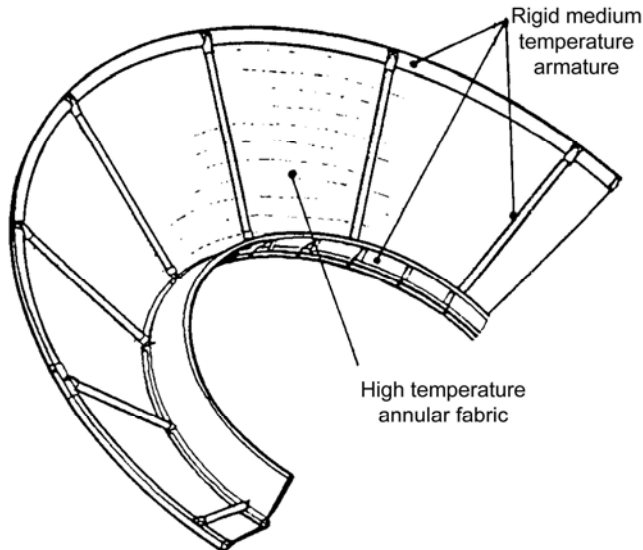


Figure 70.21-1 - Cassini-Huygens: Stretched carbon skin decelerator

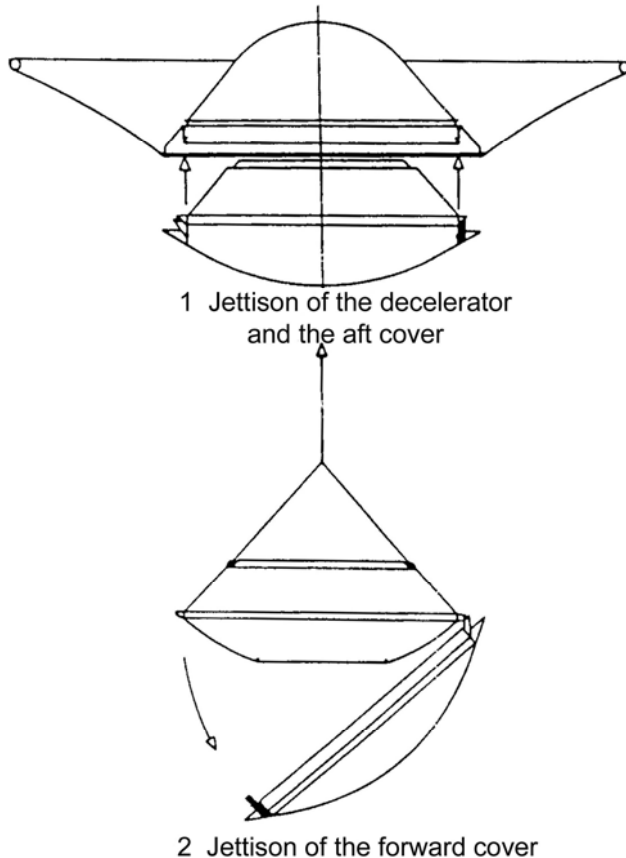


Figure 70.21-2 - Cassini-Huygens: Separation sequence

70.22 PRORA: USV – unmanned space vehicle

70.22.1 Background

70.22.1.1 RLV development approach

The majority of RLV reusable launch vehicle programmes worldwide are based on the well-known logic leitmotiv:

Frequent access to space → Reusability → Cost reduction

RLV development involves extensive use of flight demonstration. Instead of expensive, highly system-integrated flight vehicles, future research needs vehicles to be simpler and less costly. The emphasis is then the flight demonstration of a particular set of technologies and cost-effective operations, rather than full-scale vehicle system development of production, mission-sized, spacecraft. Consequently, this approach enables sub-scale, unmanned, autonomous, or remotely piloted, vehicles to be flight tested at reduced cost and risk.

Various reasons, ranging from technical to political, led to the main geographical areas involved in these activities approaching the problem in differing ways, i.e.:

- USA approach, which is generally the most advanced and traditional, has always been based on a comprehensive integration of ground data with flight experimentation. It has profited from various actions both in the civil and military field. However, from time to time, this approach suffers from top-level decisions, e.g. cancellation of X33 and X34.
- Japan, although adopting the US approach, has limited it to a particular project, i.e. Hope, with has already made three flight tests with another two envisaged.
- ESA in Europe has lacked flight experimentation compared with the US. Both institutional and industrial sectors now talk of flight demonstrators; ARD being the first of these. The programmes consist of research work and technology development along with ground testing. This means that flight tests are feasible after 4 to 5 years work.

70.22.1.2 PRORA: Italian national aerospace research programme

CIRA is responsible for the Italian national aerospace research program; known as PRORA. This program involves the integration of research centre infrastructures, including a number of laboratories some of which have world-class facilities. As of December 2000, PRORA became the major instrument for research development. As a result, a decision was made to concentrate on a number of technological areas, developing scientific and technological knowledge whilst making use of the available laboratories and facilities, and integrating the ground testing capabilities with flight test beds (FTBs) to provide technological demonstration.

For space technologies, activities were identified based on the premise that space plane-type vehicles, e.g. SSTO-HTHL, will become the means of access to space in the long term. Such vehicles need innovation and maturation in three main areas, i.e.:

- Sustained hypersonic flight,
- Atmospheric re-entry,
- Reusability.

PRORA covers technology developments in these areas, up to their validation either on ground or on-board flight test beds. FTBs can be used in different ways, i.e.:

- Experimental models in themselves (e.g. specific demonstrators),
- Vehicles on which passenger experiments can be allocated,
- System demonstrators.

Experimental flight vehicles are the critical link in the ultimate validation of design methodologies for future mission applications and of an integrated vehicle system's operational capability. Flight test often reveals and, hopefully, solves many design issues and systems problems that were not discovered during the initial design and ground test series.

In many cases, technologies and their integrated effects can only be truly evaluated in flight, because real operating envelopes and conditions can only be found under actual flight conditions.

With the aim of an incremental test objective approach, starting from a proposal made in the 1940s and renewed few years ago by Alenia Spazio, the PRORA-USV concept of an experimental vehicle, launched from a stratospheric balloon, to be the best compromise between vehicle performance, test objectives and development costs.

70.22.2 USV programme

70.22.2.1 Objectives

The main objective of the programme is to provide a technological focus for research activities in the field of aerospace. Within this, the USV (unmanned space vehicle) programme aims to identify, develop and validate a number of necessary key technologies that are considered as representative of the needs for future new generation reusable space transportation vehicles. It assumes that a 'future' space vehicle is intended to fly 20 to 25 years from now; taking-off from an airport-like launch site and is operated like a civil aircraft.

70.22.2.2 Technologies

The development of an aerospace vehicle presupposes the availability of specific macro-technologies, i.e.:

- Atmospheric re-entry, where the aerospace vehicle has to cope with the typically large thermal loads encountered when re-entering Earth's atmosphere from LEO. These occur during braking from Mach 25 or so, to a few hundreds of km/h for landing.
- Hypersonic flight, where future space vehicles will fly for large parts of its mission at speeds much greater than the speed of sound. They also have to manoeuvre safely under such conditions and cope with high thermal loads generated by atmospheric friction.
- Reusability, where the most important characteristic from the operational point of view, is to behave, as far as possible, like a conventional aircraft.

Many other technology areas are also involved in the development process, e.g. propulsion, flight mechanics, stability and control, guidance and navigation, aero-thermodynamics.

70.22.2.3 USV programme structure

In order to meet the main goal, the USV programme has two main parallel activities:

- Development of technologies oriented towards medium-long term needs.
- Design and creation of flight test beds; designated FTB_1, FTB_2 and FTB_3.

The system design activities envisaged three different vehicles to demonstrate and validate, under real flight conditions, the developments made in the strategic technologies. Moreover, as each test bed hosts a small payload, the effectiveness of the concept as a real space system can also be established.

70.22.2.4 USV programme missions

Four specific missions are envisaged; known as:

- DTFT: dropped transonic flight test.
- SRT: sub-orbital re-entry test.
- HFT: hypersonic flight test.
- ORT: orbital re-entry test.

The missions enable testing of the significant features of the space transportation system, i.e.:

- Atmospheric re-entry, where the overall atmospheric re-entry of a winged vehicle is conducted from high altitude drop (DTFT) to sub-orbital (SRT) and LEO (ORT) conditions.
- Steady hypersonic flight, where the hypersonic horizontal steady flight of a winged vehicle (HFT) is conducted.
- Reusability, where the (even partial) capability to reuse the system in subsequent missions is demonstrated.
- Space system operations, where the basic operations of a space carrier, including payload transportation and servicing, de-orbiting, manoeuvring, return to Earth and recovery is accomplished.

70.22.3 USV systems and flight test beds

70.22.3.1 General

The development of the USV system programme is achieved with three ‘flight test beds’, designated FTB_1, FTB_2 and FTB_3. The FTB missions are aimed at testing technologies and critical phases of the typical flight of a future reusable launcher. The overall aim is to progressively validate the ‘final demonstrator’ definition. The missions envisaged also provide the scientific community with opportunities to access space.

70.22.3.2 FTB _1

The FTB_1 performs the DTFT mission, which is mainly aimed at testing the aerodynamics and flight behaviour in transonic regime. The conditions for FTB_1 are those likely to be encountered by a winged launcher stage during its atmospheric entry trajectory from orbit: These conditions are also representative of the FTB_2 SRT mission. The vehicle can accommodate a payload onboard.

70.22.3.3 FTB _2

As FTB_2 performs both the SRT and the HFT missions, this demonstrates the reusability of the vehicle.

The FTB_2 is devoted to testing the aero-thermodynamics, the flight behaviour, the controllability on sub-orbital re-entry and hypersonic horizontal flight, whilst check-out of the general system features applicable to re-entry from space, such as propelled phases, other critical mission phases. The vehicle serves as a flight test bed that carries a suitable payload.

70.22.3.4 FTB _3

FTB_3 winged re-entry vehicle has major features, such as aerodynamic efficiency, innovative thermal protection concepts, integrated flight control capabilities, oriented towards third-generation RLV (ideally HTHL/SSTO).

The FTB_3 is also intended (and will be used) as a flying facility able to perform technological and operational research in the fields of re-entry, sustained hypersonic flight and general space systems.

70.22.4 External configuration of FTB_1 and FTB_2

70.22.4.1 General

The external configuration of the FTB_1 and FTB_2 vehicle is the result of a continuous high-level system design aimed at meeting the aerodynamic, flight mechanics, and equipment allocation demands and constraints. The configurations were derived from similar existing vehicles without performing specific optimisations.

70.22.4.2 Design drivers

The overall vehicle shape was defined on the basis of aerodynamic considerations. The design driver was the need for high efficiency under the envisaged flight conditions, i.e. $L/D > 2.5$ from transonic to hypersonic ranges, together with the necessity to increase the incoming stagnation heat fluxes, in order to enable testing of innovative TPS materials.

70.22.4.3 Geometry

The geometrical constraints assumed were quite challenging from the mechanical and configuration point of view, i.e.:

- Maximum thickness of wing profile: 8%
- Nominal nose radius : < 50 mm

The fuselage dimension, that drives the vehicle size, was determined by the need to accommodate the selected baseline motor, ATK ORION 32, whilst taking into account the TPS thickness.

The solution, based on two vertical fins, was introduced in order to take into account interference with parachute deployment and structural constraints, while matching stability and control requirements.

The vertical fins are moved slightly back with respect to the wings, in order to minimise aerodynamic interference, enabling the wing flaps to work correctly.

Figure 70.22.1 shows the overall external configuration of the FTB_2 winged vehicle.

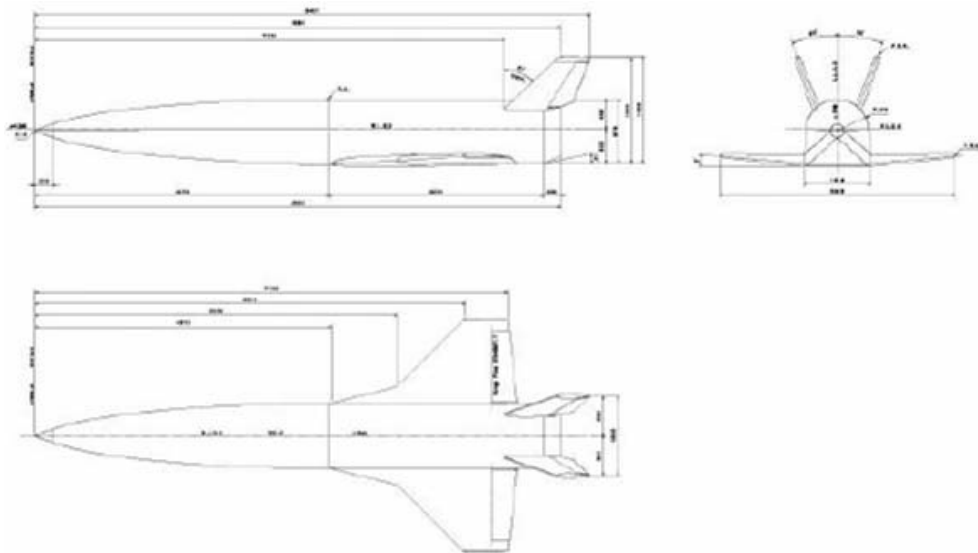


Figure 70.22-1 - PRORA – USV: FTB_2 external configuration

70.22.5 External configuration of FTB_3

70.22.5.1 General

A preliminary external configuration was obtained from a general analysis. This aimed to define major mission and system features.

70.22.5.2 Design drivers

The design drivers and constraints assumed in the design of the vehicle were:

- Envelope constraints, based on the current characteristics of the large fairing of the VEGA launcher; as shown in [Figure 70.22.2](#).
- Geometrical constraints on curvature in stagnation regions, dictated by aero thermodynamic heating thresholds not to be exceeded:
 - nose radius > 300 mm,
 - wing leading edge radius > 30 mm.
- The most slender shape possible, given the other constraints, which offers a reasonable internal space; given that there is no need for an autonomous propulsion system.

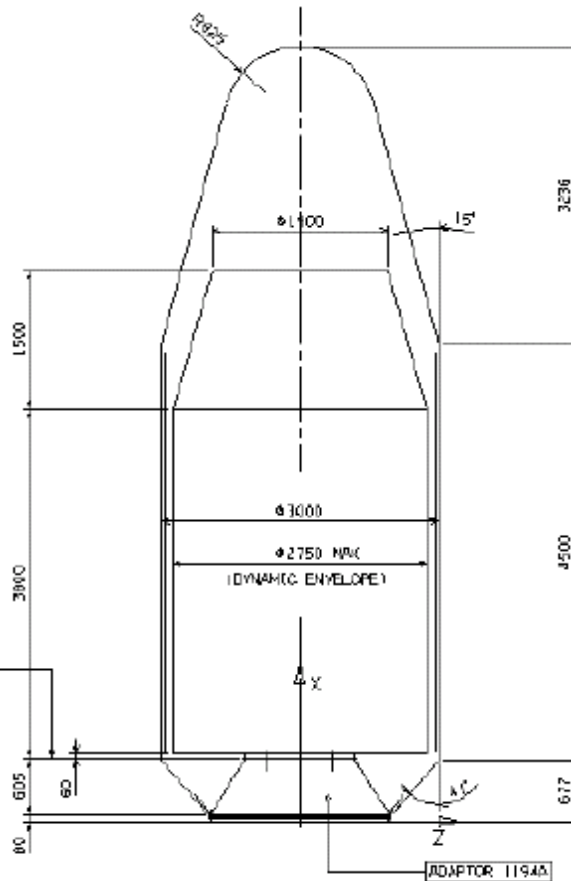
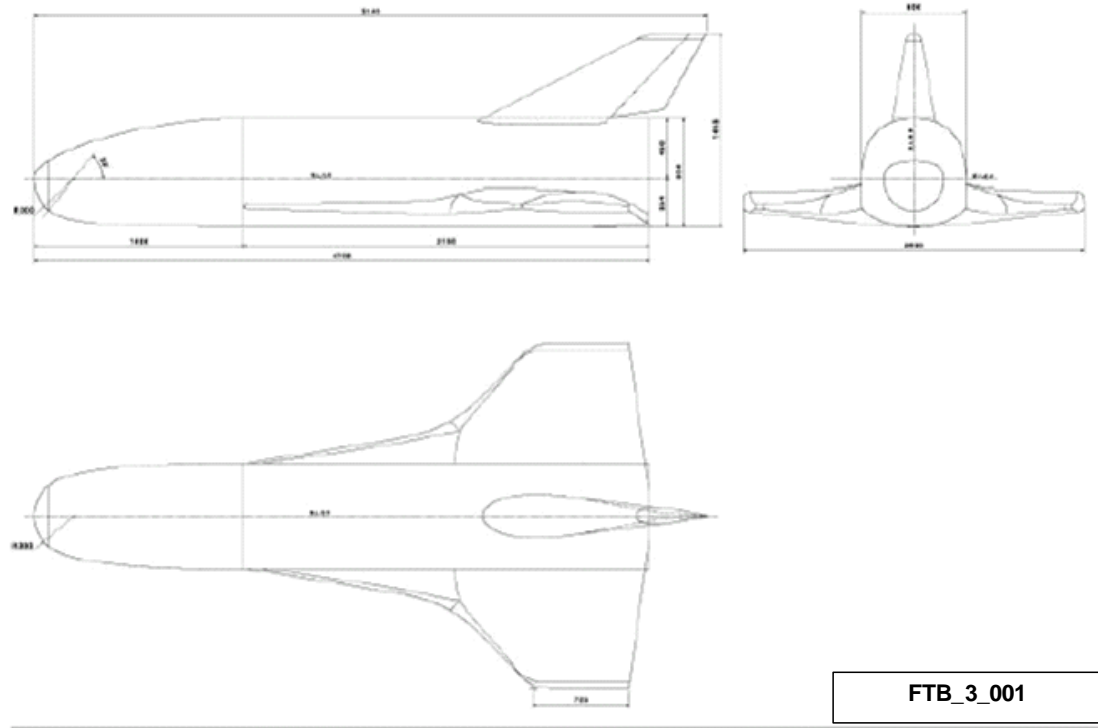


Figure 70.22-2 – VEGA launcher: Large fairing

70.22.5.3 Geometry

The FTB_3 configuration of 2005, known as FTB_3_001, is shown in [Figure 70.22.3](#).



70.23 X-38 Body flap

70.23.1 Background

70.23.1.1 Programme

The X-38 programme covered the development of the CRV (crew return vehicle) for the ISS international space station. CRV would enable an increased number of crew members on ISS. The role is currently undertaken by the Russian Soyuz TMA vehicle, which is limited to 3 crew. The X-38 development programme was cancelled in 2001.



Figure 70.23-1 – X-38: Test vehicle

70.23.1.2 European participation

The NASA X-38 programme included significant participation from European organisations, including MAN Technologie. Under ESA and DLR funding for various programmes, e.g. FESTIP, GSTP, GAP and TETRA, MAN's expertise in CMC enabled the design-development of the body flaps and associated technologies, including C/SiC materials, manufacturing, articulated and static joints and CMC mechanical fasteners, Ref. [70-34], [70-36], [70-37], [70-38].

70.23.1.3 CMC key technologies

The design and manufacture of lightweight thermo-structures, such as rigid TPS, leading edges, fins, rudders and movable control surfaces, applied to X-38, included, Ref. [70-36]:

- CMC bearings for movable hot structures.
- CMC tribology necessary for hot sliding applications.
- Oxidation protection systems for CMC materials.
- CMC fasteners for hot ceramic-to-ceramic joining.
- Hot-to-cold-structure combinations, needed for attaching hot CMC structures to cold metallic structures.
- High-temperature insulation to protect metallic structures.
- High-temperature static and dynamic seals to limit hot gas ingestion or heat transfer and to prevent overheating of structures and components.

At the cancellation of the X-38 programme, the technologies were reasonably mature, available and were qualified for 4 re-entries on X-38 V-201; an orbital prototype vehicle capable of being launched by the Space Shuttle, Ref. [70-36], [70-37], [70-38], [70-39].

The technologies can be considered for future space vehicle projects because they are suitable for most reusable vehicle TPS and hot structure concepts operating under thermo-mechanical

conditions similar to X-38. Further work is on-going within the German national ASTRA programme, Ref. [70-36], [70-39].

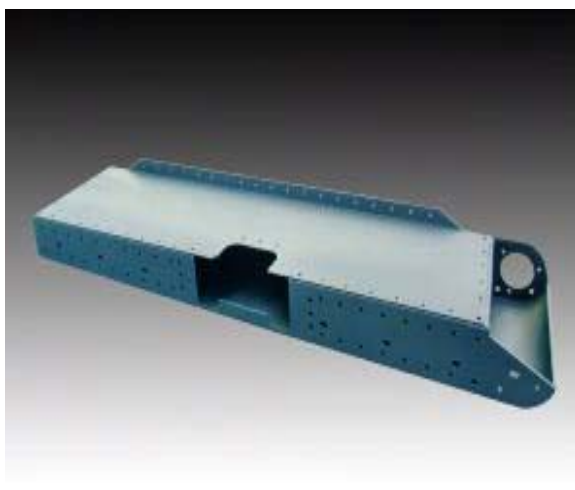
70.23.2 Body flaps

70.23.2.1 General

The X-38 test vehicle had two pairs of moveable flight control surfaces (rudders and body flaps) for the intended autonomous, controlled, re-entry and parafoil-assisted landing. Each body flap moved independently for roll and pitch manoeuvres, Ref. [70-34], [See: Figure 52.7.1]. The flap (1.4 m × 1.6 m) weighed 68kg, which is about 50% of the mass of a conventional type of flap, Ref. [70-36].

70.23.2.2 Construction

The flap structure, developed by MAN Technologie, comprises 4 box sections joined by ceramic fasteners; as shown in Figure 70.23.2, Ref. [70-36].



C/SiC box section: 1700mm × 400mm × 120mm;
wall thickness 2mm to 3mm.



Body flap assembly (4 boxes), using C/SiC
fasteners.

Figure 70.23-2 – X-38 body flap: Construction

Each box was made of C/SiC CMC, which supports high mechanical loads at temperatures up to 1600°C. Each box structure has integral features such as 'T' and 'I' stiffeners, along with plane and curved surfaces.

70.23.2.3 OPC - oxidation protection coating

An oxidation protection system is used to enable operation of C/SiC CMC in oxidising atmospheres. A multilayer OPC, initially developed during under HERMES and FESTIP programmes, was adapted and tested to meet the demands of X-38, Ref. [70-36], i.e.:

- Prevent oxygen diffusion into carbon reinforcing fibres.
- Chemical compatibility between coating and C/SiC substrate with no degradation of the substrate.

- Thermal resistance in air over a wide temperature range of 500°C to 1700°C, especially between 500°C to 750°C, and extreme plasma and hot air flow conditions at 1700°C.
- Good adherence to the substrate, with damage and spall resistance.
- Economic, industrial processing methods for applying coatings.
- Applicable to different sized and shaped parts, e.g. coating thickness.
- Suitable for C/SiC materials manufactured by different processes.

The development of OPC also considered the need for different coating thicknesses for particular components, e.g.

- Thin coatings: Mechanical fasteners, e.g. screws, nuts and washers.
- Medium coating: Large components, e.g. boxes
- Thick coatings: Highly mechanical loaded parts, e.g. bearings.

Results of various oxidation tests, including static, cyclic and post-oxidation bending, indicated that a minimum OPC thickness of 50µm will ensure material properties are maintained, with respect to RT strengths, under the stipulated exposure conditions (time and temperature). Only a small oxidation effect on residual bending strength was seen on samples exposed to the equivalent of 10 re-entries, i.e. 5 hours, at 700°C, 1200°C and 1700°C, Ref. [70-36].

The carbon fibres exposed after holes are machined in C/SiC for fasteners (bore holes) were protected using a combination of design to minimise tolerances and so limit oxidative attack, along with a slurry technique to restore the OPC coating. Repair techniques for damaged OPCs were also conducted using slurries, Ref. [70-36].

70.23.3 Mechanical fasteners

The body flap CMC components are assembled using mechanical fasteners made of C/SiC, e.g. screws, nuts and washers; as shown in [Figure 70.23.3](#), along with a cross-section of an installed test fastener, Ref. [70-36].

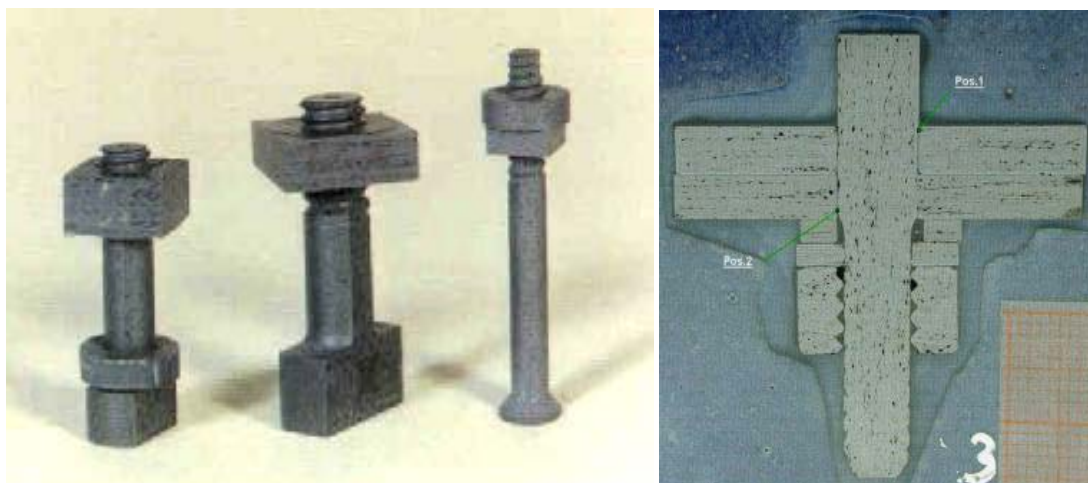


Figure 70.23-3 – X-38 body flap: Mechanical fasteners

The characteristics of C/SiC fasteners can be summarised as, Ref. [70-36]:

- Reduced mass. 4 to 8 times less than refractory metal fasteners.
- Strength of C/SiC fasteners does not reduce with temperature.
- Need protection against oxidation, so OPC applied to all fastener components prior to assembly.

Table 70.23.1 summarises the basic properties of C/SiC fasteners at 1600°C used for assembling the body flap, Ref. [70-36].

Table 70.23-1 – X-38 body flap: Mechanical fasteners – properties

Fastener diameter (mm)	Properties at 1600°C	
	Minimum tensile strength (kN)	Minimum shear strength (kN)
6	3.5	2.6
8	6.5	4.7
10	10	7.3

Fasteners capable of being installed with single-sided access were necessary for attaching the body flap covers. This was accomplished using a 'nut-strip', Ref. [70-36].

After qualification testing of an assembled body flap, evaluation of the installed fasteners showed no change in properties when compared with new fasteners, Ref. [70-36].

70.23.4 CMC to metal attachment

The CMC body flap is joined to the aft beam and structure of the X-38 vehicle, which is made of aluminium alloy. The design of this attachment took into account the mechanical loads (4 tons), body flap movements and the thermal conditions. A main objective was to prevent heat from a CMC part (designed for 1600°C) reaching the aluminium alloy part (limited to 175°C) within a path of 200mm.

Figure 70.23.4 shows the CMC to metal attachment design and the main components, Ref. [70-36].

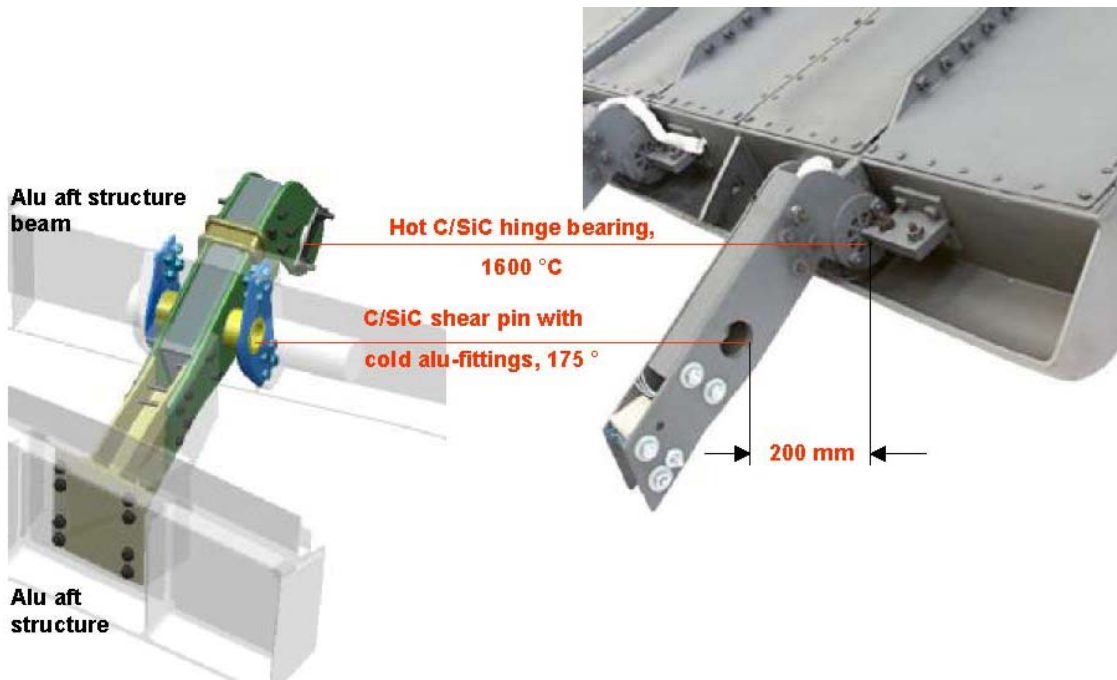


Figure 70.23-4 – X-38 body flap: CMC to metal attachment

70.23.5 Ceramic bearings

Ceramic bearings were used for mounting the flap on the vehicle aft structure, as load introduction points and in articulated joints to enable the flap to move. The flap is moved with a metal rod that is attached to the bearing. The metal-to-ceramic interface was designed for temperatures up to 1100°C and mechanical loads up to 70kN (static) and 40kN (dynamic).

Figure 70.23.5 shows the ceramic bearing, which was designed to perform under re-entry conditions, Ref. [70-36]:

- Sliding in air from RT to 1600°C.
- Retain tolerances (clearances) during local temperature differences of up to 600K.
- Resist heat-up at 300°C/minute.

The main operational demands were that, under combined thermal and mechanical loading, the ceramic bearing, Ref. [70-36]:

- Performed for 10 minutes per re-entry at >1400°C,
- Was reliable for 4 re-entries (4000 movements),
- Sustained static and dynamic loads.

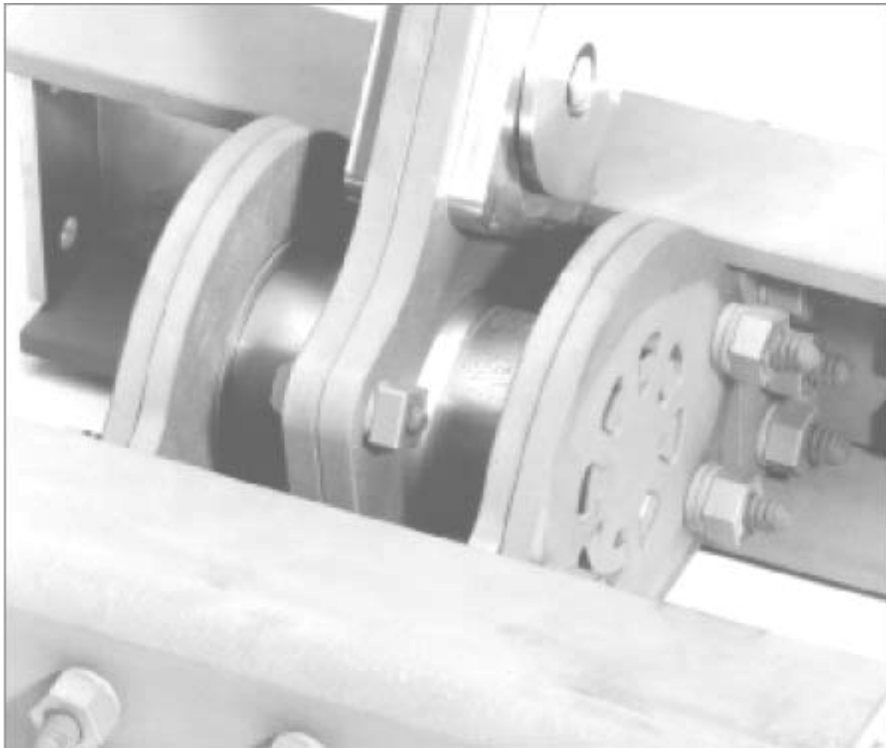


Figure 70.23-5 – X-38 body flap: Ceramic bearing

70.23.6 Ceramic seals

Static and dynamic seals developed for X-38 flight vehicle V201 have to resist a number of operational demands, Ref. [36]:

- Oxidative environment and temperatures up to 1700°C.
- Combined convective and radiation heating.
- Different thermal expansion of seal parts.
- Wear resistance, with coefficients of friction from 1.07 to 1.17.
- Component movement and rotation.
- Low pressure to high differential pressure.
- Low permeability to minimise leakage, i.e. 1×10^{-10} to $1 \times 10^{-11} \text{ m}^2$.

Static seals were applied for the nose, rudders and the leading edges of the vehicle.

Dynamic seals were used for the two movable body flaps, mainly to prevent hot gas flow through the gap between the flaps and the aft structure of the vehicle; as shown in Figure 70.23.6, Ref. [70-36].

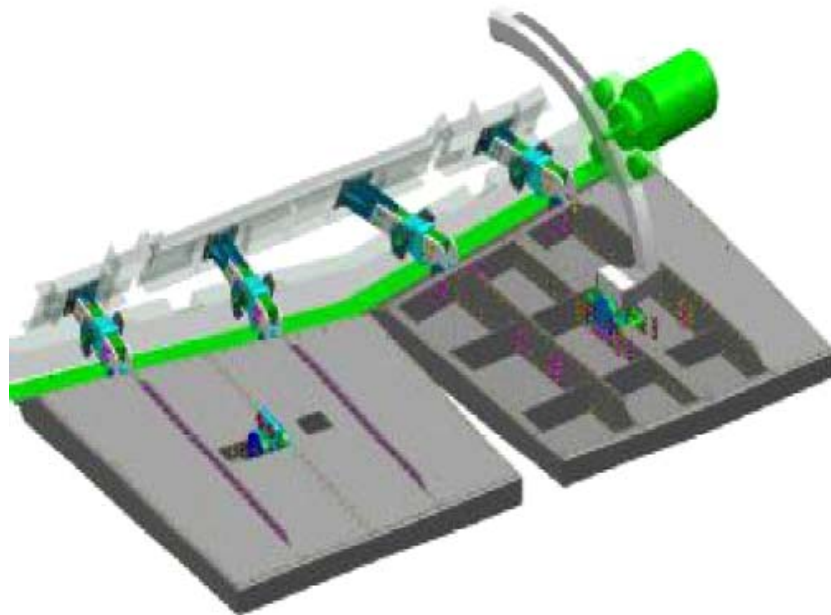


Figure 70.23-6 – X-38 body flap: Ceramic dynamic seal

Both dynamic and static seals were essentially 'stuffed ceramic fabric core'. The material and components were qualified under thermal and mechanical loads for the X-38 mission. These conditions did not damage the seals. A 20% seal pre-compression provided effective blocking of flow through the gap with less than 1% leakage. The seals survived up to 1000 scrub test cycles and remained securely attached. The seals had no effect on the movement or rotation of the ceramic components. The seals were also effective thermal barriers to limit heat convection.

70.24 X-38 Nose cap

70.24.1 Background

Figure 70.24.1 shows the various parts of the X-38 NSA nose assembly and the various participants in the design-development programme, [See also: Figure 70.23.1; 70.23 for details of the X-38 demonstrator vehicle].

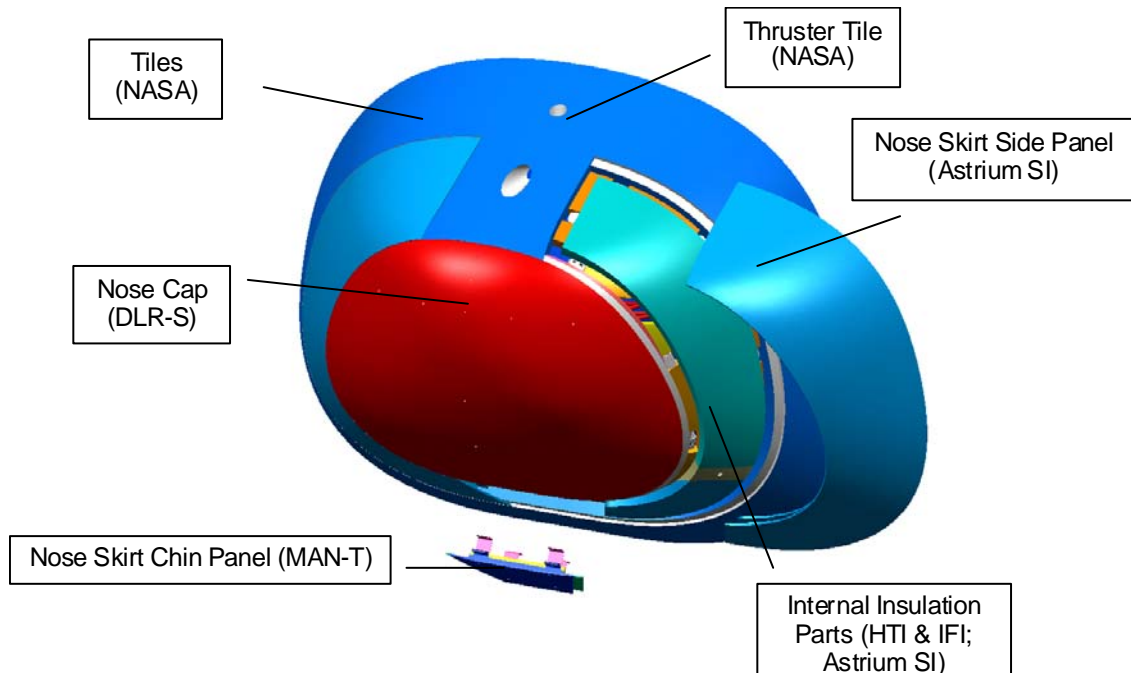


Figure 70.24-1 – X-38 Nose assembly

70.24.2 Concept

70.24.2.1 General

A TPS was developed to protect the substructure against temperatures up to 1750°C, reached in the stagnation area during re-entry. This comprised of C/SiC panels on the outer surface, with the remaining volume (between the TOML ‘outer mould line’ and SOML ‘structural outer mould line’) filled with different types of flexible insulation blankets, Ref. [70-40], [70-41]:

- IFI internal flexible insulation placed on the cold substructure, [See: 71.11].
- HTI high temperature insulation placed in the outermost region, [See: 71.23].

70.24.2.2 IFI

IFI was a side-product of the development of FEI ‘flexible external insulation’, [See: 71.11]. It is similar to FEI in that it has a blanket-like configuration. An alumina-based core fleece is covered with an alumina fabric and sewn together using an ABS alumina-boro-silicate thread. The maximum re-use temperature is 1200°C. [See: Figure 71.11.2].

70.24.2.3 HTI

Owing to the high temperatures in the outermost regions of the TPS, especially near the stagnation point, it was not possible to use existing insulation products, so a new HTI ‘high temperature insulation’ had to be developed, [See: 71.23].

70.24.3 Thermal profiles

Figure 70.24.2 shows the temperature profiles of the nose assembly and side panel at the hottest trajectory point, Ref. [70-40], [70-41].

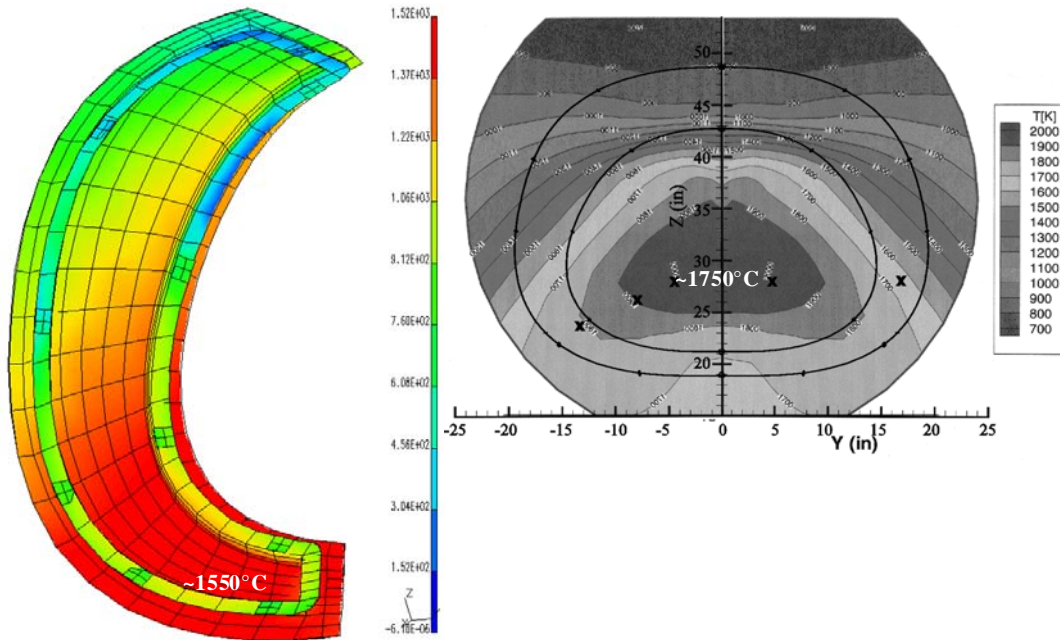


Figure 70.24-2 - X-38 Nose assembly: Thermal profiles

70.24.4 Flexible insulation design

Previous experience of FEI-type materials, including IFI, along with the results of development tests for HTI, was incorporated into the overall insulation design, Ref. [70-40], [70-41]:

- Both HTI and IFI were slightly oversized in thickness; each about 1mm. During integration of the C/SiC hard TPS parts, the insulation system was slightly compressed to account for possible thickness shrinkage.
- To account for possible in-plane shrinkage, the blanket distribution within the nose area was organised such that the interfaces between the individual blankets in the IFI and HTI area were at different locations. This ensured that the substructure was always protected by the IFI even if a small gap occurred in the hottest areas of the HTI.
- Shrinkage was only foreseen in areas where the maximum temperatures exceeded 1625°C. The HTI was divided into:
 - one large blanket covering the hottest area of the nose cap;
 - several smaller blankets in the cooler regions.
- Only one blanket had to be changed if refurbishment was necessary after one flight.

An additional intermediate HTI layer was necessary because of a variable offset between the TOML and SOML. It was made of HTI core material only (no fabric, no threads) and a variable height. This layer also further enhanced the ability to adjust the overall insulation design because its height was adapted manually to account for variations in the nominal height of the other insulation layers. Figure 70.24.3 shows the distribution of IFI and HTI within the nose assembly, Ref. [70-40], [70-41].

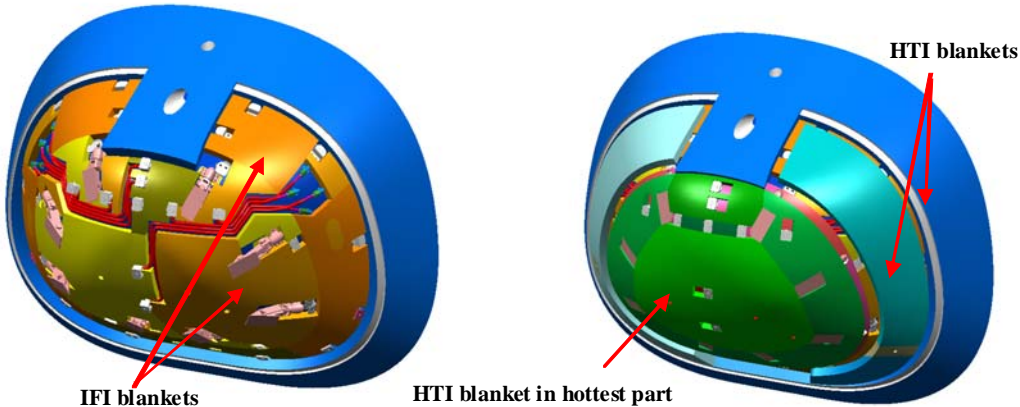


Figure 70.24-3 – X-38 Nose assembly: Flexible insulation distribution

70.24.5 Integration and qualification testing

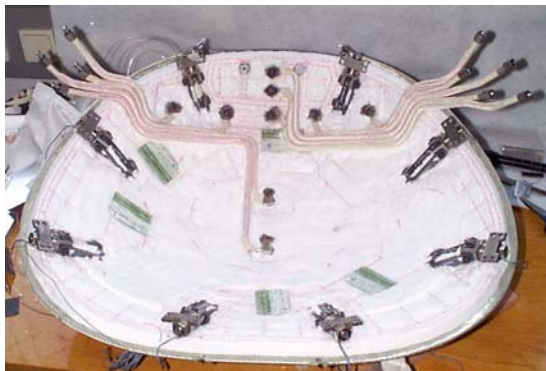
70.24.5.1 Insulation

The qualification of HTI was part of the overall nose assembly qualification test, but only items relevant to the internal insulation are described here. The testing had several steps, Ref. [70-40], [70-41]:

- Assembly.
- Thermal cycle test.
- Vibration test.
- Disassembly and visual inspection.

70.24.5.2 Assembly

Figure 70.24.4 shows the various steps in the integration of the qualification unit. All parts were assembled successfully.



HTI integration in nose cap area completed



HTI and IFI integration in nose cap area completed



IFI integration in nose skirt area completed

HTI in 'Side Panel'
(after qualification test and disassembly)**Figure 70.24-4 – X-38 Nose assembly: Flexible insulation assembly**

70.24.5.3 Thermal qualification test

The main results of the thermal qualification testing can be summarised as, Ref. [70-40], [70-41]:

- Temperatures: Levels and temperature gradients were in good agreement with those predicted.
- Displacements: Measured displacements and time-dependent deformation were in good agreement with deformation analysis.
- Thermocouples: Signals were in good agreement with prediction, with no damage or degradation of thermocouples or their fixings.

70.24.5.4 Disassembly and visual inspection

Further testing was envisaged by DLR-Stuttgart, so the nose cap was not disassembled. The observations relate only to the 'side panel' area, Ref. [70-40], [70-41]:

- Colour change to grey (partial).
- Shape:
 - no general shrinkage detected;
 - two small local gaps probably occurred during integration.
- Flexibility: No change except for the hottest areas, where a slight embrittlement of the blanket surface occurred.

70.24.5.5 Conclusions

The overall conclusions drawn from the qualification test can be summarised as, Ref. [70-40], [70-41]:

- Thermal test was successfully performed with no deviations reported
- Insulation system worked as expected
- No damage or degradation was detected on HTI blankets in the 'side panel' area; $T_{max} = 1550^{\circ}\text{C}$.
- HTI was qualified for use on X-38.

The decision on the multiple-use capability of HTI was deferred until after disassembly of the post-tested nose cap.

70.24.6 Summary

70.24.6.1 Development

The internal flexible insulation system used in the X-38 nose area needed the development of HTI 'high temperature insulation'. A series of development tests enabled the selection of materials and the blanket configuration, [See: 71.23].

The tests also provided input to the overall insulation design, which is capable of accommodating uncertainties in blanket thickness as well as small gaps in the HTI, if these occur, [See also: 71.23].

70.24.6.2 Status

Although it remains to be clarified whether the HTI is capable of multiple use, it was nevertheless qualified as part of the overall insulation system for flight on X-38 in the nose assembly qualification test.

The insulation flight hardware was shipped to NASA. The X-38 nose cap, with its HTI and IFI insulation blankets, was successfully assembled in the nose structure of the X-38 vehicle; as shown in Figure 70.24.5, Ref. [70-40], [70-41].

Unfortunately NASA cancelled the project when the integration of vehicle V201 was 90% complete.

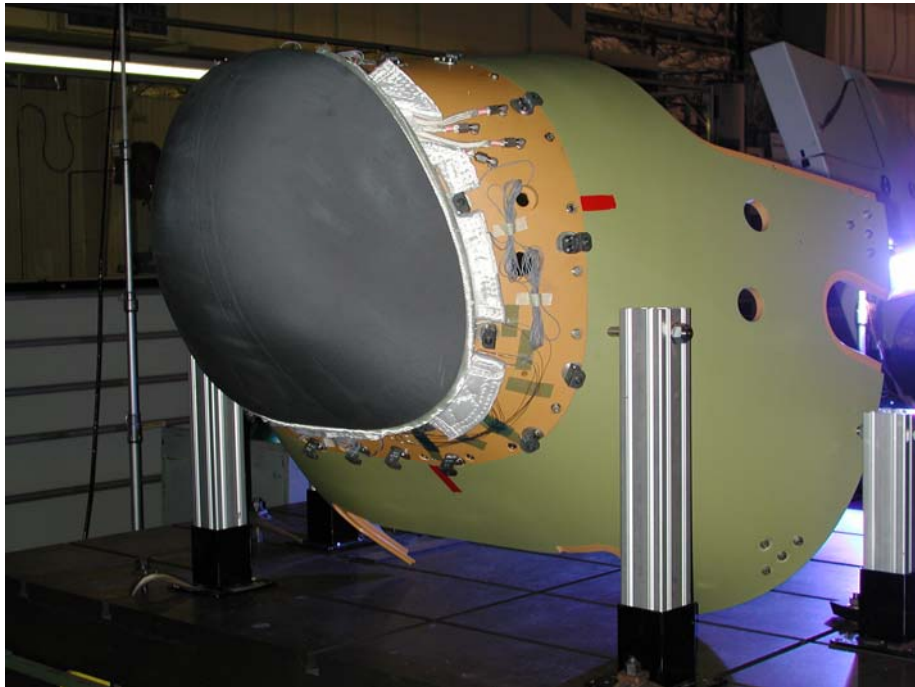


Figure 70.24-5 – X-38 Nose cap with insulation mounted on vehicle nose structure

70.25 Aerobrake: Deployable CMC decelerator

70.25.1 Background

70.25.1.1 Planetary missions

Both NASA and ESA planetary missions anticipate payloads with a greater mass and volume. This means the aerobraking system will have to be larger than that possible within existing payload carriers, e.g. an 8 m to 9 m diameter aerobrake for a Mars mission, but contained within a 4 m launcher payload fairing. The constraint of available launcher volumes led to the concept of deployable aerobraking systems. A potential candidate for a deployable heat shield is a foldable hot structure aeroshell made of CMC, Ref. [70-42], [70-43].

Another possible application is for a foldable stabiliser for a small ISS payload re-entry capsule, Ref. [70-42], [70-43].

70.25.1.2 Objectives

The main objectives for deployable CMC decelerators can be summarised as, Ref. [70-42], [70-43]:

- Lightweight load-carrying aeroshells and thermal protection of space probes in order to maximise the scientific payload.
- CMC technology is sufficiently mature, due to qualification of some TPS and hot structures, to enable its consideration for innovative designs for planetary probes, i.e. better mass performance, particularly for the external aeroshell.
- Functional reliability and the demands for cleanliness and low contamination are very important for scientific or manned probes.

- ESA-funded studies have shown that CMC aeroshells, when compared with ablator-type heat shields, can withstand the high thermal shock conditions during entry into an atmosphere and can also resist dust erosion.
- CMCs provide a high margin of safety against micrometeoroids during transfer or orbital phases. CMCs have high damage tolerance against micrometeoroid and debris impact during atmospheric entry.

70.25.2 Mars ISRU mission ‘in-situ resource unit’

The application example chosen for a preliminary investigation of the design concept for a foldable hot structure decelerator was the Mars ISRU mission, which has a Viking-type (biconic) deployable aeroshell. The lander mass is assumed to be 8.2 tons, including 1.5 tons for the deployable heat shield. The folded part with the payload and central rigid aeroshell cannot exceed more than about 4.8 m and the unfolded aerobrake decelerator structure needs to be about 8.5m diameter, Ref. [70-42], [70-43].

70.25.3 Mars ISRU mission – Concept

70.25.3.1 Aero-assist aeroshell configuration

A constraint for a Martian aeroshell concept is the need for a certain level of control for landing accuracy. If this is a design-driver for the aeroshell, then the heat shield and foldable decelerator can have a suitable aero-assist configuration.

The dimensions of the folded and unfolded aeroshell are similar to the axis-symmetrical Viking version. The disadvantage of this concept, compared with a symmetrical version, is the higher tooling cost for both the central heat shield and the decelerator TPS panels. The largest panel of the decelerator in this version is about 1.9 m, which is a suitable size regarding the mechanical load level for each panel and the manufacturing feasibility.

70.25.3.2 Central heat shield

The options for the design of the central heat shield were subjected to a mass trade-off study, Ref. [70-42], [70-43]:

- Cold structure, covered with low-density ablator tiles, with deployable ablator coated aluminium panels.
- Cold structure, covered with C/SiC CMC TPS panels attached using PM1000 alloy stand-offs. This configuration was qualified up to flight hardware level for X-38 for a very lightweight panel wall thickness of 1.6 mm for temperature up to 1600°C.

Table 70.25.1 summarises the mass trade-off for both concepts. The cost of each concept is similar, Ref. [70-42], [70-43].

Table 70.25-1 – Deployable CMC hot structures – Mass trade-off study

C/SiC concept:	Density (g/cm ³)	Mass (kg)
C/SiC segments, stringer stiffened; Wall thickness 1.7 mm	2.2	72
FEI internal insulation; Thickness 35 mm	0.1	64
Metal fasteners and stand-offs, e.g. PM1000 alloy	-	6
C/SiC Segmented decelerator; Wall thickness 2.4 mm	2.2	239
Deployment mechanism (aluminium struts, spring-loaded): Hinges, rods, actuator ring, springs	-	69
	Total mass:	450 kg
<hr/>		
Ablator concept (excluding cold structure):	Density (g/cm ³)	Mass (kg)
Ablator; Thickness 15mm	0.6	219
Deployable aluminium panels; Wall thickness 2 mm	2.8	461
Ablator on deployable aluminium panels; Thickness 10 mm	0.6	357
Deployment mechanism (aluminium struts, spring-loaded): Hinges, rods, actuator ring, springs	-	69
	Total mass:	1106 kg

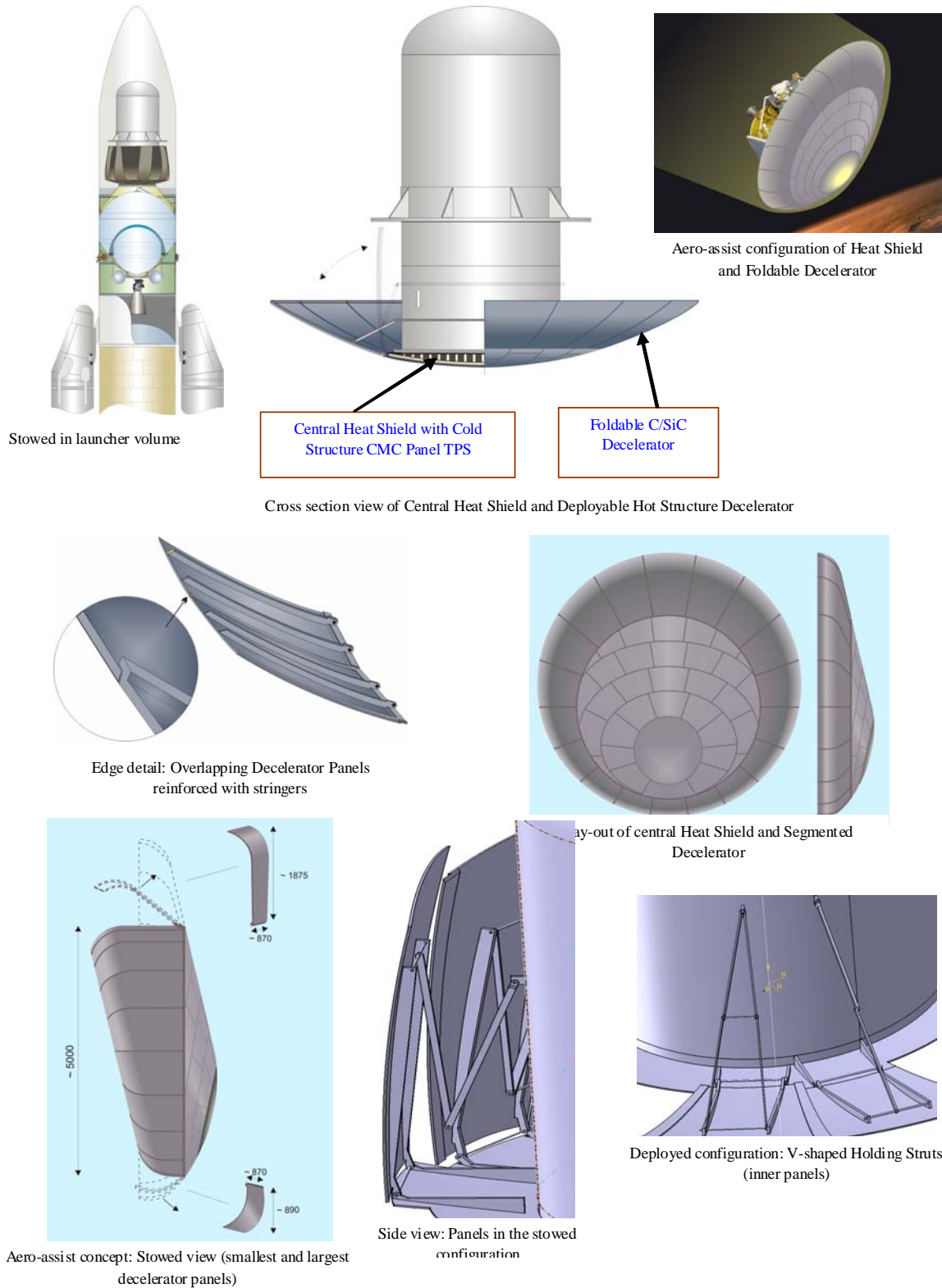
An advantage of a CMC heat shield compared with an ablator system is that it is a clean, non-polluting, material suitable for use in the Mars environment, which is a subject of considerable scientific importance. An oxide-based ceramic TPS panel is of interest where the temperature is less than 1100°C because production costs of oxide-based CMC is about 50% less than C/SiC.

Figure 70.25.1 illustrates the overall C/SiC concept, along with some of the design details of stowed and deployed configurations, Ref. [70-42], [70-43].

70.25.3.3 Foldable decelerator

Previous experience with the manufacture and qualification of large TPS panels (X-33 and X-38 programmes) showed that ultra-lightweight C/SiC panels are feasible for the structural configurations proposed.

The foldable decelerator structure is divided into 20 separate C/SiC panels with a wall thickness of about 2.4 mm. The conical shape of the decelerator provides a self-stiffening effect if the panels are connected at the outer edges after unfolding. The panels are stiffened by stringers, integrally fabricated into the composite structure, to resist initial pressure and acceleration loads on individual stowed panels without the benefit of the cone stiffening effect, Ref. [70-42], [70-43].



Reproduced courtesy of Astrium (L)

Figure 70.25-1 – Deployable CMC hot structures - Mars ISRU mission

70.25.3.4 Unfolding and deployment

The folding mechanism can be a simple, reliable, spring-loaded mechanism. The segmented conical decelerator is supported by unfolding struts and the opened shape can be backed to a self-stiffening system by a locking device around the outer edges of the panels. Around the edge of the central heat shield, the 20 decelerator panels are mounted in two concentric layers such that they can be folded towards the spacecraft to reduce the stowed volume. The outside panel rests against the overlapping inside panel gaining torsional stiffness from the V-shaped struts. In this way the outside panels only need a strut for deployment, so providing simplicity and potential weight-saving.

The folding struts control deployment and form a structural element in the deployed configuration. Form locking joints, not included in the concept described, ensure that the struts cannot fold back on themselves once deployed.

The inner panels have V-shaped struts in order to provide torsional stiffness to the panels. As the outer panels are able to support themselves on the overlaps with the inner panels, they are supported by simpler struts to save weight and reduce complexity.

The second function of the overlap ensures that no gaps occur between the panels through which hot gases can penetrate.

The deployment mechanism can be actuated to deploy all panels simultaneously, or using individual actuators to provide a synchronised movement.

A simple spring-actuated system, as used in deployable antenna structures, is the baseline concept. The deployment mechanisms have damping devices to control the deployment speed, e.g. by eddy currents.

70.25.4 Mars ISRU mission – Environmental aspects

70.25.4.1 Micrometeoroids and debris impact

Micrometeoroids striking the single wall hot structural decelerator do not cause serious damage to the structure or shape. The results of hypervelocity impact tests on CMC structural materials showed that the impacted area and size of the resulting holes do not disturb the aerodynamic flow or damage the structure significantly, Ref. [70-42], [70-43].

Even if the size of the impacted hole is about 4 times larger than the impact particle size, the damage zone is not enlarged significantly by the heat flux and dynamic pressure conditions during entry into the atmosphere, Ref. [70-42], [70-43].

From preliminary M&D tests results, it is assumed that impact of particles up to about 3mm on a large decelerator of about 9 m diameter results in a fail-safe behaviour. This is to be confirmed by further tests on a demonstrator model, Ref. [70-42], [70-43].

70.26 References

70.26.1 General

- [70-1] H.W. Bergman
'Materials and Structural Concepts for New Space Transportation Systems'
SAMPE Quarterly, Vol. 22, No.1, October 1990, p51-61
- [70-2] E. Werling & J.P. Vialaniex: ESA/HPD
'Hermes Re-orientation Programme: Present Status and Main Objectives for Hot Structures and Thermal Protection Materials and Technologies'
First ESA/ESTEC Workshop on Thermal Protection Systems ESTEC, Noordwijk, 5-7 May 1993, ESA-WPP-053 (August 1993) p136-152
- [70-3] M. Yamamoto
'Conceptual Design to Heat-resistant Airframe of HOPE'
Proceedings of the International Conference: Spacecraft Structures and Mechanical Testing, ESTEC, 24-26 April 1991 ESA SP-321, p277-282
- [70-4] M. Yamamoto: NASDA
'Thermal Protection Development of Re-entry Vehicles at NASDA'
First ESA/ESTEC Workshop on Thermal Protection Systems ESTEC, Noordwijk, 5-7 May 1993, ESA-WPP-053 (August 1993) p58-63
- [70-5] S. Walmsley
'Design of HOTOL's Structure'
ESTEC Workshop - Advanced Structural Materials : Design for Space Applications, 23-25 March 1988
ESA WPP-004 (October 1988), p191-200
- [70-6] N.W. Dunbar: BAe
'Influence of TPS Performance on Future Space Transportation Concepts'
First ESA/ESTEC Workshop on Thermal Protection Systems ESTEC, Noordwijk, 5-7 May 1993, ESA-WPP-053 (August 1993) p153-159
- [70-7] R. Kochendorfer
'High Temperature Materials for Hypersonic Transport'
International Symposium: Advanced Materials for Lightweight Structures, ESTEC, 25-27 March 1992, ESA SP-336, p7-13
- [70-8] F.D. Boensch
'Design Challenges for the National Aero-Space Plane'
Proceedings of the International Conference: Spacecraft Structures and Mechanical Testing, ESTEC, 24-26 April 1991 ESA SP-321, p293-298
- [70-9] Proceedings of a NASA Workshop: Current Technology for Thermal Protection Systems, 11-12 February 1992, Langley Research Centre, Virginia. NASA Conference Publication 3157
- [70-10] J.L. Macret & P. Lautissier
'High-temperature Composites in Aerospace Activities'

ESA Symposium on Advanced Materials for Lightweight Structures,
March 1992, ESA SP-336, p367-373

- [70-11] J.F. Jamet & P. Lamicq
'Composite Thermostructures: An Overview of the French Experience'
Proceedings of HT-CMC1, Bordeaux Sept 1993
ISBN 1-85573-143-6, p735-742
- [70-12] D.M. Curry: NASA/JSC
'Space Shuttle Orbiter Thermal Protection System Design and Flight
Experience'
First ESA/ESTEC Workshop on Thermal Protection Systems ESTEC,
Noordwijk, 5-7 May 1993, ESA-WPP-053 (August 1993) p122-135
- [70-13] A. Lacombe et al
'Development of C/SiC Large Parts Technology for Aerospace Plane
Thermal Structures'
ESA Symposium on Space Applications of Advanced Structural
Materials, March 1990, ESA SP-303, p233-240
- [70-14] V.P. Timoshenko: NPO Molniya
'BURAN's Main Thermal Protection Components'
First ESA/ESTEC Workshop on Thermal Protection Systems ESTEC,
Noordwijk, 5-7 May 1993, ESA-WPP-053 (August 1993) p40-57
- [70-15] D. Desnoyer et al
'Large Thin Composite Thermostructural Parts'
Proceedings of the International Conference: Spacecraft Structures and
Mechanical Testing, ESTEC, 24-26 April 1991 ESA SP-321, p283-292
- [70-16] U. Trabandt et al
'Design of Hot Structures of Short-cycle Manufactured CMC'
Proceedings of HT-CMC1, Bordeaux Sept 1993
ISBN 1-85573-143-6, p751-758
- [70-17] U. Trabandt & J. Heitzer
'Design Concepts for Load-carrying Hot Structures for Re-entry Bodies'
ESA Symposium on Advanced Materials for Lightweight Structures,
March 1992, ESA SP-336, p65-70
- [70-18] T. Haug et al: DASA/Dornier
'Short Manufacturing Cycle CMC Heat Shields and Hot Structures'
First ESA/ESTEC Workshop on Thermal Protection Systems ESTEC,
Noordwijk, 5-7 May 1993, ESA-WPP-053 (August 1993) p202-209
- [70-19] M.J. Eiden , A. Launay & C. Buck: ESA/ESTEC/Interspace/SEP
'C/C Heatshield Development and Mechanical Performance
Verification'
First ESA/ESTEC Workshop on Thermal Protection Systems ESTEC,
Noordwijk, 5-7 May 1993, ESA-WPP-053 (August 1993) p332-337
- [70-20] German Hypersonics Technology Programme, 1993-1995
Federal Ministry for Research and Technology, Feb 1993
- [70-21] A. Russo et al: Alenia Spazio
'The CARINA Ablative Thermal Protection: Analysis, Design and
Testing'

First ESA/ESTEC Workshop on Thermal Protection Systems ESTEC,
Noordwijk, 5-7 May 1993, ESA-WPP-053 (August 1993) p82-88

- [70-22] D. Desnoyer et al
'CNSR-Rosetta - Earth return capsule'
Proceedings of the International Conference: Spacecraft Structures and Mechanical Testing, ESTEC, 24-26 April 1991 ESA SP-321, p405-414
- [70-23] J.E. Zimmer & R.A.S. Beck: Aerotherm Corp.
'Thermal Protection System for COMET Recovery Capsule'
First ESA/ESTEC Workshop on Thermal Protection Systems ESTEC,
Noordwijk, 5-7 May 1993, ESA-WPP-053 (August 1993) p76-81
- [70-24] H. Stockfleth et al: DASA/Dornier
'C/SiC Surface Protected Ablator for High Heat Fluxes'
First ESA/ESTEC Workshop on Thermal Protection Systems ESTEC,
Noordwijk, 5-7 May 1993, ESA-WPP-053 (August 1993) p289-294
- [70-25] T.J. Kowal & J.M. Caram: NASA/JSC
'Thermal Protection System Designs for Candidate Assured Crew return Vehicles'
First ESA/ESTEC Workshop on Thermal Protection Systems ESTEC,
Noordwijk, 5-7 May 1993, ESA-WPP-053 (August 1993) p104-112
- [70-26] A. Russo et al: Alenia Spazio
'The ARCV Thermal Protection: Concept Selection, Preliminary Sizing and Development Plan'
First ESA/ESTEC Workshop on Thermal Protection Systems ESTEC,
Noordwijk, 5-7 May 1993, ESA-WPP-053 (August 1993) p113-121
- [70-27] W.D. Henline: NASA/Ames
'Thermal Protection System Development and Application to Planetary Entry Vehicles'
First ESA/ESTEC Workshop on Thermal Protection Systems ESTEC,
Noordwijk, 5-7 May 1993, ESA-WPP-053 (August 1993) p5-39
- [70-28] G.E.E. Scoon, K. Keller & C. Bonnet: ESA/ESTEC/Dassault 'Aeroshell Concepts for Mars Landers'
First ESA/ESTEC Workshop on Thermal Protection Systems ESTEC,
Noordwijk, 5-7 May 1993, ESA-WPP-053 (August 1993) p97-103
- [70-29] Ch. Bonnet et al
'Stretched Skin Concept for the Entry Aerodynamic Decelerator System of Planetary Probes'
Proceedings of the International Conference: Spacecraft Structures and Mechanical Testing, ESTEC, 24-26 April 1991 ESA SP-321, p393-398
- [70-30] A. Newerla & G. Wierheim: ESA/ESTEC/Siemens KWU
'Beryllium Components for Thermal Protection Systems'
First ESA/ESTEC Workshop on Thermal Protection Systems ESTEC,
Noordwijk, 5-7 May 1993, ESA-WPP-053 (August 1993) p325-331

- [70-31] J.M. Bouilly & D. Guerrir: Aerospatiale
'Entry Testing of AQ60 for Huygens'
First ESA/ESTEC Workshop on Thermal Protection Systems ESTEC,
Noordwijk, 5-7 May 1993, ESA-WPP-053 (August 1993) p369-381
- [70-32] A. Lacombe et al: SEP
'Status on C/SiC Thermal Structures'
First ESA/ESTEC Workshop on Thermal Protection Systems ESTEC,
Noordwijk, 5-7 May 1993, ESA-WPP-053 (August 1993) p319-324
- [70-33] J. Wilson & R.J. Hussey: RJ Technical Consultants, (F)
'Structural Health Monitoring Techniques and Potential Application to
Reusable Launch Vehicles (RLV) Composite Primary Structures and
Composite Cryogenic Tanks'
Report No. RJTC-046-SHM (September 1999)
Work Order No. 16. ESTEC Contract No. 10983/94/NL/PP
- [70-34] M. Dogigli et al : MAN Technologie (D)
'Advanced Key Technologies For Hot Control Surfaces In Space Re-
Entry Vehicles'
Proceedings of 53rd International Astronautical Congress, 10th – 19th
October, 2002. Houston, Texas, USA. Paper No. IAC 02 I.3.02. Abstract:
www.iafastro.com (April 2003)
- [70-35] A. Muhlratzer & H. Pfeiffer: MAN Technologie AG, (D)
'All-Ceramic Body Flaps for Re-entry Spacecraft'
SAMPE Journal Vol. 38, No.4 (July/August 2002), p22-29
- [70-36] M. Dogigli et al : MAN Technologie (D)
'CMC Key Technologies - Background, status, present and future
applications'
Proceedings of 4th European Workshop on Hot Structures and Thermal
Protection Systems for Space Vehicles, Palermo, Italy, 26-29 November
2002
- [70-37] H. Pfeiffer & K. Peetz: MAN Technologie (D)
'All-ceramic Body Flap Qualified for Space flight on the X-38'
Proceedings of 53rd International Astronautical Congress, 10th – 19th
October, 2002. Houston, Texas, USA. Paper No. IAC 02 I.6b.01.
- [70-38] M. Dogigli et al : MAN Technologie (D)
'Qualification of CMC Body Flaps for X-38'
Proceedings of 52nd International Astronautical Congress, 1st - 5th
October, 2001. Toulouse, F. Paper No. IAF 01 I.3.02.
- [70-39] C. Röttger et al : MAN Technologie (D)
'Structure and Materials Technologies for RLV'
Paper provided by MAN Technologie (2004).
- [70-40] J. Antonenko: EADS ST GmbH
'Flexible external insulation (FEI): Performance and data for X-38 nose
cap and nose skirt application'
ESTEC Contract 15867/01/NL/MV: CCN5 (2006)
- [70-41] J. Antonenko: EADS ST GmbH

'High Temperature Insulation HTI and IFI: Performance and data for X-38 nose cap and nose skirt application'
ESTEC Contract 15867/01/NL/MV: CCN5 (2006)

- [70-42] U. Trabandt et al: Astrium (Bremen & Friedrichshafen, D)
'Deployable CMC Hot Structure Decelerator for Aerobrake'
Proceedings of 17th ADS Conference, May 2003
- [70-43] U. Trabandt & E. Monreal: EADS-ST (Bremen)/EADS-DC
'Liquid Polymer C/SiC and Potential Applications in Space Components'
Proceedings of HTCMC 5: 5th International Conference on High-temperature Ceramic Matrix Composites, Seattle, 2004

71

Thermal protection systems

71.1 Introduction

71.1.1 Application

71.1.1.1 Structures

TPS thermal protection systems control the heat energy at the surface of structures that undergo external heating. Usually heat transfer to the underlying structures is limited because these cannot withstand elevated temperatures. The main source of external heating is either re-entry into Earth's atmosphere or entry into the atmosphere of other planets. Velocities are extremely high and heating occurs by hypersonic gas flow over the external surfaces.

[See: Chapter [70](#) for vehicle descriptions; ECSS-HB-308 – Spacecraft thermal control design data]

The main uses of TPS are:

- Re-entry capsules, e.g. Apollo, [ACRV](#)'s.
- Space Shuttle orbiter and [Buran](#).
- Spaceplane concepts, Ref. [\[71-1\]](#), e.g.:
 - [Hermes](#),
 - [HOPE](#), Ref. [\[71-2\]](#); [HOPE-X](#) which is a full scale, unmanned prototype of the HOPE winged man-capable re-entry glider, Ref. [\[71-80\]](#),
 - [HOTOL](#),
 - [NASP](#),
 - [SÄNGER](#).
- Demonstrator vehicle programmes, Ref. [\[71-80\]](#):
 - [X33](#) – Flight,
 - [X34](#) – Technology,
 - [X38](#) – Lifting body, part of the CRV crew return vehicle.
- Reusable items, such as containing propellants, e.g. LH cryotanks.
- Mars landers.
- Planetary probes.

71.1.1.2 Propulsion systems

TPS is also used in the vicinity of engines and propulsion systems to control the heat generated by combustion.

71.1.2 European development programmes

71.1.2.1 Status

TPS concepts evolved from a number of European programmes mainly concerned with technology development and demonstration. Many of these technologies are now awaiting commitments to fund particular flight programmes, notably reusable launchers.

European organisations also contributed significantly to the US-based X-vehicle projects.

71.1.2.2 Examples

Some European programmes that have contributed to the overall advancement of TPS include:

- Hermes reusable spaceplane (1988-93).
- HOTOL (SSTO) and Sänger (TSTO) concepts (to 1994).
- WLC - winged launcher configurations (1992-94), Ref. [71-69].
- Integrity control for high-temperature structural applications (1992-95), Ref. [71-61]. This study covered C-SiC heat shingles, with material characteristics and NDI related to thermo-mechanical and acoustic performance.
- MSTP - manned space transportation programme (1995-98), Ref. [71-70], [71-75], [71-80], including:
 - CTV - crew transfer vehicles and ACRV - assured crew return vehicles.
 - Re-entry capsules.
 - Heatshield assemblies, e.g. CHA - ceramic heatshield assembly
 - Ablatives.
- Planetary probes.
 - Mars Lander, e.g. MARSNET.
 - Aeroshells and decelerators.
 - Cassini-Huygens heatshield constructions.
- FESTIP- future European space transportation investigations programme (1994-97: Phase 1), Ref. [71-62], [71-66].
- Re-entry flight demonstrators (from 1994)
 - EXPRESS - experimental re-entry space system capsule, Ref. [71-80].
 - CETEX - ceramic tile experiment on the EXPRESS re-entry capsule (in 1995), Ref. [71-60]: For testing a 300mm tile of CCSiC material (made by liquid phase siliconising of carbon) under extreme, ablative stagnation-point conditions. Owing to launch vehicle problems, EXPRESS did not reach the target orbit and re-entered after 2.5 orbits. The precise re-entry conditions were unknown (loss of telemetry), but post-flight analysis of

- ablation thickness indicated more severe heat flux than expected. (2.6MW/m^2), Ref. [71-80].
- MIRKA - 'mikro rückkehr kapsel' a micro re-entry capsule (in 1997), Ref. [71-78], [71-79]. The surface protected ablator (SPA) concept, consisting of an ablator material filled honeycomb with an external thin shell of CMC (CSiC) produced by lamination and subsequent pyrolysis (Dornier's PIP process).
 - ARD - atmospheric re-entry demonstrator launched from Ariane 5 (1998), Ref. [71-76], [71-80]. Contains CMC material specimens (C-SiC from MAN-MT and SEP, C-C from Aerospatiale, CCSiC from DLR); each 200mm diameter. These are mounted with ceramic fasteners on the primary ablative heatshield for in-flight, re-entry characterisation of substrate and coating performance.
- TETRA – 'technologien für zukünftige raumtransportsysteme', a DLR-funded programme in collaboration with German industry, Ref. [71-80]:
 - 'Baseline' flight hardware: C-SiC nose cap and split flaps.
 - 'Non-Baseline': heatshield panels and blankets integrated around the baseline TPS, e.g. rigid external insulation (REI)-type C-SiC panel, fasteners and internal multiscreen insulation (IMI); C/SiC panel with internal flexible insulation (IFI); flexible external insulation (FEI).
 - ALSCAP - alternative low-cost, short manufacturing cycle assessment programme, Ref. [71-80] – a parallel technology programme to develop a low-cost, serial production method for C-SiC re-entry capsule heatshield components.
 - PRORA: Italian national aerospace programme:USV – unmanned space vehicle – flight test beds, [See: 70.22]

Recent and on-going European programmes on reusable structures include:

- FTLP – future launcher technology programme (to 2001)
- FLPP – future launcher preparatory programme (2004 to 2009)
- IXV – Intermediate experimental vehicle for re-entry technologies, flight expected in 2010.

71.1.3 Concepts

There are many concepts for TPS designs described in open publications, which are based upon a range of materials.

The selection of an appropriate TPS is both mission and vehicle related.

Preference is given to proven systems with a knowledge base to work from, providing confidence in their use in new projects. This is particularly true of USA and Russian-CIS space programmes. However, there is always a drive to produce more efficient TPS concepts, not least in spaceplane development where low mass and reusability are important criteria.

Table 71.1.1 provides a summary of selected TPS candidates and their characteristics, Ref. [71-4], [71-81].

Table 71.1-1 - TPS: Summary of candidate characteristics

Criteria	Flexible surface insulation	Rigid ceramic tiles	Ceramic shingle	Metallic shingle	Multi-wall TPS panels	C-C hot structure	C-SiC hot structure
Upper temperature limit (°C)	≈ 650	≈ 1260	≈ 1300	≈ 1300	≈ 1300	≈ 1600	≈ 1600
Local application	Leeward fuselage/wings	Fuselage/ wings	Fuselage/ wings	Fuselage/ wings	Fuselage/ wings	Nose cap, leading edges, control surfaces	Static and dynamic control surfaces
Attachment	Adhesive bonding	Adhesive bonding	Screws and shear pins	Screws and bolts	Clips or studs	Screws and bolts	Nuts and bolts
Sealing	Butt joint	Ceramic fabrics	Ceramic fabrics	Sealing plates	Sliding joint + ceramic fabrics	Ceramic fabrics and rings	Ceramic fabrics, rings, springs
Manufacturing tools effort	Low	High	High	Moderate	Moderate	High	High
Maintenance/Repair effort	Low	Moderate	Low	Moderate	Low	High	High
Scatter in material characteristics	Moderate	High	High	Low	Low	High	High
Mechanical strength	Low	Moderate	High	High	High	High	High
Coating reasoning	Surface sealing	Erosion, humidity	Not relevant for SiC-SiC	Oxidation†	Oxidation†	Oxidation	Oxidation
Thickness at comparable conditions	Not applicable	Moderate	High	Moderate	Low	Not applicable	Not applicable
Thermal expansion	Low	Low	Low	High	High	Low	Low

Key: † >1000°C

The classes of materials used within TPS and thermostructural concepts are summarised in [Table 71.1.2](#), Ref. [71-3].

Table 71.1-2 - TPS and Thermo-structural designs: Material classes

External insulation	Primary structure	Internal insulation
Medium/high density ablators ($>1 \text{ MW/m}^2$)	CMC thermostructure materials ($>1000^\circ\text{C}$)	Ceramic foil multilayer insulation ($>1000^\circ\text{C}$)
Alumina/silica tiles or low density ablators	GMC, Intermetallics or Superalloy (up to 1000°C)	Lightweight ceramic fibre tiles or mats
CMC shingles with low density fibrous insulation	Titanium, Beryllium alloys & Al MMC (up to $\sim 500^\circ\text{C}$)	Metallic foil multilayer insulation ($<1000^\circ\text{C}$)
Metallic multi-wall panels with low density insulation	CFRP and aluminium alloys	Glass fibre, silica microsphere insulation ($<500^\circ\text{C}$)
Ceramic fibre flexible blankets		Rigid or flexible organic foams

Most reusable vehicle TPS concepts combine materials capable of carrying loads at high temperatures, i.e. external vehicle surfaces, with some form of insulation that protects the underlying structure from overheating. Together they form the overall TPS system.

In reusable cryotank concepts, [See: [71.19](#)], the overall TPS system includes cryo-insulation, which limits fuel boil-off and icing during pre-launch and ascent, [See: [71.22](#)].

71.1.4 Non load-carrying TPS

Types of TPS that do not carry significant loads include:

- Ablatives, [See: [71.4](#)].
- Ceramic tiles, [See: [71.5 – Orbiter](#); [71.6 – Buran](#)]
- Fibrous insulation, [See: [71.10 – IMI](#); [71.11 - FEI](#)]
- Flexible fabrics, felts and cloths, [See: [71.10 – IMI](#); [71.11 - FEI](#)].
- Rigid or flexible foam insulation, [See: [71.22](#)].

These materials provide efficient thermal insulation, but need to be optimised in terms of mass, both on an areal basis and the ‘dead mass’ contribution to the vehicle structure.

71.1.5 Load-carrying TPS

Types of TPS that do carry significant loads can be classed as thermo-structural designs, [See: Chapter 70], and include:

- Metallic-based constructions, [See: [71.8](#), [71.9](#), [71.14](#)]:
 - titanium,
 - nickel.
- Ceramic-based, [See: [71.7](#), [71.12](#), [71.17](#), [71.18](#)]:
 - CMC, e.g. C-SiC and SiC-SiC
 - carbon-carbon composites.

Load-bearing TPS is of interest because it offers mass-savings whilst providing the aerodynamic surfaces of vehicles. Of these applications, the CMC body flap concept for the X-38 test vehicle is well advanced, [See also: Chapter 52].

The body flap, produced in C-SiC material, consists of the several main elements, Ref. [[71-85](#)], [[71-89](#)]:

- flap structures (box segments, sections and cover plates),
- hinge line bearing, Ref. [[71-90](#)],
- fasteners (bolts, nuts and washers), Ref. [[71-86](#)],
- connection to EMA electro-mechanical actuator EMA, Ref. [[71-85](#)],
- sealing system, Ref. [[71-91](#)].

A CMC elevon is proposed for the X-33/RLV programme. The largest separate elements of the inboard and outboard elevon are about 1.8m × 1.3m; one assembled ruddervator has a span of about 2.4m, Ref. [[71-84](#)]. The design concept comprises:

- rib-reinforced box: upper leeward and lower windward side and rib of integrally-fabricated C-SiC composite; with oxidation protection coating,
- metallic hinge,
- metallic actuator fittings.

71.1.6 Reusable structures

The Shuttle Orbiters and other spaceplane concepts rely on the development of reusable TPS. Ideally, this is both durable and low maintenance.

The experience with the US Space Shuttle is important because maintenance of the external ceramic tiles initially proved costly. The in-service inspection of TPS needs thorough consideration. Likewise the means of joining TPS to the sub-structure.

TPS functioning at high temperatures and under oxidative or erosive conditions undergoes some degradation. Any degradation should be sustainable within the flight environment and for the number of intended flights.

The details of TPS developments within Europe and the USA are provided within several publications, e.g. USA perspective, Ref. [71-5]; European and International, Ref. [71-3], [71-6], [71-77], [71-81].

71.2 Cooling modes

71.2.1 General

TPS provides cooling for a structure and this can be achieved in a number of ways, as shown in Figure 71.2.1, Ref. [71-5].

Conventional TPS tends to use passive systems on which there is the largest knowledge base. More emphasis is placed on active cooling for advanced spaceplanes, e.g. SSTOs and scram-jet propulsion systems.

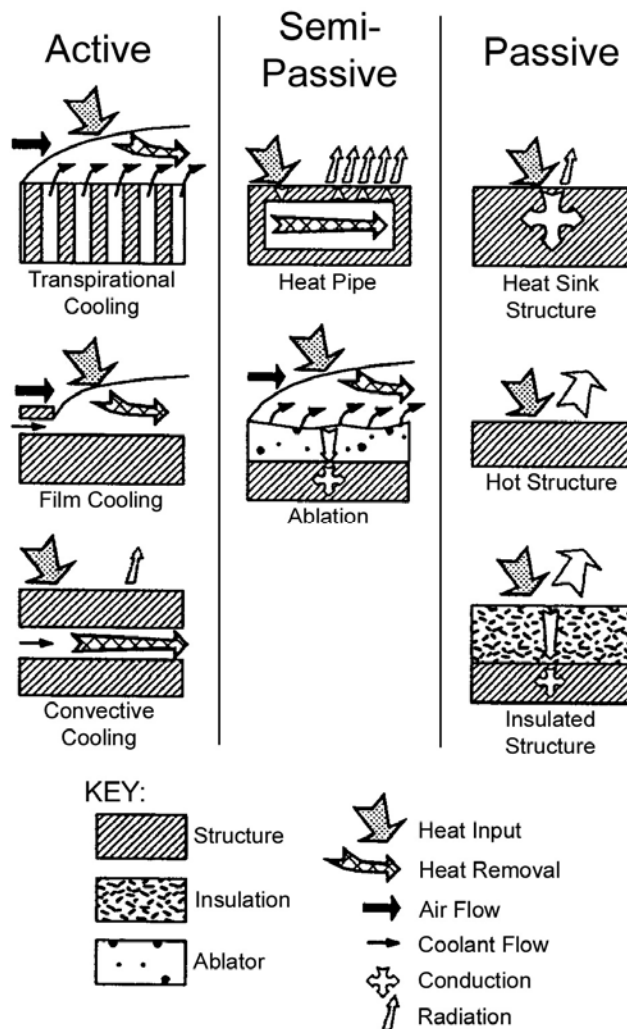


Figure 71.2-1 - TPS concepts

71.2.2 Passive TPS

71.2.2.1 Heat sinks

These rely on heat storage for preventing external heat from diffusing through the structure.

71.2.2.2 Ablatives

These use the decomposition of materials to transport (convect) heat away with the gases evolved. They are sacrificial systems, usually based on polymeric composites, which break down at high temperature leaving a charred layer with insulating properties.

71.2.2.3 Insulation systems

Principally of ceramic construction with low thermal conductivity which re-radiate a large proportion of the heat back into the environment. The emissivity and catalytic characteristics of the immediate outer surface are very important.

Thermal control variants are summarised in [Figure 71.2.2](#), Ref. [71-3].

Hot structure architecture	Protected structure architecture	Integral tank architecture
		N.A.
		N.A.

Figure 71.2-2 - Principal passive thermal control architectures

71.2.3 Active cooling concepts

71.2.3.1 Gas flow

Through the use of computational fluid dynamics (CFD), an optimum gas flow can be achieved over a surface to minimise impingement and stagnation zones. Cooler gas streams can be used to provide a laminar flow barrier over surfaces separating hot gases from the structure.

71.2.3.2 Cryogenic fuels

Cryogenic fuels, in particular liquid hydrogen, have a very high specific heat capacity. By passing fuel close to the structural surface on route to the propulsion system, active cooling can be provided, together with increased propulsive efficiency.

71.2.3.3 Liquid coolants

High heat-capacity liquids, e.g. molten sodium, have been proposed for transporting heat away from critical regions through the use of heat pipes or heat exchangers.

71.3 Early re-entry capsules

In the design of passive TPS for atmospheric entries, ablative materials have provided successful, if conservative, self-regulative solutions for early manned vehicles, Ref. [71-7], [71-8].

The materials applied were:

- Mercury: Glass fibre reinforced phenolic resin.
- Gemini: Corning DC 235 silicone composition.
- Apollo (lunar): AVCO 5026-39 HCG, an epoxy-novalac, glass fibre honeycomb reinforced material.

A low density (540kg/m^3) was achieved by the addition of silica and phenolic microballoons. Quality assurance and inspection specified that each cell of the honeycomb was filled by hand.

Apollo experienced re-entry velocities of 11.2km/s , with the TPS contributing 13.2% of vehicle mass.

Table 71.3.1 gives the mass fractions of TPS used in early capsules. Apollo experienced peak heating rates of 4.4MW/m^2 .

Table 71.3-1 – Early re-entry capsules: TPS mass fractions

Project	TPS	% of Entry mass
Apollo	AVCOAT-5026	13
Viking	SLA-561	7
Pioneer-Venus: Large probe Small probe	Carbon-phenolic	10 13
Galileo	Carbon-phenolic † Phenolic-nylon ‡	43 4
MESUR (proposed): 7 km/s entry 9 km/s entry	SLA-561 † AVCOAT-5026 & SLA-561 †	7.5 11
Key:	† Forebody only ‡ Afterbody	

Some ablatives successfully used in other programmes, Ref. [71-8] are:

- NASA Planetary Aerothermal Experiment Test (PAET) Probe: Silicone-based ablatives.

- Viking Mars Lander: A low density silicone ablator, SLA-561 with a density of 224kg/m^3 , to resist a heat flux of 0.24MW/m^2 and total heat load of 11.8MJ/m^2 .
- Pioneer Venus mission: Carbon fibre reinforced phenolic ablator construction to withstand uncertain heat fluxes ($>30\text{MW/m}^2$)
- Galileo Jupiter Probe: Carbon fibre reinforced phenolic heat shields weighing 146kg, or 46%, of the total 338kg vehicle, as shown in [Figure 71.3.1](#), Ref. [71-7].

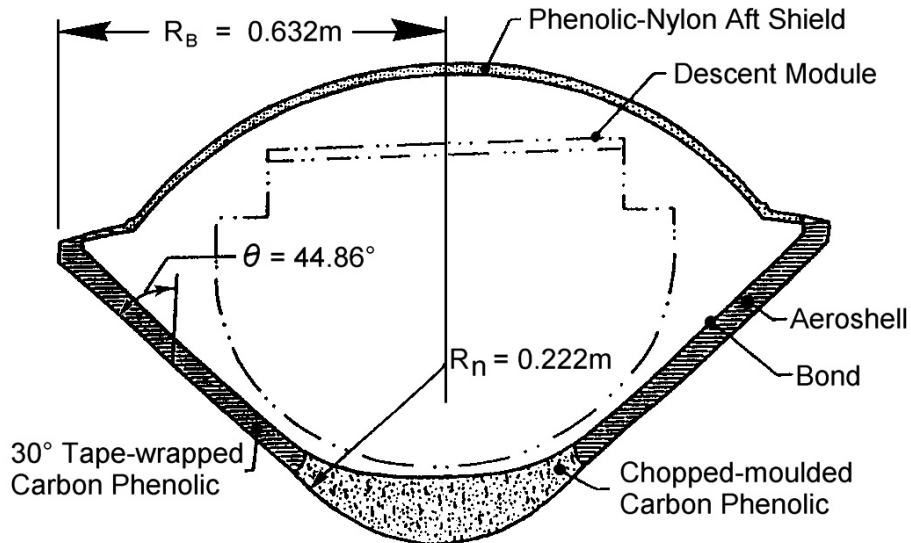


Figure 71.3-1 - Galileo entry probe

71.4 Ablative designs

71.4.1 General

For single missions, with no reusable requirements, ablatives still have a role in future space programmes, Ref. [71-58].

Figure 71.4.1 shows the basic decomposition mechanisms of ablatives, Ref. [71-8], [See also: Figure 70.15.1].

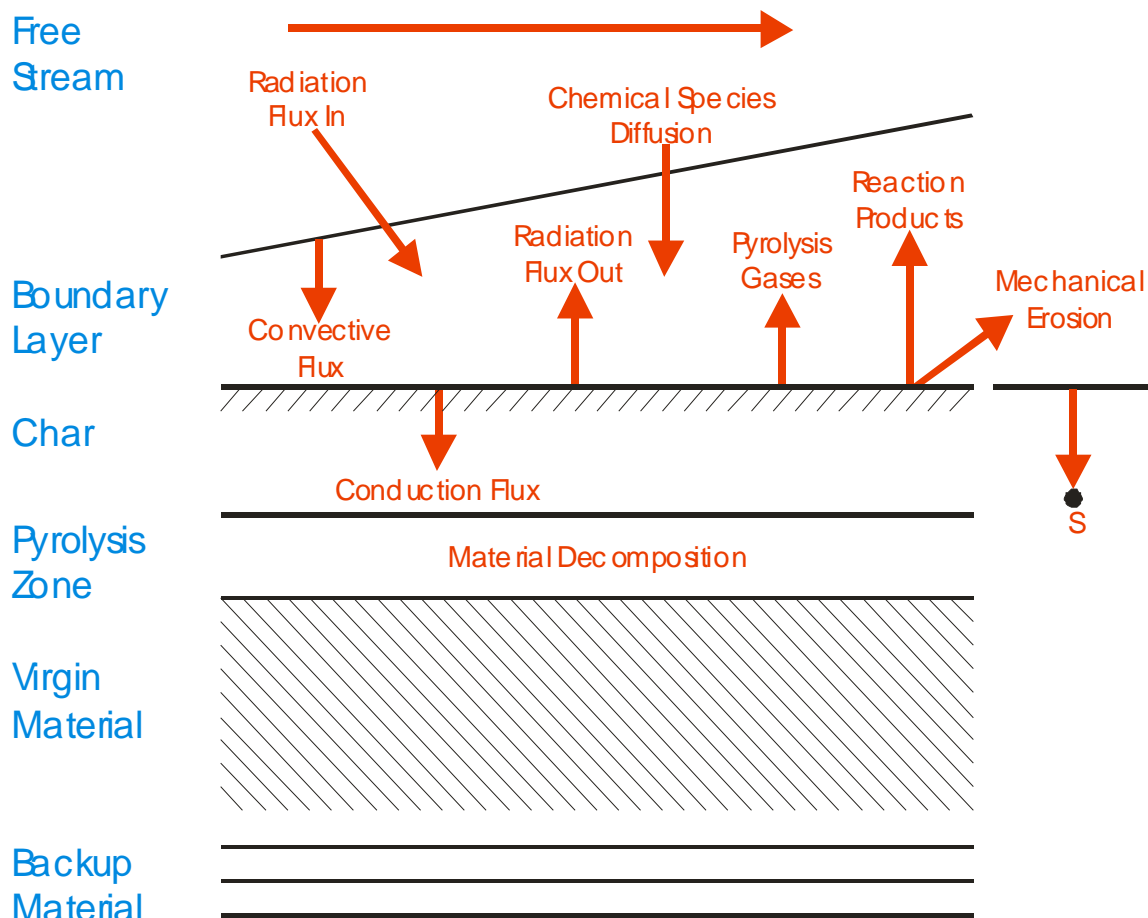


Figure 71.4-1 - Ablatives: Basic decomposition mechanisms

71.4.2 Programmes

Some examples of programmes where ablatives are used include:

- NASA Commercial Experiment Transporter (COMET) recovery capsules with two functions, Ref. [71-8]. Designed as a free-flyer concept of a pressurised recovery system (intended for 227 kg of recoverable experiments) with a non-pressurised, non-recoverable service module.
- Space recovery vehicle CARINA (CApSula di RIintro Non Abitata), by Alenia Spazio to carry and retrieve various microgravity payloads, Ref. [71-9].
- NASA/ESA ACRV, the assured crew return vehicle for the emergency return of astronauts from orbiting space stations to earth, Ref. [71-10], [71-11].
- NASA MESUR Network Mars Lander, Ref. [71-7].
- CARTEC-FT study for an Italian scientific payload carrier for re-entry experiments, Ref. [71-81].

71.4.3 Materials

71.4.3.1 Acusil: Low-density, silicone-based ablatives

Two variants under consideration for COMET and CARINA are Acusil I and Acusil II, which are derived from the Apollo-era ablatives ESA 3560HF, SLA-220. Their main characteristics include:

- Acusil I: An ablative foam composed of silicone resin, quartz microballoons, phenolic microballoons and quartz fibre. This is incorporated into a Flexcore glass fibre/phenolic honeycomb bonded to the forward structure of COMET. The material has an overall density of 480 kg/m³ and is a moderate density charring ablator for heat fluxes up to 4.5 MW/m².
- Acusil II: For use on the aft structure and end-cap of COMET. It has a similar material make-up but a density of 260 kg/m³ for low-moderate heat fluxes up to 1.1 MW/m². It remains RF transparent even during re-entry.

The CARINA concept and structural configuration shown in Figure 71.04.2, Ref. [71-9], is similar to that of COMET.

The same USA contractor produced the TPS system for COMET and studied the TPS for CARINA.

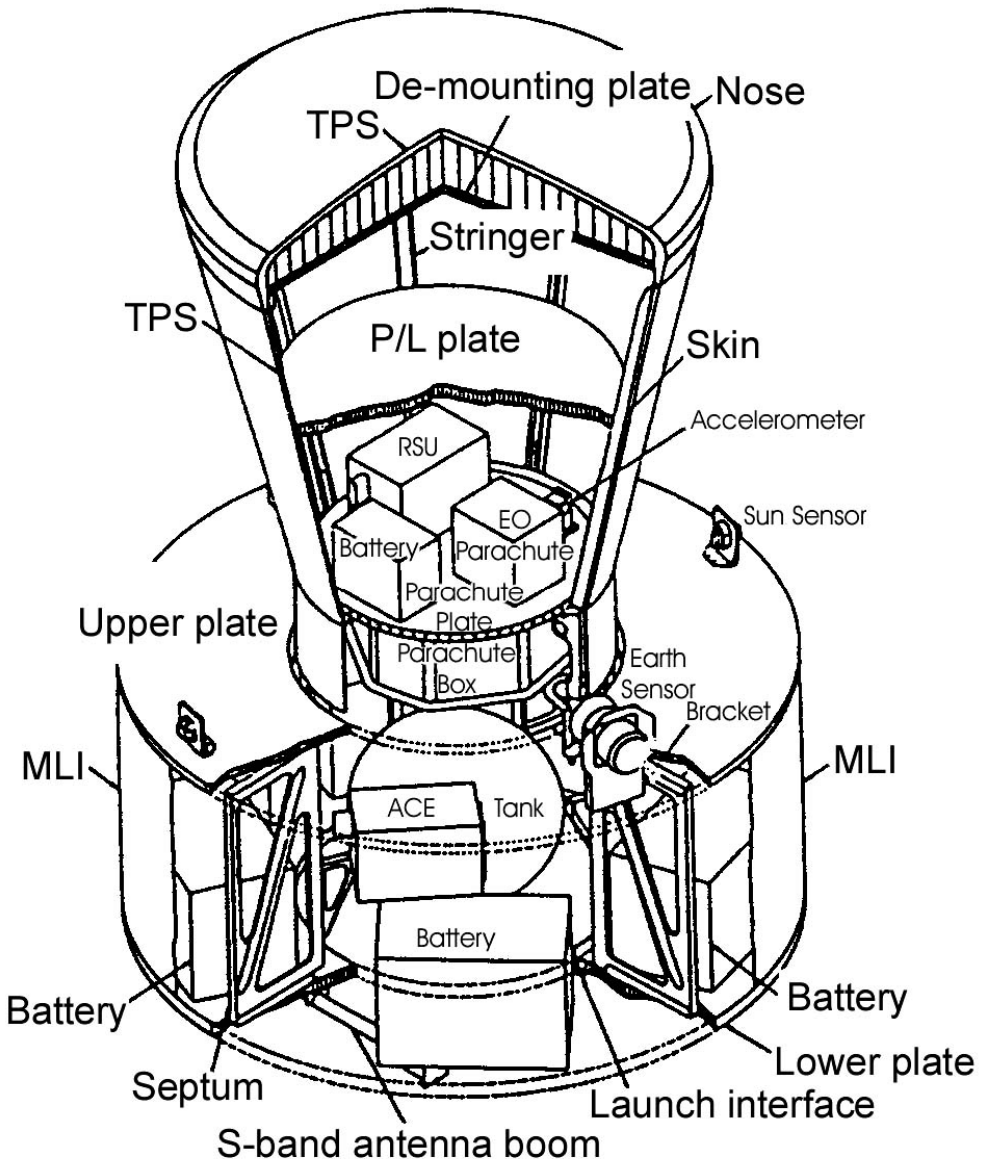


Figure 71.4-2 - CARINA: General layout

71.4.3.2 ALS051: Medium-density, silicone-based ablatives

It was developed by Alenia Spazio for the hemispherical nose cap of the CARTEC-FT spacecraft, Ref. [71-81]. The specification included:

- thermal:
 - heat flux distribution,
 - maintaining the aluminium shell below 160°C.
- general mass and dimension constraints.

ALS051 is a silicone-based ablative material supported by a glass-phenolic honeycomb. Mechanical properties are improved by adding glass reinforcement, whilst the density is reduced by the addition of phenolic microspheres. The ablative is packed into the honeycomb core and cured (at RT, or accelerated by moderate heating), followed by machining to the required thickness. Flat or curved

panels are bonded to the substructure. The properties of ALS051 are summarised in [Table 71.4.1](#), Ref. [71-81]. These were determined as part of the first qualified version of the material and used as input to Alenia Spazio [CAPSA](#), an ablative [TPS](#) design tool computer program. The ground testing programme included chemical composition, kinetic parameters and outgassing properties.

Table 71.4-1 – Ablative TPS: ALS051 properties

RT properties:	
Colour	Brick red
Density	$830 \pm 30 \text{ kg/m}^3$
Hardness	72 ± 3 Shore A
Tensile strength	3.23 MPa
Elastic modulus	37.5 MPa
Elongation	12 %
Poisson's ratio	0.43
Thermal *:	
Conductivity, at 160°C	0.056 W mK ⁻¹
Char conductivity, at 160°C	0.063 W mK ⁻¹
Specific heat, at 160°C ()	1.22 J gK ⁻¹
Char specific heat, at 550°C	1.00 J gK ⁻¹
Expansion coefficient	77.4 $\mu\text{m mK}^{-1}$
Ablative properties **:	
Mass loss, in air, to 900°C	54.4 %
Mass loss, in nitrogen, to 900°C	50.5 %
Ablation heat, by DSC, in nitrogen	3800 J g ⁻¹
Key: * convective-heating re-entry environment; ** by thermogravimetric, DSC analysis and arc-jet tests.	

Arc-jet tests on samples in air and the different nominal heating conditions expected in the CARTEC-FT environment suggested comparable performance between ALS051 and other commercially-available, qualified, ablative materials; tested from 200 kW/m² to 1000 kW/m² cold-wall heat fluxes for 150s.

The post-test samples showed no significant surface regression and retained their shape and dimensions, with a tough surface and homogeneous texture.

71.4.3.3 Epoxy resin and cork ablators

These were considered by Alenia Spazio for [ACRV](#) concepts in conjunction with the [CARINA](#) study. Acusil materials were more weight-efficient insulators than epoxy (1051 kg/m³) or cork (490 kg/m³) in modelling studies.

The modelling of ablation response is an important part of the design process for vehicle dimensioning, Ref. [71-6].

71.4.3.4 SPA - Surface protected ablator

The SPA was developed to meet the requirements of the MIRKA capsule, [See also: 70.15]. This non-reusable heat shield comprises of a conventional ablative material enclosed in a thin CMC shell.

During re-entry, the CMC shell protects the ablator from abrasion and erosion, intense heat fluxes and dynamic pressures related to the mission.

The gas produced during ablation is channelled and vents from behind the CMC shell at predetermined locations, [See also: 71.17].

71.5 Space Shuttle orbiter

71.5.1 General

The Orbiter was designed to withstand the surface temperatures shown in Figure 71.5.1, Ref. [71-12].

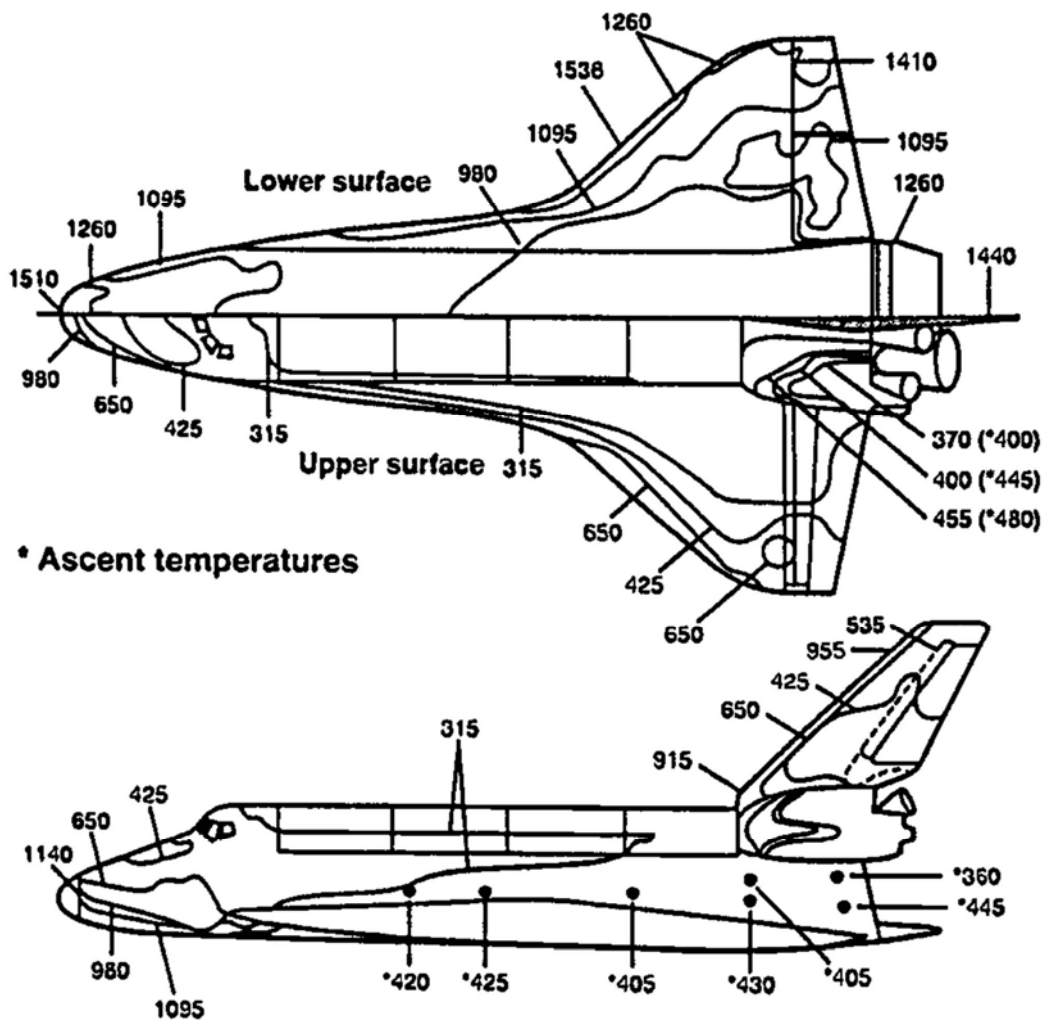


Figure 71.5-1 - Orbiter: Design surface temperatures (°C) in ascent and re-entry trajectories

Beneath the outer TPS systems lies a fairly conventional light-alloy airframe construction, with a manned flight deck and cargo-bay which is kept cool during re-entry. The airframe structure is kept below 177°C.

71.5.2 Materials and configurations

A range of TPS systems is used, Ref. [71-13], [71-14], with the coverage shown in Figure 71.5.2, Ref. [71-12].

The C-C nose cone [See: 70.9] and wing leading edges [See: 70.10] are thermo-structural elements.

[See also: 71.7 for progressive improvements in C-C materials]

Different types of ceramic insulation, classed as reusable surface insulation (RSI), cover most of the external surface of the Orbiter.

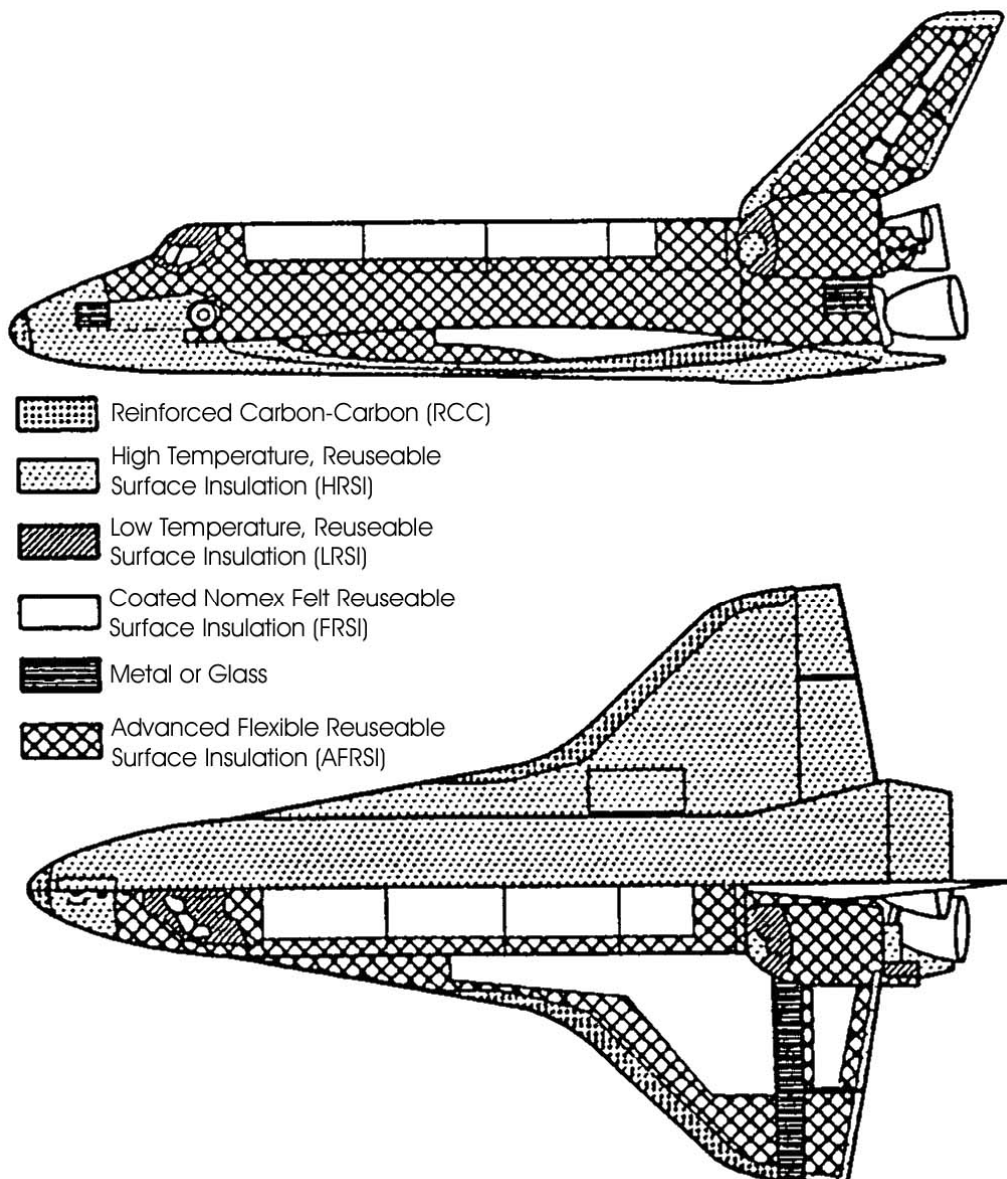


Figure 71.5-2 - Orbiter: TPS - Thermal protection systems

The temperature limits for the respective types of insulation are given in [Table 71.5.1](#), Ref. [71-12]. Some are rigid ceramic tiles, Ref. [71-12], whilst others are flexible blankets, Ref. [71-13], [71-14].

Table 71.5-1 - Orbiter: TPS material temperature limits

Type of insulation	Maximum operating temperature, (°C)		Minimum operating temperature (°C)
	100 Mission life	Single mission life	
High temperature reusable surface insulation (HRSI)	1260 † 1260 ‡	1427 1482	-128
Low temperature reusable surface insulation (LRSI)	1093	1149	-128
Fibrous refractory composite insulation (FRCI)	1260	1427	-128
Felt reusable surface insulation (FRSI)	399	482	-128
Advanced flexible reusable surface insulation (AFRSI)	816	982	-128
Reinforced Carbon-Carbon (RCC)	1482	1816	f
Thermal window pane	956	-	f

Key † : 144 kg/m³ ‡ : 352 kg/m³ f : No limit identified

The TPS systems applied to the orbiter can be summarised as:

- HRSI (high-temperature reusable surface insulation): Low density, high-purity (99.8%) silica fibre insulation rigidised by ceramic bonding. Density 144 kg/m³ or 352 kg/m³ with a black RCG (reaction cured glass) coating.
- LRSI (low-temperature reusable surface insulation): The composition is the same as HRSI, except it has a white RCG coating and a density of 144 kg/m³.
- FRCI (fibrous refractory composite insulation): The composition is the same as HRSI, but with aluminoborosilicate fibres for improved durability and a density of 192 kg/m³.
- FRSI (felt reusable surface insulation): A Nomex® felt coated with a white pigmented silicone elastomer, offering waterproofing with the specified thermal and optical properties.
- AFRSI (advanced flexible reusable surface insulation): Comprising of low density 176 kg/m³ batting (sheets for quilting) of high-purity 99.8% amorphous silica fibres. This batting is sandwiched between an outer woven-silica, high-temperature fabric and an inner lower-temperature, woven-glass fabric. The composition is stitched with a silica thread; treated with water repellent and coated with a ceramic to provide durability and resistance to damage.

The FRCI and AFRSI were later additions to the Orbiter fleet. AFRSI replaced LRSI in many places. The FRCI tiles are used in areas susceptible to handling or impact damage.

Typical RSI properties are shown in [Table 71.5.2](#), Ref. [71-12].

Table 71.5-2 - TPS: RSI Typical Properties

Property	RCG	LI-900	LI-2200	FRCI-12
Density (kg/m ³)	2195	144	352	192
Tensile strength (N/m ²):				
Through-thickness	-	1.65 x 10 ⁵	5.03 x 10 ⁵	5.58 x 10 ⁵
In-plane	2.76 x 10 ⁷	4.62 x 10 ⁵	12.4 x 10 ⁵	17.72 x 10 ⁵
Compressive strength (N/m ²):				
Through-thickness	-	1.93 x 10 ⁵	8.96 x 10 ⁵	9.10 x 10 ⁵
In-plane	6.89 x 10 ⁵	4.83 x 10 ⁵	15.86 x 10 ⁵	18.27 x 10 ⁵
Thermal expansion (10-6°C-1):				
Through-thickness	1.08	0.72	0.72	1.26
In-plane	1.08	0.72	0.72	1.26
Apparent thermal conductivity (W/m.K):				
Through-thickness: 21°C @ 10-4 atm	1.44	0.014	0.032	0.019
538°C @ 10-4 atm	-	0.045	0.059	0.049
In-plane: 21°C @ 1 atm	1.44	0.063	0.105	0.076
538°C @ 1 atm	-	0.156	0.180	0.163
Specific heat (J/kg K)	920	771	711	711
Dielectric constant	4.8	1.13	1.30	1.20
Loss tangent	0.0030	0.0004	0.0016	0.0009

The RSI ceramic tiles are bonded to the Orbiter structure with a silicone adhesive and an intermediate layer of nylon felt, as shown in [Figure 71.5.3](#), Ref. [71-12].

The nylon felt acts as a strain isolation pad (SIP) which separates the low-strength, brittle tile from airframe structural strains and deflections and subsequent critical tile stresses.

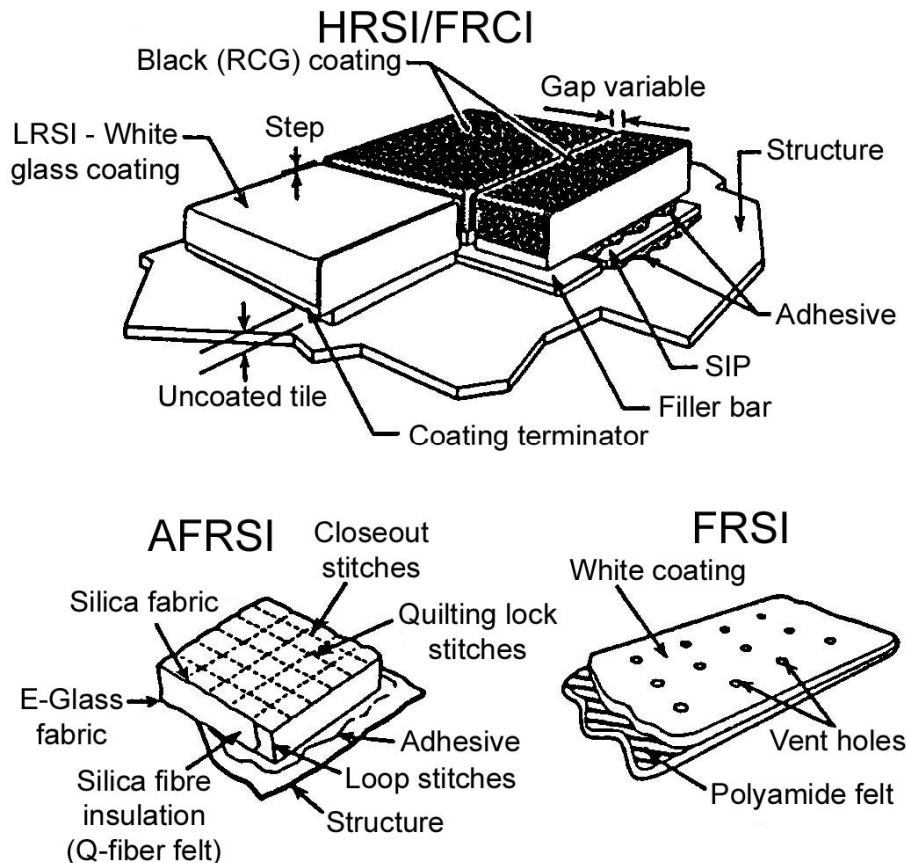


Figure 71.5-3 - Orbiter: RSI system configuration

Tiles are densified at the inner mould line to provide adequate strength at the tile-to-SIP interface. This densification enables a sufficient structural margin for the tile based on the predicted load cases.

The gaps between the tiles prevent tile-to-tile contact occurring by acoustically-induced tile movement or by contraction of the airframe in the extreme cold of space. Filler bar material at the bottom of the tile-to-tile gap is used to prevent heat penetration through the gap.

In the higher pressure gradient regions of the Orbiter, open gaps can result in ingestion of high-temperature gas during re-entry, causing local over-temperature of the various TPS components and the structure. To prevent this, two basic types of gap filler, 'pillow' or 'layer', are bonded to the top of the filler bar.

To fill the larger gaps around movable hatches and doors, thermal barriers made from the ceramic cloth filled with soft insulation and metallic springs are used.

The RSI blankets are bonded directly to the structure with a silicone rubber adhesive.

71.5.3 In-Service TPS Performance

71.5.3.1 Surface damage

Surface damage has occurred on all Shuttle flights. The damage experienced can be grouped as:

- Gap filler damage,
- Tile slumping,
- Dents,
- Gouges, and
- Chipped coatings.

These primarily result from impact by fragments during launch separation stages, icing and run-way debris. Approximately 2% to 3% of impacted tiles are replaced, whilst the remainder are repaired using standardised procedures. The loss of tiles experienced in early flights is now avoided by improved bonding techniques.

71.5.3.2 Columbia

The total loss of the Columbia in 2003 during mission STS-107 was attributed to a breach in the TPS on the leading edge of the left wing. This was caused by a piece of insulating foam that separated from an area of the 'External Tank' 81.7 seconds after launch. The foam struck the wing in the vicinity of the lower half of RCC panel No 8.

During re-entry the breach in the TPS enabled superheated air to penetrate through the leading-edge insulation and progressively melt the aluminium structure of the left wing, resulting in a weakening of the structure until increasing aerodynamic forces caused loss of control, failure of the wing, and break-up of the Orbiter, Ref. [71-97].

71.6 Buran

71.6.1 General

Buran was designed for launch into LEO by the Energia heavy-lift launcher. Early trials with TPS concepts were conducted on the BOR-4 re-entry test vehicle, Ref. [71-15].

Buran has only flown once, so does not have the operational experience of the Orbiter fleet.

The similarities between the two vehicles can be seen by comparing Figure 71.6.1, Ref. [71-15], with Figure 71.5.2.

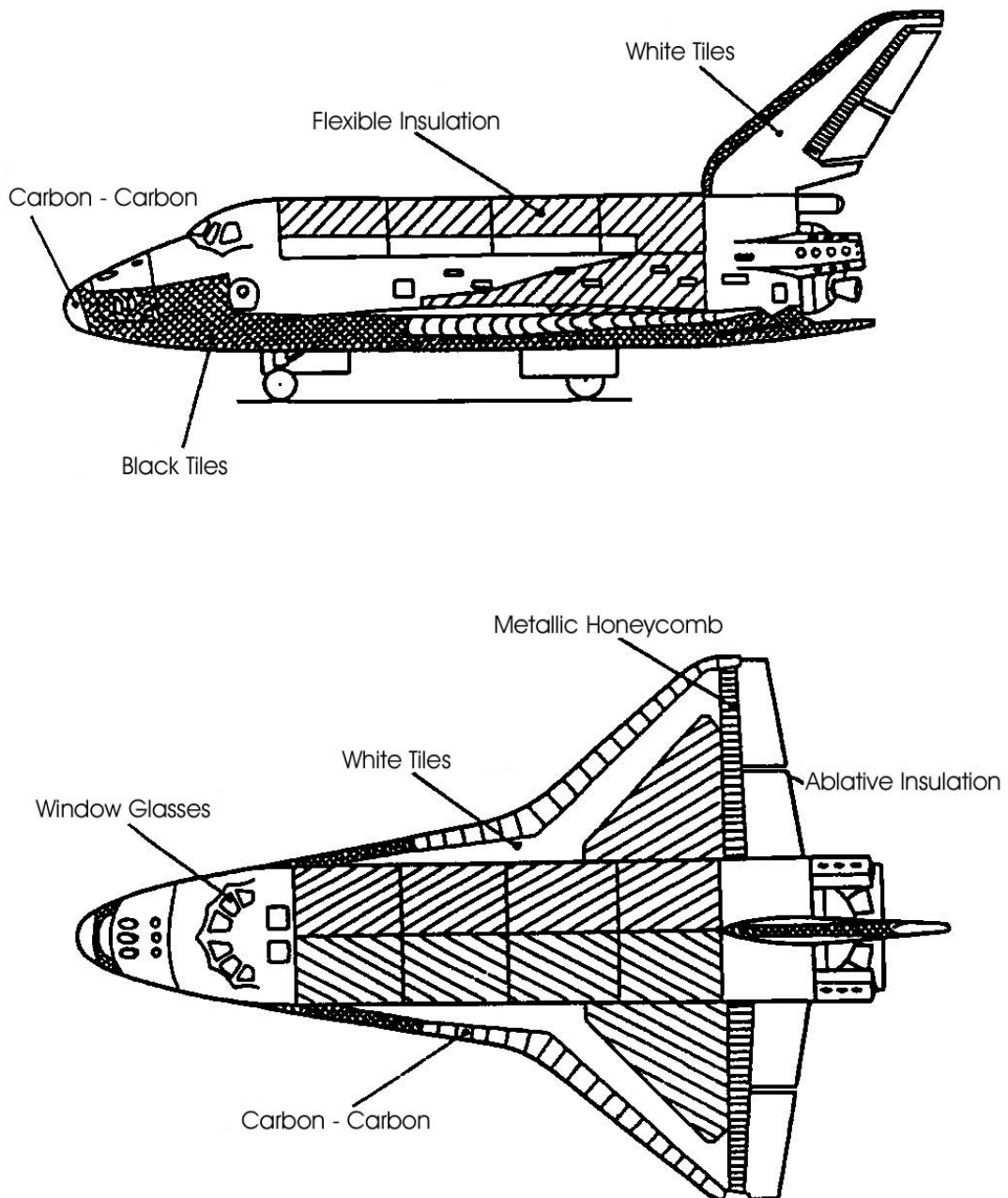


Figure 71.6-1 - BURAN: External thermal protection

Ground-based trials of TPS systems were conducted with induction and arc-jet plasmatrons. High-frequency plasmatrons with induction heating enabled the catalytic activity at surfaces to be studied.

Arc jet plasmatrons, from an earlier generation of test facilities, were used on ablative systems, [See also: 70.10 for Buran wing leading edge constructions].

71.6.2 Materials and configurations

The thermal profiles of the two vehicles on re-entry are similar, as are the distribution of TPS materials.

Buran has ceramic tiles made from silica fibres for regions experiencing temperatures between 700°C and 1200°C, with flexible insulation for zones up to 370°C.

Ablatives also appear in the design, as do external ‘thermo-resistant shields of metallic honeycomb panels’ for the 400°C to 700°C areas, Ref. [71-15]. Both of these are found on the trailing edges of the wings. Buran has 38,000 thermal protection tiles bonded to external surfaces.

71.7 Advanced carbon reinforced composites

71.7.1 Carbon-carbon composites

Carbon-carbon (C-C) composites are used in thermo-structural TPS, Ref. [71-16], [71-17], [71-18]. Their popularity continues despite the complex protection systems required for oxidation resistance, [See also: Chapter 74].

C-C composites are specified because:

- They have proven in-service performance on Shuttle Orbiter and other space programmes,
- They are the only proven structural materials capable of functioning above 1600°C,
- Carbon fibres increase in strength at high temperatures to 2500°C,
- Proven manufacturing routes exist; either resin or pitch pyrolysis, or by CVI,
- Complex constructions can be prepared with 3D or n D fibre orientations,
- They have excellent capabilities in sustaining thermal shock and thermal cycling.

Performance improvements in this class of composites have come about because of:

- The availability of improved carbon fibres,
- Different carbon fibres offering optimisation of:
 - strength,
 - modulus,
 - conductivity, and
 - thermal stability.
- Multi-dimensional fibre orientation, up to 6D.

71.7.2 ACC - Advanced carbon-carbon

To demonstrate the improvements, NASA developed ACC (advanced carbon-carbon) by 1982 to replace the earlier RCC (reinforced carbon-carbon). A 25% improvement in tensile strength was achieved, although the interlaminar strength diminished slightly for this 2D fabric composite.

Subsequent further refinements include:

- A fine tow and thin fabric combination simultaneously improves in-plane and interlaminar strengths in 2D composites,
- Optimising fibre surface treatment and sizes enables potentially high improvements in interlaminar strength,
- Through-thickness reinforcement results in property trade-offs between in-plane strength and interlaminar shear strength,
- Overall tensile strengths can be improved by 100% and interlaminar shear strengths by 200%.

These improvements give designers greater confidence in the materials for load-bearing applications, either in minimum gauge sections or high load-carrying members.

Figure 71.7.1 shows an ACC Multipost stand-off TPS concept, Ref. [71-5].

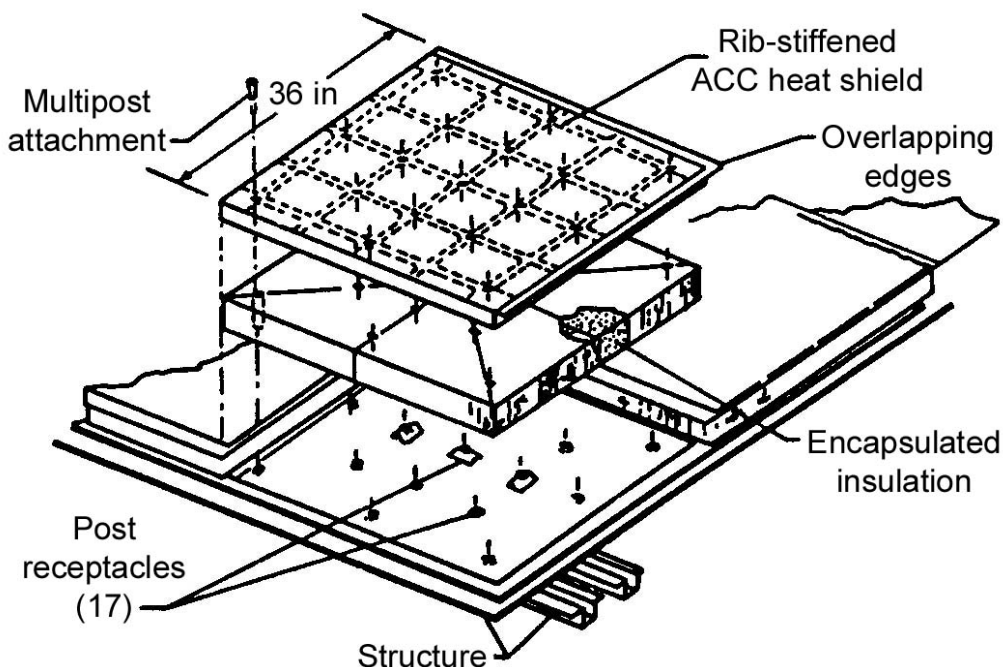


Figure 71.7-1 - TPS: ACC multi-post stand-off concept

71.7.3 Aerospaciale - Aerotiss® 2.5D

Within the Hermes programme, Aerospaciale developed a family of reinforced carbon-carbon (RCC) materials with multidirectional fibre architectures; known as Aerotiss®.

The fibre preforms (2D, 2.5D, 3D) are densified by repeated phenolic resin impregnation and cure, followed by pyrolysis to achieve the correct density. Antioxidation coatings (PAQ), based on silicon carbide, are then applied by pack cementation, CVD and silica impregnation (via sol-gel).

For the X-33 programme, BF Goodrich (formerly Rohr) is responsible for the design, manufacture and integration of the TPS. During test flights, the vehicle can reach 1300°C to 1400°C in some areas. This exceeds the reusability temperature criteria imposed for the metallic tiles that cover the majority of the vehicle. Consequently, a C-C nose cap was selected to cover all the external surfaces exposed to temperatures exceeding 1100°C during test flights and leading edges, Ref. [71-83], [71-84].

Table 71.7.1 summarises the mechanical and physical properties along with oxidation resistance of the Aerospatiale material for the X-33 nose cap, Ref. [71-83].

An evaluation sample of Aerospatiale's C-C material is included on the ARD re-entry experiment, [See also: 71.1].

Table 71.7-1 – Aerotiss® 2.5D coated carbon-carbon: Properties

A) Mechanical/Physical properties:

Properties	20°C	1500°C
Density (kg/m ³)	1550	-
Porosity (%)	<6	-
Min. tensile strength (MPa)	120	120
Tensile modulus (GPa)	75	75
Min. compressive strength (MPa)	120	120
Compressive modulus (GPa)	75	75
Min. interlaminar shear strength (MPa)	10	10
Thermal expansion coefficient (10 ⁻⁶ K ⁻¹)	-0.5	1
Thermal conductivity (Wm ⁻¹ K ⁻¹)	17	34

B) Oxidation resistance:

Temperature °C	(No. of cycles	Pressure (mbar)	Mass loss per cycle (%)
BLOX Laser heating facility			
800	10	10	0.015
1000	10	10	0.015
1450	10	10	0.015
1600	10	10	0.025
SIMOUN Arc-jet facility			
1300	5	75	0.015
1500	30	75	0.02

71.7.4 Carbon-silicon carbide composites

The use of ceramic matrix composites (CMC) in thermal protection systems originated within the Hermes programme.

An aims were to improve on that applied to the Space Shuttle, e.g.:

- higher durability (damage resistance),
- lower maintenance costs,
- lower installed mass.

This led to the separation of the thermal insulation and mechanical structure functions, Ref. [71-80].

Within the Hermes programme and subsequent European activities, a number of carbon-reinforced silicon carbide materials have been developed, manufactured and evaluated for TPS applications. Of these, several have reached full-scale component-level flight verification and have been incorporated into future re-entry vehicle programmes, Ref. [71-80].

The materials for various programmes and applications are summarised in Table 71.7.2, Ref. [71-80], [71-85].

Table 71.7-2 – CMC carbon-silicon carbide: Various TPS programmes and applications

CMC material	Source	Programme / Application
CC-SiC	DLR	ARD, [See: 71.1]
CC-SiC	DLR	CETEX, [See: 71.1]
CC-SiC	DLR	TETRA/X-38 Nosecap
CC-SiC	DLR	TETRA/X-38 REI-type panel, [See: 71.12]
C-SiC	DASA	TETRA/X-38 Large scale panel
C-SiC	MAN	ARD, [See: 71.1]
C-SiC	MAN	FESTIP - Cryogenic fuel tank TPS, [See: 71.19]
C-SiC	MAN	TETRA/X-38 REI-type panel, [See: 71.12]
C-SiC	MAN	TETRA/X-38 Split Flaps
C-SiC CVI	MAN	SÄNGER Air-intake ramp X-38 Body Flap (girders, lugs & beam parts; double-hinge, actuator bearing components; CMC fasteners)
C-SiC LPI	MAN	CHA Heatshield, [See: 71.17] SÄNGER Air-intake ramp X-38 Body Flap (cover/bottom plate parts)
C-SiC	SEP	ARD, [See: 71.1]
C-SiC	SEP	Hermes REI shingle [See: 71.12]
C-SiC [SEPCA RB-INOX 272-01]	SEP	CHA Heatshield (cassette panel) [See: 71.17; Table 71.17.1 – for material properties]

The mechanical properties and oxidation resistance of MAN materials LPI-C/SiC and CVI-C/SiC are summarised in Table 71.7.3, Ref. [71-85], [71-86].

Table 71.7-3 – CMC TPS: MAN carbon-silicon carbide - Properties

A) Mechanical properties for LPI-C/SiC, Ref. [71-85]:

Property	As-received Value	After 2.5h/1500°C/20mb argon
Tensile strength (MPa)	331	322
Tensile rupture strain (%)	0.62	0.62
Young's modulus (GPa)	61	60
ILSS (MPa)	26	28
Bending strength (MPa)	280	285

B) Approximate Mechanical Properties for CVI-C/SiC, [0/45] lay-up for CMC fasteners, Ref. [71-86]:

Property	Value
Tensile strength (MPa)	280
ILSS (MPa)	40
Translaminar shear strength (MPa)	140
Tangent modulus, parallel to lay-up (GPa)	80
Tangent modulus, perpendicular to lay-up (GPa)	25
Thermal expansion, parallel to lay-up (10^{-6} K $^{-1}$)	2-3
Thermal expansion, perpendicular to lay-up (10^{-6} K $^{-1}$)	4-5

C) Oxidation resistance for LPI-C/SiC and CVI-C/SiC: Plasma Arc Jet tests by NASA JSC, Ref. [71-85]:

Temperature (°C)	Pressure (mbar)	Time (mins)	ΔG (%)
LPI-C/SiC			
1660-1788	136	27	-1.47
1538-1933	92	13	-1.84
CVI-C/SiC			
1538-1621	92	11	-0.66
1471-1971	110	13	-0.43

71.8 Durable metallic TPS

71.8.1 General

These concepts centre on the use of titanium or nickel-based materials to create radiative stand-off TPS. The better known examples are:

- Titanium multiwall (M/W) versions, and
- Superalloy honeycomb (SA/HC).

Durable implies that they are less prone to damage than their ceramic counterparts.

These systems have been considered for Sänger in Germany, Ref. [71-4], [71-19], [71-20], [71-21] and for USA programmes.

As with all TPS concepts, there are many construction permutations. The metallic concepts with low areal mass can compete with the other TPS solutions.

71.8.2 Multiwall TPS

Metallic multiwall TPS consists of thin (30 μm to 100 μm), dimpled foils which are diffusion bonded at the dimples. Several layers with plane shear foils, combined with an optional layer of internal multiscreen insulation (IMI), make up a multiwall panel, as shown in Figure 71.8.1, Ref. [71-20].

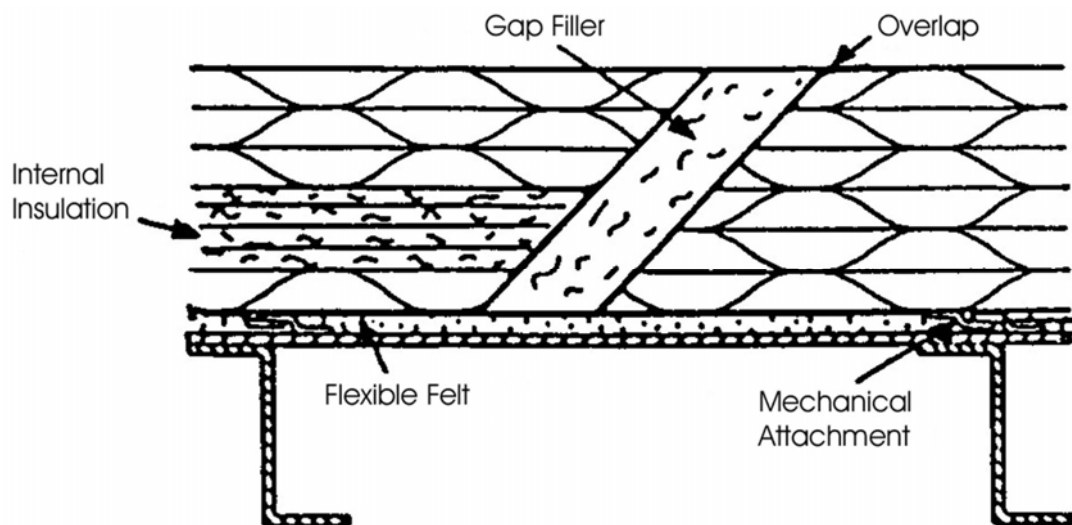


Figure 71.8-1 - TPS: Multiwall panel scheme

Several parameters can be varied:

- dimple pattern, e.g. grid spacing,
- foil thickness,
- foil material:
 - Ti alloys (to 600°C),
 - Ni alloys (to 1000°C),
 - Mo alloys (to 1300°C).
- bulk density range 100 kg/m³ to 250kg/m³,
- optimised designs can have an areal mass as low as 9kg/m².

The multiwall panels are mechanically attached to the cold sub-structure with clips or studs. The emissivity and oxidation resistance of the foils is given serious consideration to ensure that the TPS is fully reusable.

Materials evaluated in trials include:

- Ti-6Al-4V titanium alloy,
- Inconel IN 718 nickel alloy,

- Haynes 188 cobalt alloy,
- TZM molybdenum alloy.

More advanced materials such as Ti1100, with SPE/DB processing, or titanium aluminides can also be used.

There is greater confidence in the reproducible behaviour of metallic materials than their ceramic counterparts. This is used to promote the metal-based TPS concepts.

NASA have supported the development of various metallic concepts, Ref. [71-22], [71-23], [71-24], [71-25], [71-26]. The titanium multiwall version is much as described above. The Ti dimpled foil is bonded together with a liquid-interface-diffusion (LID) technique.

The superalloy honeycomb concept consists of an Inconel 617 honeycomb outer panel with 127 μm face sheets, layered fibrous insulation, and a titanium honeycomb inner surface panel with 152 μm face sheets.

The edges of the two metallic concepts are covered with 76 μm beaded closures to form panels 300mm square.

71.8.3 Developments

71.8.3.1 General

Further developments in multiwall concepts were made by DASA (formerly MBB Ottobrunn) regarding the winged and fully-reusable ESA WLC TSTO reference vehicle, Ref. [71-69].

The combination of dimpled foils with internal insulation (IMI), [See: 71.10] has been examined further to characterise the behaviour. The anticipated use was for the protection of a CFRP composite integral liquid hydrogen tank.

71.8.3.2 Construction

- 4 flat foils + 3 dimple layers Haynes 188:
 - Upper surfaces coated with ~10 μm alumina deposited by physical vapour deposition (PVD).
 - Emissivity of 0.7 (0.65 after 10 hours at 900°C).
- 40 mm IMI thickness (less than 30 kg/m³) with 9 silica quartz layers, each 4.4mm thick, separated by Inconel 600 foils. The two hottest foils were gold coated with a TiN diffusion barrier.
- Two further flat foils plus a dimpled layer backed the IMI, enabling fixing to the substrate.
- Total thickness of 60mm, with areal density of 10kg/m².

Care needs to be taken when handling these thin layer materials and the assemblies cannot be over-compressed during integration.

71.8.3.3 Mass distribution

For boxed test panel (total weight 563 grams):

- Upper and lower multiwall package: 227g (40.3% of total mass).
- Metallic cover sheet and border profiles: 86g (15.3%).
- Metallic box structure: 51g (9.1%).
- Fibrous insulation (IMI plus fillers): 69g (12.3%).
- Re-radiative screens (eight 25 μm Inco 600 foils, two with gold coatings): 81g (14.4%).
- Panel attachment clips: 33g (5.9%).
- Brazing material: 16g (2.8%).

71.8.3.4 Limitations

The construction limitations included, Ref. [71-69]:

- Uncoated Haynes and Inconel sheets undergo surface oxidation above 650°C.
- Uncoated pure nickel re-radiation foils (screens) surface oxidise above 500°C.
- Oxidation leads to an increase in emissivity.
- The dimple layer configuration undergo local elastic buckling for excessive thermo-mechanical loadings, e.g. at heating or cooling rates greater than 3°C/sec.
- Fatigue cracking: Lifetimes of 25 missions for orbital stage and 80 missions for first stage.

71.8.3.5 Surface emissivity

Surface emissivity can be adjusted by applying dedicated coatings:

- High emissivity at outer panel surface.
- Low emissivity for screens, sidewalls and internal multiwall elements.

Material characteristics include:

- Bright nickel foil has a lower emittance (initially 0.09 rising to 0.41) than Inco 600 (from 0.14 increased to 0.22) even if moderately oxidised, but has a 150°C lower temperature stability. Inco 600 is preferred if foils beneath 15 μm can be obtained to control mass.
- Gold coated Inco 600 screen material has a favourable emittance provided that the surface roughness caused by a diffusion barrier layer can be reduced.
- Fully oxidised nickel foil has a lower than expected emittance of 0.39 at 600°C.
- Emissivity values have a small effect on the overall behaviour as the most sensitive parameters are IMI thermal capacity and package dimensions, i.e. depth.

71.8.3.6 Static mechanical tests

Tests conducted on the multiwall configuration showed:

- Multiwall shear tests: strength varied between 16.8MPa and 18.5MPa which compared well with that predicted by FE analysis.

- Clip attachment tensile test: an average areal strength over entire panel of 42kPa was 5 to 6 times design level load.
- Bending strength: Multiwall package and sidewalls demonstrated adequate bending strength.

71.8.3.7 Acoustic noise test

The multiwall panel sustained a 40 minute acoustic noise test to 165dB (Shuttle noise spectrum), with minor damage recorded at dimple bonding points and at fixation points to the test facility (locking spring and bearing clip). This damage can be avoided by minor design changes, Ref. [71-69].

71.9 Titanium-based composites

71.9.1 NASP

The NASP programme placed considerable investment in:

- TMC (titanium matrix composites) with SCS SiC monofilament reinforcement,
- Titanium aluminides,
- Titanium aluminide matrix composites.

These materials are intended for the airframe, external skin and propulsion system. They are also appropriate for consideration in thermo-structural TPS because they offer better stiffness-to-weight and strength-to-weight characteristics than conventional unreinforced titanium alloys.

[See also: Chapter 47 for TMCs; Chapter 49 for intermetallics]

71.10 Internal multiscreen insulation (IMI)

71.10.1 Concept

71.10.1.1 General

Internal multiscreen insulation (IMI) development was initiated under the Hermes programme as an integral part of the Rigid External Insulation (REI) concept, i.e. IMI is between the cool substructure and external TPS skin (C/SiC or metallic) but forms part of the REI shingle, Ref.[71-27], [71-28].

More recently, IMI has been included in other vehicle programmes, e.g. McDonald Douglas SSTO 'Delta Clipper' and NASA's Lockheed-Martin 'Venture Star', Ref. [71-87].

71.10.1.2 Materials and construction

IMI consists of a series of lightweight ceramic screens, coated with an ultra-thin layer of noble metal.

The screens are separated by fibrous alumina or silica spacers, which also serve to minimise convection. The assembly of the screens and spacers produces an IMI with high thermal efficiency, Ref. [71-28].

The foils are prepared from alumina fibre fleeces impregnated with an alumina sol. After pyrolysis, the resulting alumina-alumina composite characteristics are:

- Porous matrix: 55% micro-pores (50nm), density 1.7g/cm^3 .
- Foil areal mass: 35g/cm^3 , $40\mu\text{m}$ thick.

A noble metal coating (a few 100 nm thick) is applied to each side of the foils, i.e. gold: melting point 1060°C ; platinum: melting point 1769°C . This provides a high reflectivity to an incident heat flux, by multiple reflection and re-radiation.

To ensure thermal stability and durability, an oxide (patented) is applied on the ceramic prior to noble metal coating.

The IMI concept is adaptable by varying the:

- material selection,
- density of fibrous layers,
- thickness and number of fibrous layers,
- number and areal mass of screens,
- material and type of low emittance coatings on the radiative screens.

The possible IMI combinations provide a wide range of options for various surface temperature and vehicle requirements; typically with highest mass savings between 600°C to 1700°C , Ref. [71-87].

Figure 71.10.1 shows the basic design concept, Ref. [71-87].

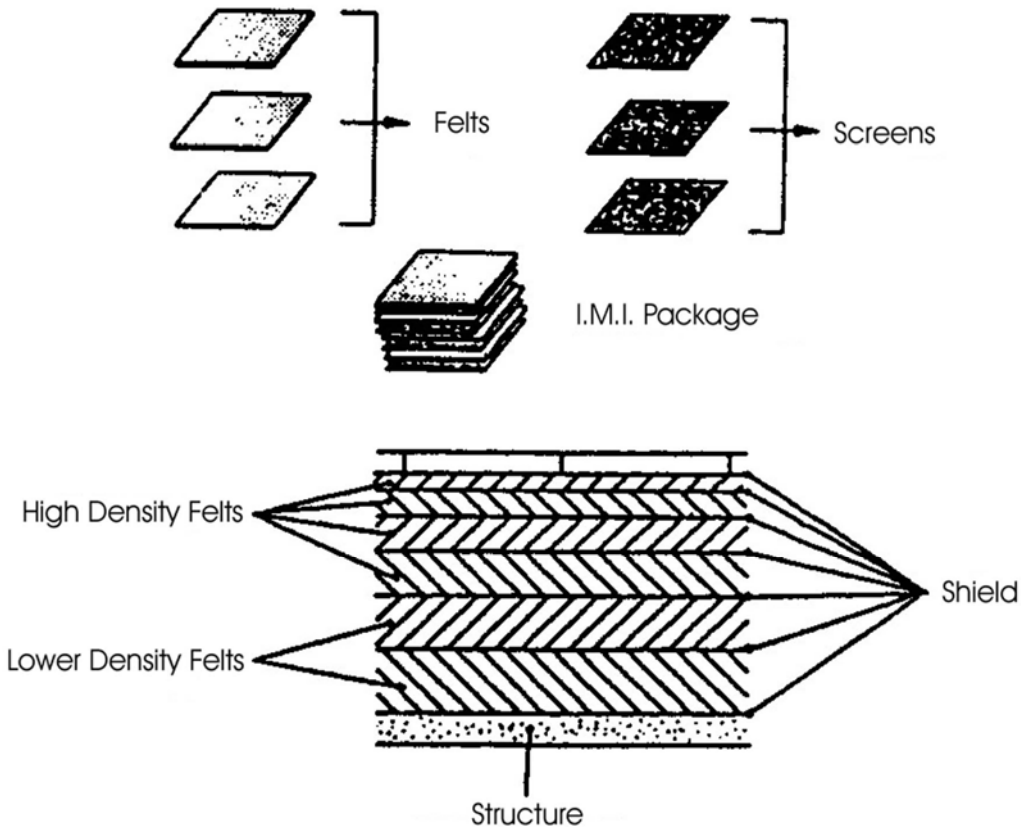


Figure 71.10-1 - TPS: IMI design concept

Table 71.10.1 lists some of the material candidates for different applications, Ref. [71-87].

Table 71.10-1 - TPS: IMI material candidates for different applications

Operational temperature range (°C)	Felt spacer material (Bulk density, kg/m³)	Screen substrate	Screen coating
<600	Low density Quartz (<17)	Alumina	Gold
600 - 900	Low/medium density Quartz (>17)	Alumina	Gold
900 – 1050	Low density alumina (25 – 35)	Alumina	Gold
1050 – 1450	Medium density Alumina (35 – 45)	Alumina	Platinum
1450 - 1700	High density Alumina (50 – 60)	Alumina	Platinum

71.10.1.3 Theory

Each reflective screen contributes to the attenuation of radiative heat transfer by a thermal radiative resistance proportional to:

$$\left(\frac{2}{E}\right)^{-1} \quad [71.10-1]$$

Where:

E *thermal emittance.*

The primary performance parameter for IMI screen development:

$$\frac{\left(\frac{2}{E}\right)^{-1}}{m} \quad [71.10-2]$$

Where:

E *thermal emittance.*

m *mass of screen per unit area.*

The total conductivity of an IMI package is the sum of the three main components:

- air conductivity,
- solid material conductivity, and
- radiative conductivity.

71.10.2 Development and characterisation

71.10.2.1 General

Under the Hermes programme, extensive analysis and testing of IMI and REI was undertaken, Ref. [71-87]:

- Theoretical modelling, developed for:
 - predicting the thermal transport behaviour, Ref. [71-6],
 - mass sensitivity studies, design layout and optimisation (thermal and mechanical vehicle specifications).
- Manufacture of sub- and full-scale IMI components: Fabrication and integration feasibility, improve manufacturing routes and produce test samples.
 - Screens, foils and spacers,
 - Integrated packages (350mm x 350mm x 100mm).
- Material characterisation and testing: Model prediction validation and performance under launch, re-entry, long-term ground and space conditions.

71.10.2.2 Thermal tests

These considered the:

- High temperature stability and optical performance after thermal ageing under defined temperature/pressure conditions (long-term single mission and cyclic).
- Thermal performance (cyclic re-entry pressure/thermal trajectories).
- Conductivity (ageing).

71.10.2.3 Material characterisation

The properties investigated were:

- Conductivity (material, parallel and perpendicular).
- Heat capacity (material).
- Permeability.
- Humidity and moisture absorption.
- Thermal shock and freezing.
- Salt water exposure and chemical compatibility.
- Emission.

71.10.2.4 Mechanical performance

The properties evaluated were:

- Mechanical load.
- Compression test
- Residual resilience (spring-back).
- Vibro-acoustic loads.
- Flexural tests.
- Venting tests.

71.10.2.5 Integration and assembly tests

This considered the:

- Integration, assembly and disassembly.
- Handling, inspection and refurbishment.

71.10.2.6 Non-destructive inspection

The evaluation of :

- X-ray inspection.
- Preload control and measurement.

71.10.2.7 Results

Table 71.10.2 summarises the main results of the IMI insulation elements and REI assembly, Ref. [71-80], [71-87].

Table 71.10-2 – TPS: Summary - IMI characterisation test results

Test type	Test conditions (representative)	Results
Thermal:		
Complete REI	10 missions, reentry profile up to 1200°C	Demonstrated thermal function of REI; temperature of cold structure met requirements.
IMI alone:		
Au-coated screens	>120 missions/in air/900°C	Effective thermal emissivity: 0.16
Pt-coated screens	>10 missions/in air/1450°C	Effective thermal emissivity: 0.4
Thermal Shock: IMI	+150/-200°C	No degradation in mechanical or optical properties
Humidity: IMI	38°C/70°C; 90-100% water	<1% water absorption
Chemical: IMI	salt water, acid rain, acids	No degradation of material No change in optical performance
REI:		
Gas Flow/Venting: REI	Ascent profile (1 bar to 1 mbar in 120s)	No damage to REI or IMI
Static Pressure: REI	95 mbar external & internal overpressure	No damage to REI or IMI
Vibration: REI	Wide band sine sweep 4 to 2000Hz in 3 directions	No damage Significant damping by IMI
Acoustic: REI	Wide band acoustic load, 50-2000Hz up to 154 dB for >30 missions	No damage
	5 missions (10 min.) for extreme overload at 165dB	No damage
Additional tests: Representative of SSTO environments		
NASA-LaRC facility	Acoustic: 125 to 168 dB	No degradation
Wright-Patterson	Thermal (quartz lamp): to 1600°C	No degradation

71.10.3 Potential applications

The TETRA programme includes REI-type TPS systems that include IMI insulation. These have also been proposed for the X-38 programme, Ref. [71-80].

In addition, IMI has been proposed for consideration within the TPS systems of:

- HOPE-X: IMI placed within the hollowed-out, baseline silica tile.
- X-33: Replacement of fibrous internal insulation materials (Saffil alumina) with IMI within the baseline TPS (metallic shingle-type). Mass studies indicated a significant saving over 'traditional' insulation materials; with a potential ~17% saving (based on net installed mass of an integrated panel).
- X-34: IMI insulation as part of the proposed C/SiC TPS panel array.

71.11 Flexible external insulation (FEI)

71.11.1 General

FEI materials have been developed and characterised for TPS applications within various programmes:

- Hermes.
- MSTP programme:
 - Crew transfer vehicle (CTV).
 - Crew return vehicle (CRV).
- ARD programme.
- Future reusable vehicles.

71.11.2 Design concept

FEI-TPS consists of an assembly of light-weight, quilted, flexible insulation blankets, as shown in Figure 71.11.1, Ref. [71-30].

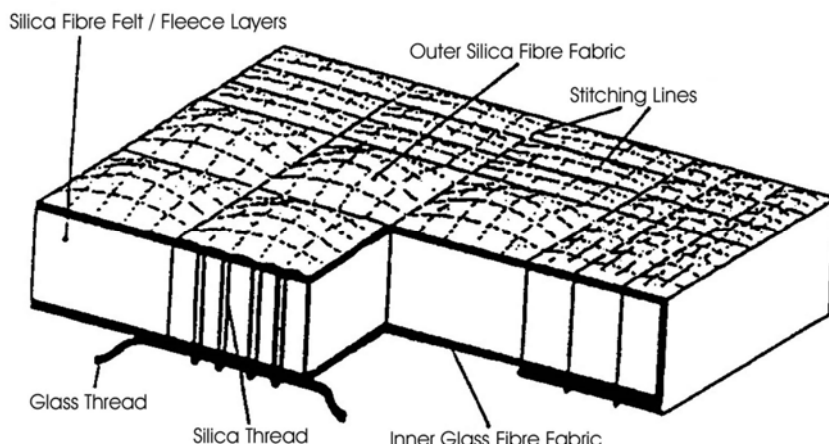


Figure 71.11-1 - TPS: Schematic of FEI blanket

71.11.3 Key features

These are:

- Blankets are constructed of ceramic, silica or glass fabrics, sewing threads and micro-fibre fleeces or felts:
 - Insulating fleeces or felts are enclosed in fabrics and stitched together, with threads of the same material.
 - Application temperatures and structural load levels determine the materials selected.
- The thermal capabilities of the FEI system have been extended to 1300°C by using aluminoboro-silicate (ABS).
- Stitching (20mm x 20mm square pattern) fixes the blanket shape and thickness. During sewing, the insulation core is compressed giving a blanket with improved stiffness and quasi-elastic properties.
- Established manufacturing technology can produce:
 - plain blankets: from 100mm x10mm x 5mm to 5000mm x 2500mm x50mm.
 - cylindrical and spherical blankets: minimum radius 500mm.
 - gradient blankets: with variable thickness.

The shape is fixed during sewing.

- Blankets are bonded to the primary structure by RT-curing silicone adhesive (RTV).
- Surface coating of the external surface provides:
 - enhanced emittance,
 - specified absorptance properties,
 - reduced permeability
 - increased stiffness.
- Water repellent (silane-based) avoids rain or moisture ingress.

The types of mechanical loads anticipated for each component of the FEI are shown in Table 71.11.1, Ref. [71-32].

Table 71.11-1 - TPS: Mechanical loads and sources on FEI components

FEI component	Type of Loading				
	Differential pressure (FEI/Atmosphere)	Acoustic noise (Ascent/Descent)	Aerodynamic (Flutter)	Manufacturing process (Pre-tension)	Other
Core	-	Compression Fatigue	Compression Fatigue	Compression	-
Outer fabric, inc. coating	Tension	Tension Fatigue	Tension Fatigue	Tension Local Forces	Erosion
Sewing thread	Tension	Tension Fatigue	Tension Fatigue	Tension Local Forces	Erosion
Lower fabric	-	-	-	Tension Local Forces	-

71.11.4 Product range

Table 71.11.2 summarises the FEI options available; with application temperatures from orbital minimum -150°C to +1200°C during re-entry, Ref. [71-88].

The product codes designate the limit temperature for multiple reuse, nominally 100 re-entry cycles under moderate structural loads, Ref. [71-88]. This generally restricts the application of FEI to the rear surfaces of winged re-entry vehicles and capsules.

Table 71.11-2 – FEI-TPS product range

Product code	Core	Thread	Fabric	Comments
FEI-300	Aramid fibre felt (Nomex, Kevlar).	Aramid		Development product, within ESA/ESTEC TRP programme. Similar to, but improved temperature capability, FRSI (Space Shuttle).
FEI-450	Aramid felts Polybenzimidazole (PBI) fibre-felts	PBI or silica		Development product, within TETRA programme for X-38 applications.
FEI-650	Silica felt	ABS	ABS	Similar to AFRSI (Space Shuttle), but improved mass advantage with FEI.
FEI-1000	Ceramic microfibre felt	ABS	ABS	
FEI-1100	Ceramic microfibre felt	ABS	ABS	Higher alumina content in fibres gives improved temperature capability.
IFI-1100	Alumina fleece	(50mm x 50mm sewing pattern)		Derivative of FEI-1100. Used under stand-off panel TPS, aerothermal, acoustic & aeroelastic loads are carried by the panel. IFI has better insulation but lower load resistance.

Key: ABS = alumino-boro-silicate

71.11.5 Hermes

71.11.5.1 General

Flexible External Insulation (FEI) was developed as TPS in the Hermes programme, Ref. [71-29], [71-30], [71-31], [71-32]. Intended for the leeward surfaces, it was capable of use up to 650°C under moderate to high acoustic loads, Ref. [71-88]. The Hermes FEI consisted of a number of quilted silica blankets, directly bonded to the primary structure.

In general, Hermes FEI was similar to the AFRSI system found on the Space Shuttle Orbiter, [See: 71.6].

The quilted FEI blankets are characterised by a surface waviness of the order of 2mm and an increased permeability (compared with other TPS). This restricts the FEI to locations with a comparably thick boundary layer, low to moderate pressure gradients and low aerodynamic surface requirements. In general, such conditions are found on the leeward sides of vehicles during re-entry.

High acoustic loading is a critical design driver, along with excitation of the outer cover by airflow possibly leading to uncontrolled oscillations (flutter).

Initial tests with early FEI constructions showed catastrophic failure at high overall acoustic sound levels of around 168dB. Failure was attributed to an erosion process between hard coating particles and the silica thread or fabric. This prompted an improvement in the construction by changing the coating formulation and application process, Ref. [71-32].

71.11.5.2 Prequalification tests

The prequalification of FEI-650 and to a certain extent FEI-1000 and FEI-1100 was successfully completed for the Hermes spaceplane. The blankets were subjected to the test sequence, Ref. [71-88]:

- Thermo-physical tests: including catalycity, plasma erosion up to 1100°C.
- Thermo-acoustic test, with loads, to 950°C surface temperature with 156dB OASPL (overall acoustic sound pressure level) acoustic noise, 5.3kPa stagnation pressure.
- Thermal cycling: 30 cycles in air, 20 mins. exposure at 650°C.
- Dynamic response (NDI).
- Acoustic noise test: stepwise increase of loads; 158dB/10 mins. + 163dB/10 mins. + 186dB/10mins.
- Acoustic noise ageing test: 158dB/20 mins.
- Flutter test (transonic): $Ma = 0.3\text{-}1.1$, $p_o < 47\text{kPa}$ (tangential flow), with 160dB OASPL acoustic noise.
- Flutter test (supersonic): $Ma = 0.3\text{-}2.6$, $p_o < 93\text{kPa}$ up to $Ma=3.2$, $p_o < 213\text{kPa}$.

71.11.5.3 Status

FEI-650 blanket was verified for:

- 120 cycles under loads corresponding to 650°C limit temperature and 158dB OASPL acoustics.
- Extreme conditions: 800°C ultimate temperature and 165dB OASPL acoustics.

FEI-1100 blanket tested to:

- 30 cycles up to 1100°C, 168dB acoustic loads/10 mins.

71.11.6 MSTP programme

71.11.6.1 General

FEI development continued after the Hermes programme to cover its possible use on crew transfer vehicle (CTV) or crew return vehicle (CRV).

In the MSTP programme FEI blankets were developed to replace the ablative TPS on the leeward conical surface of a Viking-shaped CTV or CRV capsule. From 1994-96, the functional behaviour of flexible insulation blankets was studied to increase confidence in their integrity for operational use, Ref. [71-73]. These FEIs have been successfully qualified with limit temperatures up to 1100°C and ultimate temperature of 1300°C; on 4 ascent/re-entry cycles, Ref. [71-88].

71.11.6.2 Crew transfer vehicle (CTV) specification

Specifications for a Viking-shaped CTV capsule were:

- Trapezoidal shaped blankets, 1m x 1m tapering to one end.
- Options for 650°C (FEI-650) and 1000°C (FEI-1000) operation.
- 20mm x 20mm square sewing patterns (ceramic threads) to integrate insulation core (fleece or felt) with outer fabrics.
- Ceramic fabric for outer heat resistance and woven glass fabric for underside surface.
- Blanket is pretensioned when compressing the insulation core and held in place with pattern sewing.
- Blanket premoulded to curvature of the conical surface of the CTV.
- Blankets bonded to substructure with RTV silicone adhesive.

71.11.6.3 FEI characterisation

The assessments made on materials, components and blankets were, Ref. [71-73], [71-88]:

- Thermal conductivity measurements for alumina-silica hybrid felt, fleece core materials and for entire blankets from 300°C to 1200°C and air pressures ranging from vacuum to one atmosphere. TsAGI, Russia demonstrated their excellent insulation performance.
- Gas permeation studies at NLR (cold) and TsAGI (hot, in an arc-heated wind tunnel) confirmed that when after applying a coating to the outer fabric.. The effect of typical pressure gradients experienced during capsule ascent and re-entry were not shown to be significant.
- From arc-jet wind tunnel tests the influence of surface discontinuities has been assessed. Local overheating remains within safe limits for gaps between blankets of up to 2mm and steps up to 3mm. Steps to 4.8mm can be tolerated by correct shaping of the blanket-to-blanket borders.

71.11.6.4 Structural tests

The testing and inspection included:

- Acoustic noise screening tests with stepwise increases; 155dB, 160dB and 165dB for four minutes each showed that FEI-650 and FEI-1100 survive without failure.
- Shear and peeling tests on the silicone bond between blanket and aluminium substructure gave adequate strength up to the maximum permissible surface temperature of 180°C.
- X-ray methods (used during manufacturing) and infra-red thermography (after assembly and integration on the capsule) were demonstrated to be suitable NDI techniques for detecting:
 - core density variations,
 - ceramic thread failure,
 - metallic foreign part inclusion,
 - water uptake,
 - delamination of silicone bond line.

71.11.6.5 Material and process characterisation

The various parameters evaluated can be summarised as:

- The high-temperature strength retention of fabrics and threads were investigated after exposure to temperatures in the range 800°C to 1400°C. The alumina constituents showed reasonable strength retention to 1200°C, whilst silica constituents were limited to 900°C. This complied well with the temperature resistance demonstrated in arc-jet and plasma-jet tests where blankets had been exposed between 1300°C for 2.5 minutes and 900°C for 50 minutes.
- The effect of salt exposure and subsequent annealing was measured on the strength reduction of fabric and thread.
- The compression behaviours of a silica core and two ceramic cores (one stiff and one soft) have been determined in the as-received state and after annealing at 1100°C. The compression strength varied depending on the arrangement of the fibres.
- The silicone adhesive to aluminium shear strength behaviour was assessed with respect to surface pre-treatment (cleaning, abrasion and chromatising), filler addition (glass micro-balloons), temperature and humidity. Surface pre-treatment was significant at room temperature, but decreases as temperature increases. Increasing the micro-balloon content decreases the shear strength.
- The silicone adhesive showed no uptake of water, and the FEI was unaffected by exposure to monomethylhydrazine (MMH) vapour.

71.11.6.6 Design verification

This covered the prequalification for the environment sequence from launch to re-entry and landing; with 4 blankets 150mm x 300mm x 20mm tested to simulate launch unprotected on top of Ariane 5.

The test sequence applied was:

- Ground environment:
 - rain simulation,
 - humidity,
 - thermal cycling,
 - saline atmosphere, where the silica core (FEI-650) was more prone to moisture absorbtion.
- Ascent environment:
 - Acoustic test: 4 minutes overall sound pressure level (OASPL) of 168dB at IABG, Munich. Some broken threads were found for blankets previously given ground environment exposure.
 - Flutter test in high speed wind tunnel (HST) and supersonic wind tunnel (SST) at NLR. The nominal test envelopes are given in Table 71.11.3, Ref. [71-73]. All samples were stable throughout the tests, even those with low-level acoustic damage.
- Re-entry environment:
 - Plasma test: near tangential plasma flow to simulate hot re-entry, undertaken at TsAGI with the VAT-1104 plasmatron. The temperature cycle for top surface was equivalent to 4 nominal re-entries of 650°C to 1000°C for a total of 16.8 minutes; plus one extreme re-entry of 800°C to 1200°C for 4.2 minutes. No damage occurred except for discolouration.
 - Acoustic tests at 134dB OASPL for 4 minutes and 146dB for another 4 minutes. No deterioration was observed.

Table 71.11-3 – TPS: FEI nominal flutter test envelopes

High speed wind tunnel (HST)	Supersonic wind tunnel (SST)
$0.5 < \text{Mach} > 1.1$	$1.31 < \text{Mach} > 2.31$
$15 \text{ kPa} < Q < 50 \text{ kPa}$	$57 \text{ kPa} < Q < 88 \text{ kPa}$
$101 \text{ kPa} < P_0 < 202 \text{ kPa}$	$134 \text{ kPa} < P_0 < 299 \text{ kPa}$
Key: Q = dynamic pressure; P_0 = static pressure	

71.11.6.7 Status

From the results of the testing, FEI-650 and FEI-1000 have demonstrated their resistance to the severe environment. They are considered as prequalified for one manned flight on the conical rear surface of the Viking-shaped CTV capsule, Ref. [71-88].

71.11.7 ARD programme

71.11.7.1 General

The ARD (atmospheric re-entry demonstrator) capsule is an Apollo-shaped structure, downscaled by $\sqrt{2}$, with an ablative TPS.

For in-flight validation, samples of FEI-650 and FEI-1000 were flown on the conical rear of the ARD, integrated with the ablative TPS, Ref. [71-88]. Integration into ARD took place in September 1995 with launch in 1998 on Ariane flight V-503, Ref. [71-88].

71.11.7.2 Design verification

On ARD's conical upper section, FEI samples are integrated with the ablative TPS, i.e. FEI-650 in an area of relatively low thermal loading; FEI-1000 was closer to the heat-shield, therefore hotter.

Since the FEI samples form part of the overall capsule TPS (i.e. not redundant), a delta-qualification was needed which also considers the FEI-to-ablator interface. The tests used were:

- Ascent acoustic noise: AR-5 ascent spectrum, 148dB OASPL.
- Aerothermal:
 - One re-entry cycle: 1260°C/2.5 mins.
 - Endurance: 1050°C/10 mins. (4 re-entry cycles).
- Re-entry acoustic noise: Re-entry spectrum with 148dB OASPL.

Flight samples are preshaped, whereas qualification samples are flat.

71.11.7.3 Status

The test samples showed:

- excellent post-test condition.
- discolouration due to copper- and iron-based substances in the wind tunnel.
- no deterioration of FEI due to flow of char from the ablator to the forward edge.

The qualification was successful and the FEI experiment was released for flight.

71.11.8 Future reusable vehicles

Large surfaces on the leeward side of future reusable launch vehicles are exposed to moderate thermal loads, corresponding to surface temperatures below 500°C. At such locations, mass savings are possible with the light-weight FEI blankets under development, optimised for limit temperatures of 300°C and 400°C, Ref. [71-88].

The FEI approach is adaptable and versatile. Radiative heat transfer can be reduced with further development to include reflective screens and metallised fibres within the overall construction.

FEI is currently confined to areas having:

- low surface roughness requirements.
- low to moderate requirements for combined thermal, structural and aerodynamic loads.
- moderate erosive environments (plasma and particles).

71.11.9 Verified performance

FEI has been developed and prequalified for application on the leeward surfaces of vehicles, e.g. the conical upper surface of a Viking-shaped CTV vehicle; ARD capsule.

Compared with an ablator, FEI offers a number of advantages, including:

- Low areal mass of 4.2 kg/m² for a thickness of 20 mm.
- Negligible outgassing (CVCM <0.01).
- Negligible degradation of FEI components in LEO.
- Ease of spacecraft's thermal control by choice of thermo-optical properties, adjusted by FEI coating.
- Adaptability for specific interfaces, e.g. TPS for nozzles and HF transparent antenna.

Further work is intended on FEI-1000 to improve the waterproofing and high emittance coatings for single-use capsule applications, Ref. [71-88], together with further investigation of NDI techniques.

Table 71.11.4 summarises the verified performances related to multiple, reuse applications, Ref. [71-88].

Table 71.11-4 – FEI-TPS: Summary of verified performances

Requirement/Load	FEI-1100	FEI-1000	FEI-650
Limit temperature, °C	1100	1000	650
Ultimate temperature, °C	1300	1200	800
Salt	not tested	yes	yes
Rain	not tested	yes	yes
Humidity	not tested	yes	yes
Plasma-jet	yes	yes	yes
Vibration	Covered by acoustics		
Acoustic noise, after thermal ageing	153dB/4 mins	168dB/10mins	155dB/20 mins + 168dB/10mins
Aeroelastic (flutter)	not tested	No flutter excitation $Ma = 0.5\text{-}2.3$ $Q = 15\text{-}88\text{kPa}$	No flutter excitation $Ma = 0.5\text{-}3.2$ $Q = 15\text{-}107\text{kPa}$

71.11.10 IFI - Internal flexible insulation development

71.11.10.1 Background

During the X-38 nose cone and chin strap design-development, the need was identified for flexible fibrous insulation placed under the CMC shell to protect the substructure, where temperatures of up to 1750°C are reached in the stagnation area during re-entry, [See also: [70.24](#) - X-38 nose cap].

The development of the overall TPS system for the nose assembly was a collaborative exercise conducted by Astrium SI, DLR Stuttgart and MAN Technologie in Germany, Ref. [[71-95](#)].

71.11.10.2 Concept

The X-38 nose cap TPS system comprised, Ref. [[71-95](#)]:

- Rigid C/SiC panels (outer surface).
- Flexible insulation blankets to fill the remaining volume:
 - HTI high temperature insulation on the outermost region, [See: [71.23](#)].
 - IFI internal flexible insulation on the cold substructure.

Both the flexible insulation components were developed by Astrium SI (Bremen), now EADS-ST GmbH.

[See also: [70.24](#) - X-38 nose cap]

71.11.10.3 IFI materials and configuration

IFI has a blanket-like configuration, similar to FEI, comprising an alumina-based core fleece covered with an alumina fabric and sewn together using an alumina-boron-silicate ceramic thread; as shown in [Figure 71.11.2](#), Ref. [71-95]. It was developed as a spin-off from work on FEI. The maximum operating temperature is 1200°C.

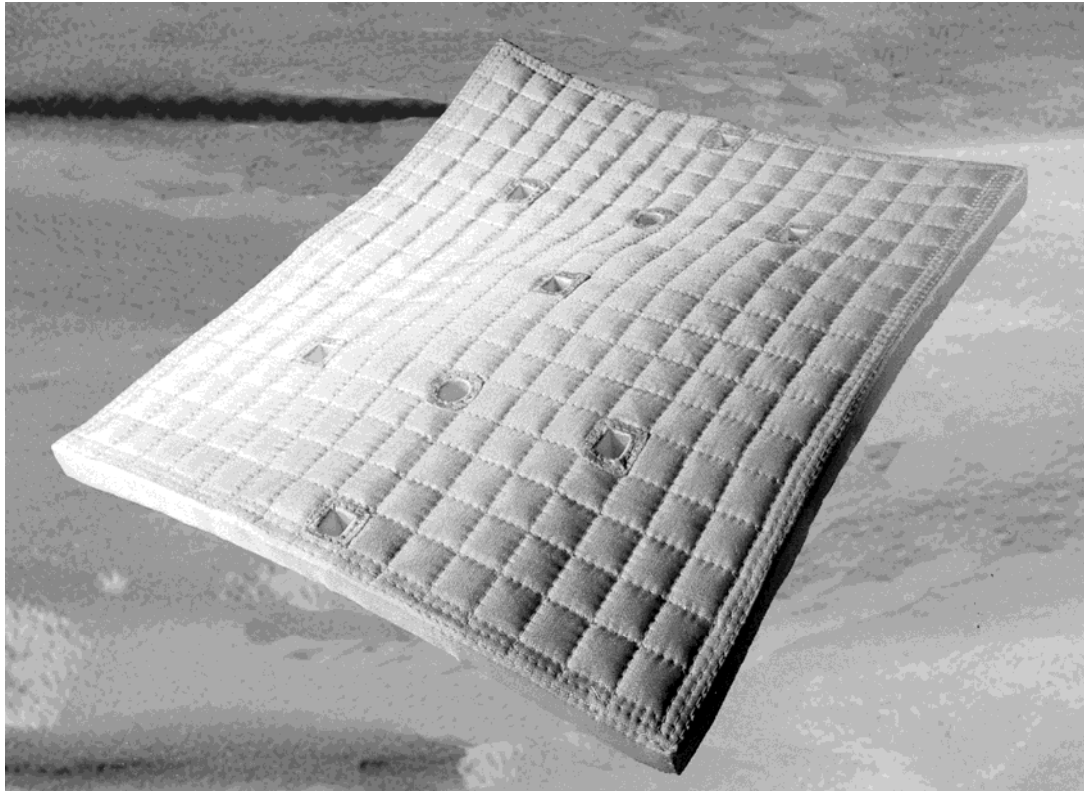


Figure 71.11-2 - TPS: IFI internal flexible insulation blanket

[Figure 71.11.3](#) shows the IFI blanket configuration within the X-38 nose cap, along with the various attachment points and interfaces, Ref. [71-95].

[See also: [70.24 - X-38 nose cap](#)]

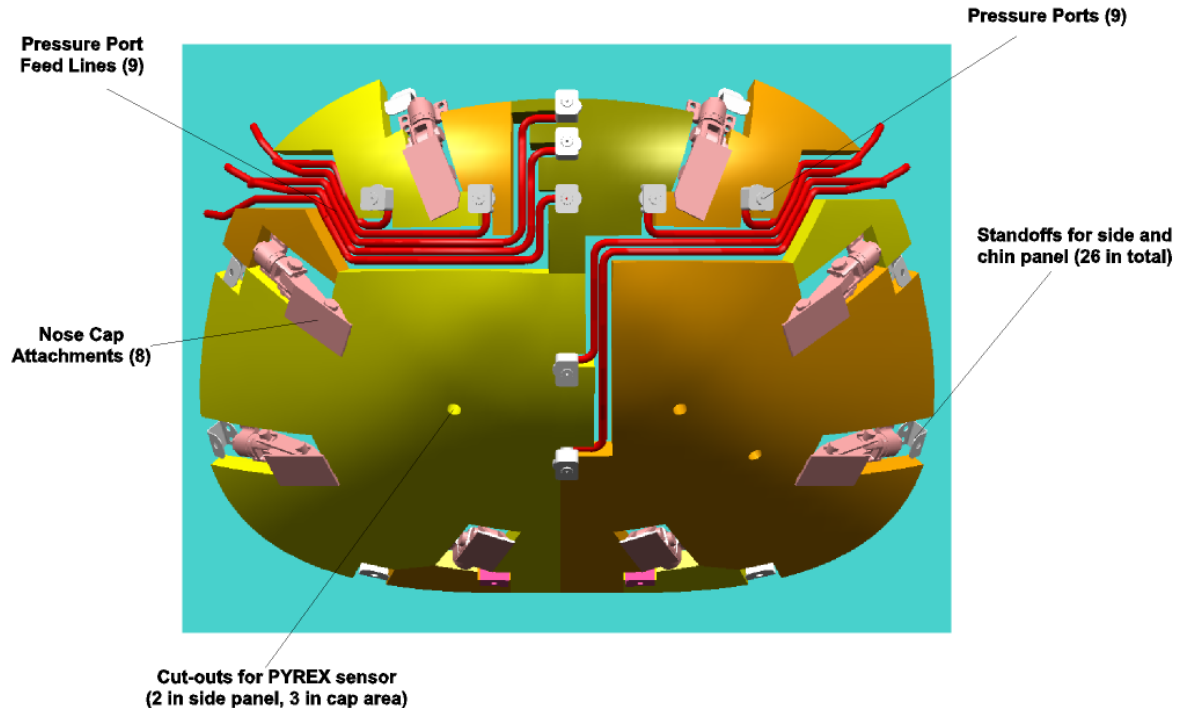


Figure 71.11-3 - TPS: IFI blanket configuration in X-38 nose cap

71.12 CMC shingles

71.12.1 Hermes design concept

71.12.1.1 General

Within the Hermes programme the development of rigid external insulation (REI) concepts consisted of, Ref. [71-33], [71-34], [71-80]:

- rigid outer thin shell of C-SiC CMC, to withstand aerodynamic surface pressure loads, thermodynamic stresses and environment (waterproofing, debris impact, handling).
- light-weight internal fibrous insulation, e.g. internal multiscreen insulation (IMI), [See: 71.10], to optimise heat transfer to the underlying vehicle structure.

Each TPS unit formed a shingle which interlocked with its neighbour and was attached to the substructure. This concept was deemed to offer greater durability than the ceramic tiles developed for the Shuttle Orbiter and reduced maintenance requirements. Since the expected average surface temperatures of Hermes were higher by some 100°C to 200°C, the need was for more efficient TPS. Each Hermes vehicle was anticipated to have approximately 800 shingles. The operating temperature range envisaged was 650°C to 1300°C.

Different manufacturing routes led to demonstrator shingles produced by SEP, Ref. [71-35], MAN Technologie, Ref. [71-34], [71-36] and Dassault Aviation, Ref. [71-33], [71-37].

The basic design described is that envisaged at the end of the Hermes project. Figure 71.12.1 shows the basic construction and method of retention, Ref. [71-33].

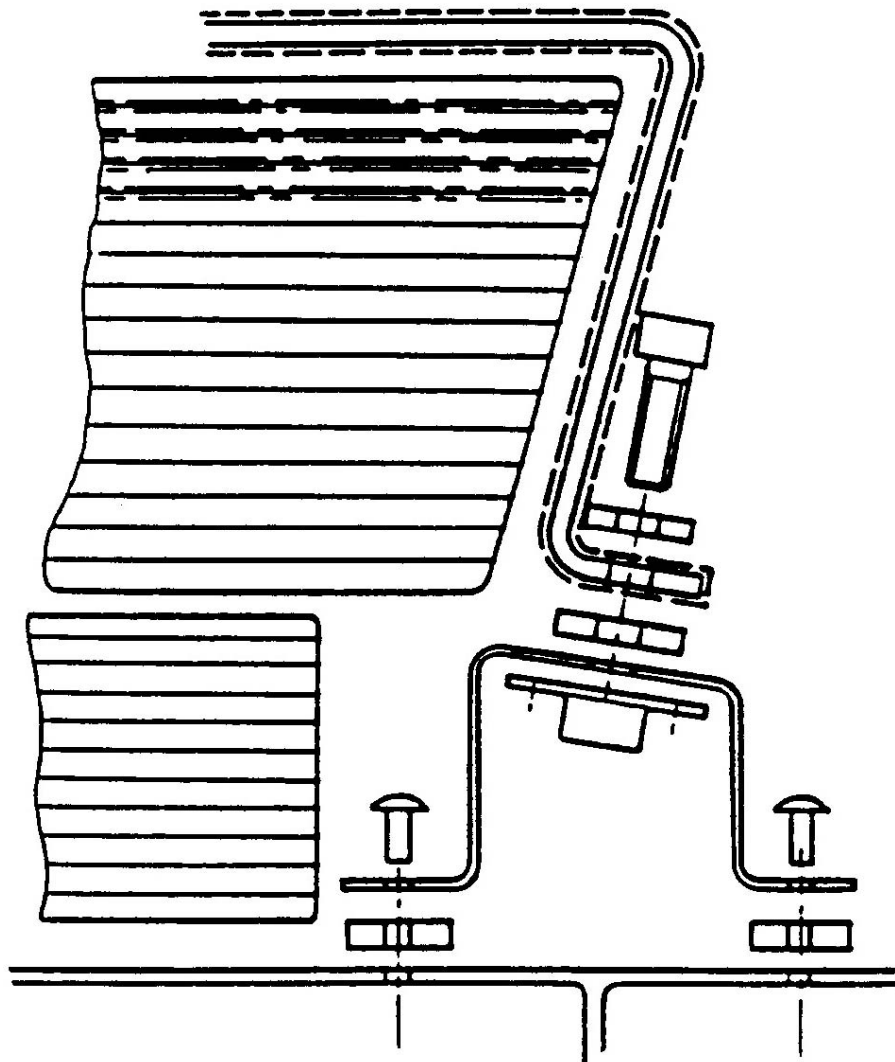


Figure 71.12-1 - TPS: Hermes CMC shingle support cross-section

71.12.1.2 Shingle construction

Each shingle has four types of component:

- one monolithic C-SiC panel, 1mm thick with a 50mm to 60mm high flange on all four sides,
- four metallic supports onto which the panel is mechanically attached with fasteners,
- layers of ultra-light IMI, and
- seal system, including:
 - external seal, ensuring aerodynamic shape continuity and preventing sneak-flows, whilst enabling self-venting in the presence of differential pressures.
 - internal barrier, ensuring the partitioning between the cavities under each shingle.

71.12.1.3 Performance criteria

These were specified as, Ref. [71-65]:

- maintenance of smooth aerodynamic surface to avoid premature boundary layer transition,
- high surface emissivity of 0.85,
- use of non-catalytic coatings to prevent exothermic recombination of dissociated chemical species,
- resistance to oxidation and other operational environments over 30 flights (15 years),
- ability to withstand acoustic excitation on launch (155dB) and aero-acoustic excitations during transonic-supersonic phases (up to 165dB in some places).
- typical temperature range of 600°C to 1450°C, Ref. [71-80].
- maximum temperature for the cold structure of 175°C.
- maximum deformation during re-entry of $\pm 2\text{mm}$ to maintain aerodynamic shape.
- minimum frequency of the first eigenmode greater than 100Hz.
- areal mass of 11.9kg/m² for the TPS.

Table 71.12.1 summarises the mass breakdown for the Hermes REI-shingle subcomponents, Ref. [71-80].

Table 71.12-1 – Hermes TPS REI-shingle mass breakdown

Subcomponet	Unit mass (kg/m ²)
C-SiC shingle + coating	3.73
Internal multiscreen insulation (IMI)	1.9 – 4.0
Joints, fasteners and supports	1.84
Seals and pressure barriers	0.88
Total:	8.35 – 10.45

Comprehensive testing confirmed the predicted system performance and provided information for further improvements, Ref. [71-80].

[See: Table 71.10.2 for results of REI evaluation]

71.12.2 TETRA/X-38 programme panels

71.12.2.1 General

Based on the initial Hermes concept, REI-type TPS panels, destined for the X-38 vehicle, are, Ref. [71-80]:

- C-SiC panel with IFI (DASA):
- large panel, approximately 1082mm × 600mm to 1160mm.
- C-SiC panel, fasteners and IMI (MAN Technologie).

- C-C/SiC panel, fasteners and IMI (DLR/MT)

71.12.2.2 Large C-SiC panel

Investigations showed mass savings possible for larger TPS panels than those previously envisaged on vehicles, Ref. [71-80].

The X-38 vehicle has 18 baseline TPS silica tiles replaced by a single, C-SiC panel. This covers an area of about 0.95m².

Some of the main features of this panel include:

- external C-SiC trapezoidal panel.
- internal flexible insulation (IFI), density 110kg/m³.
- attached by 7 edge and 1 central fastener to the underlying composite honeycomb structure.
- mass estimate of integrated panel and insulation system: 11kg/m² to 12kg/m².
- design specification:
 - Nominal surface temperature: about 1050°C (150kW/m²).
 - Maximum pressure loads: up to 7.4kPa.

The ground-test programme to validate flight readiness is shown in Table 71.12.2, Ref. [71-80].

Table 71.12-2 – TETRA/X-38 TPS: C-SiC panel qualification test matrix

Test type	Aim	Conditions
Acoustic	Characterisation of dynamic properties (sub-scale panel)	158 dB to 168 dB (progressive wave tube)
	Qualification of full-scale panel	163 dB (PWT)
Vibration	Qualification of full-scale panel	Sine and random vibration
Thermo-mechanical 1	Verification of flight loads	Combined thermal & mechanical loads (cyclic)
Flutter	Verification of stress/strain	Wind tunnel ($Ma = 0.5\text{--}1.3$; $P_{dyn} = 30 \text{ kPa}$ to 50 kPa)

71.12.2.3 Lightweight shingles

Based on the developed shingle concept, the X-38 programme includes the application and verification of two different material types, i.e. LPI-C/SiC (MAN) and C-C/SiC (DLR), both with IMI.

The CMC shingle-systems are intended to replace TPS baseline tiles.

The main features of the panel are:

- trapezoidal, 232mm × 314mm; surface area 522cm².
- volumetric envelope 72.9mm (for layout, shingle and insulation).
- underlying structure temperature limit: 175°C.
- design approaches (under evaluation): thin-walled shingle (~1.5mm), rib-stiffened (to reduce thermal deformation and carry 7.4kPa aerodynamic surface pressure).
- estimated areal mass: 6.3kg/m² to 7.3kg/m², including all attachments, insulation and seals.

The first flight-ready components are not mass-optimised. They have inherently high mechanical and thermal margins.

Each panel is instrumented to assess in-flight TPS performance and to obtain additional data on the environment.

The ground-test programme is shown in [Table 71.12.3](#), Ref. [71-80].

Table 71.12-3 - TETRA/X-38 TPS: Shingle qualification test matrix

Test type	Aim	Conditions
Vibration	Qualification of full-scale panel	Sine and random vibration
Thermal	Assess reaction of integrated system	Re-entry thermal loads (cyclic)
Thermo-mechanical	Verification of combined flight loads	Combined thermal and mechanical loads (cyclic)

71.12.3 SPFI - Surface protected flexible insulation

71.12.3.1 Background

SPFI is a thermal protection system for future re-entry vehicles which is under development by EADS-ST (Germany). It is aimed at protecting the windward side of vehicles against high heat fluxes experienced during re-entry into Earth's atmosphere, Ref. [71-94].

Development of SPFI is based on the experience with FEI (flexible external insulation) technology gained by EADS-ST during the European HERMES space vehicle program, [See also: [71.11](#)].

71.12.3.2 Concept

The SPFI concept aims to extend the application of fibrous insulation materials to the windward side of re-entry bodies. Such materials are currently limited to use on the leeward side.

The advantages of fibrous insulation, e.g. homogeneous load introduction, flexibility against thermal expansion and deformation of substructure are retained to the maximum extent possible. In order to use fibrous insulation on the windward side of re-entry vehicles, surfaces need to be aerodynamically smooth with good pressure tightness to prevent hot gas penetration. In the case of SPFI, this is achieved using a thin sheet of ceramic material on the outer surface of the insulation. The main features aims of SPFI development include, Ref. [71-94]:

- lightweight,
- low cost,
- simple to assemble,
- easy to integrate and maintain,
- multiple use, i.e. for reusable vehicles.

The manufacturing of comparatively large SPFI panels is envisaged, i.e. up to 0.5m × 0.5m. [Figure 71.12.2](#) shows a small panel and a large panel assembly, Ref. [71-94].

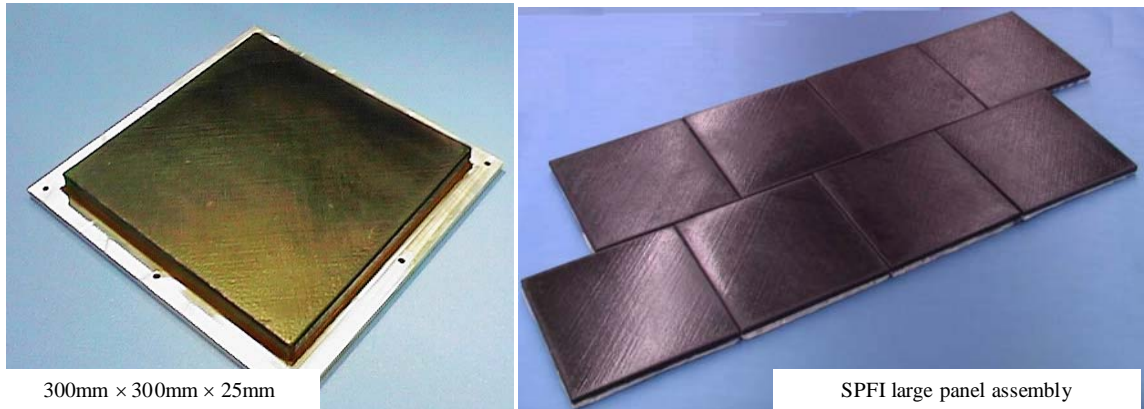


Figure 71.12-2 – SPFI surface protected flexible insulation panel

71.12.3.3 Description

SPFI is based on an FEI blanket, which comprises fabrics, threads and felt made from ceramic materials, [See: [71.11](#)]. The outer surface of the FEI blanket is covered by a thin CMC sheet to provide aerodynamic smoothness and pressure tightness. A coating is applied to the external face to protect the CMC against environmental degradation and to provide the necessary thermo-optical properties, i.e. absorptance and emittance. Depending on the mission, the interior of the SPFI, as well as the external surface, can be waterproofed to minimise water absorption during mission preparation and launch.

SPFI is bonded to the substructure of the vehicle using a room temperature curing adhesive, which is said to enable easy integration and maintenance of the TPS. [Figure 71.12.3](#) shows the design and constituent materials of SPFI, Ref. [[71-94](#)].

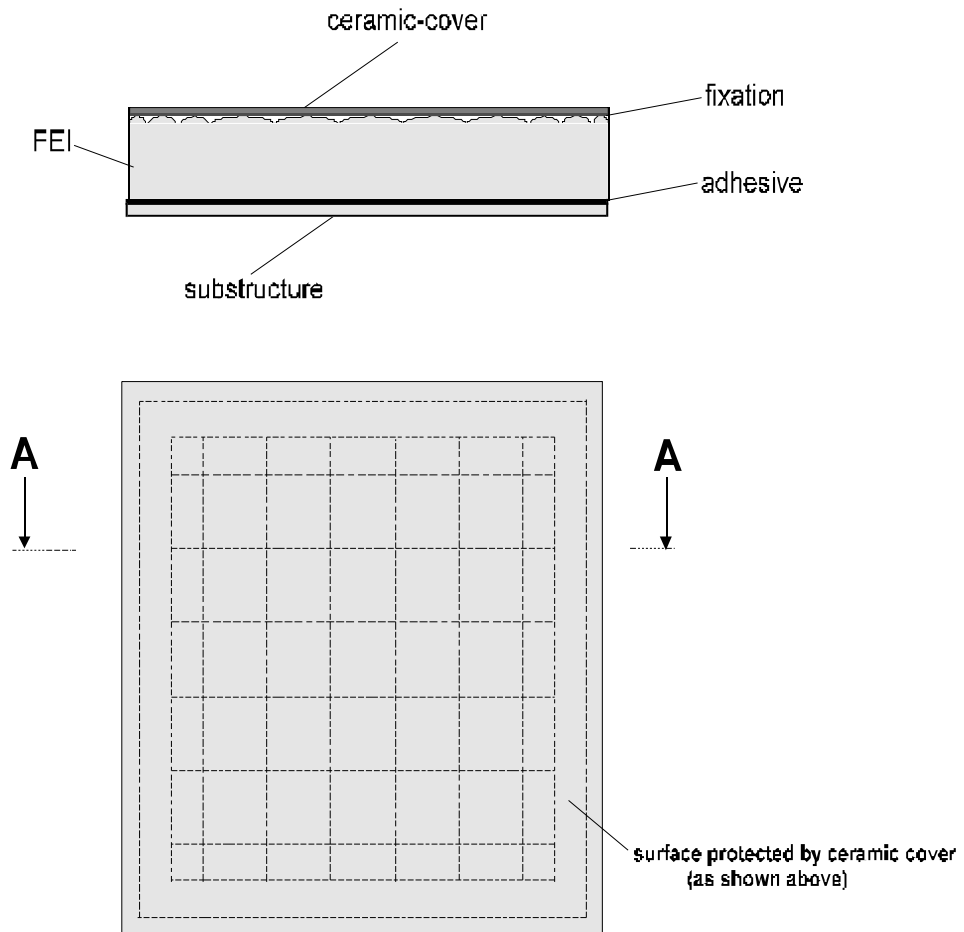


Figure 71.12-3 – SPFI Surface protected flexible insulation: Design

71.12.3.4 Characteristics

The main performance characteristics for the development of SPFI include, Ref. [71-94]:

- Outer surface temperature: > 1400°C.
- Mechanical loads: Acoustic noise > 160 dB OASPL.
- Application on areas with high thermal loads.
- High insulation performance for vacuum to 1 bar.
- High thermal shock stability.
- High emittance surface combined with low catalicity.
- Erosion resistant surface.
- Reusability.

71.12.3.5 Structural design

SPFI comprises of a flexible felt insulation and a highly temperature-stable ceramic cover plate bonded to the insulation. The thin fibre-reinforced cover plate, about 1mm thick, improves the performance of the thermal insulation because, besides being a protection against abrasive media such

as dust, ice and rain, it can sustain much higher pressure loads (aerodynamic pressure) than the unprotected insulation. As the load-carrying part, the cover distributes the pressure load over the complete surface of the SPFI panel. The load is then transmitted to the substructure via the insulation.

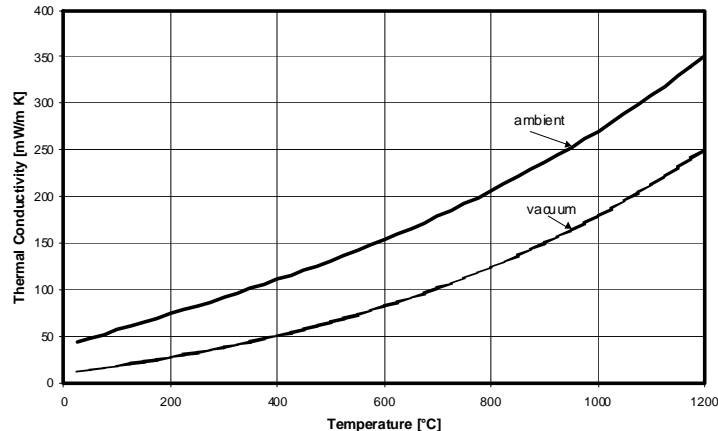
The structural characteristics of SPFI, e.g. strength and dynamic response, were investigated under pressure and temperature loads using FE models (assuming that it behaves like a plate on an elastic foundation). The effects of different lay-ups of reinforcing fibres and the influence of bent plate edges on distortion with increasing temperature and pressure loads were analysed. Different types of bonding constraint on the insulation were also evaluated.

71.12.3.6 Thermal design

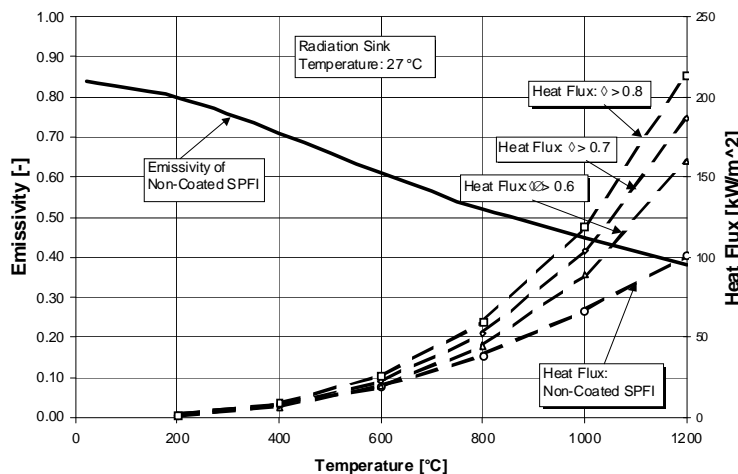
During the initial re-entry phase at high velocities and low gas pressures, radiative heat transfer is the dominant heat transfer path through the fibrous core. The contribution of gas conductance increases with increasing gas pressure. Radiative heat transfer depends on the optical properties of the fibre material, the fibre diameter and the prevailing orientation of the fibres with respect to the radiation direction. Radiative heat transfer is a minimum if the fibres are randomly oriented in a plane perpendicular to the radiation direction. For the envisaged temperature range of up to 1200°C, alumina-based ceramic fibres are most suitable. The selected fibre fleece consists of 3.3µm fibres (average diameter), which is close to the optimum derived by theory (2µm to 3µm). During manufacture, the fibrous core is compressed to a packing density of about 110kg/m³.

Figure 71.12.4 summarises the thermal performance of SPFI, Ref. [71-94]. The main thermal characteristics can be summarised as:

- Thermal conductance, which confirmed the thermally advantageous fibre orientation perpendicular to the heat transfer direction under vacuum conditions and at ambient gas pressures (10⁵ Pa).
- Radiative heat transfer, which follows the typical T³ law of heat transfer in fibrous insulation under vacuum conditions. The contribution of gas conductance to the total heat transfer becomes noticeable at gas pressures exceeding 100 Pa. At nearly 10⁴ Pa gas conductance is fully developed.
- Surface temperature (external): Since the heat flux through the SPFI is comparatively low, the external surface temperature results first of all from the equilibrium of the aero-convective and radiated heat fluxes. For the specified limit and ultimate temperatures of SPFI, the emissivity determines the tolerable heat loads and hence the possible locations on a re-entry vehicle where SPFI can be applied.
- Emissivity: Since the CMC cover has a strong emissivity decrease at elevated temperatures, it means that non-coated SPFI items can only be exposed to aero-convective heat fluxes up to 100kW/m² (T = 1200 °C). To use SPFI as TPS on higher thermally loaded areas of the windward side of space vehicles the emissivity-temperature behaviour of SPFI needs to be improved by using a coating. The allowable aero-convective heat fluxes are likely to exceed 200 kW/m² at T = 1200 °C; assuming constant hemispherical emissivities greater than 0.8.
- External emissivity coating system, which uses ceramics that exhibit high emissivities throughout the temperature range, excellent adhesion to the ceramic cover and extremely low catalycity. The emissivity-temperature behaviour of the coating system was determined by extrapolation of angular spectral emissivity measurements at room temperatures to higher temperatures, taking into account the Planckian spectra at elevated temperatures and confirmed by hemispherical emittance measurements on coated SPFI samples at elevated temperatures. The results showed that coated SPFI has emissivities exceeding ε = 0.8 at temperatures above 200 °C.



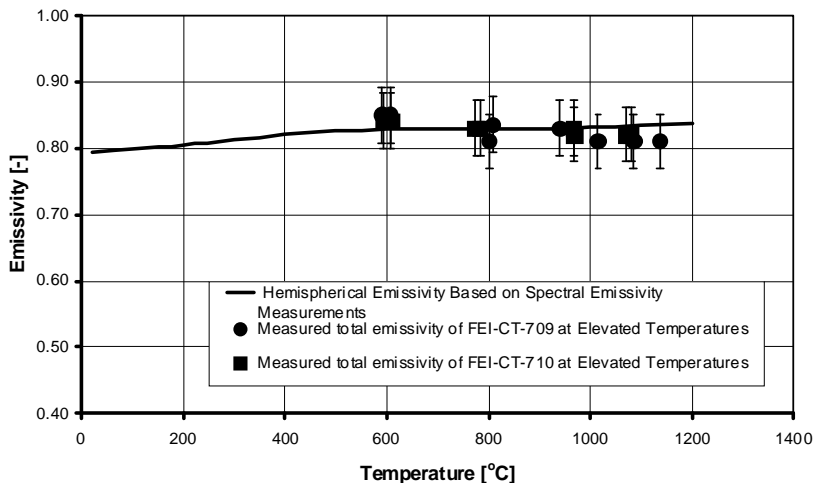
Thermal conductivity



Non-coated SPFI:

Emissivity with temperature

(hemispherical emissivity v. temperature) and aero-convective heat flux.



Coated SPFI:

Emissivity v. temperature

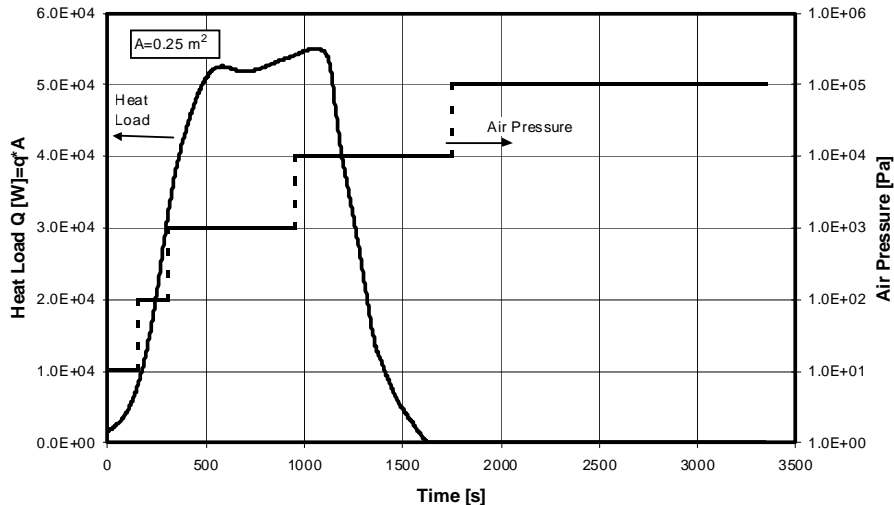
Figure 71.12-4 – SPFI: Summary of thermal performance

To illustrate the performance of SPFI as TPS for a typical reusable spacecraft, an SPFI-TPS system was designed for the external heat load and pressure timeline depicted in [Figure 71.12.5 \(A\)](#).

The 0.5 m × 0.5 m SPFI panel was bonded onto a 1.92mm thick aluminium sheet, which represented the cold structure of the vehicle. Assuming that the peak temperature of the aluminium cannot exceed 177°C during flight and 192 °C after landing, an SPFI thickness of 39 mm thick was needed. The temperature with time profile of the SPFI cover and centre, along with that of the aluminium sheet are

shown in Figure 71.12.5 (B). The maximum temperature of the aluminium plate (173°C) is reached at $t = 2727$ seconds, which is after the vehicle has landed, i.e. at $t = 2450$ s.

A: Heat load and pressure timeline during re-entry:



B: Temperature profile of SPFI cover, centre and aluminium sheet:

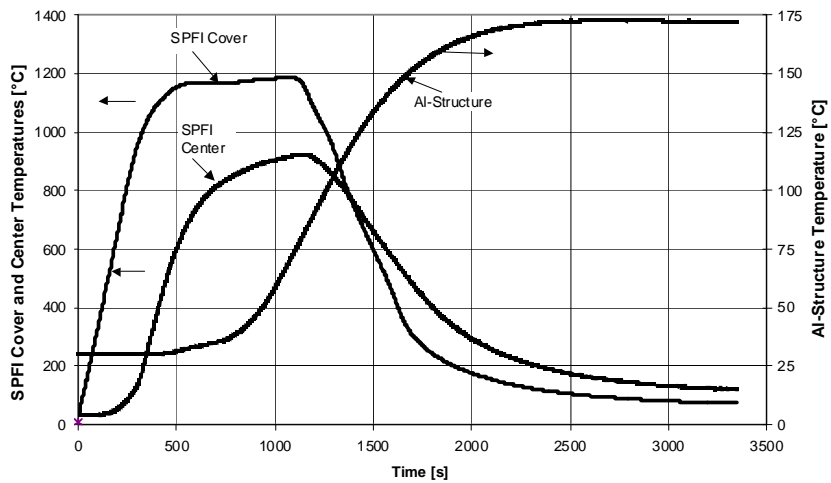


Figure 71.12-5 – SPFI: Thermal performance during vehicle re-entry and landing

71.12.3.7 Properties

The most important TPS thermal characteristics are, Ref. [71-94]:

- pressure-dependent thermal conductivity: Measurements of heat conductance under various gas pressures and temperatures were conducted in a high-temperature guarded flat plate calorimeter.
- emissivity of the outer surface. Hemispherical emittance measurements were carried out under vacuum as well as atmospheric conditions for the stipulated temperature range.

When using micro-fibrous insulation materials, a compromise always has to be found between thermal, e.g. extinction coefficient, and structural characteristics, e.g. load carrying capability, damping factor. Extensive investigation was performed previously which resulted in a material with

high thermal conductivity coupled with adequate structural properties. The emissivity of the outer surface generally needs to be as high as possible and be nearly constant over the entire application temperature range.

71.12.3.8 Structural tests

From experience of the qualification of the FEI flexible external insulation in the HERMES-MSTP program, [See: 71.11], it was assumed that SPFI is sensitive to aerodynamic pressure loads and most sensitive to the acoustic noise excitation specified for launch and re-entry of a future reusable spacecraft. Consequently, the verification of SPFI load-carrying components mainly used high level acoustic noise testing. The acoustic noise qualification level was 165dB, although some test facilities offer 160dB. Pressure tests are also envisaged, they will be completed in a later phase.

Prior to the qualification tests, an SPFI characterisation phase was undertaken by testing small samples with variations in the fixing process. All samples were subjected to a thermal heat treatment at 1200°C before the tests. It was obvious that an adequate fixing between the cover plate and the flexible insulation was a challenge. The samples showed good performance at 160 dB, but disintegrated at higher loads. This was rectified by modification of the manufacturing process and changes in the SPFI layout and test sample size (300mm × 300mm) prior to thermal treatment and testing.

Before and after the thermal loading, the dynamic behaviour of samples was characterised by a shaker test to check the fixings. [Figure 71.12.6](#) summarises the shaker test set-up and results for an intact sample (test 1) and a delaminated sample (test 2), Ref. [71-94].

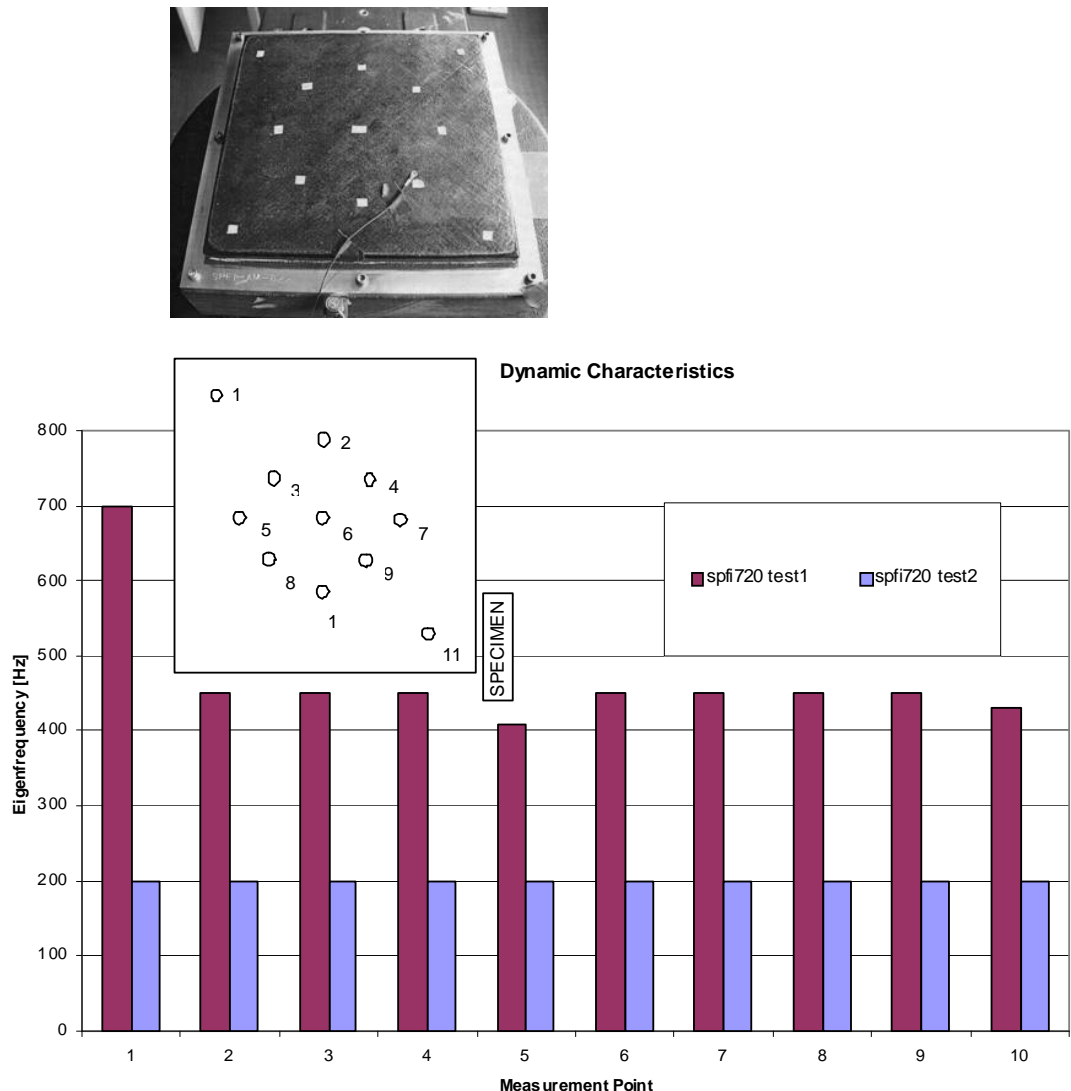


Figure 71.12-6 – SPFI: Structural performance - Shaker test

The structural qualification, originally intended to be carried out at Wright Laboratories (USA), was eventually conducted at IABG PWT in July 1998 using two samples. The total run time for each test was 33.5 minutes at an OASPL of 160 dB.

Figure 71.12.7 shows the spectral distribution and OASPL. To indicate the performance limits of SPFI, one of the two samples was subjected to higher acoustic loading, i.e. OASPL 163dB for 10 seconds, then OASPL 167 dB where sample damage occurred at about 15 seconds, Ref. [71-94].

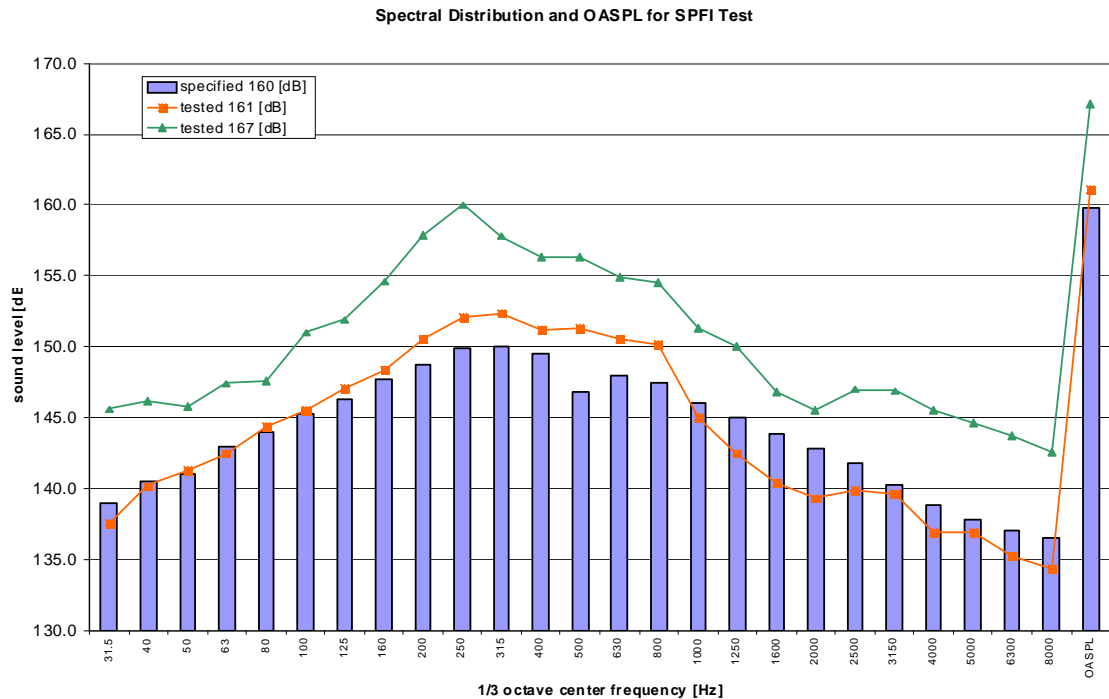


Figure 71.12-7 – SPFI: Structural performance – spectral distribution and OASPL

71.12.3.9 Thermal tests

The results of the various thermal-related tests conducted as part of SPFI development are summarised in Table 71.12.4, Ref. [71-94].

Table 71.12-4 - SPFI: Thermal property evaluation

Test	Test conditions	Results
Thermal shock Thermal cycling	Temperature range: 400°C to 1200°C Temperature increase: 4K/s to 6K/s Number of cycles: up to 50	Withstood severe loads without any damage or degradation.
Plasma erosion (1) Catalycity (1)	Stagnation point: 50 mm diameter samples: 800°C /1000°C @ 35 min 1000°C /1200°C @ 9 min	Very good resistance against plasma erosion. Weight losses were less than 0.04%. Nearly non-catalytic behaviour, $K_w < 1\text{m/s}$.
Arc jet re-entry (2)	Tangential plasma flow: Non-equilibrium plasma flow at high velocity. Earth atmosphere gas composition. Temperature and exposure identical to stagnation point tests.	No physical degradation of samples. Mass losses less than results from 'stagnation point'. No change to emissivity characteristics. Slight surface discolouration.
	Medium-size sample panel, 300mm × 300mm. Nearly tangential flow configuration, $\alpha = 4.5^\circ$. Surface temperature 800°C @ 20 min (Cycles 1,2). Surface temperature 1150°C @ 15 min (Cycles 4 to 6)	No noticeable damage after test (visual inspection). Only minor flaking of the surface coating was seen. Some colour changes. Surface emissivity not affected.. Better than predicted insulation performance as measured by substructure temperature, i.e. Cycle 1,2 (800°C): 130°C to 145°C (160°C predicted); Cycles 4-6 (1050°C): 170°C (185°C predicted)

Key: (1) High enthalpy plasmatron facility (TsAGI VAT-104); (2) 20 MW panel test facility (NASA AMES)

71.12.3.10 SPFI performance summary

The main performance-related features of SPFI can be summarised as, Ref. [71-94].

- Maximum temperature, with tests up to 1200°C conducted using Astrium and DLR facilities:
 - Multiple use: 1200°C.
 - Short duration: 1400°C.
- Temperature cycle tests, conducted at DC, DLR and foreign facilities: up to 30 cycles @ 1000°C (1200)°C.
- Plasma tests:
 - Catalycity measurements in Plasmatron of TsAGI.
 - Re-entry tests, conducted at NASA-AMES Panel Test Facility.
- Acoustic tests, conducted at IABG facility: up to 163 dB (160 dB > 30 min) in IABG facility.
- Emissivity measurements: RT, 500°C to 1200°C.
- Heat conductance measurements: 500°C to 1200°C.
- Maximum dimensions: up to 600 mm × 600 mm; thickness 20 mm to 50 mm.
- Preliminary sizing: weight: ~ 8.5 kg/m²; thickness: ~ 30 mm.
- Materials: All ceramic, with CMC cover and alumina-based fibrous components.
- Qualification status: All important tests with respect to the relevant TPS environment were successfully performed on SPFI panels.

The development performed so far shows that SPFI is a promising TPS having significant advantages compared with conventional thermal protection systems. Verification of performance under the most important environments (loads) confirmed the theoretical considerations and expectations. SPFI has now been further improved by mass reduction without loss in structural performance. As a next step, the design and verification of performance with respect to the TPS assembly, i.e. larger scale SPFI panels, is envisaged.

71.12.3.11 SHEFEX flight experiment

An SPFI experiment flew in October 2005 on the German TPS demonstrator SHEFEX; as shown in Figure 71.12.8, Ref. [71-94]. The experiment provided a successful demonstration of the capabilities of SPFI as windward-side TPS in a simulated re-entry environment.

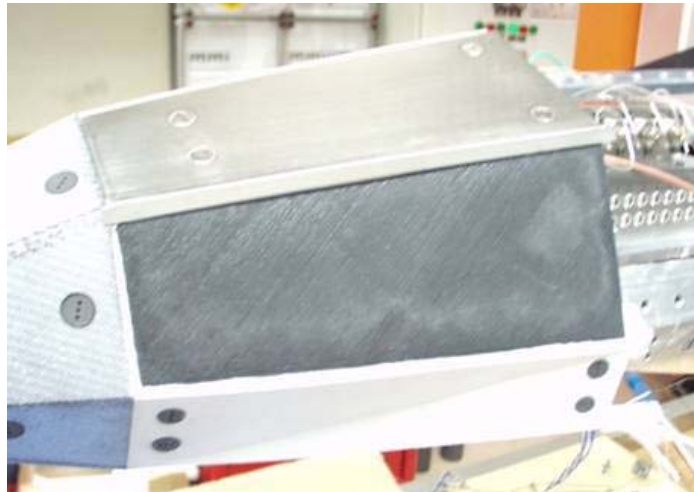


Figure 71.12-8 – SPFI: SHEFEX TPS demonstrator

71.13 Heat pipes

71.13.1 General

Heat pipes provide solutions to thermal problems associated with stagnation regions at leading edges on hypersonic aerospace vehicles. Development of heat pipe technology has a long history in the USA (over 25 years), Ref. [71-38], [71-39].

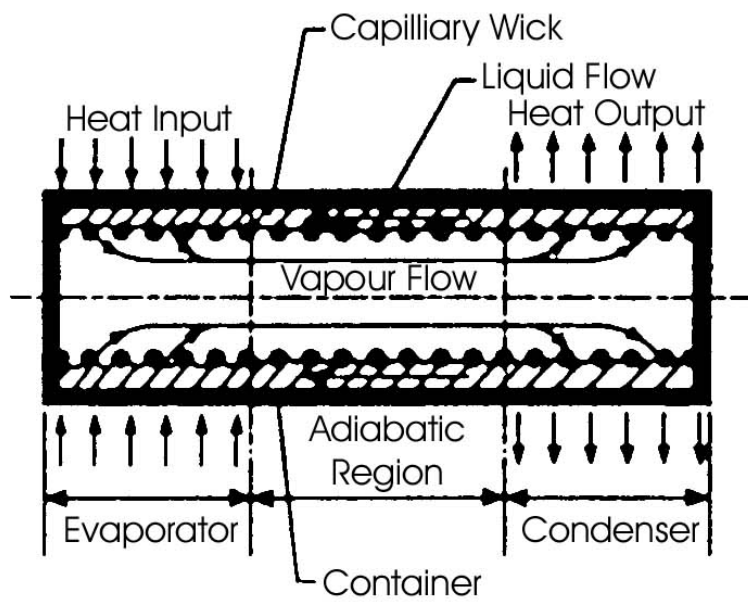
Heat pipes are self-contained, two-phase heat transfer devices comprising of a:

- container,
- wick,
- working fluid, e.g. sodium or lithium.

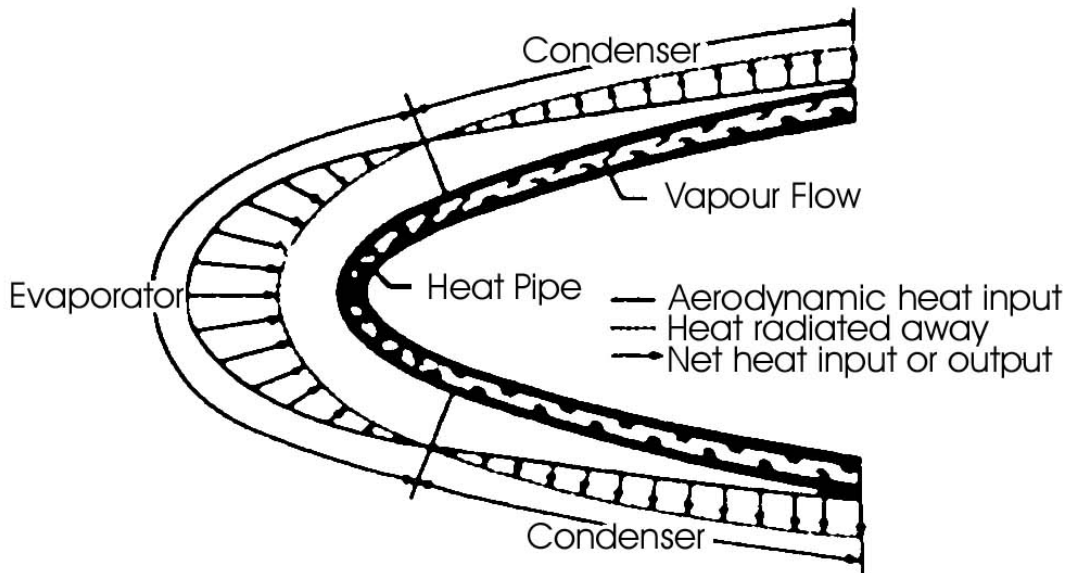
Local heat input to one section of the heat pipe (evaporator region) is conducted through the container and into the wick-working fluid matrix, where it is absorbed by the evaporation of the working fluid. The heated vapour flows to a slightly cooler section of the heat pipe where the working fluid condenses and releases heat. The heat is then conducted through the wick-working fluid matrix and the container and is rejected.

If applied to a stagnant-heated wing leading-edge, heat pipes transport the high net heat input region to cooler aft surfaces, raising the temperature there above the radiation equilibrium temperature and thus rejecting the heat by radiation.

A diagrammatic representation is shown in [Figure 71.13.1](#), Ref. [71-38].



A : Schematic of Heat Pipe Operation



B : Heat Pipe Cooling on Leading Edge

Figure 71.13-1 - Heat pipe: Operation principle for leading edge cooling

71.13.2 Shuttle-type heat pipe cooled wing leading edge

This is an early type, produced circa. 1973. A one-half scale heat-pipe-cooled wing leading-edge test model was constructed. The dimensions were 150mm span, 560mm chord length and 330mm high. It consisted of 12 sodium-filled heat pipes brazed to each other and to the inner surface of a thin 0.5mm Hastelloy-X skin. The heat pipes were circular-section Hastelloy-X with a 12.7mm outer diameter, a wall thickness of 1.27mm and a wick thickness of 0.88mm. The wick consisted of seven alternate layers of 100- and 200- mesh stainless steel screen in a concentric annulus design. The skin was coated with a high-emissivity ceramic paint to facilitate heat rejection by radiation.

71.13.3 Sodium-Hastelloy-X heat pipe for advanced space transportation system

A heat pipe 1.82m long was constructed for orientation normal to the leading edge as depicted in [Figure 71.13.2](#), Ref. [71-39]. This concept dates from circa. 1986.

The heat pipe was intended to reduce leading edge temperatures from 1925°C to 980°C.

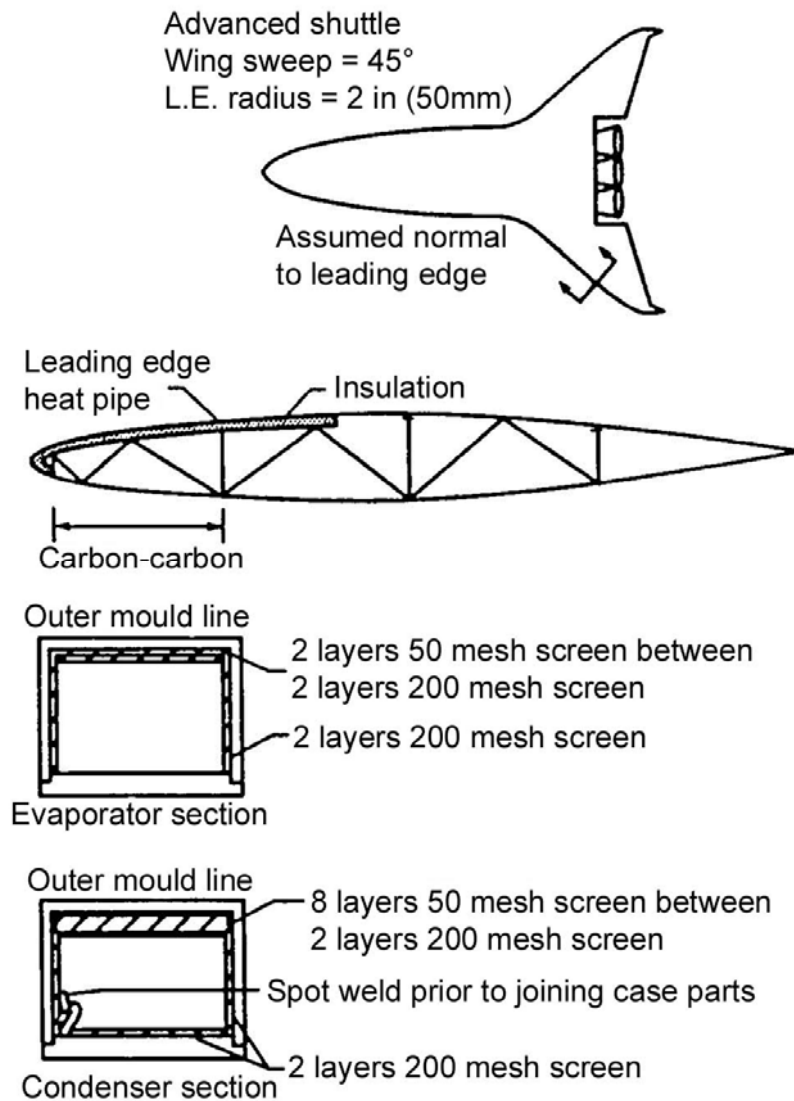


Figure 71.13-2 - Heat pipe: Wing leading edge design for advanced space transportation system

71.13.4 Refractory metal-CMC heat pipe for NASP

Within the NASP programme (from 1991), the concept moved to embedding refractory metal heat pipes in a CMC structure.

The total package is then protected from oxidation by a SiC overlay coating. Additional hydrogen fuel cooling can be incorporated in conjunction with a heat exchanger, as shown in Figure 71.13.3, Ref. [71-38].

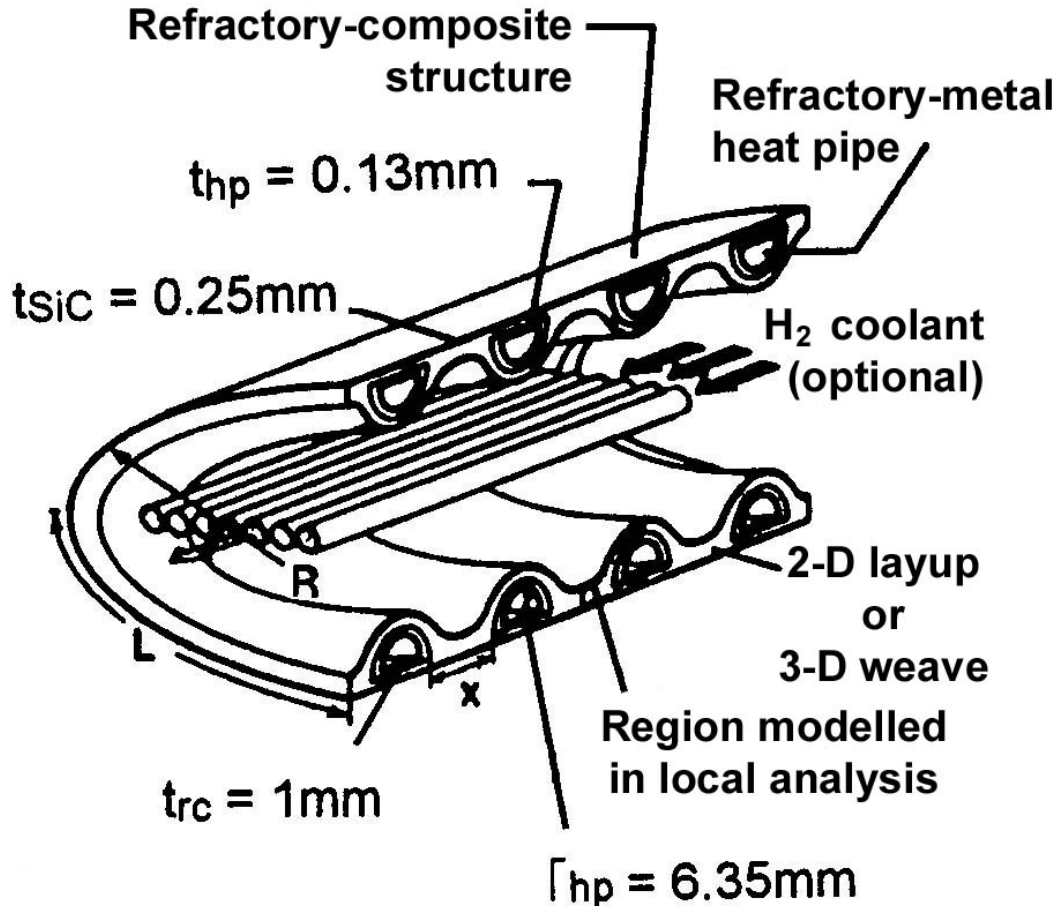


Figure 71.13-3 - Heat pipe: NASP wing leading edge

The concept has been modelled extensively, Ref. [71-39]. Tungsten heat pipes embedded in 3-D C/SiC are the initial preferred materials. Alternatively, Mo-47Re alloy was suggested instead of tungsten for the D-channel section tubes.

71.14 Cooled panels

71.14.1 General

Convection cooling is a method of limiting structural temperatures by circulating a coolant through the vehicle structure. The majority of expertise lies in the USA through development programmes such as the X-15 and NASP, Ref. [71-40].

Convection cooling is accomplished by circulating coolant through passages in the structure to absorb the aerodynamic heating. Almost the entire incident heating is transferred through the outer skin into the coolant. If the heat is transferred to the fuel before it is burned, the system is called a regenerative cooling system.

In the other active cooling methods, [See: Figure 71.2.1], both transpiration- and film-cooling operate on a principle similar to that of ablation; coolant ejected from the surface blocks most of the aerodynamic heating from reaching the structure. These two concepts use an external pumping system to bring coolant from a remote reservoir and eject it from the surface.

Transpiration cooling involves ejecting the coolant through a porous surface, whereas in film cooling the coolant is ejected, from discrete slots, parallel to the aerodynamic flow. The mass penalties associated with the expendable coolant usually limit these concepts to small, highly-heated regions.

Two different convective cooling systems are shown in [Figure 71.14.1](#), Ref. [71-40]. Both transfer heat to the fuel but the indirect version is more complex.

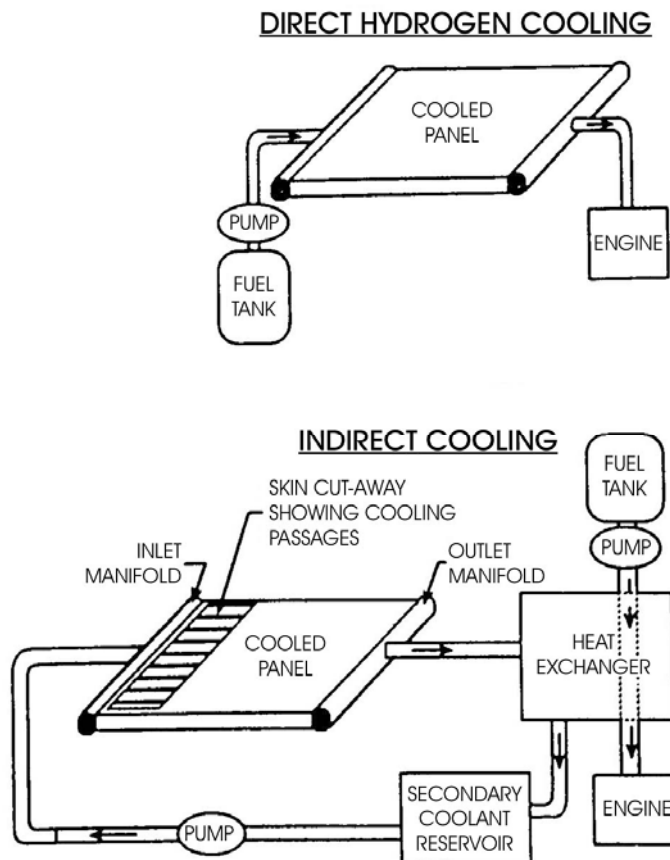


Figure 71.14-1 - Convective cooling systems

71.14.2 Demonstrator units

The USA has produced a series of demonstrators over a period of 30 years, Ref. [71-40]:

- 1960s:
 - 610mm x 1220mm hydrogen cooled Haynes L-605 nickel alloy panel.
 - 510mm x 760mm regeneratively cooled ram-jet combustion chamber and nozzle in brazed Hastelloy and Rene 41 alloys.
 - HRE (hypersonic research engine) hydrogen-cooled structures. Studies used Waspalloy, Hastelloy X, Inconel 617, 625 and 718, and Nickel 201. The concepts are shown in [Figure 71.14.2](#), Ref. [71-40]. The materials experienced temperatures up to 870°C on test panels 355mm x 460mm. The Palniro family of gold-palladium-nickel brazing alloys were used.

- 1970s: AISD (airframe integrated scramjet) produced the development of HRE concepts to extend life and maximise efficiency. Studies centred on full depth superalloy honeycomb structure with a brazed cooling jacket adjacent to the hot gases.
- 1980s: Scramjet engine fuel injection strut was in Inconel 718 and Nickel 201. The strut has a 300mm streamwise chord x 730mm long.

Obtaining sufficient fatigue life for structures of this type remains a problem as the intended vehicle Mach levels increase.

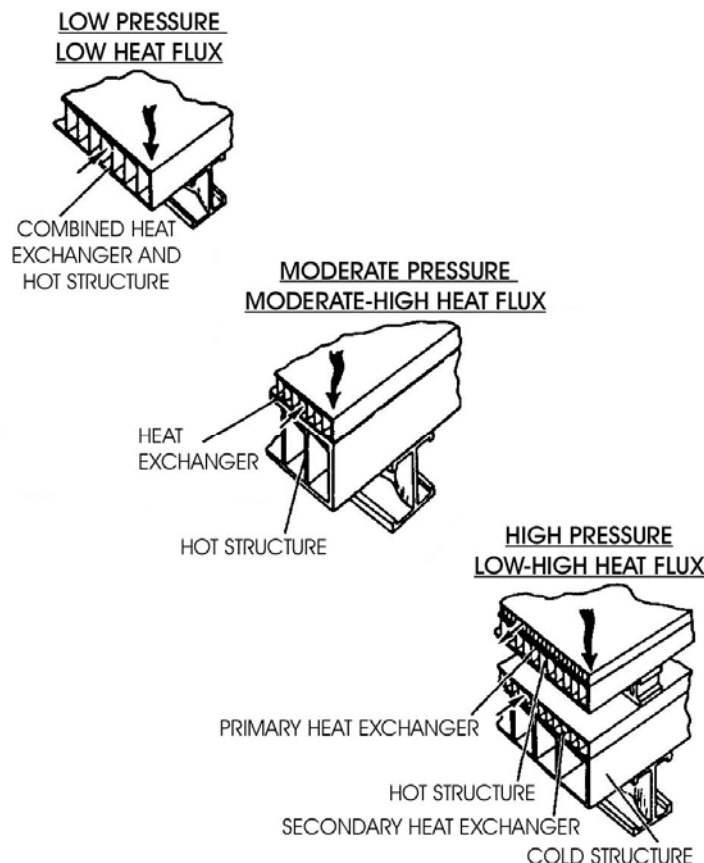


Figure 71.14-2 - Cooled structure: Design concepts

71.14.3 Active cooling on NASP

71.14.3.1 General

A variety of concepts are being studied for active cooling at a number of locations on NASP, [See: Figure 70.7.1]. Numbers relate to ascent conditions.

71.14.3.2 Titanium D-groove panels

It was designed for an inlet ramp as an integral metallurgically-bonded combined heat-exchanger and structural design, as shown in Figure 71.14.3, Ref. [71-40].

The constituent parts and materials were:

- Panel Dimensions: 584mm × 610mm.
- Outer face sheet: SiC/Ti (TMC).
- Etched sheet: Ti-14Al-21Nb.
- Honeycomb: Ti-15V-3Cr-3Sn-3Al.
- Manifold-edge: Ti-6Al-2Sn-4Zr-2Mo.
- Inner face sheet: SiC/Ti (TMC).

A summary of the main features and performance included:

- Design: 100 Btu/ft²sec, (-); 100 lb./in. (17.5 N/mm); 2000 psi (13.8MPa) LH₂ coolant.
- Failed: Prior to test, during panel precooling with N₂.
- Conditions: 0 Btu/ft²sec, 0 lb./in., 340 psi (2.3 MPa) N₂ at 20-40°F (-6°C to 4.4°C)
- Residual stress: 55 ksi (379MPa); Critical crack length: 0.040 in. (1.02mm)

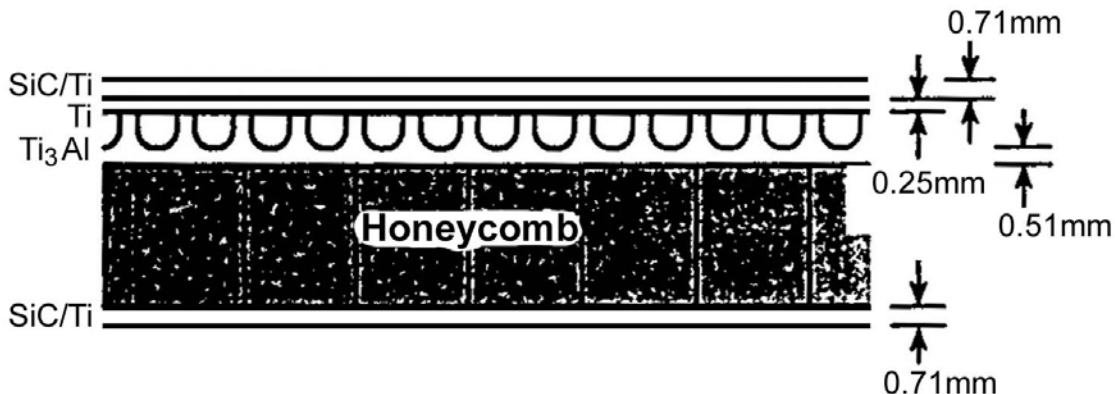


Figure 71.14-3 - NASP: SiC-Ti-Titanium aluminide D-groove panel

71.14.3.3 Beryllium skinned tube panels

These are actively-cooled panels for an external nozzle application. This concept has a non-integral beryllium skinned tube heat-exchanger, mounted onto a four-sheet titanium SPF/DB sandwich structure.

A 9-slide mechanism is used to compensate for differential thermal expansion between the heat exchanger and the titanium sub-structure. Dimensions: Beryllium skin/tube panels 533mm × 584mm, with SPF/DB titanium substructure 533mm × 584mm.

71.14.3.4 Beryllium platelet components

A series of 55 D-shaped grooves were chemically milled into a 1.78mm beryllium plate. An orifice was electrical discharge machined (EDM) into the end of each channel.

A 0.76mm close-out sheet was brazed to the chemically milled plate. A variable area manifold was then brazed to each end of the heat-exchanger panel, along with a beryllium egg-crate structure. Manifold inlet and outlet tubes were brazed to the manifold.

Dimensions: Components 150mm × 150mm.

71.14.3.5 Graphite fibre-reinforced copper panel

The Cu/Gr panel was made from two mated, symmetrical, grooved panels. Each half panel used a symmetrical ply lay-up consisting of an outer copper foil layer, two plies of Cu/Gr (90°) and three plies of Cu/Gr (0°).

In total 56 nickel tubes were embedded within the two half-sheets to limit the diffusion of hydrogen into the copper composite. The graphite fibre specified was the high thermal conductivity P-130X.

Dimensions: Panel 150mm x 150mm.

71.14.3.6 C-SiC/Refractory metal tube heat-exchangers

Mo-50Re tubes were combined with C-SiC skins for a very high temperature, non-integral cooled structure. The materials have very similar coefficients of thermal expansion.

71.15 Beryllium TPS

71.15.1 General

Beryllium has excellent mechanical efficiency in terms of stiffness to weight, good thermal conductivity and can be used at temperatures in the range 600°C to 800°C, [See: Chapter 51].

In conjunction with the high specific heat capacity, such characteristics render beryllium suitable for heat-sink TPS concepts.

Beryllium is appropriate for short-duration thermal loads and moderate heat fluxes such as those experienced on some atmospheric re-entries, e.g. Cassini-Huygens probe exploration of the Saturn moon Titan.

71.15.2 Cassini-Huygens heat shield: Phase A configuration

71.15.2.1 Main components

The main components are the:

- Forward heatshield of the fore cone and nose cap (total 21.75kg),
- Rear section after cone (9.3kg), maximum dimension 1.65m,
- Insulation (8.7kg),
- Nose cap diameter 650mm in one-piece construction.
- The fore cone in six assembled pieces is shown in Figure 71.15.1 and Figure 71.15.2, Ref. [71-41].
- The two alternative design concepts considered were, Ref. [71-41], [71-42]:
 - Solution 1: Hot structure without additional support,
 - Solution 2: Additional support provided by a connection to the main platform.

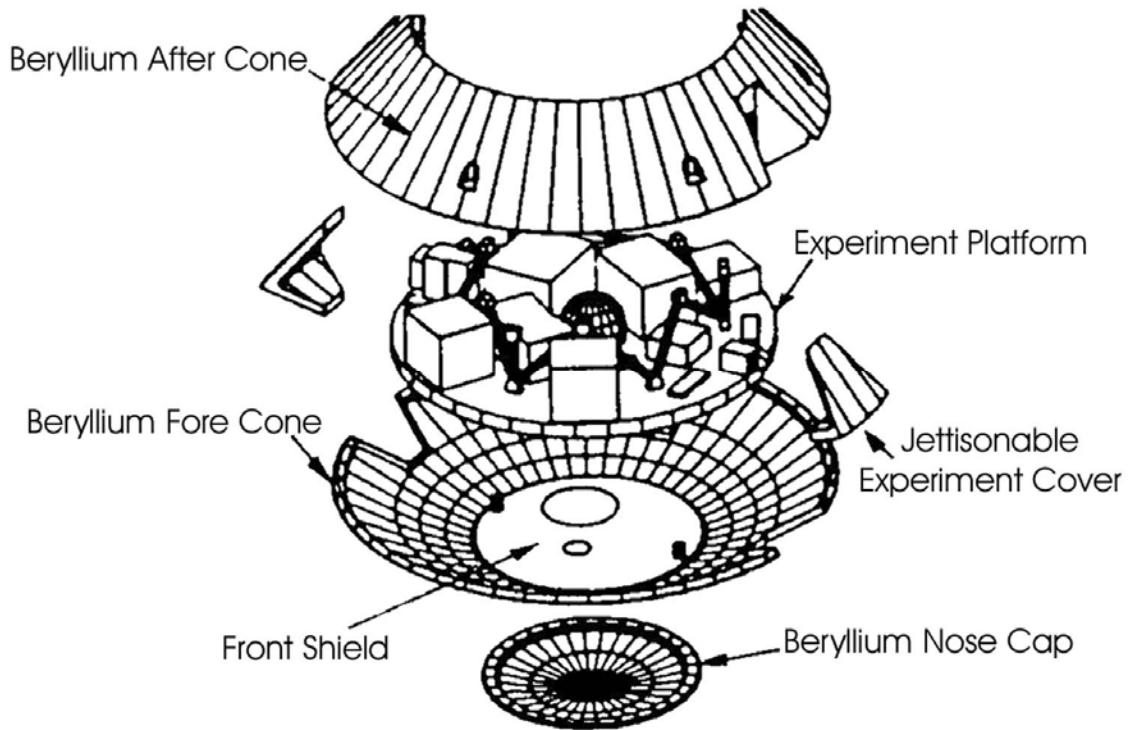


Figure 71.15-1 - Cassini-Huygens: Exploded view

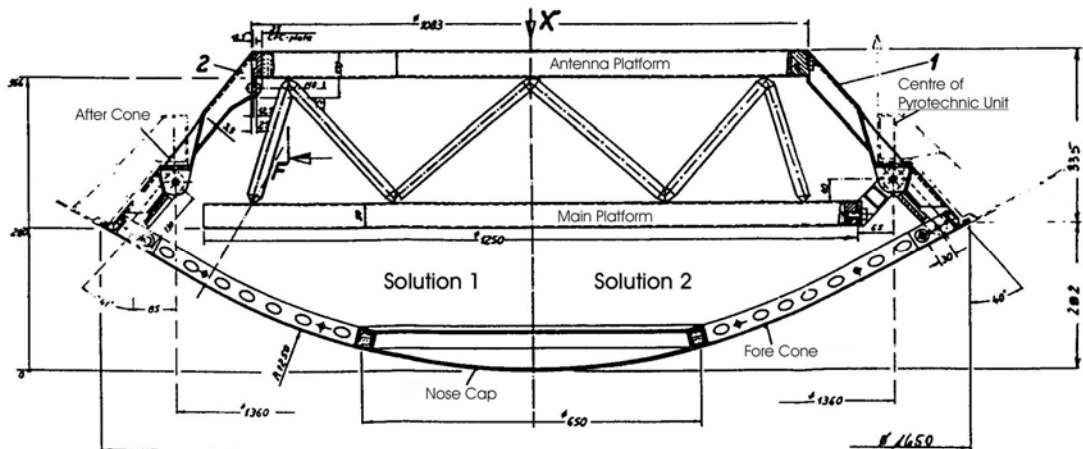


Figure 71.15-2 - Cassini-Huygens: Beryllium TPS design solution

71.15.2.2 Material selection

The beryllium materials selected were:

- Structural grade S-200F,
- Hot-rolled sheet grade SR-200E.

71.15.2.3 Operating conditions

The conditions can be summarised as:

- Heat flux of 0.46 MW/m^2 at stagnation point for 60s duration,

- +13.8 g on launch and -25 g deceleration on re-entry,
- Design goal frequency 24Hz minimum,
- Nose cap temperature below 530°C (6mm wall thickness),
- Nose cone temperature below 770°C (3mm wall thickness).

A carbon-carbon TPS design for the same application had a total mass of 41.2kg compared with 39.75kg for the beryllium version.

71.16 Aerobrakes

In some re-entry vehicles the forward facing surface is designed to provide additional vehicle braking in addition to acting as TPS, Ref. [71-43], [71-44].

The term aerobrake is used to describe this thermo-structural entity.

[See: 70.21]

71.17 Heat shields

71.17.1 General

With the significant developments in C-C, C-SiC and SiC-SiC technologies for spaceplanes, uses for these materials are being expanded to items such as heat shields for re-entry vehicles, Ref. [71-45], [71-46], [71-47]. A CMC heat shield is being studied for the MARSNET entry probe, [See: 70.13].

71.17.2 SEPCORE® TPS concept

The design and feasibility of a C-SiC probe heatshield has been studied by SEP using the SEPCORE® TPS concept, Ref. [71-59].

As an extension of the technology developed under the Hermes programme, a low mass heat shield was conceived combining a thin ablative layer on a 2mm thick C-SiC structure which protects fibrous insulation.

The Comet nucleus sample return (CVSR or Rosetta) mission provided the performance parameters for an ERC (Earth return capsule, [See: 70.17]). The re-entry conditions were specified as

- Initial velocity 15 km/s.
- Re-entry angle 11°.
- Peak deceleration 55g.
- Peak heat flux at stagnation point 10MW/m² at 50kPa pressure.

The ablative material was a dense, charring, high-density carbon-phenolic composite. The properties were:

- Emissivity: 0.85 to 0.90.

- Density: 1480kg/m².
- Specific heat at 2500K: 277J/kg.K.
- Conductivity at 2500K: 7.59W/m/K.

The C-SiC components were to be made by liquid resin infiltration and pyrolysis followed by CVI. Behind this was to be the IMI internal multiscreen insulation from Hermes. The full heatshield limits the main capsule structure to 27°C (300K).

The baseline TPS concept comprised of an ablative and an insulator to give a total mass of 190kg. Whereas the SEPCORE design produced an architecture mass budget of 120kg, comprising of 40kg for the C-SiC, 70kg for ablative heatshield and 10kg of insulation. This produced a 70kg (37%) mass saving.

A 1/5 scale mock-up was produced with a diameter of 300mm. Consideration was given to 120° radial T-stiffener configurations, fixation points and ablative bonding with RTV silicone material.

71.17.3 Ceramic heatshield assembly (CHA)

71.17.3.1 General

From 1994-96, as part of the MSTP programme, a demonstrator CHA (ceramic heatshield assembly was designed, manufactured and tested, Ref. [71-70], [71-71], [71-72].

The concept was applied to a Apollo-type Viking capsule in the form of a reusable shingle-type construction that evolved from the Hermes technology programmes.

Such technology can be applied to the CTV crew transfer vehicle.

71.17.3.2 Design concept

The design was a development of the shingle REI (rigid external insulation) technology developed under the Hermes programme, Ref. [71-65].

The main elements are, Ref. [71-80]:

- thin, rigid outer CMC panel:
 - C-SiC SEPCARB-INOX® 272-01 (SEP).
 - LPI-C/SiC (MAN Technologie).
- moderate weight, fibrous insulation: alumina (Al_2O_3) and silica (SiO_2).
- attachment, inter-panel close-outs and seals:
 - Waspalloy bolts (to primary capsule structure).

The two specific panel configurations selected for detailed design, analysis, manufacturing and testing were, Ref. [71-80]:

- Corner edge: A double-curved, integrally stiffened designed for a maximum heat flux of 1050kW/m² and surface temperatures of 1700°C. Dimensions: 450mm x 450mm x 50 mm; 2mm membrane; 108mm radius.

- Cassette panel: Trapezoidal shaped, bidirectionally curved panel with a ‘suitcase’ internal flange: Incident heat fluxes 600kW/m² and surface temperatures of 1600°C. Dimensions: 352mm to 427mm x 345mm; 2mm skin thickness.

The TPS concept was subjected to detailed analyses of the thermal, thermo-mechanical, dynamic, stress, flutter, aerothermal and humidity behaviours. The main performance specification is stated in ‘HT-TS-G-1-MSM: Thermal Protection System Technical Requirements and Environmental Specification’.

71.17.3.3 Design drivers

These can be summarised as:

- Thermal loads: For the standard element, dimensioning was based on the stagnation area heat load. With a safety factor of 1.5, the resulting flux of 600kW/m² and an emissivity more than 0.75 gives an equilibrium external surface temperature of 1630°C.
- Mechanical loads: Derived from the Ariane 5 launcher.
- Static longitudinal acceleration: 4.25g.
- Maximum sinusoidal excitation: 2.5g.
- Maximum acoustic load: 144dB.
- Aerodynamic surface.
- Maximum allowable steps between adjacent elements: +3/-2mm.

71.17.3.4 Detailed design

The three zones or ‘Typical Design Areas’ were assessed with respect to the heat shield geometry and thermal loads as a whole were the:

- standard area (with stagnation).
- corner area (including leading edge).
- central area.

Figure 71.17.1 shows the 5400mm diameter CHA heat shield assembly. It was segmented into one centre element, five circular panel rows of standard elements (124 elements in total) and an outer row of 36 corner elements, which contain the leading-edge and form the interface to the conical area of the capsule, Ref. [71-65].

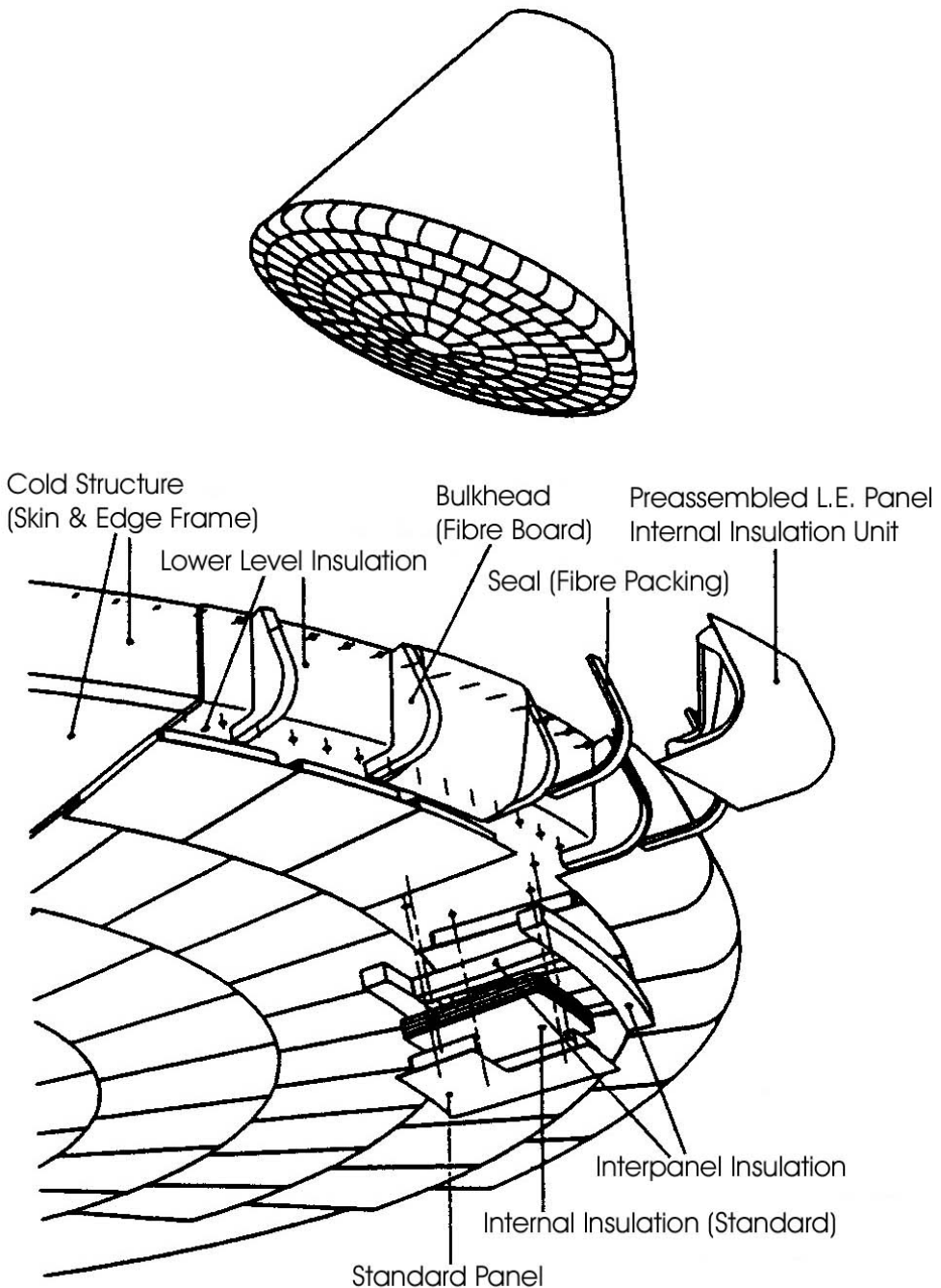


Figure 71.17-1 - CHA - Ceramic heatshield assembly

71.17.3.5 Standard panel configuration

The principal features are:

- Double-curvature of the surface, closed sidewalls and inward directed flanges.
- Panel height: 50mm.
- Overall heatshield thickness: 80mm.
- C-SiC thicknesses: 2mm (membrane) and 3mm (flanges).

71.17.3.6 Insulation

Three different insulation layers of high-flexibility alumina-silica mats were established as the optimum configuration, as shown in [Figure 71.17.2](#), Ref. [71-65]. This took account of conductive, radiated and convective heat transfer, i.e.:

- High-density (125kg/m^3) HKM 1650 insulation keeps the heat pulse away from the fixation points.
- Low-density (25kg/m^3) Saffil LD intermediate layers provide a boundary layer at the panel flanges and assist with assembly.
- The lower layer Saffil HD (75kg/m^3 density) reduces heat flow into the cold structure.

The fibrous insulations were each characterised across the temperature range for heat conductivity, specific heat capacity, ageing effects and bulk density, Ref. [71-63].

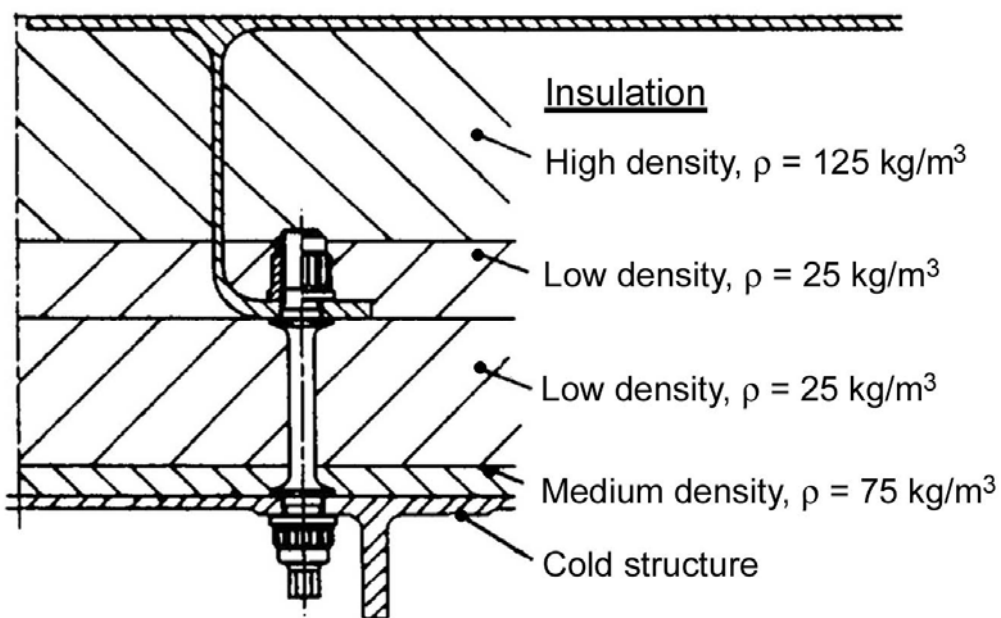


Figure 71.17-2 – CHA: Insulation and bolt assembly

71.17.3.7 Fittings

Contradictory structural and thermal demands made the choice of attachments difficult.

Six Waspalloy bolts were chosen, each 32.5mm long, with threaded connections to the cold structure and panel flanges.

The near-edge configuration of the attachments minimises the deflection of the panel membrane. Four bolts were deemed to provide inadequate support to resist dynamic and static displacements. Whereas eight bolts induced excessive heat transfer and stiffness disadvantages.

71.17.3.8 Mass breakdown

[Table 71.17.1](#) summarises the mass contribution of the various CHA subcomponents produced by MAN Technologie, Ref. [71-80].

The contributors to the mass of the system were broadly:

- panel (47.5%);
- insulation (47.5%);
- fixings (5%).

Given that the total area of shield was 28.3 m² and had a total mass of 355 kg, the average superficial areal density was 12.55 kg/m².

Table 71.17-1 – CHA: Subcomponents mass breakdown

Subcomponent	Unit mass (kg/m ²)	
	Corner Edge	Cassette
Panel Configuration		
C-SiC shingle + coatings	5.52	6.33
Insulation (HKM1650+ Saffil-25/-75)	5.90	5.66
Joints, fasteners & supports	0.54	0.60
TOTAL:	11.96	12.59

71.17.3.9 Verification by analysis

The results of the various analyses can be summarised as:

- Thermal analysis revealed that the aluminium substructure remains below 170°C and the fasteners below 900°C during the specified heat load of the re-entry trajectory.
- Stress analysis took account of thermal expansion, vibration and acoustic loads. Static pressure tests demonstrated that the panel's surface deformation was within specified tolerances; local stress concentrations at bolt seatings left sufficient safety margins with respect to material strength properties and maximum stresses did not coincide with maximum temperatures.
- Venting and gas flow analysis was undertaken to assess hot gas flow inside the CHA element during ascent and re-entry.
- Aerothermal computations revealed heat fluxes were lower than originally specified at the corner element so lowering maximum temperatures. The pressure gradient on a panel was lower and a 3mm step between panels was not critical with respect to a transition from laminar to turbulent flow.
- Humidity analysis assessed the significance of humid launch environments at Kourou on the behaviour of the fibrous insulation.
- Flutter analysis revealed it can be regarded as negligible.

71.17.3.10 Panel manufacture

The number of panels manufactured for test and evaluation were:

- One feasibility panel used to detect and resolve any manufacturing problems.
- One prototype panel used for humidity tests.
- Four conceptual design panels used for functional tests.

Each baseline panel was trapezoidal in shape; 500mm × 300mm × 400mm. The external CMC subcomponent manufacturing process was:

- SEP used a combined liquid resin impregnation with pyrolysis, followed by CVI chemical vapour infiltration, Ref. [71-72].
- MAN used a LPI low-pressure infiltration process, Ref. [71-80].

Fibrous preforms were made in the shape of the respective components, costs being lower than classical CVI processing with graphite tooling.

A quasi-orthotropic lay-up of 0°/90°/±45° was used. The main characteristics of SEPCARB-INOX® 272-01 are given in Table 71.17.2, Ref. [71-72].

[See also: Table 71.7.3 for properties of MAN LPI- and CVI-C-SiC materials]

Table 71.17-2 - SEPCARB-INOX 272-01: Properties

Property	At 23°C As made	At 23°C Aged*	At 1500°C As made
Tension	σ	200 MPa	195 MPa
	ε	0.85%	0.85%
	E_0	70 GPa	60 GPa
Compression	σ	210 MPa	150 MPa
	ε	0.32%	0.38%
	E_0	70 GPa	55 GPa
ILSS	τ	20 MPa	15 MPa
Translaminar shear τ		100 MPa	75 MPa
		500°C	1000°C
Thermal expansion Δl/l		0.065%	0.19%
Key: * = Aged at 1500°C for 15 minutes.			

71.17.3.11 Panel testing

The test programme assessed the effect of load combinations at various mission stages to give a comprehensive insight into CHA behaviour. These covered launch (vibration + acoustic), re-entry (thermo-acoustic + thermal) and launch + re-entry (static pressure).

The details of the functional tests are listed in [Table 71.17.3](#), Ref. [71-70].

Table 71.17-3 – CHA: Functional test matrix

Functional test	Test objectives	Test conditions
Modal analysis: - speckle pattern interferometr y - hammer pulse	Measurement of panel eigenmodes	Low power excitation from 70 to 2000 Hz
Sinusoidal vibration	launch & re-entry loads: - measurement of vibration responses and strains - damping effects of insulation	Vibration in three directions: 0°, 45°, 90° up to 3g.
Acoustic: nominal, overload and thermo-acoustic	Exposure to specified launch and re-entry loads (include. safety factors)	156 dB. 162 dB @ RT. & 144 dB @ 1100°C for four mission lives
Thermal tests	Exposure to specified launch and re-entry loads (include. safety factors)	Re-entry loads @ 1650°C with low and atmospheric pressure
Static pressure	Identify strength and stiffness values	200 hPa external and internal overpressure on panel membrane
Humidity	Effect of Kourou climate conditions and possible condensation	15 days Kourou temperature and humidity cycles
Plasma	Investigate hot gas flows and convective heating	Arc jet up to 1200°C with surface pressure gradient
Mission load sequence	Combined mission life cycle loads	Vibration, acoustic, thermal and static pressure loads

The thermal tests revealed the temperature against time profile given in [Figure 71.17.3](#), Ref. [71-70].

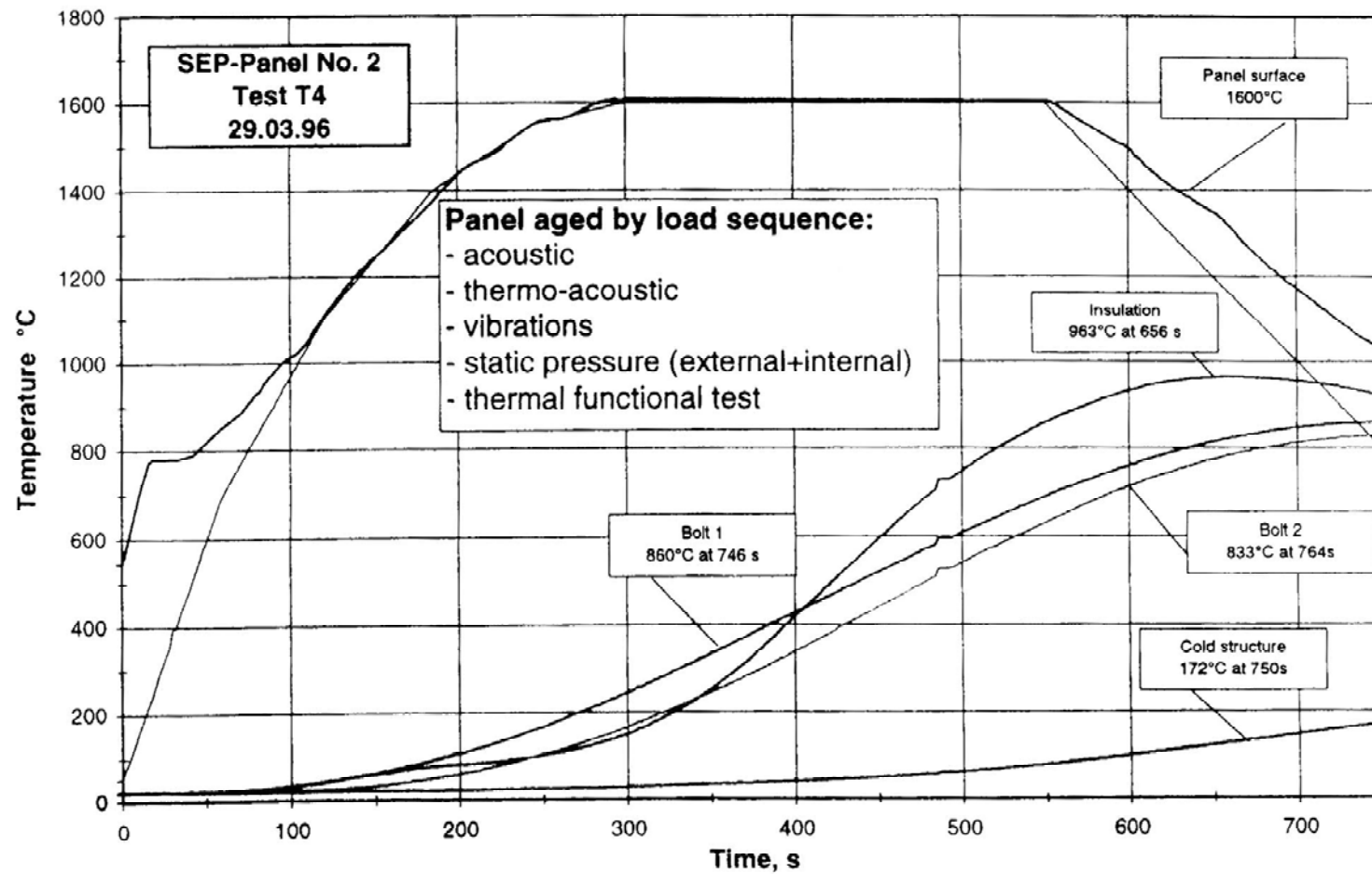


Figure 71.17-3 – CHA-element: Temperature profiles during full mission testing

The results of the other testing can be summarised as:

- No critical loads were generated in vibration and acoustic tests.
- The $\pm 200\text{hPa}$ static pressure applied on the panel membrane resulted in a reversible membrane deformation of 7mm, with no material degradation. Stresses between 86MPa (tension) and -82MPa (compression) were induced.
- Gas flow tests demonstrated sufficient venting of the CHA element during ascent and re-entry.
- A 15 day period of temperature and humidity cycles equivalent to a Kourou environment did not induce a condensation build-up, once an equilibrium amount of 28g within each CHA element had been reached after 5-days.
- The CHA element subjected to a single mission acoustic load spectrum heated for a total of 59mins. up to 1200°C survived with some degradation.
- Plasma oxidation tests verified the materials capability of withstanding 4 re-entry cycles in the range 1600°C to 1650°C , whilst retaining integrity. Hot gas ingress and sneak flows into the CHA-element did not compromise integrity despite inducing small temperature rises.

The testing confirmed the CHA single-mission capabilities and optimism that it can be reused, provided that external surface oxidation protection is used and suitable NDI techniques are available for an integrated CHA.

71.17.3.12 Leading edge element

The leading edge is highly loaded during re-entry, with heat fluxes on the middle part of the small radius expected at 700kW/m^2 (or 1050kW/m^2 when a 1.5 safety factor is applied).

Owing to these high fluxes, internal radiation in a free cavity behind the C-SiC outer skin was adopted. This was a means of reducing temperature build-up from insulation in direct contact with the C-SiC. The optimum cavity arrangement was determined.

The main features of the leading edge were:

- The maximum deformations occur 550 seconds into re-entry, with a 2.17mm displacement in the radial direction and 1.6mm thermal expansion in the circumferential direction. These are within acceptable limits.
- Maximum stresses in the panel membrane are in the range of $\pm 51\text{MPa}$.
- At 300 seconds into re-entry, maximum stresses in the C-SiC flange reach 205MPa (tensile) and -198MPa (compressive); the maximum allowable being -198MPa.
- Maximum computed in-plane shear stresses are 58MPa, against an allowable of 100MPa.

71.17.4 MIRKA - Micro re-entry capsule

71.17.4.1 General

The MIRKA capsule is a 1m diameter sphere of 150kg mass. ‘piggy-backed’ on to the FOTON capsule, as shown in Figure 71.17.4, Ref. [71-73]. It is serviced by FOTON and separates for a (ballistic) re-entry, Ref. [71-78], [71-79].

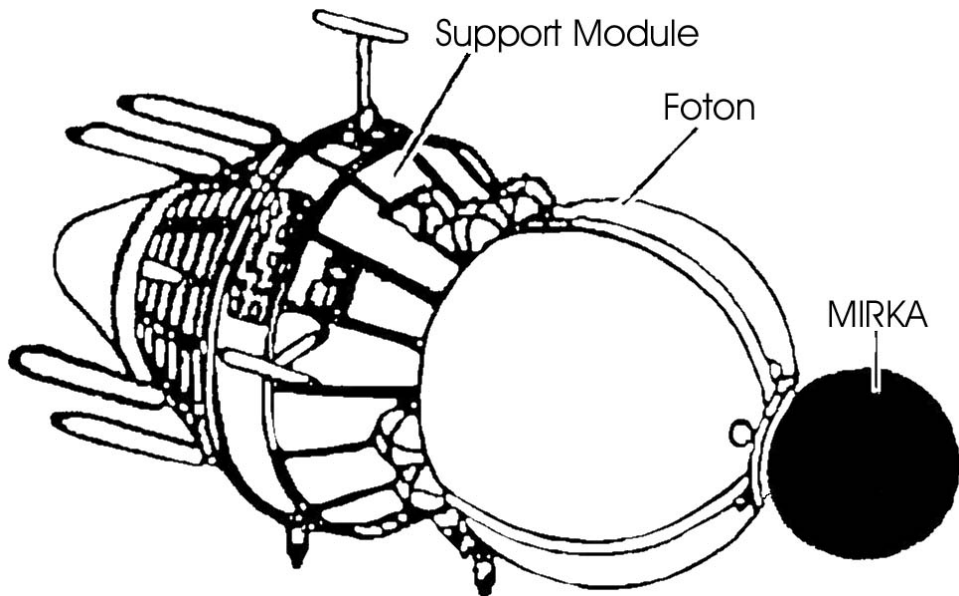


Figure 71.17-4 – MIRKA/FOTON: Configuration

The flight mission (1997) included instrumentation of both the heat shield and the capsule to investigate the environmental conditions and the verification of predictive tools.

71.17.4.2 Design concept

The main design features of the SPA, a non-reusable surface protected ablator heat shield capsule are:

- Two non-metallic hemispheres forming the load-carrying structure and SPA heat shield, which consisted of:
 - Carbon fibre laminate (1mm thick) with a thin copper mesh (on CFRP) for static discharge, local reinforcement (higher wall thickness) and stringers.
 - Honeycomb core filled with ablator material (Dornier DO 31/F); core-to-ablator 30mm thick in front and 20mm on rear hemisphere.
 - External layer: C-SiC CMC hemisphere, nominally 1.3mm thick but increased to 3.5mm locally at the stagnation point. The parachute cover has the same construction.
- Equatorial aluminium frame.
- Rear-side cover housing the cylindrical parachute box.
- Connection of hemispheres at the equator by steel screws (inner CFRP shells) and TZM-molybdenum alloy screws (ceramic hemispheres).
- During re-entry, the CMC layer separates from the ablator, but remains in place at the stagnation point (by a pressure sensor tube) and at the rear by flexible fixation elements.
- Gases liberated by the ablator during re-entry cool the backface of the CMC layer. They are channelled to vent at the capsule's equator (front hemisphere) and collar (back hemisphere).
- Compared with a traditional ablator concept, SPA has a reduced ablative material thickness, so reduces mass. This can be in the order of a 20% mass reduction for an optimised SPA.
- Mass of heat shield, including reinforcements for equipment attachment and interfaces with FOTON: ~60kg.
- Intended for missions with steep re-entry (high heat flux, short duration).

71.17.4.3 Test programme

Various test samples, for both development and verification tests, were prepared and tested by ISAS and TaAGI (Moscow), Ref. [71-79]. The tests and main observations can be summarised as:

- Initial test (40mm thick sample): 3.8MW/m² cold wall heat flux, 0.7bar: After 80 seconds, no surface regression was seen. Maximum backwall temperature: 80°C.
- MIRKA concept samples suffered from early CMC layer separation due to internal pressure and thermal expansion. Further test samples suffered from 'blow-through' between the fixing bolts and the heatshield sample.
- Final predevelopment test sample:
 - Withstood Mach 3 with 0.5bar dynamic pressure and 2500°C (stagnation point) with no visible recession.
 - About 0.1mm of the original 1.4mm thick CMC was oxidised.
 - Resisted 2.3MW/m² applied in 0.1 second.
 - Rear surface temperature 100°C.
 - Temperature gradient: 2400°C over a distance of 130mm, plus resistance to thermal shock.
 - Ablator char: ~9mm.
- Qualification tests, Ref. [71-78]:
 - Prevents burn-through at 1.4MW/m² and 500mbar dynamic pressures for more than 80 seconds without significant degradation.

71.17.4.4 Flight performance

MIRKA was launched in October 1997, spent two-weeks in LEO (inactive), re-entered and landed near Orsk. The heat shield survived re-entry without damage or burn-through and was intact on landing. The rear-side damage, visible after recovery, was due to parachute drag over rough ground, Ref. [71-78], [71-79].

71.17.4.5 Proposed applications

Potential applications include:

- Scientific earth re-entry probes.
- Planetary probes.
- Manned rescue capsules.
- Low-cost interchangeable parts for highly loaded areas of reusable vehicles.

71.17.5 ALSCAP - Alternative low-cost, short-manufacturing-cycle ceramic assessment programme

71.17.5.1 General

A major concern with CMCs is the high capital cost of process equipment, high manual labour costs and long-duration processing cycles for composite densification. ALSCAP, the alternative low cost,

short manufacturing cycle ceramic assessment programme was undertaken as part of MSTP between 1994 and 1996, Ref. [71-80].

71.17.5.2 Materials and manufacturing

It centred on the MAN Technologie liquid phase infiltration (LPI) and pyrolysis (PIP) processes for C-SiC, with an optimised fibre coating. Prepreg lay-up was achieved using the PRT placement of relaxed fibre technique. The programme aimed to improve existing resin pyrolysis C-SiC materials produced by MAN pre-1994, Ref. [71-61]. The main aims were:

- Target properties: Tensile strength of 200MPa, a Young's Modulus of 60GPa, with strain to failure of 0.3%. ILSS of 10MPa for a maximum use temperature of 1600°C.
- Performance matching of comparable material produced by CVI.

The material was compared with C-SiC materials made by Aerospatiale and SEP using resin pyrolysis and CVI, and Dornier using repeated resin impregnation and pyrolysis. The non-reusable capsule heatshield was used as the demonstrator.

Acceptable material performance is stated in HT-SOW-G401-1-HPD.

71.17.5.3 Characterisation and testing

The programme produced:

- Characterisation samples: 3mm 0°/90° T800 C-SiC, before and after thermal ageing (1500°C in argon), 156 samples. The tests methods to CEN TC-184-8 used were:
 - Tension and compression,
 - Shear, notched and three-point bend,
 - Four-point bending,
 - Tension and compression for 0°/90° drilled samples.
- Conceptual design testing (120 samples) for:
 - Tension, bend, shear and pull tests on T-stiffener to skin joint specimens,
 - Bend tests on angle specimens,
 - Tensile tests of drilled bearing samples,
 - Tensile tests on variable thickness samples.
- Thermo-physical tests (30 samples) are summarised in Table 71.17.4.
- Oxidation tests (48 samples):
 - Undertaken by DLR (L2K plasma arc wind tunnel test) and ONERA (BLOX) 3 oxidation tests by radiative heating with 1700 W CO₂ laser). These gave similar results.
 - Heating between 800°C to 1500°C in air pressure range 10mbar to 200mbar, for multiples of 5-minutes.
 - Low mass loss (~3%) at high temperature (10 minutes at 1500°C), but loss increases as atmospheric pressure increases from 10mbar to 100mbar.
 - C-SiC does not need oxidation protection for a single re-entry.

- Slurry oxidation coating applicable to manned vehicles with an additional manufacturing cost of 20% incurred.
- Flight demonstrators, 2 units of 200mm diameter for ARD.
- CHA leading-edge panel demonstrators, 2 panels:
 - Medium sizes, double-curvature and complex design,
 - Aluminium tool for panel and GFRP intermediate tool for stringer,
 - NDI by ultrasonic transmission.

Table 71.17-4 – ALSCAP: Thermo-physical data for C/SiC

Property	Fibre orientation	Measurement data		
		100°C	1000°C	1500°C
Thermal diffusivity (cm ² /s)	Parallel	730	489	461
	Transverse	334	210	198
Coefficient of thermal expansion (x 10-6/K)	Parallel	1.16	2.19	2.68
	Transverse	4.06	5.72	6.23
Specific heat (kJ/kg K)	-	0.9	1.4	1.6
Thermal conductivity (W/m K)	Parallel	11.33	12.62	12.18
	Transverse	5.24	5.48	5.29

71.17.5.4 Programme conclusions

The main conclusions can be summarised as:

- Material performance: 30% better than expected and comparable to C-SiC produced by CVI.
- Material properties:
 - Tensile strength: 270MPa;
 - Young's Modulus: 84GPa;
 - Strain to failure: 0.5%;
 - ILSS: 20MPa.
- Excellent high temperature behaviour without ageing.
- Suitable for complex and large, hot structural parts.
- Manufacturing cost around 3-times that for CFRP polymer composite structural components.
- Low-cost slurry oxidation protection applicable.
- Short manufacturing cycle of 8-weeks for demonstrator leading edge panels.

71.18 Aeroshell

71.18.1 General

An aeroshell is the forward facing shield of an atmospheric entry vehicle, such as Mars Lander, Ref. [71-48]. It withstands a short aero-thermodynamic heating period followed by a hard or semi-hard landing.

The aeroshell shape is important in determining the aerodynamic and heat flux characteristics during re-entry, Ref. [71-48].

Figure 71.18.1 shows a design concept investigated by ESA and Dassault Aviation, Ref. [71-48].

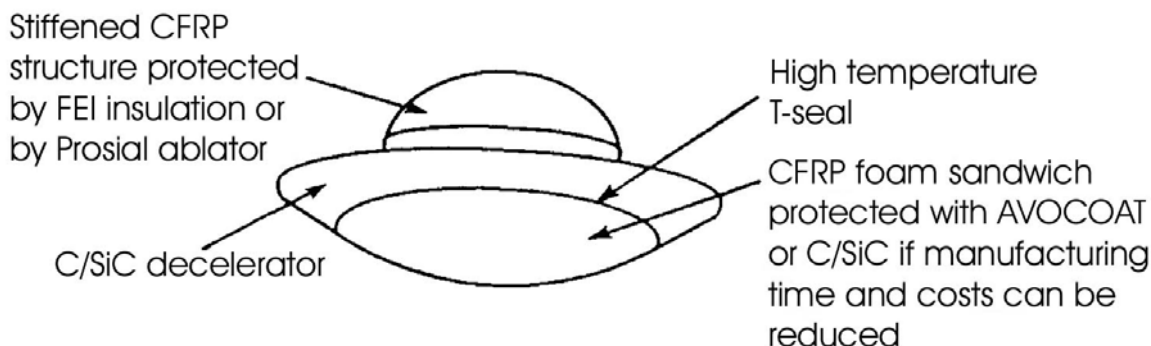


Figure 71.18-1 – Aeroshell: Design concept

71.18.2 Semi-integrated aeroshell TPS (S.I.A.T)

SIAT was a co-operative programme between Dassault-Aviation and DASA/Dornier, covering activities from 1994 to 1996 on the design of future Mars landing probe aeroshell and thermal protection concepts, Ref. [71-67], [71-68]. This continued the investigations initiated in a previous STAMP programme; the study on technology of aerobraking for Mars penetrators.

The design which was assessed was a front aeroshell based on an ablator-protected CFRP cold structure for the front shield and a non-protected C-SiC hot structure for the aerodynamic decelerator.

The aim of the programme was to demonstrate:

- The ability to manufacture the as-designed self-stiffened C-SiC part.
- The prevention of hot gas penetration at the front shield to decelerator interface.
- Confirmation of the ability to withstand thermal shock, thermo-chemical environments and dust erosion in the Martian atmosphere.

71.18.3 Demonstrator aeroshell design

71.18.3.1 General

A 1/3 scale demonstrator was produced, using scale-reduction principles to preserve the validity of the tests:

- Full-scale thickness of material sections (skin thicknesses and insulation) were applied to retain the same thermal response.
- A simple scale reduction of mesh width and curvature radii was not used as this would have modified the load levels.
- The scaled down demonstrator retained the same curvature for the spherical and conical parts as the full-scale design and the same mesh width for the decelerator. This required a shape modification, the half-cone angle being opened from 60° to 80°.
- The demonstrator was reduced to one conical mesh whereas the full scale decelerator would have three.
- The internal edge of the scaled conical C-SiC part was still suitable for assessing the stiffener integration.
- The results of acoustic testing were representative of the skin local-mode excitations.

71.18.3.2 General architecture

General features of the design are shown in [Figure 71.18.2](#) and [Figure 71.18.3](#), Ref. [71-67], some notable points are:

- The spherical ablator-covered CFRP central shell, terminating in an attachment ring.
- A decelerator represented by a non-protected C-SiC conical outer part fastened to a primary metallic structure with integral circular stiffener and semi-flexible titanium attachment tabs.
- A simplified seal arrangement with a reduced parts count and a flexible seal between the C-SiC part and the Inconel seal support.

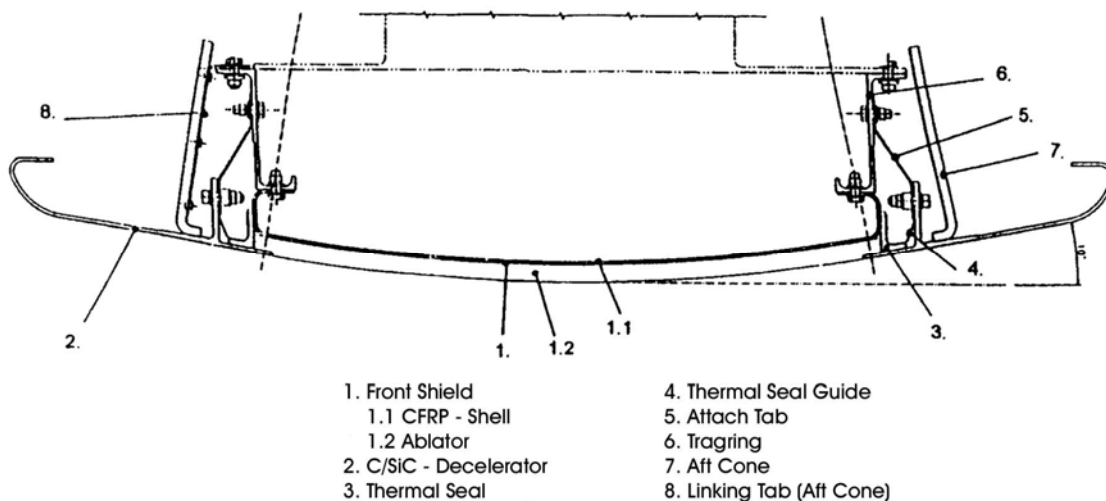


Figure 71.18-2 – Aeroshell: SIAT test model assembled cross-section

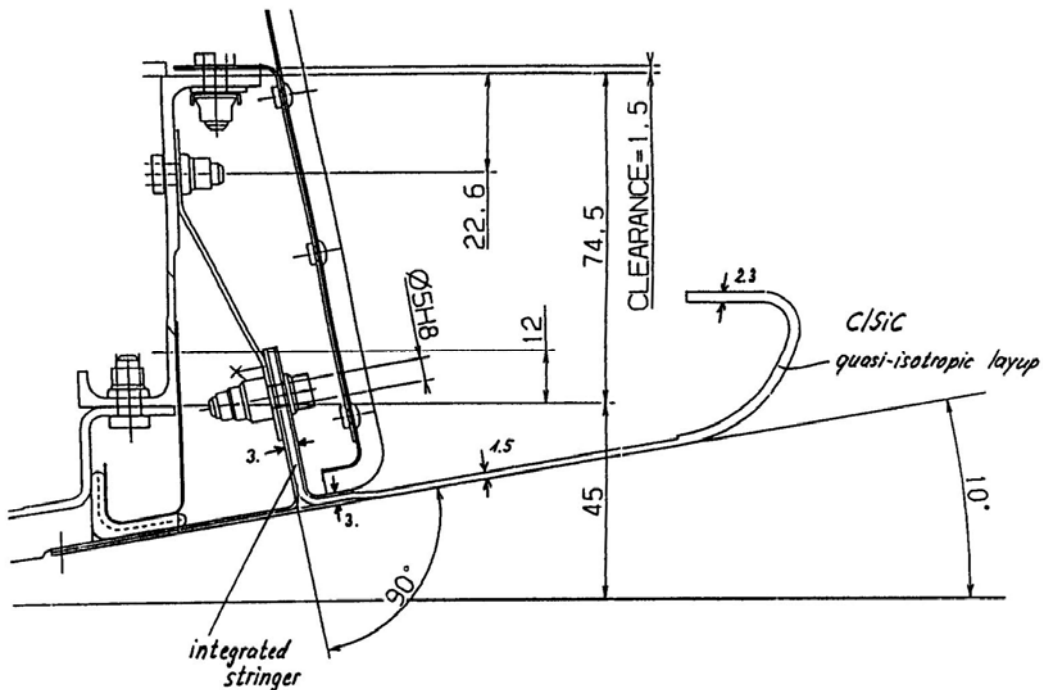


Figure 71.18-3 – Aeroshell: Down-scaled demonstrator design features

71.18.3.3 Thermal

Thermal analysis covered all forms of heat transfer, i.e.:

- conduction in solid parts,
- natural convection,
- radiation for critical areas.

The predicted and actual temperature distributions are shown in [Table 71.18.1](#), Ref. [71-67].

Table 71.18-1 - Aeroshell demonstrator: Predicted and actual temperatures

Area: Backface or behind shield		Material allowable	Actual measured temp. (°C)	Solar test samples	Plasmatron test samples	Predicted temperatures for demonstrator			
						Nominal heating. Theoretical C-SiC thickness	Actual heating. Theoretical C-SiC thickness	Nominal heating. C-SiC thickness + 15%	Actual heating. C-SiC thickness + 30%
1.8mm C-SiC skin middle	right side	1500	978 ⁽¹⁾	-	-	1064	-	-	-
	other sides	1500	805/857	-	-	1064	1018	966	919
2.7mm C-SiC stiffener top	right side	1500	850 ⁽¹⁾	-	-	867	-	-	-
	other sides	1500	633/694	690	551 ⁽⁴⁾	867	802	733	676
1.8mm C-SiC stiffener top	right side	1500	327 ⁽¹⁾	-	-	401	-	-	-
	other sides	1500	306/319	-	-	401	365	361	356
1.5mm CFRP shell centre		250	96	100	180	148 ⁽²⁾	158	-	-
Inconel seal support		800	240/260	-	-	495 ⁽³⁾	419	392	370
Aluminium structure		175	70	-	-	71	-	-	-
Key	(1)	Right side of demonstrator experienced slight overheating as it was introduced into the solar spot.							
	(2)	Ablator thickness sized for CFRP to reach 250°C under ultimate levels (test levels were limit levels only).							
	(3)	A conservative hypothesis for modelling, assuming inadequate sealing from hot gases.							
	(4)	A low temperature explained with low observed catalycity rate for C-SiC.							

All temperatures were within the capabilities of the respective materials. The Mars entry heating profile is very rapid, taking less than 60 seconds in total. This prevents the surface materials from reaching equilibrium conditions. Hence the actual temperatures experienced at any point on the structure are very sensitive to the applied heat flux against time profile.

Structural analysis showed stress levels from combined thermal and pressure loadings to be within the material allowables.

The only problem revealed by analysis was a significant opening (0.9mm), under thermal loading, between the ablative layer and the C-SiC inner-edge overlapping ring on the interface area.

To avoid any local overheating, the length of the overlapping ring was reduced in the final design to restrict the opening to 0.4mm. Gas tightness was maintained by the flexible seal between the C-SiC and Inconel seal support.

71.18.3.4 Critical load cases

These were:

- A diffuse-noise acoustic test (142dB OASPL) simulated launch (INTESPACE test centre, France).
- A differential pressure test ($\Delta P = 140\text{mbars}$) simulated the pressure loading of the aeroshell during the aerobraking phase (tested at Dornier).
- A thermal shock test (heat-up and cool-down to a maximum of 440kW/m^2) was carried out at the main solar furnace of the Plataforma solar de Almería, Spain.

71.18.3.5 Material samples test campaigns

Thermo-optical property measurements (emissivity and solar absorptivity) and thermal shock tests on C-SiC and ablator-covered CFRP disks were carried using solar furnace heating (ETCO-Odeillo test centre, France).

The details can be summarised as:

- The disks consisted of CFRP with 5mm, 10mm or 15mm ablative layers.
- The heat flux profile was simplified to:
 - a linear heating phase of 15 seconds,
 - static heating for 7.5 seconds at maximum level (440kW/m^2 for limit level, 560kW/m^2 for ultimate level) and
 - a linear cooling phase of 15 seconds,this approximated to the stagnation point heating profile.

This testing showed that:

- Optimal ablator thickness (giving a temperature of 250°C in the CFRP) was found to be between 5mm and 10mm, which compared well with the prediction of 8mm.
- Surface recession of the ablator was low, $\sim 0.1\text{mm (0.1g/cm}^2)$.

Plasmatron testing was conducted at TSNIIMASH (Russia); a 1MW high-frequency induction gas-heating facility, with high enthalpy CO₂ plasma simulating Mars atmosphere penetration (97%CO₂).

The back-face of the C-SiC reached 550°C, compared with 760°C during solar furnace tests. The rear surface of the ablator-covered BMI disc reached 180°C, compared with 100°C for the solar furnace.

Higher mass losses of 0.29g/cm² were recorded. The under-heating of the C-SiC was explained by a low catalytic rate. High rates of CO₂ dissociation reduced the peak heat flux value from 400 kW/m² to 150kW/m².

Dust impact erosion testing was carried out at the Max Planck Institute, Heidelberg, Germany. This simulated an entry velocity of 6km/sec with dust particles from 0.2µm to 20µm, at altitudes up to 60km:

- An electromagnetic accelerator was used to project iron particles with a mean diameter of 1µm in a vacuum at 7km/sec.
- Equivalence rules were applied as the iron particles did not have the same size and density as those anticipated on Mars

Using thin gold witness layers applied to the surfaces of the C-SiC and ablator it was possible to predict erosion levels of 12µm for C-SiC and 700µm (0.7mm) for the ablator during entry. An additional 1mm of ablator thickness was found to be necessary.

71.18.3.6 Manufacture

Dornier manufactured the aeroshell demonstrator unit. The procedures used were:

- C-SiC self-stiffened part produced by low-cost polymer infiltration and pyrolysis (PIP) process:
 - T800 fibres applied in 6k rovings with a thin film coating of approximately 150nm to 200nm of carbon prior to prepreg manufacture.
 - After automated prepreg lay-up and vacuum bagging, the green part was cured at 15bar and 110°C.
- BMI CFRP (M40 fibres) front shield assembly allowing temperatures up to 250°C. Lay-up of 0°/±60° produced by placement of relaxed fibre technique (PRT).
- A moulded 10mm AblaDor DO-31-F lightweight-phenolic-ablative layer was bonded to the front shield using a heat-stable resin. This ablative is a flexible honeycomb core, filled with phenolic microballoons and silica fibres.

71.18.3.7 Testing

For the demonstrator test campaign, limit load levels were applied (i.e. flight loads x 1.1). Testing was conducted in the order of criticality.

- Static differential pressure test:
 - Achieved by controlled air pumping of a back cavity adapted to the demonstrator shape.
 - Outer edge of decelerator was free to preserve the normal load path through the demonstrator structure.
 - Progressive loading and unloading sequence was applied every 20mbars up to 140mbars, with vertical measurements taken at the centre, at the C-SiC/ablator interface and at the decelerator edge every 120°.

No structural damage was recorded, although the overall stiffness of the C-SiC was lower than predicted, by 25%. This was attributed to a change in the carbon coating applied to the carbon fibres prior to composite pyrolysis.

Air leakage through the central heat-shield-to-C-SiC decelerator interface seal was measured at 0.8 litres/second at a pressure of 110mbars for a seal length of 1150mm. A solution was proposed modifying the seal support to reduce leakage. This did not impair proof of concept.

- Acoustic noise, simulating the Ariane 4 fairing:
 - The testing assessed the structural-skin dynamic response, which was considered to be the most sensitive part of the construction with respect to the decelerator fixing system.
 - Good quality acoustic excitation was sought for establishing the C-SiC skin eigenmodes. The INTESPACE 1100m³ reverberating chamber was selected to provide pure diffuse noise over 200Hz.
 - The demonstrator was hard mounted on a rigid body and fitted with accelerometers and strain gauges.

Hammer excitation tests established the eigenfrequencies, with the first at around 160Hz.

No noticeable damage resulted from acoustic excitation and the stress levels were well below the material allowables.

- Thermal shock test:
 - Concentrated solar flux was projected perpendicular to the front surface
 - Side reflectors were added around the test item to correct the incident heat-flux at the edges and to simulate the local aerodynamic over-heating expected during flight.
 - The required effective heat flux of 440kW/m² on the C-SiC was achieved with a solar flux of 600kW/m², once allowance was made for solar absorptivity, heliostat uniformity and angular corrections.

Ablator pyrolysis produced abundant smoke, but no consequential damage or over-temperatures were recorded.

Local thermal inertia was significant because of the short thermal exposure, and higher than anticipated temperatures (by 200°C) were recorded at thermocouples because of the use of a ceramic cement to bond the thermocouples to the C-SiC.

71.18.3.8 Conclusions

- The basic validity of the design was proved.
- Seal leakage during static pressure tests showed the need for a slight redesign of the seal support.
- The low surface catalycity of C-SiC may be impaired by surface contamination resulting from ablator pyrolysis.
- The use of an oxidation protection coating on the C-SiC was shown to be necessary.

71.19 Cryogenic tanks

71.19.1 General

The majority of future launcher programmes are considering the use lightweight, reuseable propellant tanks. LH liquid hydrogen is the most likely choice of fuel for such vehicles, [See also: [29.11](#), [70.12](#)]

Cryogenic tank protection systems need to resist the various rigorous conditions encountered during launch, flight and re-entry for the intended life of the tank structure.

The concept of the overall cryogenic tank protection system comprises:

- Thermal protection system, during reentry into the atmosphere.
- Cryogenic insulation, to reduce boil-off of LH propellant and avoid frost or solid air forming on the tank surface, so increasing vehicle mass during pre-launch and accent phases.

Both the TPS thermal protection system and the cryogenic insulation and the contribute to the overall heat transfer across the tank wall.

Cryogenic insulation and TPS concepts were investigated within the European reuseable launcher programmes, FESTIP and FTLP, Ref. [\[71-92\]](#), [\[71-93\]](#).

71.19.2 European programmes

71.19.2.1 FESTIP

The integration of TPS with cryogenic tank constructions for future reusable space transportation systems was part of the FESTIP programme. It considered tanks suitable for LH and LOX fuels made from CFRP materials or aluminium-lithium alloys, Ref. [\[71-62\]](#), [\[71-64\]](#), [\[71-66\]](#).

[See also: [29.11](#), [70.12](#)]

The research and development improved the supporting technologies for prolonged flight operations using TPS systems based on C-SiC rigid external insulation or metallic constructions.

71.19.2.2 C-SiC oxidation protection

The features of C-SiC internal and external oxidation protection systems for use up to 1300°C included:

- Outer CVD SiC coatings.
- Thermo-viscous external and internal sealing layers with refractory particles.
- Fabrication techniques using infiltration, slurry and sol-gel processes.
- Examination of the high temperature effects of hydrogen and water vapour.

71.19.2.3 IMI internal multiscreen insulation

Some of the features of the highly-reflective ceramic IMI internal multiscreen insulation (IMI) included, [See also: [71.10](#)]:

- Designed for improved operational use above 1200°C towards 1700°C.
- Variable thickness platinum coatings, 300nm to 1000nm.
- Yttrium interlayers, platinum alloys and variations in PVD coating conditions.

71.19.2.4 Refractory metals and aluminide oxidation protection

Oxidation protective coatings for refractory metals and titanium aluminides considered:

- Overlay and diffusion barrier coatings for niobium, tantalum and molybdenum alloys.
- Preoxidation, siliconising, aluminising and CoCrAlY coatings for TiAl.

71.19.2.5 ODS alloys

Some ODS oxide dispersion strengthened aluminium alloys were considered.

71.19.3 Concepts: TPS panel array

The concept is shown in [Figure 71.19.1](#), Ref. [\[71-80\]](#). It was developed by DLR and MAN, [See also: Chapter [52](#)].

The main features are, Ref. [\[71-80\]](#):

- C-SiC integrally-stiffened panel, produced by LPI-C/SiC process. Panel size: 400mm × 400mm; skin thickness 1.5mm; mass 3.72kg/m².
- C-SiC omega-shaped stand-off attachments, produced by LPI-C/SiC process.
- C-SiC fasteners and central post (rivet).

Testing of multi-panel arrays took into account the integrated panel performance and the integrity of all of the subcomponents.

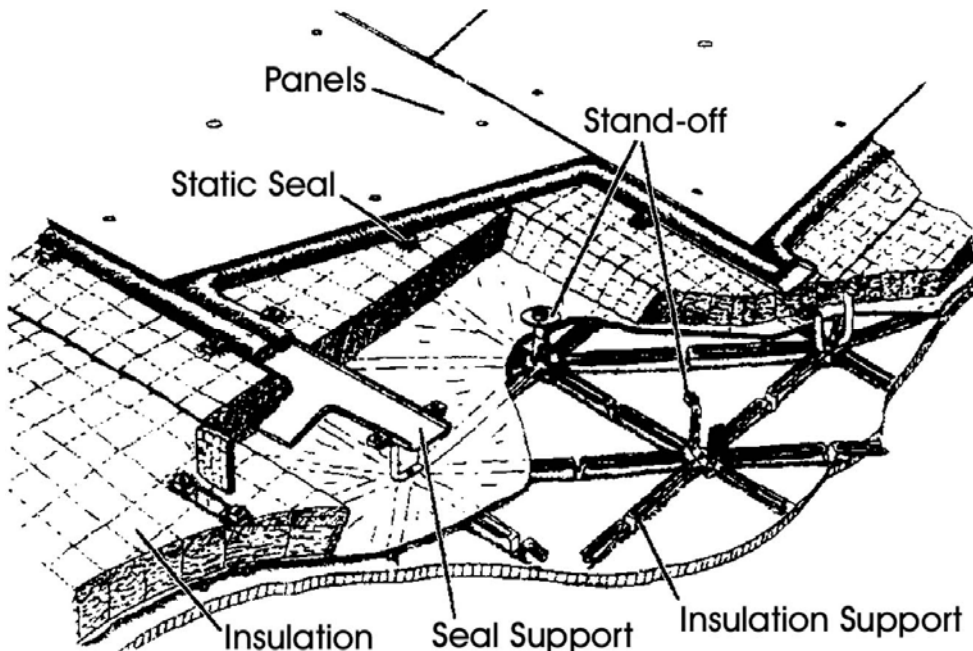


Figure 71.19-1 – TPS panel array concept: Cryogenic tanks

71.19.4 Concepts: LH tank cryogenic insulation

The research work, a FESTIP-funded project between ESTEC and Daimler-Chrysler (Bremen), investigated several commercial polymer foams for cryogenic insulation of LH tanks. One aim was to provide a ranking system for potential polymer foams for cryo-tank insulation, [See: [71.22](#)].

General technical considerations for the polymer foam materials are given in [Table 71.19.1](#), Ref. [[71-92](#)].

[See: [71.22](#) for evaluation of some commercial polymer foam grades for cryotank insulation]

Table 71.19-1 – Cryogenic insulation: Technical considerations for LH tank concepts

	Cryo-concept 1 (external insulation)	Cryo-concept 2 (internal insulation)	Comment
Maximum pressure difference	1 bar	static and dynamic loads from LH.	
Thermal cycles	Large range, e.g. -253°C to +150°C		Where +150°C is the temperature of the structure underneath the TPS.
Maintenance and repair	Low	Low	Between flights
Foam compressive strength (MPa)	0.1	0.3	
Strain	High		Foam not brittle at low temperatures
Foam density (kg/m³)	-	40 to 100	Foam strength is affected by density. A lower end value can provide mass saving.
Foam thermal efficiency	Low value		where: Thermal efficiency = (density × thermal conductivity). Ranking parameter to aid mass optimisation
Foam thermal expansion coefficient (/K)	between 35 and 55		To cope with CTE mismatch between foam and tank structure
Foam gas permeability	Low	Low	Indicates the need for a high closed-cell content, e.g. >90%
Other	CFC-free processing of foams		

Figure 71.19.2 shows two concepts for LH cryo-tank protection, Ref. [71-92].

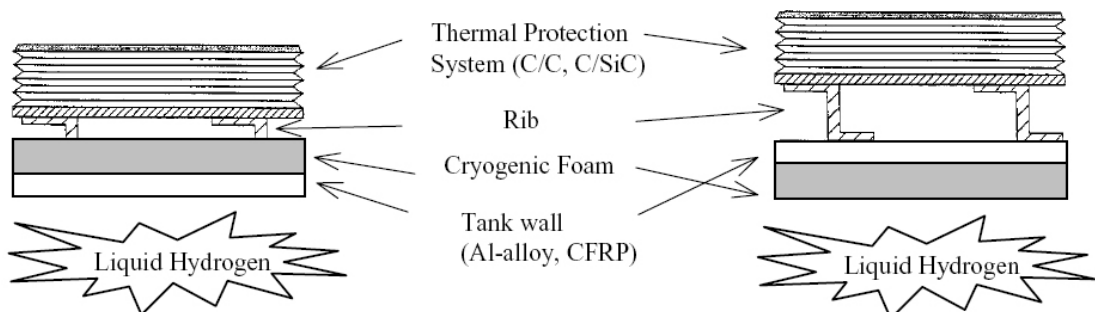


Figure 71.19-2 – Cryogenic insulation: LH tank concepts

Whilst both concepts met most of the thermal demands, a main difference between the concepts is the location of the insulation foam, for mechanical reasons, i.e.:

- Cryo-concept 1, where the foam is on the external surface of the tank wall. The foam experiences atmospheric pressure and vacuum. An open-cell foam was first considered for this concept because of the low forces involved. It also offered sufficient flexibility to cope with thermal expansion mismatch at the tank wall interface and enabled venting under vacuum. However, air condensing in the open-cells at low temperatures was problematical.
- Cryo-concept 2, where the foam is on the internal surface of the tank wall. It meant that the tank wall acts as a heat-sink, enabling the insulation thickness and mass to be reduced. The foam needs to support both static and dynamic loads from the fuel. A closed-cell foam was considered because of its higher strength and also because closed-cells limit the migration of hydrogen into the foam and evaporation. Purging, to prevent humidity, using dry-air or heated nitrogen instead of helium was seen as an advantage. A main concern was that any particles of foam that became detached for the insulation were likely to contaminate the fuel delivery system.

71.20 TPS mass budgets

71.20.1 Allocation

The design of TPS systems is highly mission dependent. Some of the factors which determine the designs and materials allocated are, Ref. [71-49], [71-50], [71-51]:

- Reusability requirements,
- Anticipated heat fluxes (MW/m^2),
- Duration of thermal loading,
- Total heat input (MJ/m^2),
- Peak surface temperatures,
- Locations of hot spots, e.g. leading edges, stagnation points.

71.20.2 Examples

Mass budgets for TPS systems used in the past have ranged between 6% and 44% of the total structural mass of the spacecraft. The 44% figure is exceptional, resulting from the very high heat fluxes anticipated for that particular mission. However, typical mass budgets are in the 5% to 20% range, so there is still a considerable incentive to save mass by the use of efficient protection systems.

Thermo-structural TPS performs a joint role and therefore complicates these mass budget figures, [See: Chapter 70].

The examples of TPS designs given in Chapters 70 and 71 illustrate the range of protection methods available.

71.21 TPS verification

The precise flux conditions found during each re-entry cannot be predicted with total certainty. Sufficient margin is therefore made in design to cope with the unknown factors.

The verification of these TPS designs by analysis and ground testing is therefore important, Ref. [71-52] to [71-57], [71-61], [71-63], [71-65] to [71-67], [71-70], [71-73], [71-74].

[See also: 86.7 for some European test facilities]

71.22 Polymer foam cryogenic insulation

71.22.1 General

71.22.1.1 Expendable ‘single-shot’ launchers

Polymeric foams are commonly used as insulation on the external surfaces of cryogenic tanks for expendable launchers. When compared with other potential materials, polymeric foams were chosen on the basis of mechanical stability, cost and simple manufacturing and application.

71.22.1.2 Reusable launchers

For reusable launchers with fast turn-round times, degradation caused by repeated use and re-entry cycles means that insulation materials previously applied to expendable tanks cannot be used without re-evaluation of their long-term performance. A study conducted under the FESTIP programme, Ref. [71-92], [71-93], evaluated a number of commercially-available polymer foams as potential insulation in reusable LH cryotank concepts, [See: 71.19].

71.22.2 Polymer foam characteristics

Whilst offering low density and low thermal conductivity characteristics, polymeric foams generally have poor mechanical performance, high gas permeability and high thermal expansion/ contraction. Their high CTE can provoke problems, such as cracking or disbonds where polymeric foams are bonded to metals.

Polymeric foams can be classed by polymer-type and cell structure, Ref. [71-92]:

- Thermoplastics, which tend to soften between 70°C and 120°C. In many cases they become brittle at cryogenic temperatures. Polymers commonly used for foams include polystyrene (rigid) or PVC polyvinyl chloride (flexible).
- Thermosetting, which include urea-formaldehyde and phenolic (both rigid with poor properties at low densities), and polyurethane (flexible). Of these, flexible polyurethanes retain good properties at cryogenic temperatures and tend not to become brittle.
- Rigidity, which depends on the polymer structure within the processed foam along with foam-related characteristics, such as cell morphology. In general, a rigid foam is one in which the polymer is in a crystalline or amorphous state, i.e. below its Tg. Consequently, a flexible foam has a polymer above the crystalline melting point or above its Tg.

- Cells, which decrease both the density and strength compared with the non-foamed polymer, but provide a higher flexural modulus-to-density. Cells within foams can be open or closed. Open-cell foams are usually flexible, whereas closed-cell foams tend to be rigid. In commercial foams, mixtures of closed and open cells are often present. Depending on the processing, cells can contain air, a gas or a mixture of both.

The properties of materials at extreme low temperatures are often poorly quantified. Even less is known where the thermal cycling range is very wide, e.g. from -253°C to +150°C, which is an expected temperature range for some cryotank concepts, Ref. [71-92].

[See: [Table 71.19.1](#)]

71.22.3 Properties

71.22.3.1 Mechanical

The mechanical properties to consider for polymer foam cryogenic insulation materials include, Ref. [71-92]:

- compressive behaviour, including strength, modulus and deformation.
- tensile behaviour, including strength, modulus and deformation.
- temperature-related effects on the mechanical properties, such as operational temperature range, thermal cycling and thermal shock. In general, both modulus and strength increase with decreasing temperature. This tends to produce brittle fracture in tension and progressive crushing in compression. At very low temperatures, when the gas condenses in the cells, the resulting pressure change can deform the cellular structure and modify the deformation behaviour.

71.22.3.2 Physical

The main physical characteristics of interest in polymer foam cryogenic insulation materials are, Ref. [71-92]:

- Thermal conductivity, which is a combination of the polymer thermal properties and the gas and air contained within the foam cell structure. At cryogenic temperatures, the gases contained in the cells can condense, affecting the thermal conductivity. This is known as 'cryopumping'. Removing the air in the cells, by vacuum or by purging with another gas, such as helium, can affect thermal conductivity. Helium is used because it has a lower condensation temperature than hydrogen.
- Thermal expansion coefficient, which is important when materials with differing CTEs are joined. In the case of polymer foams bonded to metal tank structures which undergo wide thermal cycling, mismatch of CTE can provoke shear failures along the bondline at the tank metal surface or cracking in the insulation normal to the tank surface. Reduction of cracking by use of foams containing a low level of short-fibre reinforcement has been considered.
- Gas permeability. Where the foam is in direct contact with hydrogen, hydrogen absorbed by the foam can affect the thermal conductivity or embrittle it.
- Flammability. Some foams have a fire retardant component added to improve self-extinguishing characteristics. This can be necessary because at low temperatures the presence of

oxygen-rich condensate within an oxidisable organic foam could provoke an explosion. The type of fire retardant used needs to ensure that a burning foam material does not have increased toxicity.

71.22.4 Materials

71.22.4.1 Material selection

Most commercial polymer foams are developed for industrial needs rather than the rigorous demands of reusable space systems. A first screening, largely based on manufacturers' data, for good thermal insulation at high and low temperature, identified materials for further investigation. These are summarised in Table 71.22.1, Ref. [71-92].

Table 71.22-1 - Cryogenic insulation: Polymer foam candidate materials

Properties (1)	AIREX® Alusuisse Airex AG (CH)		SOLIMIDE® Jehier Spatial (F)	ELASTOPOR® Elastogran GmbH (D)
Type	PEI - polyetherimide		PI - polyimide (densified)	Polyisocyanurate
	Thermoplastic	Thermoplastic	Thermoplastic	Thermoset
Tg (°C)	217 amorphous	217 amorphous	(2)	150 (4)
Cell structure (% closed cells)	>95	>95	60 to 90	>97
Foaming agent (6)	not stated	not stated	not stated	not stated
Density (kg/m³) (5)	80	110	70	62
Mechanical response	Elastic-plastic Rigid	Elastic-plastic Rigid	Elastic- plastic Flexible	Elastic-plastic Rigid
Modulus, compressive, RT (MPa)	54	94	-	-
Modulus, tensile, RT (MPa)	52	78	-	-
Strength, compressive, RT (MPa)	1	1.7	0.14 (3)	0.32
Strength, tensile, RT (MPa)	1.8	2.7	0.53	0.5
Thermal conductivity, RT (W/mK)	37	27	15	23

Key:

- (1) Manufacturers' data
- (2) No Tg or melting before thermal decomposition at about 500°C
- (3) 40% deflection, parallel.
- (4) softening point
- (5) Commercially available densities.
- (6) Proprietary manufacturers' information (not disclosed)

71.22.4.2 Evaluation

Each candidate material was subject to a series of evaluations, including, Ref. [71-92]:

- Microscopy to determine the internal structure of the foam, e.g. cell distribution, cell shape, average cell dimensions, cell wall thickness, variations in cell structure throughout the foam.
- Mechanical properties, at -197°C (liquid nitrogen), 23°C and 150°C, to determine elastic limit, tensile and compressive modulus, tensile and compressive strength and elongation to fracture (using ISO standard test procedures).
- Mechanical properties, post-thermal cycling, using compression tests only.

71.22.4.3 Foam structure

From the microscopy, the internal structure of Elastopor® polyisocyanurate foam appeared somewhat anisotropic due to the presence of elongated cells in the foaming direction compared with the perpendicular direction. Both Airex® grades and Solimide® foams showed an isotropic internal foam structure.

71.22.4.4 Foam mechanical properties

Table 71.22.2 provides a summary of the mechanical test results for the candidate materials, Ref. [71-92]. The values determined during testing by ESTEC tend to be lower than the manufacturers' data.

For the intended LH cryotank concepts, [See: 71.19], Elastopor® polyisocyanurate and Airex® polyetherimide grades met the necessary strength between 196°C and 150°C, i.e. the target compressive strength of 0.3 MPa. The results at -196°C are only indicative of the material performance at the true service temperature of -253°C. Hence, for contact with LH, the brittleness and high stiffness of the Airex 110kg/m³ grade and Elastopor could be problematic.

Solimide® densified polyimide, whilst exhibiting good elongation characteristics, did not have sufficient strength for use in internal cryotank insulation applications.

No significant changes were noted in the compressive mechanical properties of materials after thermal cycling between -180°C and +150°C. No microcracks or other damage was observed visually in specimens after thermal cycling. A concern was that brittle materials experiencing thermal shock were likely to crack.

Table 71.22-2 - Cryogenic insulation: Polymer foam mechanical properties

	Commercially-available polymer foam grades			
	AIREX® 80 kg/m³ R82.80	AIREX® 110 kg/m³ R82.110	SOLIMIDE®	ELASTOPOR® H2130/14
	Polymer type	PEI - polyetherimide	PEI - polyetherimide	PI - polyimide (densified)
	Compressive properties (4)			
Modulus (MPa):				
-196°C	20.08	27.20	0.51	15.81
+23°C	19.18	24.25	0.31	12.99
+150°C	13.02	20.23	0.24	7.33
Strength (MPa):				
-196°C	1.61	2.48 (3)	0.05 (3)	0.99
+23°C	1.13	1.95	0.03 (3)	0.67
+150°C	0.60	1.07	0.02 (3)	0.40 (3)
Elongation (%):				
-196°C	5.35	7.20	14.64	4.25
+23°C	4.55	6.55	14.10	3.70
+150°C	3.73	4.68	12.80	3.50
Tensile properties (4)				
Modulus (MPa):				
-196°C	47.03	70.13	2.77	14.36
+23°C	32.74	44.99	1.86	5.62
+150°C	14.25	26.18	2.43	-
Strength (1) (MPa):				
-196°C	1.70	2.49	0.18	0.21
+23°C	1.86	2.96	0.19	0.19
+150°C	1.18	1.70	0.20	-
Elongation (2) (%):				
-196°C	5.13	3.87	6.87	2.80
+23°C	7.27	7.83	10.60	4.05
+150°C	18.27	26.47	12.73	-
Key:	(1) UTS	(3) Strength at 10% compression		
	(2) Ultimate elongation	(4) Average values of at least 3 samples		

71.22.5 Ranking of polymer foam cryogenic insulation

71.22.5.1 Criteria

A number of interrelated characteristics of polymer foams need to be considered for their use as insulation materials in reusable LH tanks. These characteristics are proposed as criteria for use in ranking potential materials for cryotank applications; where, in general, the higher the number the better.

The criteria, known as 'quality grade numbers', along with the values obtained for the materials investigated, are summarised in [Table 71.22.3](#), Ref. [71-92]. The values given are for room temperature and need to be determined at both high and low temperatures.

The closed-cell content of foams is important in both externally and internally-applied insulation for LH tanks. For internal insulation, hydrogen penetration of the foam can affect thermal conductivity. In cases where interaction between hydrogen and the insulation results in embrittlement, a surface coating applied to the foam is an option, but this increases the mass and complexity of the insulation system. It also complicates the quality assurance, in-service inspection, maintenance and repair activities.

Table 71.22-3 – Cryogenic insulation: Ranking criteria and values

Criteria ⁽¹⁾		
1	$\frac{1}{\rho \times \lambda}$	Indicator for light-weight, high-performance insulation.
2	$\frac{f_{comp}}{\rho \times \lambda}$	As for criteria 1, but also takes into account the material compressive strength, e.g. applicable to internal tank insulation supporting loads from fuel.
3	Low-to-high temperature resistance (°C)	Indicator of resistance to structural degradation over a wide temperature range; usually measured by DSC dynamic scanning calorimetry or TGA thermogravimetric analysis techniques.
4	Closed-cell content	Indicator of material cell stability and gas permeability.

Key: (1) where: f_{comp} = foam compressive strength (MPa); ρ = material density (kg/m^3); λ = thermal conductivity ($\text{W}/(\text{mK})$)

Ranking of polymer foams at 23°C:

Criteria ⁽¹⁾	AIREX® 80 kg/m ³	AIREX® 110 kg/m ³	SOLIMIDE®	ELASTOPOR®
1	0.34	0.34	0.95	0.70
2	0.38	0.66	0.03	0.47
3	-190 / 180	-190 / 180	-250 / 250	* / 180
4	high	high	low	high

Key: * not stated (1) Criteria 1 and 2 use manufacturers' data for density and thermal conductivity

71.22.5.2 Summary

Based on the experimental data, the main conclusions were that:

- Airex® 80 grade appeared the best suited for internal insulation.
- Airex® 110 grade, although having high strength, was brittle at low temperature.
- Elastopor® showed adequate strength for internal insulation, but was brittle at low temperature.
- Solimide® has insufficient strength and stiffness for internal tank insulation but is a candidate for external uses.

71.22.6 Further work

Further work was proposed for the two best materials from the initial evaluation stage to complete the data for actual service temperatures, i.e. mechanical and thermal performances at liquid hydrogen temperatures.

For actual applications, some other important factors to consider include:

- Selection and performance of bonding materials and suitable processes for attaching insulation to tank structures, either internally and externally.
- Long-term effects of liquid hydrogen contact on foam materials (internal insulation), e.g. to establish if a surface coating is necessary and the implications for the overall concept, e.g. mass and complexity.
- Effects of space or other environmental interactions on the long-term performance of foams applied externally to tank walls and beneath TPS.
- Means of inspection, maintenance and repair for the overall cryotank protection system, i.e. tank insulation plus TPS system.

71.23 High temperature insulation (HTI)

71.23.1 Background

In the X-38 nose cone and chin strap design-development, the need was identified for flexible fibrous insulation, under the CMC shell, to protect the substructure. External temperatures of up to 1750°C are reached in the stagnation area during re-entry. The development of the overall TPS system for the nose assembly was a collaborative exercise conducted by Astrium SI (now EADS-ST GmbH), DLR Stuttgart and MAN Technologie in Germany.

The overall X-38 nose cap TPS system comprised, Ref. [71-95], [71-96]:

- Rigid C/SiC panels (external surface).
- Flexible insulation blankets, which were used to fill the remaining volume between the substructure and the C/SiC nose shell. Different types of insulation were used , Ref. [71-95], [71-96].
 - IFI (internal flexible insulation) on the cold substructure. This was an spin-off from existing FEI blankets, [See: 71.11].
 - HTI (high temperature insulation) on the outer regions, which was a new development to provide higher thermal performance than existing FEI and IFI products.

The flexible insulation components were developed by Astrium SI (Bremen), Ref. [71-95], [71-96]; [See also: 70.24 – X-38 nose cap].

71.23.2 Development factors

71.23.2.1 Objectives

The development aim of the HTI was to produce an insulation material that kept the temperature at the inner, IFI interface within the specified limits. HTI needed to be flexible and to retain its flexibility at elevated temperatures with potential multiple-use capabilities, Ref. [71-95], [71-96].

Any gaps that form due to shrinkage will reduce the insulation performance, so, to meet the objectives, this had to be avoided. Tests focussed mainly on the selection of appropriate materials to avoid shrinkage, Ref. [71-95], [71-96].

HTI development involved some difficult and complex challenges, which are discussed further, Ref. [71-95], [71-96].

71.23.2.2 Technology-related

The various technology-related factors included, Ref. [71-96].

- Fibrous ceramic materials tend to become brittle and begin to lose flexibility at the extremely high temperatures experienced in the X-38 nose skirt (up to 1550°C) and nose cap (1750°C).
- Potential multiple-use capability: If feasible, large areas of reusable HTI can be a means of reducing refurbishment costs.
- Complex manufacturing due to complex shapes and small radii, i.e. 3D geometries, many cut-outs and radii around 500mm.

71.23.2.3 Technical-related

Various technical factors are considered including, Ref. [71-96]:

- Size restrictions: Unlike FEI, both HTI and IFI blankets are not only restricted at their sides (x - and y -direction), but also in thickness. Hence, manufacturing tolerances are stricter because there is less room to compensate for manufacturing inaccuracies.
- Large number of sensors: The HTI design had to accommodate a multitude of sensors, some penetrating insulation layers, e.g.
 - ‘standard’ thermocouples,
 - acoustic emission, from Kayser-Threde,
 - PYREX sensors, from the Institute for Space-Systems IRS, Stuttgart University,
- Large number of interfaces: Several crucial structural hardware items interface with the insulation, e.g.
 - Stand-offs for side and chin panels.
 - Nose cap attachments.
 - Pressure ports.
 - Feed lines.
- Complex nose assembly integration procedure: Owing to limited access from the inside of the X-38 vehicle for integration, special care was needed during design to ensure access to all relevant components at each step of the integration procedure.

71.23.2.4 Configuration-related

The various configuration factors included, Ref. [71-96].

- Large number of international partners involved in the project.
- Insulation parts were last in the chain, so any design change within the nose area usually had a direct affect on the insulation design, e.g. crucial items, such as the positions of the side panel stand-offs and the routing of the pressure port feed lines, were changed several times, comparatively late in the project.

71.23.3 Development approach

71.23.3.1 Test philosophy and plan

The various development tests performed included, Ref. [71-96]:

- Characterisation of a range of materials, e.g. resistance to thermal ageing, shrinkage, strength (compressive and tensile).
- Material selection, based on the results of characterisation tests identified those best suited for the application.
- Additional tests in different configurations, e.g. additional thermal cycling and compression tests, a plasma test, a random vibration test and a temperature gradient and thermal conductivity test.

Table 71.23.1 summarises the development tests for HTI. The flow diagram for testing is shown in Figure 71.23.1, Ref. [71-96].

Table 71.23-1 - TPS: HTI development tests for X-38 nose cap assembly

Test	Objectives	Test Parameter	Test Article	Facility
Thermal Stability	Characterisation of HTI materials (shrinkage, compressibility, tensile strength)	<ul style="list-style-type: none"> • $1300^{\circ}\text{C} < T < 1750^{\circ}\text{C}$ • Various time duration ($20 \text{ min} < t < 2 \text{ h}$) 	Various Al_2O_3 - and ZrO_2 -based felts, fabrics, threads	EADS-ST Bremen
Thermal Stability of Protection Layers	Characterisation of additional HTI protection layers (shrinkage, compressibility)	<ul style="list-style-type: none"> • $1300^{\circ}\text{C} < T < 1750^{\circ}\text{C}$ • 3 temperature cycles 	Hafnia-based felts	EADS-ST Bremen
Random Vibration Test	Characterisation (structural integrity) after Random vibration loads	<ul style="list-style-type: none"> • X-38 Random Vibration Design Environment 	Selected Al_2O_3 - and ZrO_2 -felts and fabrics	EADS-ST Trauen
Plasma Test	Characterisation of HTI blankets (shrinkage)	<ul style="list-style-type: none"> • $1200^{\circ}\text{C} < T < 1900^{\circ}\text{C}$ • $p_{\text{static}} = 2\text{-}4 \text{ mbar}$ • $p_{\text{stagn.}} = 53 \text{ mbar}$ 	HTI blankets	DLR Cologne
Thermal Conductivity at High Temperatures	Characterisation of HTI core material (thermal conductivity at high temperatures)	<ul style="list-style-type: none"> • $T < 1750^{\circ}\text{C}$ • $3 \text{ Pa} < p < 10^5 \text{ Pa}$ 	Al_2O_3 -based core material	TsAGI, Russia
Temperature Gradient Test	Functional verification by exact characterisation of HTI shrinkage at various temperatures	<ul style="list-style-type: none"> • $1350^{\circ}\text{C} < T < 1750^{\circ}\text{C}$ • 3 temperature cycles 	HTI blankets (final configuration)	EADS-ST Bremen

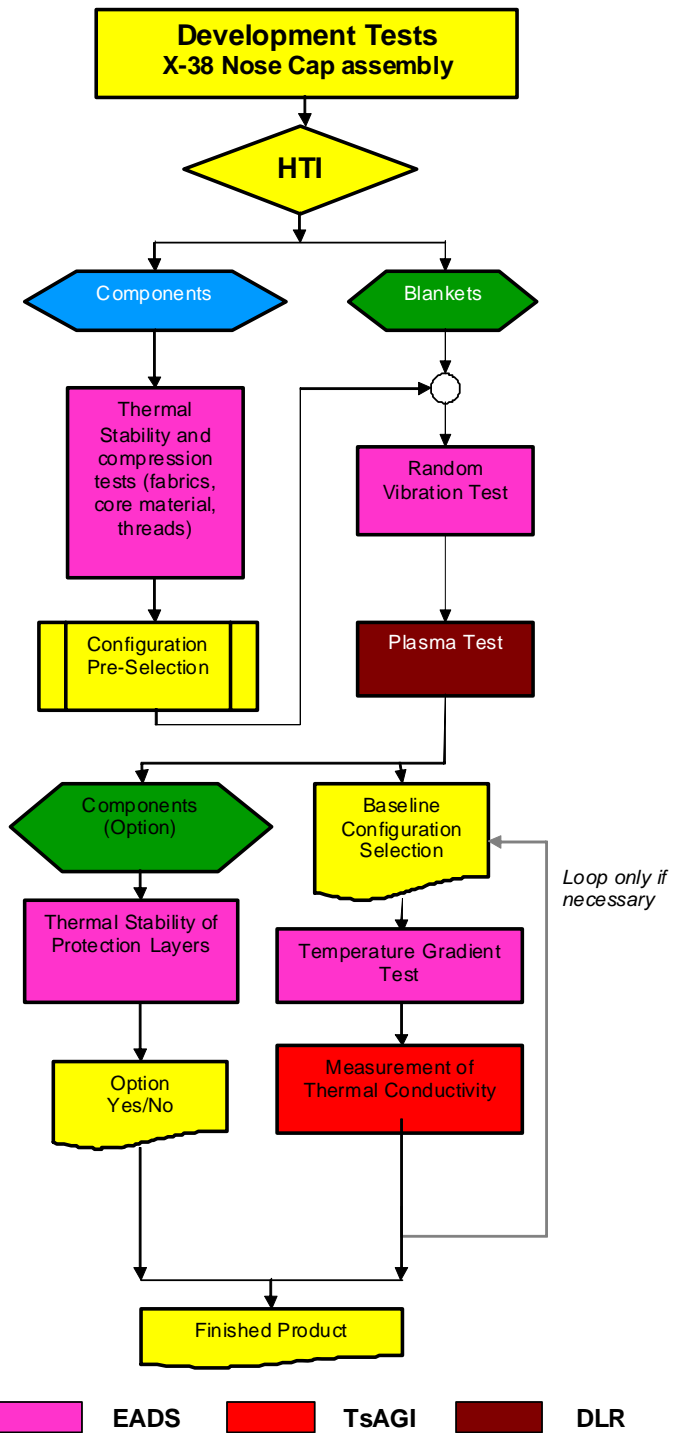


Figure 71.23-1 - TPS: Flow diagram of HTI development testing for X-38 nose cap assembly

71.23.4 Materials

The range of different types of ceramic fibre felts, fleeces, fabrics and threads examined at the start of the HTI development are given in [Table 71.23.2](#), Ref. [71-96].

Table 71.23-2 - TPS: HTI candidate materials

	Name	Composition	Density (kg/m ³)
Fibre Felts and Fleeces	ERN-CV-5A	Alumina-based	30-120
	ERN-CV-7A		
	ERN-CV-11A		
	ERN-CV-12A		
Fabrics	ERN-CV-13Z	Zirconia-based	300
	-	Hafnia-based	300
	ERN-CT-10A6	Alumina-based	-
	ERN-CT-11Z4	Zirconia-based	-
	-	Hafnia-based	-
Threads	ERN-CF-7A3	Alumina-based	-

71.23.5 Testing

71.23.5.1 General

The results from two important tests had a major effect on the final HTI design, Ref. [71-96]:

- Thermal cycling test, which was the basis for the material selection process.
- Temperature gradient test, using HTI blanket samples in their final configuration under 'quasi-realistic' temperature cycling.

71.23.5.2 Thermal stability

Thermal stability and compression tests were divided into these major steps, Ref. [71-96]:

- Step 1: Shrinkage and compression behaviour after thermal ageing at elevated temperatures (between 1400°C and 1750°C) of different fibre felt materials.
- Step 2: Test parameters adapted to [X-38](#) mission conditions and applied to materials selected from the previous step.
- Step 3: Influence of the duration of thermal ageing and the various temperature cycles on felts. Samples of ceramic fabrics and threads were aged under similar conditions and later subjected to a tensile strength testing.
- Step 4: Hafnia (HfO_2) felt and fabric was also examined as a possible protective layer for the actual HTI blanket, in the area where temperatures exceed 1600°C. It was not considered as an [HTI candidate material](#) because of its high price.

[Table 71.23.3](#) summarises the results of the thermal stability evaluation of candidate HTI materials, Ref. [71-96].

Table 71.23-3 - TPS: HTI thermal stability test results

Thermal stability test step (1)	T (°C)	Result	Comment
	1400	Shrinkage: Virtually no effect on samples was detected. Embrittlement: ERN-CV-13Z is slightly affected at the temperature.	ERN-CV-13Z was excluded from further thermal testing due to embrittlement at 1400°C. Data from the 'Random Vibration Test' confirmed decision.
	1600	All samples show high shrinkage, especially perpendicular to main fibre direction (20% - 40%). ERN-CV-13Z (zirconia-based) exhibits high brittleness.	Shrinkage levels indicate test conditions are critical for materials. Test conditions adapted to simulate better the foreseen mission, i.e. duration of thermal ageing reduced to 60 min (3 re-entry cycles, qualification); Detailed temperature grid for testing was chosen.
	1750°C	Shrinkage increased (20% - 70%)	Detailed recording of test sample dimensions for precise material shrinkage data, i.e. before and after thermal ageing.
	Below 1550°C	Shrinkage: Alumina-based (ERN-CV-11A) virtually none; Alumina-based (ERN-CV-5A; ERN-CV-12A) less shrinkage than in Step 1	-11A and -12A: ~1-2% even negative shrinkage, i.e. increase in thickness, measured in some cases.
		Above 1550°C	At 1750°C, shrinkage of all samples is drastically reduced compared with Step 1 (about 2-3% in x- and y-direction, 13-23% in z-direction).
	1400°C	ERN-CT-11Z4 (zirconia-based) fabric lost nearly all its mechanical strength.	ERN-CT-11Z4 omitted from test programme.
	1450°C	Alumina-based fabric: tensile strength reduced to 30% of the value at RT. Alumina-based thread: tensile strength reduced to 25% of original value.	Alumina-based fabric and thread: Maximum use temperature below 1450°C.
	-	Hafnia-based material: very low tensile strength at all temperatures	Similar to the zirconia-based fabric, impossible to test after exposure to temperatures of 1600°C due to high brittleness.

Key: (1) Table 71.23.2 'Materials'; (2) Fabrics and threads (Step 1 and Step 2).

71.23.5.3 Material selection based on thermal stability

The results of the thermal stability test programme enabled selection of the most suitable materials for HTI along with observations relating to the design and integration of insulation for the intended application. The findings can be summarised as, Ref. [71-96]:

- Zirconia-based felt (ERN-CV-13Z) exhibits high brittleness and shrinkage at temperatures as low as 1350°C. Despite its superior insulation properties, it was omitted from further testing.

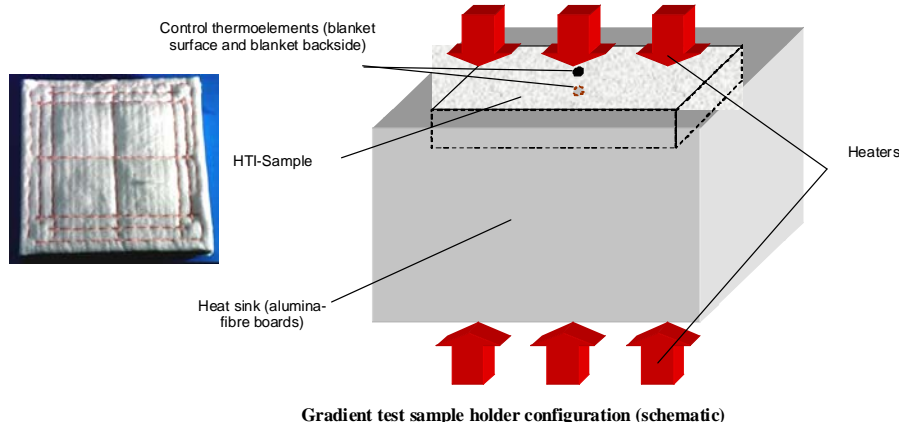
- Alumina-based materials (ERN-CV-5A, -11A and -12A) appear suitable for the application as flexible seals and was considered best suited as core material. They were subjected to further testing.
- Alumina-based ERN-CV-11A was not considered suitable for the HTI because of the higher silica content, which causes high shrinkage at elevated temperatures.
- ERN-CT-10A6 fabric (alumina-boro-silicate) exhibits far better residual strength after thermal ageing than zirconia-based fabric (ERN-CT-11ZA), which was omitted from further testing.
- The material needs to be pre-compressed to prevent excessive shrinkage. Owing to the integration sequence and geometrical restraints, the HTI cannot be compressed during integration. Therefore, ERN-CF-7A3 threads are used to compress the core material. A partial or complete failure of the threads during the hot phase does not affect the performance of the HTI, since the blanket can expand once it is integrated into the ceramic structure.
- The blanket density needs to be as high as possible in order to reduce the radiative conduction. However, manufacturing restraints meant that the density was limited to 140kg/m³.

71.23.5.4 Temperature gradient test

Based on the findings of the stability test in the general material selection process, the objective of the gradient test was to define the HTI blanket configuration and refine the test parameters to optimise testing in the critical temperature range.

To accurately simulate re-entry conditions, both the maximum temperatures and the temperature gradients through the insulation are reproduced.

Figure 71.23.2 shows the gradient test experimental set-up, the parameters and the sample configuration, Ref. [71-96].

**Parameters:**

Run No.	Temperature levels at upper surface (°C)	Temperature levels at lower surface (°C)	Temperature gradient (°C)	Duration, (min)
0	1255	792 to 879	465-375	10
1	1625	1271 to 1349	355-275	10
2	1725	1430 to 1500 (1)	295-225	10
3	1725	1529 to 1650 (1)	195-0	30
4	1725	1725 (2)	-	30
5	1650	1650 (2)	-	10

Key: (1) extrapolated; backside thermocouple removed at 1360°C; (2) without test fixture

Sample configuration:

Test Sample	Outer and inner fabric	Thread	Core	Core density (kg/m³)	Dimensions (mm)
HTI-903					
HTI-904					
HTI-905					
HTI-906					
HTI-907	No fabric	ERN-CF-8A3	ERN-CV-5A	142	150 × 150 × 20

Figure 71.23-2 - TPS: HTI temperature gradient test set-up, parameters and sample configuration

The results of the gradient tests can be summarised as, Ref. [71-96]:

- No shrinkage for temperatures up to 1250°C
- At 1625°C, decrease in thickness amounted to less than 0.5 mm. Shrinkage in the main blanket plane was up to about 1 mm in each direction.
- Decrease in thickness at higher temperatures remained below 1.5 mm, even after prolonged exposure (30 min at 1750°C).
- The material at the edges was not compressed to the same density as the majority of the blanket due to the sewing pattern. Therefore, 'true' shrinkage is probably less than the measured value.
- Shrinkage in the main blanket plane increases as temperature increases from 1 mm at 1625°C to about 2 mm after 30 min at 1750°C. However, a disproportionate amount of this shrinkage, is probably due to the reduced density at the blanket edges. Therefore, larger blankets, having relatively reduced edge effect, could show less shrinkage.

71.23.6 Summary

Considering all of the factors described, HTI in its present baseline configuration, i.e. core material only, no blankets and compressed by sewing with alumino-boro-silicate thread, is suitable for operation on a single-use vehicle such as X-38.

Using a shrinkage-tolerant design, i.e. an over-sized IFI (internal flexible insulation), [See: 71.11], along with compression of the insulation materials during integration, the decrease in thickness can be compensated for and the formation of gaps can be avoided.

In-plane shrinkage is less crucial. If a gap forms in HTI, the substructure is still protected by the IFI, which is only locally over-heated for a short time. This generally only results in a local increase in stiffness and embrittlement of the cover fabric in the small area affected.

Verification of HTI, along with the overall insulation concept, formed part of the X-38 NSA nose structure assembly qualification test. The question of whether HTI can be partially or completely re-used was deferred until after disassembly of the NSA qualification sample.

[See also: 70.24 – X-38 Nose cap]

71.24 References

71.24.1.1 General

- [71-1] 'Thermal Protection for Hypersonic Transports' Aerospace Engineering, July 1991, p9-11
- [71-2] M. Yamamoto: NASDA 'Thermal Protection Development of Re-entry Vehicles at NASDA'. First ESA/ESTEC Workshop on Thermal Protection Systems. ESTEC, Noordwijk, 5-7 May 1993. ESA-WPP-053 (August 1993) p58-63
- [71-3] K. Keller: ESA/ESTEC 'European Thermal Protection Developments'. First ESA/ESTEC Workshop on Thermal Protection Systems ESTEC, Noordwijk, 5-7 May 1993. ESA-WPP-053 (August 1993) p64-73
- [71-4] H. Grallert & K. Keller 'Metallic Thermal Protection Concept for Hypersonic Vehicles'. J.Aircraft, Vol. 28, No. 6, p410-416
- [71-5] Proceedings of a NASA Workshop: Current Technology for Thermal Protection Systems, 11-12 February 1992, Langley Research Centre, Virginia. NASA Conference Publication 3157
- [71-6] First ESA/ESTEC Workshop on Thermal Protection Systems ESTEC, Noordwijk, 5-7 May 1993 ESA-WPP-053 (August 1993) 420 pages
- [71-7] W.D. Henline: NASA/Ames, (USA) 'Thermal Protection System Development and Application to Planetary Entry Vehicles'. First ESA/ESTEC Workshop on Thermal Protection

- Systems ESTEC, Noordwijk, 5-7 May 1993. ESA-WPP-053 (August 1993) p5-39
- [71-8] J.E. Zimmer & R.A.S. Beck: Aerotherm Corp.
'Thermal Protection System for Comet Recovery Capsule'. First
ESA/ESTEC Workshop on Thermal Protection Systems ESTEC,
Noordwijk, 5-7 May 1993
ESA-WPP-053 (August 1993) p76-81
- [71-9] A. Russo et al: Alenia Spazio, (I)
'The CARINA Ablative Thermal Protection: Analysis, Design and
Testing'. First ESA/ESTEC Workshop on Thermal Protection Systems
ESTEC, Noordwijk, 5-7 May 1993. ESA-WPP-053 (August 1993) p82-88
- [71-10] T.J. Kowal & J.M. Caram: NASA/JSC, (USA)
'Thermal Protection System Designs for Candidate Assured Crew Return
Vehicles'. First ESA/ESTEC Workshop on Thermal Protection Systems
ESTEC, Noordwijk, 5-7 May 1993.
ESA-WPP-053 (August 1993) p104-112
- [71-11] A. Russo et al: Alenia Spazio, (I)
'The ARCV Thermal Protection: Concept Selection, Preliminary Sizing
and Development Plan'. First ESA/ESTEC Workshop on Thermal
Protection Systems ESTEC, Noordwijk, 5-7 May 1993.
ESA-WPP-053 (August 1993) p113-121
- [71-12] D.M. Curry: NASA/JSC, (USA)
'Space Shuttle Orbiter Thermal Protection System Design and Flight
Experience'. First ESA/ESTEC Workshop on Thermal Protection Systems
ESTEC, Noordwijk, 5-7 May 1993. ESA-WPP-053 (August 1993) p122-135
- [71-13] H. Goldstein
'Reusable Thermal Protection System Development - a Prospective'.
Proceedings of a NASA Workshop: Current Technology for Thermal
Protection Systems, 11-12 February 1992, Langley Research Centre,
Virginia.
NASA Conference Publication 3157 p1-18
- [71-14] D.M. Curry
'Thermal Protection Systems - Manned Spacecraft Flight Experience'.
Proceedings of a NASA Workshop: Current Technology for Thermal
Protection Systems, 11-12 February 1992, Langley Research Centre,
Virginia
NASA Conference Publication 3157 p19-42
- [71-15] V.P. Timoshenko: NPO Molniya, (Russia)
'BURAN's main Thermal Protection Components'. First ESA/ESTEC
Workshop on Thermal Protection Systems ESTEC, Noordwijk, 5-7 May
1993.
ESA-WPP-053 (August 1993) p40-57
- [71-16] P.O. Ransone et al
'Recent Advances in Carbon-Carbon Substrate Technology at NASA
Langley Research Centre'. Proceedings of a NASA Workshop: Current
Technology for Thermal Protection Systems, 11-12 February 1992,
Langley Research Centre, Virginia.

NASA Conference Publication 3157 p131-148

- [71-17] C.W. Ohlhorst et al
'Current Research in Oxidation-Resistant Carbon-Carbon Composites at NASA Langley'. Proceedings of a NASA Workshop: Current Technology for Thermal Protection Systems, 11-12 February 1992, Langley Research Centre, Virginia. NASA Conference Publication 3157 p149-168
- [71-18] M.J. Eiden et al: ESA-ESTEC\Interspace\SEP, (F)
'C/C Heatshield Development and Mechanical Performance Verification'. First ESA/ESTEC Workshop on Thermal Protection Systems ESTEC, Noordwijk, 5-7 May 1993.
ESA-WPP-053 (August 1993) p332-337
- [71-19] W. Keinath & P-J. Winkler
'Development of Fabrication Methods for Metallic Multilayer Structures'. ESA Symposium on Space Applications of Advanced Structural Materials, March 1990, ESA SP-303, p241-246
- [71-20] H. Grallert & K. Keller
'Multiwall Thermal Protection System: Engineering aspects'. ESA Symposium on Space Applications of Advanced Structural Materials, March 1990.
ESA SP-303, p227-232.
- [71-21] D. Alwes: DARA, (D)
'Application of TPS in German Projects'. First ESA/ESTEC Workshop on Thermal Protection Systems ESTEC, Noordwijk, 5-7 May 1993.
ESA-WPP-053 (August 1993) p89-96
- [71-22] J.L. Shideler
'Predicted and Tested Performance of Durable TPS'
Proceedings of a NASA Workshop: Current Technology for Thermal Protection Systems, 11-12 February 1992, Langley Research Centre, Virginia
NASA Conference Publication 3157 p97-130
- [71-23] R.K. Clark et al
'Thermal Control/Oxidation Resistant Coatings for Titanium-Based Alloys'
Proceedings of a NASA Workshop: Current Technology for Thermal Protection Systems, 11-12 February 1992, Langley Research Centre, Virginia
NASA Conference Publication 3157 p169-188
- [71-24] J.L. Shideler et al
'Verification Tests of Durable Thermal Protection System Concepts'. AIAA Paper 84-1767, June 1984
- [71-25] W. Blair et al
'Re-design and Fabrication of Titanium Multiwall Thermal Protection System (TPS) Test Panels'.
NASA CR-172247, 1984
- [71-26] W. Blair et al

'Fabrication of Pre-packaged Superalloy Honeycomb Thermal Protection System (TPS) Panels'
NASA CR-3755, 1985

- [71-27] L. Costamagna et al: Alenia Spazio, (I)
'Internal Multiscreen Insulation Analysis and Design Approach'. First ESA/ESTEC Workshop on Thermal Protection Systems ESTEC, Noordwijk, 5-7 May 1993
ESA-WPP-053 (August 1993) p302-306
- [71-28] K. Handrick et al
'Fibre-reinforced Ceramic Foils for a Lightweight Thermal Insulation'. Proceedings of HT-CMC1, Bordeaux Sept. 1993. ISBN 1-85573-143-6, p759-766
- [71-29] J. Bolz: MBB/ERNO, (D)
'On the Mechanical Development of the Flexible External Insulation (FEI) for Hermes Spaceplane'. ESA Symposium on Advanced Materials for Lightweight Structures, March 1992. ESA SP-336, p277-284
- [71-30] U. Rieck & L. Kampmann
'Material advances for lightweight TPS'. ESA Symposium on Advanced Materials for Lightweight Structures, March 1992. ESA SP-336, p285-290
- [71-31] U. Rieck & L. Kampmann
'Ageing behaviour of Ceramic Components used for Thermal Protection Systems'. Proceedings of ECCM6, Bordeaux Sept. 1993. ISBN 1-85573-142-8, p371-378
- [71-32] J. Antonenko et al: DASA/ERNO, (D)
'Advantages and Restrictions of Flexible Thermal Protection Concepts'. First ESA/ESTEC Workshop on Thermal Protection Systems ESTEC, Noordwijk, 5-7 May 1993. ESA-WPP-053 (August 1993) p295-301
- [71-33] C. Petiau
'The Challenge of Hermes TPS Shingles'. Proceedings of the International Conference: Spacecraft Structures and Mechanical Testing, ESTEC, 24-26 April 1991
ESA SP-321, p299-308
- [71-34] E. Werling & J.P. Vialaniex: ESA/HPD
'Hermes Re-orientation Programme: Present Status and Main Objectives for Hot Structures and Thermal Protection Materials and Technologies'. First ESA/ESTEC Workshop on Thermal Protection Systems, ESTEC, Noordwijk, 5-7 May 1993
ESA-WPP-053 (August 1993) p136-152
- [71-35] A. Lacombe et al: SEP, (F)
'Status on C/SiC Thermal Structures'. First ESA/ESTEC Workshop on Thermal Protection Systems ESTEC, Noordwijk, 5-7 May 1993
ESA-WPP-053 (August 1993) p319-324
- [71-36] K.H. Weber: MAN Technologie, (D)
'Applications of Ceramic Insulation for Weight Reduction of Re-entry Vehicle Thermal Protection Systems'. First ESA/ESTEC Workshop on Thermal Protection Systems ESTEC, Noordwijk, 5-7 May 1993

- ESA-WPP-053 (August 1993) p307-318
- [71-37] C. Petiau & A. Ajarrista: Dassault Aviation, (F)
'Concurrent Design of Thermal Protection Systems'. First ESA/ESTEC Workshop on Thermal Protection Systems ESTEC, Noordwijk, 5-7 May 1993.
ESA-WPP-053 (August 1993) p210-221
- [71-38] T.D. Swanson
'Advanced Two-Phase Heat Transfer Systems'. Proceedings of a NASA Workshop: Current Technology for Thermal Protection Systems, 11-12 Feb 1992, Langley Research Centre, Virginia. NASA Conference Pub. 3157, p251-290
- [71-39] C.J. Camarda & D.E. Glass
'Thermostructural Applications of Heat Pipes for Cooling Leading Edges of High-Speed Aerospace Vehicles'. Proceedings of a NASA Workshop: Current Technology for Thermal Protection Systems, 11-12 February 1992, Langley Research Centre, Virginia.
NASA Conference Publication 3157 p291-318
- [71-40] H.N. Kelly & M.L. Blosser
'Active Cooling from the Sixties to NASP'
Proceedings of a NASA Workshop: Current Technology for Thermal Protection Systems, 11-12 February 1992, Langley Research Centre, Virginia.
NASA Conference Publication 3157 p189-250
- [71-41] H. Leder et al
'Beryllium Thermal Protection Technology'. Proc. International Conference: 'Spacecraft Structures and Mechanical Testing', ESTEC, 24-26 April 1991.
ESA SP-321 October 1991,p399-404
- [71-42] A. Newerla & G. Wierheim: ESA/ESTEC/Siemens KWU
'Beryllium Components for Thermal Protection Systems'. First ESA/ESTEC Workshop on Thermal Protection Systems ESTEC, Noordwijk, 5-7 May 1993.
ESA-WPP-053 (August 1993) p325-331
- [71-43] D. Desnoyer et al
'Large Thin Composite Thermostructural Parts'. Proc. International Conference: 'Spacecraft Structures and Mechanical Testing', ESTEC, 24-26 April 1991.
ESA SP-321 October 1991,p283-291
- [71-44] Ch. Bonnet et al
'Stretched Skin Concept for the Entry Aerodynamic Decelerator System of Planetary Probes' Proceedings of the International Conference: Spacecraft Structures and Mechanical Testing, ESTEC, 24-26 April 1991.
ESA SP-321, p393-398
- [71-45] T. Haug et al: DASA/Dornier, (D)
'Short Manufacturing Cycle CMC Heat Shields and Hot Structures'. First ESA/ESTEC Workshop on Thermal Protection Systems ESTEC, Noordwijk, 5-7 May 1993.

ESA-WPP-053 (August 1993) p202-209

- [71-46] U. Trabandt et al
'Design of Hot Structures of Short-cycle Manufactured CMC'.
Proceedings of HT-CMC1, Bordeaux Sept. 1993
ISBN 1-85573-143-6, p751-758
- [71-47] U. Trabandt & J. Heitzer
'Design Concepts for Load-carrying Hot Structures for Re-entry Bodies'.
ESA Symposium on Advanced Materials for Lightweight Structures,
March 1992, ESA SP-336, p65-70
- [71-48] G.E.E. Scoon, K.Keller & C.Bonnet:
ESA/ESTEC/Dassault 'Aeroshell Concepts for Mars Landers'. First
ESA/ESTEC Workshop on Thermal Protection Systems ESTEC,
Noordwijk, 5-7 May 1993.
ESA-WPP-053 (August 1993) p97-103
- [71-49] N.W. Dunbar: BAe, (UK)
'Influence of TPS Performance on Future Space Transportation Concepts'.
First ESA/ESTEC Workshop on Thermal Protection Systems ESTEC,
Noordwijk, 5-7 May 1993. ESA-WPP-053 (August 1993) p153-159
- [71-50] C. Cornault & A. Paret: Dassault Aviation
'Non-linear Analysis for Optimisation of Thermal Protection Systems'.
First ESA/ESTEC Workshop on Thermal Protection Systems ESTEC,
Noordwijk, 5-7 May 1993. ESA-WPP-053 (August 1993) p246-251
- [71-51] H.K.H. Grallert & K. Vollmer: DASA, (D)
'TPS Mass Estimation for Advanced TSTO Vehicles by means of a 3D
Surface Integration of Temperature Distribution'. First ESA/ESTEC
Workshop on Thermal Protection Systems ESTEC, Noordwijk, 5-7 May
1993.
ESA-WPP-053 (August 1993) p252-257
- [71-52] N.A. Anfimov & V.B. Knotko: Tsniimash, (Russia)
'Testing and Verification of Re-entry Vehicle Thermal Protection'. First
ESA/ESTEC Workshop on Thermal Protection Systems ESTEC,
Noordwijk, 5-7 May 1993.
ESA-WPP-053 (August 1993) p350-355
- [71-53] K.K.O. Bär & W.W. Jarzab: IABG, (D)
'Qualification Testing of Thermal Protection Systems Test Technologies
and their Applications'. First ESA/ESTEC Workshop on Thermal
Protection Systems ESTEC, Noordwijk, 5-7 May 1993.
ESA-WPP-053 (August 1993) p356-362
- [71-54] A. Ajarrista & C. Petiau: Dassault Aviation, (F)
'Verification and Acceptance of Thermal Protection Systems'. First
ESA/ESTEC Workshop on Thermal Protection Systems ESTEC,
Noordwijk, 5-7 May 1993
ESA-WPP-053 (August 1993) p341-349
- [71-55] J.M. Bouilly & D. Guerrir: Aerospatiale, (F)

'Entry Testing of AQ60 for Huygens'. First ESA/ESTEC Workshop on Thermal Protection Systems ESTEC, Noordwijk, 5-7 May 1993.
ESA-WPP-053 (August 1993) p369-381

- [71-56] M. Kornmann & D. Richon: Battelle Europe, (CH)
'A Simple Rig for Thermal Tests of TPS in Realistic Atmosphere'. First ESA/ESTEC Workshop on Thermal Protection Systems ESTEC, Noordwijk, 5-7 May 1993.
ESA WPP-053 (August 1993) p388-391
- [71-57] E. Semerad et al: ÖFS/ARC, (Austria)
'Programme of Material Assessment Relevant for Thermal Protection Systems'. First ESA/ESTEC Workshop on Thermal Protection Systems ESTEC, Noordwijk, 5-7 May 1993. ESA-WPP-053 (August 1993) p392-398
- [71-58] H. Stockfleth et al: DASA/Dornier, (D)
'C/SiC Surface Protected Ablator for High Heat Fluxes'. First ESA/ESTEC Workshop on Thermal Protection Systems ESTEC, Noordwijk, 5-7 May 1993.
ESA-WPP-053 (August 1993) p289-294
- [71-59] T. Arnold et al
'The SEPCORE® TPS Concept: A Lightweight Modular Thermostructural Heatshield for Atmospheric and Planetary Entry Systems'. Proceedings of the International Symposium on Advanced Materials for Lightweight Structures '94.
ESA WPP-070, March 1994, p 227-234
- [71-60] H.Hald & P.Winkelmann
'Ceramic Tile Experiment (CETEX) for the EXPRESS Capsule'. Proceedings of the International Symposium on Advanced Materials for Lightweight Structures '94
ESA WPP-070, March 1994, p 621-626
- [71-61] Dornier GmbH/ Battelle, (D/CH).
'Integrity Control for High Temperature Structural Applications'. Europe/Aerospatiale combined programme, Phases 1 and 2, ESTEC Contract 8807/90/NL/PP(SC), Final reports 1993 & 1995
- [71-62] FESTIP '95-'96 : Technology Developments in Materials Mid-Term Review, 28 & 29 May 1996, ESTEC
- [71-63] G.H.Fauvel
'Experiences in experimental investigations on thermal characterisation of lightweight fibrous insulation for re-entry spacecraft TPS.' Conference on Spacecraft Structures, Materials & Mechanical Testing, Noordwijk, NL, 27-29 March 1996. ESA SP-386, Vol. 3, p1049-1056
- [71-64] H.Hald et al
'Design of a CMC-based thermal protection system for the cryogenic tank of a reusable space transportation system'. Conference on Spacecraft Structures, Materials & Mechanical Testing, Noordwijk, NL, 27-29 March 1996. ESA SP-386, Volume 3, p1057-1064
- [71-65] D.G.Sygulla

- 'Experiences in design and testing of ceramic shingle thermal protection systems: A review'. Conference on Spacecraft Structures, Materials & Mechanical Testing, Noordwijk, NL, 27-29 March 1996.
ESA SP-386, Volume 3, p1257-1266
- [71-66] FESTIP Yearly Workshop: Compilation of presentations, 17th and 18th October 1996 at ESTEC, Noordwijk, NL.
- [71-67] Dassault Aviation & Dornier, Daimler-Benz Aerospace, (D)
'Semi-Integrated Aeroshell TPS (S.I.A.T Study)' Final Report. Document DGT No.67933, September 30th 1996
ESA Contract 11208/94/NL/FG
- [71-68] Dassault Aviation & Dornier, Daimler-Benz Aerospace, (D)
'Semi-Integrated Aeroshell TPS (S.I.A.T Study)'. Final Presentations & Executive Summary, October 4th 1996.
- [71-69] Deutsche Aerospace Study on Thermal Protection for Advanced Launchers - ESA WLC TSTO configuration.
Final report for period 1992-93 for work conducted by DASA-RT (formerly MBB Ottobrunn); DASA-RS (Dornier), DASA Central Laboratories (Ottobrunn); IABG (Ottobrunn); ARC - Austrian Research Centre (Seibersdorf); Alenia (Turin).
- [71-70] MAN Technologie AG, (D)
'Manned Space Transportation Programme (MSTP) - Ceramic Heatshield Assembly (CHA)'. Technical Synthesis Report HT-TN-G402-0028-MAN, October 1996.
- [71-71] MAN Technologie AG et al., (D)
'Manned Space Transportation Programme (MSTP) - Ceramic Heatshield Assembly (CHA)'. Executive Summary Report. MAN Technologie AG with SEP; Dassault; IABG; IMFT Macaero; ZAE Würzburg; OEFZ Seibersdorf; NPO Molniya; TSAGI. September 1996
- [71-72] SEP- Société Européene de Propulsion, (F)
'Manufacturing of C-SiC Panels for the Ceramic Heatshield Assembly (CHA) for MSTP'. Executive Summary GPE/DC 96 31 369, June 1996
- [71-73] Daimler-Benz Aerospace, Bremen, (D)
'MSTP Technology Phase 1 - Flexible External Insulation (FEI)'. Executive Summary Report, February 1996.
ESA Contract No.11082/94/F/BM
- [71-74] Daimler-Benz Aerospace, Raumfahrt Infrastruktur (Dornier).
'Alternative Low Cost Short Manufacturing Cycle Ceramic Assessment Programme (ALSCAP)' Final Report: Test Assessment Report HT-FR-G401-001-DOR. November 1996. ESA Contract No: AO/1-2897/94/F/BM
- [71-75] ALSCAP Final Presentations at ESTEC: 1st October 1996. Contributions from:
i) Daimler-Benz Aerospace, Dornier & MAN Technologie
ii) SEP & Aerospatiale: Demonstration part manufacturing
iii) DLR: Oxidation tests.
iv) M3D (Battelle): Mechanical testing
v) ONERA: BLOX oxidation tests

- vi) ÖFZ Seibersdorf: testing of thermophysical properties.
- [71-76] P. Demuysère et al
'A.R.D Structures Development and Manufacturing'. Conference on Spacecraft Structures, Materials & Mechanical Testing, Noordwijk, NL, 27-29 March 1996. ESA SP-386, Volume 3, p1367-1374
- [71-77] Proceedings of the Second European Workshop on Thermal Protection Systems, Stuttgart, 23-25 October 1995.
ESA-WPP-103
- [71-78] D. Scheulen et al: Dornier Satellitensysteme, (D)
'The Surface Protected Ablator Heatshield of MIRKA: Development, qualification & flight results'. Third European Workshop on Thermal Protection Systems Noordwijk, NL, 25-27 March 1998.
- [71-79] H. Stockfleth: Daimler-Benz, (D)
'Development, Performance & Application Potential of the Surface Protected Ablator Concept used for the MIRKA Reentry Capsule Heatshield'. Third European Workshop on Thermal Protection Systems Noordwijk, NL, 25-27 March 1998.
- [71-80] M. Giegerich et al: MAN Technologie, (D)
'Flight Test Verification of Current Generation Ceramic-based TPS'. Third European Workshop on Thermal Protection Systems Noordwijk, NL, 25-27 March 1998.
- [71-81] Proceedings of the Third European Workshop on Thermal Protection Systems, Noordwijk, NL, 25-27 March 1998.
- [71-82] B. Fornari et al.: Alenia Spazio, (I)
'ALS051: An Ablative Material for Reentry Capsules'. Second European Workshop on Thermal Protection Systems Stuttgart, 23-25 October 1995,
ESA-WPP-103
- [71-83] B. Capdepuy et al : Aerospatiale, (F)
'2.5D C/C: A robust material for reusable launcher application to X33 nosecap'. Third European Workshop on Thermal Protection Systems Noordwijk, NL, 25-27 March 1998.
- [71-84] U. Trabandt et al: Daimler-Benz/BF Goodrich, (D)
'CMC Elevon Design Concepts for X-33/RLV' [Abstract].
Third European Workshop on Thermal Protection Systems Noordwijk, NL, 25-27 March 1998.
- [71-85] A. Muhlratzer et al : MAN Technologie, (D)
'Design & Manufacture of CMC Components for Reentry Vehicles'. Third European Workshop on Thermal Protection Systems, Noordwijk, NL, 25-27 March 1998.
- [71-86] H. Lange & M. Bickel: MAN Technologie, (D)
'CMC fasteners for Hot Structures'.
Third European Workshop on Thermal Protection Systems Noordwijk, NL, 25-27 March 1998.
- [71-87] K. E. Handrick: MAN Technologie, (D)
Private Communication, April 1997.

- [71-88] J. Antonenko et al : Daimler-Benz, (D)
'Recent Advances of the Flexible External Insulation'.
Third European Workshop on Thermal Protection Systems Noordwijk,
NL, 25-27 March 1998.
- [71-89] H. Pfeiffer & D. Roos: MAN Technologie, (D)
'CMC Body Flap for NASA's X-38 Test Vehicle'.
Third European Workshop on Thermal Protection Systems Noordwijk,
NL, 25-27 March 1998.
- [71-90] M. Dogigli et al : MAN Technologie, (D)
'CMC Hinge Joints for Hot Structures'.
Third European Workshop on Thermal Protection Systems Noordwijk,
NL, 25-27 March 1998.
- [71-91] H.G. Wulz et al: Daimler-Benz, (D)
'Dynamic Sealing of Hot CMC Control Surfaces'.
Third European Workshop on Thermal Protection Systems Noordwijk,
NL, 25-27 March 1998.
- [71-92] 'Thermomechanical assessment of Polymeric Foams dedicated to Liquid Hydrogen Tank Insulations'
ESA-ESTEC Metallurgy Report No. 2607 (December 1999); PDF file date:
Jan 2000
- [71-93] 'Characterisation of polymeric foams for the insulation of cryogenic tanks on reusable launchers'
AMTT - Aerospace Materials Technology Testhouse, Seidersdorf;
Contract No: ERBFMGECT980141; PDF file date: July 2000
- [71-94] W. P.P. Fischer: EADS ST GmbH
'Surface Protected Flexible Insulation SPFI - A new Oxide Ceramic based TPS'
ESTEC Contract 15867/01/NL/MV: CCN5 (2006)
- [71-95] J. Antonenko: EADS ST GmbH
'Flexible external insulation (FEI): Performance and data for X-38 nose cap and nose skirt application'
ESTEC Contract 15867/01/NL/MV: CCN5 (2006)
- [71-96] J. Antonenko: EADS ST GmbH
'High Temperature Insulation HTI and IFI: Performance and data for X-38 nose cap and nose skirt application'
ESTEC Contract 15867/01/NL/MV: CCN5 (2006)
- [71-97] 'The Columbia Accident Investigation Board Report'
108th Congress Science Committee Hearing – September 2003
<http://commdocs.house.gov/committees/science/>
Publication No.: hsy89216.000

72

SPF/DB titanium designs

72.1 Introduction

72.1.1 General

Superplastic forming is a single-shot manufacturing technique applied to complex designs usually with integral stiffening. When combined with diffusion bonding, the process becomes particularly versatile. Combined design, manufacturing and materials selection can produce cost-effective constructions.

Titanium alloys have been the preferred materials, starting with Ti-6Al-4V. Aluminium alloys can also be used but the diffusion bonding is more difficult, owing to the tenacity of the oxide film.

72.1.2 Aircraft components

There are numerous potential applications for SPF/DB titanium in aircraft constructions. When it has been applied, the cost effectiveness of the process has been the main driver rather than any inherent need to use the high-temperature characteristics of titanium. The ability to use minimum gauge sections in conjunction with the good stiffness and strength characteristics of titanium has negated its higher density compared with aluminium alloys or CFRP. The route has been identified as offering technical solutions to some spacecraft requirements where stability, but not high-temperature performance, is necessary, Ref. [72-1], [72-2].

72.1.3 Space applications

The high-temperature capabilities of titanium materials are more important in spaceplane applications and the SPF/DB route is the preferred manufacturing method. In the drive to use materials at the highest possible temperatures, more advanced alloys than Ti-6Al-4V have been employed, including titanium aluminides.

This chapter highlights the type of components and structures already made by the Ti SPF/DB route and the possible applications for the newer materials.

72.2 Basic SPF/DB process

72.2.1 Superplastic forming

SPF uses the ability to slowly deform and elongate a material by several hundred percent. When the material in sheet form is clamped between the faces of a steel mould it can be pressurised to conform to the internal mould profile. Titanium alloys deform in the temperature range 900°C to 1000°C. Deformation strain rates are slow and controlled, so processing can take several hours.

72.2.2 Diffusion bonding

When two sheets are pressed in contact and heated to a sufficient temperature, diffusion bonding (DB) occurs, giving a joint which is metallurgically undetectable. Bond strengths are equivalent to those of the parent alloy. If a masking material is used, only exposed areas are bonded. Stacks of masked sheets are pre-bonded before being placed in the SPF mould facility.

The process can encompass two to four sheet configurations, as shown in Figure 72.2.1, Figure 72.2.2 and Figure 72.2.3. The four sheet construction enables complex integral stiffening and double wall thickness to be produced by enabling additional bonding to occur in conjunction with the forming cycle. These are from the 'Thin Sheet' route, however, 'Massive' diffusion bonding can be used on thick plate for load bearing structures such as firewalls.

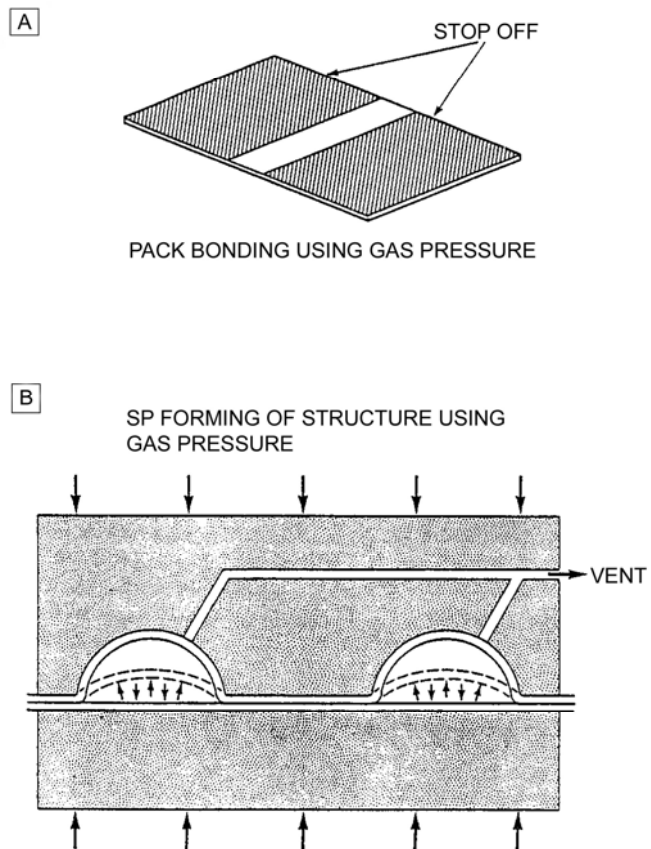
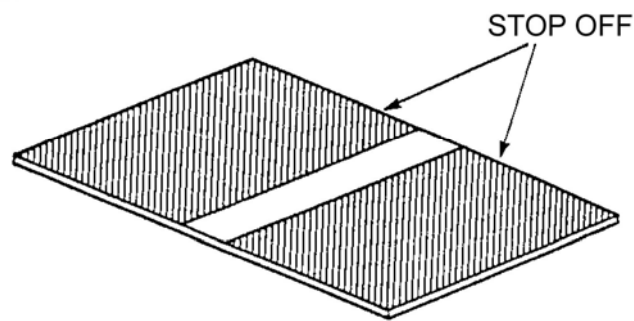
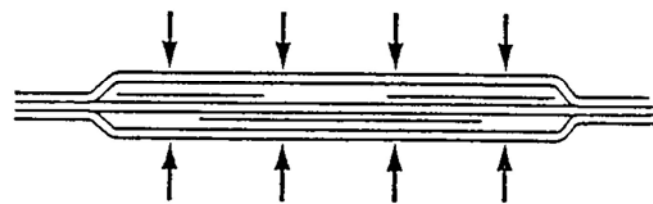
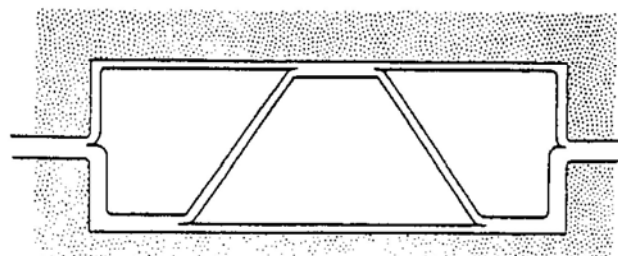
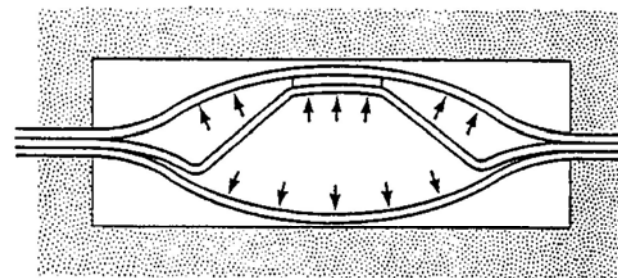


Figure 72.2-1 - SPF/DB: Two sheet configuration

A CORE SHEET**B** PACK BONDING**C** FORMING**Figure 72.2-2 - SPF/DB: Three sheet configuration**

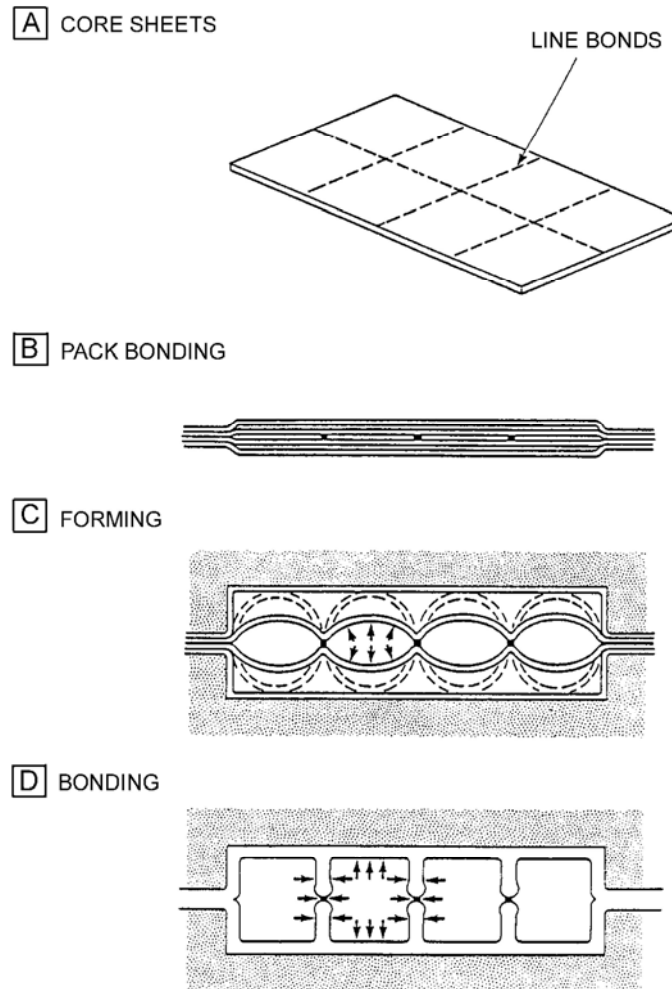


Figure 72.2-3 - SPF/DB: Four sheet configuration

72.3 Process attributes

The essential features of the SPF/DB process which make the manufacture of titanium structures cost and weight effective are:

- the process employs simple titanium starting blank forms;
- simultaneous forming and joining processes are independent of component size;
- parts counts are reduced;
- fasteners and adhesives are eliminated;
- stabilising features can be introduced at low cost;
- a material with high specific properties and corrosion resistance can be used;
- it is attractive for medium production runs of between tens and several hundreds of units per annum.

These attributes have been defined by aircraft manufacturing practices, where the majority of the experience and facilities are found.

72.4 Titanium alloys

The α - β titanium alloy Ti-6Al-4V remains the most popular choice for SPF/DB primarily because of its wide availability. There is no reason why other alloys cannot be used as Table 72.04.1 indicates, Ref. [72-3]. However, availability of sheet in the desired thickness is a limiting factor.

Table 72.4-1 - Titanium alloys: Superplastic characteristics

Alloy	Test temperature (°C)	Strain rate ($\times 10^{-4} \text{ s}^{-1}$)	Strain Rate sensitivity factor (m)	Elongation (%)
Commercially pure Ti	850	1.7	-	115
α-β Alloys				
Ti-6Al-4V	840-870	1.3 to 10^{-3}	0.75	750-1170
Ti-4.5Al-5V	850	8	0.70	700-1100
Ti-6Al-2Sn-4Zr-2Mo	900	2	0.67	538
Ti-4.5Al-5Mo-1.5Cr	870	2	0.63-0.81	>510
Ti6Al-4V-2Ni	815	2	0.85	720
Ti-6Al-4V-2Co	815	2	0.53	670
Ti-6Al-4V-2Fe	815	2	0.54	650
Ti-5Al-2.5Sn	1000	2	0.49	420
Near β and β Alloys				
Ti-15V-3Sn-3Cr-3Al	815	2	0.5	229
Ti-13Cr-11V-3Al	800	-	-	<150
Ti-8Mn	750	-	0.43	150
Ti-15Mo	800	-	0.6	100

A problem with the availability of the more advanced alloys was encountered during processing studies at Dornier. Successful forming trials were undertaken with, Ref. [72-4], [72-5]:

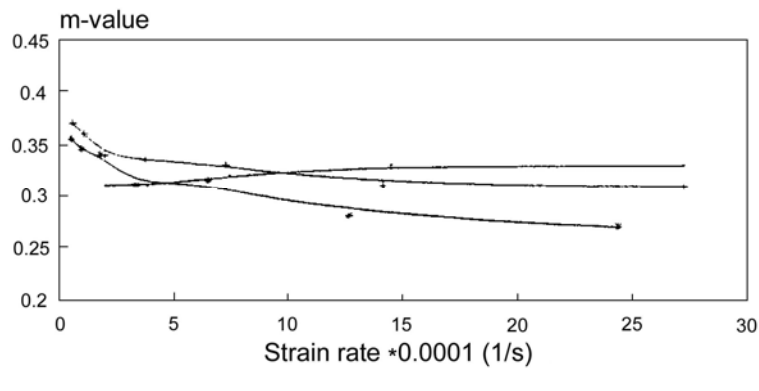
- IMI 829,
- IMI 834 (successor to IMI 829), and
- Timet Ti 1100.

[See also: Chapter 47]

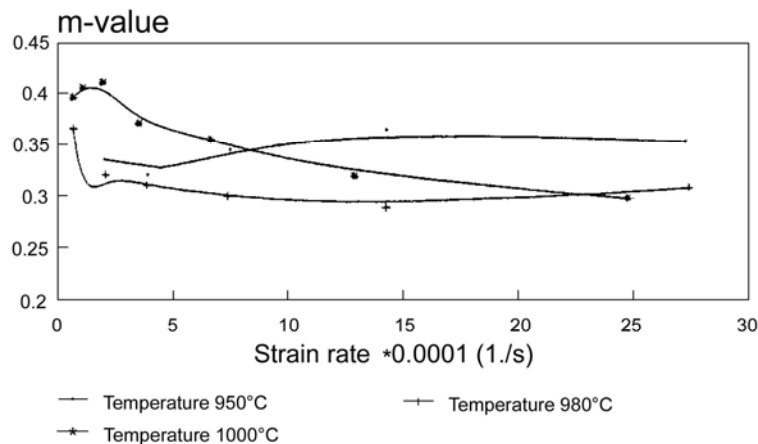
The results of the formability trials for IMI 834, Ref. [72-6], are given in Figure 72.04.1.

IMI 834 is best formed at 1000°C with a forming pressure of 2MPa for 3 hours.

[See also: Figure 47.04.1]



A: IMI 834 m-values, L-direction



B: IMI 834 m-values, L-T direction

Figure 72.4-1 - Superplastic forming: Strain rate sensitivity in formability trials on Ti alloy IMI 834

72.5 Aluminium alloys

The SPF of aluminium has been applied to serial production of aircraft parts, Ref. [72-4]. Supral® is a well-established aluminium sheet suitable for forming.

Other alloys formed include:

- 5083 Al-Mg-Mn,
- 7475 Al-Zn-Mg-Cu, and
- Aluminium-lithium 8090 Al-Li-Mg-Cu.

[See also: Chapter 46]

SPF parts made from aluminium include:

- Dornier 228 aircraft panels
- Airbus A320 7475 fuselage inspection door
- A320 tail cone
- Aircraft fuselage sections in 8090 alloy
- Sine wave spars for vertical stabilisers

72.6 Access doors and ducting

72.6.1 General

The first SPF titanium items to be manufactured by BAe for an Airbus aircraft were TIG welded slat track and jack cans which were installed in the A310 aircraft in early 1982. These were followed in 1984 by underwing access doors for all subsequent A320, A330 and A340 aircraft, Ref. [72-7].

72.6.2 Slat track/jack cans

These are located in the front spar of the A310 aircraft at two positions in each wing where, uniquely on the A310, both the slat operating tracks and jack ends penetrate through the spar and into the fuel tank, as shown in Figure 72.06.1, Ref. [72-7].

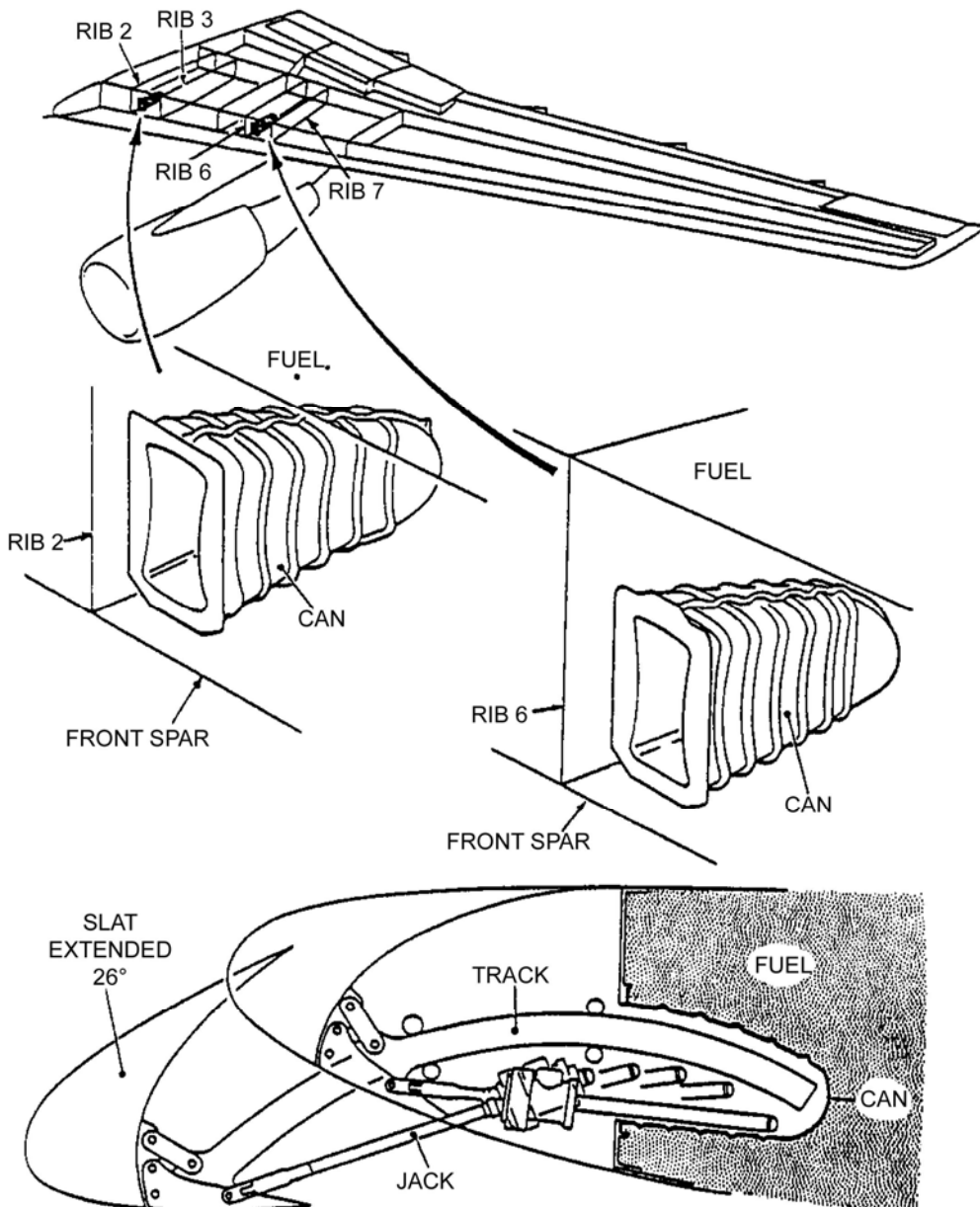


Figure 72.6-1 - SPF/DB titanium alloy: Slat track and jack for Airbus A310

This results in a space envelope requirement for the can of approximately rectangular cross section 500mm x 250mm x 120mm. The unit has to withstand the critical condition of resistance to fuel surge pressure in the wing associated with a crash landing. In this condition the unit has to remain fuel tight, Ref. [72-7].

The basic concept for this can is an integrally-stiffened, four-sided tapered box with a radius end. The starting thickness for the sheet titanium is 1.8mm which in places can be thinned to 0.7mm by forming. Tolerances of better than $\pm 0.25\text{mm}$ can be maintained on the 500mm dimension.

72.6.3 Underwing access doors

The underwing access doors are full SPF/DB constructions. These doors are located at regular intervals along the underside of the wing fuel tanks, as shown in Figure 72.06.2, Ref. [72-7].

There are 24 units on the A310 aircraft. The doors are either:

- load bearing, or
- non-load bearing.

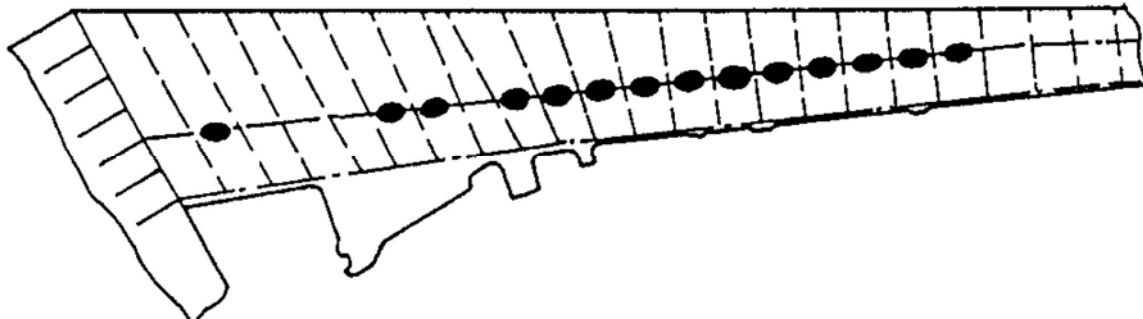


Figure 72.6-2 - SPF/DB Ti: A310 underwing access door locations

The approximate door size is 500mm in length and 300mm in width, with an oval form and door depths varying according to the local wing skin thickness.

Additional requirements which influenced design included:

- fuel pressure loading of 4.5bar in a crash situation,
- pressure fatigue resistance,
- anti-fret performance,
- provision of door clamping arrangement,
- lightning strike and fire resistance,
- impact resistance from run-way debris.

Initial blank sheet thicknesses were 0.8mm, giving minimum finished thicknesses of 0.3mm to 0.4mm.

The design incorporated several features:

- Integral stiffeners between bolt holes and across the shortest span, terminating short of the seal groove to retain seal integrity.
- Peripheral buttresses, locally thickened to support bolt loads.
- Convolutions formed on the upper pressure face, which are more structurally efficient than a flat skin.
- Short swage type stiffeners around the upper periphery to stiffen the panel edges.

72.6.4 Other SPF/DB components

- Ducting for Tornado fighter aircraft.
- Dornier pulley box for commercial aircraft.

72.7 Spars and stiffened panels

Various aircraft components have been proposed for manufacture by SPF/DB titanium, because of the ability to integrate stiffeners in whatever configuration is required in the available space, e.g. shear panels and sine-wave spars.

For NASP and Sänger type constructions, there is a heavy commitment to the more versatile titanium technologies for intermediate temperature structures.

Stiffened skin panels in the higher performance α - β and β alloys and titanium aluminides are candidates for SPF/DB.

72.8 Struts and cylinders

BAe undertook a study on the possibility of applying SPF/DB to thin walled struts and cylinders for spacecraft, Ref. [72-2].

The versatility of the process was investigated for fluted and corrugated designs.

It was concluded that SPF/DB titanium designs can compete technically with more widely used CFRP or aluminium alloy constructions in satellite structures.

72.9 Leading edges and lateral fins

BAe demonstrated the ability to produce their 125-series 800 aileron in SPF/DB titanium alloy.

For in spaceplanes, both Dornier Luftfahrt and Dassault Aviation have produced wing leading edges in Ti-6Al-4V, Ref. [72-4], [72-5].

Dornier used a modified four-sheet technique to compensate for the change in section depth moving in the direction away from the front surface, as shown in Figure 72.09.1, Ref. [72-5].

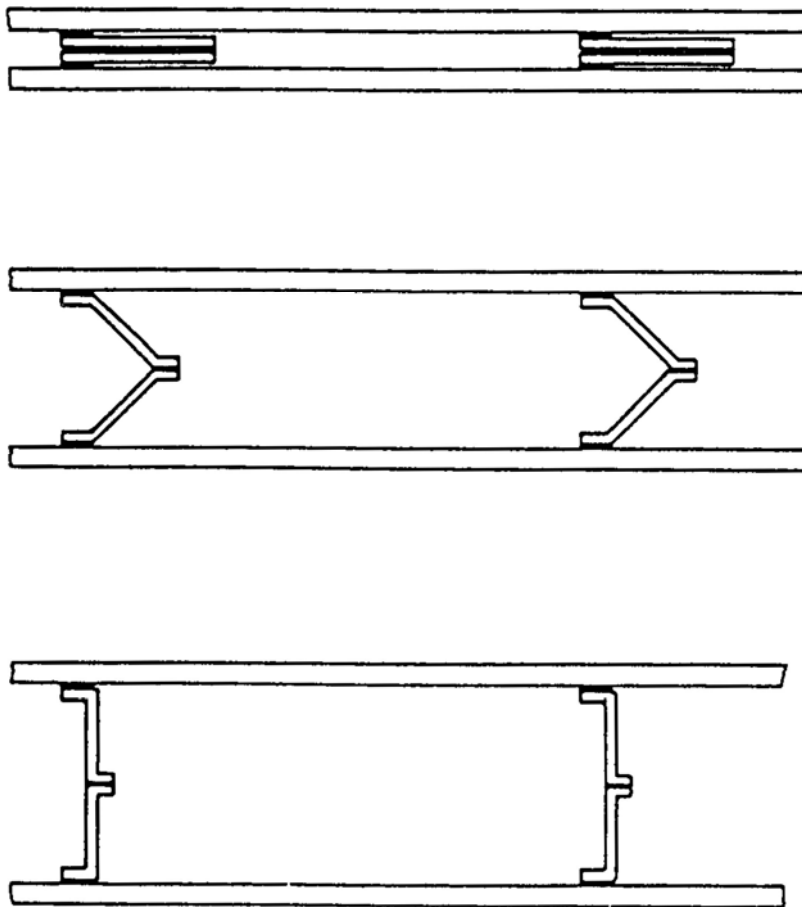


Figure 72.9-1 - SPF/DB: Principle of four-sheet technique for leading edge

72.10 Firewalls

Thick section bulkheads and firewalls have been formed by SPF.

The primary benefits over machined plate versions are the reductions in machining costs and material wastage.

72.11 Pressure vessels

Pressure vessel shells have been made by SPF with diameters up to 1000mm. The shells are subsequently seam welded to form the full sphere. Such pressure vessels are used on the Shuttle Orbiter.

SPF replaced machining of shells from a solid block of alloy on the grounds of reduced costs.

The cold rolling of β alloys, such as Ti-15-3-3 as undertaken by MAN Technologie, can be a cheaper process than SPF because it avoids high temperatures (900°C to 1000°C).

72.12 Cost aspects

SPF/DB titanium components are promoted on the basis of mass- and cost-efficiency.

For the serial production of aircraft components, cost savings of 40% to 50% are claimed over more intensive metal and composite fabrication routes.

The cost savings are application dependent, and mainly apply where complex integrally-stiffened designs are needed within restricted dimensions.

72.13 European facilities

Within aircraft construction, SPF/DB technology tends to be applied only where other fabrication routes cannot produce cost-effective designs because of component shape complexity.

Companies with the expertise and facilities to produce components of up to several metres in size include:

- Alenia Aeronautica (Turin, I).
- British Aerospace (Filton, UK).
- Dassault Aviation (F).
- Dornier Luftfahrt (D).

Space applications requiring only a few items of any one design favour the SPF/DB method, in particular, spaceplane developments.

72.14 References

72.14.1 General

- [72-1] A.K. Green
'Guidelines for the Use of Superplastic Forming of Metals in Spacecraft Construction'
Fulmer Research Laboratories (FRL) Report R878/3A/January 1982 and supplement FRL Report R878/19/July 1985. ESTEC Contract 5497/83/NL/PB(SC)
- [72-2] C.R. Parkinson
'Application of SPF/DB to Spacecraft Structures'
BAe Filton Report, July 1985
ESTEC Contract 5588/83/NL/PB(SC)
- [72-3] Metals Handbook, Volume 2, Tenth Edition
Properties and Selection: Non-ferrous Alloys and Special Purpose Materials
ASM International, ISBN 0-87170-378-5(V.2), 1990
- [72-4] G. Broden
'SPF/DB - A Manufacturing Technique for Lightweight Structures'

ESA Symposium on Advanced Materials for Lightweight Structures,
March 1992, ESA SP-336, p149-154

- [72-5] 'Advanced Materials for Space Transportation'
Dornier GmbH - Battelle Europe Final report, June 1992
ESTEC Contract 8807/90/NL/PP(SC)
- [72-6] G. Broden
'Investigation of SPF/DB Properties of the High Temperature Alloy IMI
834'
Dornier Luftfahrt GmbH Report SY20-220/93, August 1993 ESTEC
Contract 70/87/NL/PP - Work Order No.22
- [72-7] M.H. Mansbridge
'The Introduction of Titanium Superplastically Formed and Diffusion
Bonded Components into Service on Airbus Aircraft'
22nd International SAMPE Technical Conference, November 6-9 1990,
p224-236

73

Propulsion technologies

73.1 Introduction

This chapter highlights the use of advanced structural materials in space propulsion system programmes.

For spaceplanes, more advanced propulsion systems have been proposed which extend materials to the limits of their capabilities. The baseline materials for many single mission and reusable engines are derived from gas turbine developments. Those materials covered have either been applied to, or are intended for use in:

- Launcher engines,
- Shuttle Orbiter engines (SSME),
- Advanced propulsion for SSTO or TSTO spaceplanes,
- Air breathing engines,
- Ramjets or Scramjets,
- Thrusters.

73.2 Propulsion unit requirements

73.2.1 Launcher engines

73.2.1.1 Ariane 5 single mission launcher

The A5 engine specification includes:

- single-cycle, high-temperature excursion with LH/LOX fuel mixture,
- capable of test firings and multiple starts.

73.2.2 Shuttle engines

The SSME, along with its fuel turbopumps, has to withstand multiple firings equivalent to 50 missions, with some refurbishment at defined intervals.

73.2.3 Spaceplane engines

For NASP, Sänger and HOTOL, these include:

- ramjets,
- turbo ramjets,
- scramjets, and
- air breathing engines.

The specification includes:

- extended multiple firings, with reuse for 50 operations,
- engine integrated into the airframe of the vehicle,
- resolve gas flow and cooling problems by efficient design.

73.2.4 Thrusters

For orbit control of satellites and spacecraft, the thrusters withstand thousands of high-temperature firings of short duration (a few seconds) with oxidising combustion gases.

73.2.5 Nozzles

The main combustion zone for engine designs experiences an extremely hot, high-velocity gas environment.

73.3 Fuels

73.3.1 General

These are grouped as either solid or liquid propellants. To propel large vehicles, such as spaceplanes, more efficient hydrogen-oxygen (LH₂/LOX) fuel systems are used.

73.3.2 Solid propellants

These are primarily found in launcher solid boosters. The booster casings are normally steel constructions; reused for Shuttle launches. A typical propellant mixture is:

- Ammonium perchlorate,
- Aluminium powder, and
- Polymer binder.

73.3.3 LH/LOX

Each fuel constituent is kept in separate tanks. After mixing, they are ignited and release high-energy exhaust gases. This usually requires using a twin turbopump arrangement which delivers the two constituents to a thrust chamber for combustion.

The combusted gas temperatures are extremely high; 2500°C to 4000°C. Gas flows are managed to limit the engine internal surface temperatures. Active cooling of engine surfaces can be needed.

Material selection for engine construction considers both the effects of hydrogen and oxidation.

73.3.4 Monopropellants

These, along with bipropellants, are primarily used with smaller thrusters for spacecraft control. The fuels combust spontaneously when released.

73.3.5 Bipropellants

A typical mixture is:

- a nitrogen oxide, e.g. nitrogen tetroxide (NTO), and
- monomethyl hydrazine (MMH).

Combustion temperatures approach 2400°C.

73.4 Ariane 5

73.4.1 General

Ariane 5 is the latest in the series of Arianespace launchers. The propulsion systems have evolved from the Ariane 2, 3 and 4 systems to provide increased launcher lift capacity.

The main units are:

- MPS solid rocket motor
- Main Vulcain engine
- HM 7 third stage engine

73.4.2 MPS solid rocket motor

73.4.2.1 General

The boosters are assembled by Europropulsion at the launch site in Kourou, French Guiana. The P230 version contains 230 tonnes of solid propellant.

The main technologies are:

- Steel cases: D6AC (19.7 tonnes), produced by MAN Technologie,
- EPDM rubber thermal protection, with Kevlar reinforcement (4.9 tonnes),
- Elastomer seals for joints,
- Nozzle: Carbon-carbon composite throat (1.5m diameter). Total nozzle mass is 6.1 tonnes.

73.4.2.2 MPS specification

The specification includes:

- Overall length: 26.7m,
- Maximum internal pressure: 60 bar,
- Burn time: 130 seconds,
- Specific Impulse: 272 seconds,
- Thrust: 5250kN.

73.5 Vulcain engine

73.5.1 General

The Vulcain high-thrust cryogenic engine uses a gas generator cycle, in which liquid oxygen and hydrogen are fed to its combustion chamber by two pumps, each driven by a turbine supplied with hot gases by a single gas generator, Ref. [73-1]. The gas generator is fed concurrently with the main chamber, generating gases at a relatively low temperature. Figure 73.5.1 shows the main components.

High-temperature combustion takes place in the main chamber, cooled by liquid hydrogen circulating through channels in the double-wall, nickel-alloy chamber before being injected for combustion. The divergent section of the nozzle is cooled by the dump cooling method, in which a small fraction of the hydrogen fuel is used as a cooling flow and ejected without burning.

The Vulcain engine is a European development, with SEP as the prime contractor.

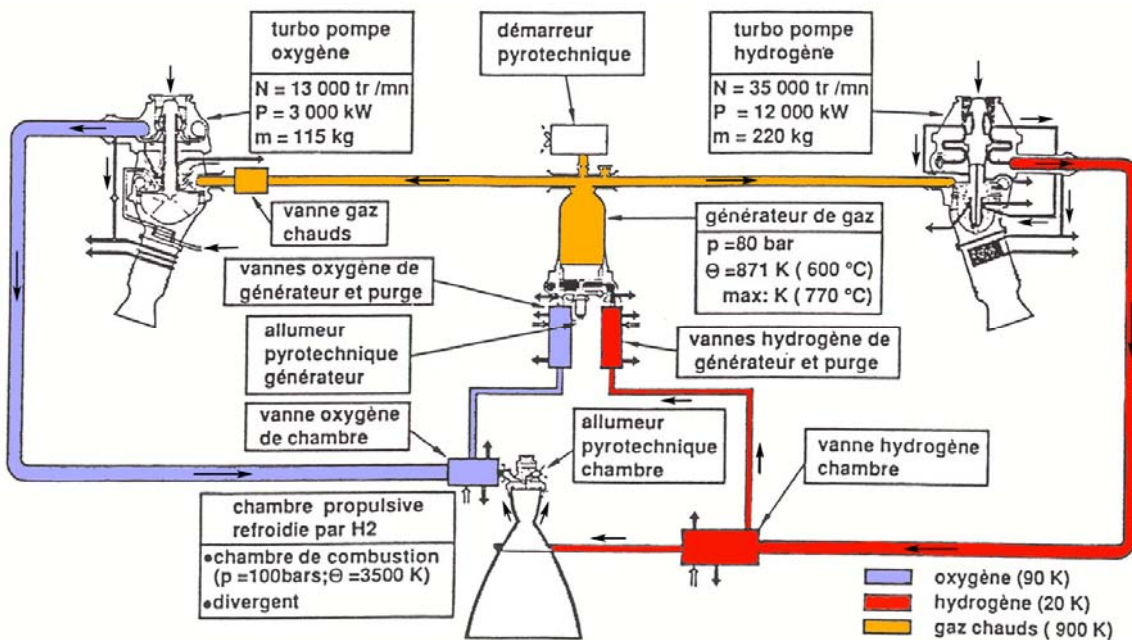


Figure 73.5-1 - Vulcain engine: Schematic diagram

73.5.2 Specification

The main features can be summarised as:

- Fuel: Burns 155 tonnes of LH/LOX fuel, with tanked LH at 20K and LOX at 90K,
- Thrust: 1120kN in vacuum,
- Chamber pressure: 109bar,
- Specific impulse: 430 seconds,
- Thrust chamber length: 3m,
- Nozzle exit diameter: 1.76m
- Total engine mass: 1500kg,
- Turbopumps:
 - Hydrogen; 34000 rpm, developing 11.3MW power,
 - Oxygen; 12900 rpm, developing 2.9MW power,
- LH/LOX ratio: 5.3:1,
- Gas speeds: 4000m/s.

73.5.3 Materials

The materials used in the construction withstand temperatures in the range -253°C to +725°C. Other factors include:

- Thermal expansion behaviours, over the extreme temperature range.
- Material embrittlement can be caused by:
 - cryogenic temperatures, and
 - presence of hydrogen.
- Nickel alloys are extensively used for the cold and hot regions, e.g. Inconel 600, 625, 718 and Waspalloy.
- Titanium alloys are used for the spinning parts of the hydrogen turbopumps.
- Three types of seals were developed (USEP, VSEP, RLSEP) for assembling the engine. These gave good spring-back retention and were of the energised variety, [See: 75.4]
- The main expansion chamber consists of a helical hydrogen cooled Inconel 600 jacket that sustains through its wall the full thermal gradient of -253°C to +725°C in a few tens of millimetres. The immediate combustion chamber is nickel electroplated copper alloy (Narloy) that is also actively cooled with hydrogen.
- The engine uses an igniter nozzle, Ref. [73-2].

73.6 HM 7 engine

73.6.1 General

The HM 7 engine was used for the third stage of Ariane 4 with a thrust of 62kN and is in effect a smaller version of the Vulcain engine, Ref. [73-3]. The thrust chamber is shown in Figure 73.6.1, Ref. [73-3].

The immediate combustion chamber could be extended with a dump cooled nozzle consisting of spirally arranged tubes made from Inconel 600 welded on their outer edges.

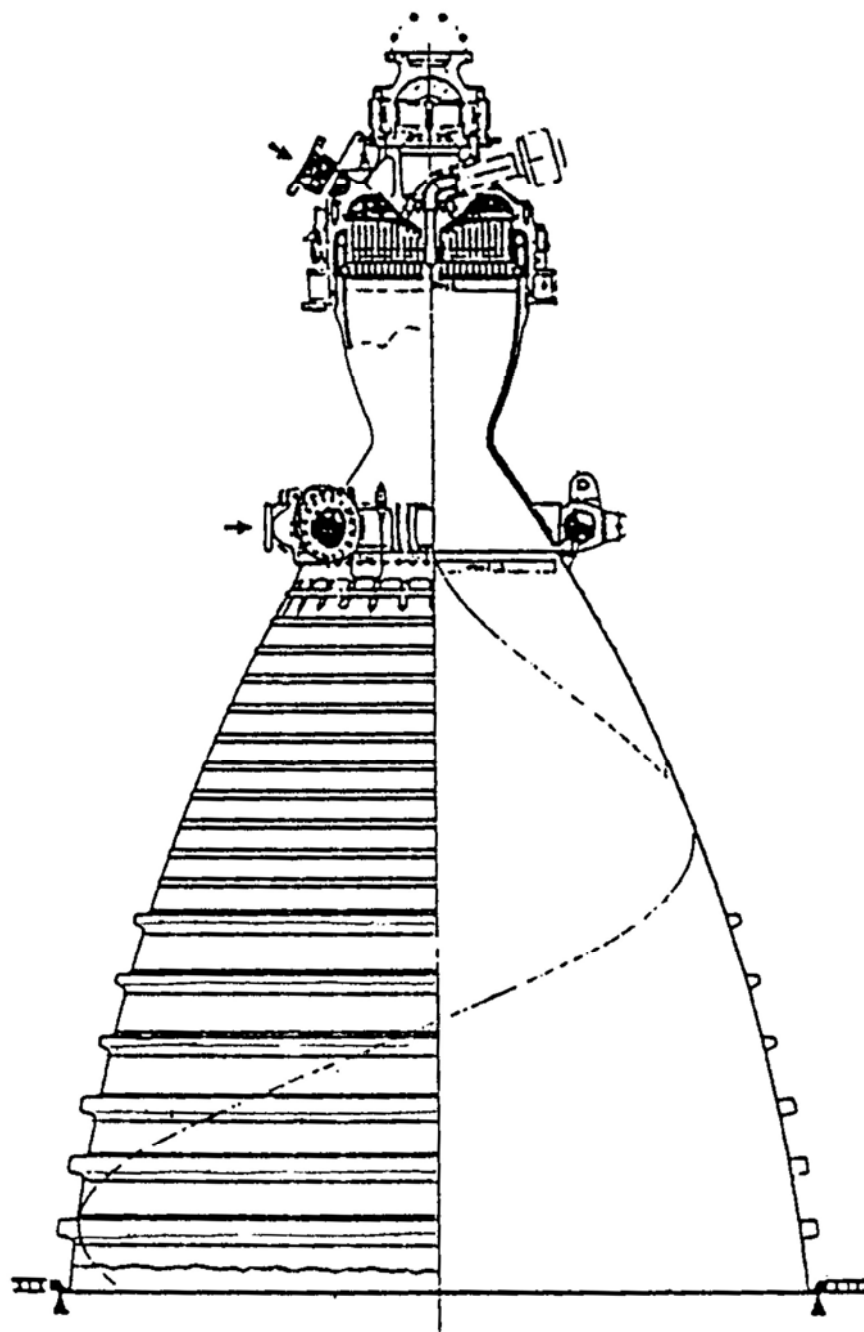


Figure 73.6-1 - Ariane 4 HM 7 engine: Thrust chamber

73.6.2 Nozzle geometry

The features included:

- Length: 1200mm,
- Maximum diameter: 990mm,
- Construction: 242 individual nickel tubes,
- Nickel tube wall thickness: 320 μm ,
- Welding: A total of 13000 operations on 700m of weld,
- Total mass: 31kg.

SEP made a CMC demonstrator nozzle for the HM 7 engine.

73.7 Mage 2 motor

The motor is used to place satellites into orbit and relies on bipropellant fuel (MMH/N₂O₄) stored in tanks, Ref. [73-4].

The motor case comprises of two isotensoid, geodetically-wound domes and a cylindrical section. The pressure vessel is connected via an adapter skirt and flange to the satellite structure. The igniter and the carbon-carbon nozzle are fixed at the polar opening interface fittings.

The materials used in the construction include:

- Metal tank:
 - maraging steel (X2 18Ni 8Co 5Mo).
 - stainless steel (X12 17Cr 7Ni, AISI 301/X2 19Cr 11Ni, AISI 304L). Stainless steels are cryoformed.
 - titanium (Ti-15V-3Cr-3Al-3Sn, Ti-15-3, Ti-6Al-4V).
The Ti-15V-3Cr-3Sn β -alloy is cold rolled.
- Overwrapping: Kevlar reinforced epoxy, [See: Chapter 29].

73.8 Nozzles

Nozzles are largely based on graphite or carbon-carbon constructions intended for short-duration single firings, Ref. [73-6].

In reusable engines, such as ramjets, wholly carbon-based materials lack oxidation resistance for long-term exposure to oxidising gas streams.

Ramjet nozzles in C-SiC have been evaluated and show that they have the basic structural integrity to survive thermal shock, but the effects of hot gas erosion have yet to be resolved, Ref. [73-7].

A variety of nozzle coatings have been evaluated for their ability to withstand hot erosive gas flows, Ref. [73-8], including the more exotic high-temperature ceramics, such as hafnium oxide.

73.9 Space Shuttle Main Engine (SSME)

The SSME is a reusable LH/LOX burning engine manufactured by Rocketdyne, USA. It experiences a similar thermal cycle to that of the Vulcain engine but is capable of reconditioning for multiple uses.

SSME experiences a combination of severe low cycle fatigue (LCF) and high cycle fatigue (HCF), in a hydrogen environment which causes acute concern.

Typical conditions for key components include:

- HPFTP: High pressure fuel (methane/hydrogen) turbopump, 823°C at 39MPa fuel pressure.
- HPOTP: High pressure oxidiser turbopump, 578°C at 39MPa .
- HPFTB: First stage high pressure fuel turbopump blade (uncooled) made in directionally solidified MAR-M-246 alloy rotating at 36000 rpm.

Experience with SSME assists in designing more advanced propulsion systems for SSTO vehicles, e.g. NASP.

73.10 Air breathing engines

73.10.1 General

Various concepts for air-breathing engines, ramjets and scramjets have been put forward for advanced propulsion systems.

All the concepts have some major requirements and problems to be tackled, including Ref. [73-9], [73-10], [73-11]:

- How to use the fuel stored on the vehicle most efficiently.
- How to optimise the amount of fuel carried and make best use of the oxygen in the earth's atmosphere to minimise the load of oxygen fuel at the initial point of launch.
- Designing engine configurations to handle extremely high gas flow velocities (4500+ m/s) through the engine and over the surface of the spaceplane.
- Having the ability to predict those gas flows and defining cooling requirements.
- Adjusting engine inlet profiles to capture air and then switching to LOX fuel intake.
- Selecting lightweight materials to fulfil different functions in the engine, where expectations are:
 - Maximum surface temperatures approaching 2500°C,
 - Heat fluxes of 17MW/m², and
 - Noise levels of 180dB.

Most advanced propulsion systems are at an early point in their development and are confined to small-scale but expensive nozzle, Ref. [73-12], combustor and inlet demonstrators in conjunction with material development programmes, Ref. [73-10].

The NASP programme has a baseline ramjet configuration, as shown in Figure 73.10.1, Ref. [73-10].

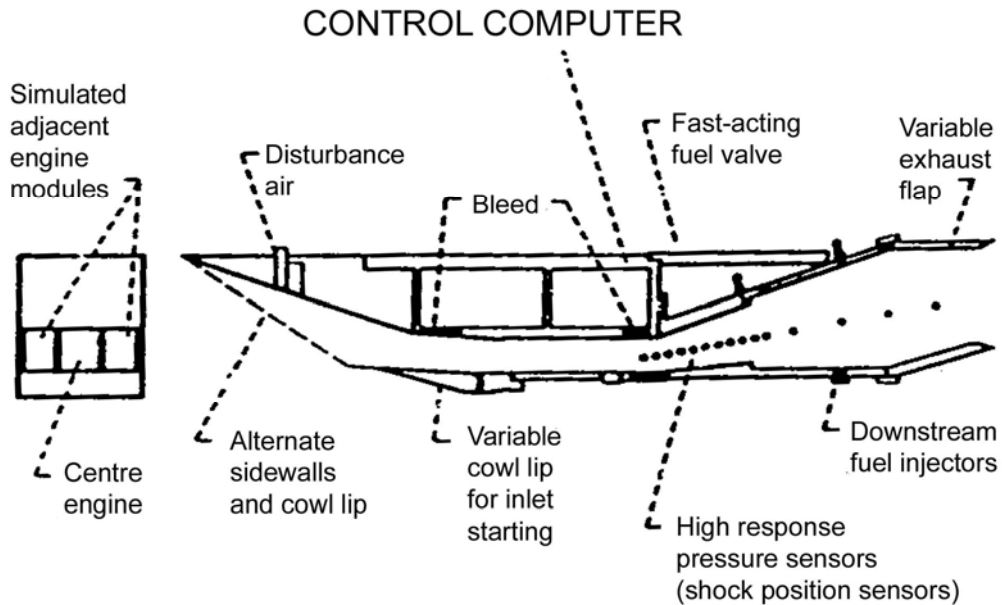


Figure 73.10-1 - NASP: Modified government baseline engine configuration

73.10.2 NASP nozzle development

The nozzle has a variable geometry and uses the vehicle aft end as an expansion surface. The nozzle is highly over-expanded at low to moderate supersonic speeds and hence causes drag. The external burning of fuel is one way of reducing drag. The nozzle functions in an exhaust gas stream at 1925°C.

Small-scale ramjet designs are under development for hypervelocity military missiles, Ref. [73-13]. The use of CFD analysis techniques to predict gas flows is vital in understanding engine design, Ref. [73-14].

73.10.3 European ramjet technology

Both The Netherlands, Ref. [73-15], and Germany, Ref. [73-7], have ramjet technology demonstration programmes. This has resulted in the development of a high temperature vitiator (HTV) which uses methane combustion to preheat the air before it enters the ramjet, Ref. [73-15].

The HTV is made of AISI 310 stainless steel or TZM, with a MoSi₂ ceramic coating.

Combustion gas temperatures can reach 1750°C.

73.11 CMC rocket stator

SEP have manufactured CMC stators, Ref. [73-16]. The geometry is equivalent to that of the metallic versions used in the Ariane HM 7 engine, [See: 73.6].

The CMC stators were developed to raise the gas temperatures from 625°C to 1325°C and so increase the specific impulse of the engine.

Each stator was assembled from two parts:

- central part, which included the hub and 23 vanes, and
- external ring, which interfaced with the turbine housing.

The rings are carbon fibre cloth, densified with SiC by CVI.

Two variants of the CMC stators are shown in Figure 73.11.1, Ref. [73-16].

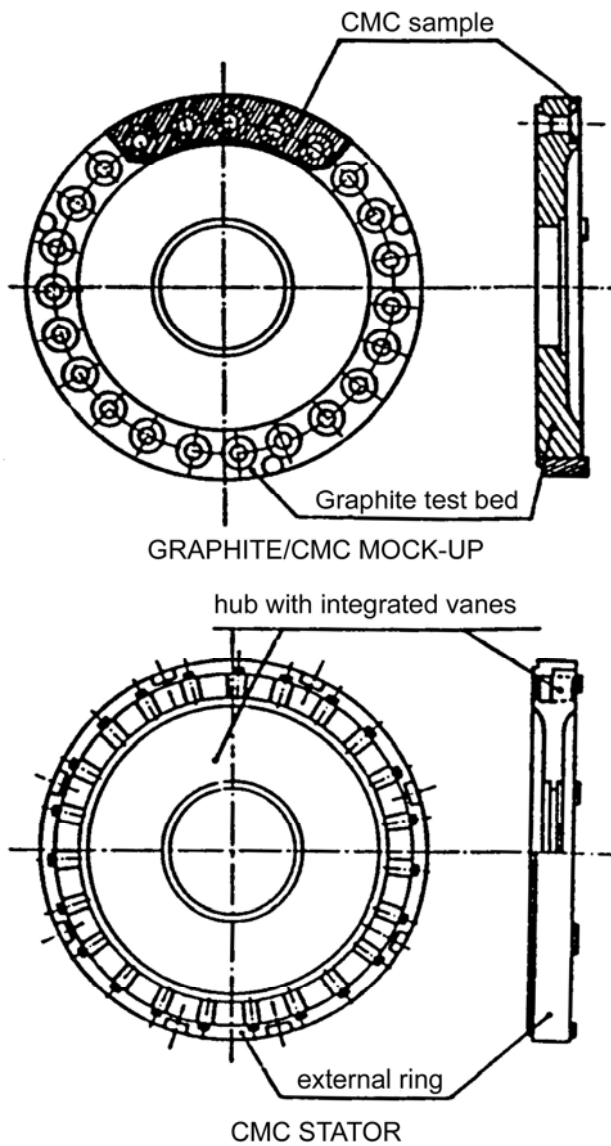


Figure 73.11-1 - Rocket stator CMC components

The rings were successfully tested with a kerosene and air fuel mixture where:

- thermal power transmitted to the vanes on start-up was 2.3MW/m^2 ,
- accumulated firing times of 3000 seconds were achieved,
- maximum calculated induced stress in the material was 110MPa , i.e. approximately 50% of ultimate,
- multiple firings were sustained.

73.12 Metal thrusters

Spacecraft control thrusters delivering up to 6000N are usually metallic constructions with a refractory metal for the hot throat region. This has traditionally meant niobium alloy with a disilicide slurry coating for oxidation protection. This construction is limited to operating temperatures of 1400°C, if prolonged life is to be guaranteed during thousands of thermal cycles, Ref. [73-17].

Increasing the maximum operating temperature can improve the efficiency of the thruster and fuel load combination. This can now be achieved by using iridium-coated rhenium constructions, Ref. [73-18].

A 15 hour life has been claimed with the throat operating at 2200°C, for over 100,000 thermal cycles, with MMH/NTO bipropellant. The intention is to scale up from 22N to a 445N thruster system.

73.13 CMC thrusters

The feasibility of producing spacecraft and Hermes thrusters in CMC materials was studied, Ref. [73-19], to complement metal thrusters, [See: 73.12].

SEP have manufactured a number of thrusters in SEPCARBINOX® C-SiC and CERASEP® SiC-SiC for 5N, 20N, 200N and 6000N units, Ref. [73-18]. These have been fired with wall temperatures of 1700°C

73.14 References

73.14.1 General

- [73-1] J. Gastal & J.R.L. Barton
'VULCAIN : A Cryogenic Engine for Ariane 5'
Proceedings of the Hydrogen Conference, Paris, 22-25 June 1992 EE92V
93022
- [73-2] J.E. Buter & G.K. Troost
'Results of Post-firing Examinations of Igniter Nozzles of the Vulcain
Engine'
ESA Symposium on Space Applications of Advanced Structural
Materials, March 1990, ESA SP-303, p273-274
- [73-3] D.B. Wolf & R.C. Nicolay
'Welded Nozzle Extension for Ariane Launch Vehicles'
Meeting: Welding in Space and the Construction of Space Vehicles by
Welding, Maryland, USA, 24-26 September 1991, p230-246
- [73-4] R. Forster
'Application of Advanced Structural Materials in Propellant Tanks and
Pressure Vessels'
ESA Symposium on Space Applications of Advanced Structural
Materials, March 1990, ESA SP-303, p261-266
- [73-5] P. Donguy & J. Broca
'High Temperature Composite Materials for Rocket Propulsion'.
Application of Advanced Material for Turbomachinery and Rocket
Propulsion

- AGARD Conference, 3 - 5 October 1988, AGARD-CP-449
Paper 23, ISBN 92-835-0498-4
- [73-6] E.v. Gellhorn et al
'Silicon-Carbide Coated Carbon-Carbon - An Advanced Material for Rocket Systems'
Application of Advanced Material for Turbomachinery and Rocket Propulsion. AGARD Conference, 3 - 5 October 1988
AGARD-CP-449, Paper 19, ISBN 92-835-0498-4
- [73-7] H. Hald
'Development and Real Test of a Ramjet Nozzle made of Liquid-silicon-infiltrated C/SiC'
ESA Symposium on Space Applications of Advanced Structural Materials, March 1990, ESA SP-303, p283-292
- [73-8] G.R. Adamczyk
'Thermal Protection Using Very High Temperature Ceramics'
Proceedings of a NASA Workshop: Current Technology for Thermal Protection Systems, 11-12 February 1992, Langley Research Centre, Virginia. NASA Conference Publication 3157 p63-76
- [73-9] Aeropropulsion 91
Proceedings of a NASA Conference, NASA Conference Publication 10063
- [73-10] R.R. Weiss & D.S. MacKay
'Future of Space Propulsion'
AIAA-92-1699
- [73-11] W.J.D. Escher et al
'Status of NASA's Earth-to-Orbit Propulsion Technology Program'
Space Technol. Vol.13, No. 5, p457-466, 1993
Also Paper IAF-91-258, Oct 1991
- [73-12] C.J. Trefny et al
'Overview of NASP Nozzle Research'
Paper 7 of Aeropropulsion '91
- [73-13] Airbreathing Propulsion for Missiles and Projectiles
AGARD Conference, 11-15 May 1992, AGARD-CP-526
ISBN 92-835-0685-5
- [73-14] CFD Techniques for Propulsion Applications
AGARD Conference, 27-31 May 1991, AGARD-CP-510
ISBN 92-835-0659-6
- [73-15] S.R. Birjimohan et al
'Verification of a High Temperature Vitiator'
First ESA/ESTEC Workshop on Thermal Protection Systems ESTEC, Noordwijk, 5-7 May 1993, ESA-WPP-053 (August 1993) p363-368
- [73-16] J. Berque & J.M. Georges
'Test of a CMC Liquid Propulsion Rocket Engine Turbine Stator'
AIAA-92-3131
- [73-17] Application of Advanced Material for Turbomachinery and Rocket Propulsion. AGARD Conference, 3 - 5 October 1988

AGARD-CP-449, ISBN 92-835-0498-4

- [73-18] R.H. Tuffias et al
'CVD Fabrication Applied to Advanced 2200°C Chemical Rocket Combustion Chambers'
Surface Modification Technologies IV, Eds.T.S. Sudershan et al The Minerals, Metals & Materials Society, 1991, p855-864
- [73-19] A.C. Mathieu & E. Soler
'CMC Materials for a High-performance 20N Thruster'
ESA Symposium on Space Applications of Advanced Structural Materials, March 1990, ESA SP-303, p277-282

74**Protective coatings**

74.1 Introduction

Protective coatings are important in high-temperature applications. As their development and processing are application dependent, they form an important part of component design.

Coatings are applied to those surface areas of finished components experiencing arduous service conditions.

[See also: [47.10](#) for coatings applied to titanium alloys]

[See also: [48.9](#), [48.10](#), [48.11](#), [48.12](#), [48.13](#) and [48.14](#) for superalloy coating types and their influence on design]

[See also: [54.4](#) for C-C oxidation protection systems]

The characteristics required of coatings are complex and inter-dependent. Some of the factors to consider include:

- ease of processing,
- adhesion to the substrate,
- protective coverage of the substrate,
- desired life expectancy,
- predictable behaviour.

Most coatings perform a sacrificial role in protecting a substrate that cannot otherwise survive the operating environment.

Features of coatings include:

- physical and chemical coating composition usually changes through its working life,
- progressive coating consumption occurs by oxidation and environmental corrosive species in the environment,
- a diffusion transition zone exists between coating and substrate,
- they are expected to sustain thermal shock and cycling.

Coating technology is an extremely complex subject; Ref. [74-1], [74-2], [74-3] discuss this in greater depth.

This chapter details coatings and high-temperature applications relevant to space programmes, such as:

- Aerodynamic surfaces of spaceplanes, e.g.
 - Ti,
 - TMC,
 - C-C constructions, and
 - C-SiC and SiC-SiC.
- Propulsion system components, e.g.
 - Ti materials,
 - Ni alloys,
 - CMCs, and
 - C-C.

[See also: Chapter 70 for thermo-structural designs; Chapter 71 for TPS; Chapter 73 for propulsion technologies requiring coatings]

Most high-temperature coating development comes from the requirements of gas-turbine engines. Space programmes rely heavily on that accumulated experience.

The life of gas-turbine engines far exceeds those of space structures or propulsion units. However, this is offset by higher operating temperatures in space systems.

74.2 Coating functions

74.2.1 General

Coating functions are linked to the intended applications and described here in fairly simplistic terms. The substrate material and the coating functions drive its selection. The process technique for depositing the coating is also important because it determines:

- coating composition,
- coating thickness,
- ability to apply multi-layers (multiplex),
- overall coverage in surface recesses and cooling passages.

74.2.2 Application requirements

74.2.2.1 Spaceplane aerodynamic re-entry surfaces

The considerations include:

- oxidation protection,
- low surface catalicity,
- high surface emittance,
- resistance to high surface fluxes, typically up to 10MW/m^2 ,
- resistance to high velocity gas erosion,
- thermal shock resistance,
- life expectancy of 50 hours at highest temperature for 100 thermal cycles.

74.2.2.2 Propulsion systems

The considerations include:

- oxidation protection,
- resistance to hydrogen embrittlement, for LH/LOX systems,
- high surface emittance,
- resistance to high surface fluxes, variable, but can reach 50MW/m^2 ,
- resistance to high velocity gas erosion,
- thermal shock resistance,
- thermal insulation of substrate, as in thermal barrier coatings (TBC),
- life expectancy dependent on single or re-usable mission requirements.

74.3 Passivation

74.3.1 General

Passivation is the simplest form of protective coating and readily occurs with some materials. It results from the exposure of the surface to an oxygen-containing environment whereupon the immediate surface layer of the material oxidises.

The process is limited to a very thin surface layer (submicrometre) as the oxide formation inhibits further penetration of oxygen to the underlying material.

If the temperature of the substrate is raised sufficiently then the passivation can be overcome and more penetrative oxidation results.

74.3.2 Materials

Both titanium and aluminium alloys passivate immediately on exposure to air at room temperature.

Silicon carbide when heated above 800°C in air undergoes a surface conversion to silica (SiO_2), which forms a protective layer to inhibit further oxidation. The formation of an oxide layer resists oxygen penetration to the substrate, and is an important part of high-temperature-coating formulation. Some protective oxide scales offer greater penetration resistance than others.

74.3.3 Coating adhesion

Assuming that the appropriate coating formulation to inhibit oxidation and corrosion is identified, it has to adhere to the substrate during the required operational life. Adhesion is best achieved by diffusion bonding to the substrate.

As the coating can have a coefficient of thermal expansion (CTE) very different from that of the substrate, an intermediate bonding layer can be needed in order to obtain a more gradual transition.

Given all the combined functions of a coating, many are multiplex (multi-layer) systems designed for specific applications.

Figure 74.3.1 indicates some properties of coating and substrate combinations, which can be controlled to ensure optimum performance, Ref. [74-1].

Properties are controlled to ensure optimum performance for any given application.

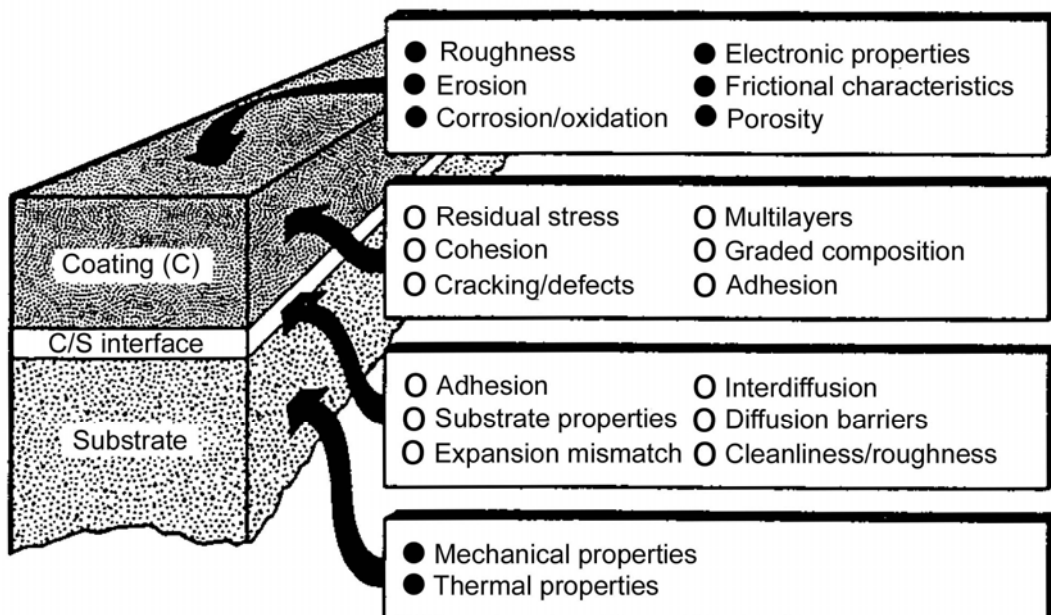


Figure 74.3-1 - Coatings: Properties of coating, substrate and interface

74.4 Basic coating types

74.4.1 General

The basic types of coating are viewed in conjunction with the available processing routes, Ref. [74-1], [74-2].

[See: 74.5]

74.4.2 Diffusion coatings

These are obtained by diffusing an element, e.g. Al, Cr, Si, into the surface of a substrate, whereupon a reaction occurs and the surface is converted to a compound, e.g. Ni to NiAl as in superalloys or C to SiC in C-C composites.

The coatings are thin so as to control the residual stresses. They form an integral part of the substrate and are well bonded, [See: 88.10].

74.4.3 Overlay coatings

74.4.3.1 General

An overlay results from the direct deposition of a coating formulation onto a substrate. A transition exists between the two phases unless diffusion can be induced between the two by thermal treatment. Obtaining good adhesion between two dissimilar materials is essential but problematical.

Overlay coatings can be applied to most substrates by many routes, e.g. PVD, CVD, thermal spraying, as slurries or sol-gels.

74.4.3.2 MCrAlY type

These are specially formulated for application to superalloys, usually nickel-based alloys, applied as overlay coatings. Their composition can be adjusted to assist diffusion bonding and are formulated for specific aggressive environments.

74.4.3.3 Thermal barrier coatings (TBC)

TBC formulations are designed to provide thermal insulation to the substrate and are usually applied to superalloys. Their function reduce the operating temperature of the substrate so that greater efficiency can be gained by using a higher temperature gas stream.

74.5 Coating processes

74.5.1 General

Most coating processes have been developed for gas-turbine-engine requirements, Ref. [74-1], [74-2]. These in turn have been adapted in many ways to achieve improvements in:

- coating composition,
- reduced residual stresses,
- reduced coating porosity,
- mass production requirements,
- surface coating coverage, and
- cost reduction.

In most coating processes, the components are placed in a controlled environment during deposition, e.g. within a vacuum chamber. Large items (several metres in size) can prove difficult to coat.

[See also: Chapter 88 for manufacturing techniques]

74.5.2 Slurry coating

74.5.2.1 General'

These are the simplest to apply and are fired to give the final coating. The facilities required are basic, but control of the process to give even deposition can be difficult.

The slurry is usually formulated from powders (coating composition), a binder and a solvent. The route is similar to that for sol-gel processing, [See also: 88.16].

74.5.2.2 Applications

These include:

- Glassy-phase outer layer for C-C protection systems, e.g. Tetraorthoethylsilicate (TEOS) pyrolysed to silica.
- Disilicide coatings applied to niobium and tantalum attitude control thrusters.

74.5.3 Physical vapour deposition (PVD)

74.5.3.1 General

A coating formulation is transported from a source through a gas phase, or vacuum, and deposited onto the substrate. This is commonly achieved by:

- evaporation,
- sputtering, or
- ion implantation.

Complex shapes are rotated because deposition occurs adjacent to the source on the immediately exposed surfaces. Poorly accessible regions cannot be coated, [See: [88.20](#)].

74.5.3.2 Applications

Coating nickel alloy components with MCrAlY compositions.

74.5.4 Enhanced physical vapour deposition (PVD)

The limitations of the basic PVD method, [See: [88.20](#)], can be reduced by the introduction of additional energy sources, including:

- plasmas,
- lasers,
- reactive sputtering,
- argon discharge,
- electron beam evaporation, and
- ion implantation.

74.5.5 Thermal spraying

74.5.5.1 General

Thermal spraying is the generic name for a family of processes used to produce thick overlay coatings. A material, often in powder form, is heated rapidly in a hot gaseous medium and simultaneously projected at high velocity onto the substrate. The well-known processes include:

- wire spraying,
- electric arc spraying,
- powder flame spraying,
- 'D' gun (detonation) combustion,
- high-velocity flame spraying (HVFS), and
- plasma spraying.

[See: [88.19](#)]

74.5.5.2 Applications

TBCs on nickel alloy components.

74.5.6 Chemical vapour deposition (CVD)

74.5.6.1 General

CVD relies on a controlled gas-phase chemical reaction to deposit the desired element or binary compound. The classical CVD method is by thermal activation of the optimum gas composition in the optimum low pressure environment. If the temperature is too high, poor adhesion results, due to high residual stresses in the coating.

CVD has excellent 'throwing-power' enabling comprehensive coating coverage on recesses and channels, [See: [88.21](#)].

74.5.6.2 Applications

As CVD is limited to elements and simple compounds, it is predominantly used for overlay coatings such as:

- deposition of SiC overlay coatings on C-C or C-SiC composite components,
- applying constituents for a multiplex coating, including:
 - TiB₂,
 - Si₃N₄,
 - C, and
 - AlN.
- applying refractory metal coatings for oxidation and erosion protection of nozzles and thrusters, e.g.:
 - tungsten (W),
 - rhenium (Rh), and
 - iridium (Ir).

74.5.7 Enhanced chemical vapour deposition (CVD)

Owing to the temperature limitations of some substrate and coating combinations, an additional energy source can be beneficial for some CVD methods in order to maintain lower substrate temperatures. The additional energy can be provided by:

- plasmas,
- lasers, and
- microwaves.

74.5.8 Other processes

These include:

- Pack cementation process for diffusion coatings.
- Electroplating, e.g. Cu and Ni
- Electroless deposition, e.g. Ni

74.6 Coatings: Titanium components

74.6.1 NASP

74.6.1.1 General

Titanium has been proposed for much of the exposed surface of NASP, Ref. [74-4]. For the life requirements of the spaceplane, surface coatings are used to provide:

- oxidation resistance,
- high emissivity, and
- low surface catalysis.

The coating therefore has a thermal control function in addition to providing protection. Various process routes have been studied for applying coatings, Ref. [74-4].

74.6.1.2 Reactive slurry coatings

The typical coating is an intermetallic layer, 25 μm to 50 μm thick, formed by furnace-baking a slurry onto the titanium substrate.

74.6.1.3 Multi-layer glass coatings

A more complicated system has a combined PVD/CVD-deposited thin reaction barrier (Al-SiBX) formed with the titanium. This is converted by heating to a two-phase, self-healing, sol-gel glass containing silica and alumina. During the conversion, the coating thickness is reduced to 2 μm .

Such coatings were applied to titanium aluminide materials (Ti-14Al-21Nb) and tested at 982°C in air, under cyclic conditions, and proved very efficient.

Similar coatings were applied to Beta 21S titanium alloy; the matrix material for Ti/SiC continuous fibre composites (TMC). Testing at 800°C under thermo-cyclic conditions, demonstrated the excellent oxidation resistance of this alloy and coating combination.

74.7 Coatings: Superalloy components

74.7.1 General

Superalloy components are primarily used in the propulsion systems of launchers and spaceplanes.

The family of alloys have working temperatures up to about 900°C for prolonged periods and can be operated to 1100°C for short periods.

74.7.2 Aluminide diffusion coatings

These are widely used to protect nickel- and cobalt-based superalloys for gas turbine applications, Ref. [74-5], [74-6].

The process is limited to aluminium as the diffused element, but it can be beneficial for other elements, e.g. chromium or yttrium.

Diffusion coatings are usually applied as pre-treatments in conjunction with other coatings, [See: 48.10].

74.7.3 MCrAlY overlay coatings

74.7.3.1 General

These coatings now constitute the primary protection system for Ni-, Co- and Fe-based superalloys, [See also: 48.11].

In the coating formulation, M represents the base alloy, Ni, Co or Fe, whilst the others are the oxide scale formers. Typical coating thicknesses are 40 μm to 70 μm .

MCrAlY coatings can be applied under controlled conditions by, Ref. [74-5]:

- electron beam physical vapour deposition (EB-PVD), or
- plasma spraying.

MCrAlY bond coats are used with thermal barrier coatings (TBC), [See: 74.8].

74.7.3.2 Oxidation resistance

The oxidation behaviour of MCrAlY coatings depends on various factors, including:

- coating composition,
- temperature,
- oxygen partial pressure,
- time, and
- thermal cycling.

A typical oxidation sequence starts with the formation of transient oxides, before a continuous stable oxide layer (chromia or alumina) has formed underneath. The diffusion of oxygen and metallic species being very slow in chromia and even slower in alumina, this layer ensures the oxidation resistance of the alloy.

The presence of chromium (10wt.% to 20wt.% Cr) reduces the Al level (10wt.%) necessary to form a protective alumina scale. Alumina scales formed within the coating lack adhesion under thermal cycling conditions. To improve the adherence of the alumina scale, an 'active element' such as yttria is incorporated in small amounts (less than 1wt.%).

[See: Table 48.11.1 for commercial coating formulations]

74.7.3.3 Hot corrosion

Coating developments for gas turbines also counter hot corrosion effects caused by fuel contaminants such as alkaline phosphates. This can be combated with cobalt additions (20wt.% Co) to the MCrAlY formulation.

Fuel contaminants can be avoided in space applications by using purer fuel compositions, so improving the coating's life expectancy.

74.8 Thermal barrier coatings (TBC)

74.8.1 Ni-based superalloy components

74.8.1.1 General

The benefits of applying thermal barrier coatings to extend performance include:

- higher gas temperatures,
- lower cooling flows, and
- reduced temperature transients on the metal surface.

This prolongs the life of gas turbine engines and improves space propulsion systems by enabling an increase in gas temperatures and improved engine efficiency, Ref. [74-7] to [74-13].

74.8.1.2 Coating formulation

TBCs are usually zirconia-based, either partially- or completely stabilised by additions of Y_2O_3 , MgO or CaO . Zirconia (ZrO_2) has a good compromise between low thermal conductivity and a high CTE close to that of nickel alloys. A 6wt.% to 8wt.% Y_2O_3 is optimum for good thermal cycling resistance. Spalling is the primary mode of failure to be avoided. However, several hundred thermal cycles have been sustained up to 1100°C in air, with bondcoats of 100 μm and a topcoat of 200 μm , Ref. [74-15]. Porosity levels determine the conductivity and thermal shock resistance, Ref. [74-16], [See also: 48.12].

74.8.1.3 Coating application

TBCs can be applied by plasma spraying or EB-PVD over a MCrAlY bondcoat, Ref. [74-9], [74-14].

[See also: 74.7 for MCrAlY coatings]

74.8.2 Shuttle Main Engine HPFTP blades

TBCs have been actively studied for extending the life of blades in the high-pressure fuel turbopump (HPFTP) on the space shuttle main engines, Ref. [74-26].

Tests were conducted with LH/LOX fuel combustion and the metal blade temperature was lowered by some hundred °C.

74.8.3 Fibre-reinforced TBC's

Preliminary work on adding fibre reinforcements to TBCs is considered as a means of improving their integrity under thermal cycling, Ref. [74-17], [74-18].

The concept of graded composition coatings has also shown to improve integrity, Ref. [74-19], [74-20].

74.8.4 Coating technology

Improvements are being made in coating technology for different substrate alloys, Ref. [74-21], [74-22], enabling thicker coatings to be deposited, Ref. [74-23].

74.8.5 Seals

TBCs are also applicable to abradable seals between moving parts where gas seals need to be maintained, Ref. [74-24]. An ultimate operation goal of 1200°C is sought, Ref. [74-25].

74.9 Carbon-Carbon: Oxidation protection

74.9.1 General

C-C composites are the only recognised thermo-structural materials for prolonged use in the temperature range 1700°C to 2500°C, despite their need for complex oxidation protection schemes.

Significant oxidation can occur at temperatures as low as 500°C. The protection systems are complex to guarantee complete coverage of the C-C substrate at all temperatures.

[See also: [54.4](#)]

74.9.2 Applications

Typical applications include:

- nose cones and wing leading edges of spaceplanes,
- TPS and heat shields for re-entry vehicles,
- components for gas turbine engines.

[See also: Chapter [70](#) and Chapter [71](#)]

74.9.3 Coating systems

Both the duration and number of thermal cycles in a high-temperature and oxidising environment influence the complexity of the protection system.

Gas turbine requirements are particularly stringent because life expectancy is measured in thousands of hours with a similar number of thermal cycles. Whilst temperatures can be higher for space applications, life expectancy is considerably lower.

Numerous protection schemes have been proposed, developed and tested. The general conclusion is that a multilayer coating scheme is essential for any guarantee of extended life.

Common terms for these coating systems include:

- Duplex,
- PAO (protection against oxygen), Ref. [74-27],
- OPS (oxidation-protection system), Ref. [74-28],
- Multiplex, [See also: 74.10]

74.9.4 Basic problem

C-C composites have a very low CTE, conferred by the fibres. All applied ceramic, refractory or inorganic coatings capable of sustaining the high temperatures have higher CTEs. Consequently, the coatings crack when cooled, enabling oxygen to penetrate which causes oxidation and spalling.

Sealing phases are used to fill the crack gaps and maintain a protective covering. Coating layers resistant to oxygen penetration are essential for longer life requirements.

74.10 Multiplex coatings

74.10.1 General

The basic configuration of a multiplex coating is shown in Figure 74.10.1, Ref. [74-28]. Such a system is applied to the entire final component.

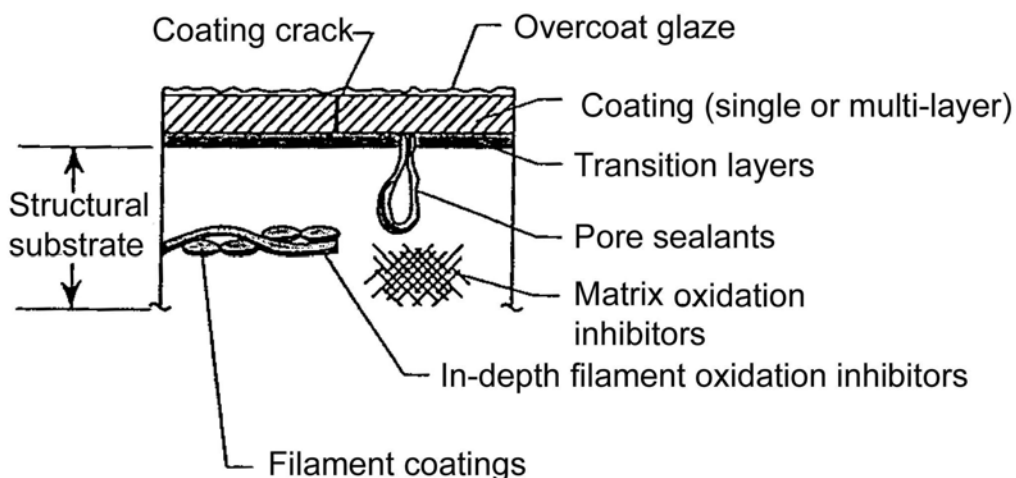
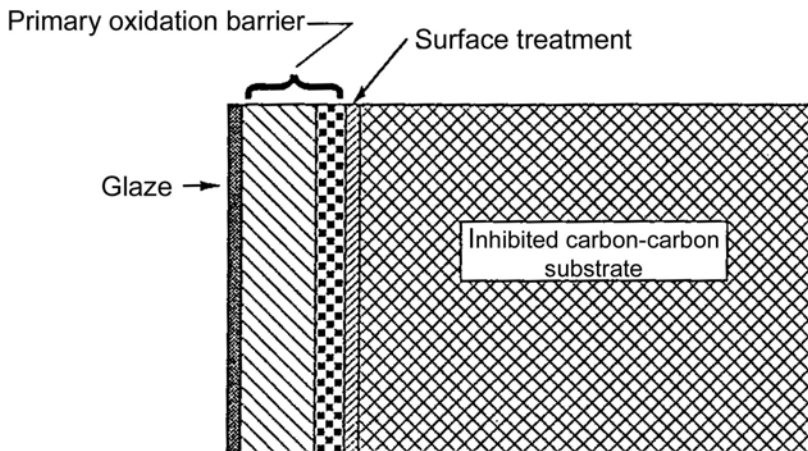


Figure 74.10-1 - Multiplex coatings: Basic configuration

74.10.2 Constituents

74.10.2.1 Inhibited C-C substrate

Glass-forming phases in the carbon matrix, introduced at the time of composite manufacture, act as a final oxidation barrier if oxygen penetrates the external (primary) barrier.

Boron and silicon additions are preferred, as they form low melting point glasses.

74.10.2.2 Surface treatment

To provide adhesion for the main barrier, a SiC diffusion coating is usually placed at the immediate surface of the substrate.

74.10.2.3 Primary oxidation barrier

Silicon carbide is the preferred overlay coating for the greater part of the primary barrier. Additional stable oxides can be applied, for oxygen penetration resistance. The primary barrier can be deposited as many thin layers to reduce residual thermal stresses, Ref. [74-29].

74.10.2.4 Outer glaze

The outer glaze is usually a special glass or sealant formulated to be fluid at intermediate temperatures when cracks in the primary barrier are still open. Whilst fluid, the glaze remains adhered to the lower coating under high gas flow velocities.

The crack and sealing mechanisms of an oxidation protection system are shown in [Figure 74.10.2](#), Ref. [74-28].

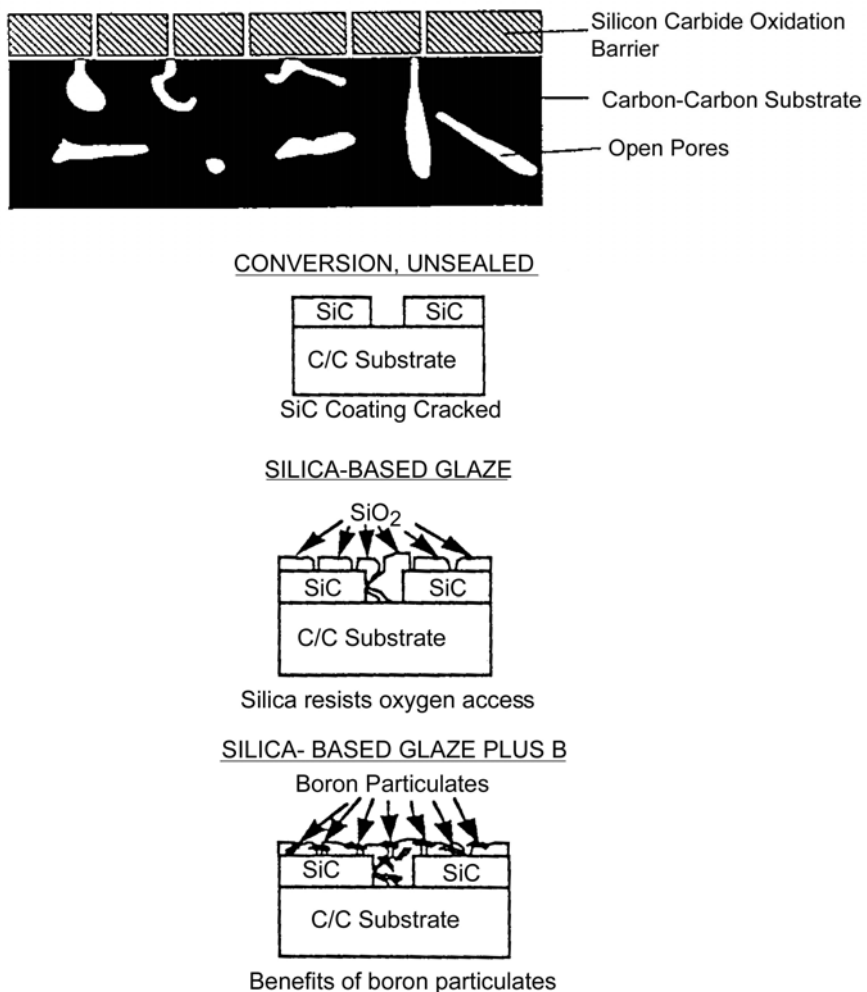


Figure 74.10-2 - C-C multiplex coatings: Crack and sealing mechanisms

74.10.3 Application examples

74.10.3.1 Buran and Space Shuttle

Classical multiplex silicon carbide coating systems were used on the nose cones and wing leading edges, Ref. [74-30], [74-31].

74.10.3.2 Hermes

The oxidation resistant C-C INOX® from Aerospatiale was proposed for the Hermes nose cone, Ref. [74-27].

In addition to oxidation resistance, the coating system also had to conform with emissivity and catalyticity requirements.

The proposed sequence was:

- SiC diffusion (silicidation) coating,
- adaptation layer of aluminium nitride (AlN),
- external alumina oxygen barrier.

These were intended to resist a maximum temperature of 1800°C at 15mb pressure. At this high temperature, a SiC overlay is no longer a viable option because it volatilises.

74.10.3.3 NASP

The intended C-C material is the ACC version, with or without inhibitors, Ref. [74-28].

Oxidation resistance to 1540°C has been demonstrated for the sequence of coating materials, i.e.:

- SiC diffusion (conversion) coating, with or without boron,
- SiC overlay coating,
- Low CTE ceramic NZP (sodium-zirconium-phosphate family),
- Boron carbide precursor to give a boric oxide glaze.

This coating system is limited to temperatures below 1800°C. Extending the operational temperature to 2500°C requires ultra-stable ceramics, such as Hafnium compounds, Ref. [74-32].

74.11 Coatings: C-SiC and SiC-SiC

74.11.1 General

Whilst these composites contain a lower proportion of carbon than C-C, they are still prone to oxidation.

74.11.2 C-SiC

The carbon fibres are not totally encased in SiC because the CTE mismatch between the two materials induces microcracking in the matrix. The surface is sealed to prevent oxygen ingress if the material is to have a prolonged working life.

A SiC overlay coating followed by a glaze is usual. The temperature is limited to about 1800°C.

74.11.3 SiC-SiC

This composite system contains a thin carbon coating on the fibre to maintain its toughness. In addition, the fibre is unstable at temperatures above 1200°C and is protected from oxygen.

The same protection system as for C-SiC is advisable for prolonged use in the temperature range 1000°C to 1300°C.

74.12 Carbon-Carbon: Surface coatings

74.12.1 Dimensionally stable structures

74.12.1.1 General

Owing to their low coefficients of thermal expansion, C-C composites are of interest for structural applications requiring dimensional stability, e.g. space telescope components.

Aerospatiale developed a range of C-C materials with an approximate CTE value of $-1.10 \times 10^{-7}/^{\circ}\text{C}$ under the ESA DSS dimensionally stable structures programme.

The materials, known as DSS C-C, have been considered for the manufacture of space reflectors, e.g. PLANCK and MASTER satellite mirrors, Ref. [74-33].

In addition to the long-term dimensional stability in the service environment, e.g. under combined mechanical loads and thermal effects (cycling and gradients), other important characteristics for space reflectors include, Ref. [74-33]:

- geometrical (shape) tolerances.
- surface roughness.

The as-manufactured, DSS C-C composites developed for this application do not meet the geometrical tolerances or surface roughness imposed for PLANCK and MIRROR-type reflectors.

Consequently, methods for improving these characteristics were investigated, Ref. [74-33]:

- Machining: This method is not appropriate because it cuts through the reinforcement fibres near the surface and so affects the (quasi-isotropic) properties of the C-C.
- Coating: A coating system, of one or more layers, applied to the material surface can be machined to correct the overall shape dimensions and meet the surface roughness requirements of the part.

Use of a coating means that an evaluation of 'material + coating' is necessary with respect to the overall application requirements, including, Ref. [74-33]:

- Property mismatch (between coating and substrate) can cause deformation during manufacture or in-service, e.g. CTE, stiffness.
- Process-related effects: deposition of a coating can affect the substrate or cause deformation. Thickness, coverage and defects form part of the quality control of coatings.
- Chemical compatibility: at interfaces (substrate-to-coating) and the interface between any intermediate layer and external (reflective) coating.
- Reliable bonding at interfaces.
- Ability to machine coating to meet surface roughness requirements and reflectivity (polishing).
- Long-term stability in service.

Coating technologies developed for test samples have to be scaleable to real reflector dimensions.

74.12.1.2 Types of coatings

Of the various technologies evaluated, most materials considered for coatings have a greater CTE than the DSS C-C substrate. Therefore the coating's modulus is kept as low as possible to avoid a "bimetallic strip" effect.

Figure 74.12.1 shows the basic multi-layer concept developed by Aerospatiale, Ref. [74-33].

This is capable of producing coatings of the necessary thickness, e.g. ~2mm for PLANCK/MIRROR size reflectors.

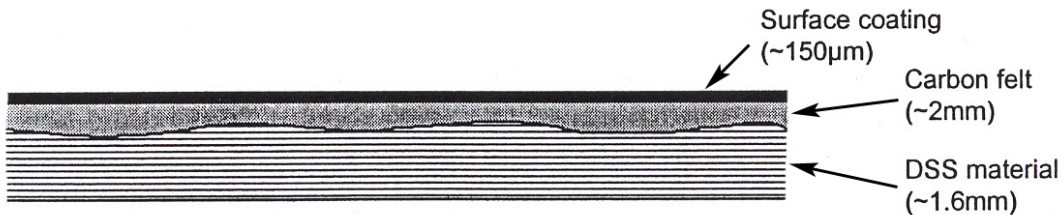


Figure 74.12-1 – Coatings: Dimensionally stable carbon-carbon – concept

The function of each layer within the coating is, Ref. [74-33]:

- Felt (~2mm thick): A carbon-based material, with low CTE and low mechanical properties, bonded to the DSS C-C substrate. This is used to correct any geometrical deviations in the substrate surface and can be machined to the final dimensions.
- Surface coating (~150µm thick): Because the machined surface of the carbon felt is too rough, an external coating is applied that can be polished to meet the surface roughness and reflectivity specification.

Figure 74.12.2 summarises the various materials considered for each part of the multi-layer coating, Ref. [74-33].

Multi-layer coating components

Substrate	2D DSS C-C					
Felt	Short carbon fibres (T-800, 500µm), impregnated with phenolic resin. Layer thicknesses: 0.5 to 3mm.					
Surface coating	Glass	Al ^[1]	Ge ^[1]	Sb ^[1]	Si ^[1]	Ti ^[1]
	SiC ^[2]	SiO ₂ ^[2]	Carbides ^[3] , e.g. TiC, TaC, Cr ₃ C ₂ .			

- Key:** [1] Selected only on their elemental properties: chemical stability, hardness, melting point and (stiffness, $E \times CTE$) factor, which indicates the stress level within the layer. Only Al coatings were evaluated, using vacuum evaporation and PVD deposition techniques.
- [2] Deposition using low-frequency CVD plasma processing techniques. Both evaluated.
- [3] Deposition possible by PVD techniques. Not evaluated.

Figure 74.12-2 – Coatings: Dimensionally stable carbon-carbon – Potential materials

74.12.1.3 Reflective coating deposition methods

A consideration of the various possible outer surface coating materials and methods can be summarised as:

- Glass provides high chemical stability, low CTE and the ability to polish the surface. It was rejected mainly because of problems associated with processing temperatures and subsequent effects on the substrate.
- PVD or an ‘evaporation under vacuum’ technique were considered to be the most promising techniques for aluminium deposition. After further evaluation these were rejected because the Al deposit infiltrated the porous felt layer and gave poor surface coverage.
- PECVD (plasma enhanced chemical vapour deposition) was identified from an evaluation of potential coating techniques for SiC and SiO₂. This process produced the required coating thickness (by single or repeated depositions), but without affecting the substrate properties because PECVD uses a low process temperature.

[See also: 74.5 – Coating Processes]

74.12.1.4 Reflective coating quality

Cracks, poor adherence and poor coverage occurred in thick ($>50\mu\text{m}$) PECVD-SiO₂ coatings.

PECVD-SiC coatings 200 μm thick were deposited on substrate samples (60mm x 100mm). These showed the presence of cracks after polishing. Cracking was attributed, not to the polishing stage, but to stresses within the initial coating arising from its thickness.

The options explored for repairing the cracks were the deposition of, Ref. [74-33]:

- A series of thin layers (each 80 μm to 100 μm thick).
- An additional thin layer (40 μm) to fill existing cracks in the previously applied thick layer.

Of these, the second option successfully filled large cracks and produced an acceptable surface roughness after polishing.

74.12.1.5 Coated DSS manufacturing methods

The proposed manufacturing route for the multi-layered system, i.e. DSS C-C substrate + carbon felt (2mm) + reflective surface coating (150 μm); involved, Ref. [74-33]:

- Preimpregnated felt applied to the 2D preimpregnated DSS material.
- Polymerisation under vacuum and carbonisation (both substrate and felt layer).
- Densification by CVI carbon (both substrate and felt layer).
- Surface machining of the densified carbon felt layer.
- Deposition of a reflective surface coating.
- Polishing of the reflective surface coating.

During the development of the manufacturing method a number of problems were encountered which were resolved by modifications in the initial processing stages.

One major modification was in the process timings for the CVI densification stage to minimise CTE differences between the substrate and felt.

The final manufacturing process is summarised in Figure 74.12.3, Ref. [74-33]. This requires some further optimisation before its validation on demonstrator parts.

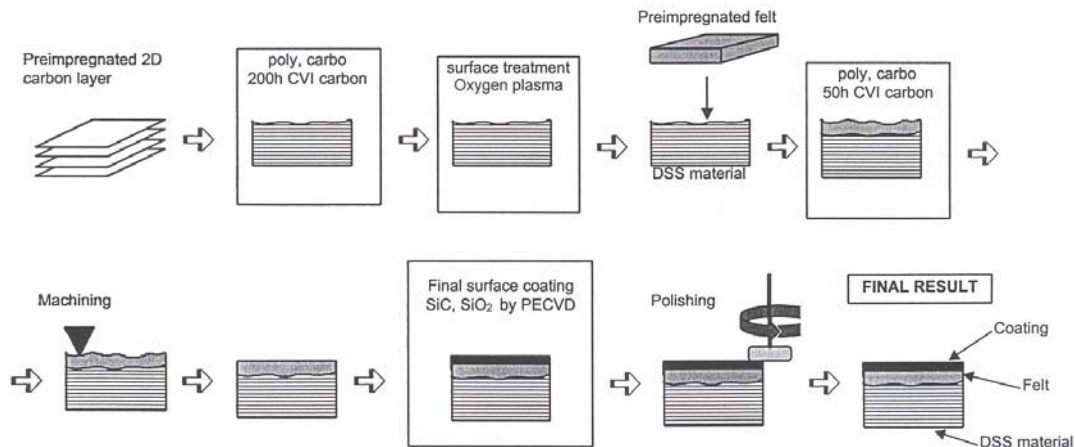


Figure 74.12-3 – Coatings: Dimensionally stable carbon-carbon – Manufacturing method

74.13 References

74.13.1 General

- [74-1] 'Advanced Surface Coatings: A Handbook of Surface Engineering'
Editors: D.S. Rickerby & A. Matthews. Chapman and Hall
ISBN 0-412-02541-8, 1991
- [74-2] M.G. Hocking et al
'Metallic and Ceramic Coatings: Production, High Temperature Properties and Applications'
Longman Scientific & Technical, ISBN 0-585-03305-5, 1989
- [74-3] High Temperature Surface Interactions
AGARD Conference Proceedings No.461. Ottawa
23-28 April 1989
- [74-4] R.K. Clark et al
'Thermal Control/Oxidation Resistant Coatings for Titanium-Based Alloys'. Proceedings of a NASA Workshop: Current Technology for Thermal Protection Systems, 11-12 February 1992, Langley Research Centre, Virginia. NASA Conference Publication 3157 p169-188
- [74-5] R. Mevrel
'High Temperature Protective Coatings: Recent Trends'
Paper 12, AGARD Conference Proceedings No.461. Ottawa, 23-28 April 1989
- [74-6] Application of Advanced Material for Turbomachinery and Rocket Propulsion. AGARD Conference Proceedings 3 to 5 October 1988
AGARD-CP-449, ISBN92-835-0498-4
- [74-7] W. J. Brindley & R. A. Miller
'TBCs for Better Engine Efficiency'
Advanced Materials & Processes, 8/89, p29-33

- [74-8] M.F. Gruninger & M.V. Boris
'Thermal Barrier Ceramics for Gas Turbine and Reciprocating Heat Engine Applications'
Proceedings of the International Thermal Spray Conference & Exposition, Orlando, 28 May - 5 June 1992, p487-492
- [74-9] H. Lammermann & G. Kienel
'PVD Coatings for Aircraft Turbine Blades'
Advanced Materials & Processes, 12/91, p18-23
- [74-10] S.M. Meier et al
'Ceramic Thermal Barrier Coatings for Commercial Gas Turbine Engines'
JOM, 43, (3), p50-53, Mar 1991
- [74-11] H-D. Steffens & R. Kaczmarek
'Thermal Barrier Coatings for Heat Engines'
Welding in the World, Vol. 28, No. 11/12, p224-230, 1990
- [74-12] E.R. Novinski
'THSP Coatings Save Aircraft Engines'
Welding Design & Fabrication, April 1991, p26-28
- [74-13] P. Vincenzini
'Zirconia Thermal Barrier Coatings for Engine Applications'
Industrial Ceramics, Vol.10, No.3, 1990, p113-126
- [74-14] W. Lih et al
'Effect of Pre-Aluminization on the Properties of ZrO₂-8wt.% Y₂O₃/Co-29Cr-6Al-1Y Thermal-Barrier Coatings'
Oxidation of Metals, Vol 38, Nos 1/2, 1992, p99-124
- [74-15] J.A.M. Boogers et al
'Thermal Shock and Oxidation Resistance of Ceramic Coatings'
Paper 12, AGARD Conference Proceedings No.461. Ottawa
23-28 April 1989
- [74-16] H.D. Steffens et al
'Thermal Barrier Coatings: Some Aspects of Properties Design'
Proceedings of the 4th National Thermal Spray Conference Pittsburgh,
USA, 4-10 May 1991, p289-294
- [74-17] D. Harris
'Composite Thermal Barrier Coatings'
Proceedings of the 4th National Thermal Spray Conference Pittsburgh,
USA, 4-10 May 1991, p363-369
- [74-18] R.P. Tolokan & G.P.Jarrabet
'Ceramic TBS/Porous Metal Compliant Layer'
Proceedings of the Current Technology for Thermal Protection Systems,
USA, p89-96
- [74-19] F. Jamarani et al
'Compositionally Graded Thermal Barrier Coatings for High Temperature Aero Gas Turbine Components'
Surface and Coatings Technology, 54/55 (1992), p58-63
- [74-20] J. Musil et al

'Plasma Spraying Deposition of Graded Thermal Barrier Coatings'
Proceedings of the International Thermal Spray Conference & Exposition,
Orlando, 28 May - 5 June 1992, p525-530

- [74-21] J. Verrier et al
'Improvements in Thermal Barrier Coatings for Gas Turbine Components'
Proceedings of the 4th National Thermal Spray Conference, Long Beach,
USA, 20-25 May 1990, p545-550
- [74-22] A. Faure-Geors & Z. Wang
'Thermal Cyclic Response of Yttria-Stabilised Zirconia-MCrAlY Thermal Barrier Coating Produced by Electron-Beam Vacuum Evaporation'
3rd International SAMPE Metals Conference, October 20-22, 1992 pM253-M265
- [74-23] H. Wang et al
'Flame Rig Testing of Thermal Barrier Coatings'
Protective Coatings: Processing and Characterisation
The Minerals, Metals & Materials Society, 1990, p155-163
- [74-24] T.E. Strangman
'Thermal Strain Tolerant Abradable Thermal Barrier Coatings'
ASME 91-GT-39
- [74-25] Bo-Chen Wu et al
'Performance Improving Mechanisms of Zirconia/Pack-aluminized MCrAlY Thermal Barrier Coatings. Part 1: Performance of TBCs Specimens'
MRL Bull. Res. Dev., Vol. 6, No. 1 (1992), p71-80
- [74-26] J.A. Nesbitt
'Thermal Response of Various Thermal Barrier Coatings in a High Heat Flux Rocket Engine'
Surface and Coatings Technology, 43/44 (1990), p458-469
- [74-27] O. Franc & J.-L. Macret
'Oxidation-inhibited Carbon-Carbon Materials'
ESA Symposium on Space Applications of Advanced Structural Materials, March 1990, ESA SP-303, p87-90
- [74-28] C.W. Ohlhorst et al
'Current Research in Oxidation-Resistant Carbon-Carbon Composites at NASA Langley'
Proceedings of a NASA Workshop: Current Technology for Thermal Protection Systems, 11-12 February 1992, Langley Research Centre, Virginia. NASA Conference Publication 3157 p149-168
- [74-29] W. Huettner et al
'Oxidation-inhibited Carbon-Carbon: A Candidate Material for Hot Structures'
ESA Symposium on Space Applications of Advanced Structural Materials, March 1990, ESA SP-303, p91-96

- [74-30] A.N. Gordeev et al
'An Induction Plasma Application to BURAN's Heat Protection Tiles
Ground Tests: Part I'
SAMPE Journal Vol.28, No.3, May/Jun 1992, p29-33
- [74-31] A.N. Gordeev & M.I.Yakushin
'The Thermochemical Stability of Carbon-Carbon using an Anti-oxidation
coating for BURAN: Part II'
SAMPE Journal Vol.29, No.2, Mar/Apr 1993, p27-31
- [74-32] H.G. Maahs
'Carbon-Carbon Composites'
Chapter 16 of Proceedings of the Flight-Vehicle Materials Structures and
Dynamics Conference on Assessment and Future Direction. ASME
publication. Volume 3, p307-332, 1991
- [74-33] T. Salmon: Aerospatiale, (F)
'Improvement of the Surface State of Carbon/Carbon Composites for
Space Mirror Applications'
Report No. NT 38112/SI/LR-AQ. Final Report (March 1999).
Work Package on ESA Contract with ERA Technology, UK.

75

Seal technology

75.1 Introduction

75.1.1 Uses

Seals are used in the assembly of components involved with fluid flow or pressure, for both static and dynamic environments. Their functions differ greatly in terms of:

- Loads (static and dynamic).
- Temperature performance,
- Compatibility with different:
 - materials,
 - fluids.
- Life expectancy,
- Ease of installation and maintenance.

The reliability of seals operating in aggressive environments is essential. A seal failure usually results in a serious loss of performance or even endangers the integrity of a structure; as seen with Challenger.

75.1.2 Structural assemblies

Some of the seal technologies for structural assemblies and particularly those experiencing high-temperature excursions are described by example, including:

- Gap filling seals between TPS tiles or shingles on space planes,
- Structural seals between segments of solid boosters,
- Sliding interfaces of articulating engine panels,
- Assemblies in combustion engines, thrusters and nozzles.

Such seals tend to be either high-temperature metal alloys, often nickel-based, or forms of ceramics, e.g. often braids or ropes.

Two important functions of seals are providing compliance and gap-filling under thermal expansion mismatch conditions.

75.1.3 Dynamic seals

Dynamic seals, as found with rotating shafts, are not included in this chapter, with the exception of some reference documents, Ref. [75-1], [75-2].

Silicon carbide is a particularly good dynamic seal material that can operate at high temperatures. It can be used as a surface coating on a CMC carrier.

75.1.4 Materials

Seal technology uses a range of materials:

- polymers (elastomers or rubbers), in metal housings, [See: 75.3].
- metals,
- ceramics.

Experience of elastomers and the design of seals that operate in aggressive industrial environments provide useful insight of seal performance for some space applications, [See: 75.7]. The particular demands of the space environment and operating conditions of elastomer seal-containing systems needs a full and thorough evaluation, [See: ECSS-Q-70-71].

For extreme high-temperature applications, such as within TPS systems, metals or ceramics are used.

75.2 Structural seals

The structural seals that have received a considerable amount of attention are those used in the assembly of solid rocket boosters.

Failure of such seals led to the loss of the Space Shuttle Challenger Orbiter during launch when combustion gases forced their way through sealed joints in the casings. These seals are made of elastomeric materials. In the case of the Challenger accident, they lost flexibility as a result of the cold launch-pad conditions. These seals experience:

- mechanical load (transmitted between booster casings),
- vibration (during launch),
- the internal pressure caused by fuel combustion,
- a thermal transient,
- relative movement (between casings).

This is a representative group of requirements in many sealing applications.

75.3 Seal materials

75.3.1 General

Seal applications are demanding and materials selection is generally based on material forms with a proven, predictable performance.

Nickel alloys and ceramic-based seals are used in high-temperature applications. Some grades of elastomeric materials are suitable for space applications whereas other are not, [See: [ECSS-Q-70-71](#)]

Materials used for seals in space applications can be grouped as:

- Nickel alloys in the form of spring seals, [See: [75.4](#)].
- Fibrous ceramics, usually used in the form of braids, felts or cloths, [See: [75.5](#)].
- Silicon carbide for rotating (shaft) seal wear facings, [See: [43.12](#)].
- Graphite sheet e.g. Hermes winglet-to-rider connections (600°C) and control surface assemblies (400°C), [See: [75.6](#); [43.10](#) for graphite materials].
- Elastomers, which have proven uses in both general engineering and severe industrial environments. There are two basic groups:
 - Thermoset, commonly known as vulcanising, which are described in detail, [See also: [75.7](#) for elastomeric seals; [30.14](#) for Ariane 5 vibration mount example].
 - Thermoplastic, which are processed like plastics, but are not cured (vulcanised) during moulding. These behave broadly similarly to vulcanised rubbers, but they are not widely-used for engineering applications because of some property deficiencies, e.g. low softening temperatures and concerns over their long-term stability.

75.3.2 Elastomers

75.3.2.1 Essential characteristics

Elastomers are a subgroup of the polymer materials. Polymer materials comprise long chain-like molecules, formed by chemically-linking low molecular weight monomers in repeated sequences. The other main subdivision of polymers comprises the various plastics, i.e. thermoplastics and thermosets.

The terms 'elastomer' and 'rubber' are synonymous for all practical purposes. Both terms can refer to either the:

- raw base polymer, or
- final fully formulated and vulcanised material, as used in a moulded engineering component.

Elastomers are characterised by their elasticity, i.e. their ability to undergo easy, and essentially reversible, deformation to high strains. This reversibility needs to be rapid when the load is removed.

Elastomers are softer than other solid materials, having Young's moduli generally in the range 1MPa to 100MPa. Most practical engineering rubbers are near the bottom end of this range.

Except at very high stresses, elastomers maintain constant volume on deformation - like a fluid. Therefore, deformation of rubber components, is accompanied by significant changes in shape. The

incompressibility is the result of the very high ratio between their high bulk modulus, and the low shear modulus. A common misconception is that the incompressibility is due to their having a Poisson's ratio very close to 0.5. In fact, this is only true at very small, or 'classical', strains. For a rubber band stretched by 100%, the 'Poisson's ratio' (the ratio of lateral contraction to longitudinal extension) is about 0.3. Consequently, it is better to use the bulk modulus, rather than Poisson's ratio, in calculations with higher stresses (where compressibility becomes significant).

75.3.2.2 Crosslinking

Polymers are made up by the intermingling of long chain-like molecules; not unlike a bowl of spaghetti. To confer thermal and elastic stability on the material, it is necessary to introduce crosslinks. These are occasional chemical bonds between adjacent molecular chains such that a 3D network is formed.

The introduction of the crosslinks prevents chains from just slipping past one another under stress. The process by which the crosslinks are introduced involves the application of chemicals and heat and is known as vulcanisation or curing.

Most practical elastomers used in engineering are vulcanised during moulding, the exceptions are:

- thermoplastic elastomers,
- rubber-type compounds, which are not described here, e.g. potting compounds, sealants and foams, which either do not cure or 'cure-in-place', [See: [ECSS-Q-70-71](#)].

75.3.2.3 Temperature effects and glass transition

An understanding of the thermal properties of elastomers is greatly assisted by knowing a little about their behaviour at the molecular level.

[Figure 75.3.1](#) shows a schematic diagram of a rubber network. It comprises long chain molecules, joined together occasionally by crosslinks. Between the fixed points the chain molecules are in a constant state of random motion and take up a highly kinked configuration which is constantly changing.

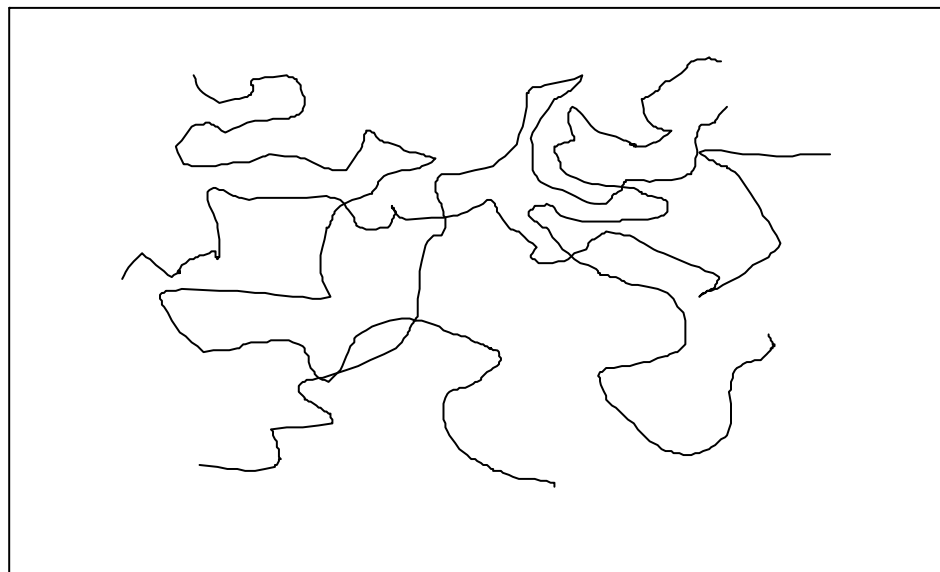


Figure 75.3-1 – Elastomers: Schematic of crosslinked rubber molecular network

The large potential deformations in elastomers can occur because, under stress, these highly-kinked molecules are able to straighten out, perhaps to several times the kinked length. The chainlike molecules themselves are highly flexible and offer little resistance to this, provided that the temperature is high enough.

Each elastomer has a glass transition temperature (T_g) below which the chains are no longer flexible. Below the T_g an elastomeric polymer feels, and behaves, like a glass or brittle polymer. Above T_g , the polymer has rubbery properties. In practice the transition is not sharp; transformation from rubbery to glassy properties can take place over a temperature range, which varies from elastomer to elastomer, but is often several tens of $^{\circ}\text{C}$.

Examples of T_g -related elastomer characteristics are:

- Natural rubber (cis-polyisoprene); a general purpose elastomer with a T_g around -70°C . It is widely used in engineering applications and has a useful rubbery temperature range from -30°C to 100°C , approximately.
- FEPM (tetra-fluoroethylene-propylene) is a specialised high temperature and oil resistant rubber with a T_g around 0°C . Although its upper service temperature can exceed 200°C , the high T_g reduces its versatility because it loses its rubbery properties at and below normal ambient temperatures.

Table 75.3.1 gives T_g values for a number of elastomers.

Table 75.3-1 – Elastomers: Typical glass transition temperatures

Polymer-type	Glass transition temperature ⁽¹⁾ , T_g ($^{\circ}\text{C}$)
Cis-polybutadiene	-108
Natural rubber (polyisoprene)	-70
Butyl rubber (polyisobutene isoprene)	-65
SBR (styrene-butadiene rubber)	-61
Neoprene WRT TM DuPont (polychloroprene)	-49
Nitrile rubber (38.5% acrylonitrile)	-24
FEPM (tetra-fluoroethylene/propylene)	0

Key: (1) Typical values because the glass transition temperature is not uniquely defined. T_g values depend on the measurement method.

In general, increasing the oil and chemical resistance properties of elastomers, and increasing their high-temperature resistance, reduces their strength and decreases their elasticity at lower temperatures.

It is important to realise that elastomer properties are more temperature-dependent than those of most other engineering materials, and that the important in-service properties are those at the service temperature. Manufacturers' published data do not always make this clear, but it is a key consideration in the selection of materials, [See: [ECSS-Q70-71](#)].

75.3.3 Types of elastomers

75.3.3.1 Formulation

An engineering elastomer is a chemically and physically bonded composition of several ingredients, vulcanised ('cured') together, usually with the application of pressure and heat in a suitably shaped mould. Broadly the composition comprises:

- Base elastomer; the type of rubber which forms the basis of the compound, e.g. natural rubber or nitrile rubber. It is often a single type, but can be a blend of two or more base elastomers.
- Crosslinking chemicals; the original crosslinking chemical for natural rubber was sulphur. This is still widely used in natural and other rubbers. However, many other chemicals can now be used to produce crosslinking.
- Vulcanisation promoters (accelerators); chemicals designed to assist and speed up the crosslinking process, usually at elevated temperatures.
- Antidegradants; chemicals, e.g. antioxidants, antiozonants, and UV-absorbers, which reduce the susceptibility of the vulcanised elastomer to atmospheric and other forms of degradation.
- Extenders; usually oils incorporated in small amounts to ease processing, or in large amounts to confer special properties on the rubber, e.g. high speed racing tyres where the oil content can exceed the weight proportion of base elastomer.
- Fillers; incorporated in the compound to increase the stiffness or strength and abrasion resistance. Carbon black is by far the most common filler, which is why most rubber components are black in colour. Different carbon blacks are characterised by their particle size and by their 'structure', i.e. the tendency of the particles to aggregate into groups. The choice of carbon black type can have important consequences for the physical properties of the vulcanisate.

Elastomers for use in space applications need careful consideration of the formulation details; however this is generally classed as proprietary information, so is difficult to obtain.

The space environment can affect the constituents of elastomers, e.g. extending oils and plasticisers can be unstable under vacuum.

The compatibility of elastomers with contacting substances can only be established with a full knowledge of those substances and the service conditions, e.g. temperatures and pressures. Fillers can be leached from elastomers and contaminate equipment.

[See: [ECSS-Q-70-71](#)]

75.3.3.2 Base elastomer-types and characteristics

There are many different base elastomeric polymers from which engineering components can be manufactured. A small number of the commonest elastomers and elastomer-types are described in [Table 75.3.2](#).

[See: [ECSS-Q-70-71](#) for elastomers not suitable for space use]

Table 75.3-2 – Elastomers: Summary of common materials and characteristics

Material ⁽¹⁾	Comments
Natural rubber (NR) ⁽¹⁾	High-strength, general purpose rubber. The high strength derives mainly from its ability to crystallise partially under strain.
Chloroprene rubber (CR)	High-strength, general purpose synthetic rubber; commonest trade name Neoprene® by DuPont, which can also crystallise under strain.
Styrene butadiene rubber (SBR) ⁽¹⁾	Probably the commonest synthetic general purpose rubber. It needs the incorporation of reinforcing fillers to achieve good strength.
Nitrile rubber (NBR) ⁽¹⁾	A rubber with high resilience and good wear resistance. It has good aliphatic oil and fuel resistance at very modest cost.
Hydrogenated nitrile rubber (HNBR)	An outstanding general purpose oil and chemical resistant rubber. Temperature range depending on ACN content to 180°C and beyond. Often a better choice than more expensive ‘specialist’ rubbers.
Fluorocarbon rubber (FKM) ⁽¹⁾	Available in a number of grades, with good oil and chemical resistance and good heat resistance up to above 200°C.
Perfluoroelastomer (FFKM) ⁽¹⁾	Extremely expensive specialist rubbers with very high heat and chemical resistance; up to about 300°C. They have, however, a high minimum working temperature and poor physical properties compared with the general purpose rubbers.

Key: (1) Tensile properties, [See: [Figure 75.3.2 \(23°C\)](#); [Figure 75.3.3 \(100°C\)](#)]

75.3.3.3 Tensile

[Figure 75.3.2](#) shows the typical tensile strengths of five common elastomers at ambient temperature. It can be seen that, as the heat and oil resistance of the elastomer increases, the tensile strength decreases.

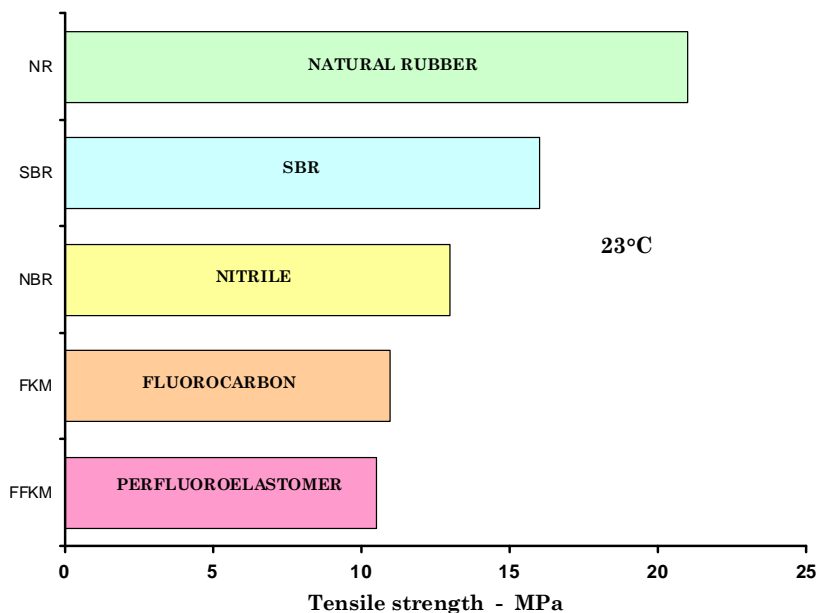
**Figure 75.3-2 – Elastomers: Typical tensile strength at 23°**

Figure 75.3.3 shows that the tensile strengths at 23°C have almost halved at 100°C. Even at 100°C, which is at or near the highest practicable service temperature for natural rubber, it is still stronger than the heat-resistant rubbers at 23°, and still maintains its lead in terms of tensile strength.

It is important to appreciate that 'heat resistance' in rubbers refers to resistance to chemical attack (ageing). It does not refer to the maintaining of physical properties at high temperature. The importance of knowing the physical properties at the service temperature cannot be overemphasised. Heat-resistant elastomers have important uses in extreme conditions, but they cannot be used unless they are essential, because their physical properties are generally inferior.

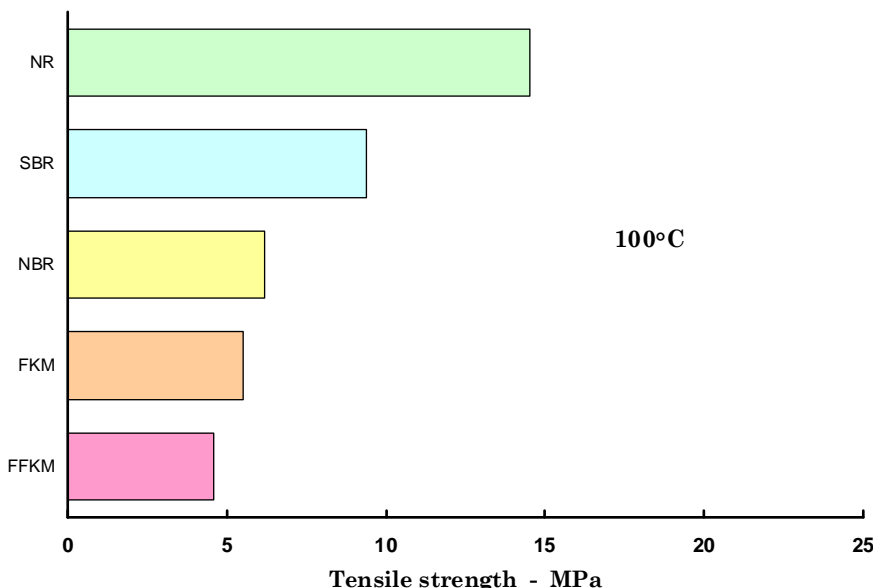


Figure 75.3-3 – Elastomers: Typical tensile strength at 100°C

75.3.3.4 Fluid resistance: Liquids

Contact between an elastomer and a liquid can have three different effects, possibly occurring simultaneously:

- swelling, which is the absorption of liquid into the elastomer,
- leaching, which is the removal of chemical species from the elastomer into the liquid,
- chemical attack (in some cases).

In some solvents, the swelling of some elastomers can be spectacular, resulting in very large increases in volume, accompanied by weakening and possible disintegration. The potential for swelling can generally be predicted from a property known as the solubility parameter. The rubber and liquid each has a solubility parameter, a thermodynamic property, and tables of these are given in standard reference works. If the rubber and the liquid in contact with it have differing solubility parameters then little swelling occurs. If, however, the solubility parameters are similar then swelling usually occurs and tests are carried out to determine the extent and whether this is compatible with the intended service. Where solubility parameters are not available in the literature they are measured in the laboratory.

The solubility parameter of a mixture of two (or more) miscible liquids is different from the solubility parameters of the individual components. Thus a rubber can swell in a mixture of two liquids, even though it does not swell in either of them alone. Other factors can reduce swelling even when the solubility parameters are similar, e.g. slink density, Tg and filler loading.

Many elastomeric components are used in contact with oil. All elastomers are swollen by oil but a number are described as 'oil resistant' to a greater or lesser degree. Resistance depends on the nature of the oil, and elastomer manufacturers publish data on this. However, component size can be just as important as the intrinsic oil resistance of the elastomer. Natural rubber (NR) is generally regarded as having very poor oil resistance and it is true that a thin strip of NR swells and becomes weak very quickly, e.g. a matter of hours in vehicle engine lubrication oil. Yet experience shows that automotive engine mounts can survive for many years in an oily environment. This is simply because they are protected by their bulk. Penetration of oil, or any liquid, into rubber is proportional to the square root of time. For example, trebling the thickness increases oil resistance (in terms of time taken to complete swelling) by a factor of three squared, i.e. nine times.

A low viscosity motor oil fully swells a 1mm thick strip of natural rubber in 70 hours, but it takes 20 years for the same oil to fully swell a 5cm thick block (given that the block is constantly and fully immersed in the oil for the whole of this time).

Correct material selection for elastomers can be complex, involving a simultaneous review of several properties and not just the property of immediate interest. For example, in a situation where contact with oil is intermittent, use of an oil-resistant elastomer can actually reduce component life because these materials are likely to have lower strengths, particularly at elevated temperatures.

75.3.3.5 Fluid resistance: Gases

Oxidation, by attack from oxygen in the air, is the commonest form of degradation in rubbers under normal atmospheric conditions. Antioxidants are incorporated into most elastomer formulations to combat this. The only other common gas which is aggressive to some elastomers is hydrogen sulphide, H₂S, which is encountered in offshore oil installations and attacks the elastomers chemically.

Under pressure, rubbers can absorb very large amounts of gas. The rate of diffusion is generally much higher than that for liquids. The amount of gas absorbed is proportional to the pressure (up to a limit where gas densities approach liquid densities). At high pressure the dissolved gas volume (measured at standard temperature and pressure) can be 100 or more times the volume of the elastomer. There is no problem whilst the gas remains dissolved but, if the external pressure suddenly drops, the gas can come out of solution and expand with spectacular and devastating consequences. This is known as explosive decompression, [See: 75.7].

75.3.3.6 Thermal cycling

Within the operating temperature range of an elastomer, the effects of temperature are normally reversible. For example, if the stiffness of an elastomer is measured at 23°C, and the measurement repeated after excursions to its highest and lowest operating temperatures, the original stiffness is unchanged.

When an elastomer is under stress, e.g. in a sealing ring, temperature cycling to elevated temperatures can increase the rate at which sealing force is lost. This is a purely physical effect, where heating the elastomer enables relaxation to take place which would occur much more slowly at lower temperatures, Ref. [75-9], [75-10].

In the long term, temperature cycling does not increase the total amount of sealing force lost, but it occurs more quickly.

[See: [ECSS-Q-70-71](#); [ECSS-Q-ST-ST-70-04](#)]

75.3.3.7 Radiation

Much work has been done on the effects of both non-ionizing and ionizing radiation on elastomers; particularly within the nuclear industry, Ref. [75-11], [75-12]. Although a full review is beyond the scope of this handbook, ionizing radiation damage varies mainly with the polymer, but to some extent also with the compounding ingredients. Additives (antirads) can reduce the effects.

It is believed that, to a first approximation, damage is independent of dose rate and type of radiation. Thus, damage is primarily a function of the total absorbed energy.

Ultra violet radiation is universally damaging to elastomers causing bond cutting, similar to attack by oxygen. In space UV is not reduced by absorption in the ozone layer, so shielding is normally needed for elastomeric components.

[See: [ECSS-Q-70-71](#); [ECSS-Q-ST-70-06](#)]

75.3.3.8 Vacuum

Elastomers, in general use, usually contain an excess of compounding ingredients that remain unreacted after vulcanisation. These species are not bound into the polymeric network, so are volatile to a greater or lesser degree. The presence of volatiles becomes a problem in a vacuum environment, as they diffuse to the surface and can be released as contaminants that can potentially damage other equipment. Vacuum conditions generally have no effect on elastomer properties.

Careful consideration of the compound formulation, and emphasis on complete vulcanisation can reduce unreacted species to very low levels.

Outgassing tests measure both the loss of weight of a sample when subjected to vacuum conditions, and the collected volatile condensable material.

[See: [ECSS-Q-70-71](#); [ECSS-Q-ST-70-02](#)]

75.3.4 Viscoelasticity

Elastomers are not perfectly elastic, their properties are viscoelastic.

Although rubber has many of the properties of an elastic solid it also behaves in a liquid-like, or 'viscous' manner. Under load, it flows with time - albeit slowly. If rubber is held at constant deformation the initial stress decays with time. The flow and stress decay are referred to as creep and stress relaxation. If a strip of rubber is stretched and then retracted, the retraction curve does not follow perfectly the extension curve; as shown in [Figure 75.3.4](#), where the area within the loop represents energy lost within the cycle, i.e. hysteresis.

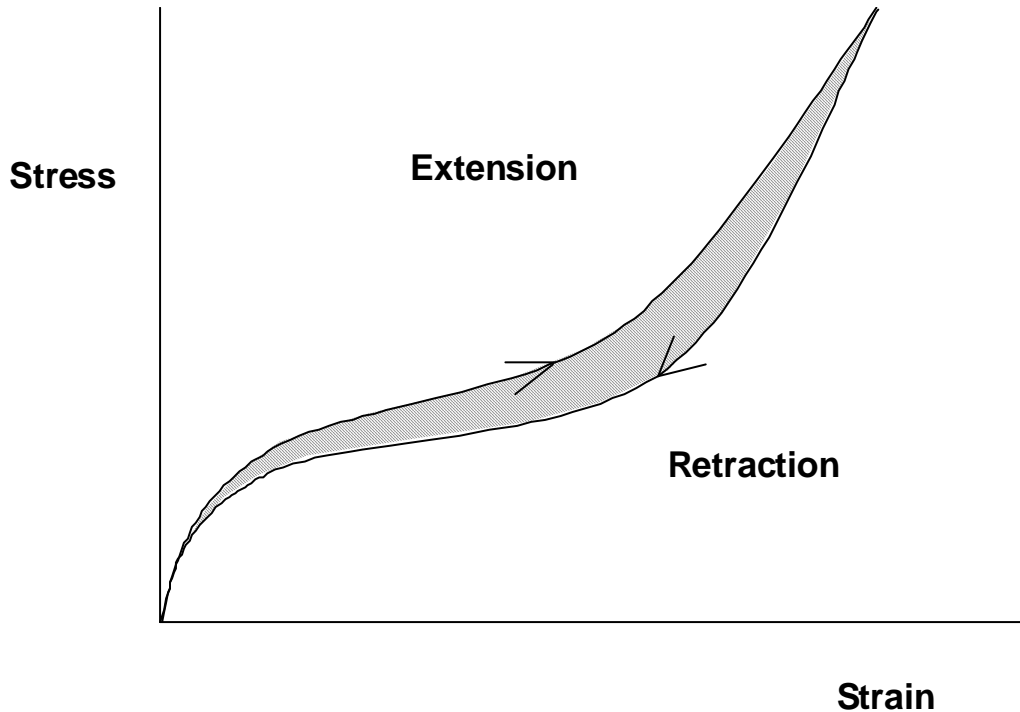


Figure 75.3-4 – Elastomers: Viscoelasticity – hysteresis effect

For many practical purposes in engineering design the non-elastic effects are ignored, so that, for example, a ‘modulus’ is quoted which enables the calculation of stiffness for a component.

When considering the long term behaviour of components under stress, then account needs to be taken of viscoelastic effects. Viscoelastic considerations are also of much greater significance in dynamic applications when the stresses or strains on the elastomeric component are varying constantly with time under cyclic loading.

Where appropriate, the viscoelastic nature of elastomers is mentioned with respect to their physical properties.

75.3.5 Physical properties

75.3.5.1 General

The physical properties of elastomers most likely to be important in engineering applications are (with ISO standards relating to each property):

- hardness (ISO 48),
- elastic moduli (ISO 48),
- tensile strength and elongation-at-break (ISO 37),
- tear strength (ISO 34),
- resilience and dynamic properties (ISO 4662, 4663, 4664),
- compression set (ISO 815),
- stress relaxation or creep (ISO 3384, 8013).

75.3.5.2 Hardness and elastic modulus

The hardness of an elastomer is usually the first physical characteristic described, e.g. 75 hard nitrile rubber sealing ring. The hardness is measured by a special instrument with a spherical indentor which pushes into the rubber following a strict time regime, and which reads directly in hardness units. These instruments are highly accurate and reproducible when used carefully.

The units of hardness used are usually international rubber hardness degrees (IRHD). Previously 'Shore' hardness was used, and the Shore A 'durometer' is still in use in the USA. Shore A and IRHD scales agree numerically to within a few degrees over most of the range.

Subjectively, an elastomeric specimen which feels soft to the touch and can be easily indented by a finger is probably 40 IRHD or below. Common rubber hoses or tyres are usually in the range from 50 to 80 IRHD. Harder elastomers are frequently used in seals, and show only slight flexibility.

Hardness is a very useful measure in general discussion, but for accuracy it is necessary to specify a modulus. Specifications for engineering components are based on modulus rather than hardness, but, on no account, specify both because they are not uniquely related.

Young's modulus can be measured in tension at small strains. However, as the stress-strain curve in tension is non-linear it is more usual in engineering to use shear modulus (generally designated G), based on the more linear shear stress-shear strain characteristic.

Compression modulus is to some extent a function of the shape of the component, not simply a material property, [See: Design].

In shear, the relationship between stiffness and modulus is a simple one. The shear stiffness K_s of a block of rubber of cross section A and thickness t is thus related to the shear modulus by:

$$K_s = \frac{GA}{t} \quad [75.3-1]$$

75.3.5.3 Tensile strength and elongation at break

Rubber is rarely used in tension in engineering applications. It is used almost entirely in compression or shear or in a combination of the two. The ultimate strength properties are, however, best measured in tension, so tensile tests are important in quality control. These tests are frequently used to determine changes in properties after ageing; an accelerated method of determining the resistance of the rubber to deterioration with time.

The test sample, to National or International standard dimensions, is usually dumb-bell (or 'dog-bone') shaped, where the material under test is the narrow, straight, central section. The sample is pulled by the test machine at a fixed rate, with stress and strain automatically recorded. The data includes the stress at fixed points, e.g. 100%, 200%, 300%, elongation (incorrectly, but universally, referred to as, e.g. the '100% modulus', '200% modulus' in the rubber industry), the extension at break, the stress at break and the tensile strength.

Modulus measurements tend to be very reproducible between nominally identical samples. Breaking strain and tensile strength are, however, always rather variable because these properties depend on the size and distribution of naturally occurring flaws in the rubber, and these always have a statistical distribution. To determine representative values, 3 to 5 replicate tests are usually necessary.

75.3.5.4 Tear strength

Fatigue due to repeated stressing is a common mode of ultimate failure in components. A parameter known as tearing energy is used in calculations related to such failure, and this can be measured in the laboratory by tear testing.

A commonly used test is the 'trouser tear' where a slit is cut in a rectangular test sample taken from a thin sheet of rubber, so that the two sides of the slit look like the legs of a pair of trousers. The edges of the two legs are gripped in the upper and lower jaws of a test machine and pulled apart so that tearing occurs at the stress concentration at the junction of the legs. If the legs are stiff enough such that their extension is negligible, then this shape of test sample gives a very simple method of determining tearing energy, T , because:

$$T = \frac{2F}{t} \quad [75.3-2]$$

Where:

F = measured force to produce tearing;

t = test piece thickness

The higher the tearing energy the greater the resistance to tearing.

75.3.5.5 Resilience and dynamic properties

If an elastomer was a perfectly resilient material, then a rubber ball dropped onto a very hard surface would rebound to the same height from which it was dropped. Its resilience would be 100%. In fact, rubber is a viscoelastic material with real resilience less than 100%. Energy is lost during the collision of the ball with the hard surface, and most of this lost energy converted into heat.

This characteristic is of importance when rubber is used as a spring material, e.g. in vibration isolators. Generally in such applications, high resilience is needed, both to increase the effectiveness of the isolation, and to prevent heat build-up in the spring, [See also: Vibration isolation].

The viscoelastic nature of rubber is also important under dynamic loading because the response of the material is then dependent both on its elastic properties and its viscous properties, the latter introducing a time dependence and energy loss. Although a detailed treatment of the behaviour of elastomers under dynamic conditions (cyclic loading) is beyond the scope of this handbook, a broad outline of dynamic properties is provided so that various important parameters can be defined.

Metal springs are essentially linear in their behaviour, i.e. stress is proportional to strain. In shear, gum elastomers, i.e. those not containing any fillers, are reasonably linear, but when substantial quantities of filler are present, as in most engineering compounds, some non-linearity occurs, and damping (energy loss) increases.

The various dynamic moduli and other parameters defined are substantially accurate for deformations of constant amplitude, but the values are different at different amplitudes.

The parameter used to describe the amount of damping in a rubber specimen under sinusoidal dynamic motion is 'tan δ ', the loss factor or loss tangent, where:

$$\tan \delta = \frac{G''}{G'} \quad [75.3-3]$$

Where:

- G' : *the in-phase or elastic component of the shear stress, known as the storage modulus.*
- G'' : *the out-of-phase or viscous component of the shear stress, known as the loss modulus.*

The absolute value of the complex modulus, G^* , which is used to replace static modulus in common equations, is given by:

$$|G^*| = \sqrt{G'^2 + G''^2} \quad [75.3-4]$$

Other parameters which can be encountered in descriptions of elastomer behaviour are:

- Logarithmic decrement, Λ , which is the natural logarithm of the ratio between successive amplitudes of the same sign in a damped free oscillation.
- Damping ratio, u , which is the ratio between actual damping and critical damping. Critical damping is the damping needed at the borderline condition between oscillatory and non-oscillatory behaviour.

$$\begin{aligned} u &= \frac{\Lambda}{2\pi\sqrt{1+\frac{\Lambda^2}{4\pi^2}}} \\ &= \sin \arctan\left(\frac{\Lambda}{2\pi}\right) \end{aligned} \quad [75.3-5]$$

This can usefully be approximated as $\frac{1}{2} \tan \delta$ for small values of δ .

Rebound resilience, R , is the ratio of the output energy to input energy for a moving mass impacting a rubber block (or a rubber ball impacting a hard surface).

An approximate equation relating R to $\tan \delta$ is:

$$R = e^{-\pi \tan \delta} \quad [75.3-6]$$

Further information on resilience and the dynamic properties of rubbers are found in standard text books, Ref. [75-13].

75.3.5.6 Compression set

Compression set is a measure of the lack of recovery of the original dimensions of a rubber component which has been held in a deformed state for some time.

The original purpose of the test was to ensure that rubbers are fully vulcanised. If a manufacturer, in order to save time and costs, undercures an elastomer, then this can be detected in a compression set test.

In test standards, a cured rubber pellet of a specified size is placed under compression, usually 20%, in a special fixture. The fixture is then placed in an air oven at a fixed temperature, often 100°C, for a fixed time, often 1 day or 7 days.

At the end of this time the fixture is removed and dismantled. Measurements are made on the test samples after 30 minutes recovery at room temperature. Loss of height of the sample compared with its original height is the basis for the measurement of 'set'.

Compression set is expressed as:

$$\text{set} = \frac{t_0 - t_r}{t_0 - t_s} \times 100\% \quad [75.3-7]$$

Where:

t_0 : the initial thickness,

t_s : the compressed thickness,

t_r : the recovered thickness.

If the rubber was undercured, then further crosslinks form during the ageing under compression. When the compression load is removed, these crosslinks oppose recovery to the final height, and the sample shows more compression set than one which had been cured fully before the test.

Compression set is also often used as a guide to the suitability of a component for its purpose; particularly for components such as sealing rings. However, in this context it is, at best, only a guide. More sophisticated tests are generally necessary for sealing applications, involving measurement of retention of sealing force; particularly under varying temperature or pressure conditions, [See: [75.7](#) for elastomer seals].

75.3.5.7 Physical creep and stress relaxation

Given that rubber is a viscoelastic material, it has both elastic and viscous properties. The viscous properties are those which lead to creep and stress relaxation:

- Creep - if a rubber component is held under constant load, the strain increases slowly with time.
- Stress relaxation - if the component is held at constant deformation, its stress decays slowly with time.

Rates of creep and stress relaxation can be related to one another by reference to the local slope of the stress-strain curve for the deformation, Ref. [\[75-14\]](#).

At normal ambient temperatures, creep and stress relaxation are predominantly physical phenomena, associated with rearrangement and slippage of the molecular network under stress. There can also be chemical components to creep and stress relaxation when chemicals affect rubbers, these are increasingly evident at elevated temperatures.

Quantitatively, creep and stress relaxation are expressed in the same way; as presented in Eq [75.3-8] (creep) and Eq [75.3-9] (stress relaxation):

$$\text{creep} = \frac{\Delta e}{e_0} \% \quad [75.3-8]$$

Where:

Δe : change in strain,

e_0 : initial strain

Similarly,

$$\text{stress relaxation} = \frac{\Delta \sigma}{\sigma_0} \% \quad [75.3-9]$$

Where:

σ : stress.

The ‘initial’ values of stress and strain are usually taken as the values at one minute, but other origins can be used. Rates of creep and stress relaxation are only mildly temperature dependent in the normal rubbery range. In contrast to chemical effects, physical rates reduce slightly with increasing temperature.

Figure 75.3.5 shows the result of a simple creep test where a weight is hung on an elastic strip at ambient temperature and the change in extension is measured with time. It shows that the rate of creep reduces rapidly with time. However, if the data are re-plotted using a logarithmic axis for time, an interesting and useful effect is observed. Figure 75.3.6 shows the same data plotted against a log time.

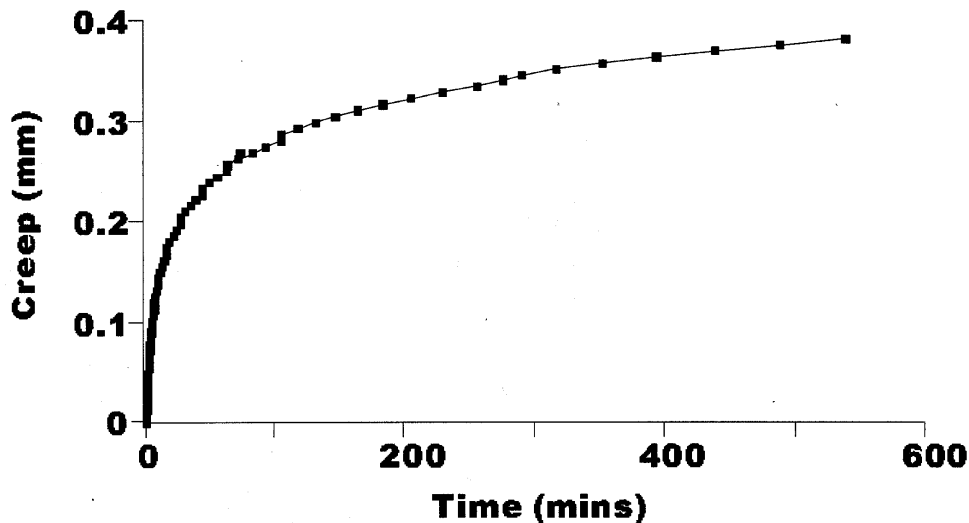


Figure 75.3-5 – Elastomers: Creep of a weighted rubber strip

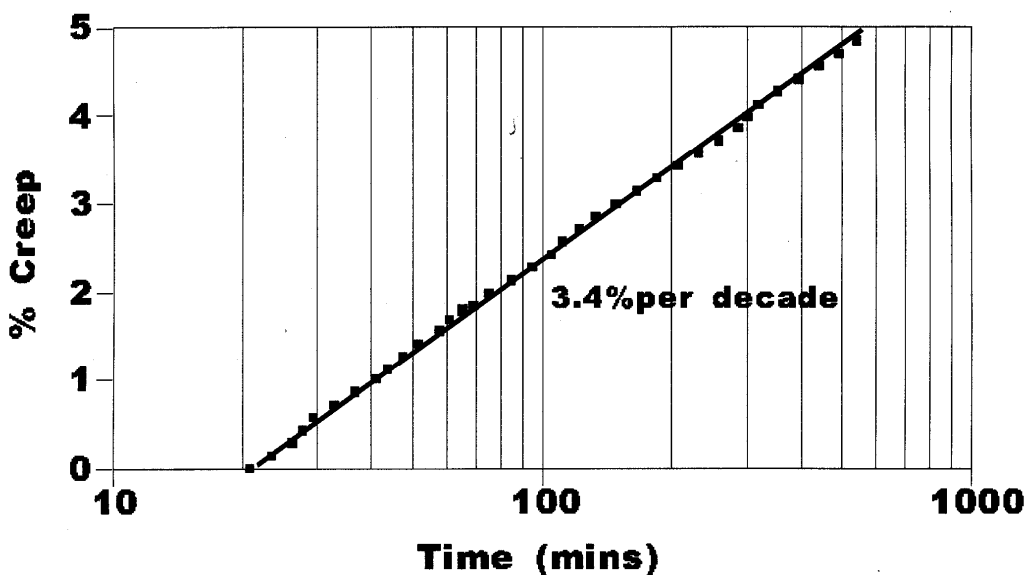


Figure 75.3-6 – Elastomers: Creep of a weighted rubber strip (logarithmic time)

Figure 75.3.6 shows that the plot is now linear, which is always approximately the case for plots of physical creep or stress relaxation of elastomers against logarithmic time.

The percentage creep is the same for any factor of ten increase in time, say 10 minutes to 100 minutes, or 2 months to 20 months. This provides a convenient way of expressing comparative creep (or stress relaxation) rates, as so-many-percent per decade of time, e.g. a rate of 3.4% per decade (10-years), as stated on Figure 75.3.6.

Total physical creep in the lifetime of a component can be estimated by undertaking similar tests and extrapolating the results to the service life.

75.3.6 Chemical properties

75.3.6.1 Heat resistance

Degradation of elastomers at elevated temperatures is usually oxidative.

Oxidation is a chemical reaction, and as such the rate approximately doubles for each 10°C rise in temperature. Oxidation rates, however, are governed by the availability of sufficient oxygen to sustain the reaction. In bulky elastomeric components, even at high temperature, the rate of reaction can be 'diffusion controlled', i.e. the rate of reaction is determined not just by the temperature, but by the rate at which oxygen can diffuse into the component.

Figure 75.3.7 shows the relative oxidation rate at 110°C for strips of natural rubber of varying thickness from 0.25mm to 7mm, Ref. [75-15].

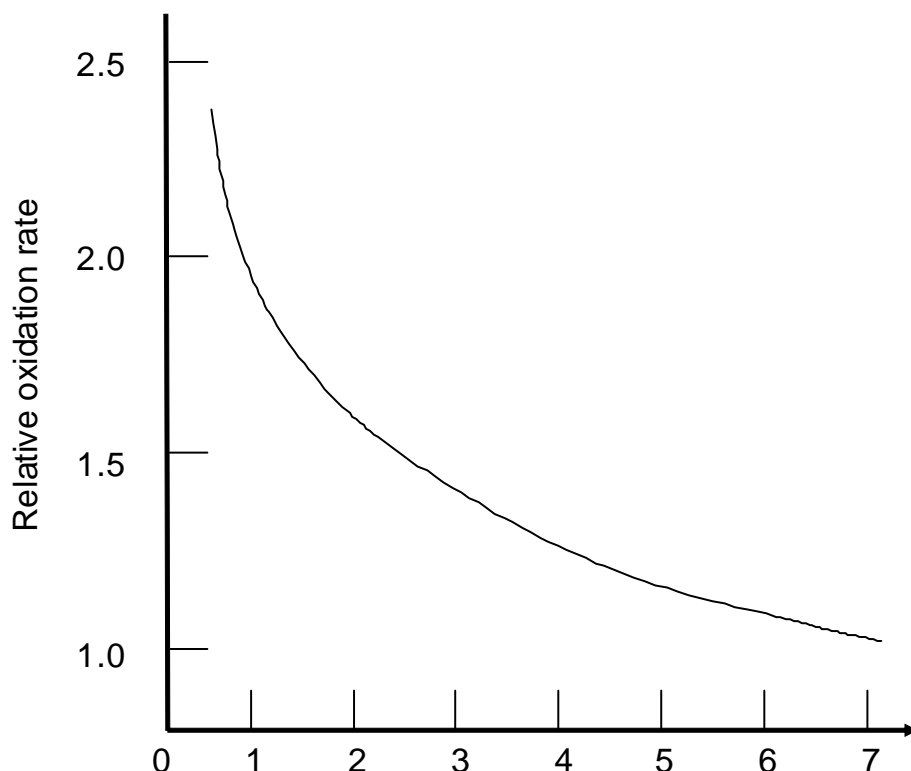


Figure 75.3-7 – Elastomers: Effect of sample thickness on oxidation rate at 110°C

The shape of the curve (left-hand side) shows that, at 110°C, the rate is governed by diffusion control even for the thinnest specimen. The average rate of oxidation in a 7mm strip is only half of that in a 1mm strip, and the rate is even lower for thicker sections.

Some elastomers form a resinous skin during long-term atmospheric exposure. This skin can take-up oxygen and protect the interior of the component, but this is normally only effective in static applications because the skin cracks under cyclic conditions.

In selecting an elastomer for an application it is necessary to take a balanced approach. When choosing a material for a substantially bulky component, it can be counterproductive to choose an unnecessarily heat-resistant elastomer. The gain in heat resistance is usually only achieved by accepting a loss in physical properties associated with heat-resistant rubbers, so that the two factors –

heat resistance and physical properties – need to be carefully balanced. Model tests, and the use of past experience, can be needed in order to optimise selection.

75.3.6.2 Low temperature resistance

The effects which low temperatures have on the stiffness and resilience of rubber were believed to be responsible for the Challenger Space Shuttle disaster in January 1986, where leakage of fuel past elastomeric O-ring seals led to the fatal explosion, although issues with the design of the sealing system were also questioned.

There are three low temperature effects to be aware of, i.e.:

- glass transition, T_g
- contraction,
- crystallisation.

The stiffness of elastomers below the T_g glass transition can be up to 1000 or more times its value in the rubbery region, [See also: Elastomers - temperature effects].

Elastomers are generally not used at temperatures which are not comfortably above their glass transition temperatures, both because of stiffening and because of increased creep and stress relaxation.

The coefficient of thermal expansion (and contraction) of elastomers is generally around 10 times greater than that of steel. Elastomeric seals in steel housings therefore shrink significantly in relation to the size of the housing when the temperature is reduced.

Thus, for example, the effects of contraction, reduction in resilience, and stiffening act together to reduce the effectiveness of an elastomeric seal as temperatures fall, [See: [75.7](#)].

Crystallisation is a completely separate effect. Elastomers can become partially crystalline under strain, due to the lining up of molecular chains. The effect is most noticeable in natural rubber and polychloroprenes, such as Neoprene™ from DuPont. These two elastomers can become significantly crystalline at low temperatures even in the absence of strain.

Crystallisation generally occurs slowly, but can lead ultimately to a 100 fold increase in elastic modulus, and a sharp increase in creep and stress relaxation rates. Crystallisation is reversible on heating, although a higher temperature can be necessary for reversal than that at which crystallisation commenced.

Crystallisation in natural rubber is not generally a problem until temperatures fall below about -15°C. It can occur in polychloroprene from about 0°C downwards. The extent of the crystallisation is strongly dependent on the chemistry of the vulcanising system. Crystallisation problems can often be overcome by changes to the grade of the elastomer or the formulation of the compound, without needing to change in the base elastomer.

75.3.6.3 Chemical resistance

Chemical degradation of an elastomer can be caused by a number of agents, including:

- Oxidation in air, particularly at higher temperatures.
- Hydrogen sulphide gas.
- Liquids, of which many are detrimental, e.g. ionic attack by amines on some elastomers, free radical reactions and even attack by water at high temperatures.

A method of determining the extent of attack on a particular elastomer is by the use of chemical stress relaxation (or creep) measurements. Chemical relaxation is brought about by chemical attack which actually breaks the molecular chains, or the crosslinks which give stability to the network (crosslink scission).

Physical creep and stress relaxation, [See: [Figure 75.3.5](#)], are negligibly temperature dependent in the normal working range. However, chemical relaxation is linear with time and is strongly temperature-dependent, increasing in rate with rising temperature, because it is a chemical reaction.

In a stress relaxation test the total relaxation can be expressed as:

$$\frac{\Delta\sigma}{\sigma_0} = A \log(t/t_0) + B(t - t_0) \quad [75.3-10]$$

Where:

- A:* is the physical contribution, given as physical rate in percent per decade.
B: is the chemical contribution, given by chemical stress relaxation rate in percent per unit time (usually per minute).

The result of a stress relaxation test can be analysed by fitting it to the expression in [Equation \[75.3-10\]](#).

The chemical rate can be most readily determined at elevated temperatures where the chemical reaction occurs more quickly. It is usually impracticable, in terms of time taken, to measure it at ambient temperature.

If the chemical rate, *B*, is measured at a number of elevated temperatures, and the logarithm of this rate is plotted against the reciprocal absolute temperature, then a straight line is normally obtained; known as an Arrhenius plot. This consists of straight lines provided that the processes involved in the phenomenon do not change fundamentally as a result of temperature change, e.g. not appropriate if the temperature changed so much that the material passed through a transition. [Figure 75.3.8](#) shows an Arrhenius plot in which a good straight line was obtained based on four measured experimental points. It shows the test temperatures, i.e. 195°C, 155°C, 130°C, and 100°C, and the line extrapolated to room temperature, 23°C.

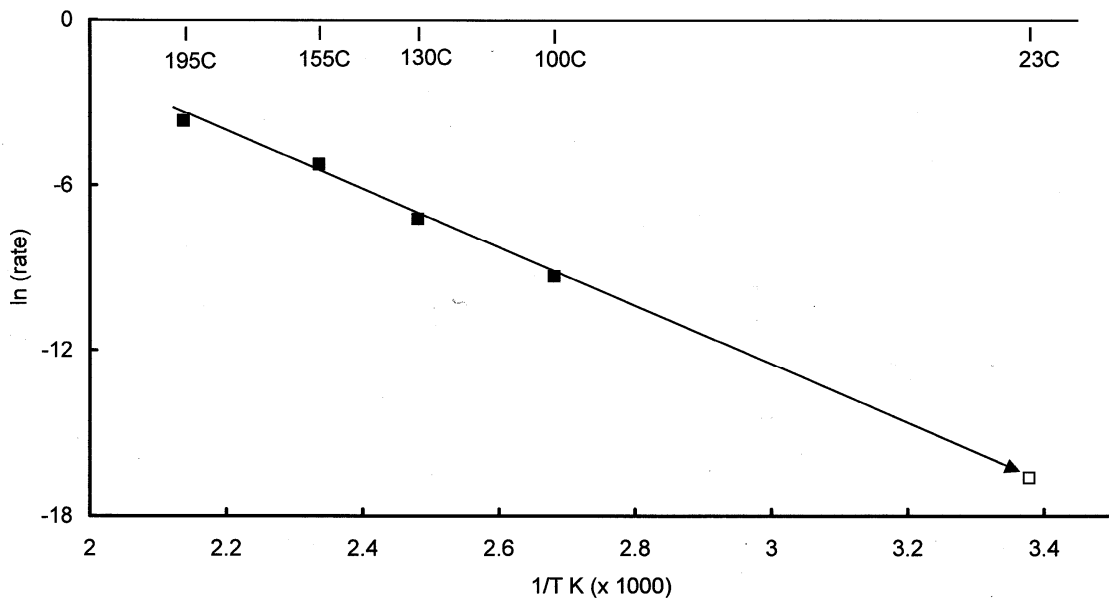


Figure 75.3-8 – Elastomers: Arrhenius plot example

The creep rate at 23°C can be read from the graph (antilog of -16.5 i.e. 6.8×10^{-6} % per minute). The total creep at room temperature for any given time can then be calculated.

Arrhenius plots are a useful way of predicting the rate of processes which are slow at operating temperature, but which can become important over the service life.

75.3.7 Rubber-to-metal bonding

A large number of rubber components are bonded to metal. Plain rubber blocks slip at the loaded surfaces, leading to an uncertain compression stiffness. Fixing to other components is facilitated by the presence of metal end-plates to the rubber component.

Bonding after vulcanisation is possible, but often uncertain in quality. For the best bonds, adhesion is usually achieved during the vulcanisation process. Metal surfaces are prepared, usually by grit blasting and degreasing, and then coated with adhesive; most often a two-part system comprising primer and adhesive. Under the pressure applied during moulding of the part a very strong bond can be achieved.

Special 'peel test' samples are made to determine the strength of the bond. A strip of rubber is then pulled away from the bond and the force to do this is measured. For engineering purposes the quantitative measure of the peel strength is less important than the mode of failure. For the best bonds, tearing always occurs in the rubber and not at the bond interface. This is the ultimate criterion as the bond strength cannot exceed the strength of the rubber.

75.3.8 Engineering design with elastomers

75.3.8.1 Fundamental aspects

Elastomers are rarely used in tension in engineering applications. Most components operate in shear or compression or a combination of the two, occasionally in torsion or bending.

Except for seals, washers and tyres, most elastomeric engineering components are strongly bonded to metal plates during the vulcanisation process to provide surfaces through which the load can be applied, and to prevent the rubber from slipping at the loaded surfaces.

75.3.8.2 Shear stiffness of simple blocks

The shear stiffness, K_s , of a bonded rubber block, such as that shown in [Figure 75.3.9](#) is given by Eq [75.3-11]:

$$K_s = \frac{GA}{t} \quad [75.3-11]$$

where:

A: the cross sectional area.

G is the shear modulus of the rubber.

t: thickness

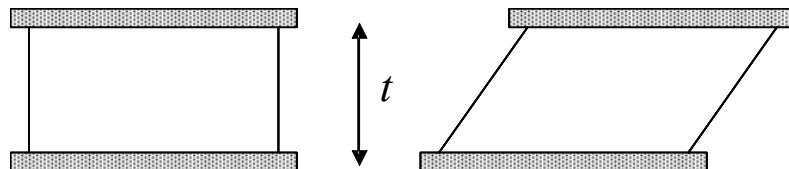


Figure 75.3-9 – Elastomers: Simple rubber block in shear

The expression applies for any plan shape, e.g. square, rectangular, circular. However, if the ratio of thickness to plan dimension exceeds about 0.25, then the block acts as a column and allowance for bending needs to be made.

75.3.8.3 Compression stiffness of simple blocks

If a block, [See: [Figure 75.3-9](#)] is subjected to compression, the compression stiffness, K_c , is given by a similar expression:

$$K_c = \frac{E_c A}{t} \quad [75.3-12]$$

Where:

E_c : compression modulus.

A : the cross sectional area.

t : thickness

The compressive modulus is not just a material property, but is dependent on both the intrinsic stiffness of the rubber and the shape of the block.

Rocard first described compression characteristics of rubber blocks of various shapes, e.g. circular and elliptical cylinders, rectangular blocks, and short and long parallelepipeds. The expressions now used include a parameter known as the shape factor, S , which is the ratio of one loaded area of the block to the total force-free area. This is key to all calculations involving the compression of elastomeric components.

- Circular section block, S is given by:

$$S = \frac{\pi r^2}{2\pi rt} = \frac{r}{2t} \quad [75.3-13]$$

- Rectangular block S is given by:

$$S = \frac{lb}{2(lt + bt)} \quad [75.3-14]$$

Where:

l : length

b : breadth (width)

Rocard's equation for compression modulus E_c is then given by:

$$E_c = 3G(1 + 2S^2) \quad [75.3-15]$$

The equation is a good approximation for most engineering rubbers in the hardness range 60 IRHD to 80 IRHD, [See also: Physical properties – hardness].

For shape factors above about 2.5, i.e. squat blocks, a good approximation is:

$$E_c = 5G S^2 \quad [75.3-16]$$

A more detailed treatment of the compression stiffness of blocks can be found in Ref. [75-16].

75.3.8.4 Compression stiffness of laminated blocks

Laminated rubber blocks comprise a number of discrete rubber layers divided by horizontal metal plates to which the rubber is strongly bonded. These are very widely used in applications from simple anti-vibration machine mountings to anti-seismic base isolation systems which protect buildings and other structures from earthquakes, [See also: 30.14 for the design-development of Ariane 5: LEC laminate elastomeric components].

The key advantage of laminated block-type components is the ability to control independently, by design, the shear and compression stiffnesses. The compression stiffness is controlled by the thickness and number of the laminations, i.e. exploiting shape factor effects, while the shear stiffness is controlled only by the area and total height of rubber in the block.

Figure 75.3.10 shows two blocks of the same plan section and having the same total height of rubber, hence the same shear stiffness. Block B, however, is divided into 7 layers.

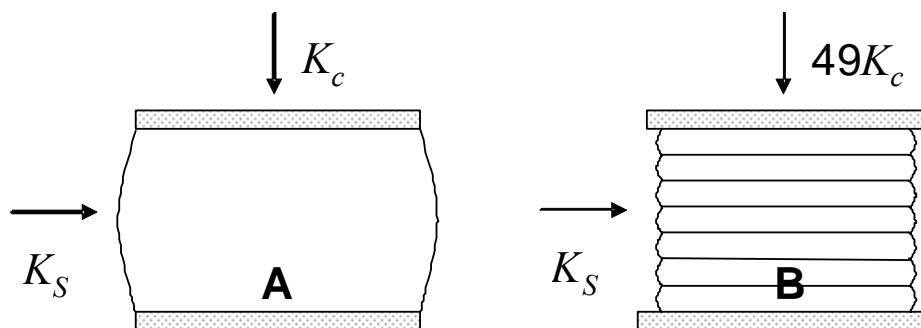


Figure 75.3-10 – Elastomers: Increasing compression stiffness by lamination

Given that the compression stiffness of a squat block is approximately proportional to the shape factor, S , squared. To a first approximation, block B has 7^2 , i.e. 49 times, the compression stiffness of block A. This enables great versatility in design and this can be further exploited by using, for example, an opposing pair of tilted blocks. The vertical load then deforms the laminated block both in the stiff compression mode and the relatively softer shear mode. Thus, by changing the angle of tilt a wide variety of compliances in both the vertical and horizontal directions can be obtained.

Although elastomers have very high bulk moduli and so are relatively incompressible, the compressibility does become significant at high shape factors.

When the compression modulus of a block exceeds about 10% of the bulk modulus, E_∞ , which is typically from 1000MPa to 2000MPa, then the effective compression modulus, E_{eff} becomes:

$$E_{eff} = \frac{E_c}{1 + (E_c/E_\infty)} \quad [75.3-17]$$

75.3.8.5 Torsion stiffness

Torsion is a less common mode of deformation in engineering applications, but can be useful in some vibration isolation applications when a relatively soft mode of deformation is needed. The assumption is made that the ends of the torsion annulus are strongly bonded to metal plates; as shown in Figure 75.3.11.

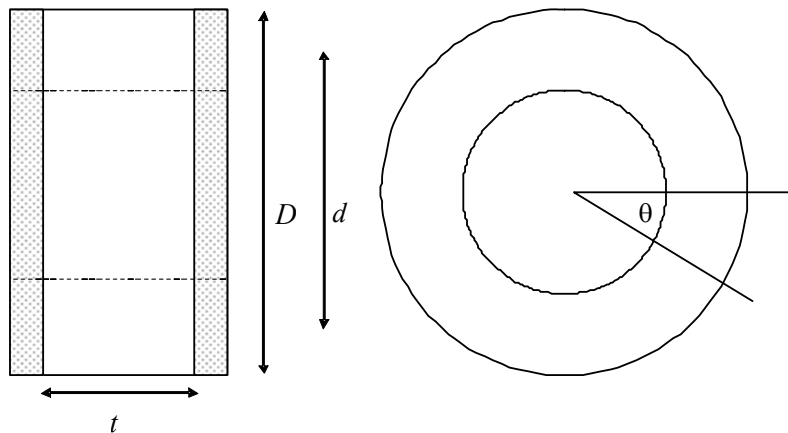


Figure 75.3-11 – Elastomers: Elastomeric torsion disc

The torsional stiffness is given by:

$$K_{\theta} = \frac{T}{\theta} = \frac{\pi G}{32t} (D^4 - d^4) \quad [75.3-18]$$

Where:

T: torque,

θ: angular rotation in radians,

G: shear modulus as before,

t: thickness,

D: outer diameter,

d: inner diameter.

75.3.9 Finite element analysis

For many solid or laminated components made of rubber and steel, simple equations are adequate and are probably preferred for designs where stiffness and deformation characteristics are necessary, [See: Engineering design].

For components of complex shape, however, FEA finite element analysis methods can be needed to determine the stiffness and deformation characteristics. In cases where the distribution of stresses and strains is important, e.g. to detect stress concentrations, FEA is usually necessary. Special methods for FEA of rubber components have been developed. It is a valuable tool in design, but needs a different approach from FEA for small strain elasticity.

Firstly, an FEA approach needs a suitable material model for the vulcanised elastomer. In contrast to other solid materials, the strains are very much higher, and the stress-strain characteristics are non-linear. The material models are based on 'strain energy density' or 'potential', which is an expression for the energy stored in the rubber per unit volume as a function of the strain. There are a number of different equations in use for strain energy density; appropriate to different circumstances. Laboratory tests are carried out on samples of the rubber, identical in formulation and cure characteristics to those of the final product. The tests typically include uniaxial tension, uniaxial compression and pure shear.

Given the high strains involved, the material model is called a 'hyperelastic model'. The input from the laboratory tests are used in the FEA program to generate the coefficients for the chosen mathematical strain energy density model. FEA analysis can then proceed as normal, by reducing the component to a suitable mesh, and following the deformation in terms of stresses and strains.

There are some special considerations which need to be taken into account when using FEA methods for elastomers, i.e.:

- Anisotropy: Both the classical equations for stiffness, and FEA techniques, assume that rubber is isotropic, and remains so under deformation. This is normally a perfectly acceptable assumption. However, some elastomers, notably natural rubber and polychloroprene, crystallise under strain. This leads to anisotropic properties which become important when fracture analysis is undertaken, because the high strains at the tip of a crack lead to local crystallisation in such rubbers (the source of their high strength), and hence anisotropy. In cyclic deformations of strain-crystallising rubbers, the extent of crack growth in the rubber depends on the minimum and maximum strains, and whether the cycle passes through a zero strain condition. Not all FEA programs can account for this.
- Compressibility: The very high compressibility of rubber components can also lead to complications in FEA analyses. Bulk compression has an important effect on stiffness for high shape factor layers. As an example, despite the high incompressibility of rubber, approximately one third of the total compression of a bonded 40cm square block of thickness 1 cm (i.e. a shape factor of 10), is due to bulk compression - and only two-thirds due to normal bulging. Modern specialised programs enable the input of true bulk moduli to give correct solutions for high shape factor conditions.
- Creep or stress relaxation can be taken into account in some FEA procedures to enable some allowance for time-dependent effects. Laboratory data is needed in order to set rates of creep or stress relaxation for the actual material. In some cases only a somewhat simplified version of the time-dependent behaviour can be introduced into an FEA program, e.g. where both physical and chemical relaxation are present.
- Stress-softening of elastomers ('Mullins effect') is important under cyclic conditions. It is the dynamic equivalent of creep, and can be taken into account in FEA analysis.

75.3.10 Applications

75.3.10.1 General

Industrial, general engineering and aerospace applications for elastomers are similar. Some typical examples include:

- Vibration isolation, e.g. anti-vibration mounts,
- Seals, such as O-rings and gaskets, [See: [75.7](#)],
- Flexible bearings,
- Fuel hoses,
- Fuel cells,
- De-icing systems,
- Electrical insulation,
- Membranes and bladders, for fluid containment.

75.3.10.2 Vibration isolation

A major application for elastomeric components is in vibration isolation. Vibration isolators work, not by absorbing the energy of vibration, but by simply blocking the incoming frequencies by detuning.

Any mass on a spring has a natural frequency which is determined by the mass and the stiffness of the spring. The mass receives much reduced energy from the vibration if it is mounted on a spring which gives it a much lower natural frequency than the frequency of the disturbance. In this context elastomers have a distinct advantage over steel springs because of their inherent damping.

Although damping is not the main mode of operation, a small amount of damping is always necessary to avoid resonance in case stray vibrations occur in the system, i.e. a frequency different from the main disturbance. A metal spring is therefore normally twinned with a damper, but the rubber component combines these in one isolator.

Vibration isolation, using this technique, has been applied successfully to buildings, e.g. in the proximity of underground train lines or in zones susceptible to earthquakes, Ref. [[75-17](#)].

[See also: [30.14](#) – Ariane 5 vibration isolation; [95](#) – vibration control using smart systems]

75.3.10.3 Seals

Elastomers are widely used in sealing applications because they are both soft and resilient. In many cases, no alternative material is available.

The choice of elastomer for a particular seal is governed primarily by:

- working temperature range,
- fluids to which the seal is exposed.

The important factors to be considered during the design of elastomer-containing seals, include, [See: [75.7](#)]:

- pressure,
- dimensions,

- knowledge of possible causes of leakage, e.g.
 - temperature,
 - pressure,
 - changes in fluids.
 - explosive decompression; also known by rubber technologists as 'rapid gas decompression'.

75.3.11 Thermoplastic elastomers

As well as the wide range of vulcanised (thermoset) materials, thermoplastic elastomers (TPEs) are another class; so called because they can be processed like plastics. They behave broadly similarly to vulcanised rubbers, but without being vulcanised during moulding.

TPEs are a two-phase system comprising a hard thermoplastic phase and a soft elastomeric phase. Depending on the relative proportions of the two phases they can behave more like a plastic or more like a rubber. They are usually pre-compounded, so that they are processed by raising the temperature to the melting point of the system followed by a moulding process to form a suitable shape which is retained on cooling.

The best TPEs have applications which overlap with vulcanised rubbers, e.g. used for tubing in fuel lines and in aircraft glazing.

In general, TPEs do not figure greatly in technical engineering applications, as a brief excursion to the melting temperature can lead to distortion. Owing to their nature, they also have high compression set, creep and stress relaxation characteristics, Ref. [74-18].

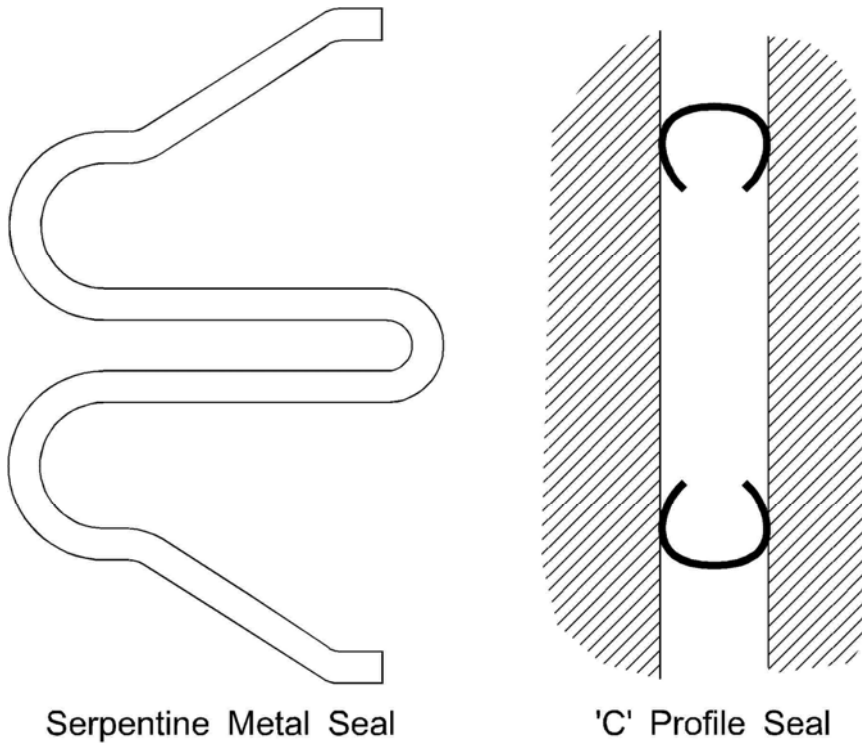
75.4 Energised metal seals

75.4.1 General

This class of seals uses a metal strip which is shaped in section to provide a compressible spring, Ref. [74-3].

The installed seal is pre-loaded in-situ (energised) and any relative movement is taken up by the elasticity of the spring. Such a system is being developed for Ariane 5 engine assemblies, Ref. [74-4], and has a 'C' profile, as shown in [Figure 75.4.1](#).

An alternative serpentine profile is also shown, Ref. [74-3] which requires less compressive force (pre-loading) than the 'C' seal.



Serpentine Metal Seal

'C' Profile Seal

Figure 75.4-1 - Metal seals: 'C' profile and serpentine

75.4.2 Materials

Appropriate materials include:

- Nimonic 90,
- Inconel X-750,
- Inconel 718, and
- Elgiloy.

Seals made from these alloys are expected to retain their spring capacity up to 800°C.

75.5 NASP engine developments

75.5.1 General

The development of the NASP engine is an example of advanced high-temperature seal technology, Ref. [75-5], [75-6].

NASP is reliant on a hydrogen-burning hypersonic engine, [See: 73.10].

Designs similar to turbojet nozzles are being considered with movable panels. The extremely hot, pressurised engine flow-path gases are prevented from escaping past the movable panels. Consequently there is a need for:

- Hinge seals, between adjacent movable panels, and
- Panel-edge seals, along each side of the movable panel.

The basic requirements are:

- Prevention of leakage of flow-path gases at 0.7MPa (100 psi),
- Resistance to gas temperatures greater than 2400°C,
- Allowance for increases in panel separation (gap) of 3.8mm.

To minimise leakage, the panel-edge seals are sufficiently pre-loaded and compliant to seal against engine wall distortions.

75.5.2 Developments

75.5.2.1 Ceramic Wafer Seal

This concept consists of multiple ceramic wafers mounted in a closely mating horizontal channel alongside the movable horizontal engine panel. The seal is pre-loaded against the engine splitter wall using an active preload system, such as a series of cooled pressurised metal bellows, as shown in Figure 75.5.1, Ref. [75-5]. The bellows push against a flexible metal backing plate that distributes the load to the wafers between the discrete circular bellows. The wafer seal conforms to engine splitter wall distortions by relative sliding between adjacent wafers.

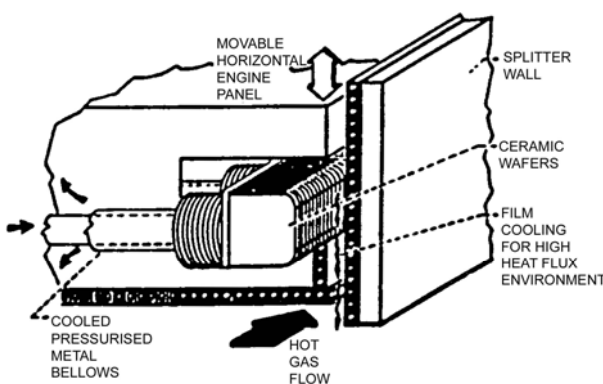


Figure 75.5-1 - NASP: Ceramic wafer seal

75.5.2.2 Braided Ceramic Rope Seal

Figure 75.5.2 shows that the ceramic wafers can be replaced by a braided rope, Ref. [75-5]. This is formed of alumina-boria-silicate (Nextel) fibres capable of sustaining 1260°C. In high heat flux environments, a pressurised coolant gas flows down the axis of the seal inflating the seal, conforming it to the engine walls and keeping it cool.

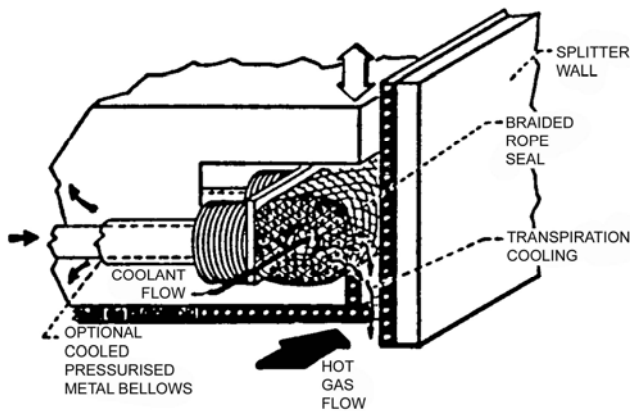


Figure 75.5-2 - NASP: Braided rope seal

All grades of Nextel fibre (Nextel 312, 440, 550 and 610) were studied to evaluate their durability for the intended 55 hours hot exposure, Ref. [75-5].

These seals are modelled to predict their performance under the most arduous conditions, where heat flux levels can reach 13.6MW/m², Ref. [75-6].

75.5.2.3 'V'-ring and 'U'-ring Seals

These are used to seal the heat exchanger panels to the non-integral, back-up structure.

Non-integral heat exchanger panels line the wetted surfaces of the NASP engine and expand while heating up to operating temperature. The heat panels glide over thin gauge, flexible seals without damaging either the seal or heat exchanger panels.

Solid lubricants such as gold and nickel are under evaluation. Representative seal materials include HS188 and Incoloy 909.

75.6 Fibrous seals

These are used on both Shuttle, Ref. [75-7], and Buran to fill the gaps between the TPS tiles, [See: 71.5].

Similar requirements were in the Hermes design for inter-shingle seals, Ref. [75-8], [See: 71.12]. The basic specification for these was:

- Dimensions: height 20mm; width 4mm and length 300m,
- Temperature: 1300°C (limit) and 1450°C (emergency),
- Emissivity: > 0.85,
- Plasma erosion resistance,
- Elastic and compliant.

The seals ageing behaviour needs to be well understood.

75.7 Elastomeric seals

75.7.1 Materials

75.7.1.1 General

Elastomers are widely used in sealing applications because they are both soft and resilient. In many cases, there is no alternative material that can be used.

The choice of elastomer for a particular seal is usually governed primarily by the:

- working temperature range, and
- the fluids to which the seal is exposed.

[See: [ECSS-Q-70-71](#) for material and process selection]

75.7.1.2 Aerospace

Although some elastomers are now claiming high-temperature resistance to 325°C or more, there is often a lack of information with respect to their physical performance at these temperatures. Temperature resistance often refers to survival rather than retention of good physical properties.

A good design ensures that the component continues to serve its function under all service conditions, rather than simply choosing an elastomer that survives high temperature or chemical attack. It is essential that this ability be verified by laboratory and field testing.

[See: [75.3](#)]

75.7.2 Design aspects

The design of the seal and its housing is principally governed by the maximum pressure to be sealed. For example, back up rings of a stiffer thermoplastic can be incorporated in a design to prevent the relatively soft elastomeric seal from being extruded into the inevitable gap around the seal housing.

The size of the seal is also very important as it can govern the rate of absorption of fluids. It is important not to over-specify in terms of heat resistance or fluid resistance. Elastomers with higher heat or fluid resistance almost invariably have poorer physical properties, particularly at higher temperatures, and they lose their rubbery properties at lower temperatures. A 'safety factor' for temperature or fluid resistance can become a 'danger factor' for sealing.

A very small amount of fluid can, in some cases, actually penetrate through the thickness of the seal by diffusion. This is only of importance in extremely critical applications, but the possibility cannot be ignored. Significant leakage normally occurs due to seepage of fluid past the outer faces of the seal, because the retained force in the seal has reduced excessively, or because of physical damage, or because of chemical degradation.

75.7.3 Causes of leakage

75.7.3.1 Static seals

Static seals, when designed competently, rarely leak in continuous use. Leakage almost always follows a change in conditions at the seal, e.g.

- temperature change,
- pressure change,
- change in composition of the fluid being sealed.

Under continuous use, seals actually perform rather better than simple predictions forecast. There are probably two reasons for this:

- adhesion of the seal to the mating surfaces over extended periods of time,
- a small amount of swelling of the seal due to contact with the sealed fluid.

Although seals are chosen on the basis of no absorption of the contacting fluid, be it liquid or gas, in fact a small amount of swelling is a major contributor to successful sealing.

75.7.3.2 Pressure-energised seals

Some seals are pressure energised, i.e. the pressure of the fluid being sealed acts to force the seal to make good contact with the sealing surfaces. However, such a seal cannot rely on pressure energization alone. It needs to seal initially before pressure is applied; otherwise a leakage path occurs from the outset and, however much pressure is subsequently applied, it is very unlikely that proper sealing is ever achieved. At best a 'bumping' technique, whereby the pressure is applied in sudden surges, is resorted to in an attempt to re-energize the seal. The Viton™ seals in the Challenger space shuttle were found not to have sealed fully, even in previous successful launches. Evidence of incomplete sealing is considered as failure and leads to a redesign.

75.7.3.3 Effect of temperature

A drop in temperature needs a seal to work harder due to reduced sealing forces and material contraction effects, Ref. [75-10], [75-19], [75-20].

The sealing force reduces because the stress in a deformed rubber component is proportional to absolute temperature. Thus, if the temperature reduces, so does the sealing force. Additionally, the seal contracts away from its housing with decreasing temperature, hence the sealing force drops still further.

The retained (reduced) resilience of the seal needs to be such that recovery of the seal from its compressed size is sufficient dimensionally, and fast enough, to maintain sealing during the temperature drop. Seals can and do achieve this, but only through knowledgeable design.

75.7.3.4 Effect of pressure

A pressure drop on a pressure-energised seal cannot reduce the sealing force to zero, or the seal does not function when the pressure is re-applied. The seal material needs sufficient recovery under the temperature conditions during pressure reduction to maintain some sealing force. Even seals which are not primarily pressure energised are usually deformed by the fluid pressure and need to recover towards their original shape in order to maintain seal contact on repressurisation.

75.7.3.5 Changes in fluids

Where the nature of the sealed fluid changes during the service life problems can occur. For example: when the UK national gas supply changed in composition the replacement gas had a smaller swelling effect on the seals. Contraction of the seals occurred resulting in leakage.

75.7.3.6 Explosive decompression

The term 'explosive decompression' as used in rubber technology is not the same as that in the aerospace industry describing loss of pressure inside an aircraft due to fuselage failure. Consequently the rubber technology term is now sometimes replaced by 'rapid gas decompression'.

A particular type of failure can occur when gases at high pressure are absorbed by an elastomer, and then the external pressure is suddenly released. This is generally known as explosive decompression (ED).

ED occurs because very large amounts of gas can dissolve in an elastomer under pressure. No problem exists while the pressure is maintained, but if the pressure is released rapidly the gas comes out of solution within the bulk of the elastomer as rapidly growing bubbles. This can lead to catastrophic failure.

Usually gas pressures of more than 100 atmospheres are thought to be necessary to produce ED, although in weaker rubbers it has been observed on decompression from 30 atmospheres to atmospheric pressure.

Two strategies are available to inhibit explosive decompression. The first of these compounds the elastomer to have the highest possible tear strength, and to have as high a modulus as is practical. Such elastomers are described as 'ED resistant', but this is just a relative term. Resistance depends on a number of factors, including the base elastomer, the contact fluids and their solubility, swelling due to absorption, the morphology of bubble formation, and the design of the housing. This last factor provides the second strategy for resisting ED damage. Elastomers are essentially incompressible. Bubbles of gas can only grow within the elastomer if the volume of the rubber can increase by the same amount. Seal housings often have considerable free volume surrounding the seal, for good reasons connected with tolerances and to provide an allowance for swelling. However, in high pressure gas applications, seals need to occupy the maximum possible proportion of the housing groove. Housing design is key to ED resistance. It is likely that a softer rubber which tightly fills its housing, with adequate anti-extrusion protection, has better ED resistance than simple reliance on 'ED resistant' elastomers.

75.7.3.7 Testing aspects

The examples given serve to define the types of testing that need to be carried out in order to qualify seals. Long-term tests are generally less appropriate than shorter-term tests in which the conditions are cycled to replicate shut-downs or failures occurring in-service. For example, temperature cycling tests have been devised where the sealing force is measured directly as the temperature is raised or lowered.

75.7.4 Aerospace applications

Aerospace applications for elastomers are similar to normal engineering applications, e.g. anti-vibration mounts, flexible bearings, fuel systems (hoses, cells), de-icing systems and in O-rings, gaskets and other types of seal.

[See: [30.14](#) for an example of elastomers used in Ariane 5]

Aerospace can, however, have much greater applications demands than are usual, e.g. higher temperatures, wider temperature extremes, very high chemical resistance, high purity to avoid contamination.

[See: [ECSS-Q-70-71](#)]

75.8 References

75.8.1 General

- [75-1] A.O. Lebeck
'Principles and Design of Mechanical Face Seals'
A Wiley-Interscience Publication, ISBN 0-471-51533-7
- [75-2] P.F. Brown
'Status of Understanding for Seal Materials'
New Directions in Lubrication, Materials, Wear and Surface Interactions:
Tribology in the 80's, Cleveland , Ohio, Apr 1983 p771-789
- [75-3] 'Metallic Sealing Ring'
UK Patent Application, GB 2 190 154 A, Nov 1987
- [75-4] 'Test Programme for Energised Metal Seals'
Work undertaken by Advanced Products N.V. Work Order No. 18
ESTEC Contract 7090/87/NL/PP
- [75-5] B.M. Steinmetz et al
'High Temperature NASP Engine Seal Development'
NASA Technical Memorandum 105641, April 1992
- [75-6] 'Seals Flow Code Development'
Proceedings of NASA Workshop, Mar 1991, NASA Conference
Publication 10070
- [75-7] D.M. Curry: NASA/JSC
'Space Shuttle Orbiter Thermal Protection System Design and Flight
Experience'
First ESA/ESTEC Workshop on Thermal Protection Systems ESTEC,
Noordwijk, 5-7 May 1993, ESA-WPP-053 (August 1993)p122-135
- [75-8] E. Werling & J.P. Vialaniex: ESA/HPD
'Hermes re-orientation programme - Present Status and Main Objectives
for Hot Structures and Thermal Protection Materials and Technologies'
First ESA/ESTEC Workshop on Thermal Protection Systems ESTEC,
Noordwijk, 5-7 May 1993, ESA-WPP-053 (August 1993) p136-152
- [75-9] C.J. Derham: MERL Ltd., UK
'Creep and stress relaxation of rubbers – the effects of stress history and
temperature changes'
Journal of Materials Science 8, p.1023-29, 1973
- [75-10] C.J. Derham: MERL Ltd., UK
'Transient effects influencing sealing force in elastomeric O-ring seals'

- Plastics, Rubber and Composites Processing and Applications Vol
26 No 3, p.129-36, 1997
- [75-11] S.D. Gehman & T.C. Gregson
'Ionizing radiation and elastomers'
Rubber Chemistry and Technology Vol 33, p.1375-1437, 1960
- [75-12] S.G. Burnay & J.W. Hitchon
'Prediction of service lifetimes of elastomeric seals during radiation ageing'
Journal of Nuclear Materials, 131, p.197-207, 1985
- [75-13] 'Testing Procedure for Measurement of Dynamic Properties of Vulcanized Rubber'
Journal of the Institution of the Rubber Industry (JIRI), April 1973
- [75-14] A.N. Gent
Journal of Applied Polymer Science.
Vol VI, No 22, p.433-441, 1962
- [75-15] C.J. Derham: MERL Ltd., UK
Proceedings of 3rd Rubber in Engineering Conference, London, 1973,
MRPRA
- [75-16] A.N. Gent & C. Hanser (Editors)
'Engineering with Rubber'
Verlag, Munich, ISBN 1-56990-299-2, 2001
- [75-17] C.J. Derham: MERL Ltd., UK
'Vibration isolation and earthquake protection of buildings'
Progress in Rubber and Plastics Technology. Vol 1 No 3 July pp14-27,
1985
- [75-18] J.R. White & S.K. De
'Rubber Technologist's Handbook'
RAPRA Technology Limited, ISBN 1-85957-262-6, 2001
- [75-19] R.K. Flitney & B.S. Nau
'Seal Users Handbook'
Air Science Company, ISBN 0906085993, 1985
- [75-20] B.S. Nau
'Fluid Sealing'
Kluwer Academic Publishers, ISBN 079231669X, 1992

75.8.2 ECSS standards

[See: [ECSS website](#)]

ECSS-Q-ST-70	Materials, mechanical parts and processes
ECSS-Q-70-71	Data for the selection of space materials and processes
ECSS-Q-ST-70-02	Thermal vacuum outgassing test for the screening of space materials
ECSS-Q-ST-70-04	Thermal cycling test for the screening of space materials and processes

ECSS-Q-ST-70-06 Particle and UV radiation testing of space materials

75.8.3 ASTM standards

[See: [ASTM website](#)]

ASTM E595 Standard test method for total mass loss and collected volatile condensable materials from outgassing in a vacuum environment

75.8.4 ISO standards

[See: [ISO website](#)]

ISO 48	Rubber, vulcanized or thermoplastic: Determination of hardness (hardness between 10 IRHD and 100 IRHD)
ISO 37	Rubber, vulcanized or thermoplastic: Determination of tensile stress-strain properties
ISO 34	Rubber, vulcanized or thermoplastic: Determination of tear strength: Part 1: Trouser, angle and crescent test pieces; Part 2: Small (Delft) test pieces
ISO 4662	Rubber: Determination of rebound resilience of vulcanizates
ISO 4663	<title not stated>
ISO 4664	<title not stated>
ISO 815	Rubber, vulcanized or thermoplastic: Determination of compression set at ambient, elevated or low temperatures
ISO 3384	<title not stated>
ISO 8013	<title not stated>

76

Integrity control of high temperature structures

76.1 Introduction

Integrity control is applied to fibre-reinforced composite materials. It determines the requirements for those materials which exhibit failure or fracture characteristics very different from those of traditional metallic materials, [See: ECSS-E-32-01 for fracture control].

The integrity control for new advanced materials, i.e. metallic and ceramic-based composites, aims to ensure that the safety of man-rated and reusable structures made from them is commensurate with that achievable by conventional metallic materials and maintained throughout their operational life.

[See: Chapters [31](#), [32](#), [33](#) and [34](#)]

This Chapter describes factors influencing the integrity of high-temperature structural materials, and includes a resumé of an [ESA](#) programme assessing the integrity control of [SiC](#)-based and [C-C](#) composites, Ref. [[76-3](#)], [[76-4](#)].

76.2 Materials

76.2.1 Integrity control

Of the numerous types of materials being developed with potential space use, Integrity control is applied to those demonstrating characteristics that cannot be adequately described by standard fracture mechanics principles, e.g. [LEFM](#). To date, these have been identified as any material containing a continuous fibre-reinforcement.

The [ESTEC](#) integrity programme, with Dornier, Battelle, Aerospatiale and Schunk, for carbon- and [SiC](#)-based composites aims to provide further information. [See: [76.7](#) and [76.8](#) for a resumé of the findings to date]

Many materials are still undergoing development, one phase of which is to establish their fracture characteristics, and integrity and fracture control requirements by combined testing and analysis. Information presented within this Chapter is preliminary, hence strictly advisory.

76.2.2 Fracture control

For materials whose behaviour can be predicted by fracture mechanics, the term 'Fracture Control' is used.

[See: ECSS-E-ST-32-01]

To date, these include some particulate-reinforced materials, some whisker-reinforced materials and the advanced metal alloys in which high-temperature strength is achieved by alloying or by dispersion strengthening through the addition of very small amounts of small particles to modify the microstructure, e.g. ODS alloys.

Care is required for directionally solidified metals or those in which other processing gives significantly anisotropic properties.

76.3 Failure characteristics

76.3.1 Advanced alloy systems

In general, all attempts to increase high-temperature strength have resulted in a lowering of ductility. As a result, the critical defect size has decreased for non-composite materials.

76.3.2 Composite materials

76.3.2.1 General

Differences exist between the failure mechanisms of those with metal and those with ceramic matrices.

76.3.2.2 Metal matrix

A metal matrix can exhibit metal fatigue-type damage; although differences between matrix and fibre combinations are significant.

76.3.2.3 Glass and ceramic matrix

Glass and ceramic matrices fail by the accumulation of microcracks to a critical level, rather like fibre-reinforced plastics, but unlike monolithic ceramics.

76.3.2.4 Fibre-to-matrix interface

Failure characteristics are influenced by the fibre-to-matrix interface, which has to be 'engineered' to provide an adequate but not too strong bond.

If bonding is too high, cracks originating in the matrix can propagate through the reinforcing fibres and failure is then brittle.

76.4 High temperature

Operation at high temperatures means that the material systems used are likely to undergo microstructural changes, as well as experiencing mechanical or thermal loading damage and surface environmental attack.

Therefore another aspect of integrity or fracture control is to ensure that the environments experienced do not cause excessive deterioration of materials during manufacture or in service. This is especially important for reusable items or manned structures.

76.5 Coatings

76.5.1 General

Depending on the intended application, coatings can be used to provide the required environmental resistance, either metallic, ceramic or mixtures of the two.

Coating integrity, which can significantly influence the operational life of the underlying material, is established under representative conditions which are often difficult to simulate.

76.5.2 Manufacturing

Manufacturing processes can significantly affect the evenness of coating thickness and residual stresses. The process temperature and conditions (CTE mismatch between substrate and coating materials) and the way the coat is deposited affect the crack and spall resistance.

The material system can be very complex, e.g.

- carbon fibre multi-directional reinforcement in a SiC infiltrated matrix, with
- multi-layered coating deliberately engineered to vary in composition with depth.

Individual layers are often only a few micrometres thick, with the overall coating thickness within the range of 10 μm to 500 μm , depending on the type. In general, thicker ceramic coatings are used as a thermal barrier (TBC) and are applied locally, not all over the surface of the part.

76.5.3 Inspection

The techniques used have to be capable of detecting smaller defects within and on the surface of these complex and more brittle materials. Methods are under development to provide the required confidence level, i.e. minimum detectable size and probability of detection.

Numerous techniques have been proposed, each claiming detection of very small material flaws of a few micrometres. Whilst many are appropriate for laboratory evaluations, fewer are applicable for manufacturing and in-service use.

To date, openly published literature shows no systematic effort to correlate defect types, sizes and populations to structural integrity. Instead, effort has been placed in the detection of microstructural features, which are important, but represent a small proportion of the overall task.

For MMC and CMC materials, which achieve their damage tolerance by controlled instigation and propagation of 'defects', determining realistic acceptance levels is complicated by the inherent inhomogeneity of the material and by the fact that material and component are simultaneously manufactured in most cases.

76.6 Considerations

76.6.1 Mass optimisation

The reason for using these new advanced materials is that they can offer potentially significant mass-savings over competitive all metallic concepts, especially for high-temperature applications. The exact mass benefits achievable can only be optimised by:

- Understanding the failure and fracture mechanisms,
- Recognising that these mechanisms are different from those of traditional high-temperature metallic materials,
- For an equivalent safe performance, development of realistic material:
 - design allowables, and
 - safety factors.

It has been done for polymer composites. The same now needs to be done for metal- and ceramic-matrix materials. The principles and experience gained with integrity control of polymer-based composites can be applied to the newer types of composite materials. If a 'high-temperature' composite is treated like a 'high-temperature' metal, any mass benefits are compromised.

76.6.2 Approach

76.6.2.1 General

The integrity-control approach influences the:

- design of materials,
- development of manufacturing processes,
- testing and inspection techniques and methods, and
- confirmed by the verification programme, Ref. [76-1].

[See: Figure 76.7.1]

76.6.2.2 New materials

Table 76.6.1 lists factors to be considered in the development of the integrity control programme for new materials, Ref. [76-2].

Table 76.6-1 - Integrity control parameters for new materials

Technology stage	Tasks
Produceability	Material availability: <ul style="list-style-type: none"> ◆ appropriate forms and quantity ◆ raw materials, with fixed specifications & quantity ◆ second source of equivalent material
	Fabricate: <ul style="list-style-type: none"> ◆ demonstrator (detailed) parts. ◆ assemblies
	Develop NDI procedures.
Characterised manufacture and production	Preliminary manufacture and production specifications: <ul style="list-style-type: none"> ◆ acceptance standards ◆ manufacturing procedures. Identify and evaluate: <ul style="list-style-type: none"> ◆ all material characteristics uniquely dependent on features that distinguish the new material from a conventional one, and that may affect produceability & structural integrity. ◆ material performance at the extremes of material & process parameters.
Design mechanical properties	Establish material properties by test, including environment: <ul style="list-style-type: none"> ◆ strength ◆ damage tolerance ◆ creep ◆ corrosion ◆ all other (combined) environmental factors identified. Building-block process: <ul style="list-style-type: none"> ◆ coupon ◆ element ◆ sub-component. Test sufficient items to create a 'database' to: <ul style="list-style-type: none"> ◆ preclude potential failure with high confidence. ◆ permit usable mass prediction.

76.7 Case study: Developments in integrity control

An ESA-funded programme started the process of defining the integrity-control requirements for oxidation-protected C-C, C-SiC and SiC-SiC materials in thermo-structural applications, Ref. [76-3].

The study logic and integrity control approach for the work are shown in Figure 76.7.1 and Figure 76.7.2, respectively, Ref. [76-3].

[See: 76.8 for a summary of the main findings for Phase 1, and 76.9 for the activities in Phase 2]

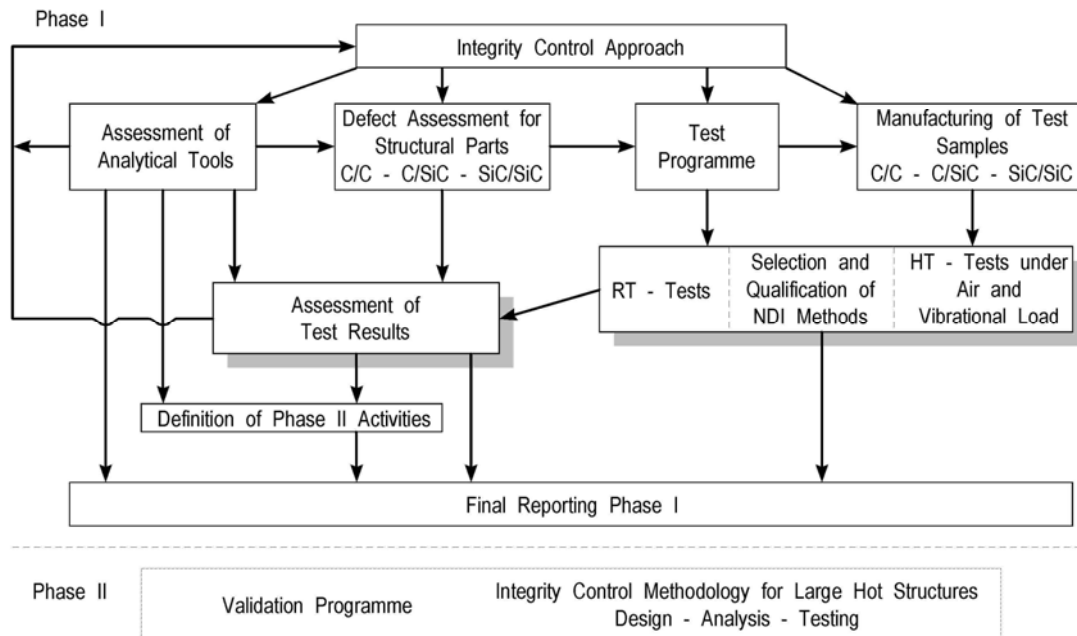


Figure 76.7-1 - Integrity control for high-temperature applications: Study logic

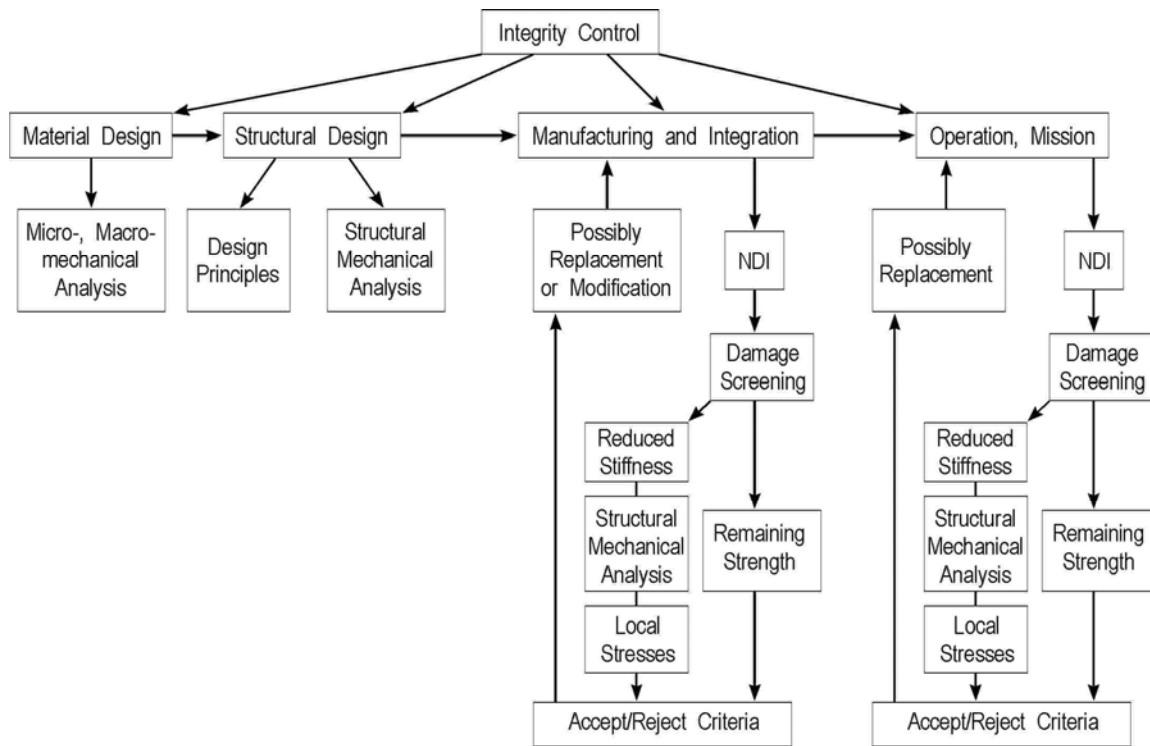


Figure 76.7-2 - Integrity control for high temperature applications: Approach

76.8 Case study: Phase 1 - Material characterisation

76.8.1 General

Phase 1 (1992-93) broadly considered the:

- ability of selected NDI methods to detect anticipated manufacturing defects and thermally induced damage, and
- proportion of maximum strength usable as an applied stress before unacceptable damage was initiated under thermo-cyclic conditions.

76.8.2 Materials, manufacturing and NDT

76.8.2.1 General

All the materials evaluated started as polymer-based composites ('green parts') that were subsequently pyrolysed. These initial laminates were evaluated by NDT prior to further processing to ensure their integrity.

Additional NDT was instigated after pyrolysis and infiltration to ensure that the manufactured high-temperature composite was satisfactory.

An external oxidation protection system was applied consisting of multiple CVD SiC layers followed by a glassy sealing coat. This protection system had also to be evaluated by NDT to ensure:

- complete coverage,
- overall integrity, and
- consistency in thickness.

This highlights a minimum of three consecutive manufacturing and NDT stages to ensure that a suitable high-temperature composite has been produced.

76.8.2.2 Carbon-Carbon

Commercially available product grade CF 222 from Schunk (G) was used. This was prepared by repeated pyrolysis and infiltration of a polymer composite followed by graphitisation.

76.8.2.3 C-SiC and SiC-SiC

The Dornier process was applied with an initial 'green' part formed by a Si-organic polymer, solvent and SiC powder combined with carbon or silicon carbide fibres during filament winding. Subsequent pyrolysis and re-infiltration steps produced the final composite.

76.8.2.4 Introduced defects

At the initial 'green part' manufacturing stage, representative defects introduced were:

- Foreign body inclusion, i.e. release film,
- Lay-up errors, i.e. cut fibres butted together,
- Excessive porosity, as a prelude to delamination.

The basic assumption was that manufacturing defects introduced at the polymer composite moulding stage cannot be rectified by any subsequent infiltration and pyrolysis steps.

76.8.3 Defect detection by selected NDI methods

76.8.3.1 General

It was recognised in advance that several NDT methods are needed, with individual methods to detect different features at various points. The broad conclusions are summarised for each stage of the processing.

76.8.3.2 Green part

This showed that:

- The use of both ultrasonic (for delaminations) and X-ray radiographic (for foreign inclusions, lay-up errors, voids) inspection can detect all likely defects.
- Appropriate ultrasonic methods (at Dornier) were through both transmission and pulse echo.

76.8.3.3 Final pyrolysed high temperature composite

This showed that:

- Only radiography is feasible for C-C to identify density variations.
- Liquid-coupled 'squirter' through-transmission, low frequency (1MHz) ultrasonics and radiography can be used for C-SiC and SiC-SiC.
- Low-frequency ultrasonics limited signal absorption, but sacrificed resolution on simulated delamination.
- Radiography detected density and thickness variations, fibre orientations and lay-up errors.
- Ultrasonics in the pulse-echo mode did not perform satisfactorily because of the high porosity content of the composites.
- Dry contact transmission mode ultrasonics (at Aerospatiale) was successful in detecting most of the introduced flaws.

76.8.3.4 Protective coatings

This showed that:

- Average coating thickness values can be calculated from the weight increase after coating.
- Prospective NDT techniques are more tentative as greater resolution is used for thin coatings, e.g. 100µm thick.
- Assessment of coating coverage requires a light reflection technique.
- Eddy current techniques (at Aerospatiale) can be applied if the main composite is a conducting material.

Eddy current works on C-C, possibly for C-SiC, but not SiC-SiC.

76.8.3.5 Unsuccessful techniques

- X-ray microfocus technique for better resolution proved unreliable and time consuming.
- IR thermography showed some success in revealing delaminations in C-SiC and SiC-SiC, but the conductivity of C-C was too high.

An automated tapping test was suggested on the final coated composite to ensure that delaminations had not been camouflaged by the addition of the protective coatings, since:

- Radiography is not realistic for delamination detection,
- Ultrasonics lack precise resolution, and coatings with metallic oxides strongly absorb the signals.

76.8.4 Maximum applied stresses

The parameters discussed are:

- μ_{\max} = maximum applied stress
- μ_{ult} = ultimate composite strength
- μ_{mc} = stress at which multiple matrix microcracking occurs

Ideally a brittle matrix composite does not experience a stress which induces significant matrix microcracking and loss of stiffness or linearity, i.e. $\mu_{\max} < \mu_{mc}$.

In reality μ_{mc} is usually low in value and there are justifications to exceed this point as the material is tolerant to a degree of microcracking. Therefore, $\mu_{mc} < \mu_{\max} < \mu_{ult}$ prevails.

The question then is how close to μ_{ult} can the applied loads go before the integrity of the composite is lost.

The application of a protective coating also limits the applied strain before cracking and spall become a problem.

Designs are therefore strain-limited for the corresponding applied stress. These composites also possess low interlaminar shear strength (ILSS), which provides an additional design constraint.

For the subsequent testing, $\mu_{\max} = 0.8 \mu_{ult}$ at maximum test temperature, i.e. 80% of ultimate, was used.

76.8.5 High-temperature tests

76.8.5.1 Test regime

The specimens underwent limited thermal cycling (1 to 4 cycles) superimposed on dynamic (0.5Hz) mechanical loading.

The basic loading and temperature regimes within a single cycle were:

- C-SiC and SiC-SiC:
 - Heated to 700°C and static load applied, then
 - 150 vibrational load cycles and stop,
 - maintaining applied load whilst temperature increases to 1100°C, then
 - 150 vibrational load cycles,
 - cooling to 700°C with static load applied, then
 - 150 vibrational load cycles,
 - all load and controlled heating and cooling removed.
- C-C:
 - Heated to 1600°C and static load applied, then
 - 300 vibrational load cycles,
 - all load and controlled heating and cooling removed.

76.8.5.2 Four point bending tests

Tests were conducted on specimens 90mm long, 20mm wide and 2mm thick; both with and without drilled holes (1.5mm or 3.0mm diameter) for various thermal exposures.

The conclusions drawn were:

- SiC-SiC, where the applied stress (149N \pm 80N applied load) equalled σ_{mc} . No detectable damage occurred during loading for specimens without holes or with 1.5mm holes. The specimens survived the test.
- SiC-SiC specimens with 3mm holes showed significant damage propagation and loss of stiffness.
- C-SiC specimens with applied stresses three times higher (450N \pm 139N load), showed similar behaviours to SiC-SiC, i.e. the 3mm hole specimen damaged considerably but the other survived.
- C-C with applied stress (226N \pm 90 N load): noticeable damage occurred in all the specimens during loading.

76.8.6 Residual strengths

76.8.6.1 SiC-SiC

- The material shows good strength retention after 1 to 4 thermo-cycles with $\mu_{\max} = 87\text{MPa}$ at 1100°C .
- NDT revealed a significant increase in matrix microcracking throughout the specimens.

76.8.6.2 C-SiC

- The applied stress $\mu_{\max} = 240\text{MPa}$, $\mu_{mc} = 216\text{MPa}$, and $\mu_{ult} = 302\text{MPa}$. The material was capable of sustaining this applied stress under thermo-cyclic conditions to 1100°C .
- NDT revealed that significant areas of microcracking and localised delamination damage were initiated in the specimens, corresponding to between 2% and 35% of specimen area. One specimen showed an 80% defective area.
- Damage areas of 50% corresponded to a loss in residual strength of 100MPa compared with similarly treated specimens with no damage detectable by NDT.

76.8.6.3 C-C

The testing regime applied at 1600°C was clearly too demanding with $\mu_{\max} = 191\text{MPa}$, against $\mu_{mc} = 140\text{MPa}$, and $\mu_{ult} = 245\text{MPa}$.

76.8.7 Analysis

The results for specimens with holes were analysed against theory and with FEA. A degree of agreement was claimed.

76.8.8 Conclusions

The main conclusions can be summarised as:

- These types of composite can be applied with high stresses in relation to their ultimate strengths and are damage tolerant for a low number of thermo-mechanical cycles.
- Low-frequency ultrasonics is a means of detecting defects, despite a reduction in resolution.
- The presence of protective coatings confuses NDT techniques in camouflaging underlying defects.

This area requires further work.

76.9 Case study: Phase 2 - Structural sub-component behaviour

Phase 2 (1993-94) undertook:

- Evaluation of a winged launcher C-SiC shingle,
- Development of analysis tools for structural parts,
- Acoustic noise tests,
- Continuation of thermo-mechanical testing, but under oxidising conditions,
- Further application of NDT,
- Update of integrity control criteria.

76.10 References

76.10.1 General

- [76-1] Dornier GmbH & Battelle
'Advanced Materials for Space Transportation Systems - Final Presentation'
ESA No. A0/1-2308/89/NL/CN. 15 April 1992
- [76-2] J.A. Harris Jnr & M.C. Van Wanderham: Pratt & Whitney, USA
'Relationships of Non-destructive Evaluation needs & Component Design'
AGARD-CP355 p.3-1 to 3-8
- [76-3] U. Trabandt et al: Dornier Deutsche Aerospace/Aerospatiale Aquitaine & Battelle Europe
'Integrity Control for High Temperature Structural Applications'
Phase 1 Final Report. ESA Contract 8807/90/NL/PP (SC)
Rider No. 1, November 1993
- [76-4] A. Pradier et al: ESTEC/DASA-Dornier/Aerospatiale Aquitaine
'Integrity Control for High Temperature Structural Applications'
First ESA/ESTEC Workshop on Thermal Protection Systems ESTEC,
Noordwijk, 5th to 7th May 1993
ESA-WPP-053 (August 1993), p.236-245

77**Defect types**

77.1 Introduction

No material is free from flaws. Likewise all structures contain defects and may experience damage during operational use, either by the propagation of existing defects or by accident. Depending on the type of material and the processing or manufacturing route used, the defects which may occur can be very different. Their size, position and population need evaluation for both the material and the intended application.

For isotropic or near-isotropic materials, a single flaw or crack will ultimately determine failure, whereas for anisotropic composites, final fracture is a result of the accumulation of cracks to a critical population density. In reaching final fracture, the structural performance (the load-bearing or environmental resistance) or the material reduces. This factor is considered during the design process and appropriate design allowances made. It also influences the operations (design) life and re-use of structures.

Defects can arise:

- In the material: from flaws or from pre-processing, e.g.
 - fibre damage during 3-D preform weaving,
 - metal inclusions from broken weaving needles.
- In manufacturing: from
 - inconsistent infiltration of metal or ceramic matrices,
 - excessive fibre attack.
- In service: from
 - propagation of existing defects, or
 - resulting from environmental degradation.

This chapter aims to highlight those defects which may occur at different stages of a structure's life. No attempt is made here to discriminate on the grounds of structural importance as this is highly application dependent.

77.2 Advanced metal alloys

77.2.1 General

In general, where property improvements do not cause pronounced anisotropy, material defects similar to those of traditional metal alloys can occur, e.g.:

- Inclusions,
- Pores,
- Cracks,
- Contamination,
- Oxidation,
- Corrosion surface damage.

Including these factors as part of the material specification, enables their potential as defects to be controlled.

77.2.2 ODS alloys

Additional factors for ODS alloys include:

- Agglomeration of reinforcing phase,
- Particle size and content.

77.2.3 SPF alloys

Additional factors for SPF alloys are the grain size and distribution.

77.3 Metal matrix composites

77.3.1 General

The integrity of MMC materials is determined by the characteristics of the reinforcement, matrix and the interface between the two. A disruption, either physical or chemical, of one or more of the constituent parts can affect material performance, hence can be considered a material defect. An integrated material development and process technology programme will aim to limit the occurrence of such defects.

77.3.2 Standard product forms

For MMC bought-in materials, such as sheet or extrusions, defect acceptance levels are determined as parts of the material specification.

77.3.3 Near-net shape manufacture

For materials manufactured simultaneously with the part, [Table 77.3.1](#) lists potential defects and their possible causes, Ref. [77-1].

Table 77.3-1 - MMC: Typical material defects

Defect	Possible cause
Reinforcement	
Volume fraction and variations	Incorrect lay-up. Process induced movement.
Particulate/Whisker	
Poor distribution	Mixing and/or processing.
Continuous fibres	
Broken/damaged	Significant for monofilaments. Care required when weaving preforms from tows. Avoid over-bending monofilaments.
Orientation and lay-up	Incorrect lay-up.
Coating material and thickness	Stipulated as part of fibre specification.
Attack by matrix	Fibre surface and process dependent.
Poor infiltration by matrix	
Reinforcement/Matrix interface	
Poor bonding Bond too strong Excessive diffusion zone Precipitation of brittle, undesirable compounds	Related to fibre surface coating and/or processing conditions. Where possible minimise processing time at high temperatures.
Matrix	
Irregular microstructure	Affected by presence of reinforcement and/or by processing conditions.
Cracking Shrinkage and tears	Matrix material and processing related.
Porosity Delamination	Poor consolidation.
Inclusions	Contamination.

77.4 Ceramic matrix composites

The integrity of CMC's is determined by the reinforcement, matrix and interface acting together. The defect types listed in Table 77.4.1 apply to ceramic, glass and carbon matrix composites, Ref. [77-2] to [77-6].

Table 77.4-1 - CMC: Typical material defects

Defect	Possible cause
Reinforcement	
Excessive attack.	Surface conditions and/or process conditions.
Reinforcement/Matrix interface	
Poor bonding.	Related to fibre surface coating and/or processing conditions. Where possible minimise processing time at high temperatures.
Too strong a bond.	Related to fibre surface coating and/or processing conditions. Where possible minimise processing time at high temperatures.
Excessive diffusion zone.	
Precipitation of brittle compounds.	
Matrix	
Irregular microstructure.	Affected by presence of reinforcement &/or by processing conditions.
Excessive cracks. (1)	Matrix material and process related.
Excessive porosity. (1)	Dust, debris or metal objects (e.g. broken weaving needles).
Inclusions.	
Key:	(1) All composites contain a certain level of matrix cracks & porosity as a result of normal manufacturing processes.
Cracking and porosity can be considered a 'defect' if:	
<ul style="list-style-type: none"> - higher than normal, e.g. > 1 0% porosity, typically. - uneven distribution. 	

CMC materials are created as near as possible to the finished component shape to avoid inducing damage by subsequent processing. The manufacturing process may comprise of several stages, notably matrix infiltration, to obtain a material of the required integrity.

77.5 Coatings

The objective of a coating is to modify the surface characteristics of a part, in such a way that environmental resistance is better than that of the substrate material. Any imperfection in a coating that allows exposure to the environment is detrimental.

Most coatings involve the use of one or more intermediate phases (layers) between the substrate and the external coating itself. The integrity of coating and intermediate layer(s) applied to seal the substrate, determine the effectiveness of a coated part. Not all coatings are required to be continuous over the part surface, e.g. thermal barrier coatings. Here the mis-location of the coating can also be classed as a defect. Table 77.5.1 lists typical defects for coatings, Ref. [77-7].

Table 77.5-1 - Coating materials: Typical defects

Defect	Possible cause
Mis-location. Thickness variations.	Process and part geometry.
Cracks: Surface breaking. Within coating.	CTE mismatch between substrate & coating. Residual stresses from: Process: Temperature gradients. Anisotropic deposited coating. Phase transformations.
Poor bonding.	Process conditions and/or surface conditions. Structure of substrate or intermediate layer. Residual stress. CTE mismatch.
Debonding.	Process conditions and/or surface conditions. Residual stress. CTE mismatch.
Variations in microstructure.	Process conditions. Service use.
Chips and scratches.	Handling. Impact. Erosion.
Porosity and voidage.	Process conditions. Contamination, including gases.

77.6 Joints

77.6.1 General

Joints are needed between either the same (similar) materials or dissimilar materials. The types of joints can be classed as:

- Fusion, or
- Mechanical fastened, including Interlocked designs.

[See: Chapter 60 - Fusion Joints, Chapter 61 - Mechanical Joints]

77.6.2 Uses

In general, mechanical fastening is appropriate for metallic-based materials and may be considered for Carbon-Carbon materials. Interlock designs and fusion may be appropriate to both metallic and ceramic-based materials. However, the exact fusion technique used varies, as shown in Table 77.6.1.

Table 77.6-1 - Fusion joints: Example of techniques and use

Technique		Comments
Metallic	Welding	Weldable metals.
	Brazing	Dissimilar or similar.
	Diffusion bonding	Either with SPF, or secondary joining.
Ceramic	Brazing	Dissimilar or similar.
	Bonding	Example: by resin pyrolysis.

77.6.3 Mechanical fastened joints

Defects arising in the materials of mechanical fastened joints may include:

- Material crushing or cracking close to the attachment; ceramic-based materials.
- Surface damage.
- Wear.

In general, these can be attributed to either errors in component geometry or the assembly technique (over or under tightening, surface damage). They are difficult to detect, especially surface damage to parts concealed in the assembled joint. This is particularly true for coated parts, e.g. fasteners, in which the coating is present to resist environmental degradation or allow disassembly after operational use at high temperatures.

77.6.4 Fusion joints

Typical defects occurring in fusion joints are shown in [Table 77.6.2](#).

Table 77.6-2 - Fused joints: Defects

Technique	Defect	Possible cause
Welding	Pores Cracks Tears Poor penetration	Material(s) Contamination Process conditions
Brazing	Pores Cracks Disbond	Process conditions Contamination
Bonding: Diffusion Resin pyrolysis	Disbond Disbond	Process conditions and/or surface contamination

77.7 Structural parts

77.7.1 General

Defects occurring during the manufacture of parts can be classed as those occurring from further processing of materials:

- Metal alloys,
- Composite materials: e.g. bought-in or near-net shape manufacture.

77.7.2 Composite materials

77.7.2.1 Shaping and machining

Potential defects are listed in Table 77.7.1.

Table 77.7-1 - Defects in composite materials after further processing

Defect	Comments
Shaping	
Broken fibres	Too tight radii
Interface failure	Deviation from ideal processing conditions
Delamination	
Matrix cracks	Poor material quality
Material fracture	
Machining	
Broken fibres	
Interface failure	Procedures require re-evaluation
Delamination	

77.7.2.2 Near-net shape manufacture

Where the material and finished part are manufactured at the same time.

[See: Chapter 87 - Integrated manufacturing]

77.8 In service

Defects arising in service can be classed as:

- Propagation of existing defects.
- Initiation and propagation of defects; from in-service conditions.
- Damage; from accidents.

The defect propagation characteristics of materials will have been evaluated during the design stage, and a judgement made on the service life of such components. Since most of materials are destined for high-temperature operation, defects initiating in service occur as a result of the combined effects of thermal and mechanical loadings and other environmental factors specific to the application, such as erosion, oxidation. Table 77.8.1 lists defects which may occur to structures and parts in service.

Table 77.8-1 - Typical in-service defects

Defects	Comments
Metallic	
Cracks.	Initiation at surfaces or internal defects. Propagation by thermal or mechanical cyclic loads. Residual stress.
Microstructure.	Temperature induced changes.
MMC's	
Cracks.	Matrix fatigue cracking.
Fibre breakage.	Matrix & Interface dependent.
Interface failure.	Thermal/Mechanical loads.
Delaminations.	Stress concentrations. Residual stress.
Oxidation.	Environment.
Matrix microstructure.	Temperature induced transformations.
Diffusion.	Temperature induced.
CMC's	
Cracks.	Initiation at surfaces or internal defects. Propagation by thermal or mechanical fatigue. Residual stress.
Fibre breakage.	Interface dependent.
Interface failure.	Thermal/Mechanical loads.
Delaminations.	Stress concentrations/Residual stress.
Oxidation.	Environment.
Matrix microstructure.	Temperature induced transformations.
Diffusion.	Temperature induced.
Coatings	
Cracks: Surface breaking.	CTE differences. Thermal/Mechanical cyclic loads.
Cracks: Internal to layer.	Impact. CTE differences. Thermal/Mechanical cyclic loads.
Debonding.	CTE differences. Thermal/Mechanical cyclic loads. Impact.
Diffusion.	Temperature induced.
Erosion.	Surface, leading to initiation of cracks. Thinning of coating.
Oxidation.	Surface, leading to initiation of cracks. Thinning of coating.
Spalling.	CTE differences. Thermal/Mechanical cyclic loads. Impact.
Mechanical/Interlock joints	
Loosening.	CTE differences. Thermal/Mechanical cyclic loading.
Diffusion.	Temperature induced. Impairs disassembly?
Cracking.	CTE differences. Thermal/Mechanical loading.
Fusion joints	
Cracking.	CTE differences. Thermal/Mechanical loading.
Debonding.	Thermal/Mechanical loading. Propagation of bondline defects.
Diffusion.	Temperature induced.

77.9 References

77.9.1 General

- [77-1] W.N. Reynolds: AERE-Harwell, UK
'Non destructive Testing Techniques for Metal Matrix Composites'
AERE-R 13040 (June 1988)
- [77-2] A. Morsh et al: Fraunhofer-Institute for NDT, Germany
'Recent Progress in High Frequency Ultrasonics in Non destructive
Testing and Acoustic Microscopy'
Nuclear Engineering & Design 128 (1991), p.83-89
- [77-3] C.B. Scuby et al: Oxford University, UK
'Non destructive Testing of Ceramics by Acoustic Microscopy'
Br. Ceram. Trans. J. 88, (1989), p.127-132
- [77-4] L.W. Kessler & T.M. Gasiel: Sonoscan Inc, USA
'Acoustic Microscopy Review: Non destructive Inspection of Advanced
Ceramic Materials'
Advanced Ceramic Materials, Vol.2,No.2, (1987),p.107-109
- [77-5] D.J. Roth et al: NASA-Lewis Research Center, USA
'Reliability of Void Detection in Structural Ceramics by use of SLAM'
Materials Evaluation 44, May 1986. p.762-769
- [77-6] C. LeFloc'h: Aerospatiale Aquitaine, France
'Non destructive Investigations of Advanced Materials (Carbon-Carbon
& Ceramic Composite Materials): WP 2-State of the Art'
Report No. NT 25 209/TA/N (18/06/90)
Prepared for Fulmer/ESA Contract No. 7090/87/NL/PP
- [77-7] P.F. Becher et al: Naval Research Lab, USA
'Factors in the Degradation of Ceramic Coatings for Turbine Alloys'
Thin Solid Films 53 (1978), p.225-235

78

Damage tolerance

78.1 Introduction

78.1.1 Materials

Damage tolerance is the ability of a material to retain an acceptable level of structural and/or environmental resistance properties under the effects of operational conditions, without risk of failing in a catastrophic manner.

78.1.2 Structure

A structure is considered damage tolerant if the amount of general degradation or the size and distribution of local defects expected during operation do not lead to structural degradation below limit-specified performance; as specified in ECSS E-ST-32-01 (previously ESA PSS-01-401).

78.1.3 Fracture mechanics

Damage tolerance extends the surface-related fatigue (or initiation) life analyses to include assessments of life remaining after crack initiation. This concept is based on the principle of fracture mechanics.

Improvements in safety and reliability have resulted from prudent application of the damage tolerance philosophy in design and development of aerospace structures and engine components, Ref. [78-1]. It is an accepted design principle for traditional metal-based applications, Ref. [78-2], and is becoming adopted for polymer composite materials.

Advanced materials and composites challenge specific current methods used for damage tolerance assessment, but the fundamental concepts are likely to remain. As new material systems, fabrication techniques and configurations are introduced, life prediction and damage tolerance principles have to be developed concurrently. Initially, the operating stress is limited to a level below which cyclic-induced damage occurs. When confidence has increased, by proving of analysis methods which describe failure characteristics better, the conservatism applied can then be reduced without affecting safety requirements, thereby enabling the new materials to compete with existing ones, Ref. [78-1].

78.1.4 Initial material quality (IMQ)

Foremost among material characterisation is the fundamental resistance to crack growth, which is quantified for life prediction.

For conventional materials a direct assessment of damage tolerance can be made on relative crack velocity against stress intensity behaviour. The intrinsic Initial Material Quality (IMQ), defined as a distribution of microstructural anomalies that might lead to failure, influences damage tolerance. This concept is helpful in quantifying the effect of defects below the current NDE detection capability.

Material inspectability, e.g. 'probability-of-detection' curves, are established for individual materials, since the processing methods can inhibit inspectability. Precaution is taken to ensure that the effect of processing on final material quality is also investigated, and reliable limits obtained. All these items combine to give 'inspection size against remaining life' predictions for specific materials and applications. This in turn forms the quantitative basis of a damage-tolerant design and life-prediction approach, Ref. [78-1].

For the new groups of high-strength, brittle materials, IMQ becomes more prominent. The initial defect tolerance could be sufficiently limiting for proof testing to become, fundamental to hardware acceptance and certification. For MMCs and CMCs, the IMQ can consist of an 'even' distribution of individual flaws, and might therefore be less important. Here the accumulation of damage, and the corresponding property loss can define life.

Failure definition differs from that customary for isotropic materials. Crack velocity versus. stress intensity can be inadequate for complex composite structures, except perhaps for unidirectional reinforcements. It can be more appropriate to consider fracture energy, or other such parameters. The definition of failure are usually different with the new materials groups.

For materials with low damage tolerance, e.g. intermetallic and conventional ceramics, proof-test life can determine component retirement; with re-proofing to establish safe return to service.

For high temperature applications, time-at-temperature or thermal-cycling duration can define life, Ref. [78-1]. It, and other application-dependent environmental factors, can also strongly influence defect initiation and propagation mechanisms, so influencing damage tolerance.

The damage tolerance of the new advanced materials is undergoing evaluation.

78.2 MMC: Particulate and whisker reinforced

78.2.1 Fatigue behaviour

78.2.1.1 General

In general, the fatigue behaviour of whisker-reinforced MMCs is superior to that of the unreinforced matrix, whereas that of particulate-reinforced MMCs is at least equivalent to the unreinforced alloy, as shown in Figure 78.2.1, Ref. [78-3].

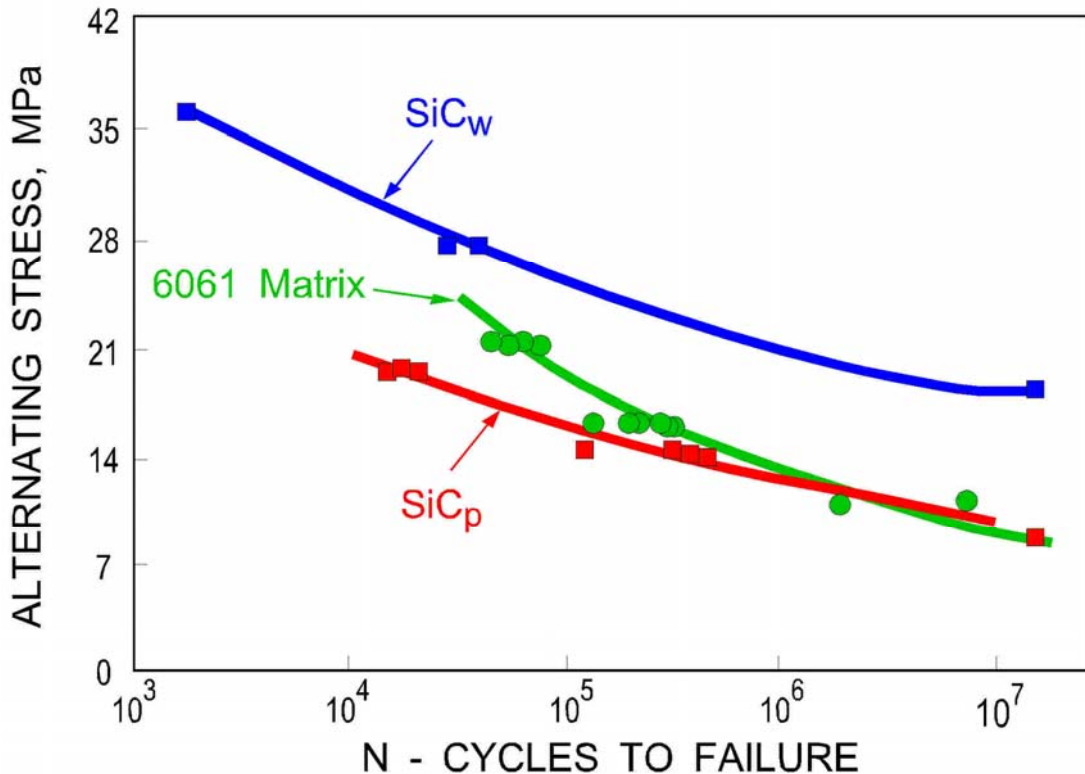


Figure 78.2-1 - Whisker and particle reinforced MMC: Fatigue response

78.2.1.2 Particulate size

The size of particle used can strongly influence fatigue performance and fracture toughness, as summarised in [Table 78.2.1](#), Ref. [78-3].

Therefore there exists an optimum size to gain most advantage over the unreinforced material. The particle content and distribution (processing) also influence MMC fracture behaviour.

Table 78.2-1 - MMC: Effect of particle size on fatigue and fracture toughness

Particulate size	Fatigue	Fracture toughness
Too small	No benefit over matrix alone.	May result in 'clumping'
Too large	Improvement, up to level where Fracture Toughness dominates.	Particulate cracking and early fracture.

78.2.2 Fracture mechanics

Studies on the applicability of Fracture Mechanics to discontinuously reinforced materials concluded that whereas the behaviour of particle-reinforced materials tends to be predictable with the aid of [LEFM](#) principles, whisker-reinforced materials show different behaviour, including sample-type dependency of results, Ref. [78-3].

78.3 CMC: Whisker reinforced

Little information on the performance of whisker-reinforced ceramics is, as yet, openly published.

A study, Ref. [78-4], to examine the high-temperature performance of SiC whisker-reinforced alumina demonstrated that for chevron-notched test specimens (considered more representative than straight-notched), the fracture resistance was independent of temperature between 20°C and 1000°C but greatly increased above 1000°C. This was attributed to crack bridging in the wake region by the SiC whiskers.

Other important conclusions were that:

- the large scatter bands for fracture toughness data were indicative of persistent crack arrest and re-initiation.
- LEFM were inadequate to describe the material behaviour.

78.4 MMC: Continuous fibre reinforced

78.4.1 Fatigue

78.4.1.1 General

Fatigue damage characteristics in MMC vary with the particular matrix, fibre and interfacial bonding properties, as summarised in Figure 78.4.1, Ref. [78-5], [78-6].

<i>Characteristic</i>	<i>Mechanism</i>	<i>Example MMC⁽¹⁾</i>
Matrix failure requires less cyclic strain than fibre	MATRIX DOMINATED FAILURE	Boron/Al-alloy
Fibre failure requires less cyclic strain than matrix	FIBRE DOMINATED FAILURE	SiC/Ti-alloy
Fibre and matrix require similar cyclic strains to failure	INTERFACE DOMINATED	Depends on fibre to matrix interface bond strength

Key: ⁽¹⁾ Different failure modes can exist between different alloy grades

Figure 78.4-1 - MMC potential failure mechanisms under cyclic loading

The characteristics of the metal matrix can determine the failure mode, as summarised in Figure 78.4.2, Ref. [78-5]. The manufacturing process used can result in residual stresses in both fibre and matrix. Depending on the precise process temperature and the CTE mismatch between fibre and matrix, residual stress levels vary within the composite. In general, they are compressive in the reinforcement and tensile within the matrix. This causes an unfavourable stress-state in the matrix for fatigue resistance.

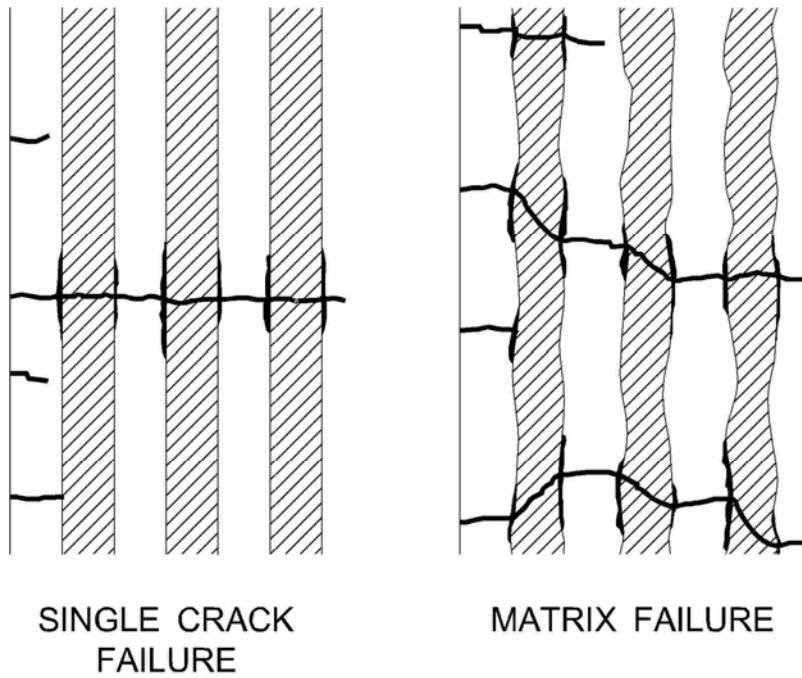


Figure 78.4-2 - Failure modes of MMC

78.4.1.2 Single crack failures

Single crack failure, also known as self-similar crack growth, occurs when the fatigue failure strains for matrix and fibre are similar, i.e.:

- when interfacial bonding is high (too high), and
- if the matrix is high strength; capable of creating a high stress concentration in the fibre ahead of the matrix.

Damage is localised at or very near the crack tip and the failure is similar to that seen in metals.

78.4.1.3 Matrix failure

Matrix failure is the gradual accumulation of fatigue damage distributed throughout the matrix without causing fibre damage, but debonding at interfaces, Ref. [78-5], [78-6]. Failure is therefore progressive and not catastrophic.

Figure 78.4.3 shows the fatigue response of a MMC showing matrix failure, Ref. [78-6].

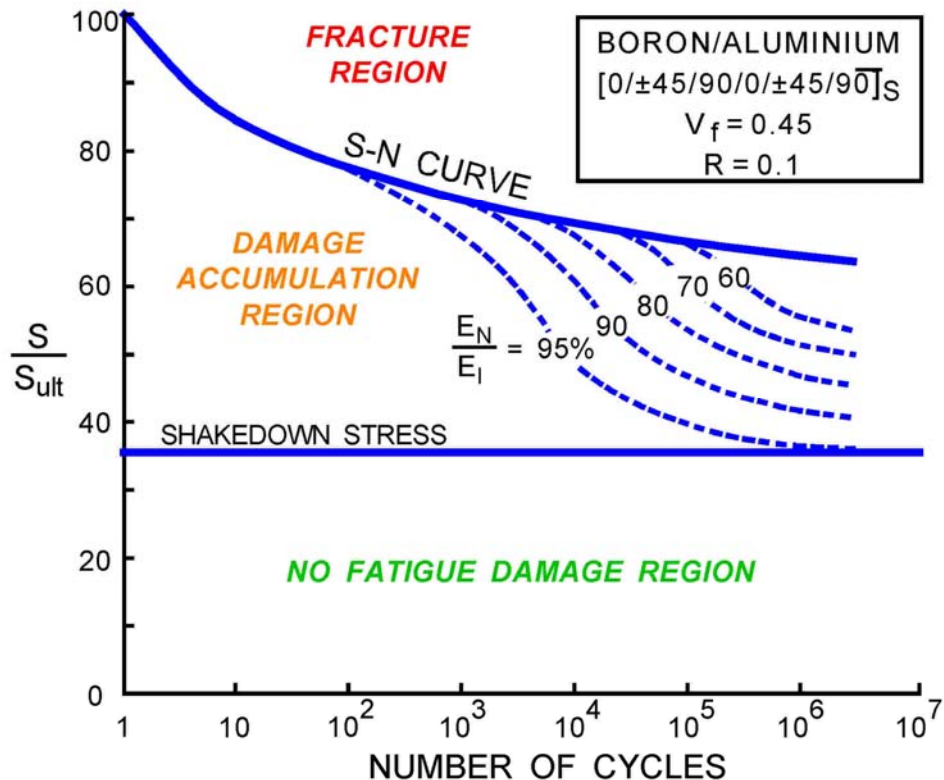


Figure 78.4-3 - MMC: Fatigue response showing matrix failure

There are three regions, [See: [Figure 78.4.3](#)]:

- Shakedown: Plastic deformation can occur during the first few cycles as the composite responds to loading. The 'Shakedown Stress' is reached if the matrix cyclically hardens to a cyclic yield stress such that only elastic deformation occurs under subsequent load cycles. Above this stress, damage initiates in the matrix, but not the fibres.
- Damage accumulation: Where fatigue cracks initiate and propagate in the matrix and cause debonding at the fibre-matrix interface; resulting in a fall in stiffness.
- Fracture region: Where the fibres fail.

78.5 CMC: Continuous fibre reinforced

78.5.1 Failure characteristics

78.5.1.1 General

In general, the failure characteristics of CMC materials are controlled by the combined action of fibre, matrix and the interfacial bonding between the two.

78.5.1.2 Fibre to matrix interface

To achieve damage tolerance, the interface is 'engineered' to prevent cracks initiating in the matrix propagating into the fibres, thus enabling a progressive failure rather than the catastrophic failure of monolithic ceramics. This is particularly difficult to achieve since the processing methods, notably

temperature at which the matrix is infiltrated, can cause significant fibre-matrix reactions at the interface. Consequently the overall 'idealised' fibre properties are never realised in a consolidated composite.

78.5.1.3 Fracture characterisation

LEFM is inadequate to describe continuously-reinforced composites. It is possible that methods developed to predict polymer-based composites are also appropriate for some materials, since their failure 'mechanisms' are similar, [See also: Chapter 33].

The complication arises when the reinforcements are multi-directional, near-net shapes, coupled with the effects of high temperatures, which can change the 'microstructure' of matrix and fibre interfaces.

As the majority of intended applications require materials and 'finished' shapes created at the same time, the opportunity for a systematic characterisation of the material is limited and, almost, redundant.

Instead assessment of damage tolerance is included in the particular application development. Apart from experience, it is unlikely that data are interchangeable for different applications.

78.6 Coatings

78.6.1 Coating performance

Damage tolerance of coatings is influenced by the performance of the constituents of the material system acting together, as summarised in Table 78.6.1.

Table 78.6-1 - Coatings: Damage tolerance aspects

Material	Characteristics for damage tolerance
Coating	Inherent material properties, e.g.: mechanical physical
	Deposition process
	Post-deposition processing, e.g.: sealing heat-treatment
Interface	Stability: mechanical chemical, and physical
	Adhesion
Substrate	Inherent material properties, e.g.: mechanical physical
	Post-deposition processing, e.g.: heat-treatment

These factors are influenced by operation in hostile environments, e.g.:

- High temperature,
- Thermal cycling,
- Erosion,
- Atmospheres, such as:
 - oxygen, and
 - hydrogen.

Application of a coating can influence the overall mechanical properties of the substrate, [See also: Chapter 74].

78.6.2 Process and material selection

78.6.2.1 General

Correct selection of materials and processing conditions minimises, Ref. [78-7]:

- Residual stress caused by CTE mismatch between coating and substrate (interface failures).
- Thermal gradients, caused by process conditions and materials CTE differences. (Spray deposition)
- Material elastic anisotropy. (Spray deposition)
- Microstructural changes, including phase transformations.

78.6.2.2 Microstructure

Control of the coating system microstructure can improve coating failure (spall) resistance, thereby improving the damage tolerance.

78.6.3 Failure characteristics

It is therefore necessary to evaluate the materials and processing parameters under realistic environmental conditions to determine damage tolerance.

Failure characteristics are normally determined by mechanical testing and analysis. Thermally-induced damage can be predicted by diffusion kinetics, if the environment is defined precisely; confirmed by metallurgical examination of failed test specimens.

78.7 References

78.7.1 General

- [78-1] T.E. Farmer & M.C.VanWanderham: Pratt & Whitney, (USA)
'Damage Tolerance Concepts for Advanced Materials & Engines'
AGARD-CP449-Application of Advanced Materials for Turbo-machinery
& Rocket Propulsion, p6-1 to 6-7
- [78-2] MIL-STD-1783 (Nov.1984). Including: Engine Structural Integrity
Program (ENSIP)
- [78-3] H.J. Rack & P. Ratnaparkhi: Clemson University, (USA)
'Damage Tolerance in Discontinuously Reinforced Metal Matrix
Composites'
Journal of Metals, Nov 1988 p55-57
- [78-4] M.G. Jenkins et al: University of Washington, (USA)
'Elevated Temperature Fracture Resistance of SiC whisker reinforced
Polycrystalline Al₂O₃ Matrix Composite'
Proceedings of 1987 SEM Fall Conference: 'Dynamic Failure',
Oct 25-28 1987 p33-38
- [78-5] V. Gerold: Max Planck Institut für Metallforschung, (D)
'Fatigue of Continuous Fibre-reinforced Metal Matrix Composites'
Proceedings of 9th Risø International Symposium on Metallurgy &
Materials Science: 'Mechanical & Physical Behaviour of Metallic &
Ceramic Composites'. 5-9 September, 1988
Risø National Laboratory, Roskilde, Denmark
- [78-6] C.R. Saff et al: McDonnell Douglas Aircraft Co., (USA)
'Damage Initiation and Growth in Fibre-reinforced Metal Matrix
Composites'
Journal of Metals, November 1988 p58-63
- [78-7] P.F. Becher et al: Naval Research Laboratory, (USA)
'Factors in the Degradation of Ceramic Coatings for Turbine Alloys'
Thin Solid Films 53 (1978) p225-235

78.7.2 ECSS standards

ECSS E-ST-32-01, Space engineering - Fracture control, previously ESA
PSS-01-401.

79**Fracture control****79.1 Introduction****79.1.1 Application****79.1.1.1 Alloys**

Fracture control is applied to materials which can be adequately predicted by Fracture Mechanics principles; [See: ECSS E-ST-32-01, previously ESA PSS-01-401].

In general, this applies to conventional alloys, but it can also be considered for new materials that incorporate a 'reinforcing' phase, provided that it does not result in significant levels of property anisotropy and that the fracture or failure mechanisms are predictable using the standard techniques.

79.1.1.2 Brittle materials

Inherently brittle materials, such as intermetallics and beryllium, affect 'Fracture Control' requirements, in that the critical defect size can be at or below the reliable limits of detection for NDE techniques.

This is especially relevant to in-service inspection where detectable size and probability of detection often differ considerably from those obtained under 'ideal' laboratory conditions, Ref. [79-1].

Work on the Fracture Control of new advanced materials is on-going.

79.2 References**79.2.1 General**

- [79-1] J. Wilson & D.P. Bashford: BNF-Fulmer, (UK)
'Inspectability In-service of Composite & Metallic Structures'
BNF Report No. R1176/D14/Jan. 1991
- [79-2] MIL-HDBK-5F (November 1990)

79.2.2 ECSS standards

ECSS E-ST-32-01, Space engineering - Fracture control

80

NDT techniques

80.1 Introduction

Various NDI techniques are evolving from the established methods for the inspection of advanced material systems for high-temperature applications. The impetus is to detect defects in brittle materials that are smaller than those in the traditional ones, i.e. high-temperature metal alloys. A further complication is that the newer materials consist of several different phases which makes characterisation difficult.

Experience of NDI of polymer-based composites is helpful, [See: Chapter 34], but other factors are considered, including:

- Defect size: Critical sizes in brittle materials can be in the 10 μm to 100 μm range, e.g. for detection by ultrasonics high frequencies are used, (>20MHz to GHz range) because the wavelength has to be comparable to the defect size to be detected.
- Overall population of defects: Isolated defects can be tolerable whereas groups, which can combine and exceed critical sizes, are not. This includes density gradients (porosity content) within CMC materials caused by poor infiltration.
- Position within component, i.e. near or within significant load-bearing paths. Applications include structural parts of complex shape with integrally created attachment or load-transfer points; e.g. spaceplane leading edge TPS.

The sensitivity of techniques is carefully established in order to enable structurally significant defects to be distinguished from an inherently complex material consisting of many small but tolerable flaws. In general, this is accomplished by integrating NDI into the material and process development stage, whereby the acceptable defect level is established for a 'good' part and confirmed by destructive testing. This then becomes a 'Reference' for all subsequent parts made.

Establishing the quality of thin coatings has always posed problems, more so when the number of layers has increased and when they are applied to parts with complex geometry, e.g. engine components, fasteners. In general, any surface-breaking defects which enable exposure to an aggressive environment need detection. Likewise, subsurface defects which can lead to premature coating failure or spall have to be identified, [See: 80.5].

For fusion bonds, weld- or braze-inspection techniques can be complicated by the need to detect small defects in shaped parts after manufacturing or in-service. Experience from the nuclear industry helps in the inspection of metal components (condensers and tubing), [See: 80.6; 80.7]. Aircraft industry experience with complex SPF/DB parts also applies to space structures, Ref. [80-18]. [See: 80.7]

Many methods described in open publications are for use only in laboratory conditions. These can form part of the overall materials and process development stages. Fewer methods are available for

post-manufacture because, in many cases, the geometry inhibits access. Fewer still have potential for in-service use.

For in-service inspection, ideally a technique is non-contact, automated, remote (for external surfaces) and with access to the part (internal structure) whilst being of the required sensitivity, e.g. critical defect size, defect population, coating thickness. This is complicated by any temperature-instigated changes to the materials, such as by diffusion or transformation of the microstructure(s). This applies to both coatings and at interfaces between reinforcement and the matrix.

No single NDI technique is capable of detecting all types of defects in a given material. Consequently, techniques are complementary. Equipment configuration, operator competence and conditions of use significantly affect the sensitivity of any particular technique.

The terminology used by various organisations world-wide varies. The term non-destructive inspection (NDI) covers NDTesting, NDEvaluation, NDCharacterisation.

80.2 Advanced metal alloys

80.2.1 General

It is envisaged that those NDI techniques applied to traditional metals and alloys are also applicable to the advanced metal alloy materials, although some level of adaptation is usually required.

80.2.2 Brittle materials

The critical defect size can be small and consequently their detection affects the selection of equipment used and its configuration.

80.2.3 Multi-phase microstructures

Materials consisting of many phases can present problems in the discrimination between defects and microstructural features which are not detrimental to structural integrity.

80.3 Metal matrix composites

Table 80.3.1 summarises NDI techniques applicable to MMCs. Precise details of the material system and equipment configuration are not given, but can be found in the cited reference.

Table 80.3-1 - NDI techniques for MMCs

Defect or measurement	Technique						
	Ultrasonic			Radio-graphy	Acoustic emission	Thermo-graphy	Eddy current
	Velocity	C-scan	Stress wave				
Reinforcement content:							
Particulate	①						
Whisker							
Continuous fibre							
Surface damage		③					
Matrix cracks				⑧		⑧	
Matrix plastic deformation					⑤⑨		
Matrix rich zones	⑦	⑦					
Porosity	②	⑦		③			① ①
Intermetallic compounds:							① ①
Fracture					⑤		
Delaminations	②	③		③②		⑧	
Fibre ends (cut or broken)				②	⑤		
Fibre lay-up	③	④		②			
Fibre: Matrix interface:			③⑥				
Failures	③				⑤		
Fibre pull-out					⑤		
Foreign inclusions		③		③			

Key: ○ Possible; ② Dye enhanced; Number inside symbol indicates Reference.

80.4 Carbon-Carbon and ceramic matrix composites

Table 80.4.1 summarises NDI techniques applicable for defect detection and measurement of C-C and CMC materials, Ref. [80-10]. It is a comprehensive listing of all the types of defects which can occur. Their detection forms part of the material and part development programme. It does not aim to identify those which are of structural importance in a finished article.

Table 80.4.2 ranks various NDI methods on their technical and economic aspects, Ref. [80-10].

Table 80.4-1 - NDI techniques for defect detection and measurement of C-C and CMC materials

DEFECT DETECTION or MEASUREMENT CAPABILITY	NDI METHOD							
	X-ray	Ultrasonic (2)	IR Thermo-graphy		Micro-wave		NMR	
Missing Fibre (1)	□	□					□	
Misaligned Fibre (1)	□	□						
Metal Inclusion (1)	□	□						
Delamination: impact	□	□	■	■	□	■		
Disbond:	□	□	□	■	■	■		
lack of bond					■			
Porosity: open	□	□						□
pore size								
Cracks	□	□						
Voids, Metal Inclusion	□	□	■			■		
Fibre Break								
Matrix Cracking					□			
Brittle Failure								
Plastic Failure								
Moisture								
Matrix Oxidation	□	□	□	■	□	□		
Blister Under Coating (3)	□	□	□	■	■	□		
Homogeneity of:								
organic binder distribution						■		□
density distribution		□	■					
boron distribution						■		
Fibre Content				□				
Measurement of:								
density		□	■					
thickness		□	■	■			□	■
fibre diameter								□
conductivity						□	□	□
Mechanical Properties				□				
Thermal Properties					□			
Electromagnetic Properties					□	□		

KEY: (1) Before densification

(2) LF: < 1 MHz

HF: 1 to 20 MHz

VHF: > 20 MHz

(3) Oxidation resistant coating, (PAO)

□ Laboratory/Manufacture

■ Maintenance

Table 80.4-2 - Technical and economical aspects of NDI techniques

NDI method	Possibility of NDI technique for:								
	Investment cost	Speed	Maintenance	Real-time	On-line	Full automation	Quantitative	Safety requirement	Availability
X-ray:									
Radiography	XX	X	N	N	N	X	N	XXX	XXX
Radioscopy	XX	XXX	N	Y	Y	X	X	XXX	XXX
Microfocus	XX	X	N	N	N	X	X	XXX	XXX
Tomography	XXX	X	N	N	N	XX	XXX	XXX	XX
Backscattering	XX	X	Y	N	N	XX	XX	X	X
Ultrasonics: ⁽¹⁾									
LF transmission	X	X	N	Y	N	X	XX	N	XXX
HF transmission	X	X	N	Y	N	XX	XXX	N	XXX
HF reflection	X	X	Y	Y	N	XX	XXX	N	XXX
VHF reflection	XX	X	N	Y	N	XX	X	N	XX
Laser ultrasonics	XXX	XXX	Y	Y	N	XX	XXX	X	X
I.R. Thermography:									
Stimulated	XX	XXX	Y	Y	N	XXX	XXX	N	XX
Photothermal	XX	X	N	Y	Y	XXX	XX	X	X
Mirage effect	XX	X	N	Y	Y	XX	XXX	X	X
Acoustic emission ⁽²⁾	XX	XX	Y	Y	Y	XX	X	N	XXX
Holographic interferometry	XXX	XXX	Y	Y	Y	XX	XXX	X	X
Neutrography	XXX	X	Y	Y	Y	XX	X	XX	X
Microwave:									
Radiometry	XX	XXX	Y	Y	N	X	XX	N	X
Near-field imaging	XX	XX	Y	Y	N	XX	XXX	N	X
Cavity perturbation	X	XXX	N	Y	Y	XXX	XXX	N	X
Eddy current	X	X	Y	Y	Y	XXX	XXX	N	XXX
β Backscattering	X	X	Y	Y	N	XXX	XX	XX	XXX
Electrical	X	X	Y	Y	N	XXX	X	N	XX
Optical	XX	XXX	N	Y	Y	XXX	XXX	X	XX
NMR	XXX	X	N	N	N	XX	XXX	XX	XX
Key: (1) Need for contact or immersion; Y: Yes; N: No; X: Low; XX: Medium; XXX: High									
(2) Need to load item									

80.5 Coatings

Table 80.5.1 summarises techniques for coating inspection. The technique used varies with the particular material system. For details of equipment configuration, see the cited reference.

Table 80.5-1 - Coatings: Inspection techniques

Coating system	Defects detectable	NDI technique (see Key)
Metallic	Cracks Bonding flaws Sulphidation Damage	C-S Impulse eddy current (a) Ref. [80-11]
Ceramic: Non conductive	-	Ultrasonics Holographic sound field imaging (b) Ref. [80-12]
Coating material	Internal flaws Thickness	Attenuating ultrasonic waves. Thermal wave testing (c) Ref. [80-11]
Interface	Flaws	VHF acoustic microscopy Ref. [80-12]

Key (a) Multi-frequency and pulsed methods to discriminate between flaw indications.
 (b) Imaging of Rayleigh waves.
 (c) Imaging by laser light (thermal).
 (d) At GHz frequencies, focused through sapphire lenses; 70µm depth, typically.

80.6 Joints

80.6.1 General

No NDI method is capable of quantifying joint strength. This is determined by testing.

80.6.2 Fused joints

An integrated testing and inspection programme aims to set up acceptance levels for features detected by the inspection technique and correlate these with strength test results. This can then be used as a comparison or reference for all subsequent inspections of manufactured joints.

The inspection of joints aims to verify that the materials of the component parts have not been seriously affected by assembly or use with the result that the assembly is unsafe.

[See: [80.7](#)]

80.6.3 Mechanically fastened and interlock joints

80.6.3.1 TPS structures

Considering the important role of TPS to the overall vehicle safety, every method used should be capable of ensuring that the connection is viable for further service, [See also: Chapter 70 and Chapter 71].

For the complex arrangements of different materials proposed in concepts, disassembly is likely to be a mandatory procedure until reliable techniques are developed and confidence is gained in in-situ NDI.

80.6.3.2 Thrusters and nozzles

Comments for TPS are also true for thruster and nozzle designs and concepts. However, disassembly can be difficult after high-temperature service use.

Where disassembly is required or possible, instrumented techniques can be used in addition to visual inspection. These are likely to be based on the methods developed for manufacture control.

Disassembly is likely to disrupt coatings, so any applied coatings are also examined.

80.7 Fusion joints

80.7.1 General

In general, standard weld and braze inspection procedures are applicable to advanced materials.

Diffusion bonded (DB) assemblies are considered as welded for the basis of inspection techniques.

Table 80.7.1 lists inspection techniques for fused joints, Ref. [80-13], [80-14], [80-15].

Table 80.7-1 - Fused joints: Inspection techniques

Joint type	NDI technique	Comments
Welded	Visual Eddy current Ultrasonic Dye penetrant Magnetic particle	Standard procedures exist for techniques. Some modifications may be necessary for advanced materials.
Brazed	Visual Eddy current Ultrasonic Dye penetrant	-
Diffusion bonded	Thermography Ultrasonic	Fighter aircraft structures, Ref. <u>[80-13]</u> Non-contact for radioactive applications, Ref. <u>[80-14]</u>

80.7.2 Thin-walled seam welded tubes

Examples of standards which exist for the inspection of high-reliability condenser tubes are given in Table 80.7.2, Ref. [80-15].

Table 80.7-2 - Standards for inspection of welded tubes

NDT Technique	Standard (1) (2)
Eddy current	ASTM B338
	SEP 1914 : German
Ultrasonic	SEP 1915 : German
	ASTM E213

Key (1) For power and nuclear industry; (2) Includes Ti alloys

The high sensitivity of eddy current techniques can lead to false defect indications, i.e. those not deemed deleterious to tube performance (structural or leak).

Test procedure modifications have been suggested to reduce apparent reject rates from false indications, Ref. [80-17], [80-15], [80-16].

80.7.3 Diffusion bonded joints

Diffusion bonding (DB) is often combined with superplastic forming (SPF) to create structural components with integral joints. Consequently the finished part can be complex in shape and contain internal features. Such structures are used in both military and civil aircraft, [See: Chapter 72].

Ultrasonic-based systems are established for defect detection. Fully, automated systems are available to inspect large, complicated shaped parts and assemblies, Ref. [80-18].

IR thermography enables whole panels to be inspected in one shot. Their accuracy and reliability is claimed to be as good as those of ultrasonic systems, provided due attention is paid to surface scratches and markings which affect surface emissivity and register as defective areas, Ref. [80-13].

80.8 References

80.8.1 General

- [80-1] R.E. Shannon et al: Westinghouse Research & Development Center, (USA)
'Non-destructive Characterisation of Metal Matrix Composites Microstructures'
Proceedings of the American Society for Composites, Symposium on High Temperature Composites. June 1989
ISBN 87762-700-2-60 p51-60
- [80-2] R.W. Pepper & T.W. Shahood Jnr: Textron Speciality Materials, (USA)
'Correlation of NDE Results on Metal Matrix & 2D C-C Composites'
Proceedings of the American Society for Composites, Symposium on High Temperature Composites. June 1989

ISBN 87762-700-2-60 p223-232

- [80-3] W.N. Reynolds: AERE Harwell, (UK)
'Non-destructive testing Techniques for Metal Matrix Composites'
AERE-R 13040 June 1988
- [80-4] W.S. Johnson: NASA-Langley Research Center, (USA)
'Screening of Metal Matrix Composites using Ultrasonic C-scans'
Journal of Composites Technology & Research, Vol.11, No.1
Spring 1989 p31-34
- [80-5] J. Awerbuch & J.G. Bakuckas
'On the Applicability of Acoustic Emission for Monitoring Damage Progression in Metal Matrix Composites'
ASTM STP 1032 :Metal Matrix Composites - Testing, Analysis & Failure Modes. 1898 p68-99
- [80-6] H.E. Kautz & B.A. Lerch: NASA-Lewis Research Center, (USA)
'Preliminary Investigation of Acousto-ultrasonic Evaluation of Metal Matrix Composite Specimens'
Materials Evaluation. May 1991 p607-612
- [80-7] R.A. Blake & H.S. Hartman: University of Delaware/DuPont, (USA)
'Computer Aided Ultrasonic Evaluation of Fiber FP Metal Matrix Composite'
Composites Technology Review, Vol.6, No.3, September 1984 p118-123
- [80-8] N. Tsangarakis et al: Army Materials & Mechanics Research Center, (USA)
'Non-destructive Evaluation of Fatigue Damage in Alumina Fiber-reinforced Aluminium'
Journal of Composite Materials, Vol.19, May 1985 p250-268
- [80-9] C. Johnson et al: University of California/Lockheed Corp., (USA)
'Acoustic Emission behaviour of Metal Matrix Composites'
Journal of Acoustic Emission 4 (2-3), 1985 p263-268
- [80-10] C. LeFloc'h : Aerospatiale Aquitaine, (F)
'Non-destructive Investigations of Advanced Materials (Carbon-Carbon & Ceramic Composite Materials): WP2-State of the Art.'
Report No. NT25 209/TA/N (18/06/90)
Prepared for Fulmer/ESA Contract No. 7090/87/NL/PP
- [80-11] H-A Crostack et al: University of Dortmund, (D)
'New Developments in Non-destructive Testing of Thermally Sprayed Coatings'
Mémoires et Études Scientifiques Revue de Métallurgie
Mai 1989 p285-295
- [80-12] H-A Crostack et al: University of Dortmund, (D)
'Recent Developments in Non-destructive Testing of Coated Components'
Thin Solid Films 181 (1989) p295-305
- [80-13] D.L. Haarvig & D.C. King: McDonnell Douglas Corp, (USA)

'Thermographic Inspection of Superplastically Formed Diffusion Bonded Titanium Panels'
SPIE Vol.934: Thermosense X (1988) p102-110

- [80-14] D.A Hutchins et al: Queens University, Ontario, Canada
'Non-contact Ultrasonic Inspection of Diffusion Bonds in Titanium'
Ultrasonics Vol.29, July 1991 p294-301
- [80-15] J. Lindemann: Mannesmannröhren-Werke AG, (D)
'Developments of the Production and NDT Methods for Welded Titanium Tubes'
Proceedings of the 5th International Conference 'Titanium Science & Technology', Vol.2, Sept.10-14, Munich, 1984 p925-938
- [80-16] H. Sakuyama & K. Taki: Nippon Mining Co. Ltd, Japan
'The Problems with the Eddy Current Test of Welded Titanium Tubes'
Proceedings of the 5th International Conference 'Titanium Science & Technology', Vol.2, Sept.10-14, Munich, 1984 p917-923
- [80-17] H. Heckhäuser et al: Vereingte Deutch Metallwerk AG, (D)
'Investigation of the Manufacturing Defects in Longitudinal Welded Ti-Condenser Tubes by NDT Methods'
Proceedings of the 5th International Conference 'Titanium Science & Technology', Vol.2, Sept.10-14, Munich, 1984 p939-946
- [80-18] USL - Ultrasonic Sciences Ltd., (UK)
'6-Axis Contour following Immersion system for Pulse Echo Inspection of SPF/DB Parts'
Extract from USL website (June 2003)

81

High-temperature testing

81.1 Introduction

Background information on the testing of advanced metallic and ceramic materials at high temperatures is provided. The response of materials to aggressive high-temperature environments is complex, with a range of degradation mechanisms possible, [See: [81.4](#)]. The extent of degradation with time establishes the material performance envelope.

A material's performance envelope is affected by the life expectancy defined for the application, e.g. a material can sustain 1000°C for many hours under inert isothermal conditions, but rapidly degrades and loses integrity under thermal cycling in an oxygen-containing environment.

High-temperature materials are often used close to their limits for short periods. Limited surface erosion is permissible in the hot gas streams of propulsion systems.

Data can be obtained from coupon testing, but this can be difficult at very high temperatures. Testing of components and assembled structures under simulated operational conditions is a very specialised activity, [See: Chapter [86](#)].

A thorough understanding of a material's behaviour is necessary before a design is finalised.

81.2 Purpose of testing

Anisotropic [MMC](#) and [CMC](#) materials present problems similar to those of [CFRP](#), i.e. use of test methods which measure the true characteristics of the material rather than a specimen-dependent parameter.

With test temperatures up to 1500°C, the construction of loading fixtures can be difficult.

Test method development is closely linked with the understanding of fracture behaviour, [See: Chapters [64](#), [65](#), [66](#), [67](#) and [68](#)].

Consequently, the results of tests are closely studied in an effort to understand microstructural features and their significance to mechanical behaviour, Ref. [[81-1](#)], [[81-2](#)], [[81-3](#)].

Testing is viewed in the context of the intended use for the resulting data. There are several levels to which the data can apply, including:

- comprehension of material behaviour,
- measurement of fundamental mechanical and physical properties, usually at ambient temperature,
- retention of properties at high temperatures,

- residual properties after mechanical loading, thermal exposure and hot corrosion, e.g. thermo-mechanical fatigue (TMF).

Residual property measurement, which covers all degradation processes, is a better measurement of a material's capabilities. It determines the validity of the material for the intended application.

Residual mechanical properties are usually significantly lower than the as-made ambient properties.

81.3 Material behaviour

81.3.1 Basic fracture modes

The important characteristics of the various advanced material groups are summarised.

[See also: Chapters 64, 65, 66, 67 and 68]

81.3.2 Metal matrix composites

81.3.2.1 Particulate reinforced (MMCp)

- Basically isotropic in behaviour,
- Initially elastic materials at low strains, then elastic-plastic to plastic, with limited ductility,
- Failure determined by particulate-to-matrix adhesion and matrix microstructure.

81.3.2.2 Fibre reinforced (MMCf)

- Highly anisotropic, low strain to failure materials,
- Fully elastic to very low strains, then complex elastic-plastic behaviour,
- Properties determined by in-situ fibre strength and modest transverse strengths between fibre and matrix.

81.3.3 Inorganic and ceramic matrix composites

81.3.3.1 Fibre reinforced (ICMCf)

This group includes GMC, GCMC, CMC and C-C materials.

- Highly anisotropic and modest strength characteristics,
- Possess high temperature, insulative, thermal shock and thermo-cyclic capabilities,
- Exhibit benign fracture characteristics, despite low overall strain to failure,
- Fibre to matrix adhesion is low to provide a de-coupling mechanism.

81.4 Degradation mechanisms

81.4.1 Materials

81.4.1.1 Metal compositions

Possible degradation mechanisms listed in order of occurrence and ultimate severity are:

- Change in microstructure,
- Grain growth,
- Brittle phase formation, including hydrogen embrittlement,
- Intergranular cracking,
- Creep,
- Fibre surface degradation (interdiffusion between metal and fibre),
- Surface oxidation,
- Hot corrosion,
- Composite embrittlement,
- Severe fractures.

81.4.1.2 Ceramic compositions

Possible degradation mechanisms listed in order of occurrence and ultimate severity are:

- Matrix microcracking,
- Growth and increase in matrix cracking,
- Fibre weakening,
- Surface oxidation,
- Protective coating consumed,
- Penetrative oxidation,
- Hot corrosive attack,
- Gross composite embrittlement.

81.4.2 Degradation rate

The degradation is increased by:

- Exposure time,
- Higher temperatures,
- Aggressive species.

81.5 Coupon testing

81.5.1 General

Measurement of the mechanical and physical properties of metallic and ceramic-based composite materials from test coupons has the difficulty of interpreting this data for bulk material properties or net-shape components. Complicating factors include:

- Anisotropy,
- Complex failure mechanisms,
- Low failure strains, and
- Measurement of properties at high temperatures.

81.5.2 Single-fibre tests

Whilst the mechanical properties of fibres are often taken as those quoted by their manufacturers, degradation occurs at high temperatures. Single-fibre tests can be used for information on:

- Changes in properties with temperature,
- Effect of oxidation by heating in air,
- Statistical distribution of strengths,
- In-situ strength within a composite.

81.5.3 Fibre push through

For ceramic composites in particular, the fracture behaviour is determined by the in-situ fibre-to-matrix bonding. The interfacial shear strength is used for theoretical calculations, so modified micro-indenter tests enable fibres to be pushed through very thin composite sections. The interfacial shear strength is calculated from the force applied and the surface area of the individual fibre.

81.5.4 Net-shape components

Many MMC and CMC components are manufactured as net-shape items. The accurate measurement of material properties is difficult where coupons are machined from a shaped item, especially with 3D or multidimensional reinforcements.

81.5.5 Flexural and ILSS testing

Flexural and interlaminar shear testing are very popular because of their simplicity. They are useful for comparison exercises between different materials. Flexural testing indicates the achievable composite tensile strength. The measurement of ILSS gives a good indication of the composite's integrity with regard to shear and compressive behaviours.

These tests do not provide design data on the true performance of composites under tensile, compressive and shear loading.

Loading jigs and fixtures for tests of these types have to withstand the test environment, i.e. high temperatures with inert gases or air.

81.5.6 Small coupon tests

The quantities of MMC and CMC materials prepared for net-shape applications can be small. This, combined with the complexity of the component or processing route, e.g. extrusion or CVI, makes small test coupons necessary.

A good understanding of material behaviour is essential to ensure that the coupons are representative of the bulk material.

81.5.7 Machining

Most MMC and CMC are difficult to machine because of their hard, abrasive nature. Diamond-tipped cutting tools are essential. Machining can cause damage. The specimen gauge length is usually polished.

81.5.8 Extensometry

The measurement of low strains at high temperatures is a specialised process. The use of bonded strain gauges or attached mechanical extensometers is not usually feasible at temperatures above 500°C or in the presence of oxidising or corrosive atmospheres.

Remote measurement techniques, e.g. laser interferometry, are essential for accurate measurement. Figure 81.5.1 shows an external scanning laser extensometry system, Ref. [81-4].

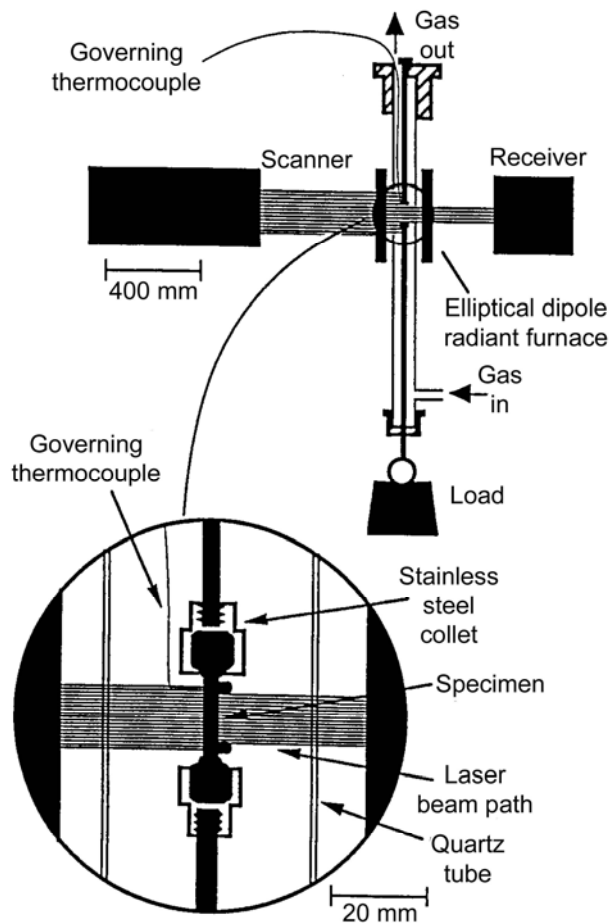


Figure 81.5-1 - Coupon testing: Scanning laser extensometry system

81.5.9 End tabs

For high-temperature tensile testing, problems in gripping the coupon can be solved by using a long specimen with a hot gauge length and two cooled ends within the grips. This enables metal end tabs to be used within the cooled grips.

Production of a suitable size test panel is needed for an 'over long' test specimen.

81.5.10 Coatings

For high-temperature applications, most CMC materials have some form of protective coating. The validity of data from a cut specimen without such a coating is questionable when the test is performed at high temperatures.

81.5.11 Material gradation

Materials manufactured by densification routes, such as pyrolysis or gas infiltration, can have a graded, through-section composition. The coupon is selected to represent the material in the component as a whole to avoid characterising solely surface or core material.

Surface coatings also form part of graded microstructures.

81.5.12 Specimen alignment

With high modulus and low strain materials, specimen alignment within loading jigs is essential if the tests are to be representative. In tensile and compressive loading, bending moments are minimised.

81.5.13 Linear elasticity

Most MMCs and CMCs retain true elasticity only to very low strain levels. Thereafter small microstructural changes introduce nonlinear characteristics, including:

- Matrix plasticity,
- Microcracking, or
- Fibre slippage.

Load, unload and re-load curves therefore show displaced hysteresis.

81.6 Mechanical properties

81.6.1 General

Mechanical test methods for continuous fibre MMC and CMC materials are based on those used for fibre-reinforced plastics. For particulate MMCs, techniques used for testing metals were the starting point.

In all cases, the complex fracture characteristics of MMC and CMC materials have proved the major hindrance in reaching common agreement on defining measured properties.

Agreement on viable test techniques is progressing. With collaborative effort on CMCs, and a number of methods are published as by standards organisations, [See: [81.8](#); [81.9](#)].

The overall uncertainty is primarily a result of the fact that:

- High-temperature composites are still evolving,
- There is a large diversity of development materials,
- Commercial availability of materials varies with time,
- Academics are generating a wide range of mathematical models to describe the complex fracture behaviour,
- There are only a few actual applications.

Only general comments on measurement of specific mechanical properties are provided because of the lack of universal agreement on mechanical test methods, [See also: [64.4](#)]

81.6.2 Tensile

81.6.2.1 General

The measurement of properties at ambient temperature eliminates the problem of temperature effects, not least because bonded aluminium tabs can be used. Agreement is usually possible on initial modulus measurement due to the linear behaviour. Once nonlinear behaviour is reached, at ~ 0.3 to 0.4% strain, the situation is more confused.

81.6.2.2 Particulate reinforced composite

In an inter-laboratory study, two particulate reinforced aluminium composites were tested and the uncertainties ($95\% \pm 2$ standard deviation) for tensile properties obtained were, Ref. [81-5]:

- Young's Modulus: ± 12 to 14%
- Proportional limit: $\pm 55\%$
- 0.2% Proof stress: $\pm 8\%$
- Tensile strength: $\pm 6\%$
- Elongation: $\pm 70\%$

By judicious manipulation of the data to a 'common procedure', the uncertainties on the proportional limits and elongation were reduced to ± 30 to 40% and $\pm 35\%$, respectively.

Machined, waisted, circular-section specimens are appropriate for particulate MMC materials.

81.6.2.3 Continuous fibre-reinforced composites

For low-failure-strain continuous-fibre composites with low overall failure strains ($\sim 1\%$), the problem is one of defining the precise point at which significant nonlinear, irreversible events occur, e.g. matrix plasticity or first ply failure. Figure 81.6.1 shows the preliminary specimen shapes for CMC materials; recommended by CEN for high temperature tests, Ref. [81-6].

With waisted specimens, the geometric changes in cross-section cannot coincide with thermal transition zones if cooled grips are used. Avoiding shear-related failure is paramount in CMC materials at changes in cross-section, Ref. [81-7].

Whether or not waisted specimens are preferable to straight edged ones is yet to be resolved for continuous fibre specimens.

Recommended for tensile properties at high temperature, inert atmospheres by CEN.

Recommended for tensile properties at high temperature, inert atmospheres (CEN standard under preparation).

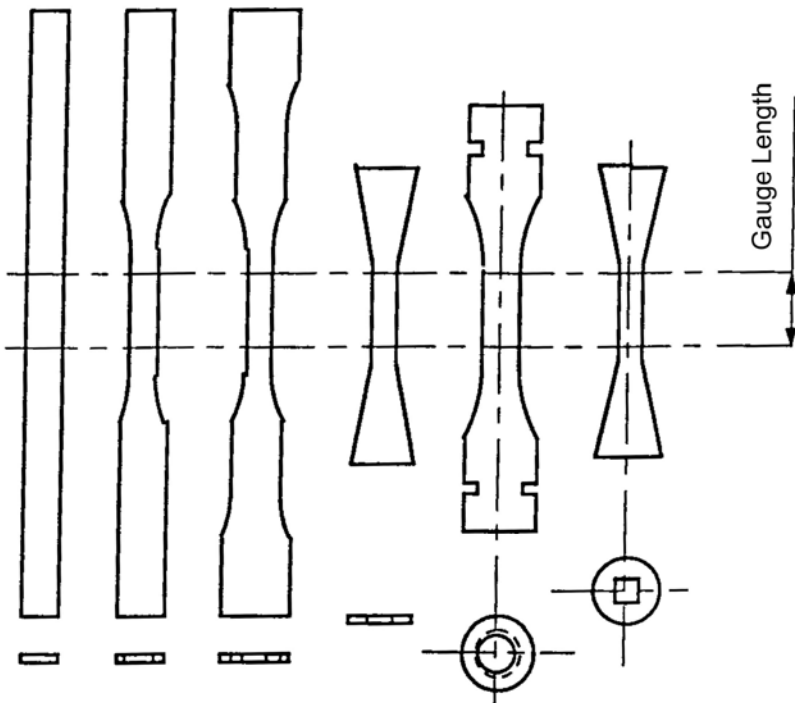


Figure 81.6-1 - CMC high temperature tensile testing: CEN recommended sample types

ASTM D 3552-77(1985) describes measurement of tensile properties for fibre-reinforced metal matrix composites, [See also: Chapter 7].

Linear regression computer analysis is gaining prominence for analysing raw test data, particularly in calculating Young's modulus from the σ/E curve.

81.6.3 Compression

81.6.3.1 Continuous fibre-reinforced composites

Compression testing of continuous-fibre composites has always been contentious. Many loading rigs have been devised to avoid end-effects and out-of-plane deflections. For room-temperature measurements, modified Celanese-type specimens and loading jigs are normally used, [See also: Chapter 7].

At high temperatures, the loading jig arrangements have to survive the test environment. Changes in specimen alignment, due to expansion, become critical between setting-up at room temperature and heating to the higher temperature.

81.6.4 Shear

Interlaminar shear strengths are relatively easy to measure on the classical short-span 3-point flexure rig.

The measurement of in-plane shear modulus and strength is far more difficult. For 2D planar composites, credence is initially given to tests which use small and simplified specimen

configurations. This implies a simple tensile loaded test with a straight edge $\pm 45^\circ$ coupon, as applied to fibre-reinforced plastics in ASTM D 3518.

As many CMC materials use fabrics, the simple system needs evaluation as to its applicability.

81.6.5 Open-hole tension

The extensive use of mechanical fastening with reinforced plastics, makes open-hole tensile testing essential for design data, particularly if the design is to undergo mechanical fatigue. Mechanical fastening is an appropriate joining technique for MMC and CMC components.

Very little published work exists on trials with open-hole specimens.

81.6.6 Fatigue

Mechanical fatigue is important for long-life applications such as gas turbine engines, advanced propulsion systems and spaceplane structures. Some fatigue work has been conducted on high-temperature materials.

[See also: Chapter 83 for thermo-mechanical fatigue (TMF)]

81.7 Fracture toughness

Fracture toughness testing has been used to examine the microstructural failure mechanisms of complex materials such as MMCs and CMCs.

Various specimen configurations have been used to create a notched section from which a crack is grown through the specimen. It is virtually impossible, because of the nature of the materials, to propagate a single crack through composites other than some particulate MMC materials. The validity of the modelling routes used to calculate fracture toughness is therefore questionable, because linear elastic fracture mechanics (LEFM) do not apply.

[See: Chapters 65, 66 and 67 for information on the fracture behaviour of MMC and CMC materials]

'R' curves describe the resistance of a material to cracking, and have some relevance in comparing materials.

Fracture toughness testing at high temperatures is generally not carried out until the room temperature behaviour is better understood. Quoted fracture toughness values for materials should be treated with extreme caution without a thorough understanding of how the testing and calculations were conducted.

It is questionable whether fracture toughness measurements have any design value, other than providing some assurance as to the material's basic 'toughness' in comparison with other options available.

81.8 Physical properties

81.8.1 General

For high-temperature applications, physical properties concerned in heat management are very important. They are quantified over representative temperature ranges for the application. Emphasis is placed on:

- Thermal diffusivity,
- Specific heat capacity,
- Thermal conductivity,
- Surface emissivity,
- Surface catalyticity.

[See: Chapter [82](#) for value changes with temperature and microstructural modifications to the materials]

81.8.2 Standards

Measurement techniques for diffusivity, conductivity and specific heat capacity have been formulated by [CEN TC184-WG4](#), [See: [81.9](#)].

81.9 Status of test standards

81.9.1 General

The impetus for the development of satisfactory test methods for [MMC](#) and [CMC](#) materials is heavily influenced by interested parties with specific technologies. The main inspiration for test method development is from technologies based on:

- Particulate reinforced [aluminium](#) composites, e.g. automotive.
- Continuous fibre [titanium](#) composites, e.g. aerospace, defence.
- Continuous fibre [GCMC](#), [CMC](#) and [C-C](#) materials, notably [C-SiC](#) and [SiC-SiC](#), e.g. space projects, often [RLV](#) concept vehicles and dimensionally-stable structures.

High-temperature testing (>1000°C) is a specialised activity and so is often restricted to a small group of laboratories.

Initiatives to provide internationally-recognised test methods for measuring the properties of [MMC](#) and [CMC](#) materials come under the auspices of:

- [ASTM](#) (USA).
- [CEN](#) (Comité Européen de Normalisation) Technical Committees (TC).
- [VAMAS](#) (Versailles Project on Advanced Materials and Standards).

Contact the specification bodies for the current status of standards.

81.9.2 Metal matrix composites

The ASTM D-30 and E-8 committees are responsible for a range of test methods appropriate to MMC materials.

VAMAS has a Technical Working Area (TWA) on MMC materials, including a 'round-robin' test programme on particulate-reinforced aluminium composites.

The UK National Forum on MMC Test Technology acts as a focal point for the exchange of information, Ref. [81-8].

81.9.3 Ceramic matrix composites

81.9.3.1 CEN TC 184 activities

The development of CEN standards is improving the European position in advanced materials. CEN TC objectives are to create standards, to adjust the work programme to meet markets needs and to work in co-ordination with ISO/TC 206. In the Vienna Agreement, the policy within CEN is that, whenever there is an appropriate ISO standard, it will be considered for adoption as a European standard.

CEN TC 184 was set up in 1989 and its activities have been driven by Europe's position as world leader in CMC technology, although the USA is the largest market. European standards organisations, via CEN, have been very active in developing and adopting standards. CEN TC 184 activities relate primarily to advanced technical ceramics for mechanical and structural applications, which divide into three main groups:

- Monolithic ceramic components, which include seals and bearings, catalyst supports, lasers, optical fibre networks and others, [See: Chapter 43].
- CMC ceramic matrix composites, including carbon-carbon composites, that by a combination of both their ceramic fibre reinforcements and their ceramic matrices properties provide high-performance advanced technical ceramics for the most demanding applications. Examples include: strong, lightweight and thermally stable components for satellites and large telescopes; durable, lightweight thermostructural components for advanced high-temperature process equipment; lightweight structural components for aerospace engines (gas turbines and rocket motors).
- Ceramics (various types of advanced technical ceramics), which are used for a wide range of applications, e.g. wear, erosion and corrosion protection, friction control, thermal and diffusion barriers. CEN TCs are developing standards for thick and thin film ceramic coatings.

For over 15 years, the technical committee CEN/TC 184 SC1 has been preparing standards for ceramic composites, with over 15 members from Germany, Italy, Netherlands, Spain, Greece, Portugal, United Kingdom, Austria, Czech Republic and France.

The standards listed, i.e. EN published or ENV pre-standards, give their status as of 2004. The lists are not exhaustive because new programmes are added on a regular basis.

81.9.3.2 Continuous fibre reinforced ceramic composites

The main CEN standards (as of 2004) are listed in [Table 81.9.1](#), where they are grouped as:

- mechanical testing methods for use at ambient or high temperatures.
- physical property methods, e.g. density and porosity.

- reinforcement characterisation methods, e.g. strength and thermophysical properties.

The standards listed cover reinforced ceramics with continuous ceramic or carbon fibres, where the reinforcement can be:

- unidirectional, in-plane, i.e. reinforcement placed in at least two directions in a single plane;
- multidirectional, i.e. reinforcement spatially distributed in at least three directions and not restricted to a single plane.

81.9.3.3 Short fibre reinforced ceramic composites

Special care needs to be taken in the selection of test standards for short-fibre-reinforced ceramics. Depending on the particular material, if the behaviour is very brittle, then a monolithic ceramic standard, as summarised in [Table 81.9.2](#), can be more appropriate than a CMC standard.

[See also: Chapter 43]

81.9.3.4 Ceramic coatings

Ceramic coatings made from various types of advanced technical ceramics are used in a range of applications such as wear, erosion and corrosion protection; friction control and as thermal and diffusion barriers. Some new standards proposed within the frame work of CEN are given in [Table 81.9.3](#).

81.9.3.5 Other properties

Standards are under development for the measurement of fibre/matrix properties, matrix properties and fibre thermo-physical properties. Some examples are given in [Table 81.9.4](#).

Table 81.9-1 - Test methods: CEN standards for advanced technical ceramic composites

Title	Standard No.
General:	
Notations and symbols	ENV 13233
Mechanical properties at RT:	
Mechanical properties of ceramic composites at room temperature – Part 1: Determination of tensile properties	EN 658-1
Mechanical properties of ceramic composites at room temperature – Part 2: Determination of compression strength	ENV 658-2
Mechanical properties of ceramic composites at room temperature – Part 3: Determination of flexural strength	EN 658-3
Mechanical properties of ceramic composites at room temperature – Part 4: Determination of shear strength by compression loading of notched specimens	ENV 658-4
Mechanical properties of ceramic composites at room temperature – Part 5: Determination of interlaminar shear strength by short span bend test (three points)	EN 658-5
Ceramic composites – Mechanical properties at room temperature – Determination of elastic properties by an ultrasonic technique	ENV 14186
Mechanical properties at high temperature:	
Mechanical properties of ceramic composites at high temperature under inert atmosphere – Determination of tensile properties	ENV 1892
Mechanical properties of ceramic composites at high temperature in air at atmospheric pressure - Determination of tensile properties	ENV 1893
Mechanical properties of ceramic composites at high temperature under inert atmosphere – Determination of shear strength by compression loading of notched specimens	ENV 1894
Mechanical properties of ceramic composites at high temperature under inert atmosphere – Determination of compression properties	ENV 12290
Mechanical properties of ceramic composites at high temperature in air at atmospheric pressure - Determination of compression properties	ENV 12291
Mechanical properties of ceramic composites at high temperature under inert atmosphere – Determination of flexural strength	ENV 12788
Mechanical properties of ceramic composites at high temperature in air at atmospheric pressure - Determination of flexural strength	ENV 12789
Mechanical properties of ceramic composites at high temperature under inert atmosphere – Determination of creep behaviour	ENV 13235
Mechanical properties at ambient temperature:	
Mechanical properties of ceramic composites at ambient temperature – Determination of in-plane shear properties	ENV 12289
Ceramic composites – Mechanical properties at ambient temperature – Evaluation of the resistance to crack propagation by notch sensitivity testing	ENV 13234
Physical properties:	
Ceramic composites – Physical properties – Determination of density and apparent porosity	ENV 1389

Reinforcements:	
Ceramic composites – Methods of test for reinforcements – Part 4: Determination of tensile properties of filament at ambient temperature	ENV 1007-4
Ceramic composites – Methods of test for reinforcements – Part 5: Determination of distribution of tensile strength and of tensile strain to failure of filaments within multifilament tow at ambient temperature	ENV 1007-5
Ceramic composites – Methods of test for reinforcements – Part 6: Determination of tensile properties of filament at high temperature	ENV 1007-6
Ceramic composites – Methods of test for reinforcements – Thermophysical properties - Part 1: Determination of thermal expansion	ENV 1159-1
Ceramic composites – Methods of test for reinforcements – Thermophysical properties - Part 2: Determination of thermal diffusivity	ENV 1159-2
Ceramic composites – Methods of test for reinforcements – Thermophysical properties - Part 3: Determination of specific heat capacity	ENV 1159-3
Key: EN - Published European standards; ENV - Pre-standards	

Table 81.9-2 - Test methods: CEN standards for advanced technical ceramics - monolithic

Title	Standard No.
General and textural properties- Part 1: Determination of the presence of defects by dye penetration	EN 623-1
General and textural properties- Part 2: Determination of density and porosity	EN 623-2
General and textural properties- Part 3 : Determination of grain size	EN 623-3
General and textural properties- Part 4 : Determination of surface roughness	EN 623-4
Thermo-mechanical properties – Part 1: Determination of flexural strength at elevated temperature	ENV 820-1
Thermo-mechanical properties – Part 2: Determination of self-loaded deformation	ENV 820-2
Thermo-mechanical properties – Part 3: Determination of resistance to thermal shock by water quenching	ENV 820-3
Thermo-physical properties – Part 2 : Determination of thermal expansion	EN 821-1
Thermo-physical properties – Part 1: Determination of thermal diffusivity by laser flash (or heat pulse) method	EN 821-2
Thermo-physical properties – Part 1: Determination of specific heat	EN 821-3
Mechanical properties at room temperature – Part 1: Determination of flexural strength	EN 843-1
Mechanical properties at room temperature – Part 2: Determination of elastic moduli	ENV 843-2
Mechanical properties at room temperature – Part 3: Determination of sub critical crack growth parameters from constant stressing rate flexural strength tests	ENV 843-3
Mechanical properties at room temperature – Part 4: Vickers, Knoop and Rockwell Superficial hardness tests	ENV 843-4
Mechanical properties at room temperature – Part 5: Statistical analysis	ENV 843-5
Methods of testing monolithic ceramics – Guidance on the sampling and selection of test pieces	ENV 1006
Monolithic ceramics – Part 1: General practice for undertaking corrosion tests	ENV 12923-1
Key: EN - Published European standards; ENV - Pre-standards; [See also: Chapter 43]	

Table 81.9-3 - Test methods: CEN standards for advanced technical ceramics - coatings

Title	Standard No.
Monolithic of test for ceramic coatings –Part 1: Determination of coating thickness by contact probe profilometer	ENV 1071-1
Monolithic of test for ceramic coatings –Part 2: Determination of coating thickness by the cap grinding method	ENV 1071-2
Monolithic of test for ceramic coatings –Part 3: Determination of adhesion by a scratch test	ENV 1071-3
Monolithic of test for ceramic coatings –Part 4: Determination of chemical composition	ENV 1071-4
Monolithic of test for ceramic coatings –Part 5: Determination of porosity	ENV 1071-5

Key: EN - Published European standards; ENV - Pre-standards

Table 81.9-4 - Test methods: CEN standards for advanced technical ceramics – others

Title	Standard No.
Cycle fatigue at room temperature	CEN 186
Cycle fatigue at high temperature in air atmosphere	CEN 187
Cycle fatigue at high temperature in neutral atmosphere	CEN 188
Elastic properties at by resonant beam method up to 2000°C	CEN 189
Transverse tension properties at room temperature	CEN 190
High temperature tensile properties of a dry tow	CEN 191
Determination of creep resistance on fibres	CEN 192

Key: EN - Published European standards; ENV - Pre-standards; CEN – in progress

81.10 Demonstrator testing

For spaceplanes experiencing severe thermal transients, it is important to evaluate assembled structures for:

- Heat fluxes,
- Thermo-acoustic fatigue,
- Expansion behaviour,
- Structural stability under combined mechanical and thermal loading.

[See: Chapter [86](#) for testing demonstrator components and structures at high temperatures]

81.11 References

81.11.1 General

- [81-1] R. Morrell & L.N. McCartney
'Measurement of Properties of Brittle Matrix Composites'
Br. Ceram. trans., 92, 1993, No. 1, p1-7
- [81-2] D.P. Bashford & R. Raynal
'Testing and Integrity of Thermostructural Ceramic Composites'
International Symposium : Space Applications of Advanced Structural Materials, ESTEC, 21-23 March 1990, ESA SP-303 p405-409
- [81-3] J. Lord & N. McCartney
'Quantitative Assessment of the Effects of Microcracking on the Properties of a Crossply CMC'
ECCM6, Bordeaux, Sept 1993, ISBN 1-85573-142-8, p497-505
- [81-4] F.H. Gordon & T.W. Clyne
'Thermal Cycling Creep of Ti-6Al-4V/SiC Monofilament Composites under Transverse Loading'
Symposium on "Residual Stresses in Composites Modelling, Measurement and Effects on Thermomechanical Properties", TMS Annual Meeting, Denver, USA, 21-25 Feb 1993
- [81-5] B. Roebuck
'Uniaxial Testing of Particulate MMC'
1992 IoP Meeting on Test Method Development
- [81-6] R. Raynal: ESA/ESTEC
'Testing Concerns of High Temperature Materials'
First ESA/ESTEC Workshop on Thermal Protection Systems ESTEC, Noordwijk, 5-7 May 1993, ESA-WPP-053 (August 1993) p404-409
- [81-7] M. Steen & J. Bressers: JRC Petten
'Mechanical Properties Testing of Continuous Fibre Reinforced Ceramic Matrix Composites: Experimental Problems and Standardisation'
First ESA/ESTEC Workshop on Thermal Protection Systems ESTEC, Noordwijk, 5-7 May 1993, ESA-WPP-053 (August 1993) p398-403
- [81-8] N.D.R. Goddard (Editor)
'Test Techniques for Metal Matrix Composites'
UK Institute of Physics Meeting Proceedings, 28 November 1990 IOP Short Meetings Series No.28, ISBN 0-85498-530-1, 1991